



HAL
open science

L'hypoxie et le métabolisme comme approche thérapeutique dans le médulloblastome

Julie Contenti-Liprandi

► **To cite this version:**

Julie Contenti-Liprandi. L'hypoxie et le métabolisme comme approche thérapeutique dans le médulloblastome. Médecine humaine et pathologie. Université Côte d'Azur, 2022. Français. NNT : 2022COAZ6007 . tel-03701533

HAL Id: tel-03701533

<https://theses.hal.science/tel-03701533>

Submitted on 22 Jun 2022

HAL is a multi-disciplinary open access archive for the deposit and dissemination of scientific research documents, whether they are published or not. The documents may come from teaching and research institutions in France or abroad, or from public or private research centers.

L'archive ouverte pluridisciplinaire **HAL**, est destinée au dépôt et à la diffusion de documents scientifiques de niveau recherche, publiés ou non, émanant des établissements d'enseignement et de recherche français ou étrangers, des laboratoires publics ou privés.



THÈSE DE DOCTORAT

L'hypoxie et le métabolisme comme approche thérapeutique dans le médulloblastome

Julie CONTENTI

Centre Méditerranéen de Médecine Moléculaire (C3M)
INSERM U1065

Présentée en vue de l'obtention du grade de docteur
en Sciences de la vie et de la santé d'Université Côte d'Azur

Dirigée par : Nathalie Mazure

Soutenue le : 15 Mars 2022

Devant le jury, composé de :

Pr Jacques LEVRAUT
Dr François VALLETTE
Dr Hélène CASTEL
Dr Matthieu ROULEAU
Dr Célio POUPONNOT

PU-PH, CHU de Nice, France
DRCE, INSERM, Nantes, France
DR2, INSERM, Rouen, France
CRCN, INSERM, Nice, France
DR2, INSERM, Paris, France

Président du jury
Rapporteur
Rapporteuse
Examineur
Examineur

L'hypoxie et le métabolisme comme approche thérapeutique dans le médulloblastome

Membres du jury :

Président du jury

Pr Jacques LEVRAUT

PU-PH, CHU de Nice, France

Rapporteurs

Dr François VALLETTE

DRCE, INSERM, Nantes, France

Dr Hélène CASTEL

DR2, INSERM, Rouen, France

Examineurs

Dr Matthieu ROULEAU

CRCN, INSERM, Nice, France

Dr Célio POUPONNOT

DR2, INSERM, Paris, France

Résumé et mots clefs

Le médulloblastome (MB) est une tumeur maligne cérébrale qui touche principalement les enfants. Elle est rarement retrouvée chez l'adulte. Parmi les quatre groupes de MB définis aujourd'hui selon des caractéristiques moléculaires, le groupe 3 est le moins favorable avec un taux de survie globale de 50 %. Les traitements actuels, basés sur la chirurgie, la radiothérapie et la chimiothérapie, ne sont pas suffisamment adaptés aux différentes caractéristiques des quatre groupes de MB.

Dans ce travail de thèse, nous avons abordé le problème du médulloblastome d'un point de vue métabolique dans un microenvironnement appauvri en oxygène, afin de se rapprocher au plus près des conditions physiologiques. L'hypoxie tumorale, et le métabolisme qui en résulte, ont été peu étudiés dans le MB. Dans ce travail, nous montrons que Hypoxia-Inducible Factor-1 alpha (HIF-1 α), sous-unité du facteur de transcription HIF-1 qui régule la réponse cellulaire. L'hypoxie, du groupe 3 des MB a soit une possible modification post-traductionnelle, soit des mutations dans le domaine PAS-A de HIF-1 α pouvant bloquer l'association avec HIF- α et entraînant un HIF-1 totalement inactif. Seul HIF-2 est alors présent pour remplacer HIF-1 dans l'activation des voies de signalisation métaboliques en condition d'hypoxie. Les données *in vitro* ont montré que l'inhibiteur pharmacologique de HIF-2 α , le PT2385, en association avec la metformine, un inhibiteur spécifique du complexe I mitochondrial, peut efficacement bloquer la prolifération et entraîner la mort des cellules du groupe 3 par rapport aux autres groupes de MB.

En parallèle, nous avons établi que les cellules du groupe 3 sont aussi plus sensibles à la phenformine, un autre inhibiteur du complexe I mitochondrial, que les cellules des autres groupes. De plus, nous avons montré que ce sous-groupe utilise différemment les deux navettes, la glycérophosphate déshydrogénase mitochondriale (mGPDH) et la navette malate-aspartate (MAS), qui permettent au NADH de se déplacer du cytoplasme vers les mitochondries, et de régénérer ainsi le NAD⁺ cytosolique. L'utilisation en combinaison de la phenformine et de l'iGP1, un inhibiteur spécifique de mGPDH, ainsi que l'association des deux inhibiteurs spécifiques des deux navettes, iGP1 et AOAA, ont clairement montré une plus grande capacité à diminuer la prolifération cellulaire et à induire la mort cellulaire spécifiquement pour les cellules du groupe 3 par rapport aux cellules des autres groupes.

Notre étude renforce l'idée d'hétérogénéité non seulement moléculaire mais aussi métabolique dans les différents groupes qui constituent le médulloblastome et apporte de nouvelles solutions thérapeutiques potentielles pour les patients du groupe 3 représentant les tumeurs les plus agressives.

Mots clefs : Médulloblastome, Hypoxie, Métabolisme

Abstract

Medulloblastoma is the most common brain cancer in children. Among the subclassification into four groups, Group 3 is the most metastatic, with a poor prognosis and for which few treatments are effective. Moreover, the genetics and biology underlying the Group 3 MB subgroup remain less clear compared to the other groups ¹. Any new markers or genetic abnormalities will allow to consider new therapeutic developments. Tumor hypoxia and consequent metabolism have been little studied in medulloblastoma (MB). In this study, we show that Group 3 MB have either a post-translational modification or mutations in the PAS-A domain of HIF-1a blocking association with HIF-1b, the subsequent entry into the nucleus, resulting in a completely inactive HIF-1. Only HIF-2 is then present to replace HIF-1 in the activation of metabolic pathways. *In vitro* data showed that pharmacological inhibitor of HIF-2a, PT2385 ^{2,3} coupled with Metformin, a specific inhibitor of the mitochondrial complex I, can efficiently block and kill Group 3 MB compared to Non-Group 3 MB. HIF-2 emerges as the key HIF isoform that is essential for Group 3 MB to respond to a hypoxic microenvironment. But it also becomes its Achilles heel, as PT2385, and others, can specifically target HIF-2 without fear of possible HIF-1 compensation.

We also established that cells in group 3 are more sensitive to Phenformin, a complex 1 inhibitor, than cells in other groups. Furthermore, we showed that this subgroup differentially utilizes the two shuttles, mitochondrial glycerophosphate dehydrogenase (mGPDH) and malate-aspartate shuttle (MAS), which allow NADH to move from the cytoplasm to the mitochondria. The use of phenformin and iGP1, a specific inhibitor of mGPDH, as well as the combination of the two specific inhibitors of the two shuttles, iGP1 and AOAA, clearly showed a greater ability to decrease cell proliferation and induce cell death specifically for cells in group 3 compared to cells in other groups. Finally, the addition of GNE-140, a potent inhibitor of lactate dehydrogenase A, potentiated the effect of the different combinations used. Our study reinforces the idea of not only molecular but also metabolic heterogeneity in the different groups that constitute medulloblastoma and provides a potential new therapeutic solution for patients in group 3 whose tumors are more aggressive.

Keywords: glycolysis; hypoxia; malate-aspartate shuttle; medulloblastoma; mitochondrial glycerophosphate dehydrogenase; mitochondrial respiration; phenformin

REMERCIEMENTS

J'aimerais tout d'abord remercier le **Pr Jacques Levrault**, qui me fait l'honneur d'être mon président du jury de thèse. Je le remercie de m'avoir guidée pendant toutes ces années et de m'avoir donnée la chance de m'épanouir dans ma vie professionnelle. Vous êtes pour moi un exemple de réussite, et j'espère pouvoir continuer à avancer et à apprendre à vos côtés.

Je tiens également à remercier les membres du jury qui ont accepté de donner un peu de leur temps précieux pour juger mon travail : mes rapporteurs **Dr Hélène Castel** et **Dr François Vallette**, ainsi que mes examinateurs **Dr Matthieu Rouleau** et **Dr Célio Pouponnot**.

Ça y est le temps de la thèse est maintenant terminé, quatre années riches en rencontres et en souvenirs. Les deux dernières années ont été particulièrement difficile pour moi, devant jongler entre mon travail de thèse et mon activité clinique d'urgentiste rythmée par une pandémie exceptionnelle, mais j'y suis arrivée et cela grâce au soutien inconditionnel de ma directrice de thèse : le Dr Nathalie Mazure.

Nathalie, je ne te remercierai jamais assez pour ton encadrement et ta rigueur scientifique sans faille, ta disponibilité et ta grande gentillesse. Tu as réussi à transformer mon esprit de médecin en un esprit scientifique, à me faire comprendre que chaque résultat est une mine d'information qu'il faut apprendre à interpréter, même si ce ne sont pas les résultats attendus, à faire grandir mon esprit. Je n'oublierai jamais nos conversations devant ce tableau blanc assis par terre au milieu du couloir, égayant la curiosité de l'ensemble du laboratoire, ou encore ces nombreux moments à réparer et réparer encore ces foutues enceintes à hypoxie. Tu aimes profondément ton travail de chercheur et ton investissement dans ton travail est énorme, j'espère avoir été à la hauteur de tes exigences.

J'aimerais remercier également l'ensemble de l'équipe 5 du C3M, qui a contribué à mon apprentissage (Mounia, Stephan, Charlotte) et tout particulièrement le **Dr Frédéric Bost** pour avoir accepté de m'accueillir dans son équipe de recherche, et avoir apporté à ce travail une lecture critique et constructive. Fred, tu es un chef d'équipe d'une extrême gentillesse et bienveillance, tu as fait de ma première expérience en recherche un moment agréable et enrichissant, grâce notamment à ton humour très personnel. Un grand merci également à **Dominique** pour sa gestion quotidienne de toutes nos commandes, sans qui aucunes expériences ne serait possible.

Un grand merci à mes acolytes du laboratoire, master, thésards, post-doc, sans qui mon parcours dans ce monde scientifique aurait été nettement moins agréable. **Nirvana**, merci de m'avoir fait découvrir le monde de la recherche. Mon année de Master II à tes côtés a été un véritable plaisir. Tu es une de mes plus belles rencontres dans ce monde « l'Hospitolo-Universitaire ». **Lucilla**, tu es partie vers d'autres aventures maintenant, mais un grand merci pour tes conseils, ton écoute, ton aide dans les manips, ton sourire, bref le bonheur à l'italienne. Je te souhaite que du bonheur sur Paris. **Monique**, tu as été une très belle rencontre, merci pour ta joie de vivre et ton soutien au laboratoire. Un énorme merci à toi **Yingbo**, pour ton aide précieuse dans les manips, j'ai toujours pu compter sur toi, et ne t'inquiète pas on va finir par réussir à te faire payer pour ton stage de Master II. Je te souhaite beaucoup de réussite pour la fin de ta thèse.

Victor (mon Tchoupi du laboratoire), nous avons débuter presque au même moment, et tu as été un véritable pilier pour moi dans cette équipe. Merci pour ton aide, ton soutien. J'espère vraiment que tu trouveras l'épanouissement professionnel que tu mérites, et encore félicitations pour ta thèse !!

Mathieu, quelle surprise de voir un chirurgien (Urologue) venir faire des Western-Blot. Ton passage dans l'équipe a été pour moi un véritable rayon de soleil. Et je reste persuadé qu'un jour tu regretteras de ne pas avoir fait une thèse de science....

Marie, merci d'avoir égayé toutes mes pauses café, merci de parler aussi fort (comme ça je t'entends dans les couloirs quand tu arrives), merci de me faire rire tout simplement. Plus sérieusement, merci de ton aide précieuse en imagerie tu es la reine du microscope.

En tout cas nos pauses en haut des escaliers, tous ensemble, à refaire le monde, à parler sans filtres de nos expériences échouées (encore une fois...), de nos contaminations en salle de culture, de nos envies de tout envoyer balader : tout ça va terriblement me manquer.

Merci à toute l'équipe médicale du service des urgences, qui a accepté que je ne sois présente dans le service que la moitié du temps. Vous vous êtes souvent demandé ce que je faisais vraiment au laboratoire, alors je vous souhaite une bonne lecture.

Je n'oublie pas les personnes présentes avant le commencement de cette thèse, sans qui rien n'aurait été possible. Je remercie sincèrement mes parents, qui m'ont inculqué de grandes valeurs : le respect, le travail, la persévérance. C'est en grande partie grâce à vous si aujourd'hui j'en suis là. Enfin je voudrais remercier la personne qui partage ma vie depuis plus de 10 ans. Laurent, tu as rendu cette étape possible, en consacrant à notre famille le temps que je n'avais pas. Tu m'as soutenu du début jusqu'à la fin, tu contribue à mon équilibre et mon bonheur, sans toi rien n'est possible. Merci encore pour tout.

Table des matières

Introduction.....	11
Chapitre 1 : Le Médulloblastome	12
I- Définition	12
II- Épidémiologie	12
III - Classification du médulloblastome	13
A- Classification histologique	13
B- Classification moléculaire	15
C- Hétérogénéité intra-tumorale	17
IV- Impact clinique de la classification moléculaire	19
A- Localisation des différents sous-groupes de médulloblastome	19
B- Stratification du risque	20
1- Potentiel métastatique	21
2- Récidive et pronostic	21
V- Stratégies thérapeutiques actuelles	21
A- La chirurgie	22
B- La radio-chimiothérapie concomitante	22
C- Les modèles pré-cliniques pour l'étude du MB	24
1- Modèles cellulaires	24
2- Modèles animaux.....	27
Chapitre 2 : L'hypoxie tissulaire	30
I- Hypoxie et cancer	32
A- Hypoxie et système nerveux central (SNC)	35
II- Hypoxia-inducible factor (HIF)	36
A- Conformation de HIF-1	37
B- Régulation de la sous-unité HIF α	39
1- Régulation de HIF-1 α	39
2- Régulation de HIF-2 α	41
C- Régulation de HIF par modifications post-traductionnelles	41
D- Autre mécanismes régulant HIF, dépendant ou non de l'oxygène	44
D - Mutations de HIF	45
III- Expression génique de l'hypoxie	46
A- Gènes cibles de HIFs	48
1- Le Métabolisme du glucose (HIF-1 >> HIF-2)	48
2- Métabolisme lipidique (HIF-2 = HIF-1)	49
3- Angiogenèse (HIF-1>> HIF-2)	49
4- Prolifération et cycle cellulaire (HIF-2 >> HIF-1)	50
5- Cellules souches cancéreuses (HIF-2>> HIF-1)	50
B- Effet compensateur HIF-1 et HIF-2	51
C- HIF et MYC	51
IV- HIF comme cible thérapeutique	52
Chapitre 3 : Le métabolisme comme approche thérapeutique	57
I- Glycolyse et phosphorylation oxydative	57
II- Voie de régénération du NAD ⁺ cytosolique	61
A- Navette Malate/Aspartate	62
B- Navette Glycérol-Phosphate	64
III- Les navettes comme cibles thérapeutiques	66
IV- Les biguanides et le métabolisme des cellules cancéreuses	67
A- Qu'est-ce que les biguanides ?	67
B- Mécanismes d'action anti-cancéreux des Biguanides	68
1- Le complexe I mitochondrial.....	68
2- La Glycérophosphate déshydrogénase mitochondriale (mGPDH)	69
C- Activation de voies métaboliques compensatrices	70

1- La Glycolyse.....	70
2- Le métabolisme de l'Aspartate, de la Glutamine et de la Sérine	71
Objectifs	74
Résultats	77
Article 1	78
I- Contexte et objectifs	78
II- Article	80
III- Figures en préparation	109
III.1 Complément Figure 1	109
III. 5 Complément Figure 4	111
IV- Conclusion et discussion de l'article 1	112
A- Analyse complexe de HIF-1 α dans le groupe 3	113
B- Par quel mécanisme le PT2385 diminue la viabilité des MB du groupe 3 ?	115
Article 2	118
I- Contexte et objectifs	118
II- Article	120
III- Figure 7 en préparation	164
IV- Conclusions et Discussion de l'Article 2	164
A- L'importance des conditions expérimentales	165
B- Quelle navette est la plus importante dans le MB ?	166
C- L'effet cumulatif des inhibiteurs de navettes	167
D- Importance de la Lactate déshydrogénase (LDH) dans le MB ?	168
Discussion générale	170
et perspectives.....	170
Annexes.....	195
Annexe 2: Co-culture of human fibroblasts, smooth muscle and endothelial cells promotes osteopontin induction in hypoxia. J cell Mol Med. 2020.	217
Annexe 3: Role of hypoxia and metabolism in the development of neointimal hyperplasia in arteriovenous fistulae. Int J Mol Sci. 2019	228
Annexe 4: Identification of a new aggressive axis driven by ciliogenesis and absence of VDAC-deltaC in clear cell Carcinoma patients. Theranostics. 2020	259

LISTE DES ABREVIATIONS

AAT	Aspartate Amino-Transferase
AcCoA	Acétyl-CoA
ADN	Acide Désoxyribo Nucléique
ADP	Adénosine DiPhosphate
AMP	Adénosine MonoPhosphate
AMPK	AMP-Activated Protein Kinase
AOAA	Acide Amino-OxyAcétique
ARN	Acide Ribo Nucléique
ARNT	Aryl hydrocarbon Receptor Nuclear Translocator
ATP	Adénosine TriPhosphate
bHLH	Basic-Helix-Loop-Helix
BNIP3	BCL2/adenovirus E1B 19 kDa protein-Interacting Protein 3
CBP	CREB-Binding Protein
ccRCC	clear cell Renal Cell Carcinoma
CDK	Cycline Dépendante des Kinases
CSC	Cellules souches Cancéreuses
CSI	Cranio-Spinal Irradiation
ESC	Embryonic Stem cell
FAD	Flavin Adenine Dinucleotide
FDA	Food and Drug Administration
FIH	Factor Inhibiting HIF
GBM	Glioblastome
GEMM	Genetically Engineered Mouse Models
GLUT	Glucose Transporter
GPDH	Glycerol Phosphate DeHydrogenase
GSK-3	Glycogen synthase Kinase-3
HAF	Hypoxia-Associated Factor
HIF	Hypoxia-Inducible Factor
HRE	Hypoxia-Responsive Element
Hsp	Heat-shock protein

IGF	Insulin-like Growth factor
IHC	Immunohistochimie
iPSC	induced Pluripotent Stem cell
LDHA	Lactate Dehydrogenase A
MB	Médulloblastome
MCT	MonoCarboxylate Transporter
MDH	Malate DeHydrogenase
NAD	Nicotinamide Adenine Dinucleotide
NLS	Nuclear localisation sequence
OCT	Organic Cation Transporter
ODDD	Oxygen-Dependant Dégradation Domain
OMS	Organisation Mondiale de la Santé
PAS	per-Arnt-SIM
PDGF	Platelet Derived Growth Factor
PDH	Pyruvate DeHydrogenase
PDX	Patient-Derived Xenograft
PHD	Prolyl Hydroxylase Domain
PI3K	Phosphatidylinositol-3-Kinases
PKA	Protéine Kinase A
pVHL	Protéine Von Hippel-Lindau
ROS	Reactive Oxygen Species
SHH	Sonic Hedg-hog
SiRNA	Small interfering RNA
SNC	Système Nerveux Central
TAD	TransActivation Domain
TCA	TriCarboxylic Acid
TGF	Transforming-Growth Factor
TNF	Tumor Necrosis Factor

Listes des Figures et Tableaux

FIGURE 1 : ANATOMIE DU CERVELET.	11
FIGURE 2 : CARACTERISTIQUES MORPHOLOGIQUES ET HISTOLOGIQUES DES DIFFERENTS TYPES DE MB APRES COLORATION A L'HEMATOXYLINE/EOSINE.	13
FIGURE 3 : VOIE DE SIGNALISATION SHH.	15
TABLEAU 1 : CARACTERISTIQUES DE CHAQUE SOUS-GROUPE DE MEDULLOBLASTOME.	16
FIGURE 4 : LOCALISATION PREFERENTIELLE, DES DIFFERENTS SOUS-GROUPES DE MB.	18
TABLEAU 2 : STRATIFICATION DU RISQUE EN FONCTION DU SOUS-GROUPE DE MB.	19
TABLEAU 3 : DIFFERENTES LIGNEES CELLULAIRES DE MB EXISTANTES (LISTES NON EXHAUSTIVES).	25
FIGURE 5 : RESUME DES METHODES ET APPROCHES TECHNIQUES DE LA MODELISATION DU MEDULLOBLASTOME.	27
TABLEAU 4 : DIFFERENTS MODELES EXISTANT DE SOURIS GENETIQUEMENT MODIFIEES.	28
FIGURE 6 : REPARTITION DU POURCENTAGE D'OXYGENE DANS L'ORGANISME HUMAIN.	30
FIGURE 7 : SCHEMA ANATOMIQUE DU CERVEAU EN COUPE SAGITTALE.	30
FIGURE 8 : CARACTERISTIQUE DES TUMEURS HYPOXIQUES.	31
TABLEAU 5 : COMPARAISON DES CONCENTRATIONS D'OXYGENE ENTRE LE TISSU NORMAL ET LE TISSU TUMORAL.	34
FIGURE 9 : IDENTIFICATION DES 10 CARACTERISTIQUES DE LA CELLULE CANCEREUSE.	35
FIGURE 10 : CONFORMATION DES DIFFERENTES SOUS-UNITES DE HIF-1.	36
FIGURE 11 : CONFORMATION DES SOUS UNITES HIF-1 α ET HIF-1 β .	37
FIGURE 12 : MECANISME DE REGULATION DE HIF-1 EN HYPOXIE.	40
FIGURE 13 : DIFFERENTS SITES DE MODIFICATION POST-TRADUCTIONNELLES AU NIVEAU DE HIF-1 α	42
FIGURE 14 : DIFFERENTS GENES DEPENDANTS DE HIF-1.	48
FIGURE 15 : MECANISMES D'ACTION DE (A) HIF-1 α ET DE (B) HIF-2 α SUR L'ACTIVITE DE MYC.	51
FIGURE 16 : DIFFERENTS COMPOSES INHIBITEURS DE HIF-1 AINSI QUE LEUR MECANISME D'ACTION.	53
FIGURE 17 : GLYCOLYSE ET PHOSPHORYLATION OXYDATIVE.	57
FIGURE 18 : COUPLAGE METABOLIQUE ASTROCYTE-NEURONE.	59
FIGURE 19 : ÉQUILIBRE SUBCELLULAIRE DU NAD ⁺ .	61
FIGURE 20 : NAVETTE MALATE-ASPARTATE.	62
FIGURE 21 : NAVETTE GLYCEROL 3-PHOSPHATE.	64
FIGURE 22 : DIFFERENTS MECANISMES D'ACTION DES BIGUANIDES (PHENFORMINE ET METFORMINE).	68
FIGURE 23 : REPROGRAMMATION METABOLIQUE POUR COMPENSER LE STRESS METABOLIQUE INDUIT PAR LE TRAITEMENT AU BIGUANIDE.	69
FIGURE 24 : ÉLECTROPHORESE SUR GEL DE DIFFERENCE BIDIMENSIONNELLE (2D DIGE)	109
FIGURE 25 : EXPRESSION DE PHD2 ET PHD3 DANS LE GROUPE 3 COMPARATIVEMENT AU GROUPE SHH.	113
FIGURE 26 : EXPERIENCE IN VIVO SUR PDX TRAITES AVEC LE PT2385.	115

Introduction

Chapitre 1 : Le Médulloblastome

I- Définition

En 1925, le neurochirurgien Percival Bailey identifia un nouveau type de gliome survenant principalement au centre du cervelet des enfants et lui donna le nom de médulloblastome (MB)(Bailey. 1925).

Il s'agit d'une tumeur primitive maligne neuro-ectodermique (PNET) du système nerveux central se développant aux dépens des cellules du cervelet, organe situé au niveau de la fosse postérieure (**Figure 1**) et essentiel aux fonctions motrices (coordination et synchronisation des mouvements) et dans une moindre mesure aux fonctions cognitives telle que l'attention, le langage, la régulation de la peur et du plaisir.

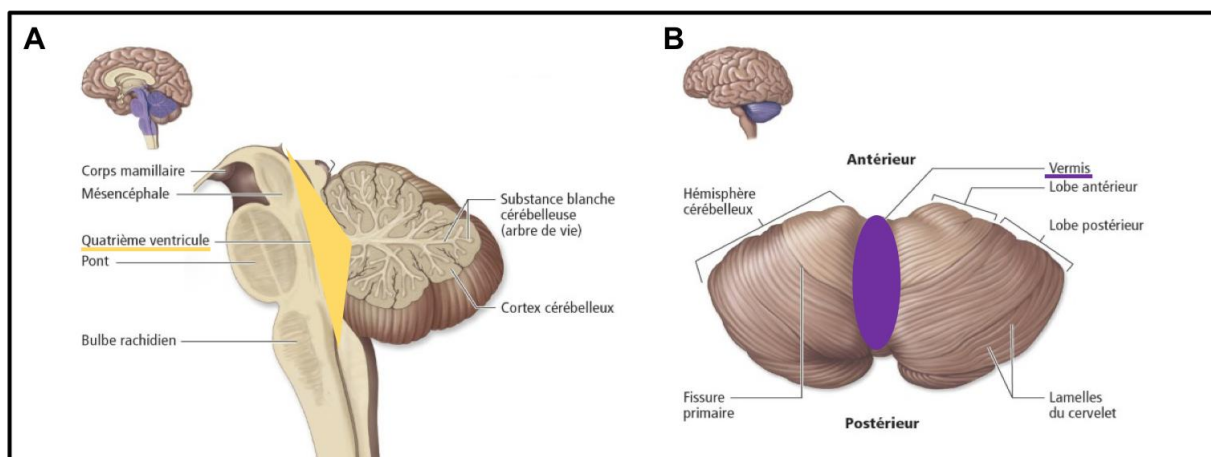


Figure 1 : Anatomie du cervelet. (A) coupe sagittale, (B) vue supérieure. (Adaptée de Biologie humaine 2009, Chenelière Éducation Inc.)

II- Épidémiologie

L'incidence du médulloblastome est de 5 à 10 cas pour 1 000 000 d'enfants correspondant à environ 150 nouveaux cas par an en France (Packer et al. 1999). Cela représente moins de 2% de l'ensemble des tumeurs cérébrales primitives. Cependant, le médulloblastome représente 40% de l'ensemble des tumeurs cérébelleuses et reste la première cause de tumeur cérébrale maligne de l'enfant. En effet, plus de 70% des médulloblastomes sont diagnostiqués durant l'enfance avec deux pics d'incidence (1-4 ans et 5-9 ans), et un âge médian de diagnostic à 6 ans. Le diagnostic est posé plus rarement à l'âge adulte avec une incidence dans cette population

de 0,05 cas pour 100.000. Le médulloblastome survient plus fréquemment chez les garçons (sexe ratio 1,8 :1) mais cette tendance peut varier en fonction du sous-type de tumeur comme nous le verrons plus tard (§ Chapitre III, Classification moléculaire).

En grande majorité, la mise en évidence d'un médulloblastome revêt un caractère sporadique, mais certaines prédispositions génétiques sont associées à la survenue du médulloblastome comme notamment le syndrome de Gorlin (naevomatose basocellulaire), le syndrome de Li-Fraumeni ou encore le syndrome de Bean (angiomatose cutanée et digestive). L'analyse d'une cohorte de 1022 patients atteints de médulloblastome a permis de mettre en évidence la présence de mutations germinales pathogènes sur les gènes *APC*, *BRCA2*, *SUFU* ou encore *PT53* dans 5,9% des cas. Les travaux décrits dans la littérature rapportent la présence d'une prédisposition génétique, avec une mutation sur le gène *SUFU* dans 28% et 9,7% des cas de médulloblastome de forme desmoplasique lorsqu'il s'agit respectivement d'enfants âgés de moins de 3 ans ou de moins de 14 ans au moment du diagnostic (Brugières et al. 2010). Cependant, le risque précis de développer un médulloblastome associé à la présence ou non de ces mutations germinales reste encore mal compris.

III - Classification du médulloblastome

A- Classification histologique

En 2007, l'Organisation Mondiale de la Santé (OMS) classe le MB dans les tumeurs neuro-épithéliales embryonnaires et distingue 4 sous-types histologiques (Siegfried et al. 2021) (Louis et al. 2007)(**Figure 2**).

La forme classique (**Figure 2A**) : il s'agit du type histologique le plus fréquent avec plus de 70% des cas. Caractérisée par des lésions à haute densité cellulaire composée de cellules aux noyaux arrondis ou ovalaires indifférenciées avec pléomorphisme cellulaire discret et un index mitotique élevé, hyper chromatiques, et aux cytoplasmes réduits, formant des rosettes de Homer Wright.

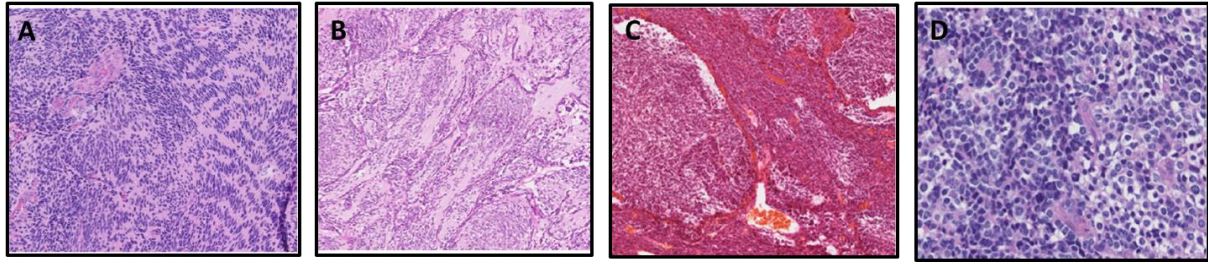


Figure 2 : Caractéristiques morphologiques et histologiques des différents types de MB après coloration à l'hématoxyline/éosine. (A) médulloblastome classique avec des arrangements palissadiques, (B) médulloblastome à nodularité extensive avec nodules clairs, (C) médulloblastome desmoplastique/nodulaire, (D) médulloblastome anaplasique caractérisé par un pléomorphisme nucléaire. (Adapté de l'article de Siegfried A et al, Neurochirurgie, 2018. (Siegfried et al. 2021)

La forme desmoplastique/nodulaire (Figure 2B) : correspond à 20% des formes de MB, elle est caractérisée par d'abondantes fibres de collagène ou de réticuline. Les nodules correspondent à des zones de maturation neuronale. Elle survient surtout chez les très jeunes enfants avec une localisation sur la ligne médiane, c'est-à-dire au niveau du vermis (Figure 1B), mais également chez l'adolescent ou le jeune adulte, alors localisée dans les hémisphères cérébelleux (Figure 1B). Le pronostic est très bon chez les jeunes enfants (Rutkowski et al. 2005).

La forme à nodularité extensive (Figure 2C) : elle est étroitement liée au MB desmoplastique/nodulaire, et représente une faible proportion des MB (3,2 à 4,2%). Elle survient chez les nourrissons et diffère de la variante nodulaire desmoplastique en présentant une architecture lobulaire nettement élargie. La composante inter-nodulaire riche en réticuline, qui domine dans la variante desmoplastique/nodulaire, est ici nettement réduite. Ce type tumoral survient chez l'enfant en bas âge, un seul cas ayant été rapporté à ce jour chez l'adulte (PMID : 26990710). Cette tumeur est surtout localisée dans le vermis (Figure 1B). Une évolution plus favorable que pour les patients atteints de MB classiques est reconnue à la fois pour la variante MB desmoplastique/nodulaire et pour le MB avec nodularité extensive.

La forme anaplasique/à grandes cellules (Figure 2D) : cette variante est caractérisée histologiquement par un pléomorphisme nucléaire marqué, un enveloppement cellule-cellule et une activité mitotique élevée, souvent avec des formes atypiques. Bien que tous les MB présentent un certain degré d'atypie, ces changements sont particulièrement prononcés et répandus dans la variante anaplasique, et correspondent à 10% des formes de MB. L'anaplasie

cytologique se traduit par une grande variabilité nucléaire, des mitoses et apoptoses fréquentes. La variante à grandes cellules présente des cellules souvent sphériques avec des noyaux ronds, une chromatine ouverte et des nucléoles centraux proéminents. Le phénotype anaplasique/à grandes cellules est associé à une amplification de MYC. Cette forme est plus agressive que les précédentes avec un pronostic plus péjoratif (Brown et al. 2000).

Une progression histologique des MB classiques aux MB anaplasiques peut être observée, au sein d'une même biopsie. Et même, si plus de 70% des cas sont considérés comme des MB classiques, la réponse aux traitements est hautement variable d'un patient à l'autre, suggérant que la forme classique est probablement très hétérogène et que la classification histologique a probablement des limites pour prédire le pronostic des patients. La difficulté à définir, dans certains cas particuliers, le sous-type histologique (hétérogénéité tumorale, matériel non représentatif, notion de desmoplasie ou de signes d'anaplasie focaux) entraîne une grande variabilité inter-observateur. L'émergence de groupes génétiquement bien déterminés a conduit à combiner la classification histologique à la classification moléculaire afin d'affiner la classification des patients atteints de MB.

B- Classification moléculaire

Depuis le début des années 2000, de multiples travaux ont permis de mettre en évidence différents profils génomiques au sein des MB (M. C. Thompson et al. 2006)(Kool et al. 2008)(Taylor et al. 2012). En 2016, l'OMS a donc réactualisé la classification des MB en y intégrant des données moléculaires en plus des données histologiques, et décrit 4 sous-groupes de MB (**Tableau 1**) (Louis et al. 2016).

- **Le groupe WNT₂**, qui est le plus rare, correspond à seulement 10% des cas et touche préférentiellement les enfants et les jeunes adultes. La suppression d'une copie du chromosome 6 ainsi qu'une mutation sur le gène *CTNNB1* codant pour la Béta-caténine sont les anomalies les plus communément retrouvées. Le **groupe WNT** présente le plus souvent une forme histologique de type classique, se situant au contact du quatrième ventricule et s'infiltrant typiquement au niveau du tronc cérébral. Le sexe ratio est de 1 pour ce groupe.
- **Le groupe SHH** représente approximativement 30% de l'ensemble des MB et présente une distribution d'âge bimodale. En effet, le groupe SHH est retrouvé principalement

chez les nourrissons (0 à 3 ans) ainsi que chez les adultes (> 16 ans). Ce **groupe SHH**, comme son nom l'indique, est caractérisé par des anomalies au niveau de la voie de signalisation Sonic Hedgehog. La plupart des nourrissons atteints de MB du **groupe SHH** sont porteurs de mutations sur les gènes *PTCH1* ou *SUFU* au niveau des lignées germinales, alors que les adultes présentent des mutations de *PTCH1* et *SMO* (**Figure 3**). Le **groupe SHH** présente le plus souvent une forme histologique de type classique ou desmoplasique/nodulaire, se situant le plus souvent au niveau des hémisphères cérébelleux chez le jeune adulte. Le sexe ratio est également de 1 pour ce groupe.

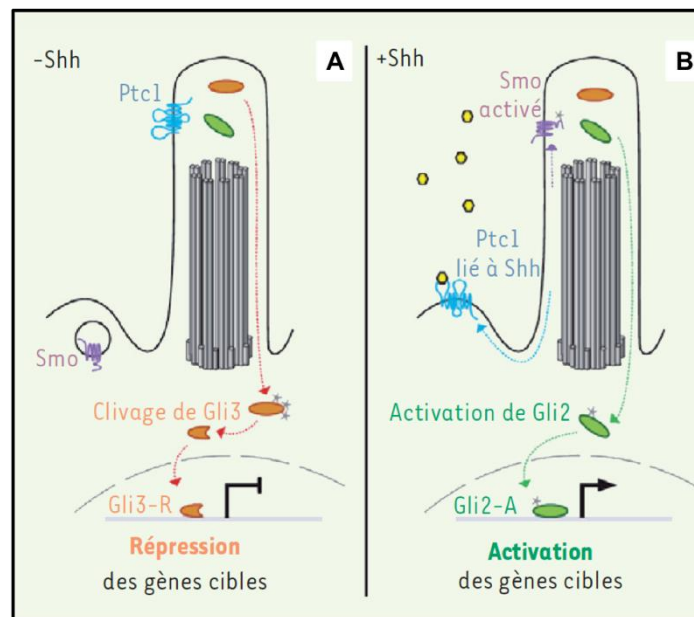


Figure 3 : Voie de signalisation SHH. (A) En l'absence de son ligand SHH, le récepteur transmembranaire Patched 1 (*Ptc1*) réprime l'accumulation de la protéine Smoothed (*Smo*), dans le cil des progéniteurs neurax. La protéine *Gli3* subit des modifications post-traductionnelles et un clivage protéolytique qui potentialise son activité de répresseur transcriptionnel (*Gli3-R*). (B) En présence de son ligand SHH fixé à son récepteur *Ptc1*, *Smo* peut s'accumuler dans le cil et activer la translocation des facteurs *Gli2* jusqu'au noyau, où il active son programme transcriptionnel. (Adaptée de l'article de Laclef C et al, *Med Sci*, 2014. (Laclef, 2014)

- **Le groupe 3** représente environ 20% de l'ensemble des MB et touche préférentiellement les hommes avec un sexe ratio de 2:1. Ce groupe est particulièrement présent chez les nourrissons ainsi que chez les enfants, mais ne se retrouve presque jamais chez l'adulte. Il est associé à une grande instabilité génomique et à une forte amplification du gène *MYC*. Le **groupe 3** se présente le plus souvent sous une forme histologique classique, mais englobe la majorité des MB anaplasiques à cellules larges

(LCA). La détection de Natriuretic peptide receptor 3 (NRP3) en immunohistochimie est considérée comme un excellent marqueur pour identifier ce groupe.

- **Le groupe 4**, quant à lui, est le plus fréquent (environ 40%). Il est caractérisé par la présence d'un isochromosome 17q (c'est-à-dire un chromosome anormal, formé de deux bras longs d'un même chromosome avec perte de l'autre bras) dans 66% des cas, et une amplification du gène *MYCN*. Il touche le plus souvent les enfants et adultes de sexe masculin avec un sexe ratio de 3:1. Le **groupe 4** est représenté le plus souvent par une forme histologique classique mais parfois par une forme anaplasique à cellules larges.



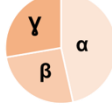
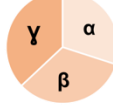
Sous-groupe	WNT		SHH				Groupe 3			Groupe 4		
	WNT α	WNT β	SHH α	SHH β	SHH γ	SHH δ	Gr 3 α	Gr 3 β	Gr 3 γ	Gr 4 α	Gr 4 β	Gr 4 γ
Proportion des sous-types												
Caractéristiques Démographiques												
Prévalence	10%		30%				20-25%			35-40%		
Age	- Enfants - Adolescents -		Nourrissons - - Adultes				Nourrissons Enfants - -			- Enfants - Adultes		
Sexe (M:F)	1:1		1:1				2:1			3:1		
Caractéristiques Cliniques												
Histologie	Classique		Desmoplasique/ nodulaire, Classique				Classique, Anaplasique			Classique, Anaplasique		
Métastases	Rare		Peu fréquent				Très fréquent			Fréquent		
Survie à 5 ans	95%		75%				50%			75%		
Pronostic	Très bon		Bon/Intermédiaire				Mauvais			Intermédiaire		
Caractéristiques Génétiques	<i>CTNNB1</i> mutation Mono chromosome 6 <i>MYC</i> +		<i>SUFU</i> mutation <i>PTCH1</i> mutation GLI2 amplification <i>MYCN</i> +				<i>Gain OTX2</i> <i>MYC</i> +++ (<i>Gr 3 γ</i>)			CDK6 amplification (<i>Gr 4 γ</i>) i17q <i>MYCN</i> + (<i>Gr 4 α</i>)		

Tableau 1 : Caractéristiques de chaque sous-groupe de médulloblastome. (Adapté de l'article de Kijima N et al, *Neurol Med Chir*, 2016. (Kijima et al., 2016)

C- Hétérogénéité intra-tumorale

Malgré les progrès sur la classification des MB et la caractérisation en sous-groupes distincts, cette affiliation n'est pas toujours corrélée à la réponse aux traitements. Des données reconnaissent aujourd'hui l'existence d'une sous-structure supplémentaire au sein des quatre

sous-groupes moléculaires, en particulier au sein des **groupes 3** et **4** (Cho et al. 2011). Ces sous-structures sont définies comme des sous-types et étiquetées α , β , *etc...* (Taylor et al. 2012).

Au sein de chaque sous-groupe primaire, des marqueurs moléculaires supplémentaires ont commencé à émerger, conduisant à des stratifications de risque plus affinées (Ramaswamy et al. 2016). Récemment, des méthodes d'analyses regroupant plusieurs types de données (expression génique, données de méthylation *etc...*) ont été développées (J. Wang and Wechsler-Reya 2014), permettant de fournir une analyse plus fine des différents groupes de MB par rapport à l'analyse de données uniques. En 2017, Cavalli *et al.* ont utilisé ces méthodes de regroupement d'analyses afin de mieux identifier l'hétérogénéité intra-tumorale, et ont mis en évidence 12 sous-types (2 pour le **groupe WNT**, 4 pour le **groupe SHH**, 3 pour le **groupe 3**, et 3 pour le **groupe 4**) (Cavalli et al. 2017). Ces sous-types ont des caractéristiques cliniques et génétiques particulières (amplifications/gains de *MYC*, *MYCN*, *OTX2*, *CDK6*, *SNCAIP* et *ACVRI*), qui permettent aujourd'hui d'affiner la compréhension du paysage génomique du MB (**Tableau 1**). Plusieurs sous-types, en particulier dans le **groupe SHH** et le **groupe 3**, présentent des différences cliniques et pronostiques claires et drastiques, ce qui permet une stratification du risque plus robuste pour les futurs essais cliniques. Parmi les 3 sous-types du **groupe 3** l'un est composé de tumeurs à forte expression de *MYC* nommées G3 γ . Ce sous-type a le plus mauvais pronostic. Le deuxième sous-type, G3 β , est surreprésenté par des tumeurs avec des altérations *GFI1*, et le dernier G3 α , par des tumeurs exprimant des gènes photorécepteurs dans lesquels on retrouve peu d'amplifications de médiateurs de la voie TGF β /Activine. En 2017, Northcott *et al.* ont démontré, sur une grande cohorte de patients atteints de MB, que les amplifications *MYC* étaient bien limitées aux patients atteints de MB du **groupe 3** (17%), tandis que les amplifications *MYCN* ont été trouvées à une fréquence comparable chez les patients atteints de MB du **groupe 3** (5%) ou du **groupe 4** (6%) (Northcott et al. 2017). Une surreprésentation significative des gènes impliqués dans les voies de signalisation Notch et TGF β a été également retrouvée dans le **groupe 3** comparativement aux autres sous-groupes. Ces études soulignent la nature hétérogène et complexe des différents sous-groupes de MB et la nécessité de continuer les efforts pour appréhender l'éventail complet des mécanismes moléculaires sous-jacents au développement du médulloblastome.

IV- Impact clinique de la classification moléculaire

A- Localisation des différents sous-groupes de médulloblastome

Étant donné que les sous-groupes de médulloblastomes (MB) sont enrichis par des altérations génétiques spécifiques et présentent des profils épigénétiques et transcriptionnels différents, on a longtemps soupçonné qu'ils provenaient de populations cellulaires ou de lignées de développement distinctes (Gilbertson et al. 2008). Des études récentes ont cherché à identifier les cellules d'origine pour chaque sous-groupe de médulloblastome. Le groupe **WNT** se développerait à partir de cellules progénitrices de la lèvre rhombique inférieure, le groupe **SHH** à partir de précurseurs de neurones des granules cérébelleuses, et le **groupe 3** proviendrait de cellules souches neurales (Gibson et al. 2010). Les cellules d'origine du médulloblastome du **groupe 4** sont restées inconnues pendant longtemps, mais une étude récente suggère qu'elles sont des progéniteurs de la lèvre rhombique supérieure (Hovestadt et al. 2019)(Lin et al. 2016). L'origine des cellules de chaque sous-groupe joue probablement un rôle dans la localisation du médulloblastome qui est là encore différente selon le sous-groupe (**Figure 4**).

La plupart des tumeurs des **groupes 3 et 4** se développent dans le vermis et infiltrent le quatrième ventricule (**Figure 3**). Les tumeurs du **groupe WNT** entrent en contact avec le tronc cérébral et se développent dans le quatrième ventricule. Inversement, les médulloblastomes du **groupe SHH** se développent principalement dans les hémisphères cérébelleux.

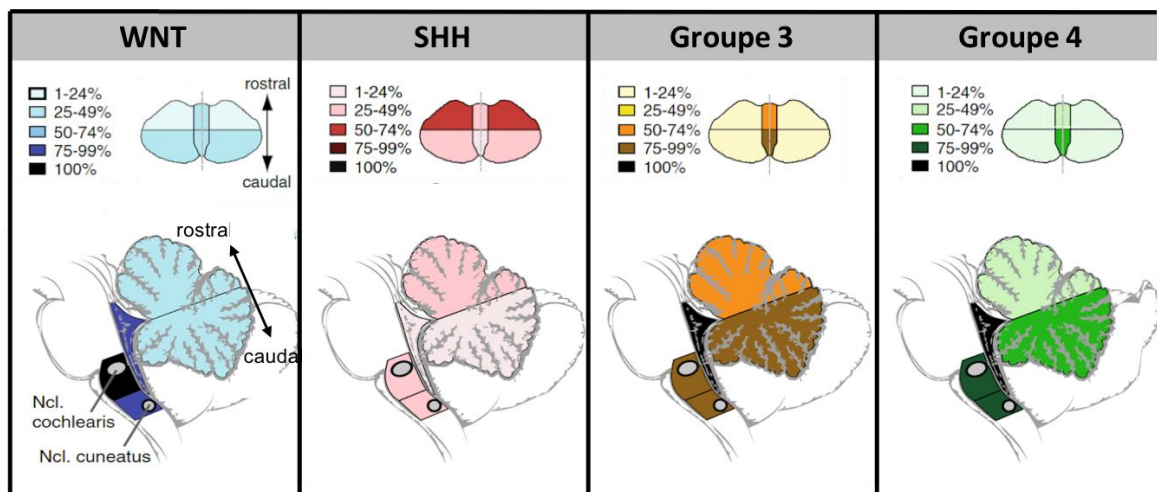


Figure 4 : Localisation préférentielle, des différents sous-groupes de MB. (Adapté de l'article de Gibson P et al, Nature, 2010. (Gilbertson et al. 2008)

B- Stratification du risque

Les patients atteints de MB ont été classiquement stratifiés en deux groupes selon leur niveau de risque sur la base des critères suivants : l'étendue de la résection, l'âge au moment du diagnostic ainsi que le statut métastatique. Les patients présentant des reliquats tumoraux > 1,5cm², âgés de moins de 3 ans au moment du diagnostic et/ou présentant une maladie métastatique étaient classés comme patients à haut risque, tandis que les autres étaient classés comme patients à risque standard. Certains sous-types histologiques, tels que les tumeurs anaplasiques et à grandes cellules, ont également été associés à un mauvais pronostic.

Parce qu'il est maintenant reconnu que le MB se compose d'au moins quatre sous-groupes moléculaires avec des caractéristiques démographiques, transcriptomiques et génomiques différents, il a été proposé de nouveaux systèmes de stratification du risque basés sur des variables cliniques, histologiques et moléculaires (Pietsch et al. 2014)(Gottardo et al. 2014). Un groupe d'experts a édité une conférence en 2015 incorporant des marqueurs moléculaires pronostiques et a suggéré une stratification du risque plus affinée pour les tumeurs touchant les enfants âgés de 3 à 17 ans (Ramaswamy et al. 2016). Les quatre catégories proposées comprennent les MB à risque faible, standard, élevé et très élevé (**Tableau 2**).

Niveau de risque	Faible (Survie > 90%)	Standard (Survie 75-90%)	Elevé (Survie 50-75%)	Très élevé (Survie < 50%)	Inconnu
WNT	<ul style="list-style-type: none"> Non métastatique Age < 16 ans 				<ul style="list-style-type: none"> Métastatique
SHH		<ul style="list-style-type: none"> Non métastatique TP53 non muté Pas d'amplification de MYCN 	<ul style="list-style-type: none"> Amplification de MYCN Métastatique 	<ul style="list-style-type: none"> TP53 muté 	
Groupe 3		<ul style="list-style-type: none"> Non métastatique Pas d'amplification de MYC 		<ul style="list-style-type: none"> Métastatique avec amplification de MYC 	<ul style="list-style-type: none"> Non métastatique avec amplification de MYC 117q Anaplasique/à grandes cellules
Groupe 4	<ul style="list-style-type: none"> Non métastatique Perte du chromosome 11 Gain du chromosome 17 	<ul style="list-style-type: none"> Non métastatique sans perte du chromosome 11 	<ul style="list-style-type: none"> Métastatique 		<ul style="list-style-type: none"> Anaplasique/à grandes cellules

Tableau 2 : Stratification du risque en fonction du sous-groupe de MB. (Adapté de l'article de Ramaswamy V et al, Acta Neuropathol, 2016. (Ramaswamy et al. 2016)

1- Potentiel métastatique

La fréquence de présence de métastases lors du diagnostic diffère selon le sous-groupe moléculaire des médulloblastomes, avec un haut potentiel métastatique pour les **groupes 3 et 4** comparativement aux **groupes WNT et SHH (Tableau 1)**. La plupart des métastases (95%) se situent au niveau du système nerveux central sous la forme de nodules au niveau de l'encéphale et/ou du névraxe ou d'une méningite tumorale (Aref and Croul. 2013). Plus rarement (moins de 5% des cas) les métastases peuvent apparaître au niveau d'autres organes comme le foie, le poumon ou les os puis la moelle osseuse (Kleihues et al. 2002).

2- Récidive et pronostic

Là encore, la fréquence de récurrence après traitements est différente selon le sous-groupe avec un risque de récurrence plus important dans les **groupes 3 et 4** comparativement aux autres groupes. Le mode de récurrence diffère également. En effet, les médulloblastomes du **groupe SHH** présentent principalement une récurrence locale, tandis que les **groupes 3 et 4** présentent des récurrences de type métastatique.

De façon assez attendue, le **groupe WNT** présente donc le meilleur pronostic avec une survie globale à 5 ans de 95%. Les patients du **groupe SHH** ont, quant à eux, globalement un pronostic intermédiaire avec une survie à 5 ans de 75% mais un risque très faible de métastases.

Les patients des **groupes 3 et 4** présentent le plus haut potentiel métastatique, avec un pronostic intermédiaire, voire pauvre, et une survie à 5 ans pouvant atteindre les 50%. Une amplification de *MYC*, dans les **groupes 3** confèrent une survie particulièrement courte avec seulement 20% des patients survivant 5 ans après le diagnostic (Tamayo et al. 2011) (**Tableau 2**). Le sous-type histologique est également corrélé à la survie sans événement à 5 ans avec une survie plus faible (57%) pour les tumeurs anaplasiques à grandes cellules (Gajjar et al. 2006a).

V- Stratégies thérapeutiques actuelles

Les approches thérapeutiques actuelles tiennent compte de deux facteurs principaux pour le choix du traitement post-opératoire : le risque de toxicité du traitement et le risque de récurrence. Le risque de toxicité du traitement est particulièrement important pour les nourrissons et les enfants de moins de 3 ans. Le risque de récurrence est considéré comme élevé en cas de maladie métastatique ou de résection sous-optimale, avec un résidu tumoral $\geq 1,5\text{cm}^2$. Trois groupes de

traitements peuvent être définis en fonction de ces critères : (i) les enfants de plus de 3 ans atteints d'une maladie à risque standard, (ii) les enfants de plus de 3 ans atteints d'une maladie à haut risque et (iii) les nourrissons et enfants de moins de 3 ans.

A- La chirurgie

La chirurgie est la première étape thérapeutique, avec une résection qui se veut la plus totale mais sans vouloir être trop ambitieuse car le risque de lésion cérébelleuse est non négligeable (Puget et al. 2009). La résection totale chez les patients atteints de MB du **groupe 4** permet un bénéfice en termes de survie sans progression par rapport à une résection subtotalaire, en particulier en présence d'une maladie à un stade métastatique. Cependant l'étendue de la résection n'est pas liée à la survie globale du MB (E. M. Thompson et al. 2016). Les objectifs primordiaux et actuels de la chirurgie restent donc l'approvisionnement en tissus pour l'analyse histopathologique et le diagnostic moléculaire, ainsi qu'une cytoréduction maximale sûre, garantissant le moins d'effets secondaires.

B- La radio-chimiothérapie concomitante

Après la chirurgie, les patients sont traités par radiothérapie sur l'axe crano-spinal avec une irradiation supplémentaire sur le site de la tumeur, avec des doses de rayonnement variables selon les groupes à risque. Les patients atteints de MB à risque standard sont traités avec une irradiation crano-spinale (CSI) de 23,4Gy sur l'ensemble du cerveau et de la colonne vertébrale, et une irradiation supplémentaire de la fosse postérieure pour une dose totale de 54 à 55,8Gy (R J Packer et al. 1999)(Wahba et al., 2013). En revanche, les patients à haut risque reçoivent une CSI de 36 à 39,6Gy avec une irradiation supplémentaire au site tumoral, pour une dose totale de 54 à 55,8Gy (Gajjar et al., 2006).

La radiothérapie est généralement initiée 30 jours après la chirurgie, car l'administration tardive est associée à une survie plus faible (Schwalbe et al. 2017). Une étude a cependant identifié une diminution de la survie globale à 5 ans chez les patients bénéficiant d'une radiothérapie initiée précocement dans les 3 semaines après la chirurgie, indiquant qu'un temps suffisant pour la cicatrisation post-chirurgicale est également primordial (Chin et al. 2018). La radiothérapie est associée à de nombreux effets secondaires, en particulier chez les enfants de moins de 5 ans (handicap neurocognitif permanent, dysfonctionnement neuro-endocrinien, troubles de la croissance, infertilité, malformations de croissance et une possible malignité secondaire) ((Silber et al. 1992)). Cependant, le report de la radiothérapie post-opératoire, même à l'ère

moderne de la chimiothérapie, est associé à une survie globale moins bonne et n'est donc pas recommandé pour les enfants de plus de 3 ans (Kann et al. 2016).

La plupart des essais cliniques les plus récents menés sur le MB a incorporé l'évaluation du risque basé lui-même sur des critères moléculaires, dans le choix de la stratégie thérapeutique permettant, dans certains cas (ex : groupe WNT à risque standard), une modification du protocole de radiothérapie avec notamment une diminution de la dose reçue par le patient (Thomas et al. 2000)(Shen et al., 2021)(Ashley et al. 2012). Des techniques récentes, comme la radiothérapie protonique semble permettre de limiter l'irradiation des tissus normaux avec une survie similaire à la radiothérapie conventionnelle (Yock et al. 2016). Néanmoins, des études supplémentaires sont nécessaires pour déterminer si la radiothérapie protonique offre un gain cognitif à long terme cliniquement significatif par rapport aux protocoles de radiothérapie par faisceau de photons (Kahalley et al. 2016).

Concernant la chimiothérapie, elle a été initialement ajoutée à la gestion du MB dans les années 1970 comme moyen d'augmenter la survie, puis dans les années 1990 comme moyen de compenser les résultats de survie inférieurs provoqués par la réduction de la dose de radiothérapie chez les patients atteints de MB non métastatique de 36,0Gy à 23,4Gy (Thomas et al. 2000). Au cours des années suivantes, la chimiothérapie s'est avérée être un complément précieux à la chirurgie et à la radiothérapie et a considérablement contribué à l'augmentation de la survie chez les personnes métastatiques et non métastatiques.

L'approche thérapeutique actuelle comprend une radiothérapie adaptée au risque et quatre cycles de chimiothérapie à dose intensive à base de Cyclophosphamide (incorporant du Cisplatine ou de la Vincristine). Ce schéma thérapeutique entraîne 85% de survie à 5 ans (IC à 95% 75-94) dans la population de MB à risque standard et 70% de survie à 5 ans (IC à 95% 54-84) dans la population à haut risque (Gajjar et al. 2006). Un autre schéma thérapeutique envisageable pour les patients à haut risque comprend une radiothérapie à dose réduite (30,6 à 23,4Gy) complétée par une chimiothérapie en tandem à haute dose (2 cycles avant et 4 cycles après radiothérapie) suivie d'une autogreffe de cellules souches. Ce schéma entraîne des taux de survie sans événement à 5 ans de 70% et une survie globale de 74% (Sung et al. 2013). Ces dernières années, les recherches sur l'optimisation des schémas thérapeutiques n'ont cessé de progresser. Une étude récente à confirmer que la combinaison de Gemcitabine et d'Axitinib, hautement cytotoxique, ne nécessitant que de faibles concentrations pico molaires lorsqu'elle est utilisée en combinaison, avait une efficacité en termes de contrôle tumoral et de survie dans un modèle de MB du groupe 3 (Schwinn et al. 2021). Dans cette étude, la Gemcitabine et

l'Axitinib ont été mieux tolérés que le régime standard comprenant du Cisplatine et du Phosphate d'Etoposide. Un autre travail récent s'intéressant à l'Axitinib (inhibiteur de tyrosine kinase puissant et sélectif des récepteurs du facteur de croissance de l'endothélium vasculaire), a montré un indice de sélectivité élevé pour les cellules de MB par rapport aux cellules normales du cervelet, en réduisant efficacement le taux de croissance des tumeurs expérimentales (Pagnuzzi-Boncompagni et al. 2021).

Un obstacle majeur à la mise en place de stratégies thérapeutiques encore plus efficaces avec le moins de toxicité possible a été jusqu'ici la gestion du MB en tant que maladie uniforme. Il est aujourd'hui indispensable d'attribuer une thérapie différentielle aux différents groupes à risque sur la base de caractéristiques moléculaires et cliniques, offrant ainsi une opportunité de personnaliser la thérapie et d'éviter un traitement excessif ou insuffisant. Par exemple, dans l'essai HIT'2000, comprenant une chimiothérapie d'induction renforcée avec une CSI hyperfractionnée et quatre cycles de chimiothérapie d'entretien (composés de cisplatine, et vincristine), la survie des patients était associée à la présence d'amplifications *MYC/MYCN*, suggérant que celles-ci pourraient être utiles dans les futures schémas thérapeutiques (von Bueren et al. 2016).

Il est urgent de découvrir de nouvelles voies médicamenteuses pour les sous-groupes présentant des taux des métastases fréquents et un faible niveau d'altérations moléculaires, tels que les MB du **groupe 3** et du **groupe 4**. Pour cela, le développement de modèles pré-cliniques *in vivo* et *in vitro* est indispensable.

C- Les modèles pré-cliniques pour l'étude du MB

1- Modèles cellulaires

Plusieurs lignées cellulaires de médulloblastome humain ont été établies *in vitro* au fil des années et ont été bien décrites (Y. Lee et al. 2003)(Ivanov et al. 2016). Sans surprise, la plupart ont été générés à l'aide de MB agressifs du **groupe 3** avec amplification de *MYC*. Bien que ces lignées tumorales humaines établies soient faciles à cultiver, sous forme de monocouches ou de sphères, et soient couramment utilisées pour évaluer l'effet de certaines thérapeutiques médicamenteuses dans les essais précliniques, une analyse moléculaire récente par séquençage de nouvelle génération a révélé que dans certains cas, ces lignées peuvent acquérir des

mutations supplémentaires et/ou perdre du matériel génétique. Actuellement, il existe environ 44 lignées cellulaires de médulloblastome établies sur une période de quatre décennies (J. Xu et al. 2015). En raison de la diversité des méthodes de caractérisation utilisées au fil des années, il peut être très difficile d'avoir une vue d'ensemble du paysage des lignées cellulaires du MB. De plus, avec la classification moléculaire actuelle du MB, il est essentiel de connaître le sous-groupe auquel appartient chaque lignée cellulaire. Par exemple, toutes les lignées cellulaires du **groupe 3** hébergent une amplification *MYC* et 50% des lignées cellulaires **SHH** classées (UW-228 et DAOY) ont une mutation dans TP53 (Ivanov et al. 2016). Alors que les tumeurs du **groupe SHH** et du **groupe 3** sont largement représentées parmi les lignées cellulaires, il existe une pénurie de modèles *in vitro* pour les tumeurs du **groupe 4** et du **groupe WNT**. Il n'y a qu'une seule paire de lignées cellulaires (CHLA-01-MED et CHLA-01R-MED), toutes deux dérivées du même patient, qui ont été classées dans le **groupe 4**, alors que plus de 40% des tumeurs du MB appartiennent à ce sous-groupe. Enfin, plus de la moitié des lignées cellulaires disponibles n'a pas été sous-typée ou caractérisée selon les normes de la classification moléculaire du MB. Il semble indispensable pour toutes les expériences futures qu'une caractérisation plus complète notamment des sous-types de MB à l'aide de la méthylation ou de l'expression génique soit réalisée.

Sous-groupe	Lignées cellulaires	Mutations	Sources
WNT	MED5R	B-catenine	
SHH	<u>DAOY</u>	CDKN2A NF1 TP53	ATCC
	<u>ONS-76</u> UW228 UW426	TP53	JCRB
Groupe 3	D341MED D384MED D425MED	Amplification de myc Amplification de myc Amplification de myc P53	ATCC Millipor Sigma
	<u>D458</u> D283MED MED8A	Amplification de myc Amplification de myc	ATCC
	<u>HD-MB03</u> MB002 Med-114FHTC Med-411FHTC	Amplification de myc Amplification de myc Amplification de myc	DSMZ BTRL BTRL
	Med-2112FHTC	Amplification de myc Isochromosome 17	BTRL
Groupe 4	CHLA-01-MED CHLA-01R-MED	Amplification de myc Amplification de myc	ATCC ATCC

Tableau 3 : Différentes lignées cellulaires de MB existantes (listes non exhaustives). Les lignées utilisées dans ce travail de thèse sont celles soulignées dans le tableau. (Adapté de l'article de Jingying X et al, J cell biochem, 2015. (J. Xu et al. 2015)

Les modèles d'organoïdes sont également une technologie émergente pour étudier les tumeurs cérébrales pédiatriques. Les organoïdes sont généralement générés avec des cellules souches embryonnaires (ESC) ou des cellules souches pluripotentes induites (iPSC) et ont le potentiel de se développer en une architecture 3D d'une manière similaire au développement tissulaire *in vivo* en raison de leur capacité à s'auto-renouveler et à se différencier. (Ballabio et al. 2020a)

Un modèle d'organoïdes cancéreux humains dérivés d'iPSC imitant l'altération génétique humaine du **groupe 3** du MB a récemment été décrit (Ballabio et al. 2020a). Cette étude met en avant l'utilité de créer des organoïdes de MB spécifiques de certains sous-groupes afin d'étudier les mécanismes moléculaires qui sous-tendent leur développement. Bien que particulièrement intéressant, le modèle des organoïdes de tumeurs cérébrales n'est pas sans limites. L'acquisition optimale du tissu tumoral repose sur une étroite coordination avec le neurochirurgien pendant l'opération pour s'assurer que le tissu viable est réséqué en bloc sans cautérisation. Une coordination étroite avec les anatomopathologistes est également importante pour confirmer le

diagnostic et limiter le laps de temps entre la résection et le traitement des tissus, ce qui est essentiel pour une fiabilité maximale de la génération des organoïdes. Dans des modèles d'organoïdes de glioblastomes, il a été rapporté la préservation partielle de la microvascularisation et des cellules immunitaires, ce qui peut s'avérer utile pour mieux comprendre le microenvironnement tumoral, mais avec, au fil du temps, une diminution de l'abondance des populations de systèmes vasculaires et de macrophages/microglies et une expression plus faible des gènes liés au système immunitaire (Jacob et al. 2020). En effet, les conditions de culture des organoïdes sont optimisées pour préserver la viabilité et la croissance des cellules tumorales, et les cellules immunitaires résidentes ont une durée de vie limitée et se diluent sans expansion, nécessitant une exploitation rapide des organoïdes après leur conception. Des travaux récents sur un modèle préclinique d'organoïdes cérébelleux humains démontrent que l'expression concomitante de Otx2/c-MYC donne naissance à des organoïdes de type MB hébergeant une signature de méthylation de l'ADN qui se rapproche des tumeurs humaines du **groupe 3** (Ballabio et al. 2020a). Dans ces organoïdes, la surexpression de SMARCA4 (chromatin remodeling ATPase) est capable de réduire l'activité tumorigène d'Otx2/c-MYC. Enfin, le traitement par Tazemetostat (inhibiteur compétitif de l'histone méthyltransférase) réduit la tumorigenèse engendrée par l'expression d'Otx2/c-MYC dans les organoïdes cérébelleux humains. Ces études démontrent que les organoïdes cérébelleux humains peuvent être utilisés efficacement pour comprendre le rôle des gènes altérés chez les patients atteints de MB et représentent un outil fiable pour développer des thérapies personnalisées (Yamazaki et al. 2021)

2- Modèles animaux

La plupart des animaux développent rarement des tumeurs cérébrales spontanées et peuvent être utilisés pour générer des modèles expérimentaux (Huszthy et al. 2012). En 2018, une étude sur la biologie des tumeurs cérébrales parrainée par le Children's Oncology Group a conduit à la génération de 30 modèles de patient-derived xenograft (PDX) de tumeurs cérébrales orthotopiques pédiatriques, y compris le MB (**Figure 5**). Ces dernières années, les modèles de souris génétiquement modifiés (GEMM) ont gagné en popularité dans la recherche sur les tumeurs cérébrales (**Tableau 4**). Contrairement aux PDX, les GEMM peuvent reconstruire l'initiation et le développement de tumeurs chez des animaux dotés d'un système immunitaire natif, d'une barrière hémato-encéphalique intacte et d'un microenvironnement non perturbé. À ce jour, la majorité des GEMM de MB sont du **groupe SHH**, générés en modifiant les gènes de

signalisation SHH, tels que *PTCH*, *SMO* ou *SUFU* ((Neumann, Swartling, and Schüller 2017), (Dobson and Gopalakrishnan 2018).

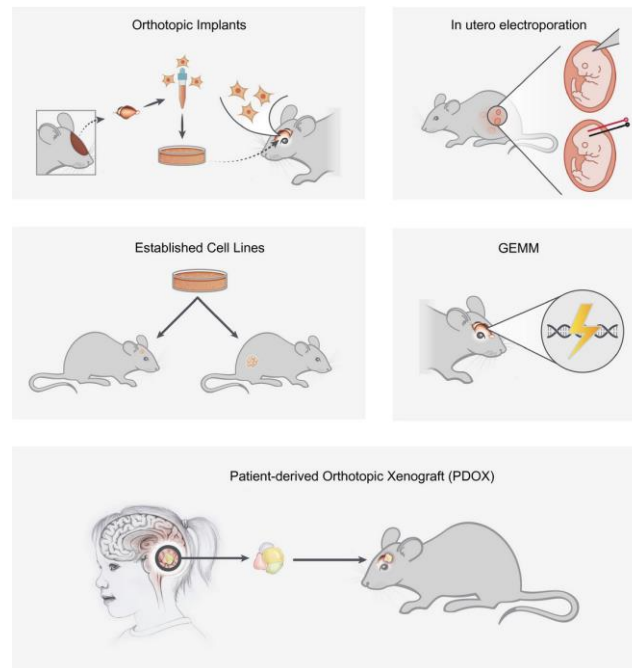


Figure 5 : Résumé des méthodes et approches techniques de la modélisation du médulloblastome. (Adapté de l'article de Roussel M.F et al, *Brain Pathol*, 2020.(Roussel et al. 2020)

L'utilisation de ces modèles pré-cliniques a permis de mettre en évidence des voies thérapeutiques intéressantes. Une étude récente a montré que la combinaison de Gemcitabine (anti-métabolite pyrimidique) et d'Axitinib (inhibiteur de protéine tyrosine kinase) présente des effets favorables sur la progression tumorale dans un modèle de xéno greffe orthotopique de MB du **groupe 3**, tout en présentant un profil de faible toxicité (Schwinn et al. 2021). D'autres travaux ont mis en évidence l'activation de la voie TGF β -Activine dans les MB du **groupe 3** (Morabito et al. 2019). Une stimulation autocrine d'Activine β serait responsable de l'activation de la voie dans un sous-ensemble de MB du **groupe 3** caractérisé par une expression élevée du gène *prostate transmembrane protein-androgen induced 1 (PMEPA1)*. Cette voie pourrait être alors une nouvelle cible thérapeutique, avec des effets prometteurs du Galunisertib (molécule utilisée en recherche clinique sur des patients atteints de glioblastome, (Brandes et al. 2016) sur un modèle de xéno greffe orthotopique de MB.

Sous-type de MB	Modèle de souris
WNT	<i>Blbp-Cre^{+/+}; Ctnnb1^{lox/lox}; Tp53^{flv/flx}</i> <i>Blbp-Cre^{+/+}; Ctnnb1^{lox/lox}; Tp53^{+/flx}; Plk3ca^{lox/lox}E545K/αE545K</i>
SHH	<i>Ptch1^{+/+}</i> <i>Ptch1^{+/+}; Math1-Cre</i> <i>Ptch1^{+/+}; hGFAP-Cre</i> <i>Ptch1^{+/+}; Math1-CreER</i> <i>Ptc1^{+/+}; p53^{-/-}</i> <i>Ptc1^{+/+}; Ink4c^{-/-}</i> <i>Ptc1^{+/+}; Kip1^{-/-}</i> <i>Ptch1^{+/+}; Hic1^{-/-}</i> <i>Ptch1^{+/+}; Ptch2^{-/-}</i> <i>NeuroD2-SmoA1 (W539L)</i> <i>Smo/smo (homozygous smoA1)</i> <i>NeuroD2-SmoA2 (S537N)</i> <i>CAGGS-CreER; R26-SmoM2</i> <i>p53^{-/-}; Sulu^{-/-}</i> <i>Trp53^{-/-}; PTEN^{-/-}</i> <i>Trp53^{-/-}; Parp^{-/-}</i> <i>Nestin-tv-α mice infected with RCAS-Shh + N-Myc</i> <i>Nestin-tv-α mice infected with RCAS-Shh + N-Myc (T50A)</i> <i>Nestin-tv-α mice infected with RCAS-Shh + Bcl2</i>
Groupe 3	<i>Gli1-TTA : TRE-MYC/N/luciferase (GTML)</i> <i>GTML; Trp53^{-/-}</i> <i>Mil4^{-/-}; Nestin-Cre</i> <i>Nestin-tv-α; Trp53^{-/-} mice infected with RCAS-Myc</i> <i>Nestin-tv-α mice infected with RCAS-Myc + Bcl2</i> <i>Co-electroporation of Myc and trp53DN into embryonic cerebellar progenitor cells</i>
Groupe 4	<i>Co-electroporation of SRC-CA and Dnp53 into E13.5 developing cerebella</i>

Tableau 4 : Différents modèles existant de souris génétiquement modifiées. (GEMM)(Adapté de l'article de Zhiqin L et al ; Front Oncol; 2021. (Li et al. 2021)

En conclusion, bien que les travaux récents nous permettent aujourd'hui de mieux appréhender la diversité moléculaire des sous-groupes de MB, la morbi-mortalité de cette pathologie tumorale pédiatrique reste très élevée. Il semble important de continuer à comprendre les mécanismes spécifiques des différents sous-groupes pouvant expliquer leur différence de pronostic, afin d'adapter et de personnaliser les stratégies thérapeutiques. Pour cela, les études expérimentales doivent pouvoir être menées dans des conditions les plus physiologiques possibles, reproduisant l'environnement dans lequel se développe la tumeur. Dans ce contexte, prendre en considération les variations d'oxygénation tissulaire semble être un aspect fondamental du processus cancéreux.

Chapitre 2 : L'hypoxie tissulaire

L'oxygène est une molécule essentielle à notre survie, son rôle premier est l'apport d'énergie à l'ensemble des cellules de l'organisme. L'air que nous respirons contient 21% d'oxygène, cet air va ensuite transiter par nos poumons à travers la membrane alvéolo-interstitiel pour se retrouver dans nos artères. Le sang artériel contient environ 13% d'oxygène, et va irriguer toutes les cellules du corps humain (**Figure 6**). La concentration tissulaire en oxygène est déterminée par la pression artérielle en oxygène et le débit sanguin d'une part, mais également par le taux de consommation d'oxygène cellulaire d'autre part qui varie d'un organe à l'autre. La condition de normoxie correspond à la valeur de pO_2 atmosphérique de 160mmHg ce qui correspond à 21% d' O_2 de l'air total. La physioxie correspond aux valeurs de pO_2 en situation physiologique au niveau tissulaire. Elle varie selon les organes mais se situe entre 15 et 68mmHg ce qui correspond à une teneur en O_2 de 2-9%. En deçà de ces valeurs, on parle d'hypoxie. Elle peut être modérée, de 8 à 38mmHg (1-5% d' O_2) ou sévère, < 8 mmHg ($< 1\%$ d' O_2), et enfin, on parle d'anoxie en la quasi-absence d' O_2 . L'hypoxie peut se rencontrer dans différentes situations physiologiques ou pathologiques. L'hypoxie tissulaire peut être causé par un faible taux d'oxygène dans l'atmosphère (hypoxie hypobare), un faible taux d'oxygène dans le sang (hypoxémie), un faible taux d'hémoglobine et/ou de globules rouges (hypoxie anémique), une diminution de la consommation d'oxygène dans le tissu (hypoxie histotoxique, comme dans l'empoisonnement au cyanure), ou par la réduction et/ou l'arrêt du flux sanguin.

Au niveau cérébral, la concentration physiologique tissulaire en oxygène varie selon les études expérimentales animales entre 4 et 7% (Zauner et al. 1995)(McKinley et al. 1996). Il existe des variations régionales considérables du flux sanguin dans le cerveau de tous les mammifères, y compris chez l'homme, qui peuvent notamment expliquer cette variabilité de concentration tissulaire en oxygène. Plus précisément, la pO_2 est plus élevée au niveau de la substance grise cérébrale et plus faible au niveau de la substance blanche, du pont et du fornix, en corrélation directe avec les débits sanguins régionaux (**Figure 7**). A noter également que les niveaux d'oxygène sont élevés dans les zones adjacentes aux plexus pia-arachnoïdien et choroïde, et dans les ventricules cérébraux (Erecińska and Silver 2001).

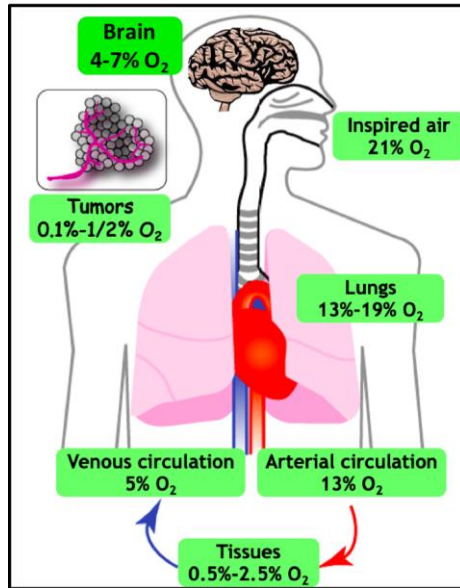


Figure 6 : Répartition du pourcentage d'oxygène dans l'organisme humain. (Adapté de Brahimi-Horn C. Hypoxia and tumor angiogenesis (dans Tumor Angiogenesis), Springer, 2008, pages 171-194)

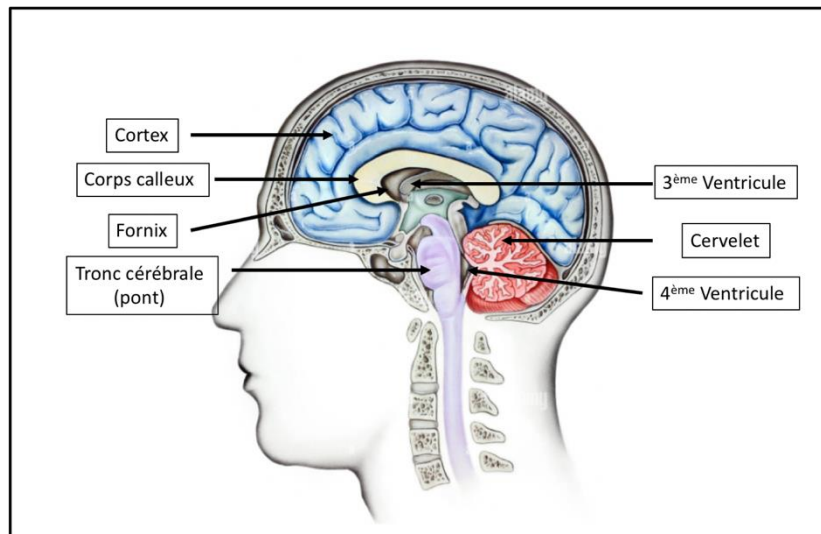


Figure 7 : Schéma anatomique du cerveau en coupe sagittale. (Adapté de Alamy banque d'image, Medical. Art.Inc).

I- Hypoxie et cancer

L'hypoxie est une caractéristique classique d'un grand nombre de tumeurs (Eschmann et al. 2005)(Yasui et al. 2010), et les cellules ont, à travers l'évolution, mis en place un système de régulation remarquable afin de survivre à cet environnement. Les tumeurs hypoxiques présentent généralement une tension en oxygène $< 10\text{mmHg}$ (**Tableau 5**). La masse tumorale se développe plus rapidement que le système vasculaire, ainsi les cellules résultant d'une prolifération intense se retrouvent rapidement dans un environnement hypoxique du fait de la distance avec les capillaires (**Figure 8**) Les cellules cancéreuses vont s'adapter à cet environnement et vont sécréter des facteurs pro-angiogéniques permettant la production de nouveaux vaisseaux et la ré-oxygénation de la tumeur, qui pourra à nouveau proliférer et créer de nouvelles zones hypoxiques. A noter cependant que cette néo-vascularisation est immature, et extrêmement perméable, rendant la perfusion tissulaire relativement inefficace et entretenant l'hypoxie tumorale (Carmeliet 2005)(Vaupel, Mayer, and Höckel 2004).

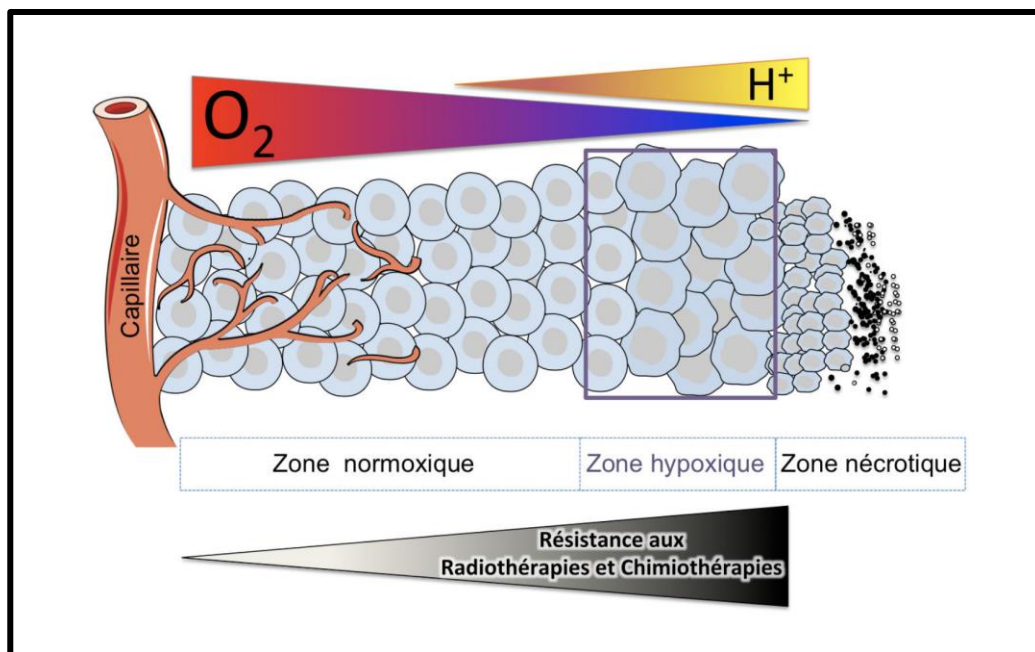


Figure 8 : Caractéristique des tumeurs hypoxiques. L'oxygène et les nutriments sont apportés par les capillaires jusqu'aux tissus. Les cellules tumorales doivent faire face à des tensions en oxygène différentes en fonction de leur distance des vaisseaux (gradient décroissant d'oxygène). En parallèle, l'accumulation d'acide lactique et de CO_2 augmentent l'acidose tissulaire (H^+) dans les zones hypoxiques. La résistance aux radio/chimiothérapies est inversement proportionnelle à la concentration en oxygène de la tumeur. (Adapté de l'article de Brahim-Horn et al, *J Mol Med*, 2007. (M. C. Brahim-Horn et al. 2007)

L'hypoxie est un facteur micro-environnemental crucial qui, en plus de définir la croissance et l'agressivité d'une tumeur, va jouer un rôle dans la non-réponse aux traitements classiquement utilisés en cancérologie (Wilson and Hay 2011). La résistance aux traitements radio/chimiothérapie est inversement proportionnelle à la tension en oxygène de la tumeur. Des lignées cellulaires de MB dans des conditions hypoxiques ont une réduction significative des dommages à l'ADN liés au traitement après un traitement par étoposide et radiothérapie (Cowman et al. 2019). En effet, la radiothérapie nécessite de l'oxygène pour créer les radicaux libres et induire les dommages de l'ADN, les cellules tumorales hypoxique ont de ce fait besoin d'une adaptation des doses d'irradiation avec des doses pouvant être 2 à 3 fois plus élevées (Graham and Unger 2018)(Whillans and Hunt 1982). L'hypoxie est également associée à une résistance à un certain nombre d'agents de chimiothérapie (ex : 5-Fluorouracil, Cisplatine, Etoposide, Bléomycine). Divers mécanismes contribuent à la résistance aux agents chimiothérapeutiques en condition d'hypoxie : (i) la surexpression des protéines d'efflux des médicaments, (ii) l'induction de l'autophagie régulée par Hypoxia Inducible Factor-1 (HIF-1) (Voir paragraphe II-A Conformation de HIF), (iii) la néo vascularisation tumorale sous-optimale (barrière de diffusion entre les vaisseaux sanguins et les cellules tumorales) (Minassian et al. 2019)(Bellot et al. 2009)(Trédan et al. 2007). Finalement, lorsqu'elle est présente, l'hypoxie conduit à un mauvais pronostic à long terme chez les patients atteints de cancer (Vaupel 2008). Cette observation a fourni la justification du développement de stratégies thérapeutique ciblées sur l'hypoxie (Bertout et al. 2008).

Il semble important que l'environnement hypoxique devienne une condition expérimentale essentielle aux essais précliniques afin de développer des stratégies thérapeutiques dans les conditions les plus réalistes.

Diverses approches sont disponibles pour étudier le degré d'hypoxie tumorale, mais aucune n'est couramment utilisée en clinique. Une mesure directe de la tension en oxygène de la tumeur est possible dans les sites tumoraux accessibles où une électrode à oxygène peut être utilisée. Cela a été couronné de succès dans un certain nombre d'études cliniques (Marianne Nordmark et al. 2005)(M Nordmark et al. 1996). Les défis actuels de cette technique incluent non seulement son caractère invasif mais également le niveau élevé d'hétérogénéité tumorale (Stone et al. 1993). Diverses approches d'imagerie transversale ont été proposées, telles que la détection par imagerie par résonance magnétique de la désoxy-hémoglobine (BOLD MRI), mais la signification biologique des paramètres utilisés pour refléter l'hypoxie et leur lien avec

le phénotype de l'hypoxie tumorale n'a pas encore été clairement établie. (Mason 2006). Des marqueurs exogènes de l'hypoxie (composés de nitroimidazole) ont été utilisés avec succès pour désigner les zones d'hypoxie au sein des tumeurs (Chapman, Franko, and Sharplin 1981). Les composés sont administrés par voie systémique et convertis en produits protéiques stables dans les zones hypoxiques. Ceux-ci peuvent être détectés par immunohistochimie (IHC) sur biopsie tumorale ou par imagerie *in vivo*, telle que la tomographie par émission de positons au 18F-Fluoromisonidazole (18F-FMISO) (Chitneni et al. 2011). Cependant, il existe un débat quant à savoir si ces composés sont suffisamment sensibles pour détecter un phénotype tumoral hypoxique, car HIF-1 est stabilisé à des tensions d'oxygène plus élevées que celles auxquelles se forment les produits protéiques du Nitroimidazole (Tuttle et al. 2007).

Les gènes qui sont régulés à la hausse ou à la baisse en réponse à l'hypoxie reflètent le phénotype hypoxique des tumeurs et peuvent fournir une mesure indirecte du niveau d'hypoxie. Leur expression peut être évaluée au niveau de la protéine, en utilisant l'immunohistochimie, ou au niveau de l'ARNm. L'étude de la réponse cellulaire à l'hypoxie au niveau moléculaire a d'ailleurs permis de mieux comprendre les mécanismes mis en jeu dans ce contexte. En 2019, le prix Nobel de Physiologie et de Médecine a été remis à trois scientifiques, Gregg Semenza, William Kaelin, et Sir Peter Ratcliffe, pour leurs travaux sur la façon dont les cellules s'adaptent aux variations d'oxygène et en particulier à l'hypoxie. Ils ont démontré que lorsque l'oxygène est insuffisant, un complexe protéique appelé Hypoxia-inducible Factor (HIF), s'accumule dans presque toutes les cellules du corps. Le rôle de cette protéine est crucial dès les premiers jours de la vie. Si un embryon n'a pas les gènes *HIFs*, il ne survivra pas au-delà de l'embryogenèse très précoce. L'hypoxie, et donc HIF, est liée à l'ensemble des caractéristiques émergentes du cancer (Hanahan and Weinberg 2011), y compris l'angiogenèse, les métastases et l'invasion, l'échappement à l'apoptose, la suppression de la réponse immunitaire et l'instabilité génomique (G L Semenza 2000)(Chang et al. 2011)(H. D. Levine and Sicé 1976)(Erler et al. 2004) (Yotnda, Wu, and Swanson 2010)(Bristow and Hill 2008) (**Figure 9**). Il va être un véritable chef d'orchestre dans l'évolution des cellules vers la malignité. A ce jour, HIF-1 est reconnu pour contrôler plus de 100 gènes. Près de 2% de l'ensemble du génome humain seraient directement régulés par HIF-1, soit par un phénomène d'induction soit de répression, pouvant orchestrer des changements phénotypiques, conduisant à la progression du cancer et à la résistance au traitement (Schito and Semenza 2016)(Choudhry and Harris 2018). Plusieurs études ont déterminé une réponse transcriptionnelle globale à l'hypoxie. Cela a généralement été effectué dans des lignées cellulaires exposées à l'hypoxie par rapport à la normoxie (21%

d'oxygène utilisé dans les laboratoires). Les gènes dont la régulation positive est significative, ou qui dépassent un seuil défini par rapport à l'expression normoxique de base, sont généralement regroupés et ont été appelés « signature d'expression génique d'hypoxie » ou « signature d'hypoxie ». Cette approche a été utilisée dans de nombreux domaines pour étudier les effets de l'hypoxie sur le système vasculaire et le système immunitaire, ainsi que sur les cellules tumorales (Jögi et al. 2004)(Aprelikova et al. 2006).

Tissus normal	Concentration moyenne en O ₂	Références	Concentration moyenne en O ₂ du tissu tumoral	Références
Cerveau	5-6%	Hoffman, Charbel et al.1996; Dings et al. 1998	1,7%	Rampling et al. 1994; Vaupel, Höckel et al. 2007
Sein	8,5%	Vaupel, Höckel et al. 2007	1,5%	Vaupel, Höckel et al. 2007; Vaupel, Schlenger et al. 1991
Rein	4,9%	Lawrentschuk, et al. 2005	1,3%	Lawrentschuk et al. 2005
Foie	4-7,3%	Leary, klinck et al. 2002; Brooks, Eastwood et al.2004	0,8%	Leary, klinck et al. 2002; Brooks, Eastwood et al.2004
Poumon	5,6%	Le Chen et al. 2006	2,2%	Graffman, Björk et al. 2001
Pancréas	7,5%	Koong, Mehta et al. 2000	0,3%	Koong, Mehta et al. 2000

Tableau 5 : Comparaison des concentrations d'oxygène entre le tissu normal et le tissu tumoral.

A- Hypoxie et système nerveux central (SNC)

Le système nerveux central est un grand consommateur d'oxygène : 15% de la consommation d'oxygène et 20% du débit cardiaque total sont centrés sur le cerveau, un organe qui ne représente pourtant que 2% du poids corporel (Ferrer and Vidal 2017). La valeur aérobie du tissu cérébral est d'environ 40mmHg dans des conditions physiologiques, alors qu'elle s'est avérée significativement plus faible dans certaines tumeurs cérébrales comme le glioblastome (GBM) (Valable et al. 2017). Dans le GBM, l'hypoxie va de légère ($pO_2 = 20$ à 4mmHg) à sévère ($pO_2 = 4$ à 0,75mmHg), en particulier dans les zones nécrotiques (Gérard et al. 2019), avec un pronostic d'autant plus sombre que l'hypoxie est sévère.



Figure 9 : Identification des 10 caractéristiques de la cellule cancéreuse. Toutes liées au facteur de transcription HIF (Hypoxia-inducible factor). En bleu clair sont ciblées les caractéristiques plus particulièrement étudiées dans notre travail.

II- Hypoxia-inducible factor (HIF)

HIF est un facteur de transcription qui appartient à la famille des bHLH (basic helix loop helix) -PAS(PER-ARNT-SIM). C'est un complexe hétérodimérique constitué d'une sous-unité α régulée par la concentration en oxygène et d'une sous-unité β (appelé également Aryl hydrocarbon Receptor Nuclear Translocator ou ARNT) constitutive est stable (**Figure 10**).

Il existe trois isoformes de la sous-unité alpha (HIF-1 α , HIF-2 α , et HIF-3 α) ainsi que deux isoformes de la sous-unité β (HIF-1 β et HIF-2 β). HIF-1 α est une isoforme ubiquitaire, à l'inverse de HIF-2 α et de HIF-3 α qui sont restreintes à certains types cellulaires. HIF-2 α a été initialement mis en évidence au niveau des cellules endothéliales, puis au niveau du rein, des hépatocytes, des macrophages, des cellules musculaires et des cellules astrocytaires (Tian, McKnight, and Russell 1997)(Wiesener et al. 2003). HIF-1 et HIF-2 ont des fonctions complémentaires en conditions physiologiques et pathologiques.

HIF-3 a été caractérisé plus récemment (Gu et al. 1998). En raison de l'utilisation de différents promoteurs, de différents sites d'initiation de la transcription et d'un épissage alternatif de HIF-3, plusieurs isoformes de HIF-3 existent. En effet, la protéine HIF-3, dans sa forme longue, fonctionne comme un activateur de transcription régulé par l'oxygène et active un programme transcriptionnel unique en réponse à l'hypoxie (Q. F. Li et al. 2006). De nombreux gènes cibles HIF-3 ont été identifiés mais l'induction hypoxique de l'expression de HIF-3 semble tissu-spécifique (Heidbreder et al. 2003), alors que certaines variantes courtes de HIF-3 agissent comme des régulateurs dominants-négatifs des actions menées par HIF-1 et HIF-2 (Maynard et al. 2005)(Pasanen et al. 2010).

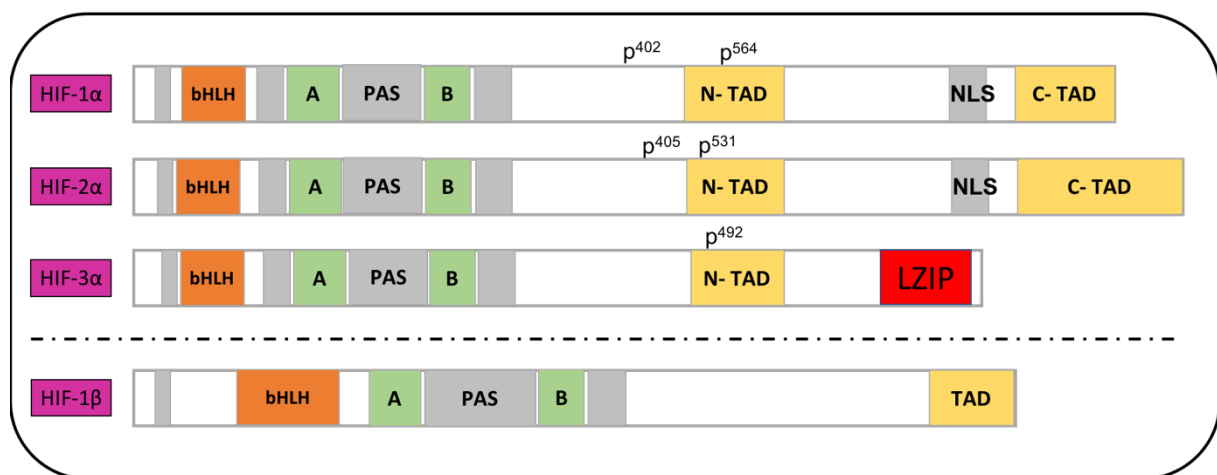


Figure 10 : Conformation des différentes sous-unités de HIF-1. (Adapté de l'article de Duan C, *Am j Physiol Cell Physiol*, 2016. (Duan. 2016). (LZIP= Leucine zipper)

A- Conformation de HIF-1

Les sous-unités α et β possèdent, à leurs extrémités N-terminales, des domaines PAS (*PER-ARNT-SIM*) (A et B) et bHLH (*basic-helix loop helix*) permettant leur dimérisation (**Figure 10**). Leurs domaines bHLH sont des domaines riches en éléments basiques, formant une structure tridimensionnelle de type hélice-boucle-hélice, permettant la dimérisation de HIF-1 α avec HIF-1 β mais également sa fixation à l'ADN.

La sous-unité α contient d'autres domaines essentiels à sa régulation. Il s'agit tout d'abord de deux domaines de transactivation, N-TAD situé au niveau des acides aminés 531-577 et C-TAD en position C-terminal au niveau des acides aminés 813-826.

La sous-unité β contient également un domaine TAD dans sa partie C-terminal mais ce domaine n'est pas impliqué dans la réponse à l'hypoxie.

Le domaine de dégradation dépendant de l'oxygène (ODD), responsable de la dégradation de HIF-1 α en normoxie, est situé entre les acides aminés 401-603 (**Figure 11**). A l'intérieur de ce domaine a été mis en évidence une séquence importante de 15 acides aminés (557-571), conservée dans la protéine homologue de HIF-1 chez la drosophile, contenant un motif *LXXLAP* déterminant pour la stabilisation de HIF-1 (Srinivas et al. 1999).

Enfin sont décrites deux séquences de localisation nucléaire au niveau de la sous-unité α . La première séquence ¹⁷RRKEKSRDAARRSKE³³ est située dans le domaine bHLH et est réprimée par le domaine PAS-B ce qui peut entraîner une rétention cytosolique de la protéine (**Figure 11**). La seconde ⁷¹⁸RKRK⁷²¹ joue un rôle majeur dans la localisation nucléaire dépendante de l'hypoxie (Kallio et al. 1998).

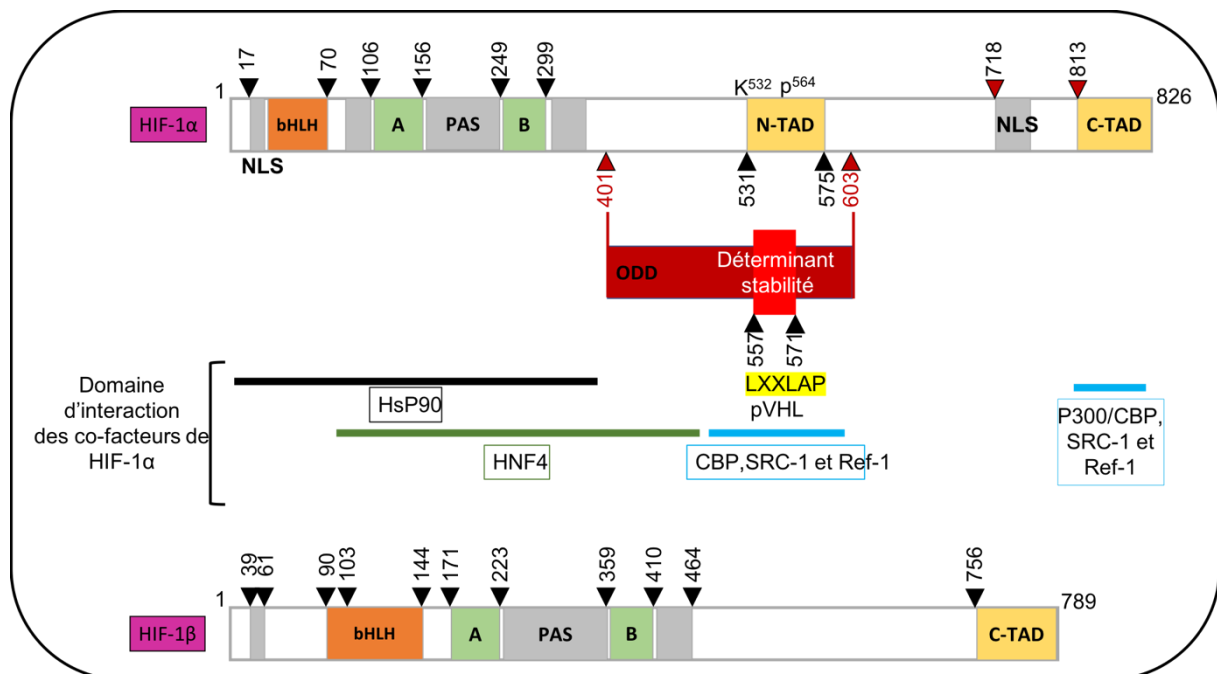


Figure 11 : Conformation des sous unités HIF-1 α et HIF-1 β . Abréviation : bHLH (basic helix loop helix), PAS ((*PER-ARNT-SIM*), TAD (domaine de transactivation), NLS (signaux de localisation nucléaire)

Chez l'homme, la région N-terminal des trois sous-unités α est équivalente mais les régions C-terminales sont différentes (**Figure 10**). Bien que HIF-1 α soit exprimé de manière ubiquitaire, l'expression de HIF-2 α est limitée à des types cellulaires spécifiques, notamment les cellules endothéliales, les cellules gliales, les pneumocytes de type II, les cardiomyocytes, les fibroblastes rénaux, les cellules interstitielles du pancréas et du duodénum, et les hépatocytes (Wiesener et al. 2003). Dans les neuroblastomes, HIF-2 α , mais pas HIF-1 α , est fortement

exprimé dans les zones bien vascularisées et l'expression de HIF-2 α favorise la croissance tumorale, les métastases, et est associée à une maladie plus agressive (Holmquist-Mengelbier et al. 2006).

B- Régulation de la sous-unité HIF α

1- Régulation de HIF-1 α

HIF-1 α est une protéine dégradée extrêmement rapidement en situation de normoxie, avec une demi-vie de l'ordre de 5 minutes (Huang et al. 1998)(G. L. Wang et al. 1995).

La sous-unité β étant constitutive et indépendante de l'oxygène, l'étape essentielle de l'activation de HIF-1 est donc la stabilisation de la sous-unité α dépendante du niveau d'oxygénation tissulaire. HIF-1 α nécessite plusieurs étapes préalables à son activation. La première est son transport dans le noyau grâce aux signaux de localisation nucléaire (NLS). Puis la sous-unité α va se dimériser avec la sous-unité β dans le noyau, grâce au motif bHLH et aux domaines PAS. Le dimère se lie ensuite à l'ADN et recrute les cofacteurs nécessaires à son activité transcriptionnelle. Pour se fixer à l'ADN, HIF, en tant que facteur de transcription, va reconnaître un motif appelé Hypoxia Response Element (HRE) dont la séquence en position 3' non codante du gène est *RCGTG* (R étant une base purine, A ou G) et recrute les cofacteurs nécessaires à son activité transcriptionnelle.

En présence d'oxygène, la sous-unité α va être hydroxylée au niveau des résidus Proline (Pro 402 et Pro 564) par les Prolyl Hydroxylase (PHDs) (Jaakkola et al. 2001)(Ivan et al. 2001) (**Figure 11**). Ces enzymes vont reconnaître le domaine ODD de HIF-1 α et hydroxyler les résidus Prolines. Cette hydroxylation va permettre ensuite la fixation de la protéine Von Hippel-Lindau tumor suppressor (pVHL) au domaine N-TAD de la sous-unité HIF-1 α . La fixation de pVHL au domaine N-TAD peut se faire qu'après reconnaissance du motif *LXXLAP* (K Tanimoto et al. 2000)(Ohh et al. 2000). Une mutation de ce motif abolirait complètement la fixation de pVHL entraînant donc une stabilisation de HIF-1 α . pVHL dirige ensuite l'ubiquitinylation de HIF-1 α et sa dégradation par le protéasome 26S (**Figure 12**). L'ajout de groupement d'ubiquitine lié à un résidu α -amine du substrat est possible grâce au groupement de trois enzymes (E1 : ubiquitin-activating-enzyme ; E2 : ubiquitin-carrier-protein; E3: ubiquitine-protéine-ligase) permettant l'activation, la conjugaison puis le transfert de l'ubiquitine. De manière générale, l'ubiquitinylation affecte l'activité, la fonction et la

localisation des protéines cibles ainsi que leur interaction avec leurs partenaires, et sert donc de véritable modification post-traductionnelle.

Une autre enzyme, dépendante de l'oxygène, a été caractérisée et joue également un rôle majeur dans la régulation de HIF-1 α : le Factor-Inhibiting HIF-1 (FIH). FIH permet l'hydroxylation d'un résidu Asparagine (Asn 803), réprimant ainsi l'activité transcriptionnelle de HIF-1 α en empêchant la liaison du coactivateur transcriptionnel p300/CBP au domaine de transactivation C-TAD (**Figure 12**). FIH n'influence pas la stabilité de HIF-1 α mais permet la modulation de sa transactivation.

Dans des conditions hypoxiques, les PHD et FIH sont inactifs en raison du manque d'oxygène suffisant (**Figure 12**). Ces deux enzymes utilisent en effet l'oxygène et le 2-oxoglutarate comme substrats dans la réaction d'hydroxylation. Cependant, ils sont très différents en ce qui concerne la concentration d'oxygène nécessaire à leur activité. *In vitro*, les PHDs ont une constante de Michaelis (Km) pour l'oxygène de 230 μ M (correspondant à 24% O₂) qui est trois fois supérieure à celle de FIH (Km de 90 μ M correspondant à 8% d'O₂) (Koivunen et al. 2004). Ainsi, à mesure que la concentration en oxygène diminue, les PHD deviennent inactives et la sous-unité HIF-1 α est par conséquent stabilisée et peut aller au noyau pour réaliser son activité transcriptionnelle. Cette activité est, comme décrite précédemment, contrôlée par des domaines d'activation transcriptionnelle (TAD) situés au niveau de l'extrémité C-terminale. L'activité du C-TAD est réprimée par l'action de FIH, mais l'activité du N-TAD est-elle complètement indépendante de FIH. Ainsi, HIF-1 α a une activité transcriptionnelle bi-fonctionnelle qui, selon l'activité de FIH, permet une activation différentielle des gènes contrôlée soit par N- soit par C-TAD (Dayan et al. 2006).

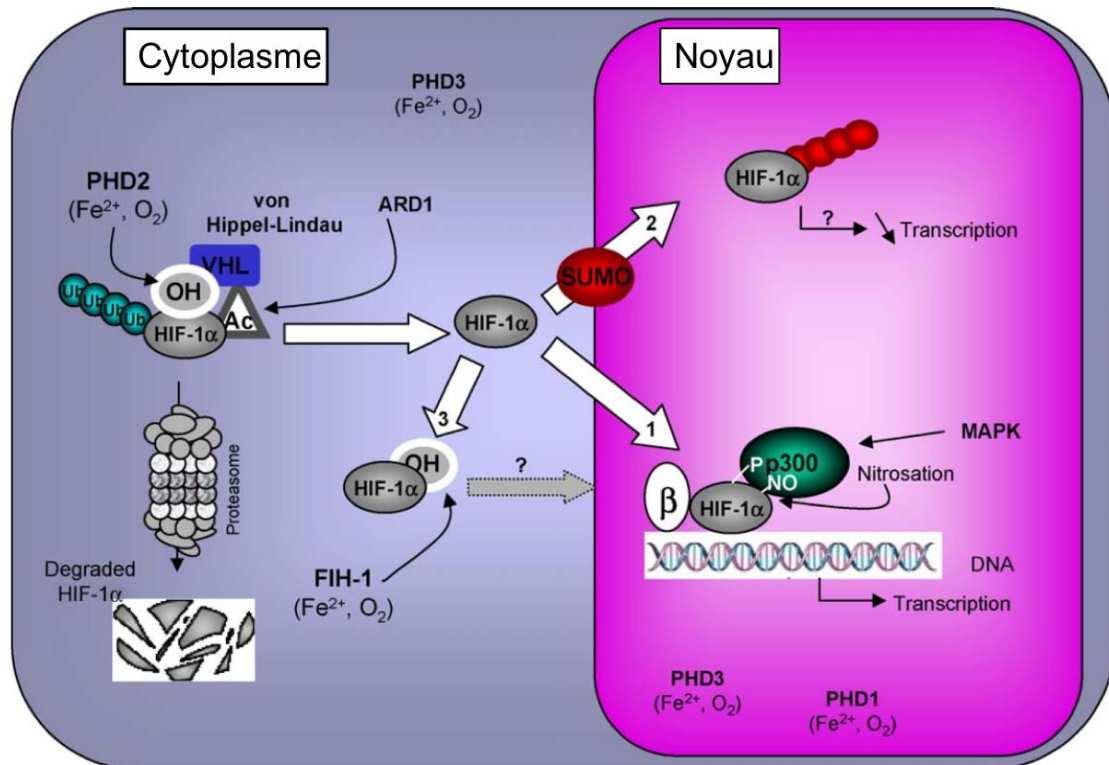


Figure 12 : Mécanisme de régulation de HIF-1 en Hypoxie. (Adaptée de l'article de C Brahim-Horn et al, Cellular Signalling, 2005. (C. Brahim-Horn et al. 2005).

2- Régulation de HIF-2α

Les voies de dégradation et de stabilisation décrites majoritairement pour HIF-1α sont différentes pour HIF-2α selon le degré et la durée de l'hypoxie (Koh and Powis 2012). HIF-2α est hydroxylé avec une efficacité beaucoup plus faible que HIF-1α, à la fois par les PHDs et FIH-1, entraînant ainsi une stabilisation et une activation de HIF-2α à un taux d'oxygène plus élevé que HIF-1α. Schématiquement, il semblerait que HIF-1α soit stabilisé pour des conditions d'hypoxie sévères et aiguë (< à 1% d'O₂) alors que HIF-2α serait activé en condition d'hypoxie modéré (< à 5% d'O₂) et chroniques (48-72h).

C- Régulation de HIF par modifications post-traductionnelles

La SuMOylation (Figure 13) : SUMO est comparable à l'ubiquitine en termes de structure moléculaire globale et de poids moléculaire (environ 11kDa), mais peut entraîner des changements distincts dans la régulation d'une protéine donnée en fonction des isoformes de SUMO (Z.-J. Han et al. 2018). Le résultat fonctionnel de la SUMOylation de HIF-1α reste

incertain. Le premier rapport sur la SUMOylation de HIF-1 α suggère que la modification par SUMO-1 augmente la stabilité et la trans-activité de la protéine HIF-1 (Bae et al. 2004). SUMO-1 a été proposé pour concurrencer l'ubiquitine pour la liaison à K391 et K477 dans les séquences consensus SUMO de HIF-1 α . Contrairement à cela, une autre étude a mis en évidence que la SUMOylation de K391 et K477 induit une diminution de l'activité transcriptionnelle, qui semble être indépendante de la dégradation de HIF-1 α sous hypoxie (Berta et al. 2007). Il a également été montré que la SUMOylation favorise la liaison de pVHL à HIF-1 α même lorsque ce dernier n'est pas hydroxylé sur les résidus Proline (402 et/ou 564) (Cheng et al. 2007). Alors que HIF-1 α et HIF-2 α sont tous deux des cibles pour la SUMOylation, moins de sites de modifications ont été identifiés dans HIF-2 α . Bien que HIF-2 α contienne deux sites consensus SUMOylation, un seul, K394, s'est avéré être conjugable par SUMO (van Hagen et al. 2010). L'ajout enzymatique de SUMO-2 a facilité la reconnaissance par les ubiquitines ligases ciblées par SUMO (pVHL et RNF4) pour dégrader rapidement HIF-2 α sous hypoxie.

La phosphorylation (Figure 13) : La phosphorylation est une modification post-traductionnelle extrêmement courante et bien étudiée, impliquant l'addition enzymatique d'un groupe phosphate à des résidus sérine, thréonine ou tyrosine sur une protéine cible. La modification de HIF-1 α par phosphorylation est abondante et à des rôles variés dans la régulation de sa stabilité, activité, localisation subcellulaire et interactions avec les partenaires de liaison (**Figure 12**). Alors que bon nombre de ces événements de phosphorylation directe se produisent indépendamment de la tension d'oxygène, les modifications au sein du domaine ODD semblent se produire exclusivement sous normoxie. La diminution d'expression de la Glycogène-synthase Kinase-3 (GSK-3) stabilise HIF-1 α , suggérant que HIF-1 α est une cible directe de GSK-3, phosphorylant des cibles dans les domaines ODD et N-TAD (Flügel et al. 2007)(Mottet et al. 2003). Bien que les sites de phosphorylation visés par GSK-3 soient différents selon le type cellulaire, cette phosphorylation induit la dégradation de HIF-1 α par le protéasome (Cassavaugh et al. 2011). Une autre kinase, la Polo-like kinase 3 (PLK3), cible HIF-1 α pour la dégradation *via* la phosphorylation directe de deux sites, S576 et S657 (D. Xu et al. 2010). Cette phosphorylation se produit en normoxie et permet la dégradation protéasomale de HIF-1 α d'une manière indépendante de pVHL. Un seul de ces sites cibles, S576, est situé dans le domaine ODD, tandis que l'autre, S657, est situé immédiatement après le NLS de HIF-1 α . Toutes les phosphorylations des HIF-1 α ne diminuent pas leurs stabilités, certaines font le contraire. Les kinases dépendantes des cyclines (CDK), et notamment CDK-

1, interagissent directement avec HIF-1 α et le phosphorylent au niveau d'un résidu sérine (S668), d'une manière indépendante de l'oxygène (Hubbi et al. 2014)(Warfel et al. 2013). CDK5, qui se distingue des autres CDK car elle n'implique pas de sous-unité cycline pour l'activation catalytique, modifie HIF-1 α en S687 et augmente sa stabilité (Herzog et al. 2016). La protéine kinase A (PKA) phosphoryle six sites différents couvrant toute la longueur de HIF-1 α *in vitro*, la phosphorylation de T63 et S692 favorisant la stabilisation indépendante de l'oxygène et augmentant l'activité transcriptionnelle de HIF-1 (Bullen et al. 2016). La localisation nucléaire de HIF-1 α peut être régulée par la phosphorylation de motif sérine en S641/S643, au sein du motif NLS, par la protéine kinase p42/44 mitogen-activated (ERK1/2) (Mylonis et al. 2008)(Mylonis et al. 2006). Cette phosphorylation favorise la localisation nucléaire de HIF-1 α et donc son activation. Tout comme HIF-1 α , la localisation nucléaire de HIF-2 α est régulée par la phosphorylation par ERK1/2 d'un résidu sérine en S672 (Gkotinakou et al. 2019).

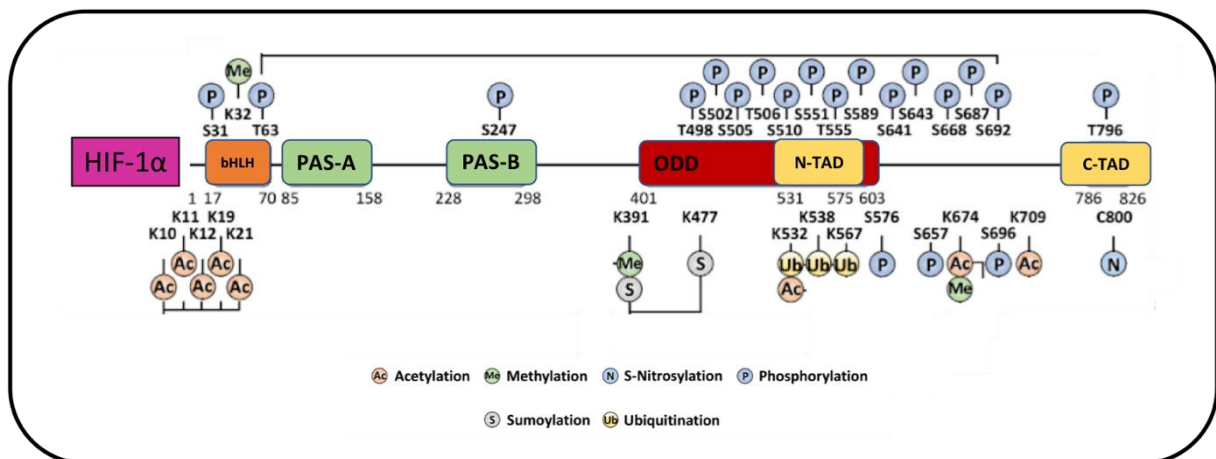


Figure 13 : Différents sites de modification post-traductionnelles au niveau de HIF-1 α . (Adapté de l'article de Albanese A et al, *Int J Mol sci*, 2020. (Albanese et al. 2020)

L'acétylation (Figure 13) : Il a été rapporté que de nombreux événements post-traductionnels d'acétylation et de dé-acétylation jouent un rôle dans la régulation à la fois de la stabilité de la protéine HIF α et de son activité transcriptionnelle. De multiples sites de la protéine HIF-1 α peuvent être modifiés par acétylation de la lysine, entraînant différents effets en aval. Par exemple, l'acétylation au sein du domaine ODD est liée à la dégradation de HIF-1 α dépendante du pVHL. Jeong *et al.* ont montré que la liaison à pVHL est favorisée par l'acétylation du résidu lysine (K532) de HIF-1 α (Jeong et al. 2002).

La nitrosylation (Figure 13) : La S-nitrosylation de C800 a été identifiée comme une modification critique pour le recrutement des cofacteurs CBP/p300 et l'activation transcriptionnelle de HIF-1 (Yasinska and Sumbayev 2003). Dans l'ensemble, la S-nitrosylation semble réguler au moins la stabilité et la trans-activité de HIF-1. Aucune donnée n'est disponible pour HIF-2.

La méthylation (Figure 13) : Le plus souvent, la méthylation des protéines se produit au niveau des résidus arginine ou lysine. La méthylation a été largement étudiée au niveau des protéines histones où elles régulent l'accessibilité de l'ADN pour la transcription. La méthylation régule également d'autres protéines, y compris HIF-1 α . La SET7/9, une mono méthyl transférase connue pour son rôle dans l'activation des gènes *via* la modification de l'histone H3, s'est avérée interagir avec HIF-1 α et méthyler plusieurs sites (X. Liu et al. 2015). La méthylation de K391 sur HIF-1 α induit sa déstabilisation (Kim et al. 2016). SET7/9 peut méthyler à la fois HIF-1 α et HIF-2 α sur les sites conservés K32 et K29 dans les domaines bHLH (Kim et al. 2016). Initialement, la méthylation de K32 pour HIF-1 α (et K29 pour HIF-2) s'est avérée induire une inhibition de la transcription indépendamment de la dégradation de HIF-1 α . Mais des résultats ultérieurs rapportent que HIF-1 α méthylé par SET7/9 serait dégradé par le protéasome 26S (X. Liu et al. 2015).

D- Autre mécanismes régulant HIF, dépendant ou non de l'oxygène

Le facteur HAF (Facteur associé à l'hypoxie, également connu sous le nom de SART1) est une ubiquitine ligase E3 qui cible HIF-1 α spécifiquement et entraîne sa dégradation par le protéasome après une hypoxie prolongée. HAF se lie également sur HIF-2 α bien que dans ce cas il augmente la transactivation de HIF-2 α sans provoquer sa dégradation. Ainsi, HAF représente un médiateur de commutation pour la réponse hypoxique de la cellule cancéreuse entre HIF-1 α et HIF-2 α et fournit une explication pour une progression tumorale améliorée sous hypoxie prolongée (Kalbag et al. 1991)(Koh et al. 2011).

Certains stimuli indépendants de l'hypoxie sont également capable de réguler HIF, il s'agit de certaines hormones comme l'insuline, les facteurs de croissances (IGF-1 ou PDGF), certains agents vaso-actif (NO, angiotensine 2), et certaines cytokines comme TNF- α . (Treins et al. 2002)(Köhl, Zhou, and Brüne 2006)(Sánchez-López et al., 2005). Ces stimuli non hypoxiques peuvent réguler la traduction de l'ARNm de HIF α , via des voies de signalisation de facteur de

croissance telles que les voies du phosphatidylinositol 3-kinase (PI3K) ou de la protéine kinase activée par les mitogènes (MAPK). Ces stimuli indépendants de l'oxygène jouent un rôle autocrine dans la prolifération, la survie ou la réparation tissulaire, permettant une adaptation précoce aux variations de l'environnement cellulaire (M. C. Brahimi-Horn and Pouyssegur 2009).

D'autres mécanismes, indépendants de l'hypoxie, peuvent agir sur la stabilisation de HIF, comme les protéines de choc thermique (Hsp). HIF-1 α , comme d'autres protéines de la famille "bHLH-PAS", est associée de manière stable à la protéine de choc thermique 90 (Hsp90). Hsp90 est impliquée dans la stabilisation de la sous-unité HIF-1 α contre l'ubiquitination et la dégradation protéasomale. A l'opposé, il a été rapporté que la protéine de choc thermique 70 (Hsp70) avait un rôle dans la dégradation de HIF-1 α induite par l'hypoxie, mais pas dans celle de HIF-2 α (W. Luo et al. 2010). Hsp70 recrute l'ubiquitine ligase pour promouvoir sélectivement l'ubiquitination et la dégradation protéasomale de HIF-1 α mais pas de HIF-2 α . Par conséquent, Hsp70 et Hsp90 ont des rôles opposés, impliqués respectivement dans la dégradation et la stabilisation de HIF-1 α .

D - Mutations de HIF

Les scénarii possibles qui peuvent perturber le rôle des domaines fonctionnels de HIF α et donc affecter son rôle en tant que principal facteur de transcription en condition d'hypoxie sont : (I) les variations au sein du domaine bHLH qui peuvent empêcher la liaison de HIF α aux sites de reconnaissance HRE dans la région promotrice des gènes cibles ; (ii) les variations au sein du domaine PAS qui peuvent affecter la dimérisation avec la sous-unité β ; (iii) les variations au sein du domaine ODD qui peuvent affecter la stabilité de la protéine en normoxie ; (iv) les variations au sein du signal de localisation nucléaire (NLS) qui peuvent avoir un effet sur la translocation de HIF α dans le noyau; et (v) les variations au sein du N-TAD et du C-TAD qui peuvent influencer l'activation transcriptionnelle de HIF et l'interaction avec ses co-activateurs. Une revue de la littérature récente sur le polymorphisme de HIF-1 α a montré que les variations présentent en dehors du domaine ODD ont également des effets fonctionnels et sont associées à des maladies et des phénotypes spécifiques (Gladek et al. 2017).

Certaines mutations de HIF-1 α et de HIF-2 α sont aujourd'hui bien décrites. Par exemple une étude du gène *HIF-2 α* sur 3 générations d'une même famille atteinte d'érythrocytose a révélé plusieurs mutations situées à proximité de l'accepteur d'hydroxyle P531, étant responsable de

la maladie (Lappin and Lee 2019). Des tests fonctionnels *in vitro* des trois mutations (M535 V, P534L et G537R) de HIF-2 α associées à l'érythrocytose, ont révélé que les trois mutants stabilisaient HIF-2 α . Récemment, une mutation gatekeeper G323E dans HIF-2 α a été identifiée comme étant responsable de la résistance à l'utilisation d'un inhibiteur de HIF-2 (PT2385) après un traitement prolongé (Courtney et al. 2020).

D'autres mutations ont été décrites sur HIF-1 α et seraient responsables d'un risque plus élevé de développer une pathologie cancéreuse. L'étude de l'ADNc de lignées cellulaires de cancer de la prostate humaine et d'échantillons de prostate solides humains a identifié la présence d'un polymorphisme dans la séquence ODD de HIF-1 α , en particulier 1772C>T, entraînant un changement d'acide aminé de la proline 582 à la sérine (P582S) (Anastasiadis et al. 2002). Cette mutation a ensuite été détectée dans les cellules germinales de patients atteints d'un carcinome rénal (Ollerenshaw et al. 2004), de carcinome épidermoïde de la tête et du cou (Keiji Tanimoto et al. 2003) et de cancer de la prostate androgéno-indépendant (Chau et al. 2005). La mutation P582S empêche la dégradation de la sous-unité HIF-1 α , et améliore l'activité transcriptionnelle de HIF-1 (Fu et al. 2005), bien qu'elle n'affecte pas l'hydroxylation de la proline 564 (Percy et al. 2003). Étonnamment, la base de données COSMIC (<https://cancer.sanger.ac.uk/>) identifie un faible taux de mutation d'environ 1,5 à 2% pour HIF-1 α (668 mutations sur 44263 séquençages de HIF-1 extrait de tumeurs de patients) et HIF-2 α (928/39561) ((Tate et al. 2019)), la plupart étant des mutation faux-sens (42%). Ce taux de mutation reste relativement stable au niveau du système nerveux central avec 1,8% de mutation retrouvées sur HIF-1 α .

III- Expression génique de l'hypoxie

Plusieurs tentatives ont été faites pour identifier des collections de gènes dont les niveaux d'expression peuvent refléter l'hypoxie tumorale et être utilisés pour corrélérer leur expression avec le pronostic ou la réponse aux traitements de certains cancers. Environ 30 signatures de gènes d'hypoxie ont été identifiées pour les cancers de l'adulte (Harris et al. 2015). Par exemple, une signature de 28 gènes liée à l'hypoxie a été validée dans le cancer de la prostate en tant que biomarqueur pronostique et prédictif de la réponse aux traitements (L. Yang et al. 2018). En 2016, un ensemble de neuf gènes (*SLCO4A1*, *ENO1*, *HK2*, *PGK1*, *MTFP1*, *HILPDA*, *VKORC1*, *TPI1*, and *HIST1H1C*) identifiés dans des échantillons de tumeurs de neuroblastomes et des lignées cellulaires de neuroblastomes hypoxique, s'est avéré être associé à des tumeurs plus

agressives représentant ainsi une nouvelle signature potentielle dans le domaine de la cancérologie pédiatrique (Applebaum et al. 2016).

L'existence de différentes isoformes des sous-unités HIF soulève la question sur la spécificité de leur action ainsi que sur le spectre des gènes cibles régulés par les différentes isoformes. Parmi les 3 isoformes de HIF α , HIF-1 α et HIF-2 α sont aujourd'hui les mieux comprises et les plus décrites. Il a été démontré que les domaines de transcription (TAD) contribuent à la spécificité des gènes cibles de HIF-1 α et HIF-2 α (Hu et al. 2007). En effet le N-TAD confère des spécificités de gènes cibles de HIF-1 α ou HIF-2 α , tandis que le C-TAD favorise l'expression des gènes cibles communs HIF-1 α /HIF-2 α . Aujourd'hui un nombre croissant de données suggère que les hétéromères HIF-1 α et HIF-2 α ont des fonctions et des rôles physiologiques distincts (Takeda et al. 2010)(Gordan, Thompson, and Simon 2007). Par exemple, à la suite de l'activation constitutive des deux isoformes dans le cancer du rein avec déficience en VHL, plusieurs éléments indiquent un rôle oncogène pour HIF-2 α , alors que HIF-1 α semble manifester des propriétés anti tumorales opposées (Raval et al. 2005)(C. Shen et al. 2011). HIF-1 α et HIF-2 α manifestent des schémas distincts d'expression en fonction des tissus (Wiesener et al. 2003) mais également une évolution temporelle d'expression différente en hypoxie (Holmquist-Mengelbier et al. 2006). Par exemple, la stabilisation de HIF-1 culmine tôt après le début de l'hypoxie, alors que celle de HIF-2 se produit plus lentement et est plus soutenue (Stiehl et al. 2012).

Comme expliqué précédemment, HIF-1 et HIF-2 se lient aux sites HRE contenant la même séquence consensus centrale 5'-RCGTG-3', afin d'activer la transcription des gènes cibles. Malgré un motif de liaison à l'ADN consensuel commun, HIF-1 et HIF-2 se lient à des ensembles de sites différents au niveau de l'ADN. Une analyse séparée de ces sites HRE a conduit à l'identification de motifs HRE distincts mais très similaires pour HIF-1 et pour HIF-2 (respectivement : M00139 annoté HIF1A, et M00074 annoté EPAS1) pouvant être responsable d'une activation de gènes cibles différents (Tausendschön et al. 2015)(Smythies et al. 2019). En effet HIF-1 et HIF-2 se comportent largement indépendamment l'un de l'autre en ce qui concerne leur liaison à l'ADN, avec la liaison de HIF-1 plus fréquemment à proximité des promoteurs et la liaison de HIF-2 plus fréquemment à distance des promoteurs (Smythies et al. 2019).

A- Gènes cibles de HIFs

Dans la plupart des types cellulaires, on a identifié des gènes activés soit uniquement par HIF-1, soit uniquement par HIF-2, ou activés à la fois par HIF-1 et HIF-2, montrant l'extrême hétérogénéité de l'activité des gènes cibles de HIFs (Mu et al. 2021). Cependant certaines voies métaboliques semblent être préférentiellement sous la régulation de l'une ou l'autre isoformes.

1- Le Métabolisme du glucose (HIF-1 >> HIF-2)

La plupart des gènes codant pour les enzymes de la glycolyse (*HK1/2*, *GPI*, *PFKL*, *ALDOA*, *TPI*, *GAPDH*, *PGK1*, *PGAM1*, *ENO1*, *PKM2* et *LDHA*) ont une transcription dépendante de HIF-1 (**Figure 13**). C'est également le cas pour les transporteurs de glucose (*GLUT1* et *GLUT3*) ((Gregg L Semenza 2012)). Ainsi en hypoxie, l'activation de HIF-1 augmente l'absorption de glucose et la sécrétion de lactate en régulant à la hausse l'expression de *GLUT1*, *GLUT3* et *LDHA*. A noter que *GLUT1* et *LDHA* sont des gènes dont la transcription peut être également régulée par HIF-2. Le lactate accumulé dans les cellules hypoxiques est exporté en extracellulaire *via* le transporteur de monocarboxylate 1/4 (MCT-1/4). L'anhydrase carbonique (CAIX) et l'échangeur Na⁺/H⁺ (NHE-1) eux aussi activés par HIF-1 sous hypoxie, vont permettre la régulation du PH intracellulaire indispensable à la survie cellulaire (Zilli and Nisi 1986).

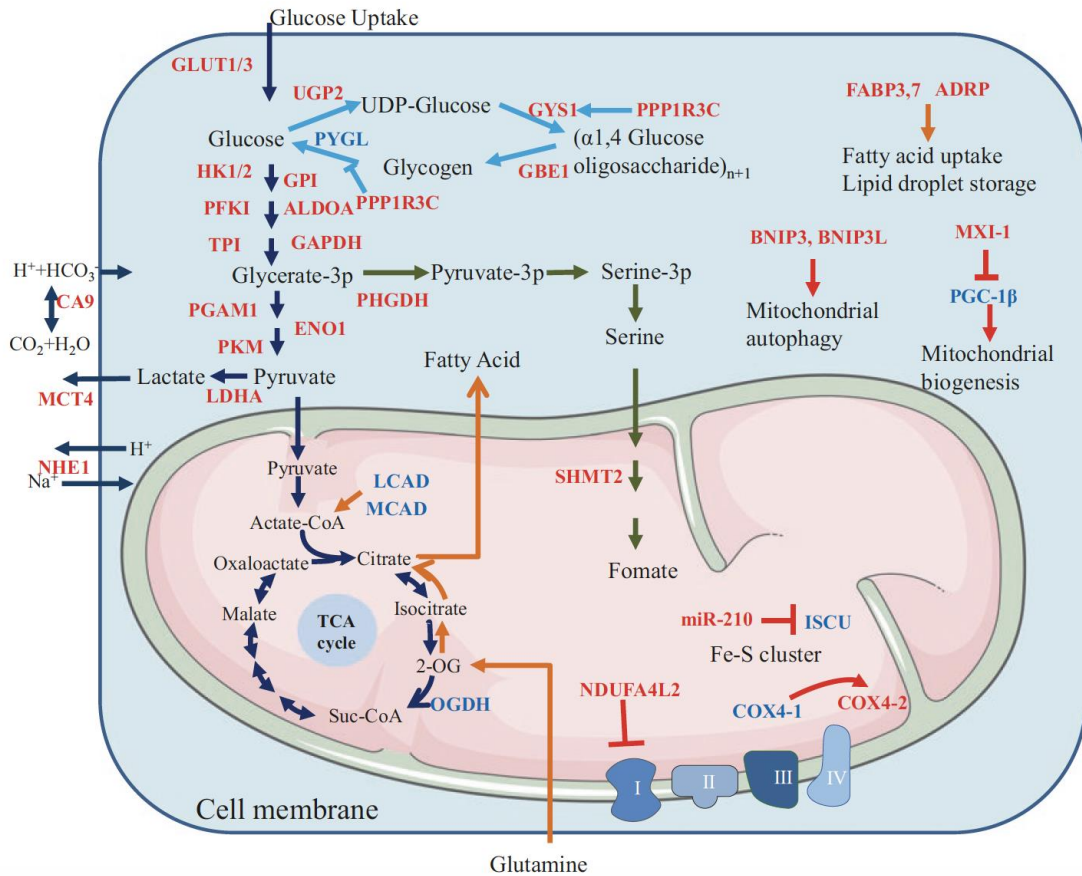


Figure 14 : Différents gènes dépendants de HIF-1. Les gènes en rouge sont ceux induits par HIF-1, et en bleu ceux réprimés par HIF-1.

2- Métabolisme lipidique (HIF-2 = HIF-1)

Le métabolisme lipidique est quant à lui régulé de manière équivalente par HIF-1 et HIF-2. En normoxie, l'Acétyl-Coa (AcCoa) dérivé du glucose est converti en citrate, puis transporté vers le cytoplasme permettant la production d'acides gras. En condition d'hypoxie, du fait du faible niveau d'AcCoA, les cellules cancéreuses vont utiliser la glutamine pour générer de l' α -cétooglutarate, qui est converti en citrate. Le passage du métabolisme oxydatif du glucose au métabolisme réducteur de la glutamine en tant que source d'AcCoA pour la synthèse des lipides dans des conditions hypoxiques dépend de HIF.

3- Angiogenèse (HIF-1 >> HIF-2)

HIF-1 fonctionne comme un des régulateurs principaux de l'angiogenèse en modulant l'expression des gènes impliqués dans la réponse angiogénique, notamment : le facteur de croissance endothélial vasculaire A (VEGF-A), le facteur dérivé du stroma-1 (SDF-1),

l'angiopoïétine 2 (*ANGPT2*), le facteur de croissance placentaire (*PGF*), le facteur de croissance dérivé des plaquettes B (*PDGF-B*) et le facteur de cellules souches (*SCF*): (Rey and Semenza 2010)). Les cellules angiogéniques dérivées de la moelle osseuse (BMDAC) sont mobilisées dans la circulation et recrutées dans les tumeurs par la sécrétion de SDF-1 et VEGF-A dépendante de HIF-1 (Du et al. 2008)(K. Lee, Qian, et al. 2009). L'inhibition de l'activité de HIF-1 altère la mobilisation des BMDAC et la vascularisation tumorale en inhibant l'expression de VEGFA et de SDF-1 (K. Lee, Zhang, et al. 2009).

4- Prolifération et cycle cellulaire (HIF-2 >> HIF-1)

HIF-2 active la transcription de multiples gènes impliqués dans le cycle cellulaire et la prolifération cellulaire, notamment *TGF- α* impliqué dans la prolifération et la différenciation cellulaire et *CCND1* impliqué dans la régulation du cycle cellulaire. HIF-1, quant à lui, active la transcription de gènes impliqués dans la prolifération cellulaire comme : l'*Insuline-like growth factor 2 (IGF2)*, ou l'*IGF binding protein 1/2 et 3*.

5- Cellules souches cancéreuses (HIF-2>> HIF-1)

Les cellules souches cancéreuses (CSC), également appelées cellules initiatrices de tumeurs, sont présentes dans divers cancers et peuvent favoriser l'apparition, la progression et les métastases tumorales (Maccalli et al. 2018). L'expression de divers facteurs embryonnaires tels que Sox2, Nanog et Oct4 par les CSC améliore leurs propriétés telles que la pluripotence et l'auto-renouvellement (Boiani and Schöler 2005). Il a été montré que la liaison directe de HIF-2 α au HRE situé dans les régions promotrices améliore l'expression de *Sox2*, *Nanog* et *Oct4* (J M Heddleston et al. 2010). Dans le Glioblastome, il a été récemment démontré que HIF-2 α peut être considéré comme un marqueur spécifique de cellules souches cancéreuses, mais également comme un facteur de transcription essentiel pour induire un phénotype de CSC (J M Heddleston et al. 2010)(John M Heddleston et al. 2009a). Bien que HIF-2 α améliore l'expression des gènes cibles nécessaires à l'enrichissement des CSC dans des conditions normoxique, HIF-1 a un potentiel plus fort pour induire des CSC dans des conditions hypoxiques par rapport à HIF-2 (Covello et al. 2006). HIF-1 et HIF-2 sont donc nécessaires au développement de CSC, en gérant différentes étapes de développement (Hajizadeh et al. 2019).

B- Effet compensateur HIF-1 et HIF-2

Aujourd'hui, la façon dans laquelle les isoformes HIFs se compensent ou entrent en compétition dans des conditions d'expression différentielle n'est pas claire. Nous avons mis en évidence, dans un travail antérieur portant sur différentes lignées cellulaires (fibroblastes, cellules endothéliales, cellules musculaire lisses), un effet compensateur de HIF-1 sur HIF-2 et *vice versa* lors de l'inactivation de l'un ou l'autre par siRNA (Sadaghianloo et al. 2020)(Sadaghianloo et al. 2021). Ce constat nécessite de plus amples recherches pour comprendre si ce phénomène est cellule-dépendant. Ces questions sont importantes non seulement pour comprendre la physiologie des réponses à l'hypoxie, mais également pour évaluer le potentiel des approches thérapeutiques ciblant spécifiquement l'une ou l'autre des isoformes HIFs.

C- HIF et MYC

MYC code pour une protéine MYC qui est un facteur de transcription régulant environ 15% de l'ensemble des gènes. Il s'agit d'un proto-oncogène qui est surexprimé dans certains cancers humains (surexpression du gène *C-myc* dans les leucémies, le cancer du sein, de l'estomac ou du poumon, surexpression du gène *N-myc* dans le neuroblastome ou glioblastome). C'est un régulateur principal de la transcription qui active ou réprime l'expression des gènes pour coordonner divers processus cellulaires, notamment la division cellulaire, la différenciation, l'apoptose, l'angiogenèse, la réplication de l'ADN, le métabolisme et la biogenèse des ribosomes. MYC en tant que facteur de transcription est connu pour activer l'expression de HIF-1 α et également de HIF-2 α , mais inversement le rôle de HIF sur l'activité de MYC est beaucoup plus complexe et différent en fonction de la sous-unité HIF-1 α ou HIF-2 α .

HIF-1 α s'oppose à l'activité transcriptionnelle de MYC au niveau des gènes cibles de MYC en interférant avec la liaison de MYC avec ses partenaires protéiques. HIF-1 α se lie à MAX et perturbe les complexes MYC/MAX, entraînant une réduction de l'expression de la cycline D2 et l'arrêt de la phase G1 (Gordan et al. 2007) (**Figure 14**). HIF-1 α induit également l'expression de MXI1, une protéine de la famille MAD, qui entre en concurrence avec MYC pour se lier à MAX, inhibant ainsi l'activité de MYC et réprimant l'expression de certains gènes cibles de MYC impliqués notamment dans la biogenèse mitochondriale ou l'apoptose (Bernardini et al. 1991)(Corn et al. 2005). HIF-1 α inhibe également directement l'activité transcriptionnelle de

MYC par compétition sur les sites de liaison à l'ADN au niveau du promoteur p21, et régule positivement l'expression de p21 (Koshiji et al. 2004). MYC et HIF-1 ont une régulation complexe jouant chacun un rôle sur l'autre, et ayant plusieurs gènes cible communs impliqués dans le métabolisme glucidique, lipidique et l'angiogenèse. Dans des conditions d'hypoxie, il a été démontré que la surexpression de MYC peut remplacer le besoin en HIF-1 pour la survie et la propagation cellulaires, en induisant glutaminolyse et lipogenèse (Munksgaard Thorén et al. 2017).

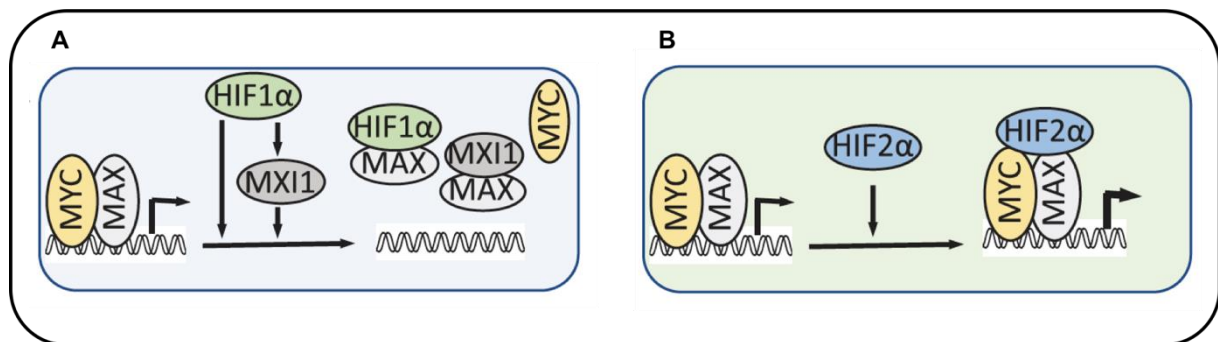


Figure 15 : Mécanismes d'action de (A) HIF-1 α et de (B) HIF-2 α sur l'activité de MYC. HIF-1 α s'oppose à l'activité transcriptionnelle de MYC alors que HIF-2 α induit l'activité de MYC. (Adapté de l'article de Yanping L et al, Front Cell Dev Biol, 2020. (Y. Li et al. 2020)

Contrairement à HIF-1 α , HIF-2 α favorise l'activité MYC en stabilisant le complexe MYC/MAX (Xue et al. 2015) (**Figure 14**). A noter que la stabilisation induite par HIF-2 α de l'hétérodimère MYC/MAX est beaucoup plus forte que la dégradation induite par HIF-1 α de MYC dans les cellules cancéreuses, conduisant à l'activation de MYC sous hypoxie (Xue et al. 2015). L'activité accrue de MYC, induite par HIF-2 α favorise la progression du cycle cellulaire et favorise la tumorigenèse dans certain cancer du rein (Ex : le carcinome rénal à cellule claire (ccRCC) (Gordan et al. 2007). En effet, dans les ccRCC déficients en VHL exprimant uniquement HIF-2 α , l'activité élevée de MYC est responsable d'une prolifération cellulaire accrue et d'une plus grande agressivité comparativement aux tumeurs exprimant HIF-1 α

IV- HIF comme cible thérapeutique

Comme décrit ci-dessus, HIFs régulent de manière majoritaire les réponses physiologiques face à l'hypoxie, initiant une cascade de mécanismes permettant à la tumeur de s'adapter à son environnement hostile, faisant de cette protéine une cible thérapeutique de choix. La

signification pronostique de certains gènes des voies HIFs a été évaluée dans les cancers pédiatriques. Dans le neuroblastome, la tumeur solide extra crânienne la plus courante chez les nourrissons, une expression plus élevée de HIF-1 α est corrélée avec un faible grade tumoral et un pronostic favorable pour le patient, tandis que l'expression de HIF-2 α est en corrélation avec un stade tumoral élevé et un pronostic défavorable (Påhlman and Mohlin 2018). A contrario, HIF-1 α est un facteur pronostique défavorable dans les cancers des os, y compris les ostéosarcomes (D. Luo et al. 2019). Dans le MB, l'inhibition de HIF-1 α semblerait diminuer la prolifération cellulaire (Marx and Panzer 1988). A noter cependant que dans cette étude, la lignée cellulaire de MB utilisée (UW402) est aujourd'hui encore non caractérisée et donc ne correspond pas à un sous-groupe de MB spécifique. Une autre cible, le transporteur de glucose 1 (GLUT1), est plus fréquemment exprimée dans les neuroblastomes de mauvais pronostic (Ramani, Headford, and May 2013). Cela démontre la signification variable de ces marqueurs d'hypoxie endogène en fonction du modèle cancéreux, et donc la nécessité de les étudier spécifiquement pour chaque tumeur, afin d'identifier les cibles thérapeutiques potentielles.

L'inhibition sélective du HIF s'est avérée être un défi, et aucun inhibiteur de HIF-1 n'a jusqu'à présent été approuvé cliniquement, très probablement parce qu'ils n'ont pas la spécificité souhaitée (Soni and Padwad 2017). Pourtant, il existe un certain nombre de molécules inhibant HIF-1 directement ou indirectement (**Figure 15**). Par exemple, l'EZN-2208, un oligonucléotide anti-sens synthétique, et l'Aminoflavone inhibent directement l'expression de l'ARNm de HIF-1 α . (Wigerup, Påhlman, and Bexell 2016). Les inhibiteurs de la voie PI3K/Akt/mTOR (Ex : Glyceolline) et les inhibiteurs de la Topoisomérase I (Ex : CRLX1-101) suppriment la traduction de HIF-1 α , tandis que les inhibiteurs HSP90 (Ex : LBH589) et HDAC inhibent la dégradation de HIF-1 α (Soni and Padwad 2017). La Geldanamycine (inhibiteur HSP90), une molécule qui inhibe indirectement l'activité HIF, a montré des résultats prometteurs dans les essais pédiatriques de phase 1 (Bagatell et al. 2007)(Weigel et al. 2007). Cependant, des toxicités limitant la dose ont été observées. Néanmoins, l'intérêt pour l'inhibition du HIF en tant que stratégie thérapeutique pour le cancer pédiatrique se poursuit, en particulier pour les tumeurs cérébrales pédiatriques. Le blocage de l'activité transcriptionnelle de HIF-1 α avec le 2-méthoxy-estradiol a augmenté l'activité cytotoxique du Cyclophosphamide et de l'Ifosfamide dans les cellules de MB du groupe SHH (Valencia-Cervantes et al. 2019). Il a été démontré que l'Acriflavine, une petite molécule sûre dotée de propriétés inhibitrices du HIF, régule négativement les voies médiées par HIF-1 α et induit la mort cellulaire dans des modèles de

gliome *in vitro* et *in vivo* (Mangraviti et al. 2017). Cependant, un essai clinique de phase II récemment mené sur les patients atteints de gliome de haut grade récidivant rapporte que l'utilisation du LBH589, inhibiteur indirect de HIF-1 α , combiné avec du Bevacizumab n'a pas significativement amélioré la survie sans progression à 6 mois par rapport au Bevacizumab en monothérapie (E. Q. Lee et al. 2015).

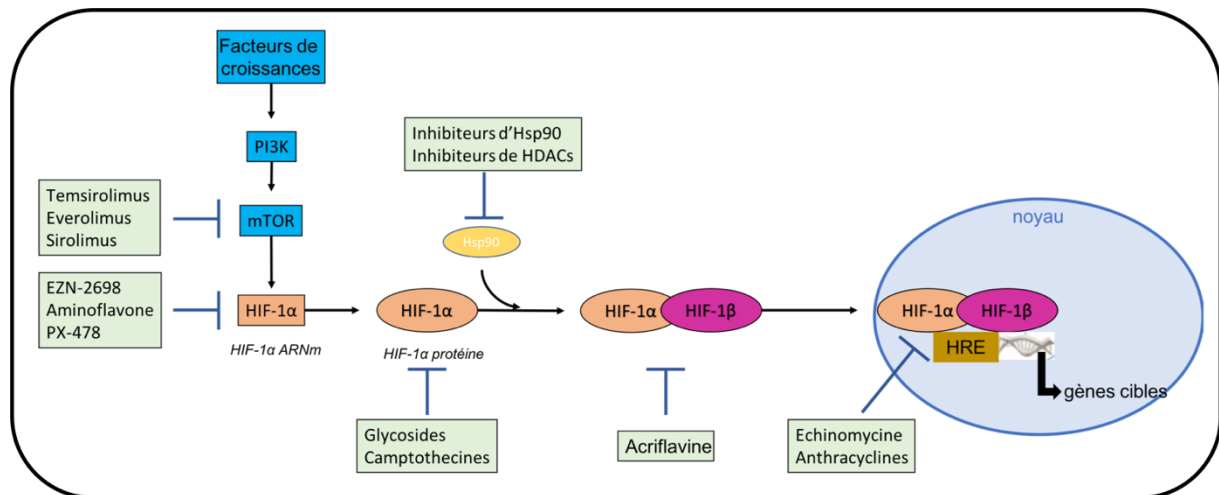


Figure 16 : Différents composés inhibiteurs de HIF-1 ainsi que leur mécanisme d'action. (Adapté de l'article de Albadari N et al, *Expert Opin Drug Discov*, 2019. (Albadari, Deng, and Li 2019))

De son côté, HIF-2 α est apparu comme une cible thérapeutique prometteuse suite à la découverte d'une grande cavité interne dans le domaine PAS-B de HIF-2 α permettant la liaison au ligand (Key et al. 2009)(Scheuermann et al. 2009), et donc une action spécifique, en particulier dans les carcinomes rénaux à cellules claires (ccRCC). Un essai de phase 3 pour le carcinome rénal à cellules claires de l'adulte est en cours avec l'inhibiteur de HIF-2 α de deuxième génération (PT2977) (Y. Yu, Yu, and Zhang 2019). Plusieurs antagonistes spécifiques de HIF-2 α (PT2385, PT2399) ont montré cependant des effets prometteurs aux cours d'essais précliniques et cliniques. Le PT2385 et le PT2399 sont des inhibiteurs sélectifs de HIF-2 α qui bloquent allostériquement sa dimérisation avec HIF-1 β . Le PT2399 inhibe efficacement la croissance tumorale dans les lignées cellulaires de ccRCC exprimant hautement HIF-2 α (Chen et al. 2016). Dans l'étude préclinique de Wallace *et al.* réalisée sur des souris atteintes de ccRCC, le PT2385 inhibe l'expression des gènes induits par HIF-2 α et entraîne une régression majeure de la taille de la tumeur. (Wallace et al. 2016). En 2018, les résultats d'un essai clinique de phase I sur le PT2385 ont montré une réponse ou une stabilité de la

maladie chez 66% des patients atteints de ccRCC, avec une bonne tolérance du composé (Courtney et al. 2018). *A contrario*, le PT2385 n'a eu aucun effet sur la réponse à la chimiothérapie lorsqu'elle est testée dans des xénogreffes dérivées de patients atteints de neuroblastome pédiatrique, ce qui implique qu'il ne s'agit peut-être pas d'une cible appropriée dans le neuroblastome (Persson et al. 2020). Les résultats des essais cliniques de phase II pour le PT2385 sont en cours de publication dans le ccRCC (NCT03108066) et le glioblastome récidivant (NCT03216499). Les résultats encourageants avec le PT2385 chez les patients atteints de ccRCC, cancer exprimant majoritairement HIF-2, nous montre qu'il y a probablement une place pour les inhibiteurs spécifiques de HIF-2 dans l'arsenal thérapeutique anticancéreux. Il est cependant indispensable de mieux caractériser les différentes pathologies cancéreuses sur leur expression HIF-1/HIF-2, qui est probablement différente au sein des sous-groupes d'une même entité tumorale.

Pour protéger les enfants des traitements expérimentaux inutiles, il est essentiel que les futurs essais cliniques chez les enfants soient fondés sur une justification solide de la combinaison d'agents ciblant l'hypoxie avec les traitements existants. Cela doit être étayé par des données précliniques solides pour stratifier les tumeurs des patients en fonction de leur niveau d'hypoxie (Bernauer et al. 2021), car comme le soulignent Yang *et al.*, les traitements modifiant les réponses à l'hypoxie (ciblant directement HIF ou les gènes/protéines cibles) sont d'autant plus efficaces que la tumeur est plus hypoxique (L. Yang and West 2019).

Comme nous venons de le décrire dans ce chapitre, l'hypoxie, et plus particulièrement son facteur de transcription principal HIF, est un point de contrôle de multiples voies métaboliques et de nombreuses caractéristiques faisant évoluer la cellule vers un processus cancéreux. Alors que HIF-1 α a été la première sous-unité à être identifiée et a été plus largement étudiée, HIF-1 α et HIF-2 α régulent ensembles des gènes impliqués dans l'angiogenèse tumorale, les métastases et la différenciation, avec des effets spécifiques au type cellulaire. Compte tenu de l'importance de l'hypoxie dans le développement tumoral, l'identification de petites molécules inhibitrices de la voie HIF reste un domaine d'intérêt croissant, et plusieurs composés prometteurs ont été identifiés. Des données précliniques suggèrent que l'ajout d'un inhibiteur de HIF au traitement standard actuel peut améliorer la survie des patients, mais l'identification des patients les plus susceptibles de répondre à ces thérapeutiques reste encore à préciser. Cette question a probablement toute son importance dans le MB, aux vues des grandes variabilités de pronostic. Comme pour toutes les thérapies anticancéreuses, le défi consistera à identifier quelle

combinaison de médicaments pour quels patients avec quel type de cancer entraînera un bénéfice thérapeutique significatif. Cibler la réponse à l'hypoxie conjointement à d'autres voies métaboliques pourrait être une approche anti-cancéreuse multimodale prometteuse.

Chapitre 3 : Le métabolisme comme approche thérapeutique

I- Glycolyse et phosphorylation oxydative

On sait depuis 95 ans que les cellules cancéreuses métabolisent le glucose différemment des cellules saines. Au début des années 1920, Otto H. Warburg a fait l'observation fondamentale que les cellules cancéreuses convertissent principalement le glucose en lactate même dans des conditions adéquates d'approvisionnement en oxygène, c'est-à-dire sans exposition à des conditions hypoxiques (Warburg, 1956). Il a attribué initialement ce trait métabolique (appelé « glycolyse aérobie » ou « effet Warburg ») à un dysfonctionnement mitochondrial, et a considéré la glycolyse aérobie comme l'altération métabolique majeure guidant les cellules vers la malignité (Warburg, 1956). Les avancées en biologie moléculaire ont révélé que cette glycolyse aérobie n'était pas uniquement expliquée par un dysfonctionnement mitochondrial détruisant ainsi le dogme proposé par Otto H. Warburg (Cairns, Harris, and Mak 2011). De plus, dans les cellules non cancéreuses, l'effet Warburg est un phénomène réversible lié à la prolifération, ce qui indique qu'il reflète les changements métaboliques associés à la prolifération plutôt qu'une caractéristique unique de malignité.

Une connexion évidente s'est faite ces dernières années entre l'effet Warburg et l'acquisition des mutations responsables de la transformation des cellules tumorales, en effet l'altération du métabolisme est une composante essentielle du mode d'action des oncogènes/suppresseurs de tumeurs (Pecqueur et al. 2013). Divers effets peuvent être engendrés sur les voies métaboliques en fonction de l'oncogène ou du suppresseur de tumeur impliqués (A. J. Levine and Puzio-Kuter 2010). Par exemple, l'activation de c-Myc induit l'expression des transporteurs de glutamine et rend les cellules dépendantes à la glutaminolyse (Wise et al. 2008). L'activation de la plupart des oncogènes tel que Ras, Myc, ou la perte/mutation des suppresseurs de tumeurs tel que P53 ou PTEN, stimulent eux la glycolyse (vander Heiden, Cantley, and Thompson 2009).

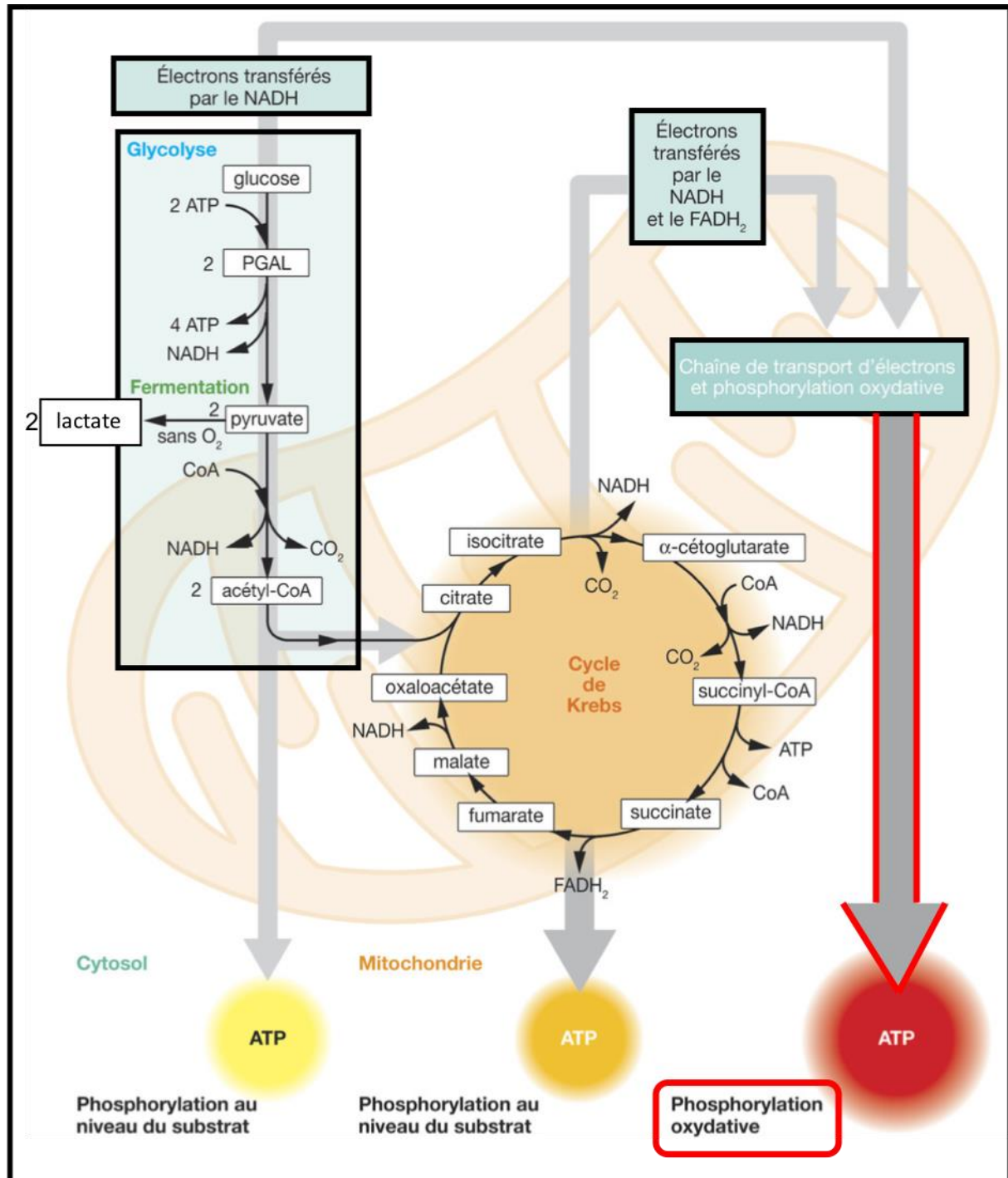


Figure 17 : Glycolyse et phosphorylation oxydative. Le pyruvate produit par la glycolyse anaérobie peut être réduit en lactate ou entrer dans la mitochondrie pour être incorporé dans le Cycle de Krebs. Après l'oxydation du pyruvate en acétyl-CoA qui produit du NADH, l'acétyl-CoA alimente le cycle de Krebs pour produire du NADH, de l'ATP et du FADH₂. Le NADH et le FADH₂ sont ensuite utilisés pour fournir des électrons à la chaîne respiratoire productrice d'ATP.

La dérégulation du métabolisme énergétique est considérée aujourd'hui comme une nouvelle caractéristique distinctive des cellules cancéreuses ("hallmark") et constitue une perspective pour le développement de nouveaux outils diagnostic ou de nouvelles thérapeutiques ciblées anticancéreuses (vander Heiden 2011). Force est de constater qu'à l'heure actuelle aucune stratégie thérapeutique ciblant le métabolisme a apporté suffisamment de preuve pour faire partie de l'arsenal thérapeutique anticancéreux de référence.

La glycolyse aérobie a été historiquement interprétée comme un passage de la phosphorylation oxydative à la glycolyse pour générer de l'ATP (Gatenby and Gillies 2004). Cette voie de production d'ATP produit moins d'ATP par mole de glucose que la phosphorylation oxydative, mais permet une génération rapide d'ATP même en cas de faible teneur en oxygène (Koppenol, Bounds, and Dang 2011) (**Figure 16**). L'énergie est dérivée de l'hydrolyse de l'ATP en ADP (ou AMP), et dépend donc du rapport ATP/ADP (ou ATP/AMP). Par conséquent, les cellules doivent continuellement oxyder les nutriments pour régénérer l'ATP afin de maintenir l'homéostasie.

En plus de fournir de l'ATP, la glycolyse aérobie génère également des fragments antioxydants comme le NADH. La régénération du pool cytosolique de NAD⁺ est une étape primordiale à la pérennisation de l'activité glycolytique au niveau cellulaire.

La production de lactate comme cul de sac énergétique de la glycolyse a longtemps été considéré comme un simple déchet glycolytique potentiellement délétère pour l'organisme car associé à l'acidification du milieu. Les études de ces dernières années placent le lactate au centre de l'homéostasie énergétique, il assure une communication métabolique entre les cellules et les tissus (Brooks 2020) En faisant la navette entre les cellules productrices et celles consommatrices, le lactate remplit au moins trois objectifs : (i) une source d'énergie majeure pour la respiration mitochondriale, (ii) un précurseur majeur de la néoglucogénèse, (iii) et une molécule de signalisation (Brooks 2020). Les lactates déshydrogénases (LDH) sont des enzymes essentielles à la transformation du pyruvate en lactate. Dans la littérature, la LDHA est souvent associée à la conversion préférentielle du pyruvate en lactate et la LDHB à la conversion préférentielle du lactate en pyruvate. Les LDHA et B sont toutes deux capables d'effectuer ces conversions de manière bidirectionnelle en fonction des concentrations respectives des différentes réactions. La LDHA est régulée positivement par HIF-1 α et dans certains cancers, la surexpression de HIF-1 α est associée à une surexpression de LDHA et à une survie significativement plus faible (Lu et al. 2013). Cette navette entre cellules

productrices et consommatrices de lactate est particulièrement importante au niveau du cerveau où le lactate correspond à un substrat énergétique majeur, permettant ainsi un couplage métabolique astrocytes-neurones (Pellerin et al. 2007) (**Figure 17**). Ainsi, la production de lactate par le cerveau en période d'hypoxie n'est pas délétère, mais plutôt un moyen de protection ou même de survie (Schurr and Rigor 1998)

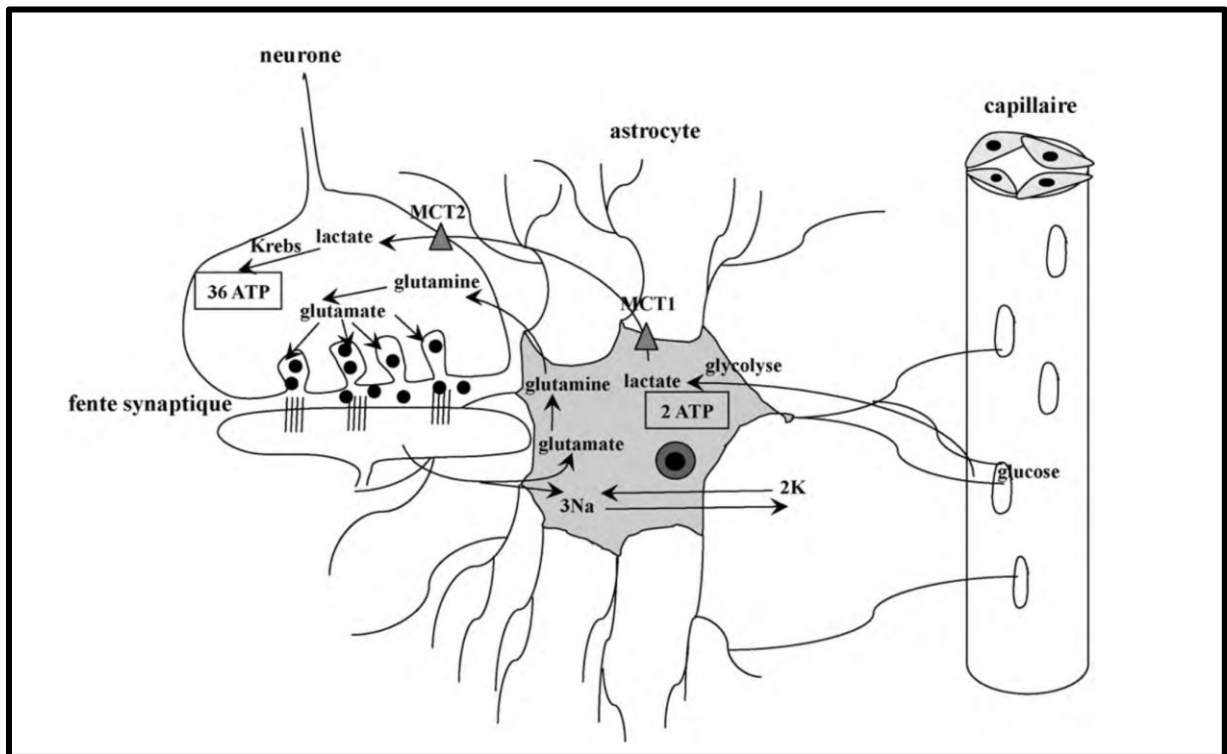


Figure 18 : Couplage métabolique astrocyte-neurone. L'astrocyte permet de faire le lien énergétique entre capillaire et neurone grâce au système de navette intercellulaire du lactate. Lors de l'activation des neurones, de fortes quantités de glutamate sont libérées dans la fente synaptique. Celles-ci doivent être rapidement recaptées pour être retransformées en glutamine, ce qui demande de l'énergie. Ce phénomène se produit au niveau de l'astrocyte. L'énergie dans l'astrocyte (ATP) est fournie par la production de lactate à partir du glucose provenant du capillaire (glycolyse). La recaptation du glutamate par l'astrocyte se fait avec pénétration simultanée de sodium qui doit être réexpulsé de la cellule en échange de potassium. Le lactate produit dans l'astrocyte va être recapté par les neurones pour rejoindre le cycle de Krebs et l'oxydation phosphorylante en présence d'oxygène pour produire l'énergie nécessaire au fonctionnement de cette cellule. (Adapté de l'article de Pellerin C et al, *Glia*, 2007. (Pellerin et al. 2007)

Comme nous venons de le voir, différentes étapes de la glycolyse produisent du NADH par la réduction du NAD⁺. Le NAD⁺ joue un rôle vital pour le transfert d'hydrogène dans le statut redox de la cellule. Le NAD⁺ reçoit un H⁺ provenant des processus métaboliques, y compris

la glycolyse, le cycle du TCA et l'oxydation des acides gras pour former le NADH. Le NADH sert donc de donneur d'H⁺ central à la synthèse d'ATP *via* la phosphorylation oxydative mitochondriale. Au-delà de son rôle vital en tant que coenzyme dans le métabolisme énergétique, le rôle important du NAD⁺ s'est étendu pour devenir un co-substrat pour diverses enzymes, notamment les sirtuines et les PARP (Imai et al. 2000)(Hopp, Grüter, and Hottiger 2019)(Cohen 2020). Le NAD⁺ et ses métabolites fonctionnent comme une plaque tournante régulatrice contrôlant un large éventail de processus physiologiques, y compris l'homéostasie redox, la stabilité génomique, le traitement de l'ARN, le métabolisme énergétique, l'immunité et l'inflammation, et l'horloge circadienne (Cantó, Menzies, and Auwerx 2015)(Gaber, Strehl, and Buttgerit 2017)(Hurtado-Bagès et al. 2020)(Sies, Berndt, and Jones 2017). La carence en NAD⁺ contribue à un éventail de maladies, notamment les maladies métaboliques, le cancer, le vieillissement et les troubles de la neuro-dégénérescence. La régénération du NAD⁺ cytosolique est essentielle à la survie cellulaire, et ceci est possible grâce à différentes voies de production.

II- Voie de régénération du NAD⁺ cytosolique

Les cellules cancéreuses ont un très faible rapport NAD⁺/NADH (Hung et al. 2011), et les changements du rapport NAD⁺/NADH sont fortement corrélés à la croissance tumorale (Gui et al. 2016). En effet, la régénération du NAD⁺ permet d'augmenter la prolifération cellulaire même lors d'altération de la phosphorylation oxydative (Sullivan et al. 2015)(Titov et al. 2016). Pour que le métabolisme se poursuive, le NADH dans le cytosol doit donc être réoxydé en NAD⁺. Puisque la membrane mitochondriale interne est imperméable au NADH et au NAD⁺, deux navettes vont agir pour transférer les équivalents réducteurs du NADH dans le cytosol vers les mitochondries : (i) la navette glycérol 3-phosphate (ii) et la navette malate-aspartate (**Figure 18**).

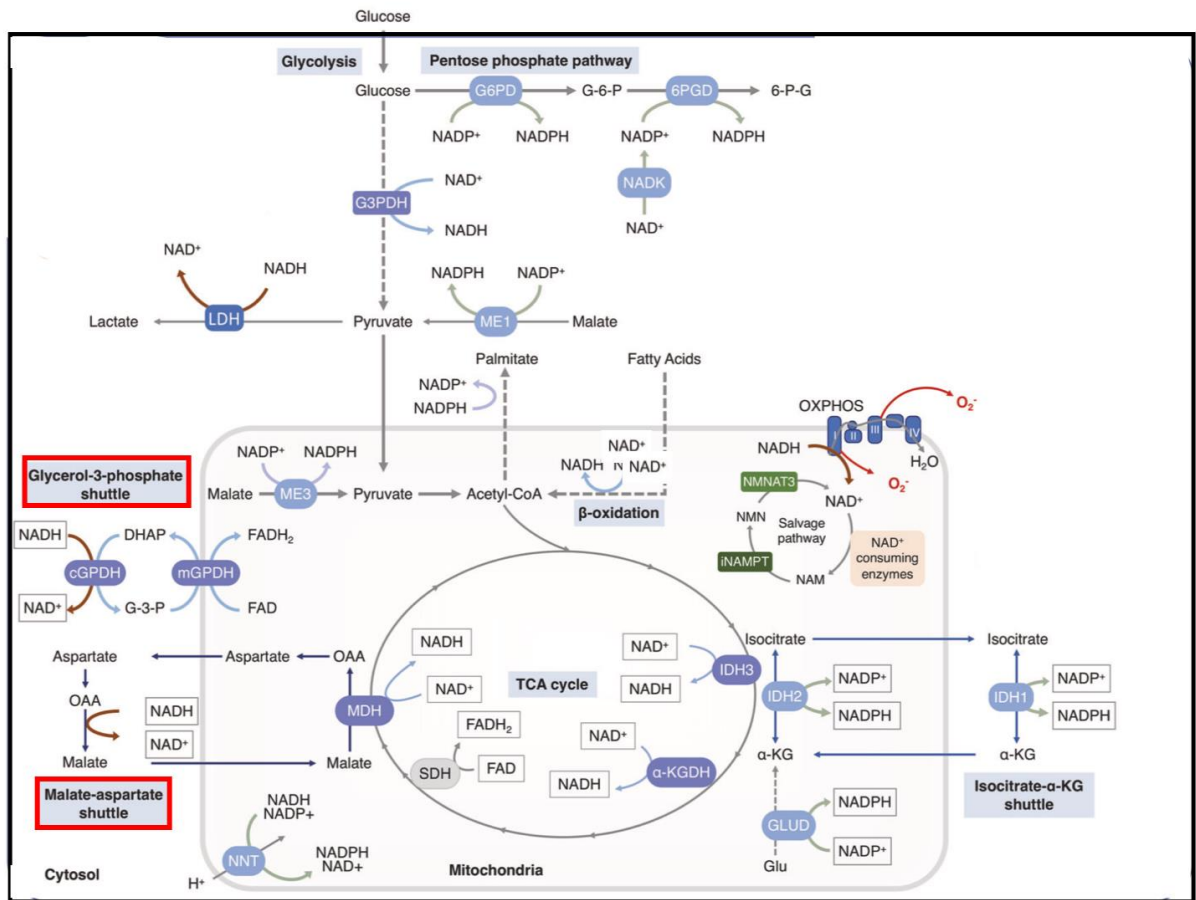


Figure 19 : Équilibre subcellulaire du NAD⁺. Le NAD⁺ peut recevoir du H⁺ pour produire la forme réduite NADH dans les processus métaboliques, notamment la glycolyse, la FAO et le cycle de Krebs (TCA cycle). Le NADH fournit une paire d'électrons pour piloter l'OXPHOS mitochondrial pour la génération d'ATP et la conversion de l'acide lactique en pyruvate. Le NADH cytosolique et mitochondrial est échangé par la navette malate-aspartate et la navette glycérol-3-phosphate. (Adapté de l'article de Xie N et al, *Signal transduction and targeted therapy*, 2020. (N. Xie et al. 2020)

A- Navette Malate/Aspartate

Plusieurs protéines participent au fonctionnement de la navette malate-aspartate, notamment le transporteur aspartate-glutamate, le transporteur malate- α -cétoglutarate et les formes cytosolique et mitochondriales de la malate déshydrogénase (MDH) et de l'aspartate aminotransférase (AAT) (**Figure 19**).

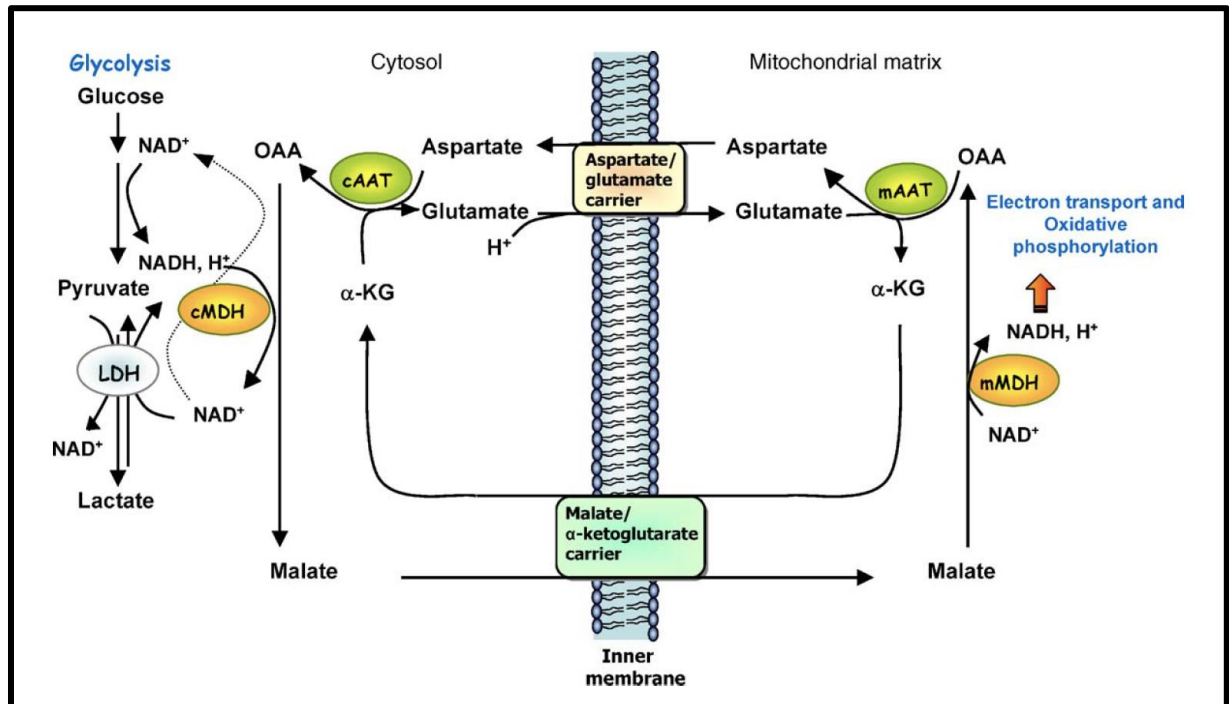


Figure 20 : Navette Malate-Aspartate. L'oxaloacétate (OAA) est converti en malate par la malate déshydrogénase cytosolique (cMDH). Le malate pénètre dans la matrice mitochondriale via le transporteur malate- α -cétooglutarate en échange d' α -cétooglutarate. Les électrons sont transférés à la chaîne de transport d'électrons lorsque le malate est oxydé en OAA par la malate déshydrogénase mitochondriale (mMDH). L'OAA est ensuite converti en aspartate par transamination avec du glutamate via l'aspartate aminotransférase mitochondriale (mAAT). L'aspartate sort des mitochondries via le transporteur aspartate-glutamate. Dans le cytosol, l'aspartate est converti en OAA par transamination avec l' α -cétooglutarate via l'aspartate aminotransférase cytosolique (cAAT) complétant la navette. Abréviations : LDH, lactate déshydrogénase ; α -KG, α -cétooglutarate. (Adapté de l'article de McKenna M.C et al, *Biochem Pharmacol*, 2006. (McKenna et al. 2006))

Cette navette agit pour transférer des électrons du NADH à l'oxaloacétate dans le cytosol formant du malate, qui pénètre dans les mitochondries en échange d' α -cétooglutarate via le transporteur malate- α -cétooglutarate (**Figure 19**). La malate déshydrogénase mitochondriale (mMDH) convertit le malate en oxaloacétate, transférant les équivalents réducteurs au NAD⁺ et formant le NADH. L'oxaloacétate est ensuite trans-aminé en aspartate via l'aspartate aminotransférase mitochondriale en conjonction avec la conversion du glutamate en α -cétooglutarate. L'aspartate quitte les mitochondries via le transporteur aspartate-glutamate en échange de glutamate cytosolique, qui pénètre dans les mitochondries. Pour compléter la navette, l'aspartate aminotransférase cytosolique convertit l'aspartate en oxaloacétate, formant simultanément du glutamate à partir de l' α -cétooglutarate. Dans le fonctionnement de cette navette, l'aspartate aminotransférase (ATT) semble être l'enzyme limitante, son activité étant plusieurs fois inférieure à celle de la MDH.

Au niveau du cervelet, l'ATT est fortement exprimé notamment au niveau des cellules granulaires mais également au niveau des processus synaptiques (Wenthold, Skaggs, and Altschuler 1986). Cependant, l'expression des enzymes indispensables au fonctionnement de la navette malate-aspartate semble diminuée dans les tumeurs cérébrales (Sytinskiï et al., 1978). L'ATT a une expression diminuée d'environ 25% dans le cas du sarcome méningé, dans les tumeurs neuro-ectodermiques et plus fortement dans les glioblastomes (Sytinskiï et al. 1978). Le taux d'aspartate intracellulaire est corrélé à la prolifération des cellules cancéreuses et semble limitant pour la croissance de certaines tumeurs *in vivo* (Gui et al. 2016)(Garcia-Bermudez et al. 2018). En condition d'hypoxie le taux d'aspartate diminue. En effet, les niveaux d'aspartate dans les tumeurs humaines primaires sont négativement corrélés avec l'expression de marqueurs d'hypoxie (Sullivan et al. 2018). La surexpression du transporteur Aspartate/Glutamate (SLC1A3) améliore la capacité de prolifération tumorale sous hypoxie dans des lignées cellulaires de cancer du poumon ou du pancréas (Garcia-Bermudez et al. 2018). Dans les glioblastomes là encore le taux d'aspartate est fortement corrélé avec l'expression de marqueurs d'hypoxie comme VEGF ou CAIX, avec une plus faible expression de l'aspartate en hypoxie. L'aspartate apparaît donc comme un métabolite limitant de la croissance tumorale sous hypoxie et pourrait être une cible thérapeutique potentielle.

B- Navette Glycérol-Phosphate

La navette glycérol 3-phosphate fonctionne également pour transférer des électrons du NADH cytosolique dans les mitochondries. Les équivalents réducteurs du NADH sont transférés à la dihydroxyacétone phosphate *via* la glycérol-3-phosphate déshydrogénase pour former le glycérol 3-phosphate (**Figure 20**). Le glycérol 3-phosphate est converti en dihydroxyacétone phosphate sur la surface externe de la membrane interne mitochondriale par la glycérol-3-phosphate déshydrogénase mitochondriale (mGPDH), et les équivalents réducteurs sont transférés au FAD, formant le FADH dans les mitochondries.

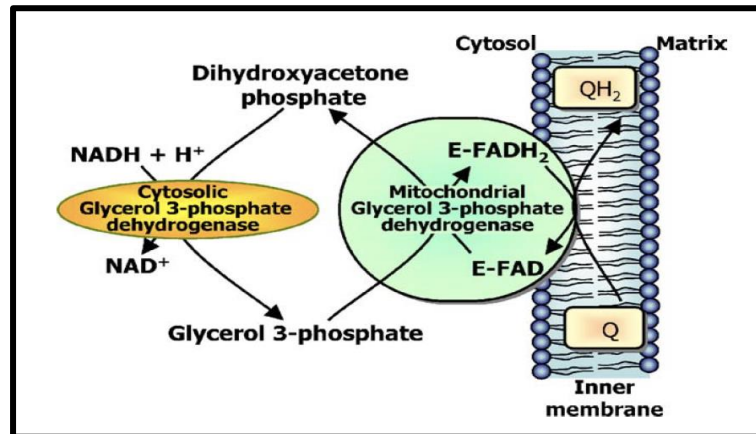


Figure 21 : Navette glycérol 3-phosphate. Les électrons sont transférés du NADH lorsque le phosphate de dihydroxyacétone est réduit en glycérol 3-phosphate. Le glycérol 3-phosphate est réoxydé en phosphate de dihydroxyacétone par la glycérol-3-phosphate déshydrogénase mitochondriale (mGPDH) qui est liée à un groupe prothétique FAD sur la face externe de la membrane interne mitochondriale et les électrons sont transférés à la coenzyme Q (Q) et pénètrent ensuite dans la chaîne de transport d'électrons. (Adapté de l'article de McKenna M.C et al, *Biochem Pharmacol*, 2006. (McKenna et al. 2006)

La mGPDH est une flavoprotéine liée à l'ubiquinone (CoQ) qui transfère les équivalents réducteurs directement du glycérol-3-phosphate dans la chaîne de transport d'électrons (Klingenberg 1970)(Yeh, Chinte, and Du 2008). Elle fait partie des neuf enzymes mitochondriales productrices d'espèces réactives de l'oxygène (ROS) (Mráček et al. 2009). Cela a été particulièrement mis en évidence dans certaines lignées cellulaires du cancer de la prostate (Chowdhury, Gemin, and Singh 2005). Le site actif de la mGPDH fait face à l'espace inter-membranaire mitochondrial. Cette orientation permet au mGPDH de coordonner le métabolisme cytosolique et mitochondrial pendant les périodes de forte activité. La mGPDH est d'ailleurs fortement exprimée dans les tissus avec des besoins énergétiques variables, notamment la graisse brune thermogénique, les fibres musculaires squelettiques de type II, le sperme, le pancréas et le cerveau (MacDonald 1981)(Koza et al. 1996).

Des études portant sur la culture d'astrocytes et de cellules granulaires cérébelleuses fournissent les preuves d'une activité importante de la navette glycérol 3-phosphate dans ces cellules (Atlante et al. 1999)(Waagepetersen et al. 2001). En effet, l'homéostasie du glucose et du lactate, qui dépend de la capacité à régénérer le NAD⁺ dans le cytosol, s'est avérée n'être que peu affectée par l'inhibition de la navette malate-aspartate dans les astrocytes, suggérant que la navette glycérol-3-P déshydrogénase était prédominante dans ces cellules.

Dans d'autres organes, et notamment au niveau du cœur, il a été montré que l'hypoxie induit l'expression de la mGPDH pour faciliter la synthèse d'ATP (Ishihama et al. 2021). L'expression de la glycérol-3-phosphate déshydrogénase cytosolique (cGPDH) est elle aussi induite en hypoxie cette fois-ci dans le cancer du rein (ccRCC), et son expression est significativement corrélée à une diminution de la prolifération cellulaire et à une meilleure survie globale (R. Liu et al. 2021). Dans les cellules de ccRCC, l'extinction de HIF-1 entraîne une réduction de l'expression de la cGPDH. Alors que le fait d'invalider HIF-2 n'a aucun impact sur l'expression de cGPDH/mGPDH. L'action de l'hypoxie sur la navette glycérol-phosphate, semble tissu dépendant, et la modulation de son activité, en ciblant notamment la mGPDH, pourrait avoir un impact sur la prolifération cellulaire (G. Singh 2014).

III- Les navettes comme cibles thérapeutiques

En raison de la dépendance des cellules cancéreuses à ce shunt entre glycolyse et phosphorylation oxydative, les protéines qui contribuent au lien entre glycolyse et OXPHOS peuvent être des cibles thérapeutiques anticancéreuses prometteuses. En ce sens, les voies de régénération du NAD^+ à travers les navettes malate/aspartate et glycérol-phosphate, sont aujourd'hui étudiées avec attention, d'autant plus que des inhibiteurs spécifiques existent.

En ce qui concerne la navette malate-aspartate, le composé le plus fréquemment utilisé pour inhiber son activité est l'acide amino-oxyacétique (AOAA). Ce composé inhibe spécifiquement les ATT cytosolique et mitochondriales. Son action inhibitrice est concentration dépendante, et a de faible concentration l'AOAA n'est que modérément puissant en tant qu'inhibiteur de l'aspartate aminotransférase (A. C. Yu, Schousboe, and Hertz 1982). Par conséquent, afin d'inhiber la navette malate-aspartate, une concentration en AOAA de 1 à 5mM est nécessaire. Cet inhibiteur a montré son efficacité sur des modèle *in vitro* et *in vivo* de cancer du sein, avec notamment une diminution de la prolifération cellulaire des cellules cancéreuses par rapport aux cellules épithéliales mammaires humaines normales, et une diminution de la croissance des tumeurs du sein sur modèle animal (Tanaka et al. 1991). Le niveau d'aspartate d'une cellule étant le déterminant clé de sa prolifération et de son arrêt du cycle cellulaire, Il semble intéressant de cibler la navette malate-aspartate en association avec d'autres traitements visant la phosphorylation oxydative afin de potentialiser leur effet (Birsoy et al. 2015a). Une étude récente montre que le déficit en phosphorylation oxydative causé soit par une hypoxie soit par

des mutations, rend les tumeurs sensibles à l'aspartate et à ses métabolites et confirme que l'effet synergiques des traitements ciblant ces deux voies (oxphos et aspartate) serait prometteur (Madala et al. 2020).

La mGPDH est une enzyme importante de la navette glycérol-phosphate qui relie la glycolyse à l'OXPPOS (Mráček, Drahot, and Houštek 2013). L'analyse de la structure de la mGPDH a permis l'identification d'un motif de base "benzimidazole-phényl-succinamide" comme étant essentiel à son inhibition. Les dérivés du Benzimidazole (composés RH02211, iGP-1, iGP-5) se révèlent être de puissants inhibiteurs de la mGPDH (Orr et al. 2014)(G. Singh 2014). En plus de ces composés pharmaceutiques spécifiques, Thakur *et al.* ont récemment montré que l'utilisation d'un traitement antidiabétique: la Metformine (voir paragraphe § III) était associée à une régulation négative de l'expression de mGPDH et à l'inhibition de la phosphorylation oxydative dans un modèle *in vitro* de cancer de la thyroïde (Thakur et al. 2018). Dans cette étude, le niveau d'efficacité du traitement par Metformine était directement lié au niveau d'expression de la mGPDH. Les cellules avec une expression élevée de mGPDH étaient majoritairement dépendantes de la phosphorylation oxydative, tandis que les cellules avec une expression plus faible de mGPDH étaient principalement dépendantes de la glycolyse. La mGPDH a également été signalée comme cible thérapeutique de la Metformine dans le foie où la suppression de l'activité enzymatique de la mGPDH par la Metformine entraîne une inhibition de la néoglucogenèse hépatique (Madiraju et al. 2014).

En association avec les inhibiteurs spécifiques ciblant les différentes voies de régénération du NAD^+ , la Metformine, médicament de la classe des Biguanides, apparaît aujourd'hui comme une possibilité dans l'arsenal thérapeutique anticancéreux, ciblant le métabolisme *via* différents mécanismes.

IV- Les biguanides et le métabolisme des cellules cancéreuses

A- Qu'est-ce que les biguanides ?

Les Biguanides sont une classe d'antidiabétiques oraux provenant de composés qui ont été identifiés dans une fleur : le lilas, plante reconnue pour ses propriétés hypoglycémiantes depuis le Moyen Âge.

Un des Biguanides, la Phenformine (N-phénylbiguanide), a été prescrit pour traiter le diabète de type 2 à partir des années 1950 mais a été retiré du marché à la fin des années 1970 en raison d'un risque accru d'acidose lactique. En 1995, la Metformine (diméthylbiguanide), un autre Biguanide ayant moins d'effets indésirables, a été approuvée par la FDA aux États-Unis et est devenue le médicament le plus prescrit dans le cadre de la pathologie diabétique (Pollak 2010). Dans les années 2000, l'analyse rétrospective de grosses cohortes de patients a révélé que l'utilisation de la Metformine était associée à un risque réduit de cancer, et que la mortalité liée au cancer chez les patients diabétiques consommant de la Metformine était également plus faible que ceux vierge de ce traitement (Evans et al. 2005)(Morales and Morris 2015). Ces observations ont rapidement placé les Biguanides comme traitement anticancéreux prometteur. Des études récentes viennent cependant tempérer l'engouement pour la Metformine comme traitement anticancéreux. Une étude clinique de phase II (TAXOMET), menée sur des patients atteints de cancer de prostate métastatique, n'a pas montré de supériorité de l'association de la Metformine au traitement classique par Docetaxel *versus* Docetaxel seul (Pujalte Martin et al. 2021).

Dans les études précliniques, la Phenformine s'avère posséder des activités anti tumorales plus puissantes que la Metformine (Shackelford et al. 2013)(Vara-Ciruelos et al. 2019) du fait de son caractère lipophile qui lui permet de traverser plus facilement la membrane cellulaire. *A contrario*, la Metformine nécessite une famille de transporteurs (OCT) pour pénétrer dans les cellules (Daugan et al. 2016), l'activité anti-tumorale de la Metformine va donc dépendre de propriétés pharmacodynamiques de perméabilité cellulaire basées sur l'expression de l'OCT (Madera et al. 2015).

B- Mécanismes d'action anti-cancéreux des Biguanides

1- Le complexe I mitochondrial

La Metformine et la Phenformine sont reconnues comme étant des inhibiteurs du complexe I mitochondrial qui ralentissent la croissance tumorale en empêchant la régénération du NAD⁺ *via* le complexe I (Wheaton et al. 2014) (**Figure 21**). Ainsi, les voies alternatives de régénération du NAD⁺ diminuent la dépendance au complexe I et favorisent la résistance à la Metformine (Gui et al. 2016). L'inhibition du complexe I conduit également à une augmentation du rapport intracellulaire AMP/ATP qui active indirectement la protéine kinase (AMPK) activée par l'AMP. L'AMPK module l'expression et l'activité de diverses enzymes impliquées dans des voies métaboliques essentielles pour la croissance et la prolifération des cellules

cancéreuses. L'inhibition de mTOR, dépendante de l'AMPK, est peut-être le mécanisme antinéoplasique le plus étudié pour les Biguanides (van Nostrand et al. 2020). L'inhibition du complexe I par la Metformine est également associée à d'autres changements métaboliques, tels que l'épuisement des métabolites du cycle de Krebs et la diminution de l'activité de HIF-1 α en condition d'hypoxie (Janzer et al. 2014)(Wheaton et al. 2014).

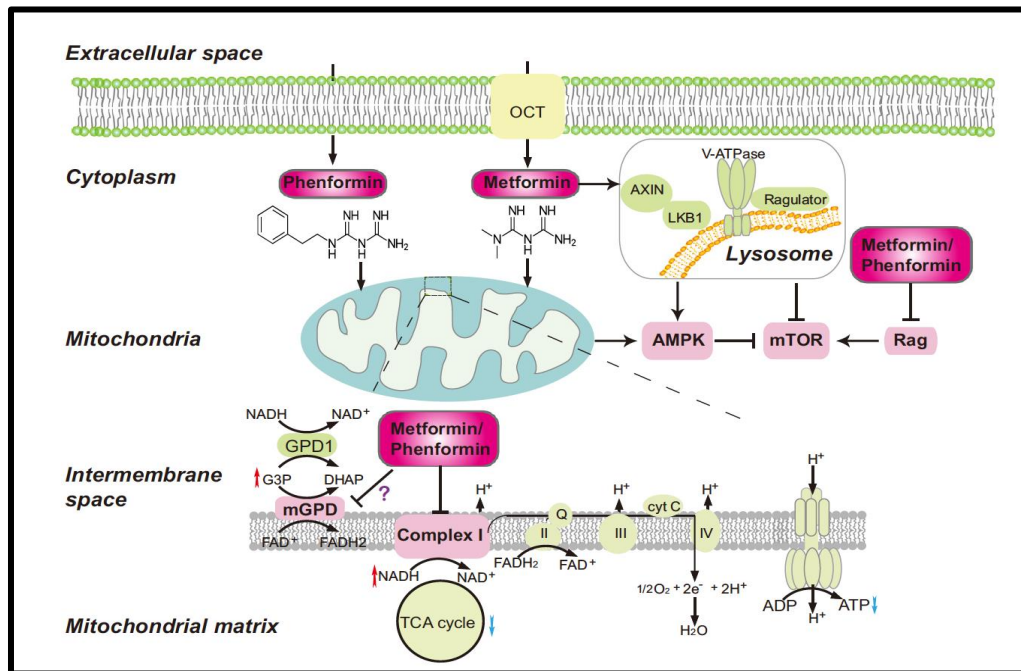


Figure 22 : Différents mécanismes d'action des Biguanides (Phenformine et Metformine). Les Biguanides pénètrent dans les cellules soit directement (Phenformine) ou via des transporteurs de cations organiques (OCT) (metformine). L'inhibition du complexe mitochondrial I par les Biguanides déclenche une augmentation du rapport l'AMP/ADP, conduisant à l'activation de l'AMPK et à l'atténuation de la signalisation mTOR. Les Biguanides inhibent également la mGPD, entraînant une perturbation de la navette glycérol-3-phosphate (G3P) et l'accumulation de NADH et de G3P. Enfin, les Biguanides peuvent activer l'AMPK et inhiber mTOR indépendamment du statut du complexe I mitochondrial. (Adapté de l'article de Zhao H et al, Trends in cancer, 202. (Zhao, Swanson, and Zheng 2021)

2- La Glycérophosphate déshydrogénase mitochondriale (mGPDH)

La mGPDH est une autre cible potentielle de l'activité anti-tumorale des Biguanides (**Figure 21**). La mGPDH et la cGPDH sont des constituants majeurs de la navette glycérol-3-phosphate (G3P), jouant un rôle important dans la régulation du potentiel redox de la cellule. Récemment, Di Magno *et al.* ont attribué à la Phenformine une action inhibitrice sur l'activité de la mGPDH dans les cellules de médulloblastome du groupe SHH. La Phenformine entraînerait des

altérations du potentiel redox cytoplasmique et une augmentation des niveaux de NADH (di Magno et al. 2020). Cependant, les preuves affirmant les effets anti-tumoraux directs des Biguanides *via* leur inhibition de la navette G3P sont toujours manquantes et d'autres études sont nécessaires pour étayer cette hypothèse.

C- Activation de voies métaboliques compensatrices

Lorsque les cellules cancéreuses sont traitées avec des Biguanides, elles subissent généralement une reprogrammation métabolique étendue pour faire face au stress métabolique induit par le médicament. Cibler ces adaptations métaboliques compensatrices pourrait permettre de potentialiser l'efficacité des Biguanides.

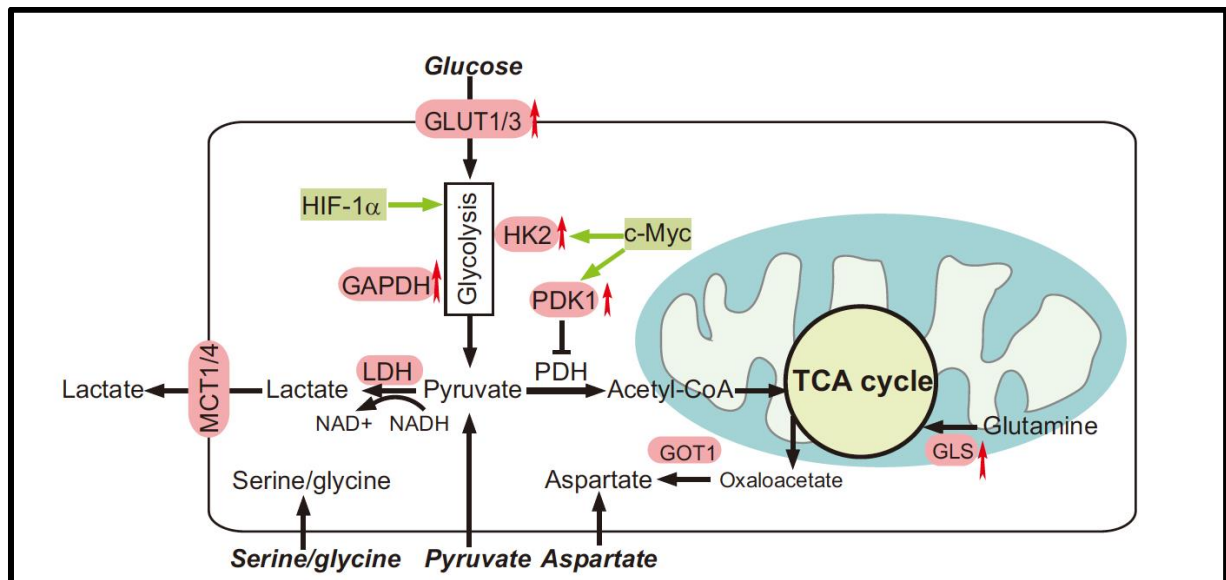


Figure 23 : Reprogrammation métabolique pour compenser le stress métabolique induit par le traitement au Biguanide. Les adaptations métaboliques comprennent la glycolyse, la biosynthèse de l'aspartate, de la glutamine et la synthèse de la sérine. Abréviations : GAPDH, glyceraldéhyde 3 phosphate déshydrogénase ; GLS, glutaminase ; HIF-1α, facteur 1 alpha inducible par l'hypoxie ; HK2, hexokinase 2 ; PDH, pyruvate déshydrogénase ; PDK1, pyruvate déshydrogénase kinase 1 ; TCA, acide tricarboxylique. (Adapté de l'article de Zhao H et al, Trends in cancer, 202.: (Zhao, Swanson, and Zheng 2021)

1- La Glycolyse

Les altérations de la glycolyse peuvent influencer les effets des Biguanides sur les cellules cancéreuses. En effet, la privation de glucose sensibilise les cellules cancéreuses au traitement par les Biguanides, soutenant fortement un rôle du métabolisme du glucose dans la réponse compensatoire à l'action des Biguanides sur le métabolisme mitochondrial (**Figure 22**). Cette

augmentation du flux glycolytique peut être expliquée par une augmentation de l'expression des transporteurs de glucose (GLUT1, GLUT3) à la surface des cellules (Litchfield et al. 2015). D'ailleurs le knockdown de *GLUT1* sensibilise les cellules cancéreuses à l'apoptose induite par la Phenformine (Leigh 1989). Et à l'inverse, la surexpression de GLUT3 a rendu plusieurs lignées cellulaires cancéreuses, initialement sensibles au Biguanide, résistantes à la Phenformine dans des conditions de faible taux de glucose (Birsoy et al. 2014). Les effets des inhibiteurs pharmacologiques sur les transporteurs de glucose ou le flux glycolytique, en combinaison avec des Biguanides, ont été largement étudiés dans divers types de tumeurs. L'inhibition de HIF-1 α en association avec les Biguanides induit une mortalité supérieure dans les cellules de leucémie lymphoblastique aiguë (LAL), et de leucémie lymphoïde chronique (LLC) (Khan et al. 2019). Le Dichloroacétate, un inhibiteur de l'enzyme glycolytique PDK, a diminué l'acidose lactique induite par les Biguanides, et amélioré leurs effets la mortalité cellulaire dans les cellules souches de gliome (Jiang et al. 2016). De plus, l'inhibition de la famille des transporteurs mono carboxylates (MCT), renforce l'activité anti-tumorale des Biguanides (Marchiq et al. 2015). La double inhibition de MCT1/MCT4 par la Syrosingopine, a potentialisé les effets létaux de la Metformine dans diverses lignées cellulaires cancéreuses, probablement par déplétion en NAD⁺ (Benjamin et al. 2018). Ces résultats suggèrent fortement que la combinaison d'un traitement par Biguanides avec des inhibiteurs glycolytiques pourrait être plus puissante que les Biguanides seuls.

MYC et HIF-1 α jouent un rôle important dans l'activation de la glycolyse (**Figure 22**), en induisant l'expression des enzymes glycolytiques, et aurait donc un effet compensateur de l'action des Biguanides. En effet l'hyperglycémie bloque la sensibilité des Biguanides dans des modèles de cancer de l'ovaire, probablement par une l'induction des enzymes glycolytiques hexokinase 2 (HK2) et pyruvate déshydrogénase kinase 1 (PDK1), qui sont fortement induite par MYC et HIF-1 α (Litchfield et al. 2015). Ces découvertes soutiennent fortement la capacité de la régulation positive de la glycolyse à agir comme une réponse adaptative pour rendre les cellules résistantes au traitement par Biguanide.

2- Le métabolisme de l'Aspartate, de la Glutamine et de la Sérine

L'aspartate est un précurseur d'acide aminé essentiel pour la synthèse de nucléotides et est donc important pour la prolifération cellulaire. Lorsque le complexe I est inhibé par un traitement aux Biguanides, la régénération du NAD⁺ à partir du NADH est limitée, altérant ainsi la

synthèse de l'aspartate. Lorsque la chaîne de transport d'électron mitochondrial est inhibée, l'ATT devient essentiel à la survie cellulaire en convertissant l'oxaloacétate en aspartate dans le cytosol, ce qui compense la diminution de la production d'aspartate dans les mitochondries causée par la Phenformine (Birsoy et al., 2015). En fait l'ATT cytosolique consomme normalement de l'aspartate pour transférer des électrons dans les mitochondries, mais, lors de l'inhibition de la chaîne de transport d'électron mitochondrial, son rôle s'inverse pour générer de l'aspartate dans le cytosol, ce qui compense partiellement la perte de synthèse d'aspartate mitochondriale.

Lorsqu'elles sont traitées avec de la Metformine, plusieurs lignées cellulaires présentent une dépendance accrue au métabolisme réducteur de la glutamine qui s'accompagne d'une diminution de l'oxydation du glucose induite par la Metformine (Fendt et al. 2013). L'inhibition de la glutaminase en combinaison avec la Metformine diminue la prolifération cellulaire, tandis que l'augmentation du flux de glutamine réduit la sensibilité à la Metformine (Fendt et al. 2013). De même, l'utilisation d'un inhibiteur de la glutaminase, le CB839, permet de potentialiser les activités anti-tumorales de la Metformine dans les lignées cellulaires de tumeurs osseuses (Ren et al. 2020).

De son côté, la sérine est un précurseur pour la biosynthèse des acides nucléiques, des protéines et des lipides. Le flux de sérine peut augmenter pour compenser la diminution de la phosphorylation oxydative induites par les Biguanides (Gravel et al. 2014). À l'inverse, l'utilisation d'un milieu pauvre en sérine améliore la mortalité cellulaire induite par la Metformine. Par conséquent, cibler les voies de synthèse de la sérine peut représenter une voie alternative pour renforcer les actions anti-tumorales des Biguanides.

En conclusion, déterminer quels aspects du métabolisme limitent la prolifération des cellules cancéreuses semble être une approche séduisante dans la recherche de nouvelles cibles thérapeutiques. Ainsi venir freiner ces activités qui fournissent des matériaux limitants pour la prolifération cellulaire est thérapeutiquement attrayant, surtout si les voies utilisées sont moins importantes dans les tissus prolifératifs normaux. La régénération du pool de NAD⁺ cytosolique, indispensable à la pérennisation de la glycolyse, est une étape essentielle à la survie de la cellule. Différents processus en assurent le fonctionnement, et récemment l'un d'entre eux (la navette glycérol-3-phosphate) a été identifié comme cible thérapeutique dans les MB du **groupe SHH** avec des résultats prometteurs. D'autres travaux sont bien évidemment

indispensables afin de comprendre le rôle de ces navettes dans le développement tumoral des différents sous-groupes de MB, afin encore une fois d'apporter une réponse thérapeutique la plus spécifique et personnalisable.

Objectifs

Le médulloblastome est la tumeur cérébrale pédiatrique la plus fréquente, avec un pronostic qui reste aujourd'hui sombre notamment pour les patients des **groupe 3 et 4**, en raison d'une faible efficacité des protocoles thérapeutiques actuels. Ce sont des tumeurs d'une grande hétérogénéité moléculaire, avec une variabilité dans leur localisation anatomique en fonction des différents sous-groupes. Nous avons émis l'hypothèse que cette différence de localisation anatomique pouvait entraîner une différence de niveaux d'oxygénation tissulaire en fonction des sous-groupes et donc une sensibilité à l'hypoxie probablement différente. Le métabolisme de la cellule cancéreuse étant en grande partie contrôlé par le facteur de transcription dépendant de l'hypoxie HIF, les différents sous-groupes pourraient présenter un profil métabolique différent, en fonction de leur niveau d'hypoxie.

Nous avons donc décidé de se rapprocher au maximum de l'environnement hypoxique tumoral du MB en travaillant à trois niveaux d'oxygénation différents : à 21% d'oxygène, qui correspond aux conditions standards d'un laboratoire, à 6% d'oxygène qui correspond au niveau de physioxie cérébrale et à 1% qui se rapproche des conditions hypoxiques du tissu tumoral.

Mieux comprendre les différences métaboliques des différents sous-groupes de MB en condition d'hypoxie est la première étape à la construction d'un protocole thérapeutique expérimental solide. S'appuyant sur les travaux récents de Di Magno L. *et al* (di Magno et al. 2020), nous nous sommes naturellement intéressés aux navettes impliquées dans la régénération du NAD⁺ cytosolique en association avec un composé antidiabétique bien connu de notre équipe de recherche, la Metformine/Phenformine. Cette approche co-ciblant la phosphorylation oxydative avec d'autres voies métaboliques compensatrices est une approche thérapeutique innovante dans le domaine du MB.

Mon projet de thèse a consisté dans un premier temps à définir la carte d'identité hypoxique de chaque sous-groupe de MB en dichotomisant les groupes en deux entités distinctes : (i) le **groupe 3**, ayant le moins bon pronostic avec la mortalité la plus haute, et (ii) le **groupe non 3** correspondants aux groupes de MB le plus étudié c'est-à-dire le groupe SHH.

- La sensibilité à l'hypoxie et donc le profil métabolique est-il différent en fonction des groupes de MB ?

En parallèle, je me suis intéressée au cours de ma thèse à comprendre quel était le processus de régénération du NAD⁺ cytosolique principal dans le **groupe 3** et dans le **groupe non 3** en condition d'hypoxie. Afin d'analyser si ces navettes pouvaient réellement être des cibles thérapeutiques intéressantes en complément d'un traitement visant la phosphorylation-oxydative.

- Quelle est la voie de régénération du NAD⁺ principal dans les différents groupes de MB ?
- Peuvent-elles être des cibles thérapeutiques intéressantes ?

Les résultats répondant aux questions ici posées, sont présentés dans la section suivante.

Résultats

Article 1

HIF-2 as a new therapeutic target in medulloblastoma Group 3

I- Contexte et objectifs

Le médulloblastome fait partie des tumeurs cérébrales malignes les plus courantes chez l'enfant. Des études récentes ont identifié quatre sous-groupes de la maladie (WNT, SHH, groupe 3 et groupe 4) qui diffèrent en termes de caractéristiques moléculaires mais également de pronostic. Plus de 70% des patients atteints de MB répondent aujourd'hui aux caractéristiques du groupe 3 ou 4 (Gajjar et al. 2021). Malgré cette hétérogénéité, la plupart des patients atteints de MB reçoivent des thérapies similaires, notamment la chirurgie, la radiothérapie et la chimiothérapie intensive. Bien que ces traitements prolongent la survie globale des patients, nombre d'entre eux décèdent encore de la maladie et ceux qui survivent souffrent de graves effets secondaires à long terme. Il est urgent de considérer que chaque patient atteint de médulloblastome puisse être sensible à différentes thérapies et que l'adaptation de la thérapie en fonction des caractéristiques moléculaires et cellulaires des différents groupes améliorera leurs résultats (Rusert et al. 2020). La totalité des recherches *in vitro* sur le MB a été réalisé dans des conditions de cultures classique, c'est-à-dire à 21% d'oxygène, ce qui s'éloigne énormément des conditions d'oxygénation physiologique au niveau du tissu cérébral. Il est évident que le métabolisme cellulaire est modifié en fonction du niveau d'oxygène disponible, et qu'il est primordial de mieux caractériser les voies métaboliques impliquées dans chaque modèle cancéreux, dans un environnement le plus proche des conditions *in vivo*.

Le niveau d'oxygénation tissulaire est extrêmement variable au sein même du cerveau, et on constate que le développement des quatre groupes de MB se situe à différents endroits du cervelet. Cette répartition anatomique pourrait entraîner une variabilité d'oxygénation rendant certains groupes plus ou moins sensibles à l'hypoxie, et positionnant le métabolisme hypoxique comme nouvelle cible thérapeutique.

Alors que l'hypoxie intra-tumorale en général est associée à un mauvais pronostic, le rôle pronostique de HIF-1 α et HIF-2 α diffère selon les types de tumeurs, pouvant avoir des effets cliniques opposés selon le type de tumeur. La surexpression de HIF-1 est associée à un

pronostic favorable dans le neuroblastome (Noguera et al. 2009), alors que l'expression de HIF-2 est un marqueur de mauvais pronostic dans le glioblastome (Zhizhong Li et al. 2009). A ma connaissance, aucune étude ne décrit aujourd'hui le rôle des HIFs dans le MB, rendant difficile le développement de thérapies ciblant l'hypoxie dans ce type de cancer.

Il nous a donc semblé important d'étudier la sensibilité à l'hypoxie des différents groupes de MB afin de mettre en évidence, si elles existent, des différences pouvant devenir la base de recherches thérapeutiques spécifiques.

II- Article

HIF-2 as a new therapeutic target in medulloblastoma Group 3

J. Contenti^{1*}, Y. Guo¹, M. Larcher², L. Mirabal², M. Rouleau³, M. Irondelle¹, V. Tiroille¹, A. Mazzu¹, V. Duranton-Tanneur⁴, F. Pedeutour⁴, I. Ben-Sahra⁵, L. Tiberi⁶, G. Robert¹, C. Pouponnot², F. Bost¹, N.M. Mazure^{1*}.

¹ INSERM U1065, University of Côte d'Azur (UCA), C3M, 151 Route de St Antoine de Ginestière, BP2 3194, CEDEX 03, 06204 Nice, France.

² CNRS UMR 3347, Centre Universitaire, Orsay, France.

³ LP2M, CNRS-UMR 7370, Faculty of Medicine, University of Côte d'Azur (UCA), 06108 Nice, France.

⁴ Laboratory of Solid Tumor Genetics, University Hospital of Nice-Côte d'Azur University, Nice, France; Laboratory of Solid Tumor Genetics, Institute for Research on Cancer and Aging of Nice (IRCAN), CNRS UMR 7284/INSERM U1081, Nice, France. Electronic address: florence.pedeutour@unice.fr.

⁵ Department of Biochemistry and Molecular Genetics, Northwestern University, Chicago, Illinois.

⁶ Armenise-Harvard Laboratory of Brain Cancer, Department CIBIO, University of Trento, Via Sommarive 9, 38123 Trento, Italy.

* Correspondence: contenti.j@chu-nice.fr & mazure@unice.fr

Medulloblastoma is the most common brain cancer in children. Among the subclassification into four groups, Group 3 is the most metastatic, with a poor prognosis and for which few treatments are effective. Moreover, the genetics and biology underlying the Group 3 MB subgroup remain less clear compared to the other groups¹. Any new markers or genetic abnormalities will allow to consider new therapeutic developments. Tumor hypoxia and consequent metabolism have been little studied in medulloblastoma (MB). In this study, we show that Group 3 MB have either a post-translational modification or mutations in the PAS-A domain of HIF-1 α blocking association with HIF-1 β , the subsequent entry into the nucleus, resulting in a completely inactive HIF-1. Only HIF-2 is then present to replace HIF-1 in the activation of metabolic pathways. *In vitro* data showed that pharmacological inhibitor of HIF-2 α , PT2385^{2,3} coupled with Metformin, a specific inhibitor of the mitochondrial complex I, can efficiently block and kill Group 3 MB compared to Non-Group 3 MB. HIF-2 emerges as the key HIF isoform that is essential for Group 3 MB to respond to a hypoxic microenvironment. But it also becomes its Achilles heel, as PT2385, and others, can specifically target HIF-2 without fear of possible HIF-1 compensation.

Group 3 MB are sensitive to oxygen variations and do not express HIF-1 target genes

Most solid cancers are subject to constant oxygen variations and have had to develop numerous responses to survive this hypoxic microenvironment^{4,5}. Medulloblastoma (MB) is not exempt. The four different subgroups that arise from the classification of medulloblastomas are not similarly geographically located in the cerebellum (Fig. 1a). We therefore compared Group 3 MB (HDMB03 and D-458) to Non-Group 3 MB (DAOY and ONS-76) and cultured these cells in three different oxygen concentrations: 21% O₂ (normoxia - Nx) which only laboratory cells will encounter, 6% O₂ (physioxia - Phx) conditions close to physiological conditions of cerebellum cells, and 1% O₂ (hypoxia - Hx) general tumor conditions. We then observed that Group 3 MB were more sensitive to low oxygen conditions resulting in higher mortality and subsequently lower proliferation in contrast to Non-Group 3 MB (Fig. 1 b-i). However, all four cell lines expressed HIF-1 α and HIF-2 α in different proportions and kinetics (Fig. 1j). Analysis of the different target genes of HIF-1 (*Ca9* and *Mct4/SLC16A3*), HIF-2 in (*Oct4/Pou5F1*), HIF-1/HIF-2 (*Ca12*, *Glut1/SLC2A1*, *Ldha*), and non-target genes of HIFs (*Ldhb* and *MCT1/SLC16A1*) showed that none of the target genes of HIF-1 alone were expressed in Group 3 MB. Similar results showing lower expression of *Mct4* were detected in data analysis from

R2: Genomics analysis and visualization platform (Suppl. Fig. 1). In addition, HIF-2 α /EPAS and HIF-2 target genes have higher expression in Group 3. Similarly, single cell meta data analysis (<https://singlecell.broadinstitute.org/>) by Manoranjan *et al.* ⁶ using primary patient-derived MB brain tumor-initiating cell (BTIC) lines showed low expression of *Ca9*, *Ca12*, *Glut1/SLC2A1*, *Mct4/SLC16A3* and *Oct4/Pou5F1* in Group 3 MB in a context of high MYC expression compared to the other MB groups (Suppl. Fig. 2). These data suggest that HIF-1 α , although present (HDMB03) or weakly present (D-458) in Group 3 cells, may be mutated leading to an inability to control these target genes.

HIF-1 α is mutated and transcriptionally inactive in Group 3 MB

Immunoblot analysis revealed that HIF-1 α from HDMB03 cells systematically showed a higher molecular weight shift estimated at about 2 to 3 kDa while HIF-1 α from D-458 cells was mostly absent or otherwise hardly visible (Fig. 2a). To better characterize these two HIF-1 α from Group 3, we first analyzed their kinetics of stabilization in Nx in the presence of MG132, a proteasome inhibitor (Fig. 2b) as well as their stability after reoxygenation (Suppl. Figure 3a-c). We determined that MG132 stabilized overall HIF-1 α from Group 3 more weakly compared to Non-Group 3 and that HIF-1 α was very rapidly degraded in D-458 cells. As for HIF-1 α in HDMB03 cells, the band with the highest molecular weight appeared much more stable in Nx even after 10 min of reoxygenation in contrast to the other cell lines. In addition, we demonstrated that both HIF-1 α from Group 3 lacked the ability to localize to the nucleus (Fig. 2c-d). Because HIF-1 α in HDMB03 is slightly different from classical HIF-1 α , siRNAs directed against HIF-1 α and HIF-2 α were used (Suppl. Figure 3d). HIF-1/2 α were invalidated in DAOY, ONS-76 and D-458 to different degrees of invalidation but confirming the specificity of HIF-1 α . However, we were unable to invalidate HIF-1 α in HDMB03. The use of another anti-HIF-1 α antibody confirmed the identity of this particular HIF-1 α (Suppl. Figure 3e). HIF-1 α was then stabilized in hypoxia in the presence of Bafilomycin or MG132 or both compounds to block any potential degradation during sample processing. Bafilomycin does not stabilize HIF-1 α in HDMB03 but the use of MG132 in hypoxia increases the stabilization capacity of HIF-1 α (Fig. 2e). A 2D gel exploration was possible allowing a finer analysis of HIF-1 α of HDMB03 compared to that of ONS-76.

Finally, HIF-1 α cDNA sequencing (i) confirmed that HIF-1 α was poorly represented in Group 3 MB and (ii) revealed specific DNA mutations in each of the two Group 3 MB lineages (Suppl. Fig. 4). However, translation of the different cDNA sequences showed that these mutations resulted only in four mutations in the PAS-A domain of HIF-1 α in D-458 cells explaining the inability of HIF-1 α to dimerize with HIF-1 β and to localize in the nucleus (Fig. 2f). Moreover, these mutations lead to a different 3D conformation suggesting the impossibility of HIF-1 α of Group 3 MB to activate its target genes (Fig. 2g). As for HIF-2 α , characterized *via* the use of HIF-2 α siRNA (Suppl. Fig. 3d) and in comparison, with HIF-2 α from 786-O ccRCC cells (Suppl. Fig.3f), it is present in all four cell lines, but more strongly induced in Hx in Group 3 MB compared to Non-Group 3 MB. Silencing of HIF-1 α or HIF-2 α resulted in compensatory effects in Non-Group 3 MB whereas no compensatory effect was observed in Group 3 MB (Suppl. Fig. 3d). Taken together, these results suggest that Group 3 MB has a nonfunctional HIF-1 resulting from post-translational modifications (HDMB03) and mutations (D-458) and that this Group 3 MB owes its response to the hypoxic microenvironment only to the ability of HIF-2 to replace HIF-1.

PT2385 sensitizes Group 3MB viability *in vitro* and affects glycolysis

We then evaluated the metabolic capacity of Group 3 MB compared to Non-Group 3 MB under the three oxygenation conditions previously described: Nx, Phx and Hx. Seahorse analyses were performed to measure glycolytic (ECAR) and oxidative (OCR) metabolisms. The four cell lines overall showed similar or better glycolytic capacity in Phx and Hx *versus* Nx (Fig. 3a-d). However, Group 3 MB showed a greater response to glucose (G) addition than Non-Group 3 MB suggesting an ability of HIF-2 directly or indirectly to manage anaerobic glycolysis. Completely unexpectedly, DAOY (Non-Group 3 MB) as well as HDMB03 (Group 3 MB) showed much greater respiratory capacities in Hx than in Phx or even Nx (Fig.3e and g, Suppl. 5) whereas it is more commonly accepted that respiration is repressed under Hx *via* activation of PDK1, the target gene of HIF-1^{7,8}, and as observed with ONS-76 and D-458 (Fig.3f and h). We then considered that the use of an HIF-2 α inhibitor could specifically target the metabolism of Group 3 MB. We therefore chose PT2385, one of the first specific HIF-2 α inhibitors currently used in clinical trials for kidney cancer and glioblastoma. The lowest concentration of PT2385 (1mM) induced cell death only in Group 3 MB (Fig. 3i). As expected, in Hx (Fig. 3j-m) and Phx (data not shown), PT2385 reduced glycolytic capacity by 35.3- and

38.2-% in HDMB03 and D-458 cells, respectively, in somewhat similar proportions to those observed with 2-DG used as a control (Suppl. Fig. 6a). The repressive effect of PT2385 was not observed in Nx (Fig. 3j-k). However, a decreasing trend was observed in Non-Group 3 MB (Suppl. Fig. 5c-d). PT2385 had no effect on respiration in Hx in either Group 3 MB (Fig. 3l-m) or Non-Group 3 MB (Suppl. Fig. 5e-f). It may, however, have increased breathing capacity in Nx as observed in HDMB03 (Fig. 3l). To completely collapse the energy intake of the Group 3 MB, we considered blocking the respiration by using Metformin (Metf), another drug widely employed to fight diabetes^{9,10}. Metformin clearly decreased the proliferation of all cells in Hx while only specifically targeting Group 3 MB viability both in Phx and Hx (Fig. 3n-o). The addition of Metformin did block respiration in Group 3 MB but only partially decreased respiration in Non-Group 3 MB (Suppl. Fig. 6b). A mirror effect on glycolysis was observed since Metformin increased glycolysis overall in Group 3 MB to compensate for the lack of energy due to the blockade of respiration but this compensatory effect was hardly observed in the Non-Group 3 MB (Suppl. Fig. 6a). These results indicate that the use of each of these compounds, PT2385 and Metformin, perfectly and specifically target HIF-2 and complex 1, respectively, in Group 3 MB, but that there is a compensatory effect that only the use in combination will be able to cancel out. Moreover, it appears that the significant biological effects of these two compounds is limited to Group 3 MB.

PT2385/Metf combo is effective *in vitro* and induces Group 3MB cell death

Treatment alone (PT2385) decreased the stabilization of HIF-1 α and/or HIF-2 α only in D-458 cells (Suppl. Fig. 7a). However, the combination of the two compounds more strongly affected the stability of both HIF- α subunits (Suppl. Fig. 7b). This resulted in decreased expression of the *Ca9-*, *Ca12-*, *Glut1-*, *Oct4-* and more slightly on *Ldha-* genes (Suppl. Fig. 7c-h). Subsequently, dual PT2385 and Metformin treatment clearly decreased proliferation in all cell lines (Suppl. Fig. 8a-b) and induced cell death more specifically in Group 3 MB in Phx and Hx (Fig. 4a-b). Invalidation of HIF-1 α in the presence of PT2385 and Metformin ultimately induced cell death in Non-Group 3 MB and not in Group 3 MB reinforcing that HIF-1 has a protective role for the cancer cell when in the presence of HIF-2 (Suppl. Fig.8c). We then showed that the coloration of the medium, a reflection of growth and lactate production, was significantly affected in three of the four cell lines (DAOY, HDMB03, and D-458) (Suppl. Fig. 8d), that all cells consumed less glucose (Suppl. Fig. 8e), and that almost all cells produced less

lactate (Suppl. Fig. 8f) following the double treatment. However, the combination worked better in the D-458 than in the HDMB03 cells. Indeed, glycolysis as well as respiration were collapsed in D-458 cells while the compensatory effect of Metformin on glycolysis was only partially blocked in HDMB03 cells (Fig. 4c-f). Dual treatment decreased glycolysis in Non-Group 3 MB but was not able to decrease respiration enough to have a deleterious effect on these cells (Suppl. Fig. 8d-g).

Together, these results strongly confirm that simultaneous blockade of glycolysis and respiration in Group 3 MB is a promising therapeutic approach.

Discussion

Here we show for the first time that cell lines belonging to Group 3 MB, the most aggressive and metastatic group, exhibit genetic modifications, mutations, of HIF-1 α leading to functional inactivation of HIF-1. The HIF-2 isoform then remains alone to respond to different oxygen variations. This makes it interesting to compare Group 3 MB with ccRCCs expressing only HIF-2, a particular type of aggressive kidney cancer. The activity of HIF-1 α , rather anti-tumor in this very particular cancer, is strongly decreased due to chromosomal deletions¹¹ or HAF activity¹² leaving HIF-2 to work fully in its pro-tumor activity. The dichotomy between HIF-1 and HIF-2 observed in ccRCCs was until now unique in the tumor field. What about medulloblastomas and especially Group 3 MB? In Non-Group 3, the presence of a functional HIF-1 coupled to HIF-2 seems to protect the tumor cells from cell death while none of the tested treatments seemed to affect them. However, what our results suggest is more that HIF-1 would introduce a survival capacity in a hostile environment like hypoxia. Therefore, what would be the interest for the tumor cell to get rid of HIF-1 α ? HIF-2 alone offers non-negligible interests. Group 3 MB has been identified by high expression of the MYC oncogene that enables rapid and aggressive tumor development¹³. Yet HIF-2 α is a formidable promoter of MYC activity while HIF-1 α tends to inhibit MYC instead. Moreover, MYC has been shown to regulate the HIF-2 α expression¹⁴. Pei *et al.* showed that MYC overexpression in stem cells had strong morphological homologies and expression profiles comparable to those of Group 3 cells¹³. Their studies suggest that MYC overexpression is a major oncogenic event for Group 3 MB: it induces tumorigenesis and then allows its maintenance and progression. However, HIF-2 is a formidable player in maintaining stem cells in an undifferentiated state *via* genes like *Oct4*, *Sox* and *Nanog*^{15,16}. In a MYC background where Oct4 would be induced by physioxia or hypoxia,

the cells would then have a strong stem cell potential even though these cells would be "adult". Since hypoxia occurs as early as the embryonic state ¹⁷, we can propose that HIF-2 may be the primary origin of oncogenic evolution of Group 3 MB, even before MYC. If the uniqueness of HIF-2 is an extraordinary advantage for the Group 3 MB tumor cell, then it becomes a perfect target to block MB tumor growth. We used PT2385, which is in phase II for ccRCC (<https://clinicaltrials.gov/ct2/show/NCT03108066>) but also for glioblastoma (<https://clinicaltrials.gov/ct2/show/NCT03216499>). Very promising results have been obtained suggesting similar results for Group 3 MB patients. Other more recent inhibitors, such as PT2399 or PT2977, could certainly provide stronger therapeutic responses. HIF-2 inhibition could then not only partially block metabolism but also affect a certain identity of stem cells. However, unlike ccRCC, it was the combination of PT2385 with Metformin that had a very strong impact on cell growth and death. Here we have proven the concept that the best targeted therapy comes from a better molecular knowledge. It seems obvious that this "hypoxic" approach will reveal other potential therapeutic targets allowing to find new drug combinations to provide the most specific and personalized therapeutic response possible.

Legends

Fig. 1. Group 3 MB are sensitive to oxygen variations and do not express HIF-1 target genes. **a**, Schematic distribution of the different MB subgroups according to the vascular system (from ref.). **b-e**, DAOY (**b**), ONS-76 (**c**), HDMB03 (**d**), D-458 (**e**) cells were incubated in 21-, 6- and 1- % O₂ for 24-, 48- and 72- h. Cell viability (%) was measured using an ADAM cell counter. **f-i**, DAOY (**f**), ONS-76 (**g**), HDMB03 (**h**), D-458 (**i**) cells were seeded at the same density and incubated in 21-, 6- and 1- % O₂ for 24-, 48- and 72- h. **j**, DAOY, ONS-76, HDMB03, D-458 cells were incubated in normoxia (Nx) for 24h and hypoxia (Hx - 1% O₂) for 24-, 48- and 72- h. Cell lysates were analyzed by immunoblotting for HIF-1 α and HIF-2 α . Tubulin was used as a loading control. **k-r**, Graphic representation of *Glut1* (**k**), *Ldha* (**l**), *Ldhb* (**m**), *Ca9* (**n**), *Ca12* (**o**), *Mct1* (**p**), *Mct4* (**q**) and *Oct4* (**r**) mRNA expression in DAOY, ONS-76, HDMB03, D-458 cells incubated in normoxia (Nx) for 24h and hypoxia (Hx - 1% O₂) for 24-, 48- and 72- h.

The 2-way ANOVA is representative of at least three independent experiments.

Fig. 2. HIF-1 α is mutated and transcriptionally inactive in Group 3 MB. **a**, DAOY, ONS-76, HDMB03 and D-458 cells were seeded at the same density and incubated in Hx (1% O₂) for 72h. Cell lysates were analyzed by immunoblotting for HIF-1 α . **b**, DAOY, ONS-76, HDMB03 and D-458 cells were seeded at the same density and incubated in Nx (21% O₂) for 18h. MG132 (10 μ M) was added for 1-, 2-, 4- and 6- h. Cell lysates were analyzed by immunoblotting for HIF-1 α . Tubulin was used as a loading control. Bottom panel, Quantification of HIF-1 α protein levels. **c**, Immunofluorescence labeling and merged images with HIF-1 α (in red) and DAPI (in blue) for DAOY, ONS-76, HDMB03 and D-458 cells incubated for 48h in Hx. **d**, DAOY, ONS-76, HDMB03 and D-458 cells were seeded at the same density and incubated in Hx (1% O₂) for 48h. Subcellular fractionation was used to identify proteins in nuclei and cytoplasm. HSP90 was used as a loading control. **e**, ONS-76 and HDMB03 cells were seeded at the same density and incubated in Hx (1% O₂) for 48h. MG132 was added 6h prior to lysis. Subcellular fractionation was used to identify proteins in nuclei and cytoplasm. Tubulin was used as a loading control. Gel 2D. **f**, Alignment of the HIF-1 α protein sequences from HIF-1 α control (sp|Q16665|HIF1A_HUMAN Hypoxia-inducible factor 1-alpha), DAOY, ONS-76, HDMB03 and D-458. **g**, Predicted model of HIF-1 α from HIF-1 α control (sp|Q16665|HIF1A_HUMAN Hypoxia-inducible factor 1-alpha), HDMB03 and D-458 (I-Tasser Protein Structure & Function Prediction <https://zhanggroup.org/I-TASSER/>).

Fig. 3. PT2385 sensitizes Group 3MB viability *in vitro* and affects glycolysis. **a-d**, ECAR in Nx (21% O₂), Phx (6% O₂) and Hx (1% O₂) for 24 h of DAOY, ONS-76, HDMB03, D-458 cells was evaluated with the XF24 analyzer. Cells were deprived of glucose for 1 h, then glucose (G) and oligomycin (O) were injected at the indicated times. The graphs are representative of at least three independent experiments carried out in octuplicate. **e-h**, Respiratory control of DAOY, ONS-76, HDMB03, D-458 cells. OCR was measured in real time with the XF24 analyzer. Cells were cultured for 24 h in Nx (21% O₂), Phx (6% O₂) and Hx (1% O₂). Cells were deprived of glucose for 1h, then glucose (G), oligomycin (O), FCCP (F), and Rotenone + Antimycin A (R/A) were injected at the indicated times. The graphs are representative of at least three independent experiments carried out in octuplicate. **i**, DAOY, ONS-76, HDMB03, D-458 cells were incubated in Hx for 72h in the absence (Control) or presence of PT2385 at 1-, 10-, and 20- mM. Cell viability (%) was measured using an ADAM cell counter. **j-k**, ECAR of HDMB03 and D-458 cells cultured in Nx (21% O₂) and Hx (1% O₂) for 24h was evaluated

with the XF24 analyzer. Cells were deprived of glucose for 1h, then glucose and oligomycin were injected. The graphs are representative of at least three independent experiments carried out in octuplicate. **l-m**, Respiratory control of HDMB03 and D-458 cells. OCR was measured in real time with the XF24 analyzer after cells were cultured for 24h in Nx (21% O₂) and Hx (1% O₂). Cells were deprived of glucose for 1h, then glucose, oligomycin, DNP, and Rotenone + Antimycin A were injected at the indicated times. The graphs are representative of at least three independent experiments carried out in octuplicate. **n**, DAOY, ONS-76, HDMB03, D-458 cells were incubated in 6 (Phx)- and 1 (Hx)- % O₂ for 72h in the absence (Control) or presence of Metformin (Metf). Cell number was measured using an ADAM cell counter. **o**, DAOY, ONS-76, HDMB03, D-458 cells were incubated in 6 (Phx)- and 1 (Hx)- % O₂ for 72h in the absence (Control) or presence of Metformin (Metf). Cell viability (%) was measured using an ADAM cell counter.

The 2-way ANOVA is representative of at least three independent experiments.

Fig. 4. PT2385/Metf combo is effective *in vitro* and induces Group 3MB cell death. **a-b**, DAOY, ONS-76, HDMB03, D-458 cells were incubated in Phx (**a**) and Hx (**b**) for 72h in (absence (Control) or presence of PT2385 (1- or 10- mM) and Metformin (Metf). Cell viability (%) was measured using an ADAM cell counter. **c-d**, ECAR of cells cultured in Hx (1% O₂) in the absence (Control) or presence of Metformin alone (Metf), PT2385 alone (1mM), PT2385 + Metformin for 24h of HDMB03 (**c**) and D-458 (**d**) cells was evaluated with the XF24 analyzer. Cells were deprived of glucose for 1h, then glucose (G) and oligomycin (O) were injected at the indicated times. The graphs are representative of at least three independent experiments carried out in octuplicate. **e-f**, Respiratory control of HDMB03 (**e**) and D-458 (**f**) cells. OCR was measured in real time with the XF24 analyzer of cells cultured for 24 h in Hx (1% O₂). Cells were deprived of glucose for 1h, then glucose (G), oligomycin (O), FCCP (F), and Rotenone + Antimycin A (R/A) were injected at the indicated times. The graphs are representative of at least three independent experiments carried out in octuplicate.

The 2-way ANOVA is representative of at least three independent experiments.

Suppl. Figure 1. a-h, Schematic distribution of the different MB subgroups according to HIF-1 α (a), CA9 (b), MCT4 (c), HIF-2 α /EPAS (d), OCT4 (e), MYC (f), VEGF A (g) and GLUT1 (h).

Suppl. Figure 2. a, tSNE of 3725 cells colored by GSVA enrichment score for the Wnt subgroup gene signature. **b-j**, Cells colored by classification for enrichment of Wnt subgroup signature. Dark red cells surpassed the 5% cutoff and are considered significantly enriched for the gene signature. Gray cells did not pass the threshold. SLC2A1/GLUT1 (b), LDHA (c), LDHB (d), CA9 (e), CA12 (f), SLC16A1/MCT1 (g), SLC16A3/MCT4 (h), POU5F1/OCT4 (i) and MYC (j). **k**,

Suppl. Figure 3. a, DAOY, ONS-76, HDMB03, D-458 cells were incubated in hypoxia (Hx) for 48h and reoxygenated for 1-, 2-, 4-, 6-, and 10- min (*). Cell lysates were analyzed by immunoblotting for HIF-1 α . Tubulin was used as a loading control. **b**, Quantitative analysis of the total HIF-1 α bands compared to tubulin. **c**, Quantitative analysis of the upper and lower HIF-1 α bands compared to tubulin. **d**, DAOY, ONS-76, HDMB03, D-458 cells were transfected with control siRNA (siCtl), siHIF-1 α , and siHIF-2 α . Cell lysates were analyzed by immunoblotting for HIF-1 α , HIF-2 α , and Tubulin was used as a loading control. **e**, ONS-76 and HDMB03 cell lysates were analyzed by immunoblotting for HIF-1 α from Invitrogen (PA5-85494) and Tubulin was used as a loading control. **f**, DAOY, ONS-76, HDMB03, D-458 cells were incubated in normoxia (Nx- 24h) and hypoxia (Hx – 72h) and compared to 786-O \pm pVHL cultured in normoxia. Cell lysates were analyzed by immunoblotting for HIF-2 α , and Tubulin was used as a loading control.

Suppl. Figure 4. a, Summary of primers used for RT-PCR. **b**, Representative experiments of RT-PCR of HIF-1 α cDNA. **c**, Alignment of the cDNA of HIF-1 α (NCBI Reference Sequence: NC_000014.9) with the cDNA of HIF-1 α from DAOY, ONS-76, HDMA03 and D-458 cells.

Suppl. Figure 5. a, Representative graph of Seahorse XF Cell Mito Stress Test Profile from Agilent. **b**, Table of the OCR parameters obtained with the Seahorse analysis with DAOY, ONS-76, HDMB03 and D-458 cultured in normoxia (Nx – 21% O₂), physioxia (Phx – 6% O₂) and hypoxia (Hx – 1% O₂) for 24h. The standard deviation is representative of at least three independent experiments. **c-d**, ECAR in Nx and Hx in the absence (Control) or presence of

PT2385 (1 μ M) for 24 h of DAOY and ONS-76 cells was evaluated with the XF24 analyzer. Cells were deprived of glucose for 1 h, then glucose (G) and oligomycin (O) were injected at the indicated times. The graphs are representative of at least three independent experiments carried out in octuplicate. **e-f**, Respiratory control of DAOY and ONS-76 cells. OCR was measured in real time with the XF24 analyzer. Cells were cultured for 24 h in Nx and Hx in the absence (Control) or presence of PT2385 (1 μ M). Cells were deprived of glucose for 1h, then glucose (G), oligomycin (O), DNP, and Rotenone + Antimycin A (R/A) were injected at the indicated times. The graphs are representative of at least three independent experiments carried out in octuplicate.

Suppl. Figure 6. a, ECAR of DAOY (first line), ONS-76 (second line), HDMB03 (third line) and D-458 (fourth line) cells cultured in Nx (21% O₂ – first column), Phx (6% O₂ – second column) and Hx (1% O₂ – third column) in presence of metformine (Metf) or 2-DG for 24 h was evaluated with the XF24 analyzer. Cells were deprived of glucose for 1 h, then glucose (G) and oligomycin (O) were injected. The graphs are representative of at least three independent experiments carried out in octuplicate. **b**, OCR of DAOY (first line), ONS-76 (second line), HDMB03 (third line) and D-458 (fourth line) cells cultured in Nx (21% O₂ – first column), Phx (6% O₂ – second column) and Hx (1% O₂ – third column) in presence of metformine (Metf) or 2-DG for 24 h was evaluated with the XF24 analyzer. Cells were deprived of glucose for 1h, then glucose (G), oligomycin (O), DNP, and Rotenone + Antimycin A (R/A) were injected at the indicated times. The graphs are representative of at least three independent experiments carried out in octuplicate.

Suppl. Figure 7. a, DAOY, ONS-76, HDMB03, D-458 cells were incubated in Hx for 72 h in absence (-) or presence (+) of PT2385 (1 μ M). Cell lysates were analyzed by immunoblotting for HIF-1 α and HIF-2 α . Tubulin was used as a loading control. **b**, DAOY, ONS-76, HDMB03, D-458 cells were incubated in Hx for 72 h in absence (-) or presence (+) of PT2385 (1 μ M) and Metformin (Metf – 10mM). Cell lysates were analyzed by immunoblotting for HIF-1 α and HIF-2 α . Tubulin was used as a loading control. **c-h**, Graphic representation of *Ca9* (**c**), *Cal2* (**d**), *Glut1* (**e**), *Oct4* (**f**), *Ldha* (**g**) and *Ldhb* (**h**) mRNA expression in DAOY, ONS-76, HDMB03, D-458 cells incubated in hypoxia (Hx - 1% O₂) for 48h in the absence (Control) or presence of PT2385 (1 μ M) or presence of both PT2385 (1 μ M) and metformin (Metf – 10mM). The 2-way ANOVA is representative of at least three independent experiments.

Suppl. Figure 8. a-b, DAOY, ONS-76, HDMB03 and D-458 cells were incubated in physioxia (Phx – **a**) and hypoxia (Hx – **b**) for 72h in the absence (Control) or presence of PT2385 (1 μ M or 10 μ M) and metformine (Metf – 10mM). Cell viability (%) was measured using an ADAM cell counter. **c**, DAOY, ONS-76, HDMB03 and D-458 cells were incubated in hypoxia (Hx) for 72h in the absence (Control) or presence of PT2385 (1 μ M) and metformin (Metf – 10mM) after transfection with siRNA to siMA (Control) or HIF-1 α (siHIF-1). Cell viability (%) was measured using an ADAM cell counter. **d**, Colorimetric assay of DAOY, ONS-76, HDMB03 and D-458 cells. Cell lines were seeded at the same density and incubated in Hx 1% O₂ for 7 days. **e-f**, Glucose (**e**) and lactate (**f**) measurements. DAOY, ONS-76, HDMB03 and D-458 cells were incubated in hypoxia (Hx) for 72h in the absence (Control) or presence of metformine (Metf – 10mM) or PT2385 (1 μ M or 10 μ M) or both. **g-h**, ECAR of DAOY (**g**) and ONS-76 (**h**), cells cultured in hypoxia (Hx) in presence of metformin (Metf – 10mM), PT2385 (1 μ M) or both for 24h was evaluated with the XF24 analyzer. Cells were deprived of glucose for 1h, then glucose (G) and oligomycin (O) were injected. The graphs are representative of at least three independent experiments carried out in octuplicate. **i-j**, OCR of DAOY (**i**) and ONS-76 (**j**) cells cultured in hypoxia (Hx) in presence of metformin (Metf – 10 mM), PT2385 (1 μ M) or both for 24 h was evaluated with the XF24 analyzer. Cells were deprived of glucose for 1h, then glucose (G), oligomycin (O), DNP, and Rotenone + Antimycin A (R/A) were injected at the indicated times. The graphs are representative of at least three independent experiments carried out in octuplicate.

STAR Methods

Cell Culture

DAOY (from ATCC - HTB-186TM) and ONS-76 (from Dr. F. Di Cunto (University of Torino - Italy)) cells were grown in Dulbecco's Modified Eagle's Medium (DMEM) (Gibco-BRL, Courtaboeuf, France) supplemented with 10% fetal bovine serum with penicillin G (50 U/mL) and streptomycin sulfate (50g/mL) where as HDMB03 (from DSMZ - ACC740) and D-458 cells, provided by Dr. C. Pouponnot (Institut Curie - France), were grown with the same medium supplemented with 20% fetal bovine serum. A BugBok workstation (Ruskin Technology Biotrace International Plc, The Science Park Bridgend, UK) set at 6% oxygen, 94% nitrogen and 5% carbon dioxide was used for physioxic conditions. A Whitley H35 hypoxystation anaerobic workstation (Don Whitley Scientific, West Yorkshire, UK) set at 1% oxygen, 94% nitrogen and 5% carbon dioxide were used for hypoxic conditions.

Pharmacological Inhibitors and Chemicals

Cells were incubated with 10 mM Metformin (Metf) to block mitochondrial Complex I, 2-DG (10mM) to block glycolysis and PT2385 (1- and 10- mM) to inhibit HIF-2 α activity. Rotenone, antimycin A, oligomycin, and 2,4-Dinitrophenol (DNP) were from Sigma, (St. Louis, MI, USA).

RNA interference

The 21-nucleotide RNAs were chemically synthesized (Eurogentec, Seraing, Belgium) and previously described (PMID: **16585195**). The siRNA sequences, all validated, were as follows: siCtl (forward) 5'-CCU-ACA-UCC-CGA-UCG-AUG-AUG-TT-3', siHIF-1 α (forward) 5'-CUG-AUG-ACC-AGC-AAC-UUGATT-3', siHIF-2 α (forward) 5'-CAG-CAU-CUU-UGA-UAG-CAG-UTT-3'.

PCR analysis

Total RNA was extracted with the RNeasy Mini Kit (QIAGEN, Hilden, Germany). The amount of RNA was evaluated with a NanoDropTM spectrophotometer (ThermoFisher Scientific, Waltham, MA USA). One μ g of total RNA was used for reverse transcription, using the QuantiTect Reverse Transcription kit (QIAGEN, Hilden, Germany), with oligo (dT)₁₅ to prime first-strand synthesis. Full-length HIF-1 α cDNAs of approximately 3.5 kb were amplified by

RT-PCR different primers represented on Suppl. Figure 4a. The HIF-1 α cDNAs were amplified and sequenced.

Quantitative real-time PCR analysis

Total RNA was extracted with the RNeasy Mini Kit (QIAGEN, Hilden, Germany). The amount of RNA was evaluated with a NanoDrop™ spectrophotometer (ThermoFisher Scientific, Waltham, MA USA). One μ g of total RNA was used for reverse transcription, using the QuantiTect Reverse Transcription kit (QIAGEN, Hilden, Germany), with oligo (dT)₁₅ to prime first-strand synthesis. SYBR master mix plus (Eurogentec, Liege, Belgium) and specific oligonucleotides (Sigma Aldrich) were used for qPCR. Primer sequences used are: *Ca9* (forward: 5'-CCGAGCGACGCAGCCTTTGA -3'; reverse: 5'-GGCTCCAGTCTCGGCTACCT- 3'), *Ca12* (forward: 5'-CTGCCAGCAACAAGTCAG-3'; reverse: 5'- ATATTCAGCGGTCCTCTC-3'), *Glut1* (forward: 5'-CTTCACTGTCGTGTCGCTGT -3'; reverse: 5'-TGAAGAGTTCAGCCACGATG-3'), *Oct4* (forward: 5'-TGGAGTTTGTGCCAGGGTTT-3'; reverse: 5'-CTGTGTCCCAGGCTTCTTT-3'), *Ldha* (forward: 5'-AGCCCGATTCCGTTACCT-3'; reverse: 5'-CACCAGCAACATTCATTCCA-3'), *Ldhb* (forward: 5'-GATGGATTTTGGGGGAACAT-3'; reverse: 5'-AACACCTGCCACATTCACAC-3'), *Mct4* (forward: 5'-ATTGGCCTGGTGCTGCTGATG-3'; reverse: 5'-CGAGTCTGCAGGAGGCTTGTG-3'); *Mct1* (forward: 5'-CACCGTACAGCAACTATACG-3'; reverse: 5'-CAATGGTTCGCCTCTTGTAGA-3') and 36B4 (forward: 5'-TGCATCAGTACCCCATTCATCAT-3'; reverse: 5'-AGGCAGATGGATCAGCCAAGA-3').

Colony-Forming Assay

Cells (5000–10,000) were plated on 60-mm dishes and incubated at 37°C, 5% CO₂ for colony formation. After 10 days, colonies were fixed with 10% (v/v) methanol for 15min and stained with 5% Giemsa (Sigma, St. Louis, USA) for 30min for colony visualization.

Respirometry and Extracellular Acidification

The cellular oxygen consumption rate (OCR) and extracellular acidification rate (ECAR) were obtained using a Seahorse XF24 extracellular flux analyzer from Seahorse Bioscience (North Billerica, MA, USA). Experiments were performed according to the manufacturer's instructions. OCR and ECAR were measured in real time in normoxia, physioxia or hypoxia.

40,000 cells were deprived of glucose for 1 h, then glucose (G–10 mM), oligomycin (O–1 μ M), 2,4-Dinitrophenol (DNP–100 μ M), and Rotenone + Antimycin A (R/A–1 μ M) were injected at the indicated times.

Glucose and Lactate Measurements

The Glucose and lactate concentrations in the supernatant of cells incubated either in hypoxia for 72h was determined by YSI Biochemistry Analyzer. Each condition was determined for 100,000 cells to express the Glucose/Lactate concentration as g/L per 100,00 cells.

Immunoblotting

Cells were lysed in 1.5x SDS buffer and the protein concentration determined using the BCA assay. 40 μ g of protein from whole cell extracts were resolved by SDS-PAGE and transferred onto a PVDF membrane (Millipore, Molsheim, France). Membranes were blocked in 5% non-fat milk in TN buffer (50mMTris-HClpH7.4, 150mMNaCl) and incubated in the presence of the primary and then secondary antibodies in 5% non-fat milk in TN buffer. Rabbit polyclonal anti-HIF-1 α antibody (antiserum 2087) was produced and characterized in our laboratory (PMID: **10551817**). The antibody against HIF-2 α (NB100-122) was purchased from Novus Biologicals (Littleton, CA). ECL signals were normalized to either β -tubulin or HSP90. After washing in TN buffer containing 1% Triton-X100 and then in TN buffer, immunoreactive bands were visualized with the ECL system (Amersham Biosciences, Buckinghamshire, UK).

Immunocytochemistry

Cells were fixed in 3% paraformaldehyde and extracted with Triton X-100. Primary antibodies included rabbit anti-HIF-1 α (PMID: **10551817**) (1:400). Alexa Fluor 594- and 488-conjugated secondary anti-rabbit antibodies (Molecular Probes, Carlsbad, CA, USA) were used at 1:400. Cells were visualized by wide-field, fluorescence microscopy using a DM5500B upright stand (Leica, Wetzlar, Germany) with a 40x oil objective NA 1.00. The cubes used were A4 (excitation filter BP 360/40, dichroic mirror 400, emission filter BP 470/40), L5 (BP 480/40, 05, BP 527/30), and TX2 (BP 560/40, 595, BP645/75). Acquisitions were done with an Orca-ER camera (Hamamatsu, Hamamatsu, Japan). Cells were also visualized using the confocal microscope, Axiovert 200M inverted stand (Zeiss, Oberkochen, Germany). Objectives 10x dry NA 0.3 and/or 40x oil 1.3 NA and/or 63x oil 1.4 NA were used. The LASER used were diode 405nm, and/or Argon 488nm, and/or HeNe 543nm. The microscope was equipped with an automated xy stage for mosaic acquisitions.

Single Cell Data Availability

The RNA-Seq data discussed in B. Manoranjan publication (PMID: [32859895](#)) have been deposited in NCBI's Gene Expression Omnibus and are accessible through GEO Series accession number GSE131473. The scRNA-seq data have been deposited in CReSCENT (<https://crescent.cloud/>; CRES-P22) and processed data is uploaded on Broad Institute Single Cell Portal https://singlecell.broadinstitute.org/single_cell/study/SCP840.

Data sources

Primary medulloblastoma RNA-seq data were obtained from 'R2: Genomics Analysis and Visualization Platform (<http://r2.amc.nl>)' in the data set 'Tumor Medulloblastoma - Pfister - 223 - MAS5.0 - u133p2'.

Statistics

Statistical analysis of all data was performed using GraphPad Prism software, version 7.0 (Graphpad Software, La Jolla, CA, USA) and expressed as means \pm S.E.M. For multiple comparisons, two-way ANOVA (post hoc Bonferroni) was done. The p-values are indicated (p<0.05 *, p<0.005 **, p<0.0005 ***, p<0.0001 ****) whereas p-values between 0.05 and 0.10 indicated a statistical tendency.

References

1. Northcott, P. A. *et al.* Medulloblastomics: the end of the beginning. *Nature reviews. Cancer* 12, 818–34 (2012).
2. Chen, W. *et al.* Targeting renal cell carcinoma with a HIF-2 antagonist. *Nature* 539, 112–117 (2016).
3. Cho, H. & Kaelin, W. G. Targeting HIF2 in Clear Cell Renal Cell Carcinoma. *Cold Spring Harbor symposia on quantitative biology* 81, 113–121 (2016).
4. Petrova, V., Annicchiarico-Petruzzelli, M., Melino, G. & Amelio, I. The hypoxic tumour microenvironment. *Oncogenesis* 7, 10 (2018).
5. Pouyssegur, J., Dayan, F. & Mazure, N. M. Hypoxia signalling in cancer and approaches to enforce tumour regression. *Nature* 441, 437–43 (2006).
6. Manoranjan, B., Adile, A. A., Venugopal, C. & Singh, S. K. WNT: an unexpected tumor suppressor in medulloblastoma. *Molecular & cellular oncology* 7, 1834903 (2020).
7. Kim, J., Tchernyshyov, I., Semenza, G. L. & Dang, C. v. HIF-1-mediated expression of pyruvate dehydrogenase kinase: a metabolic switch required for cellular adaptation to hypoxia. *Cell metabolism* 3, 177–85 (2006).
8. Papandreou, I., Cairns, R. A., Fontana, L., Lim, A. L. & Denko, N. C. HIF-1 mediates adaptation to hypoxia by actively downregulating mitochondrial oxygen consumption. *Cell metabolism* 3, 187–97 (2006).
9. Pernicova, I. & Korbonits, M. Metformin--mode of action and clinical implications for diabetes and cancer. *Nature reviews. Endocrinology* 10, 143–56 (2014).
10. Bost, F., Sahra, I. ben, le Marchand-Brustel, Y. & Tanti, J.-F. Metformin and cancer therapy. *Current opinion in oncology* 24, 103–8 (2012).
11. Schödel, J. *et al.* Hypoxia, Hypoxia-inducible Transcription Factors, and Renal Cancer. *European urology* 69, 646–657 (2016).
12. Koh, M. Y. & Powis, G. Passing the baton: the HIF switch. *Trends in biochemical sciences* 37, 364–72 (2012).
13. Pei, Y. *et al.* An animal model of MYC-driven medulloblastoma. *Cancer cell* 21, 155–67 (2012).
14. Das, B. *et al.* MYC Regulates the HIF2 α Stemness Pathway via Nanog and Sox2 to Maintain Self-Renewal in Cancer Stem Cells versus Non-Stem Cancer Cells. *Cancer research* 79, 4015–4025 (2019).
15. Covello, K. L. *et al.* HIF-2 α regulates Oct-4: effects of hypoxia on stem cell function, embryonic development, and tumor growth. *Genes & development* 20, 557–70 (2006).
16. Petruzzelli, R., Christensen, D. R., Parry, K. L., Sanchez-Elsner, T. & Houghton, F. D. HIF-2 α regulates NANOG expression in human embryonic stem cells following hypoxia and reoxygenation through the interaction with an Oct-Sox cis regulatory element. *PloS one* 9, e108309 (2014).
17. Simon, M. C. & Keith, B. The role of oxygen availability in embryonic development and stem cell function. *Nature reviews. Molecular cell biology* 9, 285–96 (2008).

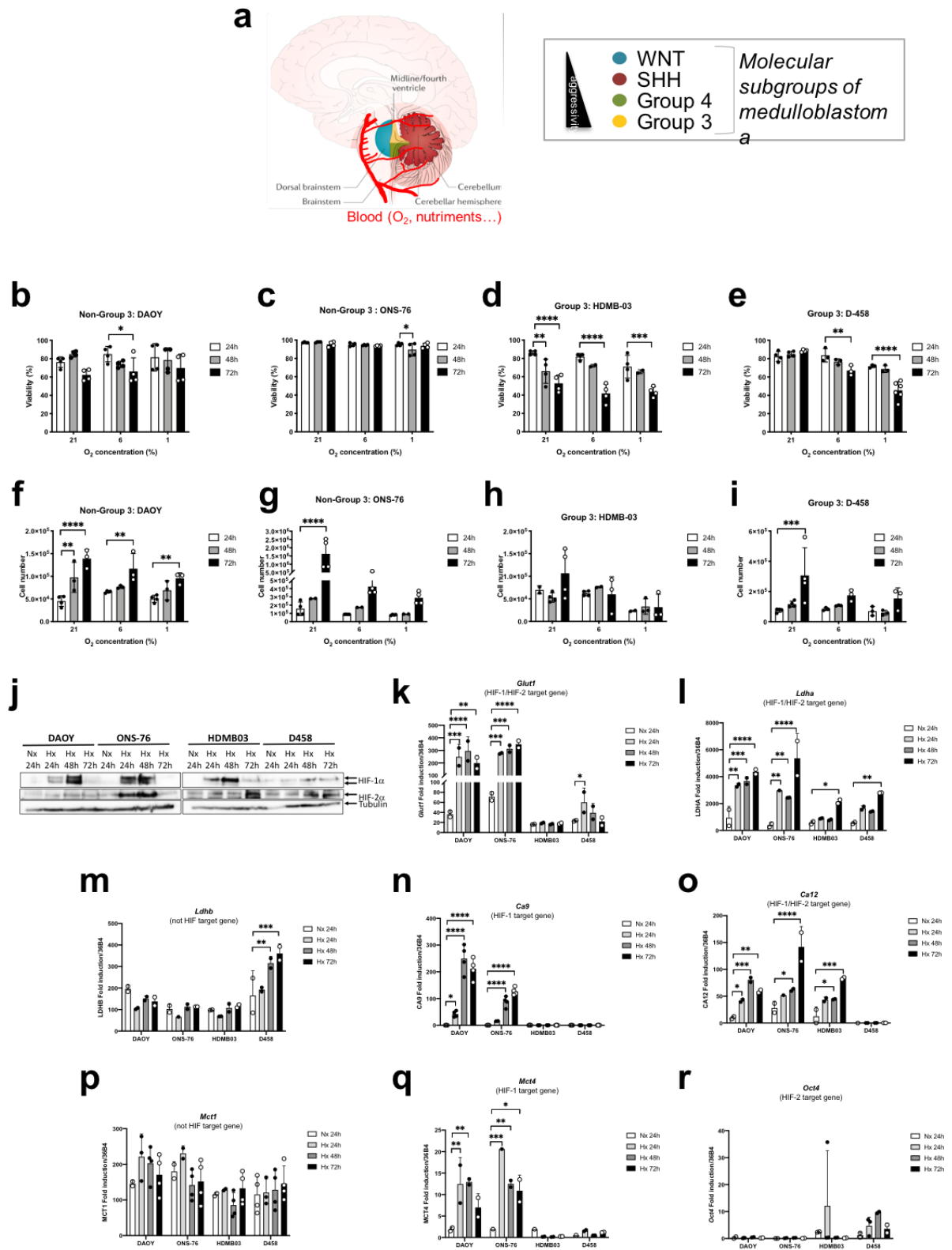


FIGURE 1

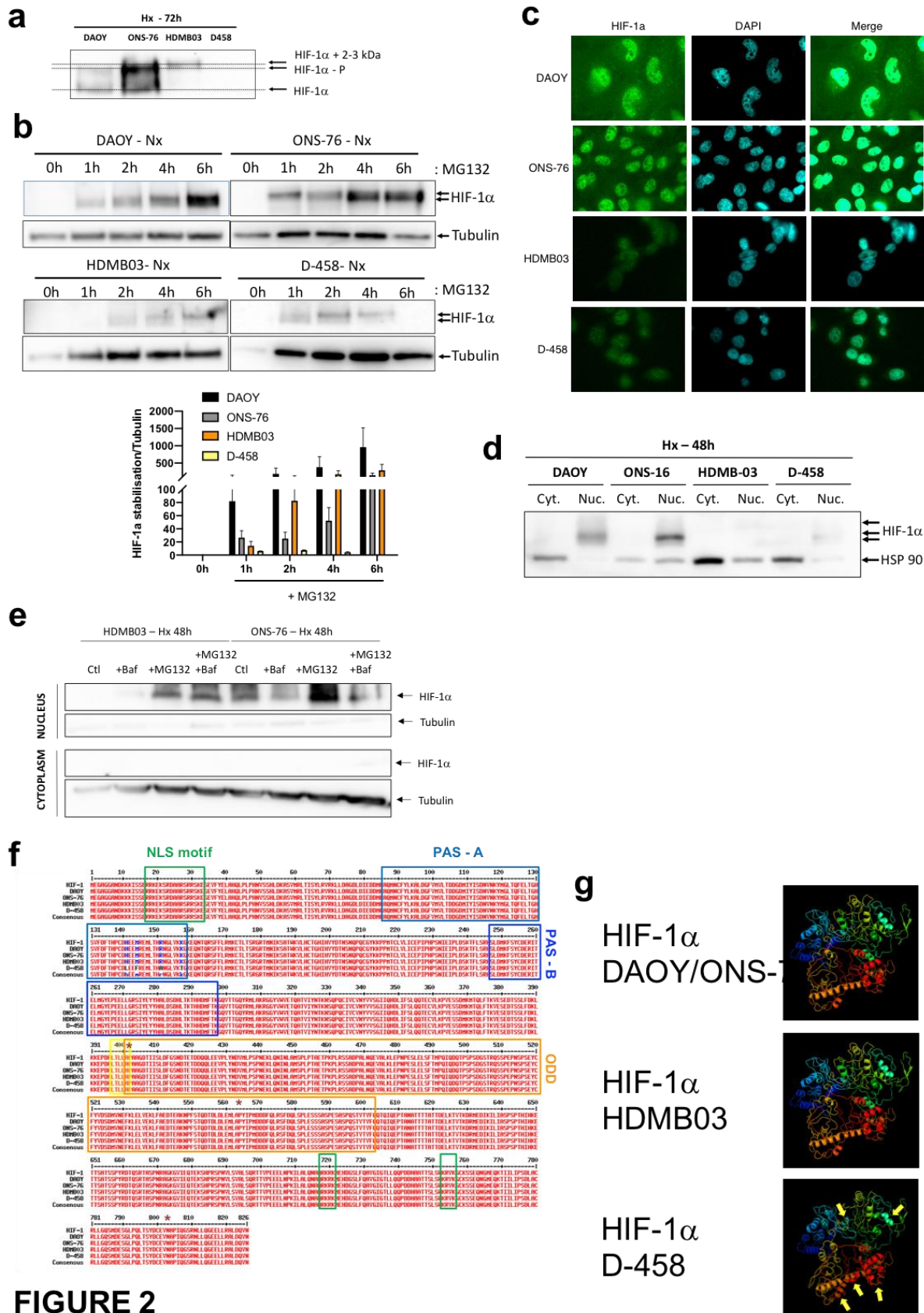


FIGURE 2

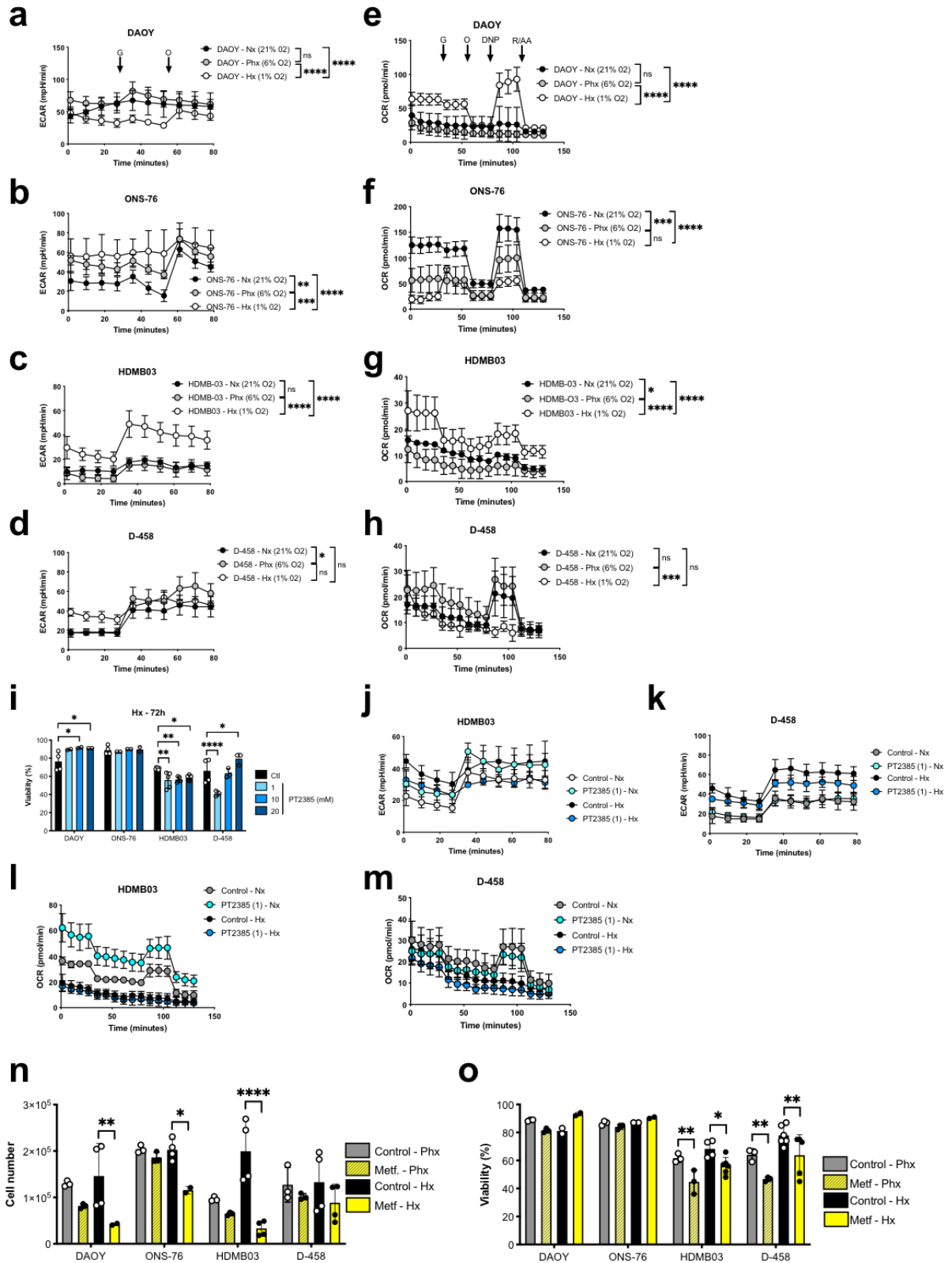


FIGURE 3

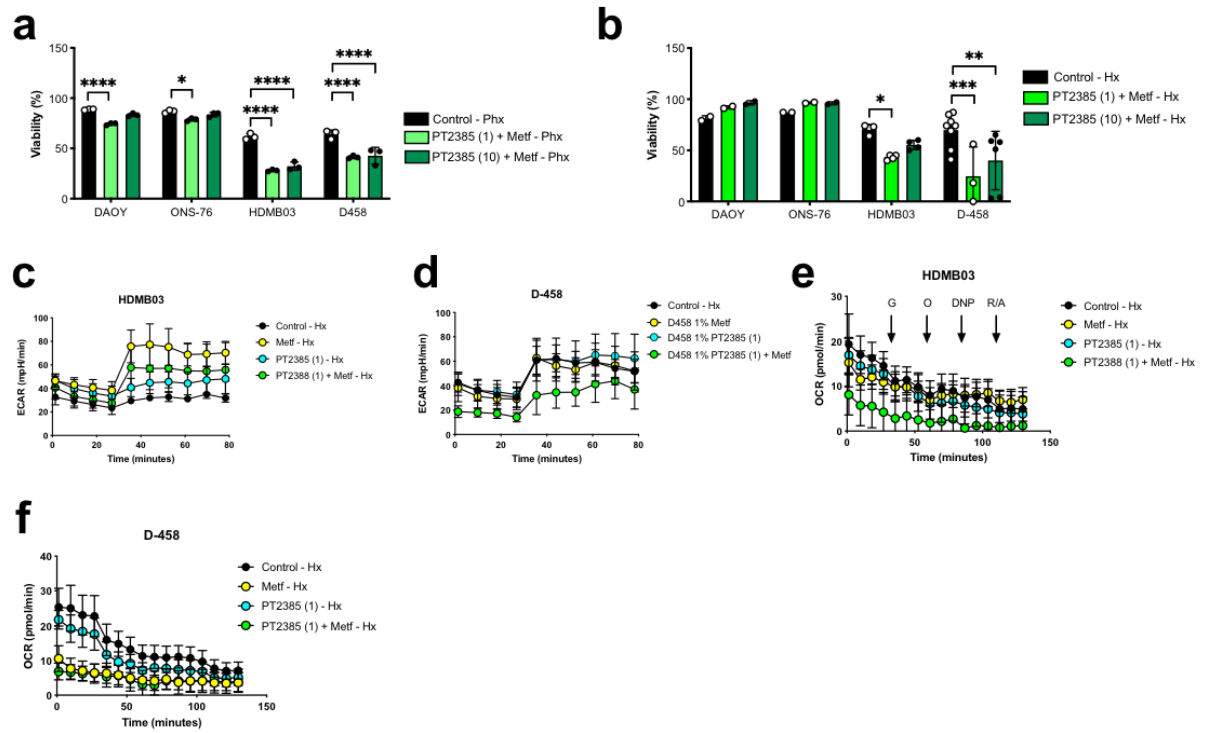
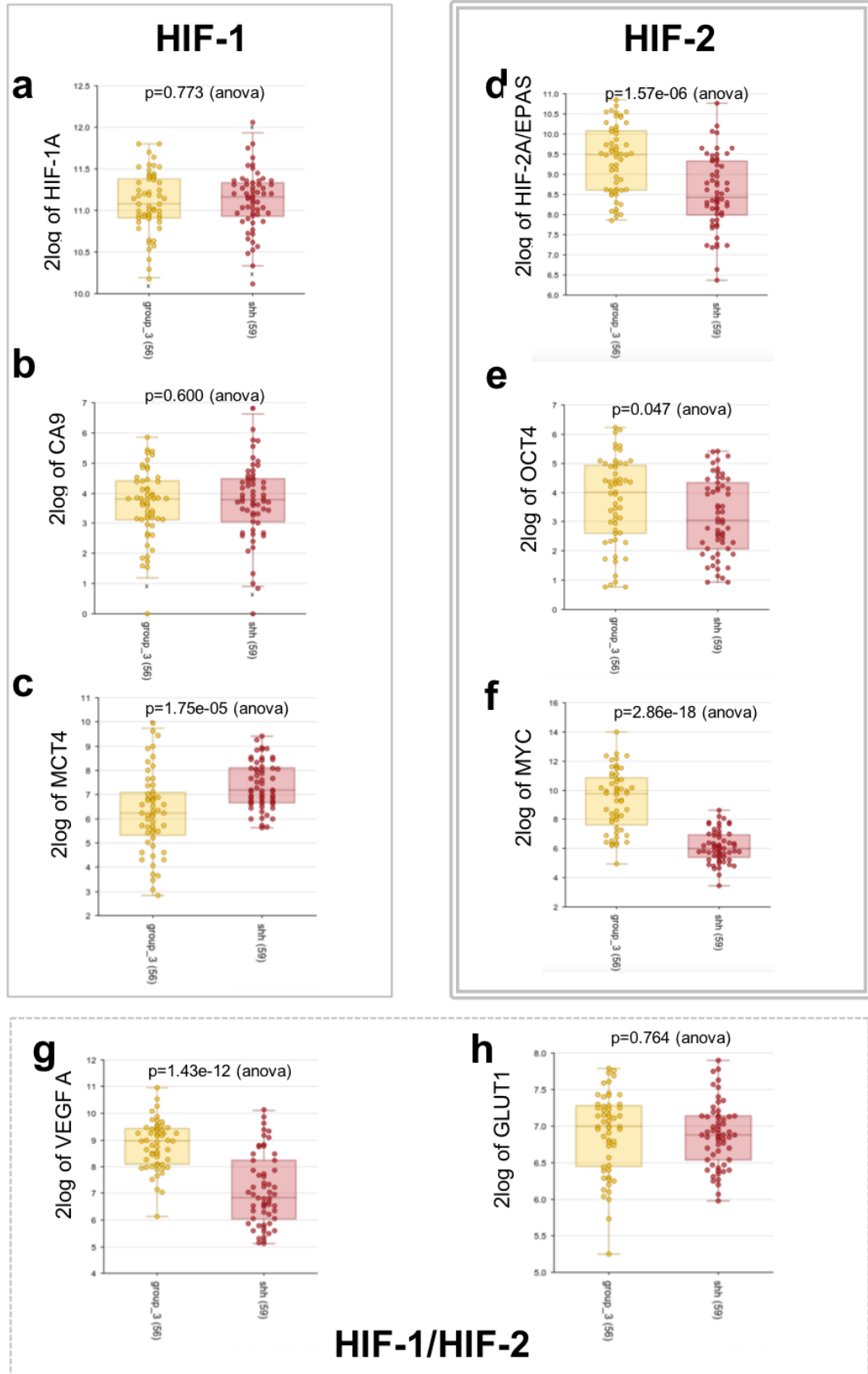
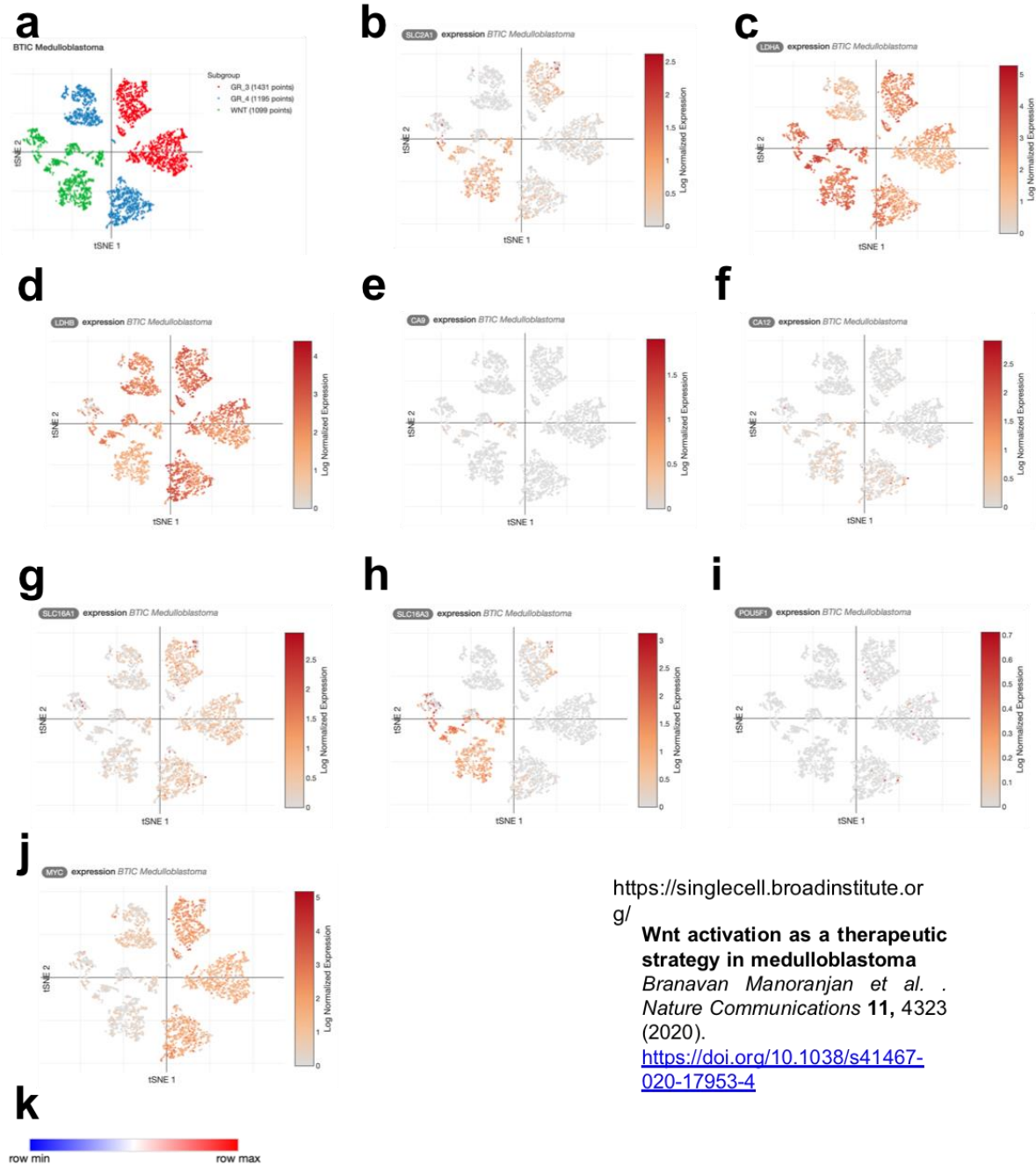


FIGURE 4

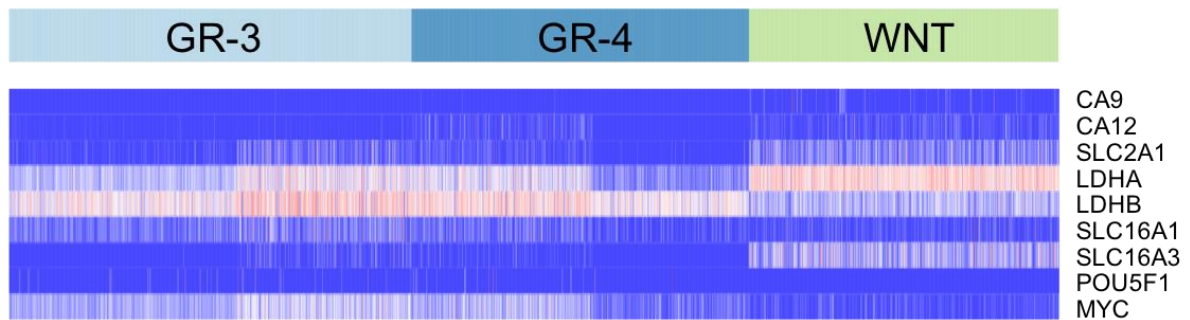


Suppl. FIGURE 1

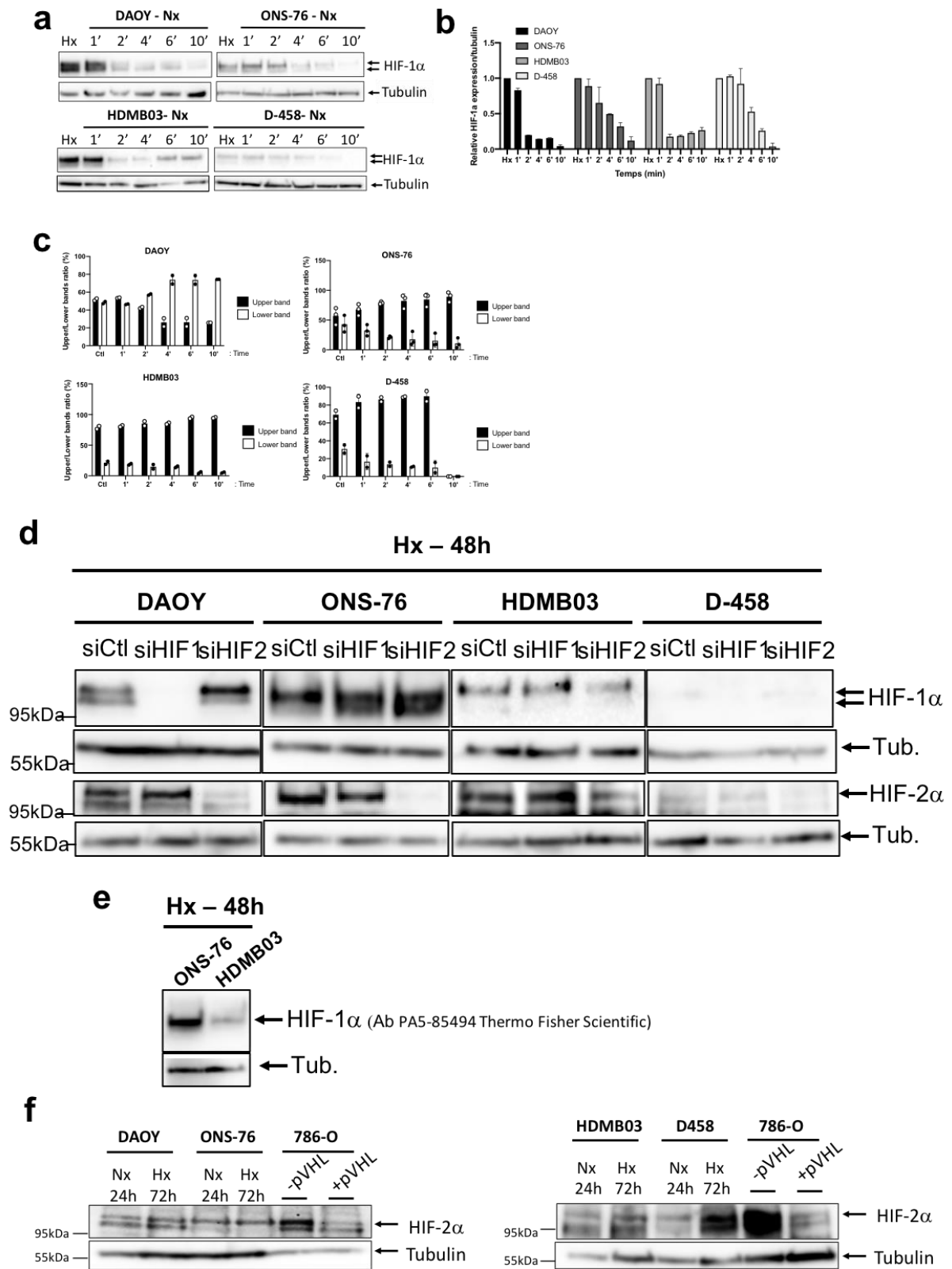


<https://singlecell.broadinstitute.org/>

g/ Wnt activation as a therapeutic strategy in medulloblastoma
 Branavan Manoranjan et al. .
Nature Communications 11, 4323 (2020).
<https://doi.org/10.1038/s41467-020-17953-4>



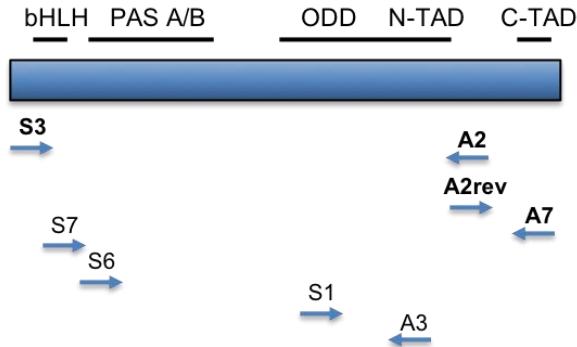
Suppl. FIGURE 2



Suppl. FIGURE 3

a

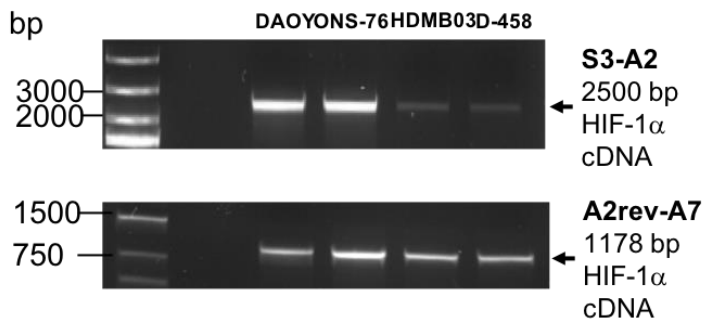
• **Positions of Primers in HIF-1 α cDNA**



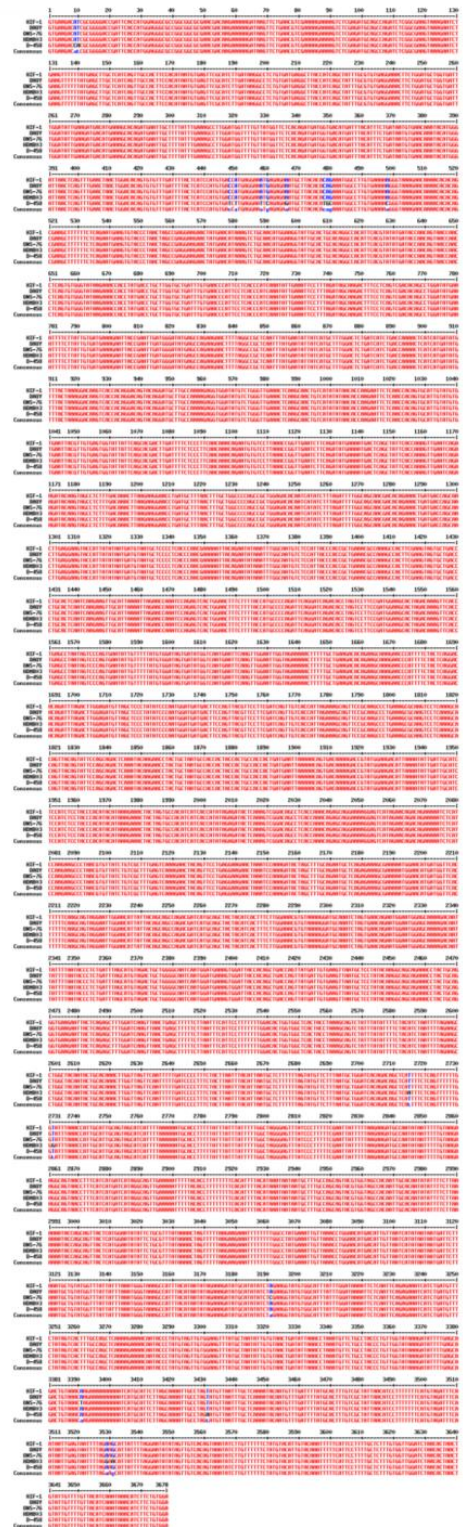
• **Primer sequences (5' to 3')**

S1 : CCCAGATTCAGGATCAGACA
 S3 : GTGAAGACATCGCGGGGAC
 S6 : TGTGACCATGAGGAAATGAGAGA
 S7 : GGATATTGAAGATGACATG
 A2rev : GTTAACTGAGCTTTTTCTTA
 A2 : TAAGAAAAGCTCAGTTAAC
 A3 : TCTAAATCTGTGTCCTCAGG
 A7 : TCCACAGAAGATGTTTATTTG

b

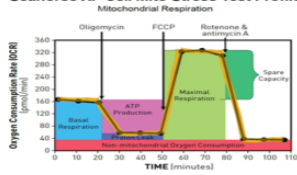


c



Suppl. FIGURE 4

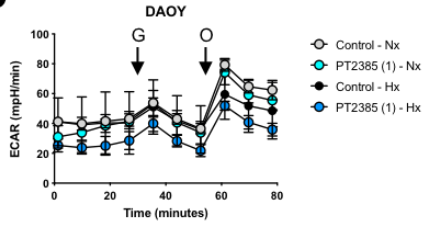
a Seahorse XF Cell Mito Stress Test Profile



b

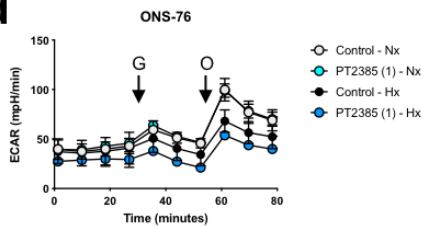
Parameters	DAOY - Nx (21% O2)		DAOY - Phx (6% O2)		DAOY - Hx (1% O2)	
	OCR	St Dev	OCR	St Dev	OCR	St Dev
Basal	8.89	3.39	6.38	1.86	42.07	5.59
Proton Leak	2.20	1.30	2.19	1.42	2.55	1.94
Maximal Respiration	5.22	10.21	1.32	0.73	71.82	15.03
Spare Respiratory Capacity	0.00	0.00	0.00	0.00	36.39	12.62
Non Mitochondrial Oxygen Consumption	14.69	1.94	10.09	1.17	21.12	3.49
ATP Production	3.09	3.77	0.02	0.75	32.88	3.76
Coupling Efficiency (%)	52.79%	25.35%	16.08%	105.40%	93.08%	4.64%
Spare Respiratory Capacity (%)	101.58%	175.74%	80.57%	70.69%	202.60%	34.23%
Acute Response	-3.60	4.89	-4.18	0.83	-6.64	1.27

c



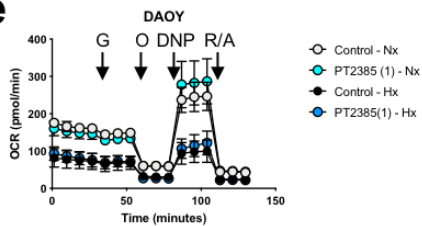
Parameters	ONS-76 - Nx (21% O2)		ONS-76 - Phx (6% O2)		ONS-76 - Hx (1% O2)	
	OCR	St Dev	OCR	St Dev	OCR	St Dev
Basal	89.63	12.52	45.58	11.75	5.29	6.75
Proton Leak	12.51	5.05	4.58	1.91	4.71	1.34
Maximal Respiration	121.09	25.11	74.20	20.28	35.89	7.85
Spare Respiratory Capacity	39.27	16.56	30.88	13.10	7.67	4.28
Non Mitochondrial Oxygen Consumption	36.61	3.24	25.64	6.62	19.81	2.18
ATP Production	69.31	10.16	38.73	11.11	23.51	6.15
Coupling Efficiency (%)	84.90%	4.86%	89.12%	4.38%	82.82%	4.69%
Spare Respiratory Capacity (%)	147.74%	17.91%	173.20%	25.95%	128.55%	16.30%
Acute Response	-7.81	1.97	-2.27	3.37	22.93	1.13

d



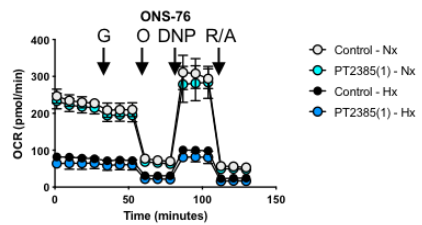
Parameters	HDMB-03 Control		HDMB03 - Phx (6% O2)		HDMB03 - Hx (1% O2)	
	OCR	St Dev	OCR	St Dev	OCR	St Dev
Basal	9.45	0.98	4.57	2.12	15.00	4.34
Proton Leak	3.06	0.38	0.62	1.06	1.41	1.86
Maximal Respiration	5.50	1.13	2.54	2.13	7.18	2.30
Spare Respiratory Capacity	0.00	0.00	1.37	1.18	2.38	2.58
Non Mitochondrial Oxygen Consumption	4.73	0.56	3.64	2.24	11.16	2.61
ATP Production	2.52	0.23	0.54	0.89	3.39	1.11
Coupling Efficiency (%)	45.27%	4.86%	43.49%	33.29%	96.18%	89.58%
Spare Respiratory Capacity (%)	98.37%	18.38%	151.47%	87.95%	203.92%	164.56%
Acute Response	-3.88	0.97	-3.41	0.84	-10.21	2.65

e

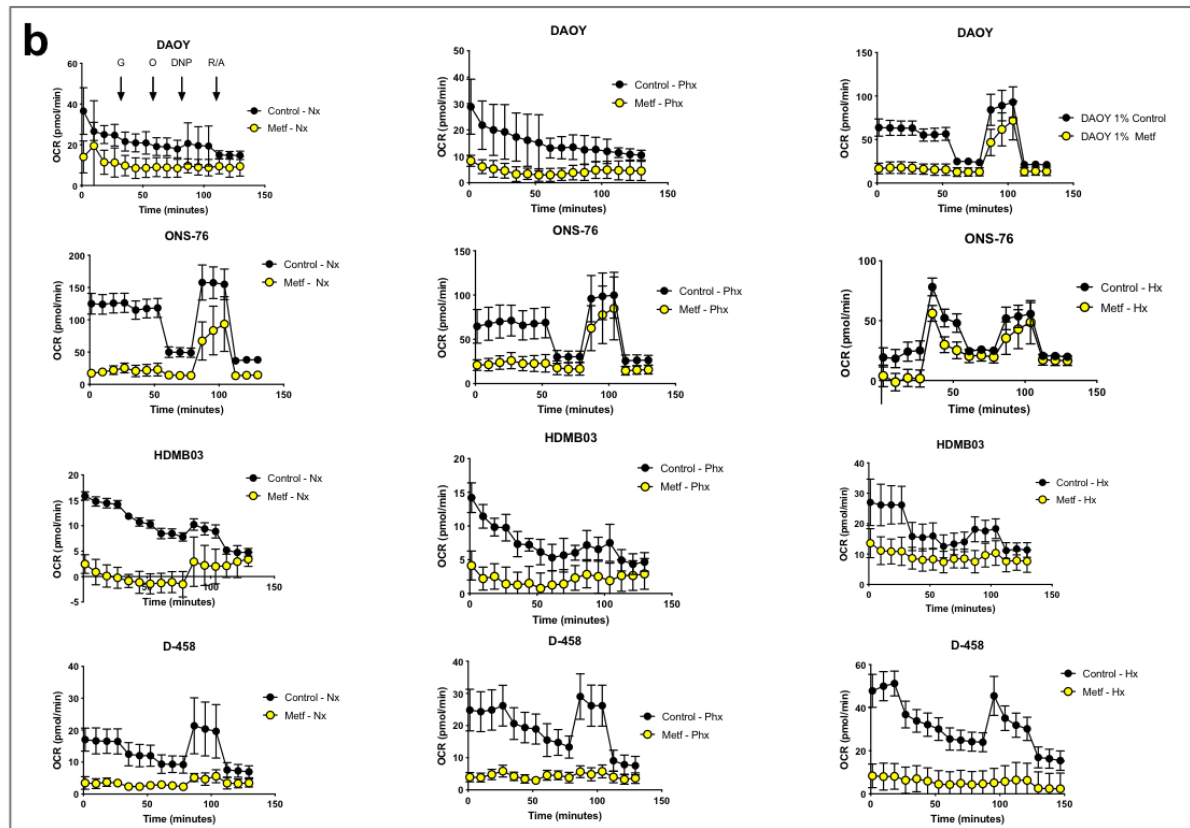
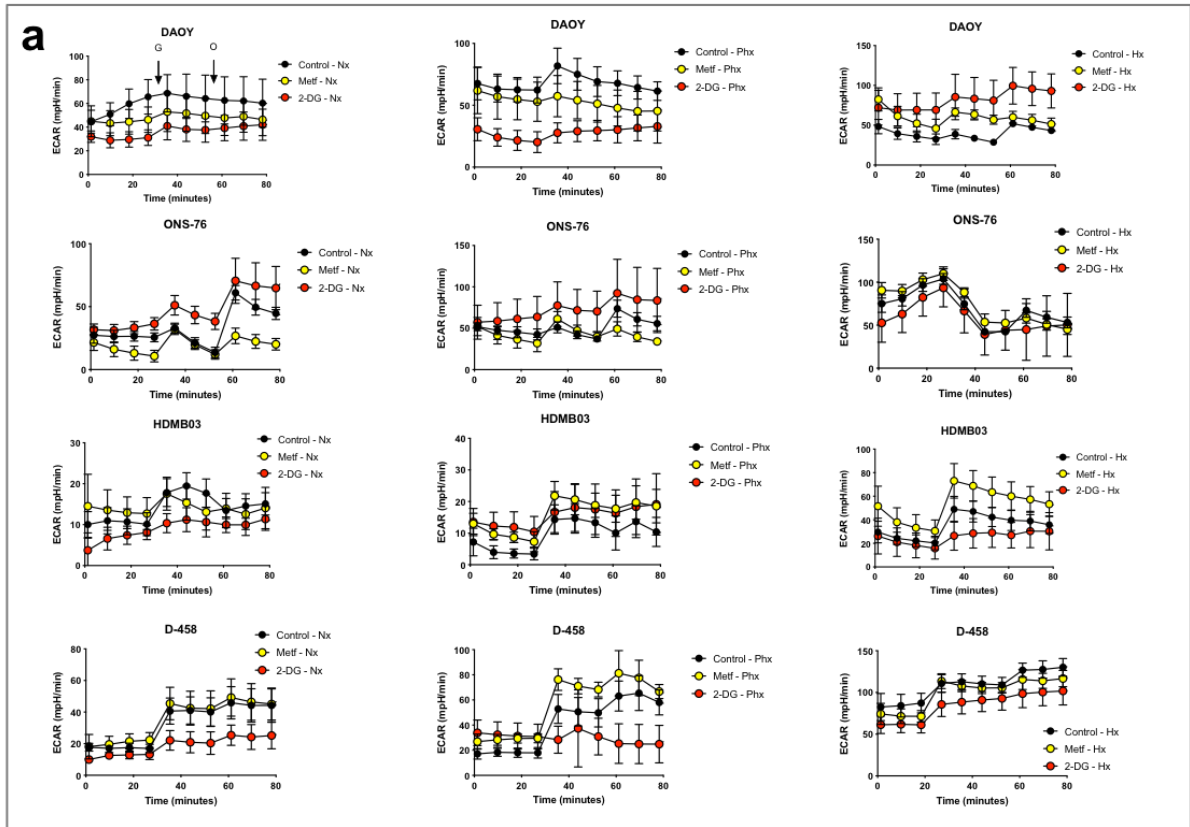


Parameters	D-458 - Nx (21% O2)		D-458 - Phx (6% O2)		D-458 - Hx (1% O2)	
	OCR	St Dev	OCR	St Dev	OCR	St Dev
Basal	9.56	3.05	17.53	4.68	6.80	1.79
Proton Leak	2.58	0.95	5.13	2.32	0.86	0.66
Maximal Respiration	16.75	6.51	19.83	6.18	2.12	1.82
Spare Respiratory Capacity	11.20	6.03	9.81	6.25	0.84	4.75
Non Mitochondrial Oxygen Consumption	7.18	1.89	7.01	2.89	6.51	1.14
ATP Production	2.97	1.55	4.89	2.10	0.42	2.29
Coupling Efficiency (%)	51.38%	14.67%	48.66%	9.38%	72.62%	28.75%
Spare Respiratory Capacity (%)	334.19%	153.81%	232.59%	118.67%	-37.70%	142.61%
Acute Response	-4.01	1.46	-7.51	2.10	-5.52	2.21

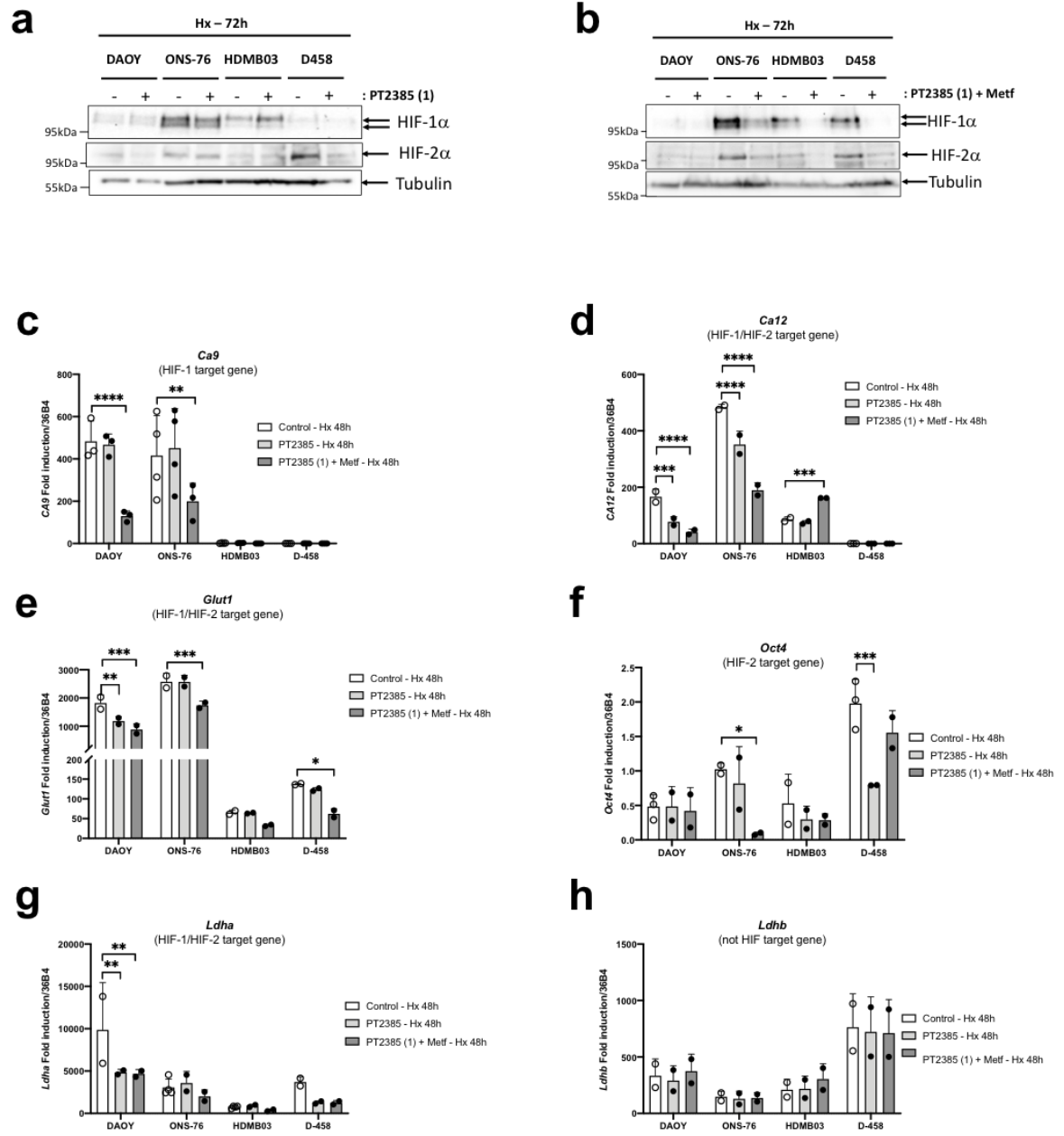
f



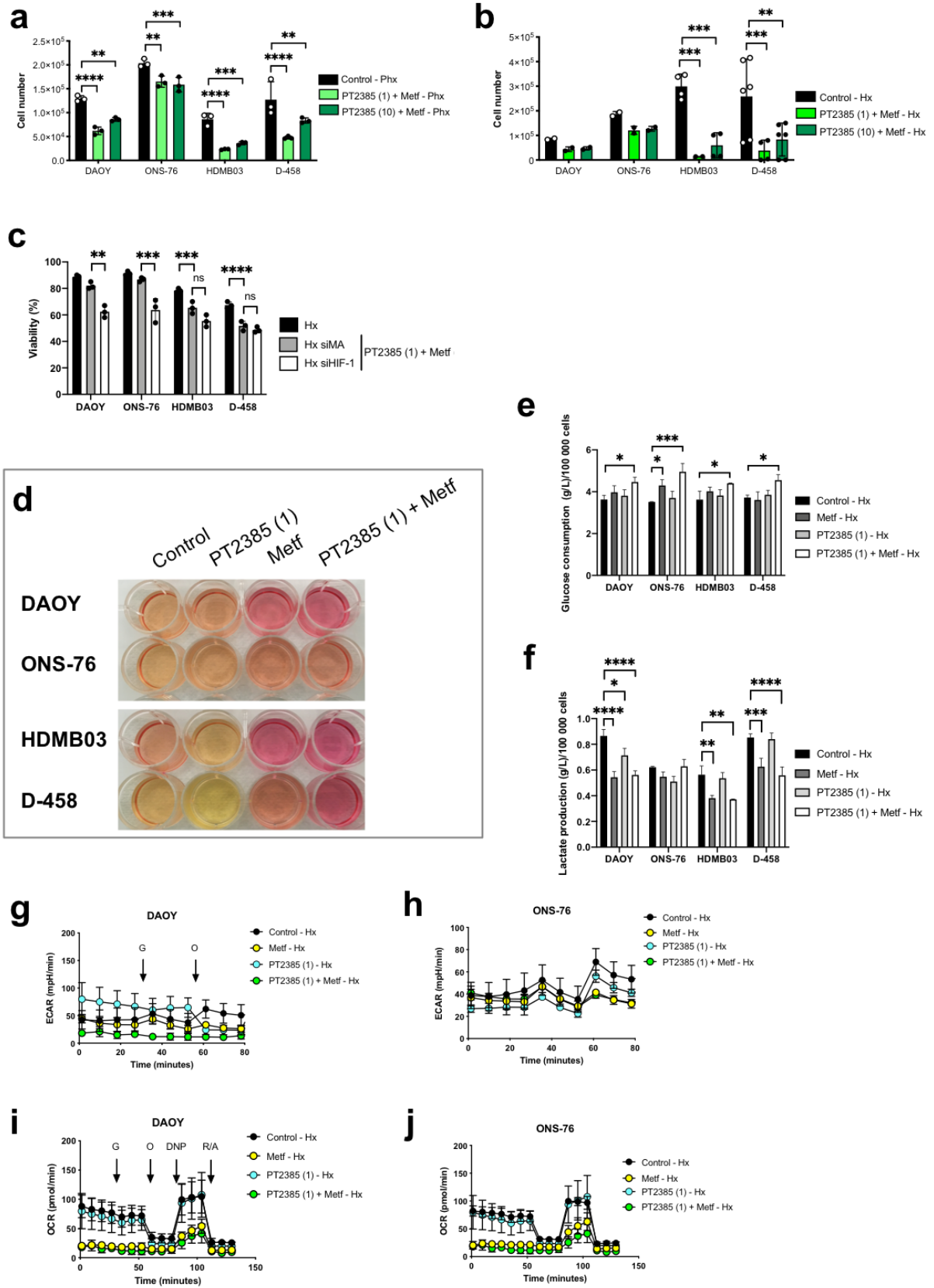
Suppl. FIGURE 5



Suppl. FIGURE 6



Suppl. FIGURE 7



Suppl. FIGURE 8

III- Figures en préparation

III.1 Complément Figure 1

Afin de compléter la Figure 1, nous sommes en train de réaliser un séquençage de l'ARN à haut débit (RNA-seq) afin de mettre en évidence une signature hypoxique particulière due aux changements dans l'expression génique de HIF-1 et HIF-2, dans les lignées de MB du **groupe 3** versus le **groupe non 3** en Nx et en Hx.

III.2 Complément Figure 2 e

Afin de confirmer la différence de taille en WB de HIF-1 α entre les ONS-76 et les HDMB-03, nous sommes en train de réaliser des électrophorèses sur gel de différence bidimensionnelle (2D DIGE, en collaboration avec Guillaume Robert, C3M, Équipe de Patrick Auberger) en hypoxie et après traitement par le MG-132 afin de stabiliser HIF-1 α . En effet, pour des raisons techniques de manipulation, le MG-132 s'est avéré indispensable pour stabiliser HIF-1 α , car ce dernier est très vite dégradé lorsque nous sortons les cellules de l'enceinte à hypoxie, même si les échantillons sont placés sur de la glace. Les résultats préliminaires (**Figure 24**) nous confortent dans le fait que le HIF-1 α des cellules HDMB03 est bien différent de celui des cellules ONS-76. Comme nous pouvons le voir, seulement deux points, présentant un poids moléculaire ainsi qu'un point isoélectrique différent du HIF-1 α classique (en rouge), sont mis en évidence dans les cellules HDMB03, points qui ne sont pas retrouvés sur le gel des cellules ONS-76. Cela vient conforter le fait qu'il existe une modification post-traductionnelle de HIF-1 α dans les cellules HDMB03 différente de celles des cellules ONS-76.

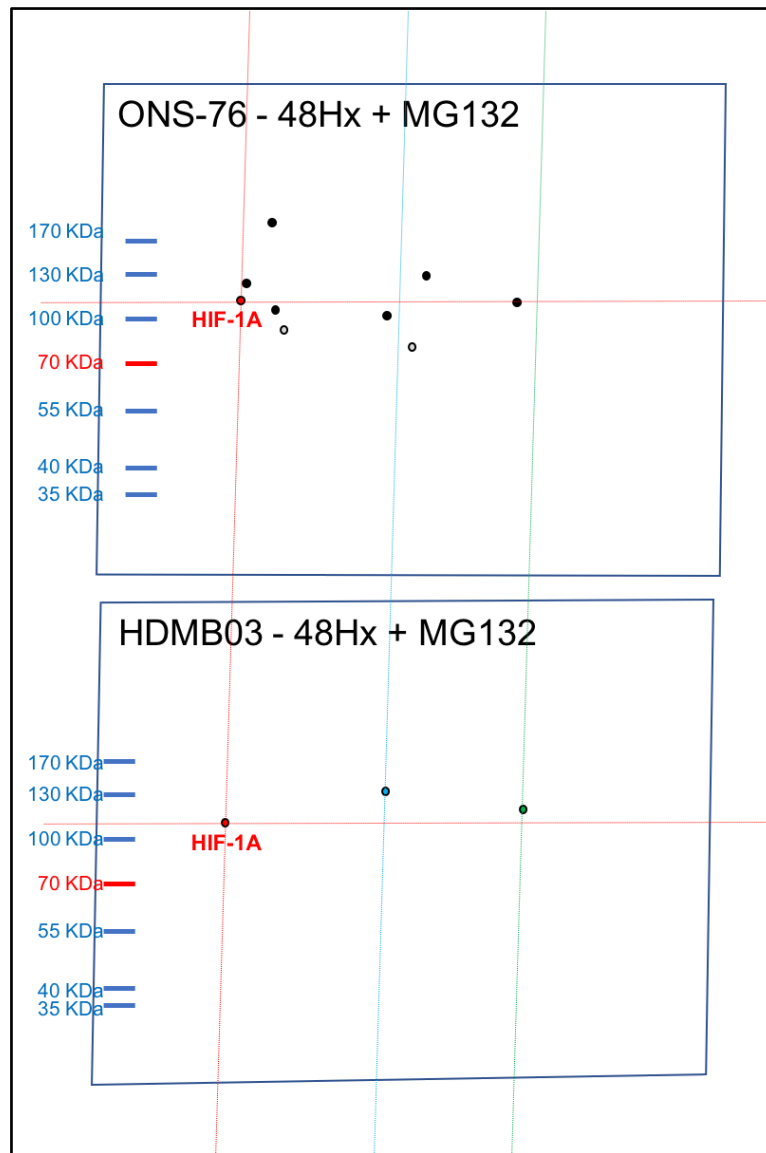


Figure 24 : Électrophorèse sur gel de différence bidimensionnelle (2D DIGE)

Cette expérience doit être répétée et couplée à une spectrographie de masse afin d'identifier la nature de la modification post-traductionnelle présente dans les cellules HDMB03.

Il est intéressant de constater que lors de l'utilisation du MG-132 (inhibiteur du protéasome) sur les cellules HDMB03 en hypoxie, nous avons été en mesure de stabiliser HIF-1 α au niveau du noyau. Nous sommes donc en train de réaliser une qPCR des cellules HDMB03 dans ces conditions afin de vérifier si ce HIF-1 α , stabilisé au noyau, est capable d'activer la transcription de ses gènes cibles.

Il est possible que le HIF-1 α des cellules HDMB03 en hypoxie soit en fait dégradé beaucoup trop rapidement pour lui permettre d'être stable, d'aller au noyau et d'activer ses gènes cibles.

Nous allons donc également tester l'activité du protéasome dans les cellules du **groupe-3** et la comparer à celle des cellules du **groupe non-3**.

III.3 Complément Figure 2 g

Quant aux cellules D-458, nous avons mis en évidence quatre mutations au niveau du domaine PAS-A pouvant entraîner un défaut de dimérisation entre les sous-unités HIF-1 α et HIF-1 β . Ceci pourrait ainsi expliquer l'inefficacité du facteur de transcription HIF-1 dans ces cellules. Nous sommes donc en train de réaliser une expérience de co-immunoprécipitation afin de confirmer notre hypothèse.

III.4 Complément Figure Suppl. Figure 3 e

Nous rencontrons actuellement des difficultés techniques pour invalider complètement HIF-1 α dans les cellules ONS-76 et HDMB03 avec notre siRNA. Nous allons donc réaliser à nouveaux une transfection de ces deux lignées cellulaires avec un pool de siRNA de HIF-1 α en espérant éteindre totalement son expression.

III. 5 Complément Figure 4

Une analyse métabolomique sur les cellules du **groupe 3** (HDMB-03 et D-458) et du **groupe non 3** (ONS-76) après traitement par le PT2385 seul, la Metformine seule, ou en association avec le Metformine, dans des conditions d'hypoxie est actuellement en cours en collaboration avec le Dr Issam Ben-Sahra à l'Université Northwestern. Nous pourrions ainsi analyser l'impact de ces différents traitements sur le métabolome du MB.

IV- Conclusion et discussion de l'article 1

Notre article met en lumière un élément clé du métabolisme hypoxique du médulloblastome, qui est l'expression différentiel des sous-unité alpha du principal facteur de transcription : HIF. En effet, nos résultats démontrent l'inactivité ou l'absence de HIF-1 α dans le **groupe 3** des médulloblastomes, faisant reposer l'ensemble du programme métabolique hypoxique du **groupe 3** sur HIF-2. Cette découverte capitale corrobore avec ce qui est aujourd'hui connu du carcinome rénal à cellules claires (ccRCC). Ce sous-groupe de cancer du rein, particulièrement agressif, exprime presque que HIF-2 α . L'activité de HIF-1 α est fortement diminuée en raison de délétions chromosomiques (Schödel et al. 2016) ou de l'activité de HAF (Koh and Powis 2012) laissant HIF-2 travailler pleinement dans son activité pro-tumorale.

Nos résultats peuvent donc avoir un impact majeur sur le développement de nouvelles thérapies, positionnant HIF-2 au centre de la cible thérapeutique des médulloblastomes les plus agressifs.

Il est communément admis que les cellules cancéreuses hypoxiques auraient un profil métabolique plutôt glycolytique, avec une respiration mitochondriale diminuée. Force est de constater que dans la grande majorité des cas (DAOY, HDMB-03 et D-458), les lignées de médulloblastome étudiées dans notre étude présentent une meilleure respiration mitochondriale en hypoxie. Cela est une découverte également intéressante car elle donne du sens à une approche globale du métabolisme comme cible thérapeutique dans le médulloblastome. L'option choisie dans notre étude de cibler, d'une part HIF-2 en utilisant un inhibiteur spécifique (le PT2385), et d'autre part la phosphorylation oxydative avec le Metformine, prend donc tout son sens dans le cas du MB.

Nos conclusions sont uniques aujourd'hui dans le paysage des recherches sur le médulloblastome positionnant HIF-2 α comme point de contrôle de la réponse métabolique hypoxique. Plusieurs points de ce travail méritent discussion et soulèvent des interrogations, et nous allons essayer d'y répondre.

A- Analyse complexe de HIF-1 α dans le groupe 3

Nos résultats mettent en avant un HIF-1 α ayant un poids moléculaire légèrement plus élevé que le HIF-1 α classique d'environ 2 à 3KDa dans les HDMB-03. Cette différence pourrait s'expliquer par une modification post-traductionnelle parmi celles présentées en Introduction (§). Malheureusement, je ne suis pas en mesure aujourd'hui de connaître avec précision le changement de poids moléculaire qu'entraînerait une phosphorylation, une nitrosylation ou encore une méthylation. Cependant, il est admis qu'une seule phosphorylation n'engendre pas un grand shift en électrophorèse. Au vu de la faible augmentation du poids moléculaire, plusieurs hypothèses pourraient expliquer cette différence (phosphorylation, hydroxylation). Nous avons donc continué les recherches en réalisant 1) une électrophorèse en 2D afin de séparer les protéines par rapport à leurs points isoélectriques et 2) une spectrométrie de masse sur HIF-1 α des cellules HDMB-03 en comparaison au HIF-1 α des cellules ONS-76 utilisées comme contrôle. Reste ensuite à comprendre comment cette modification post-traductionnelle vient déstabiliser la protéine et l'empêche donc d'activer les gènes cibles. Nous pourrions également émettre l'hypothèse que cette augmentation de taille en hypoxie serait en fait une sous-unité HIF-1 α constamment hydroxylée, même dans des conditions très pauvre en oxygène, dû à une activité intense des PHDs dans les HDMB, comme le suggère les fortes expressions des PHD2 et 3 révélées par Medulloblastoma 500 portal (Medulloblastome 500 Genomics Analysis and Visualization Platform) (**Figure 25**). Cela pourrait expliquer une dégradation permanente de HIF-1 même en hypoxie.

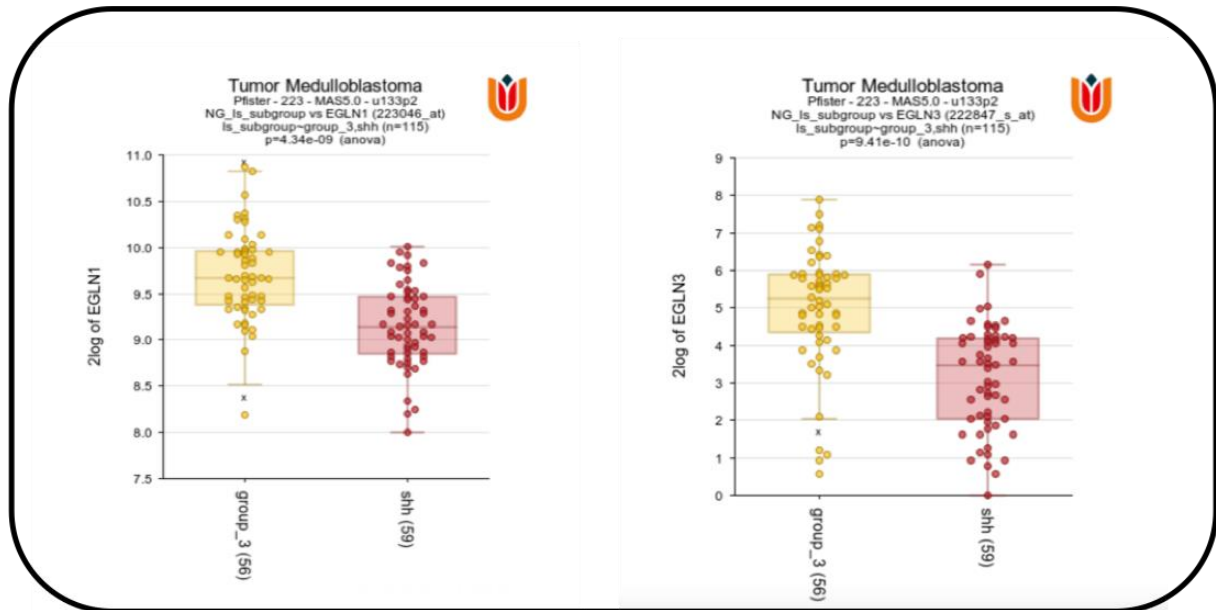


Figure 25 : Expression de PHD2 et PHD3 dans le groupe 3 comparativement au groupe SHH.

Dans tous les cas, le HIF-1 α des **groupe 3** se retrouve peu (D-458) ou pas (HDMB03) dans le noyau. Nous nous attendions alors à retrouver une mutation dans les domaines NLS, mais ce n'est pas le cas. Il serait important de refaire les analyses de séquençage pour en être sûre car l'échange d'un seul acide aminé unique du motif NLS en C-terminal entraîne une réduction spectaculaire de la capacité du HIF-1 α à s'accumuler dans le noyau en réponse à l'hypoxie (Kallio et al. 1998). Par ailleurs, nous avons mis en évidence dans notre étude des mutations dans le domaine PAS-A des cellules D-458. Ces mutations peuvent expliquer un défaut dans la dimérisation de la sous-unité HIF-1 α avec la sous-unité β et donc son incapacité à activer les gènes cibles. Afin de confirmer notre hypothèse, nous avons programmé des expériences de co-immunoprécipitation de HIF-1 α avec HIF-1 β afin de confirmer l'absence de dimérisation de la protéine.

Il semble également indispensable à ce niveau de confirmer nos résultats sur des échantillons de tumeur de patients, afin de réaliser un séquençage de HIF-1 dans des tumeurs du **groupe 3** *versus* le **groupe non-3**. Nous avons pris des contacts au niveau de différentes équipes nationales mais nous sommes en attente, les échantillons tissulaires du **groupe 3** étant rares.

B- Par quel mécanisme le PT2385 diminue la viabilité des MB du groupe 3 ?

Après avoir mis en évidence le rôle majeur et central de HIF-2 dans les MB du **groupe 3**, nous sommes naturellement tournés vers un inhibiteur spécifique de HIF-2 actuellement utilisé en étude de phase II dans le cancer du rein. Bien que nous ayons mis en évidence une diminution de la prolifération et de la viabilité dans le **groupe 3**, nous n'avons pas décrit les mécanismes qui entrent en jeu. Un article récent, utilisant le PT2385 sur des cellules dérivées de PDX de neuroblastome, a mis en évidence une réduction nette de l'expression de HIF-2 α au niveau nucléaire mais aucun effet sur les gènes cibles de HIF-2 n'a été observé (Persson et al. 2020). Une seconde étude publiée récemment, portant sur les glioblastomes, démontre globalement les mêmes résultats (Renfrow et al. 2020). Dans cette étude, le phénotype cellulaire, y compris la prolifération, la viabilité, la migration/invasion, ainsi que l'expression des gènes, n'ont pas été modifiés après le traitement par PT2385 *in vitro*. Par contre, le traitement par PT2385 a amélioré la survie globale médiane par rapport au placebo dans leur modèle *in vivo* (souris traitées par PT2385 à 10mg/kg pendant 21 jours). Dans chacune des études, l'effet compensateur de HIF-1 sur HIF-2 était mis en avant pour expliquer ces résultats. Le **groupe 3** de médulloblastome n'ayant pas de HIF-1 fonctionnel, cette piste thérapeutique reste pertinente. Contrairement aux données de la littérature, présenté ci-dessus, nous mettons en évidence dans notre travail une diminution significative de l'expression du gène *Oct-4*, gène dépendant de HIF-2, dans les cellules du **groupe 3** (D-458) traitées par PT2385 en hypoxie suggérant que l'effet de l'inhibition de HIF-2 par le PT2385 est probablement différents selon le type cellulaire.

Nous avons mené en parallèle de notre étude une expérience *in vivo* sur xénogreffes orthotopiques avec des cellules D-458 du **groupe 3** (**Figure 26**). La première série (**Figure 26A**) de 6 souris traitées par le PT2385 seul ou en association avec la Metformine a montré des résultats intéressants avec une différence à la limite de la significativité ($p = 0,08$) en faveur de l'association PT2385 + Metformine. Nous avons voulu confirmer nos résultats sur un plus grand nombre de souris (**Figure 26B**, avec 10 souris ayant reçu le traitement par PT2385 + Metformine). La seconde série n'a pas démontré de supériorité du traitement par rapport au contrôle sur la viabilité des souris. La posologie de PT2385 utilisée dans notre modèle *in vivo* était de 30mg/kg par voie orale, soit trois fois plus élevée que celle utilisée dans les études sur le glioblastome ou le neuroblastome (Renfrow et al. 2020)(Persson et al. 2020). Cependant,

devant l'absence d'effet du PT2385 dans les modèles *in vivo* de tumeur cérébrale, il semblait judicieux d'augmenter la posologie. D'autres études sur le cancer du rein utilisent des posologies variant de 50 à 100mg/kg par voie orale (C. Xie et al. 2018)(Chen et al. 2016). A notre connaissance, aucune autre étude n'avait testé le PT2385 comme thérapie sur des xénogreffes de souris de médulloblastome. Il est évident qu'il nous faudrait tester d'autres concentrations afin de trouver la bonne posologie.

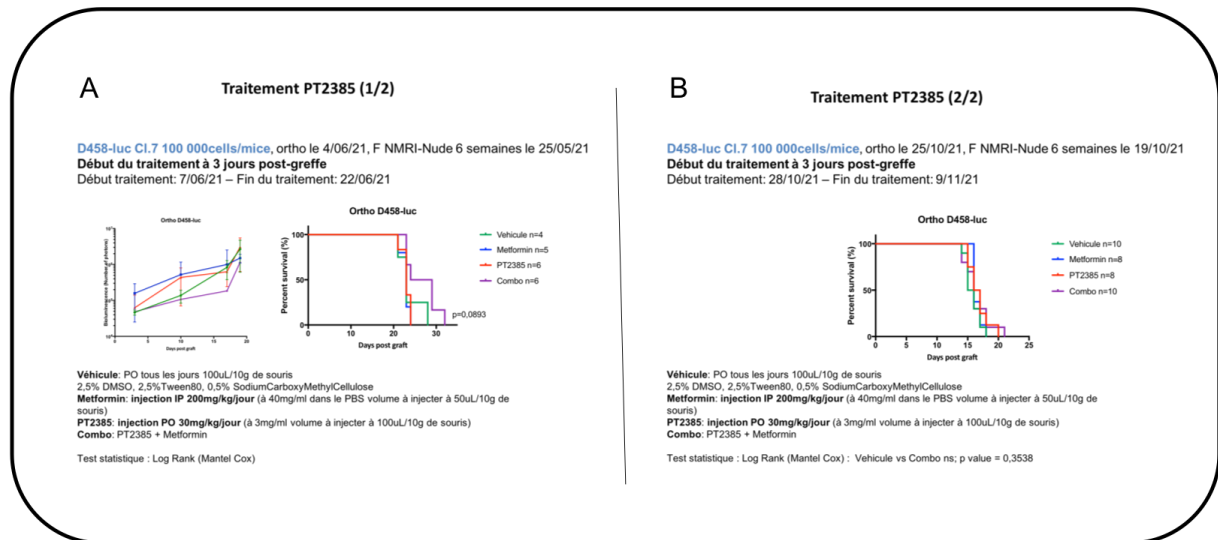


Figure 26 : Expérience *in vivo* sur PDX traités avec le PT2385.

Dans cette idée de définir avec précision la posologie la plus efficace possible en ce qui concerne le PT2385, mais également la metformine, nous avons commencé une collaboration avec l'équipe italienne de L. Tiberi (Université de Trente) qui nous permettra de tester nos schémas thérapeutiques avec différentes concentrations, sur des organoïdes cérébelleux Otx-2/c-MYC hébergeant une signature commune avec les MB du groupe 3 (Ballabio et al. 2020).

Nous avons, au travers de mon travail de thèse, ouvert une voie de recherche très séduisante, positionnement le métabolisme hypoxique, et plus particulièrement le facteur de transcription HIF-2 au centre des cibles thérapeutiques potentielles pour le MB du groupe 3. Nous savons que HIF-2 est un acteur incontournable dans le maintien des cellules souches dans un état indifférencié *via* des gènes comme *Oct4*, *Sox* et *Nanog* (Petruzzelli et al. 2014). Dans un contexte où MYC et Oct4 seraient induits en hypoxie, les cellules auraient alors un fort potentiel de cellules souches alors même que ces cellules seraient « adultes ». Étant donné que l'hypoxie survient dès l'état embryonnaire (PMID : 18285802), nous pouvons proposer que HIF-2

pourrait être à l'origine de l'évolution oncogénique du **groupe 3** des MB, même avant MYC. Si le caractère unique de HIF-2 est un avantage extraordinaire pour les cellules tumorales du **groupe 3**, il devient également une cible parfaite pour bloquer leur croissance tumorale. De nombreuses étapes sont toutefois encore nécessaires afin de pouvoir confirmer nos résultats.

Article 2

NAD⁺ pathways are a metabolic vulnerability for medulloblastoma Group 3 cells in a hypoxic microenvironment

I- Contexte et objectifs

En 2020, la lutte contre les cancers pédiatriques est devenue une préoccupation majeure et permanente de l'Institut National du Cancer. Chaque année, 2200 enfants et adolescents sont nouvellement touchés par un cancer. Il s'agit actuellement de la première cause de décès prématuré chez les enfants de plus de 1 an. Parmi les cancers pédiatriques, le médulloblastome est la tumeur primaire la plus fréquente du système nerveux chez l'enfant, entachée d'une grande morbi-mortalité en fonction du groupe de MB. L'établissement de la classification actuelle en quatre groupes distincts (WNT, SHH, groupe 3 et groupe 4) a, en très peu de temps, réorganisé la façon dont ce cancer est considéré et étudié, à la fois en recherche expérimentale et dans la conception des futurs essais cliniques (Roger J Packer 2011)(Leary and Olson 2012). Ce qui pendant de nombreuses années a été considéré en tant qu'entité tumorale unique, est désormais considérée comme quatre maladies très distinctes, chacune nécessitant des approches thérapeutiques personnalisées.

Considérant l'environnement tumoral, et donc l'hypoxie, comme un élément primordial à la compréhension de la variabilité de pronostic des différents groupes de MB, nous avons démontré (cf article 1) que les cellules tumorales du **groupe 3** ont une réponse différente à un microenvironnement hypoxique exprimant soit un HIF-1 non actif, soit une absence de HIF-1 en fonction des lignées cellulaires étudiés. Ces caractéristiques hypoxiques nous ont permis de proposer une approche thérapeutique différente selon le groupe de MB, avec une combinaison de traitement basé sur l'utilisation d'un inhibiteur de HIF-2.

Récemment, Di Magno *et al.*, ont mis en évidence que l'utilisation de la Phenformine, un médicament antidiabétique affichant une puissante activité anti-cancéreuse, provoque un effet

thérapeutique significatif par le biais d'un mécanisme redox-dépendant mais complexe I-indépendant, dans le groupe SHH des MB. La Phenformine inhiberait la glycérophosphate déshydrogénase mitochondriale (mGPD), un composant de la navette glycérophosphate, et provoquerait des élévations de la teneur en NADH intracellulaire. Nous savons que le métabolisme oxydatif du pyruvate dérivé du glucose, principal substrat énergétique du cerveau, est essentiel à son fonctionnement. Pour que le métabolisme se poursuive, le NADH dans le cytosol doit être réoxydé en NAD⁺. Si cela ne se produit pas, le rapport NADH/NAD⁺ augmente et le pyruvate est converti en lactate afin de réoxyder le NADH en NAD⁺. Puisque la membrane mitochondriale interne est imperméable au NADH et au NAD⁺, deux navettes agissent pour transférer les équivalents réducteurs du NADH dans le cytosol vers les mitochondries dans le cerveau, la navette malate-aspartate et la navette glycérol 3-phosphate. La navette malate-aspartate est considérée comme la navette la plus importante dans le cerveau (Fitzpatrick, Cooper, and Duffy 1983). Cependant l'activité de cette navette peut être extrêmement faible, voire inexistante dans les astrocytes cérébraux (Ramos et al. 2003)). Et bien que les enzymes de la navette glycérol 3-phosphate soient également présentes, il existe une controverse sur l'importance de cette navette dans le cerveau (Nguyen, Bråthe, and Hassel 2003).

Au vu de la différence de sensibilité à l'hypoxie des différents groupes de MB, et au rôle potentiel des navettes dans le développement du MB, nous avons travaillé sur l'impact des navettes glycérol-3-phosphate et malate/aspartate sur le métabolisme des cellules de MB du **groupe 3** versus le **groupe non-3** dans un microenvironnement proche des conditions physiologique de la tumeur, c'est-à-dire à 6% d'O₂ mais également en condition d'hypoxie sévère (1% d'O₂).

II- Article

NAD⁺ pathways are a metabolic vulnerability for medulloblastoma Group 3 cells in a hypoxic microenvironment

J. Contenti^{1*}, Y. Guo, M. Rouleau², A. Mazzu¹, L. Tiberi³, I. Ben-Sahra⁴, F. Bost¹, N.M. Mazure^{1*}.

¹ INSERM U1065, University of Côte d'Azur (UCA), C3M, 151 Route de St Antoine de Ginestière, BP2 3194, CEDEX 03, 06204 Nice, France.

² LP2M, CNRS-UMR 7370, Faculty of Medicine, University of Côte d'Azur (UCA), 06108 Nice, France.

³ Armenise-Harvard Laboratory of Brain Cancer, Department CIBIO, University of Trento, Via Sommarive 9, 38123 Trento, Italy.

⁴ Department of Biochemistry and Molecular Genetics, Northwestern University, Chicago, Illinois.

* Correspondence: contenti.j@chu-nice.fr & mazure@unice.fr

Abstract (240/250 words)

Medulloblastoma is a cancerous brain tumor that affects mostly children. It is rarely found in adults. Among the 4 groups defined according to molecular characteristics, group 3 is the least favorable with a survival rate of 50%. Current treatments, based on surgery, radiotherapy and chemotherapy, are however not sufficiently adapted to the different characteristics of the tumor, which are still not understood. In this study, we addressed the problem of medulloblastoma from a metabolic perspective in an oxygen-deficient microenvironment. We established that cells in group 3 are more sensitive to Phenformin, a complex 1 inhibitor, than cells in other groups. Furthermore, we showed that this subgroup differentially utilizes the two shuttles, mitochondrial glycerophosphate dehydrogenase (mGPDH) and malate-aspartate shuttle (MAS), which allow NADH to move from the cytoplasm to the mitochondria. The use of phenformin and iGP1, a specific inhibitor of mGPDH, as well as the combination of the two specific inhibitors of the two shuttles, iGP1 and AOAA, clearly showed a greater ability to decrease cell proliferation and induce cell death specifically for cells in group 3 compared to cells in other groups. Finally, the addition of GNE-140, a potent inhibitor of lactate dehydrogenase A, potentiated the effect of the different combinations used. Our study reinforces the idea of not only molecular but also metabolic heterogeneity in the different groups that constitute medulloblastoma and provides a potential new therapeutic solution for patients in group 3 whose tumors are more aggressive.

Keywords: glycolysis; hypoxia ; malate-aspartate shuttle ; medulloblastoma ; mitochondrial glycerophosphate dehydrogenase ; mitochondrial respiration ; phenformin

Introduction

Pediatric cancers have recently become a major national cause, especially in France, as this is the first cause of death by disease in children, and the third in young people (Institut National du Cancer: « Les cancers en France en 2016 – L'essentiel des faits et chiffres » - Février 2016 <http://www.e-cancer.fr/Actualites-et-evenements/Actualites/Les-cancers-en-France-en-2016-l-essentiel-des-faits-et-chiffres> dernier accès : 24 novembre 2017). Among the 3450 new cases identified each year, only 2650 young children will survive. It is also estimated that 1 child out of 440 will be affected by cancer by the age of 15. Medulloblastoma is a cancerous brain tumor, in the cerebellum. It is the most common malignant brain tumor in children, accounting for 20% of all pediatric central nervous system (CNS) tumors. Between 250 and 500 new cases of pediatric medulloblastoma are diagnosed each year in the United States. These tumors are most seen in children younger than 16 years of age and most often diagnosed between the ages of 5 and 9 years. However, medulloblastomas can be found in older adolescents and, less often, in adults. Medulloblastomas are fast growing tumors that often spread to other parts of the brain and spinal cord. Most medulloblastomas are in the middle of the cerebellum, near the fourth ventricle.

Medulloblastoma can be divided into four subgroups based on the molecular characteristics of the tumor cells: WNT- and Sonic hedgehog (SHH)- subtypes, Group 3 and Group 4. The specific subgroup of medulloblastoma affects prognosis. The WNT tumor subtypes have a very good prognosis, while the prognosis of Group 3 tumors is less favorable. The other two subtypes have an intermediate prognosis.

A better understanding of the molecular basis of medulloblastoma has led to improved survival rates in recent years. However, medulloblastoma survivors often suffer from numerous treatment-related complications. These include problems with endocrine function, cognition, hearing, fertility, and heart and lung function, as well as an increased risk of a second cancer. There is therefore an urgent need to better understand the development of this pediatric cancer for which there are still few treatments, especially for Group 3 patients. A major obstacle to the development of even more effective therapeutic strategies with the least possible toxicity has so far been the management of MB as a uniform disease. It is now essential to assign differential therapy to different risk groups based on molecular and clinical characteristics, thus providing an opportunity to personalize therapy and avoid over- or under-treatment.

We have therefore chosen to approach the MB with a metabolic prism, little used until now, and an oxygen gradient prism not used in therapy. Indeed, as the cerebellum microenvironment never presents an oxygen concentration of 21% (normoxia, Nx), we chose to consider the physiological control at 6% oxygen (physioxia, Phx) and the physiopathological conditions at 1% oxygen (hypoxia, Hx). We have recently shown that Group 3 tumor cells respond differently to a hypoxic microenvironment as HDMB-03 cells express a non-active HIF-1 and D-458 cells do not express HIF-1 α (Contenti, J – submitted article). Thus, we proposed a treatment based on the HIF-2 inhibitor, PT2385, coupled with metformin (Metf), a biguanide approved by the FDA (USA) that has become the most prescribed drug in diabetic pathology (1) and recognized as a mitochondrial complex I inhibitor (2), to block glycolysis and respiration, respectively. The use of these two compounds together allowed a strong reduction of tumor progression in mouse xenografts performed in the cerebellum, suggesting an innovative therapeutic potential.

Cancer cells have a very low NAD⁺/NADH ratio (3), and changes in the NAD⁺/NADH ratio are strongly correlated with tumor growth (4). NAD⁺ regeneration allows for increased cell proliferation even when oxidative phosphorylation is impaired (5)(6). Therefore, for metabolism to continue, NADH in the cytosol must be reoxidized to NAD⁺. Since the inner mitochondrial membrane is impermeable to NADH and NAD⁺, two shuttles will act to transfer the reducing equivalents of NADH in the cytosol to the mitochondria: (i) the glycerol 3-phosphate shuttle (ii) and the malate-aspartate shuttle.

The mGPDH is part of a network of shuttles that allow NADH, a reduced form of nicotinamide adenine dinucleotide (NAD) that plays an important role in many biological processes, to travel from the cytoplasm to the mitochondria. Indeed, the inner mitochondrial membrane being impermeable to cytosolic NADH, the NADH shuttles will then allow the transfer of the reducing equivalents of cytosolic NADH into the mitochondria, thus increasing mitochondrial ATP production. The second shuttle is the malate-aspartate shuttle (MAS). Aspartate aminotransferase (AST), a pyridoxal phosphate-dependent transaminase, is the rate-limiting enzyme for MAS. Aminoxyacetate acid (AOAA) is described as the specific inhibitor of AST, a widely used inhibitor of MAS. Similarly, iGP-1, the mitochondrial GPDH inhibitor, is considered a potent and selective inhibitor of mGPDH and not of cytosolic GPDH.

Under hypoxic conditions, it has been shown that the ratio of NADH:NAD⁺ (reduced: oxidized), in mitochondria, often increases due to the slowing of electron transport and the consequent reduction in the rate of NADH oxidation. As a result, NADH-producing reactions

in the tricarboxylic acid cycle (TCA) will decrease, reducing the rate at which the malate-aspartate shuttle can transfer NADH produced by glycolysis into the mitochondrial matrix. How hypoxia modulate the rate of the mGPDH/glycerophosphate (GP) shuttle is unknown. The NADH can then be oxidized by pyruvate which is then reduced to lactate. Since the cell cannot live with an internal acidic pH, lactate and its H⁺ proton will be exported outside the cell by the monocarboxylate transporters (MCT1 and MCT4). The acidic pH created outside the cell will be a powerful metastatic signal. Lactate dehydrogenase (LDHA), induced under hypoxia, will then reduce pyruvate to lactate. LDHB, on the other hand, will operate the opposite reaction by transforming lactate into pyruvate.

We therefore propose to test the impact of these two shuttles on the metabolism of Group 3 cells (HDMB03 and D-458), the most aggressive, *versus* non-Group 3 cells (DAOY and ONS-76, both from the SHH sub-group) in Nx, Phx and Hx microenvironments. We have shown that i) Non-Group 3 and Group 3 cells behave differently under physioxic and hypoxic conditions, ii) Non-Group 3 cells are highly adapted to drastic hypoxic conditions while Group 3 cells prefer more oxygenated conditions, iii) these two shuttles, mGPDH and Malate-Aspartate, are preferentially used by Group 3 cells and that blocking them strongly sensitizes the cells to cell death under hypoxic conditions and finally iv) targeting metabolic pathways opens new therapeutic perspectives with high potential.

Materials and Methods

Cell culture

DAOY cells were purchased from the ATTC (HTB-186TM). The ONS-76 cell line was a kind gift from Dr. F. Di Cunto (University of Torino - Italy). Both cells were grown in Dulbecco's Modified Eagle's Medium (DMEM) (Gibco-BRL) supplemented with 10% fetal bovine serum with penicillin G (50U/ml) and streptomycin sulfate (50µg/ml). HDMB-03 cell line was purchased from the DSMZ (ACC740). The D-458 cell line was provided by Dr. C. Pouponnot (Institut Curie - France).

An INVIVO₂ 200 anaerobic workstation (Ruskinn Technology Biotrace International Plc) set at 6% and 1% oxygen, 94% nitrogen and 5% carbon dioxide were used for hypoxic conditions.

Pharmacological inhibitors and chemicals

Metformin, phenformin, rotenone, antimycin A, oligomycin, and trifluorocarbonylcyanide phenylhydrazone (FCCP) were from Sigma (St. Louis, USA). iGP-1 was from Merck (Darmstadt, Germany), AOAA from Selleckchem (Houston, USA) and GNE-140 from MedChemExpress (Monmouth Junction, USA).

Respirometry and Extracellular Acidification

The cellular oxygen consumption rate (OCR) and extracellular acidification rate (ECAR) were obtained using a Seahorse XF24 extracellular flux analyzer from Seahorse Bioscience (North Billerica, MA, USA). Experiments were performed according to the manufacturer's instructions. OCR and ECAR were measured in real time in normoxia or hypoxia. Cells were deprived of glucose for 1h, then glucose (G–10mM), oligomycin (O–1µM), 2,4-Dinitrophenol (DNP–10µM), and Rotenone + Antimycin A (R/A–1µM) were injected at the indicated times. Protein standardization was performed after each experiment, with no noticeable differences in protein concentration and cell phenotype.

Phenotype MicroArray on OmnilogTM Analyzer

Metabolic profiling was studied by using the Omnilog[®] Phenotype Microarray[™] system (Biolog, Hayward, CA, USA) evaluating the cell's ability to metabolize 367 substrates. Cells were cultured for 48h in normoxia or hypoxia, then transferred at seeding densities of 20,000 cells/well to the PM-M1 to 4 plates in a phenol red-free RPMI-1640-based medium depleted of carbon energy sources (IFM1 medium, Biolog Inc., Hayward, CA, USA), supplemented with 0.3mM glutamine, 5% FCS, 100U/mL penicillin, and 100µg/mL streptomycin. Cells were then incubated for 24h at 37°C under 5% CO₂ in hypoxia or normoxia before adding Biolog Redox Dye Mix MA, sealing the plate with tape to prevent gas transfer, and incubated at 37°C in the Omnilog[®] automated incubator-reader (Biolog Inc., Hayward, CA, USA) for 24h to kinetically measure tetrazolium reduction resulting in formation of a purple color. Data was collected on a PMM Kinetics software with subtraction of the average values of three negative control wells (background), then, analysis was computed with R software (Version 3.4.4) with the *opm* package.

Steady-state metabolomics

To determine the relative levels of intracellular metabolites, extracts were prepared and analyzed by LC/MS-MS. Triplicate 10-cm plates (~80% confluent) were incubated in Hx for 72 hours. Metabolites were extracted on dry ice with 4 mL 80% methanol (-80°C), as described previously (Ben Sahra Science 2013). Insoluble material was pelleted by centrifugation at 3,000 × *g* for 5 minutes, followed by two subsequent extractions of the insoluble pellet with 0.5mL 80% methanol, with centrifugation at 16,000 × *g* for 5 minutes at 4°C. The 5-mL metabolite extract from the pooled supernatants was dried down under nitrogen gas using an N-EVAP (Organomation Associates, Inc). Dried pellets were resuspended using 20µL HPLC-grade water for mass spectrometry. A 7-µL sample was injected and analyzed using a 5500 QTRAP triple quadrupole mass spectrometer (AB/SCIEX) coupled to a Prominence UFLC HPLC System (Shimadzu) via selected reaction monitoring of a total of 300 endogenous water-soluble metabolites for steady-state analyses of samples (Yuan M Nat Protocole 2012). The normalized areas were used as variables for the univariate statistical data analysis. All univariate analyses and modeling on the normalized data were carried out using Metaboanalyst 4.0 (<http://www.metaboanalyst.ca>). Univariate statistical differences of the metabolites between two groups were analyzed using two-tailed Student *t* test.

Immunoblotting

Cells were lysed in 1.5x SDS buffer and the protein concentration determined using the BCA assay. 40µg of protein from whole cell extracts was resolved by SDS-PAGE and transferred onto a PVDF membrane (Millipore). Membranes were blocked in 5% non-fat milk in TN buffer (50mM Tris-HCl pH 7.4, 150 mM NaCl) and incubated in the presence of the primary and then secondary antibodies in 5% non-fat milk in TN buffer. Rabbit monoclonal anti-GPD2 antibody (ab188585) was from Abcam (Paris, France). Rabbit monoclonal anti-MDH2 antibody (D8Q5S) was from Cell Signaling technology. Mouse anti-β-tubulin, HSP90 and β-actin were from Sigma. ECL signals were normalized to either β-tubulin or HSP90. After washing in TN buffer containing 1% Triton-X100 and then in TN buffer, immunoreactive bands were visualized with the ECL system (Amersham Biosciences).

Gene expression microarray analysis

Normalized RNA sequencing (RNA-Seq) data produced by The Cancer Genome Atlas (TCGA) were downloaded from cbiportal (www.cbiportal.org, TCGA Provisional; RNA-Seq V2). Different parameters were available for 375 ccRCC tumor samples, with information for VHL status (methylation, mutation and deletion) {Chen, 2016 #1829;Ricketts, 2018 #1827}. We performed a differential expression analysis between patients with a “primary cilium” signature and patients with a “no primary cilium” signature using the Bioconductor package DESeq2.

The results published here are in whole or in part based upon data generated by the TCGA Research Network: <http://cancergenome.nih.gov/>.

Database analysis

To assess the effect of the presence or absence of the primary cilium in ccRCC from Cohort C, we performed a differential analysis between the group expressing the primary cilium (n=48 patients) and the group expressing no primary cilium (n=327 patients) by computing the ratio and p-values obtained with a Wilcoxon rank sum test. We then performed a functional and pathway enrichment analysis on differentially expressed genes (p-value < 0.05 and absolute ratio > 0.7) based on Reactome databases using the geneSCF tool {Subhash, 2016 #1647}. The terms are considered significant only if enriched with p-value < 0.05.

Statistics

All values are the means \pm SEM. Statistical analyses were performed using the 2-way ANOVA test in Prism. The *p* values are indicated. All categorical data used numbers and percentages. Quantitative data were presented using the median and range or mean. All statistical tests were two-sided, and *p*-values <0.05 indicated statistical significance whereas *p*-values between 0.05 and 0.10 indicated a statistical tendency.

Results

mGPDH and MAS shuttles are two important pathways used differentially in Hx in both groups

The mGPDH and mMDH are integral components of the respiratory chain and these two shuttles play an important role in cell bioenergetics (**Figure 1A**). To explore their possible roles in MB, we first interrogated the R2: Medulloblastoma 500 Genomics Analysis dataset. *GPD2* gene expression, encoding mGPDH, was different within the 4 groups (**Suppl. Figure 1A**). Its expression in Non-Group 3 (Shh) was significantly higher in comparison to Group 3. Inversely, Group 3 appears to express *MDH2*, encoding mitochondrial malate dehydrogenase (MDH2) more strongly compared to the other groups (**Suppl. Figure 1B**).

ONS-76 and DAOY cells, representative of Non-Group 3, as well as HDMB-03 and D-458 cells, representative of Group 3, were exposed for 72h to 21%- (Nx), 6%- (Phx) and 1%- O₂ (Hx). Interestingly, we observed a significant increase in mGPDH mRNA expression in Non-Group 3 after 72h of Hx while this expression was not affected in Group 3 (**Suppl. Figure 1C**). No modulation of MDH2 mRNA expression was observed under hypoxia regardless of the cell line used (**Suppl. Figure 1D**). However, the expression level of the mGPDH protein appears to be dependent on oxygen concentration only in ONS-76. (**Suppl. Figure 1E**) unlike MDH (**Suppl. Figure 1F**). However, a compensatory effect on MDH2 was observed upon invalidation of mGPDH in DAOY and ONS-76 cells (**Suppl. Figure 1E**). A similar effect was observed on mGPDH (**Suppl. Figure 1F**) upon invalidation of *MDH2* in DAOY and HDMB03 suggesting that the two shuttles are closely linked especially in Non-Group 3 cells compared to Group 3 cells.

To gain an in-depth understanding of the functional significance of the metabolic capability of Non-Group 3 and Group 3 cells, we evaluated the glycerol-phosphate (**Figure 1B** and **Suppl. Figure 2A**) and malate-aspartate (**Figure 1C** and **Suppl. Figure 2B**) pathways from the OmniLog Phenotype MicroArray to obtain the mitochondrial metabolic fingerprinting of ONS-76 and HDMB03 cells in Nx, Phx, and Hx using MitoS1 plates. ONS-76 cells showed the ability

to grow on Glycerol-3P independently of oxygen concentration while HDMB03 cells clearly grew on this compound as a function of decreasing oxygen (**Figure 1B**). ONS-76, and HDMB03 cells exhibited abilities to grow on malate under all three conditions tested (Nx, Phx, and Hx) (**Figure 1C**). We also observed that other compounds associated with malate such as acetyl L carnitine or Keto-isocaproic or leucine were readily used by HDMB in Hx. For therapeutic purposes, we favored the use of a recognized inhibitors (iGP1) and aminooxyacetate (AOAA) to block mGPDH and mMDH pathways, respectively, rather than testing siRNAs. Both inhibitors were efficient (**Suppl. Figure 1G-I**).

We then performed an unbiased metabolomic profiling on a representative cell line from each of the two groups, ONS-76 and HDMB03, in Hx (**Figure 1D and E**). ONS-76 and HDMB03 were untreated or treated with iGP1 or AOAA in Hx. Of the 262 small metabolites identified by LC/MS-MS, the steady-state levels of 50 metabolites were significantly altered in both cells treated with iGP1 or AOAA relative to control cells ($P < 0.02$). The profiles obtained are clearly different. ONS-76 cells have a metabolism that is not very mitochondrial based but very nucleotide metabolism oriented (**Figure 1D**). In the presence of iGP1, a very strong repression of deoxyribonucleotide synthesis was observed. However, when mGPDH was inhibited, products from amino acid metabolism (cystathionine and glutaminic acid), pentose phosphate pathway (d-sedoheptulose-7) and fatty acids (carnitine) were accumulated suggesting a use of these pathways to compensate for the lack of mGPDH shuttle and continue to feed mitochondria. In the presence of AOAA, the synthesis of deoxyribonucleotides was also stopped as well as a large part of the pentose phosphate pathway and the production of NADP⁺. Many compounds such as uridine, valine, leucine histidine, serine, methionine have been up regulated with a Variable Importance in Projection score between 1.29 to 1.32 suggesting the activation of the nucleotide synthesis pathway (**Suppl. Figure 1J**). In comparison to ONS-76, HDMB03 cells produce more pyruvate and asparagine suggesting that they may promote glycolysis and TCA cycle. iGP1 clearly impacted on HDMB03 metabolism *via* a reduction in the production of D-sedoheptulose-7-phosphate, D-ribose-1/5-phosphate and S-adenosyl-methionine suggesting a direct impact on the lipopolysaccharide, pentose phosphate and s-adenosylmethionine metabolic (SAM) pathways (**Figure 1E and Suppl. Figure 1K**). AOAA, on the other hand, has dramatically reversed the metabolism of the HDMB03 cells, which then seem to use or accumulate highly mitochondrial metabolites.

These results suggest that under conditions of oxygen variation the two shuttles are of importance, and that iGP1 and AOAA should globally modify the growth, and possibly the mortality, of Non-Group 3 and Group 3 cells probably differentially.

Inhibition of mGPDH increases the respiratory and glycolytic capacity of Group 3 cells

Since it is clear that mGPDH and MDH2 have a strong impact on the metabolism of MB cells under hypoxic conditions, we first examined whether the decrease in mGDPH activity had an impact on the viability, proliferation as well as the metabolism of the cells in the two groups. In the presence of 1 or 100 μM iGP1, 24- or 72-h, only a slight trend towards better proliferation was observed for ONS-76 in Phx (**Figure 2A**). The viability of Non-Group 3 cells was not impacted (**Figure 2B**). A more significant increase in proliferation was observed with HDMB03 in low oxygen concentrations (**Figure 2C**), in correlation with an increase in viability in Hx compared to Nx were characterized (**Figure 2D**).

We then hypothesized that the metabolism could be modified in favor of a better viability and higher proliferation. We thus quantified mitochondrial respiration with the Seahorse XF by measuring the oxygen consumption rate (OCR). As expected, a decay in respiration patterns between Nx, Phx and Hx (**Figure 2E-G**) in ONS-76 was observed. Basal respiration of ONS-76 cells was significantly decreased from 115.0 ± 14.3 pMoles/min in Nx to 78.27 ± 7.4 pMoles/min in Hx. ONS-76 cells showed a decrease in respiratory capacity more consistent with what is usually obtained with cancer cells subjected to hypoxic stress. Interestingly, HDMB03 showed higher basal respiration as well as a higher respiratory capacity in Hx from 18.7 ± 12.6 pMoles/min in Nx to 30 ± 13.9 pMoles/min in Hx (**Figure 2K-M**). In parallel, the basal level of glycolysis and the maximal glycolytic capacity of ONS-76 cells were similar than that in Nx, Phx or Hx (**Figure 2H-J**). HDMB03 cells appeared to have a higher oxygen-dependent glycolytic profile (**Figure 2N-P**). HDMB03 showed a higher basal glycolytic capacity in Hx (24.53 mpH/min) compared to Phx (15.20 mpH/min). In the presence of iGP1, the respiratory capacity was almost always increased in both groups (**Figure 2E-G** and **K-M**), especially in Phx, but that the glycolytic capacity was increased only in Group 3 cells (**Figure 2H-J** and **N-P**). The other cells in the Non-Group 3 and Group 3, DAOY and D-458 respectively, showed similar behavior (**Suppl. Figure 3**).

As those increases were not expected, we hypothesized that reactive oxygen species (ROS), generated by mGDPH (Mracek BBA 2013), may be inhibited by iGP1 in this way, then promoting high viability and better proliferation under low oxygen conditions. ROS were

inhibited by the use of N-Acetyl Cysteine (NAC) and we then observed, focusing on Group 3, that indeed HDMB03 and D-458 cells had a higher viability: 72.5 ± 4.8 versus 61.5 ± 7.05 and 76.3 ± 4.7 versus 51.8 ± 5.1 respectively (**Suppl. Figure 4**).

These results suggest that iGP1 allows Group 3 cells to switch to glycolysis, thereby increasing their cell growth. Although cells from Group 3 oxidizes G3P *via* mGDPH in Phx or Hx, all this activity tends to stunt the cells in their development probably due to ROS production.

Group 3 cells are more sensitive to the respiration blocking action of Phenf than Non-Group 3 cells

Recently, Di Magno *et al.* proposed a therapeutic potential for phenformin (Phenf) in medulloblastoma in the SHH group (7). The authors demonstrated that, at clinical doses, Phenf does not act at the level of mitochondrial complex 1 but rather at the level of mitochondrial glycerophosphate dehydrogenase (mGDPH). By acting on mGDPH, Phenf would then attenuate the transfer of reducing equivalents from the cytoplasm to the mitochondria leading to an increase in the lactate/pyruvate ratio and a redox-dependent inhibition of gluconeogenesis from reduced but non-oxidized substrates.

To better identify the dual function of Phenformin (Phenf) (mitochondrial complex 1 and/or mGDPH blockade) on Group 3 cells compared to Non-Group 3 cells, we compared its action in Nx, Phx, and Hx on proliferation, viability, and cell metabolism. We also used rotenone, a potent and specific inhibitor of mitochondrial complex 1, as a control. Viability and proliferation were measured. Cells were challenged with phenformin (Phenf - 100 μ M) and Rotenone (2.5 μ M).

The proliferation of ONS-76 and HDMB03 cells was strongly decreased in the presence of Phenf and Rotenone at all oxygen concentrations (**Figure 3A** and **C**). However, the impact on viability was different. Phenf slightly decreased the viability of ONS-76 by 9.1% in Nx (**Figure 3B**). In Phx and Hx, viability was restored close to 100%. Rotenone had a weak effect in Hx in ONS-76 (23%). HDMB-03 appeared to be more sensitive to Phenf (**Figure 3D**). We observed a systematic decrease in viability in Nx, Phx and Hx (39.6-, 33.5- and 26.5-%). The lethal effects of rotenone were attenuated in the presence of low oxygen concentrations. Similar effects were observed with DAOY (Non-Group 3) and D-458 (Group 3) (**Suppl. Figure 5A-D**).

As for the action of Phenf/Rotenone on the metabolism, we characterized that Phenf (3 and 100 μ M) and Rotenone blocked mitochondrial respiration in Nx, Phx and Hx in ONS-76 cells

(**Figure 3E-G**). In HDMB03 cells, Rotenone was less potent to block the respiration compared to Phenf 100 μ M (**Figure 3K-M**). Phenf 3 μ M, only tested in Hx, blocked respiration similarly to Phenf 100 μ M in both ONS-76 and HDMB03 (**Figure 3G and M**). In ONS-76 cells, a gradual, but slight, increase in glycolysis was observed with decreasing oxygen concentration for both Phenf 100 μ M and Rotenone (**Figure 3H-J**). In HDMB03 cells, only Rotenone drastically increased glycolysis as early as Phx while Phenf (3 and 100 μ M) showed no effect (**Figure 1N-P**). Like HDMB03, DAOY and D-458 also showed interesting behavior in their ability to breathe better in hypoxia (**Suppl. Figure 5E-P**).

Taken together, these results suggest a particular adaptability of ONS-76 cells in a drastic microenvironment. Indeed, significant differences has been observed in their respiratory capacity (ONS-76 *versus* DAOY/HDMB03/D-458). These results may explain why Phenf had little impact on cell death in ONS-76 cells, unlike Group 3 cells, or even DAOY cells. However, it should be noted that Group 3 cells have a greater sensitivity to Phenf than Non-Group 3 cells, both in terms of viability and proliferation. Whatever the group, Phenf at low or usual concentration seems to have a similar action to Rotenone on respiration, confirming its involvement at the level of mitochondrial complex I. However, we can already state that the mode of action of iGP-1 is different from that of Phenf, one inducing breathing, the other blocking it.

Phenf and iGP1 have a cumulative effect in Hx leading to high cell death in HDMB03 cells

Next, we examined the cumulative effect of both Phenf and iGP1 on the two groups. While proliferation was greatly reduced, the viability of Non-Group 3 cells (**Figure 4A-B**), was not impacted by the combination Phenf/iGP1 in contrast to Group 3 cells which presented a decrease in viability in Nx ($39.0\pm 8.5\%$), Phx ($23.8\pm 11.9\%$) and Hx ($12.5\pm 3.5\%$) (**Figure 4D**) as well as a decrease in proliferation (**Figure 4C**). As for the metabolism, Phenf/iGP1 combinations were able to decrease respiratory capacity in both groups (**Figure 4E**) in a similar manner to Phenf alone (**Figure 3**). However, the Phenf/iGP1 combo blocked the increase in respiratory capacity previously obtained with iGP1 in HDMB03 (**Figure 2M**). Glycolysis remained unchanged when iGP1 was added to Phenf (**Figure 4F and H**). While DAOY cells showed a similar pattern to ONS-76, D-458 cells were more resistant to the combo (**Suppl. Figure 6**).

Taken together, these results clearly showed that HDMB03 were the only cells sensitive to the Phenf/iGP1 combo since, although blocking as much respiration and glycolysis compared to

Phenf alone, the HDMB03 cells died twice more. We can then assume that the actions of Phenf and iGP1 are different.

Malate-Aspartate shuttle is used more by Non-Group 3 than by Group 3 in Hx

As previously described in Figure 1, the malate-aspartate shuttle appears to have an essential role along with the G3P shuttle. Thus, we used the malate-aspartate shuttle inhibitor, AOAA, to block mMDH activity in both groups. We also combined the two inhibitors iGP1 and AOAA in Hx to totally block both shuttles. All cells showed sensitivity to 1 mM AOAA in both proliferation (**Figure 5A-C**) and viability (**Figure 5B-D**) suggesting that cells use this shuttle equivalently. However, this was the first time we observed a real inhibitory effect on Non-Group 3 cells suggesting a greater use of Malate-Aspartate shuttle compared to mGPDH shuttle in Non-Group 3. However, the iGP-1/AOAA combination did not increase cell death or proliferation compared to conditions with only AOAA in ONS-76 (**Figure 5B**). However, the AOAA/iGP1 combination appeared to show a slight additive effect in HDBM03 cells (**Figure 5D**). Respiration analysis showed differences between the two groups (**Figure 5E and G**). AOAA alone was able to strongly decrease the respiratory capacity of Non-Group 3 cells while the results obtained with Group 3 cells clearly show the importance of using the AOAA/iGP1 combination to block mitochondrial respiration. AOAA or AOAA/iGP1 strongly decreased the glycolytic capacity of ONS-76 and HDMB03 (**Figure 5F-H**). Similar results for proliferation, cell survival and metabolism were obtained with the other cells in Non-Group 3 and Group 3 (**Suppl. Figure 7**).

Therefore, these results show a clear difference between the different groups. Metabolism of the Non-Group 3 is strongly influenced by MAS while that of Group 3, especially HDMB03 cells, relies on the two shuttles since both inhibitors are needed to observe an inhibition effect.

The combination of GNE-140 with the other combos massively kills all cells in Hx, regardless of the group to which they refer.

We then hypothesized that the other NAD⁺ production pathway generated by lactate dehydrogenase could be used when both shuttles are blocked and considered the need to block it as well. We therefore used GNE-140, which is a potent inhibitor of lactate dehydrogenase A (LDHA), to block the transformation of pyruvate to lactate but also of LDHB, which allows the reverse transformation. The results obtained with Omnilog clearly showed that both cell lines, independently of the group to which they belong, were avid for glucose but also for glucose-6

phosphate and Fructose-6 phosphate (**Figure 6A**). This ability to grow on these compounds was stronger under hypoxic conditions for Group 3 cells compared to Non-Group 3 cells, although the glycolytic profile did not appear very characteristic (**Figure 2**). However, ONS-76 and HDMB03 showed little or no sensitivity to GNE-140 in terms of proliferation and cell death, respectively (**Figure 6B-C**). Basal glycolysis and glycolytic capacity were completely abolished in Non-Group 3 cells in Hx (**Figure 6D**) resulting in a decreased proliferation. HDMB03 showed a slightly different behavior in the presence of GNE-140. The glycolytic capacity was not as reduced as in ONS-76, which may explain a low impact on proliferation (**Figure 6E**). GNE-140 had a similar effect on the other cell lines (**Suppl. Figure 8A-D**).

Finally, we decided to associate GNE140 to the different combinations previously used to block any potential for NAD⁺ production and any switch to lactate production. The addition of GNE-140 clearly potentialized the effects of iGP-1/AOAA (**Figure 6F-G**) and iGP-1/Phenf (**Figure 6H-I**) combos, regardless of the cell line used and regardless of its group belonging (**Figure 6F-I** and **Suppl. Figure 8E-H**). Both super combos, iGP-1/AOAA/GNE-140 and iGP-1-Phenf/GNE-140, massively reduced the proliferation and/or killed the Group 3 and Non-Group 3 cells, since the few colonies visible in Non-Group 3 did not grow and few or no colonies grew in Group 3.

These results strongly suggest that i) Non-Group 3 cells are much more dependent on the NAD⁺ source from pyruvate to lactate conversion than on the sources generated by mGPDH and MDH2, ii) Group 3 cells are definitely more sensitive than Non-Group 3 cells when one or more metabolic pathways are blocked in hypoxia iii) the addition of GNE-140 strongly sensitizes all cell lines, even the most refractory ones such as Non-Group 3 cells, and finally iv) we have characterized new therapeutic leads and potentially to target the most treatment refractory Group 3 cells.

DISCUSSION

Metabolism of medulloblastoma has received very little attention in recent years. However, aerobic glycolysis and lipogenesis are known to be strongly present in Shh-directed medulloblastomas, but it is not known whether these pathways are common to other subgroups (8). Activation of the WNT pathway has also been shown to increase glycolysis at the expense

of oxidative phosphorylation in normal and transformed cells outside the brain (9)(10). Obviously, the presence of MYC in the WNT group is found to participate in the increased glycolysis activity in this subgroup (11). Similarly, the detection of MYC family amplifications in Group 3 should largely direct the metabolism of Group 3 tumor cells toward exacerbated glycolysis (12)(13). Although glucose metabolism has not yet been examined in Group 3 medulloblastomas, it is therefore likely that in these tumors MYC reconfigures metabolism to favor glycolysis. However, little research has addressed the study of metabolism in the different subgroups in its environmental context of low oxygen concentrations. Bernauer's review (14) clearly explains the importance of hypoxia in the resistance process of cancer cells and the existing tools to measure directly or indirectly the presence of low oxygen concentrations. However, he did not address the issue of metabolism and its therapeutic approach in a hypoxic microenvironment, nor did he provide an oxygen concentration value in medulloblastoma but rather a comparison with other cancers. Our study therefore places for the first-time tumor cells of Non-Group 3 (ONS-76 and DAOY) and Group 3 (HDMB03 and D-458), in a laboratory setting of 21% O₂, in an estimated physiological setting of 6% O₂, and in a tumor pathophysiological setting of 1% O₂. As we have been working on the metabolic approach in hypoxia for many years in colon (15)(16) and kidney (17) cancers and have focused throughout these years on the primordial role of mitochondria in an environment that normally does not particularly emphasize them, we decided to bring for the first time a rigorous light on the metabolism of cancer cells of medulloblastoma. We have already recently demonstrated that depending on the belonging of the different groups, Non-Group 3 or Group 3, HIF-1 α can be different (Contenti, 2002 – to be submitted). Indeed, it has been shown that HIF-1 α is a classical HIF-1 α in Non-Group 3 cells (stabilization in hypoxia, molecular weight, expression...) whereas HIF-1 α in HDMB03 cells is mutated, is not expressed in the nucleus, and shows specific post-translational modifications. HIF-1 α from D-458 cells is virtually non-existent. Thus, the response to hypoxia in these two cell types depends primarily on HIF-2. However, it is known that HIF-2 is not the transcription factor that best manages hypoxia metabolism. It was therefore reasonable to assume that the responses of Group 3 cells would differ from those of Non-Group 3 cells.

Overall, did we observe differences between 21 and 6% O₂ or between 6% and 1% O₂? The answer is YES. Should we grow our cells at 6% O₂ consistently? The answer is certainly more subtle. We observed major differences with Agilent Seahorse analysis when we compared the 21% *versus* 6% conditions, e.g. the impact of Rotenone on glycolysis (ECAR) or iGP-1 on

respiration (OCR) and glycolysis (ECAR), respectively (e.g. **Figure 2** and **Figure 3**). The conclusions on the impact of Rotenone or iGP1 would then have been different depending on whether the experiments were done at 21 or 6%. We also observed that it was more difficult to reproduce identically our experiments performed at 6% O₂ compared to 21% or 1% and that we very often had large standard deviations. It then appeared to us that the cells could be torn between two worlds, that of normoxia in which the cell lines have always been artificially immersed *in vitro* and that of hypoxia where their natural tumor metabolism is better able to express itself. The conditions at 6% O₂ are certainly not linear conditions intermediate between 21% and 1%. These are the closest conditions in which the normal cell must live and adapt. The tumor cell will then be confronted with a much larger O₂ gradient under less fixed and much more dynamic conditions.

Should we then necessarily compare hypoxic cells with cells maintained in artificial normoxia or just work in hypoxia and challenge the tumor cells in the most extreme conditions to find their metabolic failures is a philosophical question that researchers have not yet resolved. However, we decided to examine a wide range of O₂ concentrations, while focusing primarily on hypoxia, where tumor cells are most resistant to therapies, and then move to organoids, a model in which environmental heterogeneity can begin to take hold.

In 2020, Di Magno *et al.* proposed a model involving an important role of glycerophosphate shuttling in Med1-MB and DAOY cells (7). They described that Phenformin at low concentrations inhibited mGPD in a complex I-independent manner, resulting in an increase in redox state and NADH levels, all of which blocked tumor growth. However, knowing that mitochondrial activity is often repressed in hypoxia *via* HIF-1 (18), we therefore hypothesized that the mechanism of action of Phenformin may have a different impact than that proposed by Di Magno (19) and that the glycerophosphate shuttle may also have a different role in hypoxia and in Group 3 cells compared to Non-Group 3.

Contrary to Rotenone, which acted according to the pattern we had envisaged, i.e. less and less effective according to the decrease in oxygen concentration, the action of Phenformine seemed to be independent of oxygen variations, at least in Group 3 cells suggesting a less intense activity of Phenf compared to Rotenone, which is a powerful mitochondrial inhibitor. Moreover, we clearly showed that in the presence of iGP1, cells proliferated much better under Physioxia and Hypoxia conditions, which we never observed with Phenformin. These results clearly demonstrate that Phenformin has a different action than iGP1 and that it does not affect the activity of mGPDH.

The two shuttles clearly showed different sensitivity to hypoxia. Both mGDPH and MDH2 mRNA and protein expressions, in Group 3, do not seem to be affected by the oxygen variations used in this study. On the other hand, MDH2 appeared to be strongly induced under hypoxic conditions in Non-Group 3 cells, both at the mRNA and protein expression levels. However, Non-Group 3 cells have a functional HIF-1 unlike Group 3 cells (Contenti, 2002 – to be submitted). We can therefore hypothesize that *MDH2* is a target gene of HIF-1 but that its regulation is disrupted by the presence of a particular HIF-1 α in HDMB03 or a non-existent HIF-1 α in D-458. Similarly, AOAA was able to show an inhibitory effect on viability and proliferation only under hypoxic conditions and not under normoxic conditions in Non-Group 3 cells (data not shown).

Interestingly, Non-Group 3 cells were the most difficult cells to target with metabolic inhibitors. Group 3 cells always reacted strongly to metabolic inhibitors (Phenf, iGP1, AOAA, GNE-140...) for the same reasons as previously mentioned, i.e., the non-activity of HIF-1, the master of metabolic regulation under hypoxia. We have thus clearly highlighted an Achilles heel of Group 3 cells: hypoxic metabolism. In addition, Group 3 cells showed high sensitivity to different NAD⁺ generating metabolic pathways. We obviously did not test all the metabolic pathways controlled by hypoxia, but it turned out that the two shuttles mGDPH and MDH2 were of such importance that they are of potential interest as therapeutic targets. We have clearly highlighted new treatment approaches that are very specific to the most emblematic group of Medulloblastomas, that of metastases and very low survival rates.

We have clearly highlighted new treatment approaches that are very specific to the most emblematic group of Medulloblastomas, that of metastases and very low survival rates. We will continue to explore these avenues in the hope of reinforcing the knowledge acquired during this study and bringing therapeutic solutions to young children affected by this devastating disease as soon as possible.

Acknowledgments

This work was supported by a grant from La Fondation Flavien and the Fondation ARC pour la recherche sur le Cancer. Y. Guo is supported by the Chinese Ministry of Research. I. Ben-Sahra is supported by the NIH R00-CA194192 and LAM Foundation grants. F. Bost and N.M. Mazure are CNRS investigators. Metabolomics services were performed by the Metabolomics Core Facility at Robert H. Lurie Comprehensive Cancer Center of Northwestern University and the Beth Israel Deaconess Medical Center Mass Spectrometry Facility of Harvard Medical School.

Author Contributions

Conception and design: J. Contenti, NM Mazure

Development of methodology: L. Kaminski, S. Torrino, Z. Djabari, E. Jaune, K. Laurent, S. Clavel, F. Bost

Acquisition of data (provided animals, acquired and managed patients, provided facilities, etc.): J. Contenti, Y. Guo, M. Rouleau, A. Mazzu, I. Ben-Sahra, N.M. Mazure.

Analysis and interpretation of data (e.g., statistical analysis, biostatistics, computational analysis): J. Contenti, Y. Guo, M. Rouleau, I. Ben-Sahra, F. Bost, N.M. Mazure.

Writing, review, and/or revision of the manuscript: J. Contenti, I. Ben-Sahra, F. Bost, NM Mazure

Administrative, technical, or material support (i.e., reporting or organizing data, constructing databases): J. Contenti, NM Mazure

Study supervision: NM Mazure

Declaration of Interests

No potential conflicts of interest were disclosed.

Figure titles and legends

Figure 1. mGPDH and MDH2 shuttles are used differentially in Non-Group 3 and Group 3 depending on the oxygen concentration. **A**, Schematic representation of the metabolic pathways driven by mGPDH and MDH2. Specific inhibitors are represented: iGP1 (mGPDH), AOAA (MDH2), Phenformin (Phenf – Complex 1) and GNE-140 (LDHA). **B**, Heatmap showing the 1 substrate that was differently metabolized by ONS-76 and HDMB03 in Nx, Phx and Hx. The color key scale for each substrate is based on dye reduction quantified by Omnilog units. A dark red color indicates strong positive substrate metabolization, a red color moderate metabolization and a green color indicates no substrate metabolization. **C**, Heatmap showing the 9 substrates or combination of substrates that were differently metabolized by ONS-76 and HDMB03 in Nx, Phx and Hx. The color key scale for each substrate is based on dye reduction quantified by Omnilog units. A dark red color indicates strong positive substrate metabolization, a red color moderate metabolization and a green color indicates no substrate metabolization. **D** and **E**. Steady-state metabolite profile of ONS-76 (**D**) and HDMB03 (**E**) cells submitted to hypoxia for 72h in the absence (Ctl Hx), or presence of i-GP1 or AOAA. Intracellular metabolites from four independent samples per condition were profiled by LC/MS-MS, and those significantly altered in treated cells, relative to control cells, are shown as row-normalized heatmaps ranked according to fold-change \log_2 (treated/untreated). The 2-way ANOVA is representative of at least three independent experiments.

Figure 2. Inhibition of mGPDH by iGP-1 increases OXPHOS and glycolysis in group 3 cells. **A** and **C**, ONS-76 (**A**) and HDMB03 (**C**) cells were seeded at the same density and incubated in 21-, 6- and 1- % O₂ for 24-, and 72- h in the absence (Ctl) or presence of iGP-1 (1 or 100µM). Cell proliferation was measured using an ADAM cell counter. **B** and **D**, ONS-76 (**B**) and HDMB03 (**D**) cells were seeded at the same density and incubated in 21-, 6- and 1- % O₂ for 24-, and 72- h in the absence (Ctl) or presence of iGP-1 (1 or 100µM). Cell viability was measured using an ADAM cell counter. **E**, **F** and **G**, Respiratory control of ONS-76 cells. OCR was measured in real time with the XF24 analyzer. Cells were cultured for 24 h in Nx (21% O₂ - **E**), Phx (6% O₂ - **F**) and Hx (1% O₂ - **G**) in the absence (Ctl) or presence of iGP-1 (1 or 100 µM). Cells were deprived of glucose for 1h, then glucose (G), oligomycin (O), DNP, and Rotenone + Antimycin A (R/A) were injected at the indicated times. The graphs are representative of at least three independent experiments carried out in octuplicate. **H**, **I**, and **J**,

ECAR in Nx (21% O₂ - **H**), Phx (6% O₂ - **I**) and Hx (1% O₂ - **J**) in the absence (Ctl) or presence of iGP-1 (1 or 100μM) for 24h of ONS-76 cells was evaluated with the XF24 analyzer. Cells were deprived of glucose for 1h, then glucose (G) and oligomycin (O) were injected at the indicated times. The graphs are representative of at least three independent experiments carried out in octuplicate. **K, L and M**, Respiratory control of HDMB03 cells. OCR was measured in real time with the XF24 analyzer. Cells were cultured for 24h in Nx (21% O₂ - **K**), Phx (6% O₂ - **L**) and Hx (1% O₂ - **M**) in the absence (Ctl) or presence of iGP-1 (1 or 100μM). Cells were deprived of glucose for 1h, then glucose (G), oligomycin (O), DNP, and Rotenone + Antimycin A (R/A) were injected at the indicated times. The graphs are representative of at least three independent experiments carried out in octuplicate. **N, O, and P**, ECAR in Nx (21% O₂ - **N**), Phx (6% O₂ - **O**) and Hx (1% O₂ - **P**) in the absence (Ctl) or presence of iGP-1 (1 or 100μM) for 24h of HDMB03 cells was evaluated with the XF24 analyzer. Cells were deprived of glucose for 1h, then glucose (G) and oligomycin (O) were injected at the indicated times. The graphs are representative of at least three independent experiments carried out in octuplicate. The 2-way ANOVA is representative of at least three independent experiments.

Figure 3. Phenf partially kills Group 3 cells compared to Non-Group 3 cells. **A and C**, ONS-76 (**A**) and HDMB03 (**C**) cells were seeded at the same density and incubated in 21-, 6- and 1- % O₂ for 24-, and 72- h in the absence (Ctl) or presence of Phenf (100μM) or Rotenone (2.5μM). Cell proliferation was measured using an ADAM cell counter. **B and D**, ONS-76 (**B**) and HDMB03 (**D**) cells were seeded at the same density and incubated in 21-, 6- and 1- % O₂ for 24-, and 72- h in the absence (Ctl) or presence of Phenf (100μM) or Rotenone (2.5μM). Cell viability was measured using an ADAM cell counter. **E, F and G**, Respiratory control of ONS-76 cells. OCR was measured in real time with the XF24 analyzer. Cells were cultured for 24h in Nx (21% O₂ - **E**), Phx (6% O₂ - **F**) and Hx (1% O₂ - **G**) in the absence (Ctl) or presence of Phenf (3 or 100μM) or Rotenone (2.5μM). Cells were deprived of glucose for 1h, then glucose (G), oligomycin (O), DNP, and Rotenone + Antimycin A (R/A) were injected at the indicated times. The graphs are representative of at least three independent experiments carried out in octuplicate. **H, I, and J**, ECAR in Nx (21% O₂ - **H**), Phx (6% O₂ - **I**) and Hx (1% O₂ - **J**) in the absence (Ctl) or presence of Phenf (3 or 100μM) or Rotenone (2.5μM) for 24 h of ONS-76 cells was evaluated with the XF24 analyzer. Cells were deprived of glucose for 1 h, then glucose (G) and oligomycin (O) were injected at the indicated times. The graphs are representative of at least three independent experiments carried out in octuplicate. **K, L and M**, Respiratory control

of HDMB03 cells. OCR was measured in real time with the XF24 analyzer. Cells were cultured for 24 h in Nx (21% O₂ - **K**), Phx (6% O₂ - **L**) and Hx (1% O₂ - **M**) in the absence (Ctl) or presence of Phenf (3 or 100μM) or Rotenone (2.5μM). Cells were deprived of glucose for 1h, then glucose (G), oligomycin (O), DNP, and Rotenone + Antimycin A (R/A) were injected at the indicated times. The graphs are representative of at least three independent experiments carried out in octuplicate. **N**, **O**, and **P**, ECAR in Nx (21% O₂ - **N**), Phx (6% O₂ - **O**) and Hx (1% O₂ - **P**) in the absence (Ctl) or presence of Phenf (3 or 100μM) or Rotenone (2.5μM) for 24h of HDMB03 cells was evaluated with the XF24 analyzer. Cells were deprived of glucose for 1 h, then glucose (G) and oligomycin (O) were injected at the indicated times. The graphs are representative of at least three independent experiments carried out in octuplicate.

The 2-way ANOVA is representative of at least three independent experiments.

Figure 4. Phenf and iGP1 combo induces high cell death in HDMB03 cells. **A** and **C**, ONS-76 (**A**) and HDMB03 (**C**) cells were seeded at the same density and incubated in 21-, 6- and 1- % O₂ for 24-, and 72- h in the absence (Ctl) or presence of iGP-1 (100μM), Phenf (100μM) or Phenf+iGP-1. Cell proliferation was measured using an ADAM cell counter. **B** and **D**, ONS-76 (**B**) and HDMB03 (**D**) cells were seeded at the same density and incubated in 21-, 6- and 1- % O₂ for 24-, and 72- h in the absence (Ctl) or presence of iGP-1 (100μM), Phenf (100μM) or Phenf+iGP-1. Cell viability was measured using an ADAM cell counter. **E** and **G**, Respiratory control of ONS-76 (**E**) and HDMB03 (**G**) cells. OCR was measured in real time with the XF24 analyzer. Cells were cultured for 24 h in Hx (1% O₂) in the absence (Ctl) or presence of Phenf (100μM) + iGP-1 (100μM). Cells were deprived of glucose for 1h, then glucose (G), oligomycin (O), DNP, and Rotenone + Antimycin A (R/A) were injected at the indicated times. The graphs are representative of at least three independent experiments carried out in octuplicate. **F** and **H**, ECAR in Hx in the absence (Ctl) or presence of Phenf (100μM) + iGP-1 (100μM) for 24h of ONS-76 (**F**) and HDMB03 (**H**) cells was evaluated with the XF24 analyzer. Cells were deprived of glucose for 1h, then glucose (G) and oligomycin (O) were injected at the indicated times. The graphs are representative of at least three independent experiments carried out in octuplicate.

The 2-way ANOVA is representative of at least three independent experiments.

Figure 5. The Malate-Aspartate shuttle is preferentially used by Non-Group 3 cells. **A** and **C**, ONS-76 (**A**) and HDMB03 (**C**) cells were seeded at the same density and incubated in 1% O₂

for 72h in the absence (Ctl) or presence of AOAA (0.3 and 1mM), iGP-1 (100 μ M) or AOAA+iGP-1. Cell proliferation was measured using an ADAM cell counter. **B** and **D**, ONS-76 (**B**) and HDMB03 (**D**) cells were seeded at the same density and incubated in 1% O₂ for 72h in the absence (Ctl) or presence of AOAA (0.3 and 1mM), iGP-1 (100 μ M) or AOAA+iGP-1. Cell viability was measured using an ADAM cell counter. **E** and **G**, Respiratory control of ONS-76 (**E**) and HDMB03 (**G**) cells. OCR was measured in real time with the XF24 analyzer. Cells were cultured for 24h in Hx (1% O₂) in the absence (Ctl) or presence of AOAA (1mM) or AOAA+iGP-1 (100 μ M). Cells were deprived of glucose for 1h, then glucose (G), oligomycin (O), DNP, and Rotenone + Antimycin A (R/A) were injected at the indicated times. The graphs are representative of at least three independent experiments carried out in octuplicate. **F** and **H**, ECAR in Hx (1% O₂) in the absence (Ctl) or presence of AOAA (1mM) or AOAA+iGP-1 (100 μ M) for 24 h of ONS-76 (**F**) and HDMB03 (**H**) cells was evaluated with the XF24 analyzer. Cells were deprived of glucose for 1 h, then glucose (G) and oligomycin (O) were injected at the indicated times. The graphs are representative of at least three independent experiments carried out in octuplicate.

The 2-way ANOVA is representative of at least three independent experiments.

Figure 6. The combination of GNE-140 with the other combos massively kills MB cells. **A**, Heatmap showing the 7 substrates that were differently metabolized by ONS-76 and HDMB03 in Nx, Phx and Hx. The color key scale for each substrate is based on dye reduction quantified by Omnilog units. A dark red color indicates strong positive substrate metabolization, a red color moderate metabolization and a green color indicates no substrate metabolization. **B** and **C**, ONS-76 and HDMB03 cells were seeded at the same density and incubated in Nx, Phx and Hx for 72h in the absence (Ctl) or presence of GNE-140 (5 μ M). Cell proliferation (**B**) and viability (**C**) were measured using an ADAM cell counter. **D** and **E**, ECAR in Hx (1% O₂) in the absence (Ctl) or presence of GNE-140 (5 μ M) for 24h of ONS-76 (**D**) and HDMB03 (**E**) cells was evaluated with the XF24 analyzer. Cells were deprived of glucose for 1h, then glucose (G) and oligomycin (O) were injected at the indicated times. The graphs are representative of at least three independent experiments carried out in octuplicate. **D** and **E**, ONS-76 and HDMB03 cells were seeded at the same density and incubated in Nx, Phx and Hx for 72h in the absence (Ctl) or presence of iGP-1 (100 μ M) + AOAA (1mM) + GNE-140 (5 μ M). Cell proliferation (**F**) and viability (**G**) were measured using an ADAM cell counter. **H** and **I**, ONS-76 (**H**) and HDMB03 (**I**) cells were seeded at the same density and incubated in Hx for 72h in

the absence (Ctl) or presence of iGP-1 (100 μ M) + Phenf (100 μ M) or iGP-1 (100 μ M) + Phenf (100 μ M) + GNE-140 (5 μ M). Viability was measured using an ADAM cell counter. **J**, Clonogenic assay of ONS-76 and HDMB03 cells. Cell lines were seeded at the same density and incubated in Hx 1% O₂ for 7 days in the absence (Ctl) or presence of iGP-1 (100 μ M) + AOAA (1mM) + GNE-140 (5 μ M) or iGP-1 (100 μ M) + Phenf (100 μ M) + GNE-140.

The 2-way ANOVA is representative of at least three independent experiments.

Supplemental

Supplemental Figure 1: A and B, Schematic distribution of the different MB subgroups according to GPD2 (mGPDH – **A**) and MDH2 (**B**). **C**, Graphic representation of *mGPDH* mRNA expression in DAOY, ONS-76, HDMB03, D-458 cells incubated in normoxia (Nx) for 24h and hypoxia (Hx - 1% O₂) for 24-, 48- and 72- h. **D**, Graphic representation of *MDH2* mRNA expression in DAOY, ONS-76, HDMB03, D-458 cells incubated in normoxia (Nx) for 24h and hypoxia (Hx - 1% O₂) for 24-, 48- and 72- h. **E**, ONS-76 and HDMB03 cells were transfected, or not (Ctl), with a siRNA control (siCtl) or siRNA to mGPDH (simGPDH) for 24h. Cells were then incubated in normoxia (Nx), physioxia (Phx) and hypoxia (Hx) for 72h. Cell lysates were analyzed by immunoblotting for mGPDH and MDH2. Hsp90 was used as a loading control. **F**, ONS-76 and HDMB03 cells were transfected, or not (Ctl), with a siRNA control (siCtl) or siRNA to MDH2 (siMDH2) for 24h. Cells were then incubated in normoxia (Nx), physioxia (Phx) and hypoxia (Hx) for 72h. Cell lysates were analyzed by immunoblotting for MDH2 and mGPDH. Hsp90 was used as a loading control. **G**, HDMB03 cells were transfected with siRNA Control (siCtl), siRNA to mGPDH (simGPDH – 100nM) or treated with iGP-1 (10 or 100 μ M) for 72h in Hx. G3P was then detected by colorimetric assay. **H**, HDMB03 cells were treated with iGP-1 (100 μ M) or transfected with siRNA Control (siCtl), or siRNA to mGPDH (simGPDH – 100nM) for 72h in Hx. Ratio of NAD/NADH was then quantify by colorimetric assay. **I**, HDMB03 cells were transfected with siRNA Control (siCtl), siRNA to MDH2 (siMDH2) or treated with AOAA (1mM) for 72h in Hx. Malate concentration was then detected by colorimetric assay. **J**, Metabolites differentiating between control (Ctl) and iGP-1 or AOAA ONS-76 treated cells in Hx (VIP>1.0, metabolites with VIP>1.5 are shown). Relative metabolite abundance is indicated in the bar, with red representing metabolite

accumulation. **K**, Metabolites differentiating between control (Ctl) and iGP-1 or AOAA HDMB03 treated cells in Hx (VIP>1.0, metabolites with VIP>1.5 are shown). Relative metabolite abundance is indicated in the bar, with red representing metabolite accumulation. The 2-way ANOVA is representative of at least three independent experiments.

Supplemental Figure 2: A, Heatmap showing the 1 substrate that was differently metabolized by ONS-76 and HDMB03 in Nx, Phx and Hx. The color key scale for each substrate is based on dye reduction quantified by Omnilog units. A dark red color indicates strong positive substrate metabolization, a red color moderate metabolization and a green color indicates no substrate metabolization. **B**, Heatmap showing the 9 substrates or combination of substrates that were differently metabolized by ONS-76 and HDMB03 in Nx, Phx and Hx. The color key scale for each substrate is based on dye reduction quantified by Omnilog units. A dark red color indicates strong positive substrate metabolization, a red color moderate metabolization and a green color indicates no substrate metabolization.

Supplemental Figure 3: A and C, DAOY (**A**) and D-458 (**C**) cells were seeded at the same density and incubated in 21-, 6- and 1- % O₂ for 24-, and 72- h in the absence (Ctl) or presence of iGP-1 (1 or 100μM). Cell proliferation was measured using an ADAM cell counter. **B and D**, DAOY (**B**) and D-458 (**D**) cells were seeded at the same density and incubated in 21-, 6- and 1- % O₂ for 24-, and 72- h in the absence (Ctl) or presence of iGP-1 (1 or 100μM). Cell viability was measured using an ADAM cell counter. **E, F and G**, Respiratory control of DAOY, cells. OCR was measured in real time with the XF24 analyzer. Cells were cultured for 24 h in Nx (21% O₂ - **E**), Phx (6% O₂ - **F**) and Hx (1% O₂ - **G**) in the absence (Ctl) or presence of iGP-1 (1 or 100 μM). Cells were deprived of glucose for 1h, then glucose (G), oligomycin (O), DNP, and Rotenone + Antimycin A (R/A) were injected at the indicated times. The graphs are representative of at least three independent experiments carried out in octuplicate. **H, I, and J**, ECAR in Nx (21% O₂ - **H**), Phx (6% O₂ - **I**) and Hx (1% O₂ - **J**) in the absence (Ctl) or presence of iGP-1 (1 or 100μM) for 24h of DAOY cells was evaluated with the XF24 analyzer. Cells were deprived of glucose for 1h, then glucose (G) and oligomycin (O) were injected at the indicated times. The graphs are representative of at least three independent experiments carried out in octuplicate. **K, L and M**, Respiratory control of D-458, cells. OCR was measured in real time with the XF24 analyzer. Cells were cultured for 24h in Nx (21% O₂ - **K**), Phx (6% O₂ - **L**) and Hx (1% O₂ - **M**) in the absence (Ctl) or presence of iGP-1 (1 or 100μM). Cells were

deprived of glucose for 1h, then glucose (G), oligomycin (O), DNP, and Rotenone + Antimycin A (R/A) were injected at the indicated times. The graphs are representative of at least three independent experiments carried out in octuplicate. **N**, **O**, and **P**, ECAR in Nx (21% O₂ - **N**), Phx (6% O₂ - **O**) and Hx (1% O₂ - **P**) in the absence (Ctl) or presence of iGP-1 (1 or 100 μM) for 24 h of D-458 cells was evaluated with the XF24 analyzer. Cells were deprived of glucose for 1 h, then glucose (G) and oligomycin (O) were injected at the indicated times. The graphs are representative of at least three independent experiments carried out in octuplicate.

The 2-way ANOVA is representative of at least three independent experiments.

Supplemental Figure 4: **A**, HDMB03 and D-458 cells were seeded at the same density and incubated in 1% O₂ for 72h in the absence (Ctl) or presence of NAC, iGP-1 (100μM) or NAC + iGP-1. Cell viability was measured using an ADAM cell counter.

Supplemental Figure 5: **A** and **C**, DAOY (**A**) and D-458 (**C**) cells were seeded at the same density and incubated in 21-, 6- and 1- % O₂ for 24-, and 72- h in the absence (Ctl) or presence of Phenf (100μM) or Rotenone (2.5μM). Cell proliferation was measured using an ADAM cell counter. **B** and **D**, DAOY (**B**) and D-458 (**D**) cells were seeded at the same density and incubated in 21-, 6- and 1- % O₂ for 24-, and 72- h in the absence (Ctl) or presence of Phenf (100μM) or Rotenone (2.5μM). Cell viability was measured using an ADAM cell counter. **E**, **F** and **G**, Respiratory control of DAOY cells. OCR was measured in real time with the XF24 analyzer. Cells were cultured for 24h in Nx (21% O₂ - **E**), Phx (6% O₂ - **F**) and Hx (1% O₂ - **G**) in the absence (Ctl) or presence of Phenf (3 or 100μM) or Rotenone (2.5μM). Cells were deprived of glucose for 1h, then glucose (G), oligomycin (O), DNP, and Rotenone + Antimycin A (R/A) were injected at the indicated times. The graphs are representative of at least three independent experiments carried out in octuplicate. **H**, **I**, and **J**, ECAR in Nx (21% O₂ - **H**), Phx (6% O₂ - **I**) and Hx (1% O₂ - **J**) in the absence (Ctl) or presence of Phenf (3 or 100μM) or Rotenone (2.5μM) for 24 h of DAOY cells was evaluated with the XF24 analyzer. Cells were deprived of glucose for 1 h, then glucose (G) and oligomycin (O) were injected at the indicated times. The graphs are representative of at least three independent experiments carried out in octuplicate. **K**, **L** and **M**, Respiratory control of D-458 cells. OCR was measured in real time with the XF24 analyzer. Cells were cultured for 24h in Nx (21% O₂ - **K**), Phx (6% O₂ - **L**) and Hx (1% O₂ - **M**) in the absence (Ctl) or presence of Phenf (3 or 100μM) or Rotenone (2.5μM). Cells were deprived of glucose for 1h, then glucose (G), oligomycin (O), FCCP (F), and

Rotenone + Antimycin A (R/A) were injected at the indicated times. The graphs are representative of at least three independent experiments carried out in octuplicate. **N**, **O**, and **P**, ECAR in Nx (21% O₂ - **N**), Phx (6% O₂ - **O**) and Hx (1% O₂ - **P**) in the absence (Ctl) or presence of Phenf (3 or 100μM) or Rotenone (2.5μM) for 24h of D-458 cells was evaluated with the XF24 analyzer. Cells were deprived of glucose for 1h, then glucose (G) and oligomycin (O) were injected at the indicated times. The graphs are representative of at least three independent experiments carried out in octuplicate.

The 2-way ANOVA is representative of at least three independent experiments.

Supplemental Figure 6: **A** and **C**, DAOY (**A**) and D-458 (**C**) cells were seeded at the same density and incubated in 21-, 6- and 1- % O₂ for 24-, and 72- h in the absence (Ctl) or presence of iGP-1 (100μM), Phenf (100μM) or Phenf+iGP-1. Cell proliferation was measured using an ADAM cell counter. **B** and **D**, DAOY (**B**) and D-458 (**D**) cells were seeded at the same density and incubated in 21-, 6- and 1- % O₂ for 24-, and 72- h in the absence (Ctl) or presence of iGP-1 (100μM), Phenf (100μM) or Phenf+iGP-1. Cell viability was measured using an ADAM cell counter. **E** and **G**, Respiratory control of DAOY (**E**) and D-458 (**G**) cells. OCR was measured in real time with the XF24 analyzer. Cells were cultured for 24 h in Hx (1% O₂) in the absence (Ctl) or presence of Phenf (100μM) + iGP-1 (100μM). Cells were deprived of glucose for 1h, then glucose (G), oligomycin (O), DNP, and Rotenone + Antimycin A (R/A) were injected at the indicated times. The graphs are representative of at least three independent experiments carried out in octuplicate. **F** and **H**, ECAR in Hx in the absence (Ctl) or presence of Phenf (100μM) + iGP-1 (100μM) for 24h of DAOY (**F**) and D-458 (**H**) cells was evaluated with the XF24 analyzer. Cells were deprived of glucose for 1h, then glucose (G) and oligomycin (O) were injected at the indicated times. The graphs are representative of at least three independent experiments carried out in octuplicate.

The 2-way ANOVA is representative of at least three independent experiments.

Supplemental Figure 7: **A** and **C**, DAOY (**A**) and D-458 (**C**) cells were seeded at the same density and incubated in 1% O₂ for 72h in the absence (Ctl) or presence of AOAA (0.3 and 1mM), iGP-1 (100μM) or AOAA+iGP-1. Cell proliferation was measured using an ADAM cell counter. **B** and **D**, DAOY (**B**) and D-458 (**D**) cells were seeded at the same density and incubated in 1% O₂ for 72h in the absence (Ctl) or presence of AOAA (0.3 and 1mM), iGP-1 (100μM) or AOAA+iGP-1. Cell viability was measured using an ADAM cell counter. **E** and

G, Respiratory control of DAOY (**E**) and D-458 (**G**) cells. OCR was measured in real time with the XF24 analyzer. Cells were cultured for 24 h in Hx (1% O₂) in the absence (Ctl) or presence of AOAA (1mM) or AOAA+iGP-1 (100μM). Cells were deprived of glucose for 1h, then glucose (G), oligomycin (O), FCCP (F), and Rotenone + Antimycin A (R/A) were injected at the indicated times. The graphs are representative of at least three independent experiments carried out in octuplicate. **F** and **H**, ECAR in Hx (1% O₂) in the absence (Ctl) or presence of AOAA (1mM) or AOAA+iGP-1 (100μM) for 24h of DAOY (**F**) and D-458 (**H**) cells was evaluated with the XF24 analyzer. Cells were deprived of glucose for 1h, then glucose (G) and oligomycin (O) were injected at the indicated times. The graphs are representative of at least three independent experiments carried out in octuplicate.

The 2-way ANOVA is representative of at least three independent experiments.

Supplemental Figure 7: **A** and **B**, DAOY and D-458 cells were seeded at the same density and incubated in Nx, Phx and Hx for 72h in the absence (Ctl) or presence of GNE-140 (5μM). Cell proliferation (**A**) and viability (**B**) were measured using an ADAM cell counter. **C** and **D**, ECAR in Hx (1% O₂) in the absence (Ctl) or presence of GNE-140 (5μM) for 24h of DAOY (**C**) and D-458 (**D**) cells was evaluated with the XF24 analyzer. Cells were deprived of glucose for 1h, then glucose (G) and oligomycin (O) were injected at the indicated times. The graphs are representative of at least three independent experiments carried out in octuplicate. **E** and **F**, DAOY and D-458 cells were seeded at the same density and incubated in Nx, Phx and Hx for 72h in the absence (Ctl) or presence of iGP-1 (100μM) + AOAA (1mM) + GNE-140 (5μM). Cell proliferation (**E**) and viability (**F**) were measured using an ADAM cell counter. **G** and **H**, DAOY (**G**) and D-458 (**H**) cells were seeded at the same density and incubated in Hx for 72h in the absence (Ctl) or presence of iGP-1 (100μM) + Phenf (100μM) or iGP-1 (100μM) + Phenf (100μM) + GNE-140 (5μM). Viability was measured using an ADAM cell counter. **I**, Clonogenic assay of DAOY and D-458 cells. Cell lines were seeded at the same density and incubated in Hx 1% O₂ for 7 days in the absence (Ctl) or presence of iGP-1 (100μM) + AOAA (1mM) + GNE-140 (5μM) or iGP-1 (100μM) + Phenf (100μM) + GNE-140.

The 2-way ANOVA is representative of at least three independent experiments.

References

1. Pollak M. Metformin and other biguanides in oncology: advancing the research agenda. *Cancer prevention research (Philadelphia, Pa)*. 2010;3:1060–5.
2. Wheaton WW, Weinberg SE, Hamanaka RB, Soberanes S, Sullivan LB, Anso E, et al. Metformin inhibits mitochondrial complex I of cancer cells to reduce tumorigenesis. *eLife*. 2014;3:e02242.
3. Hung YP, Albeck JG, Tantama M, Yellen G. Imaging cytosolic NADH-NAD(+) redox state with a genetically encoded fluorescent biosensor. *Cell metabolism*. 2011;14:545–54.
4. Gui DY, Sullivan LB, Luengo A, Hosios AM, Bush LN, Gitego N, et al. Environment Dictates Dependence on Mitochondrial Complex I for NAD⁺ and Aspartate Production and Determines Cancer Cell Sensitivity to Metformin. *Cell metabolism*. 2016;24:716–27.
5. Sullivan LB, Gui DY, Hosios AM, Bush LN, Freinkman E, vander Heiden MG. Supporting Aspartate Biosynthesis Is an Essential Function of Respiration in Proliferating Cells. *Cell*. 2015;162:552–63.
6. Titov D v, Cracan V, Goodman RP, Peng J, Grabarek Z, Mootha VK. Complementation of mitochondrial electron transport chain by manipulation of the NAD⁺/NADH ratio. *Science (New York, NY)*. 2016;352:231–5.
7. di Magno L, Manni S, di Pastena F, Coni S, Macone A, Cairoli S, et al. Phenformin Inhibits Hedgehog-Dependent Tumor Growth through a Complex I-Independent Redox/Corepressor Module. *Cell reports*. 2020;30:1735-1752.e7.
8. Tech K, Gershon TR. Energy metabolism in neurodevelopment and medulloblastoma. *Translational pediatrics*. 2015;4:12–9.
9. Esen E, Chen J, Karner CM, Okunade AL, Patterson BW, Long F. WNT-LRP5 signaling induces Warburg effect through mTORC2 activation during osteoblast differentiation. *Cell metabolism*. 2013;17:745–55.
10. Pate KT, Stringari C, Sprowl-Tanio S, Wang K, TeSlaa T, Hoverter NP, et al. Wnt signaling directs a metabolic program of glycolysis and angiogenesis in colon cancer. *The EMBO journal*. 2014;33:1454–73.
11. Thompson CB. Wnt meets Warburg: another piece in the puzzle? *The EMBO journal*. 2014;33:1420–2.
12. Kool M, Korshunov A, Remke M, Jones DTW, Schlanstein M, Northcott PA, et al. Molecular subgroups of medulloblastoma: an international meta-analysis of transcriptome, genetic aberrations, and clinical data of WNT, SHH, Group 3, and Group 4 medulloblastomas. *Acta neuropathologica*. 2012;123:473–84.
13. Pöschl J, Stark S, Neumann P, Gröbner S, Kawauchi D, Jones DTW, et al. Genomic and transcriptomic analyses match medulloblastoma mouse models to their human counterparts. *Acta neuropathologica*. 2014;128:123–36.
14. Bernauer C, Man YKS, Chisholm JC, Lepicard EY, Robinson SP, Shipley JM. Hypoxia and its therapeutic possibilities in paediatric cancers. *British journal of cancer*. 2021;124:539–51.
15. Pelletier J, Bellot G, Pouysségur J, Mazure NM. Biochemical titration of glycogen in vitro. *Journal of visualized experiments : JoVE*. 2013;e50465.
16. Pelletier J, Dayan F, Durivault J, Ilc K, Pécou E, Pouysségur J, et al. The asparaginyl hydroxylase factor-inhibiting HIF is essential for tumor growth through suppression of the p53-p21 axis. *Oncogene*. 2012;31:2989–3001.

17. Fabbri L, Dufies M, Lacas-Gervais S, Gardie B, Gad-Lapiteau S, Parola J, et al. Identification of a new aggressive axis driven by ciliogenesis and absence of VDAC1- Δ C in clear cell Renal Cell Carcinoma patients. *Theranostics*. 2020;10:2696–713.
18. Kim J, Tchernyshyov I, Semenza GL, Dang C v. HIF-1-mediated expression of pyruvate dehydrogenase kinase: a metabolic switch required for cellular adaptation to hypoxia. *Cell metabolism*. 2006;3:177–85.
19. di Magno L, Manni S, di Pastena F, Coni S, Macone A, Cairoli S, et al. Phenformin Inhibits Hedgehog-Dependent Tumor Growth through a Complex I-Independent Redox/Corepressor Module. *Cell reports*. 2020;30:1735-1752.e7.

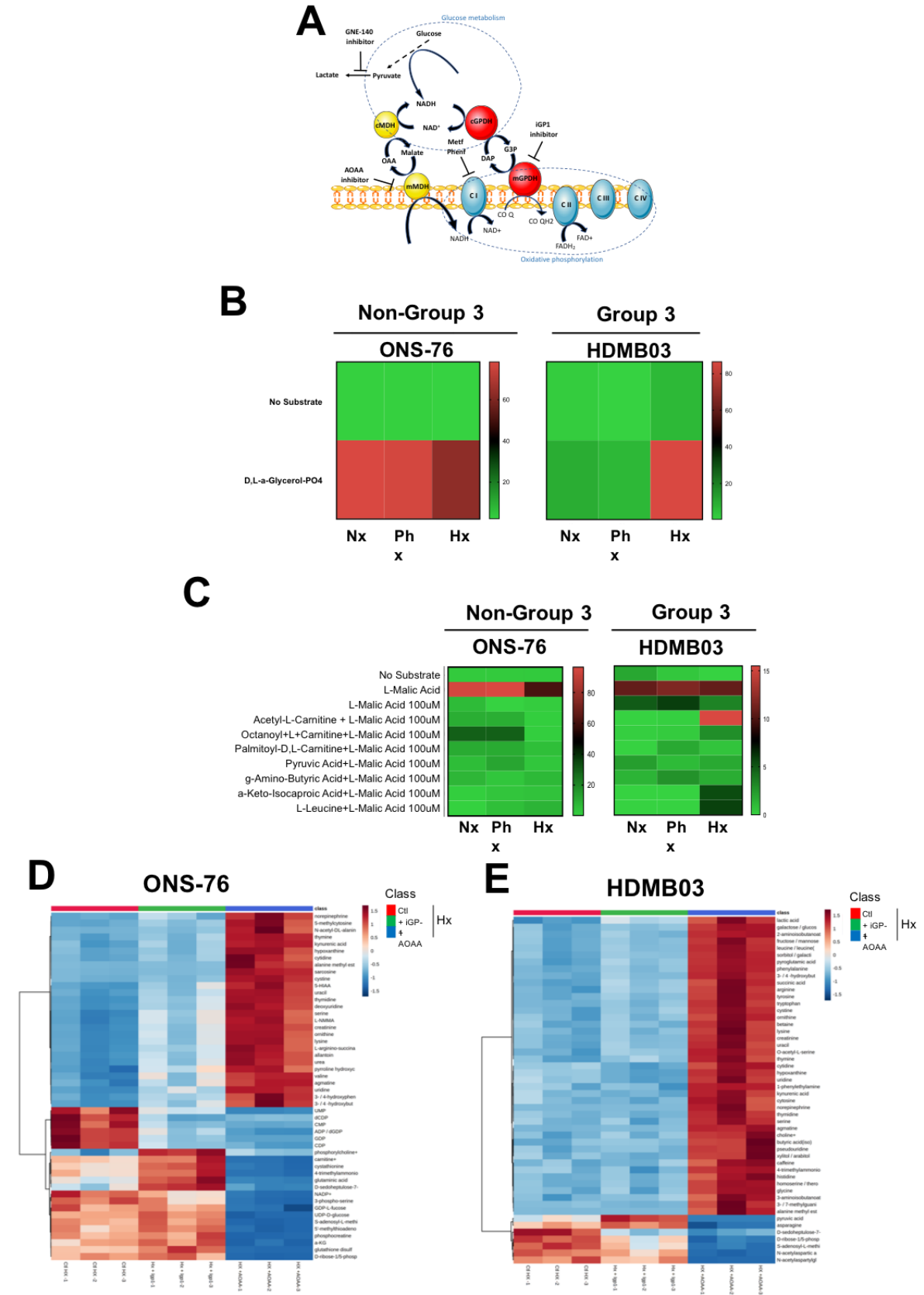


FIGURE 1

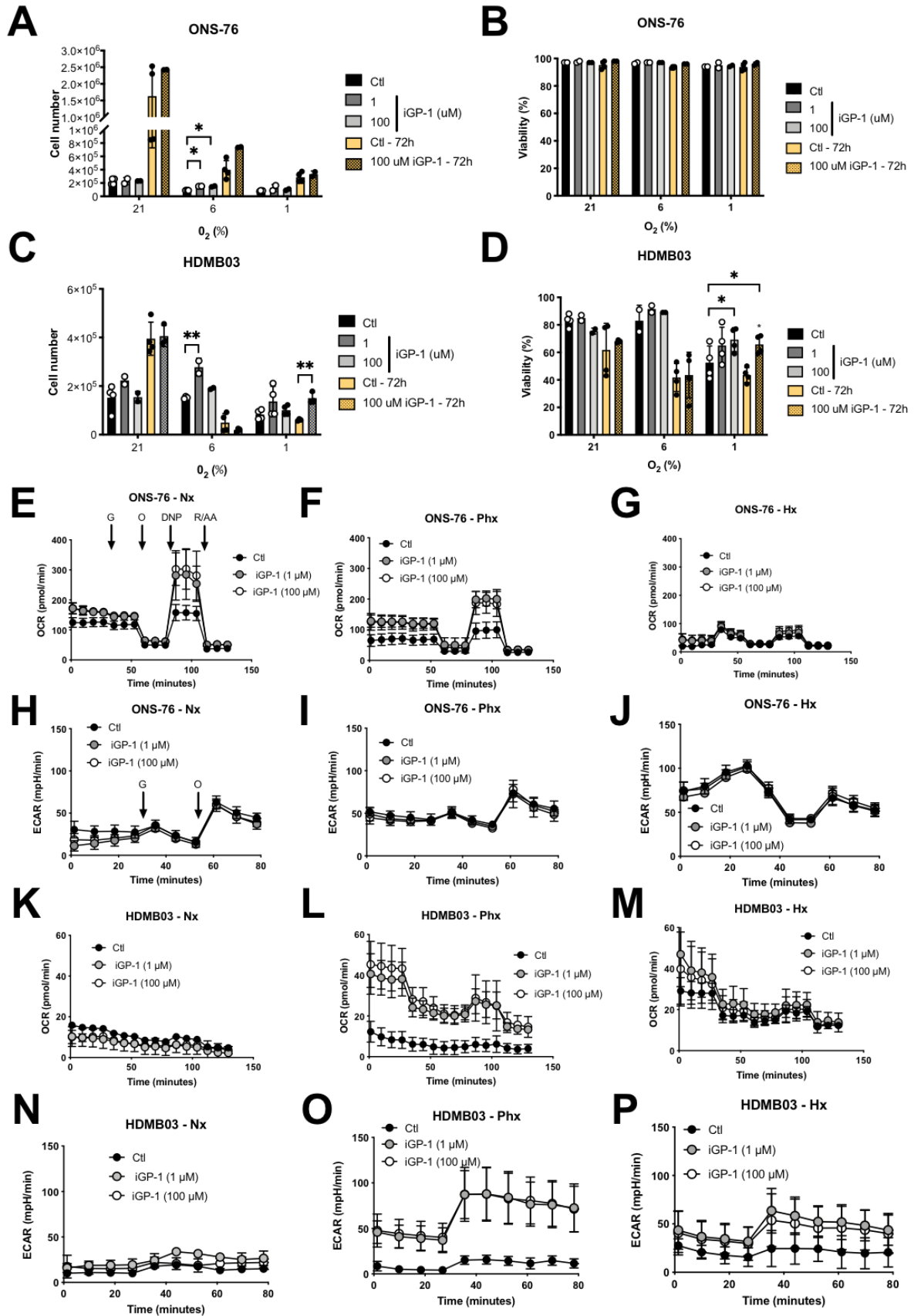


FIGURE 2

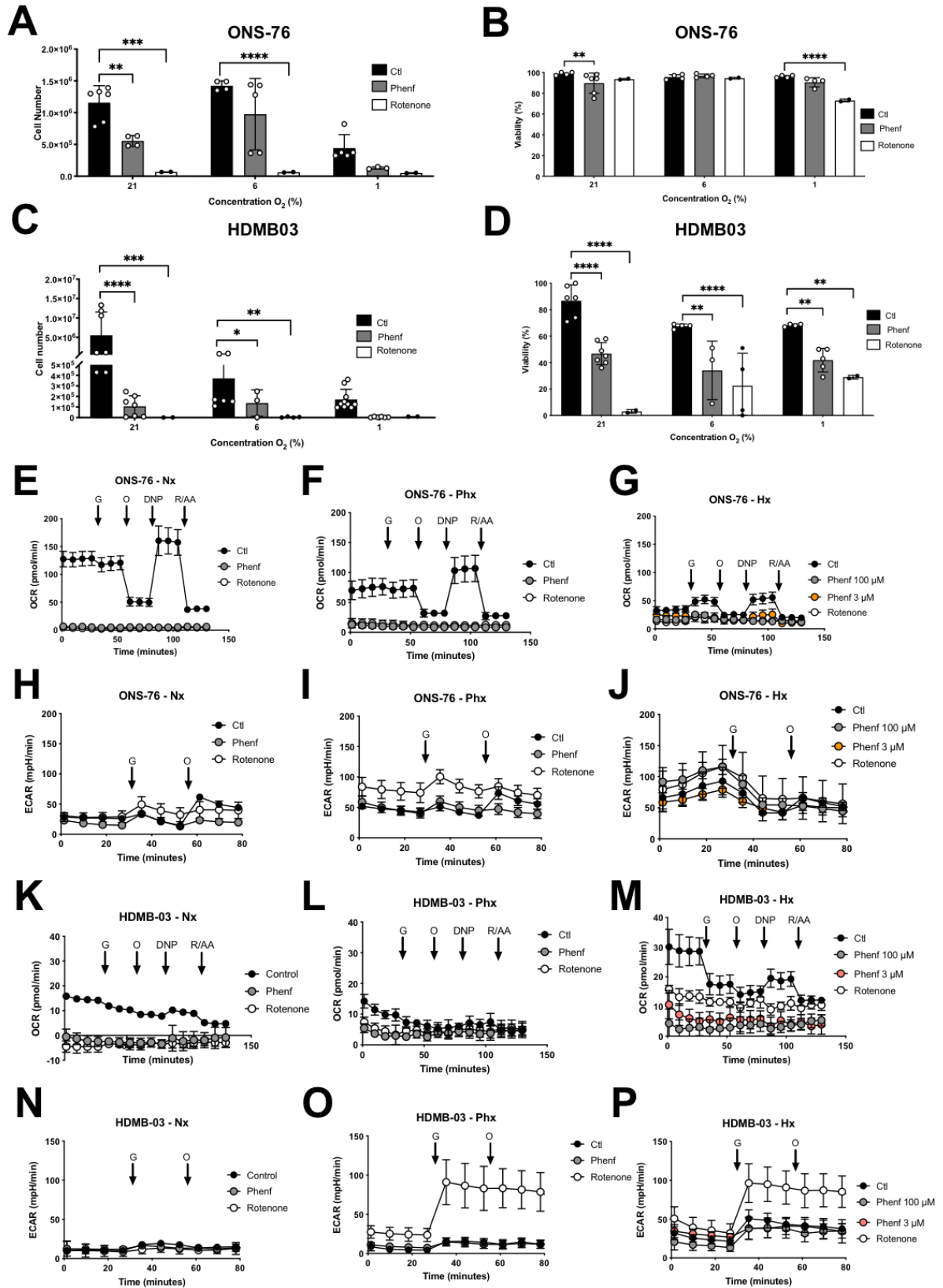


FIGURE 3

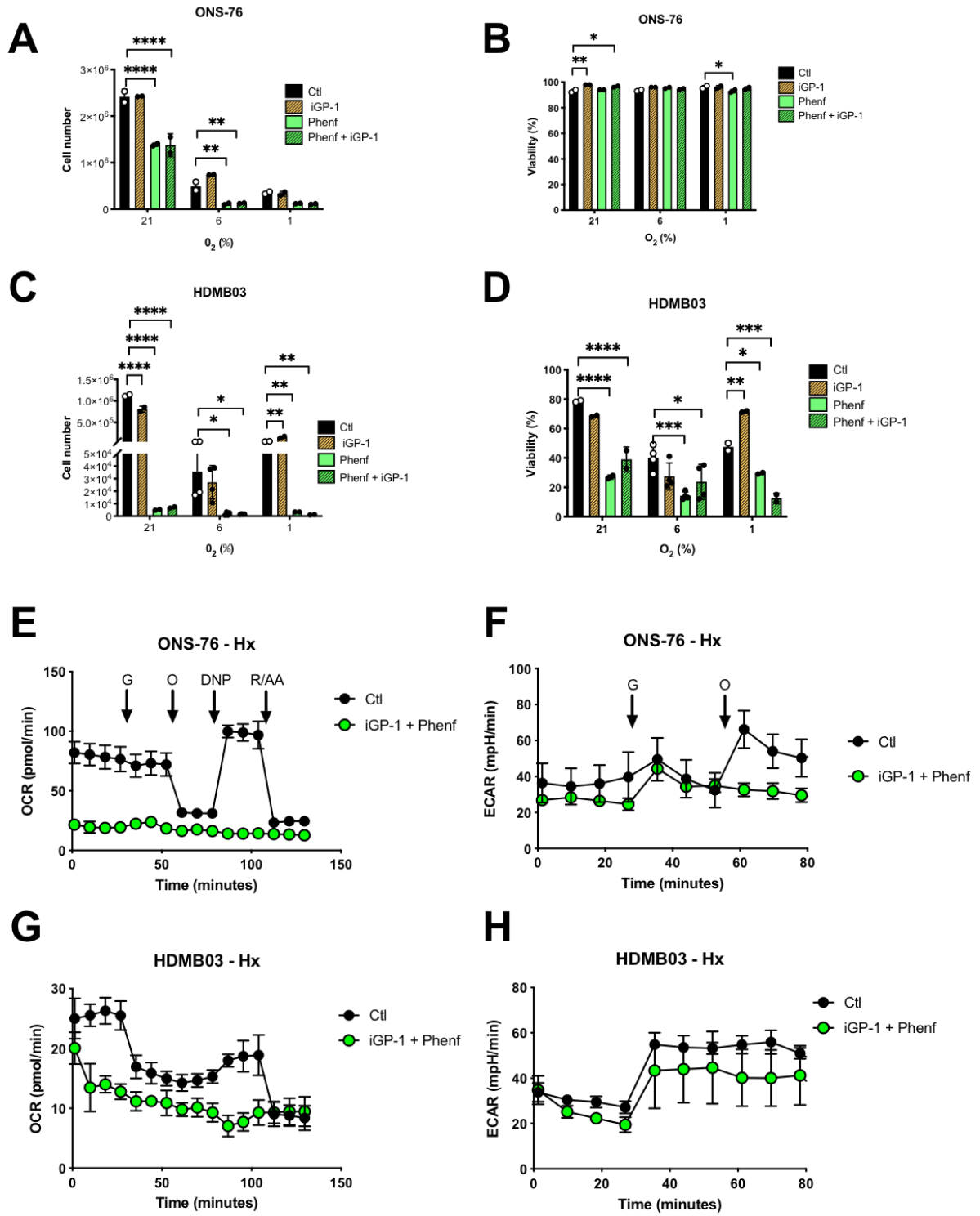


FIGURE 4

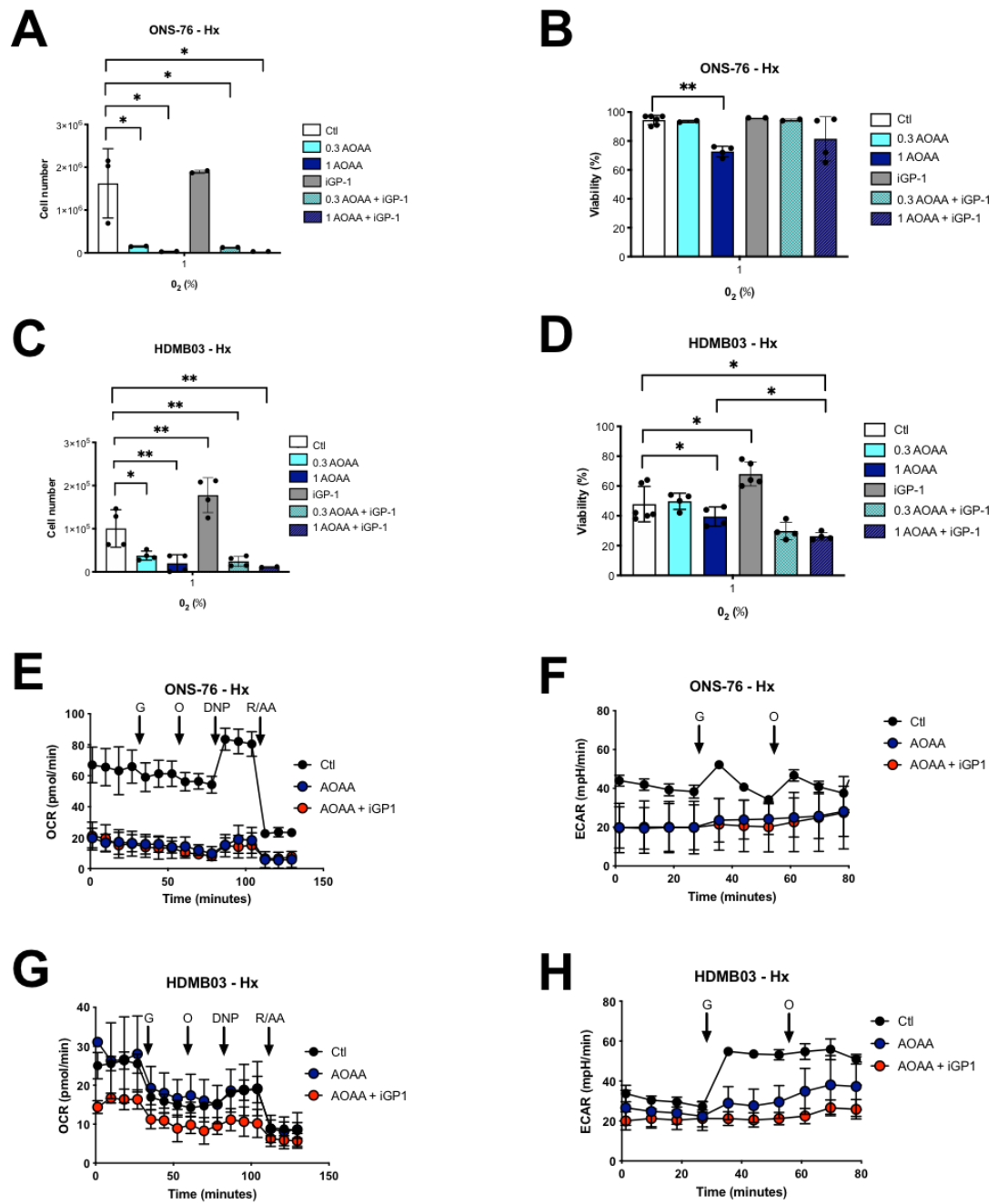


FIGURE 5

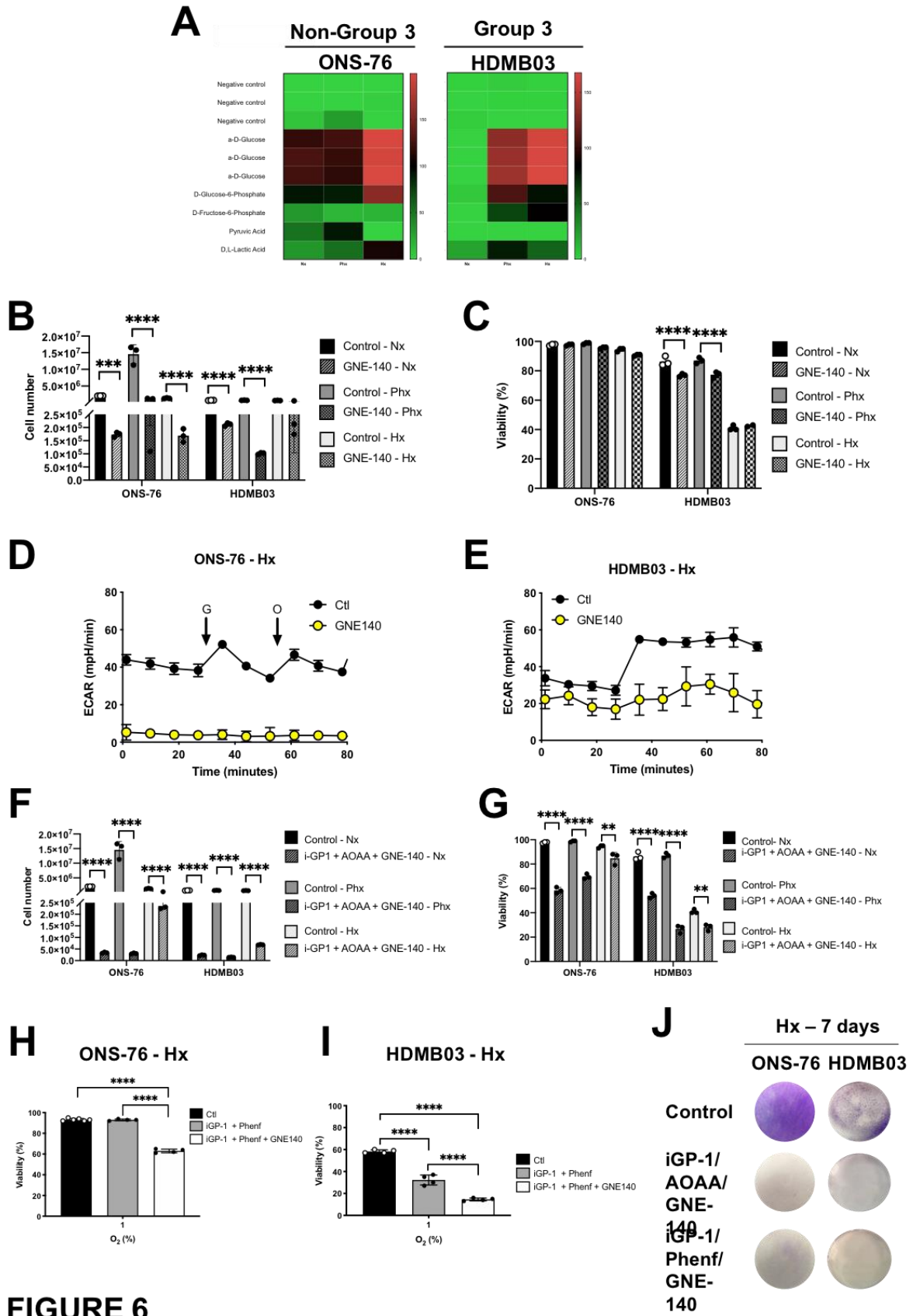
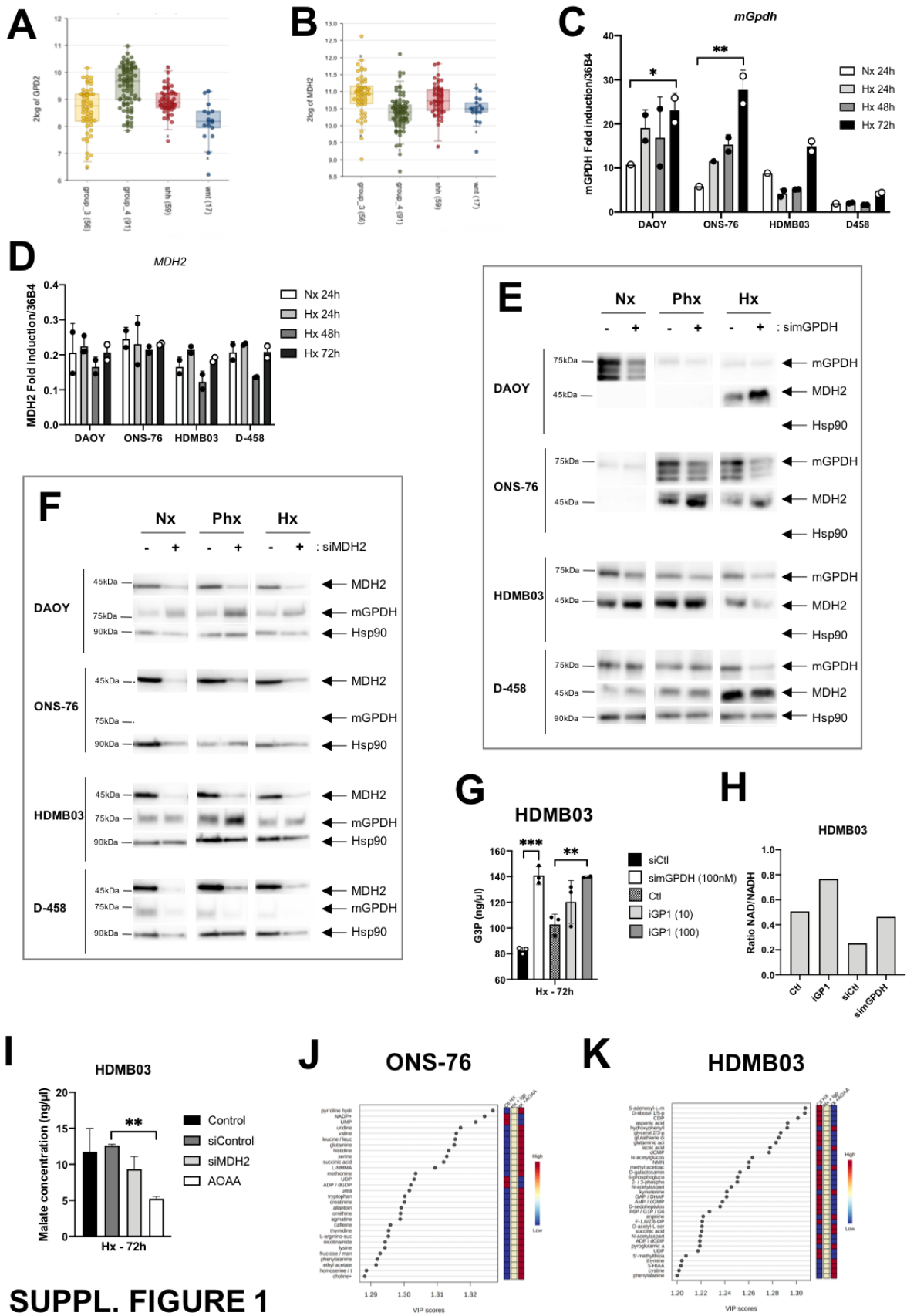
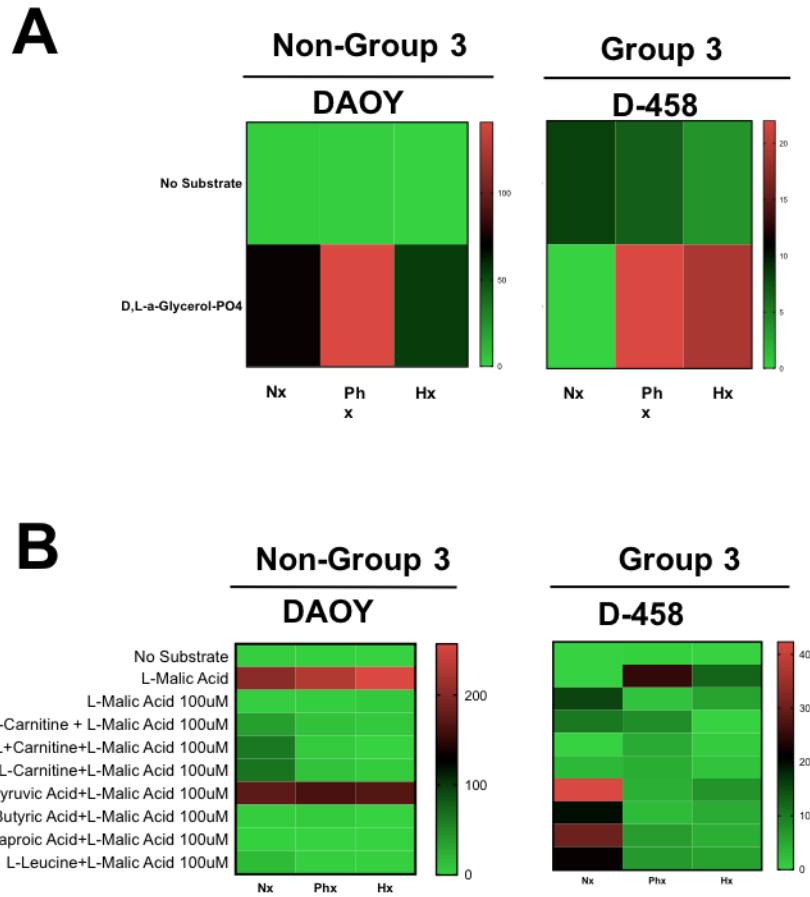
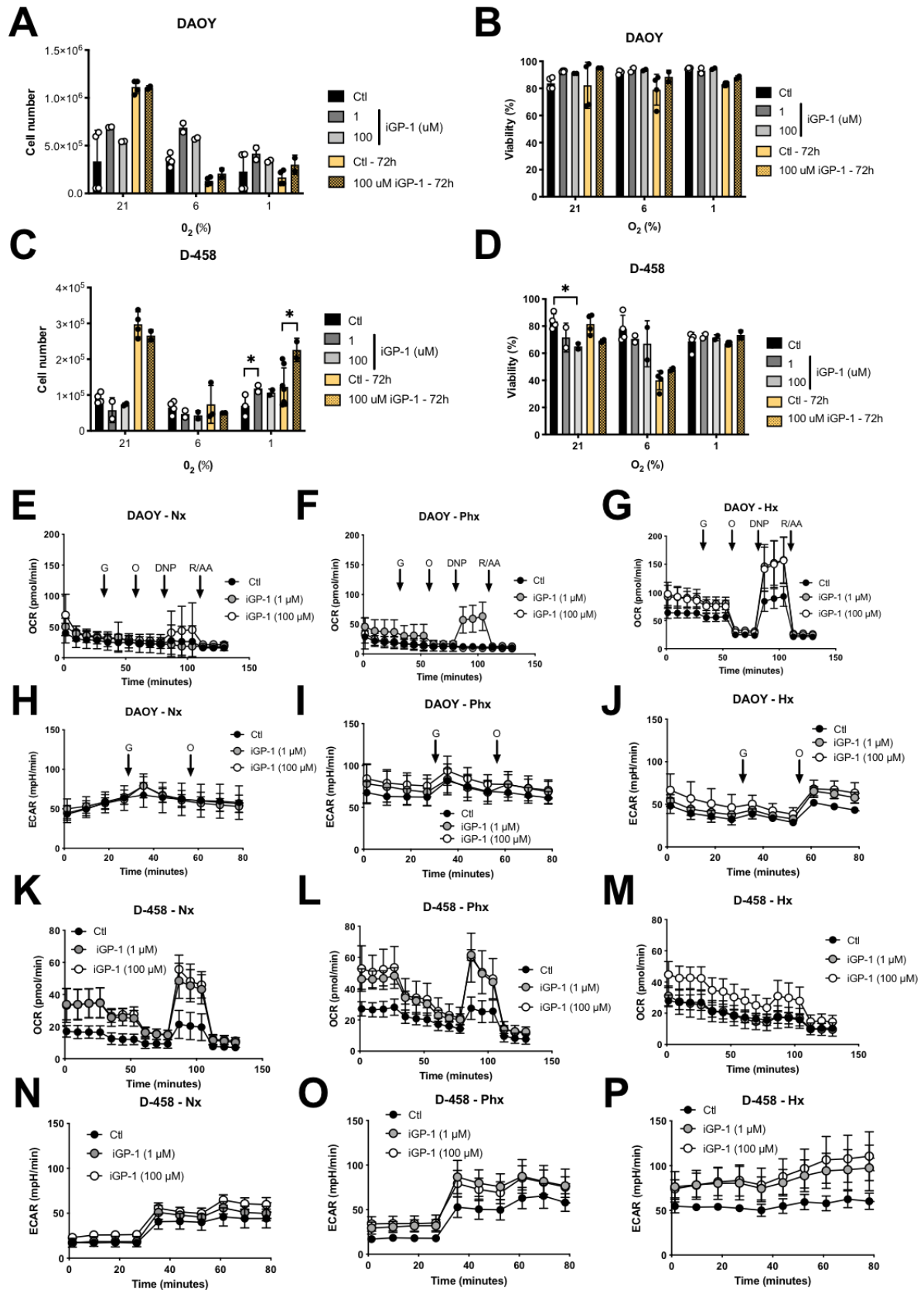


FIGURE 6



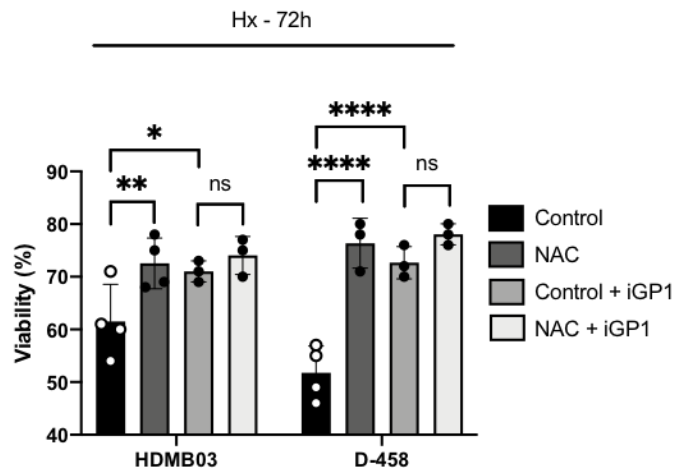


SUPPL. FIGURE 2

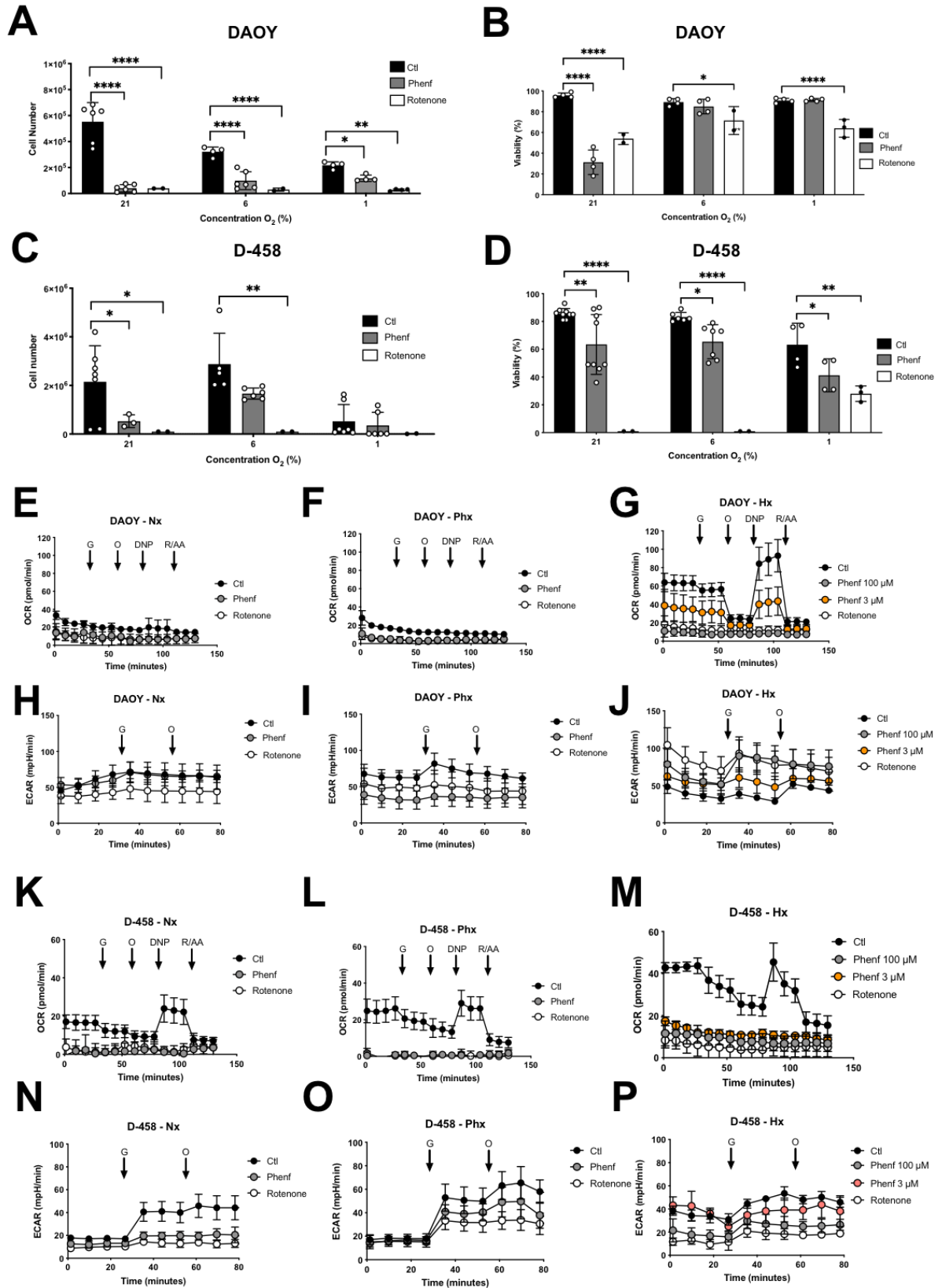


SUPPL. FIGURE 3

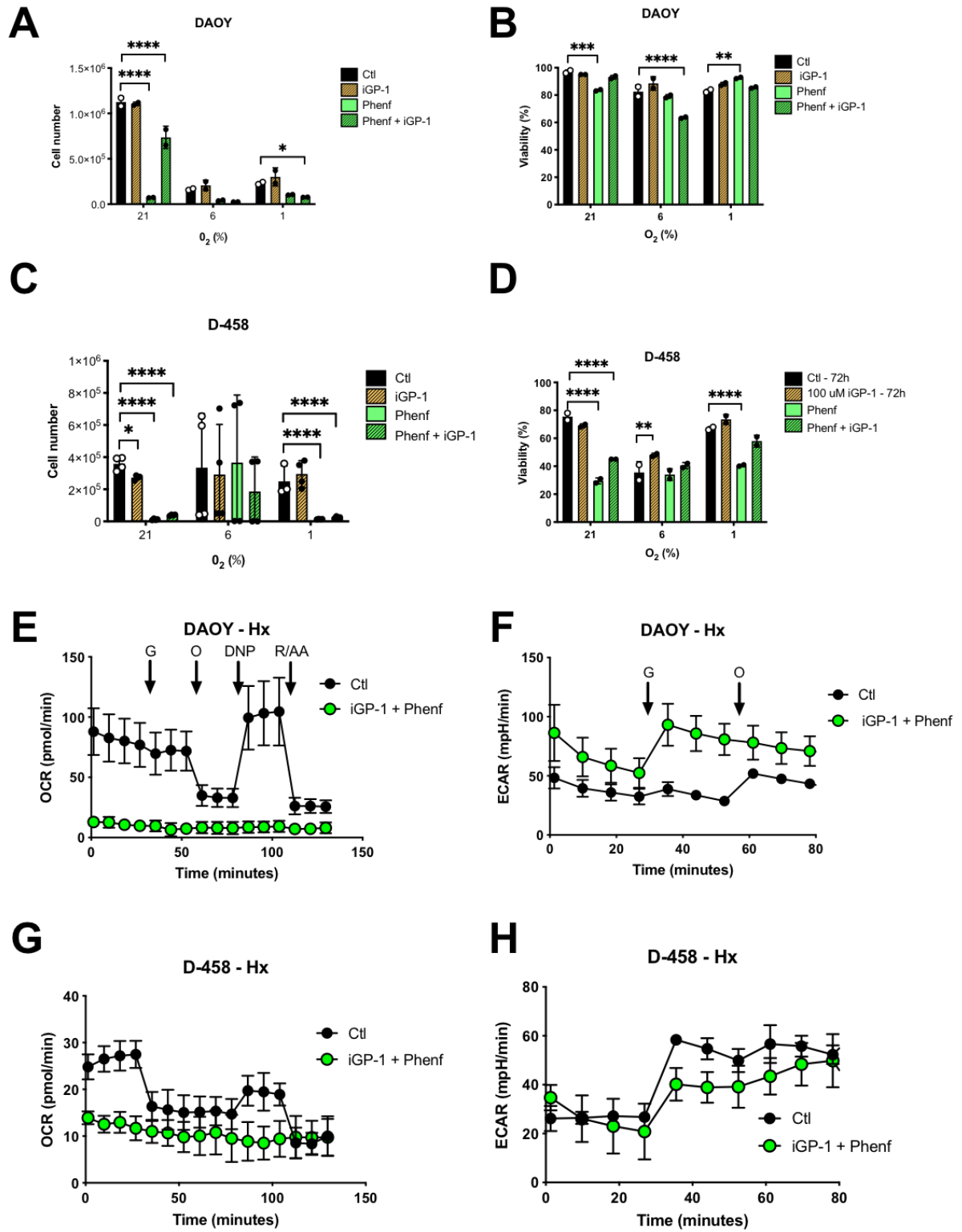
A



SUPPL. FIGURE 4

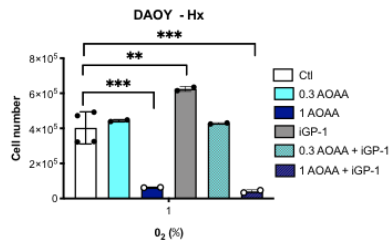


SUPPL. FIGURE 5

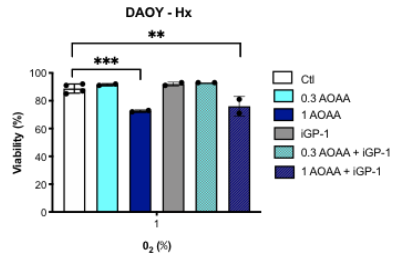


SUPPL. FIGURE 6

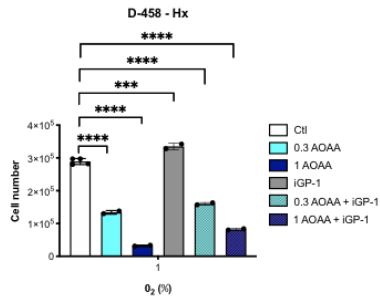
A



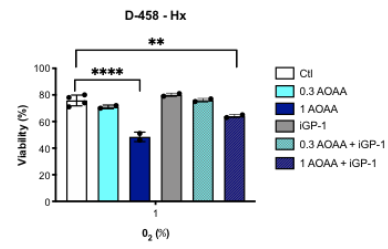
B



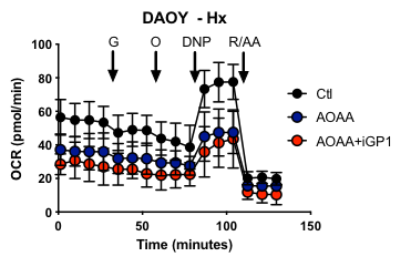
C



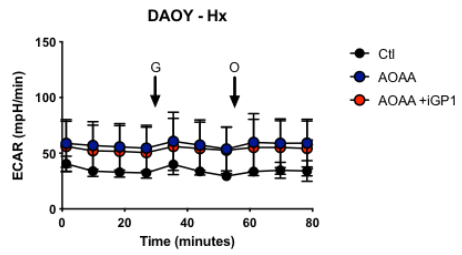
D



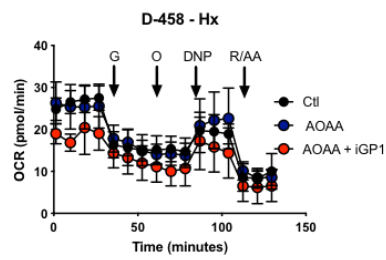
E



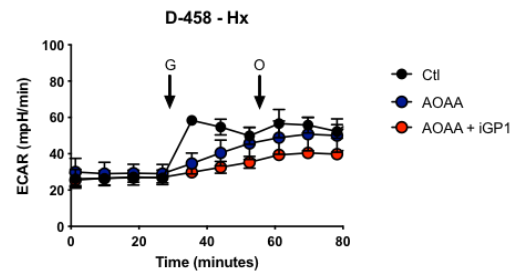
F



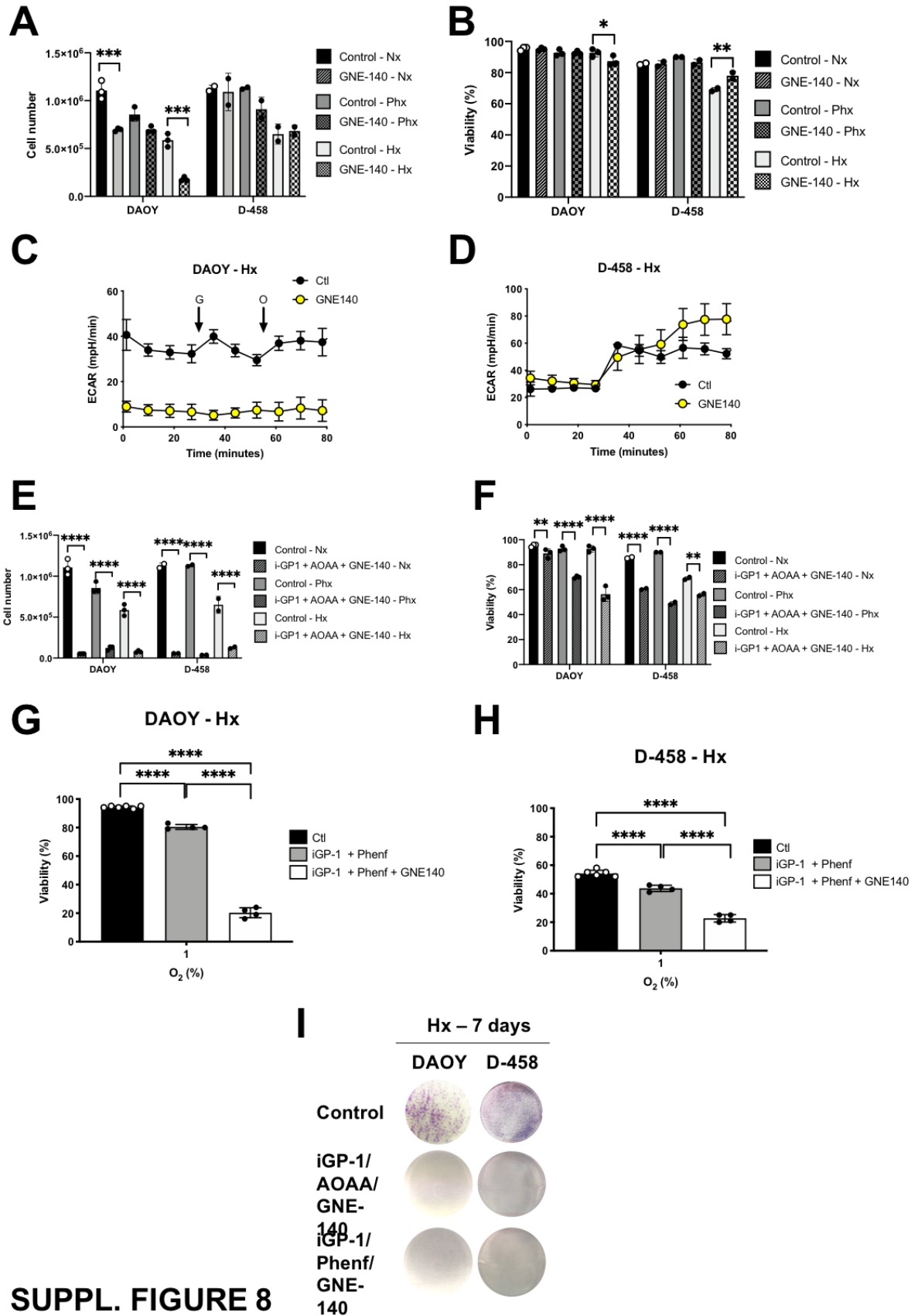
G



H



SUPPL. FIGURE 7



III- Figure 7 en préparation

A la lumière de nos résultats *in vitro* démontrant une diminution nette de la viabilité des cellules du **groupe 3** en associant (Phenformine + AOAA + GNE-140) ou (AOAA + IGP-1 + GNE-140), il semble intéressant de tester nos résultats sur un modèle expérimentale en 3D : les organoïdes. En collaboration avec l'équipe italienne de Tiberi L., nous allons pouvoir tester nos schémas thérapeutiques sur des organoïdes cérébelleux Otx-2/c-MYC hébergeant une signature de méthylation de l'ADN qui se regroupe avec les MB du **groupe 3** (Hubert et al. 2016). Les manipulations seront réalisées dans un premier temps à 21% d'oxygène, partant du principe que la structure en 3D de l'organoïde possède déjà un gradient en oxygène intrinsèque. Il a déjà été démontré dans la littérature l'existence d'un gradient de stabilisation de HIF-1 α ainsi que de ses gènes cibles dès 3 à 4 couches de cellules (Dayan et al. 2009). Ce gradient a été mis en évidence dans un modèle d'organoïdes de glioblastome, avec un marquage CAIX en immunofluorescence (Hubert et al. 2016).

Le taux de prolifération cellulaire (marquage Ki67) des organoïdes sera comparés en fonction du schéma thérapeutique : (i) Phenformine seul, (ii) Phenformine + AOAA + GNE-140, (iii) AOAA+ IGP-1+ GNE 140. Dans un second temps, nous reproduirons les mêmes manipulations mais à des niveaux d'oxygénation différents, à 6% puis à 1% d'oxygène afin de se rapprocher des conditions physiologiques cérébrales.

IV- Conclusions et Discussion de l'Article 2

Nous avons démontré dans cette étude l'importance des voies métaboliques régénérant le NAD⁺ cytosolique (navettes Malate/aspartate et Glycérol-3-phosphate) dans la croissance tumorale et la survie des cellules de MB. Ces voies métaboliques s'avèrent être un véritable talon d'Achille pour les cellules de MB du **groupe 3**, groupe ayant aujourd'hui le plus fort taux de métastases ainsi que la mortalité la plus élevée. Il existe une véritable variabilité métabolique entre les cellules du **groupe 3** et les cellules du **groupe non-3** en fonction du pourcentage d'oxygénation (21% vs 6% vs 1%). (i) Le **groupe 3** s'avère être plus sensible à la Phenformine et ce d'autant plus que les conditions d'hypoxie deviennent sévères. (ii) Il existe une variabilité de l'utilisation des navettes en fonction des groupes de MB, et du pourcentage d'oxygène. (iii) L'utilisation concomitante d'inhibiteurs spécifiques des deux navettes a clairement démontré une grande

capacité à diminuer la prolifération cellulaire et à induire une plus grande mortalité dans le **groupe 3** par rapport au **groupe non-3**.

Ces résultats soulèvent plusieurs questions auxquelles nous apportons ici des pistes de réponses.

A- L'importance des conditions expérimentales

Nous avons, dans ce travail, choisi d'aborder le problème du médulloblastome sous un angle métabolique et dans des conditions expérimentales mimant un environnement pauvre en oxygène, afin de se rapprocher le plus de l'environnement tumoral *in vivo*. Le fait d'avoir réalisé les expériences à trois niveaux d'oxygénation différent (21%, 6% et 1% O₂) est une des caractéristiques majeures de notre travail. En effet, la grande majorité des recherches *in vitro* sont réalisées à 21 % d'O₂. Bien qu'il soit de plus en plus reconnu que les études réalisées *in vitro* ne constituent pas un modèle parfait pour l'environnement *in vivo* (Hellwig, Heinrich, and Biber 2013)(Neiva, Malva, and Valero 2014)(Ransohoff 2016), peu ont tenté de combler l'écart afin de modéliser plus précisément les fonctions physiologiques *in vivo* dans un environnement *in vitro*. Une technique récente qui utilise la microscopie à phosphorescence à deux photons fournit des valeurs détaillées de la pO₂ absolue dans différents tissus (Sakadzić et al. 2010)(K. Xu et al. 2017). Cette technique a révélé la grande hétérogénéité de l'oxygénation des tissus cérébraux par région et a permis aux chercheurs de visualiser les différences dramatiques entre la pO₂ dans le cerveau par rapport à la pO₂ dans l'atmosphère (K. Xu et al. 2017). Nos résultats vont dans ce sens en montrant que le métabolisme des cellules cancéreuse de MB est drastiquement différent selon les conditions d'oxygénation, avec une meilleure phosphorylation oxydative pour les HDMB-03 en condition d'hypoxie (1% O₂) comparativement aux autres conditions (6% et 21% O₂). A l'inverse, les cellules du **groupe non-3** ont un meilleur profil métabolique en condition de normoxie (21% O₂) ou de physioxie (6% O₂). Il est important de noter que très peu d'attention a été accordée à l'effet de la tension d'oxygène sur l'action des médicaments (Bordt 2018). Pourtant l'augmentation ou la diminution de la tension d'oxygène pourrait entraîner des changements conformationnels des récepteurs, affectant ainsi la capacité d'un médicament à se lier à certains récepteurs. Ou encore, simplement modifier la cinétique de la liaison du médicament. Il se peut que l'absorption mitochondriale des médicaments soit également altérée en fonction des conditions d'oxygénation. D'ailleurs, nous mettons en évidence dans notre étude que l'effet de la Phenformine sur la viabilité des cellules du **groupe 3** est différent en normoxie et en hypoxie, quand on compare au contrôle dans chaque condition d'oxygénation. Les études futures devraient se concentrer non seulement sur la capacité des

médicaments à se lier correctement à leurs récepteurs à différentes tensions d'oxygène, mais également sur les modifications transcriptomiques et protéomiques en aval induites par la liaison des médicaments.

B- Quelle navette est la plus importante dans le MB ?

Concernant la navette malate/aspartate, nos travaux ont montré une sensibilité équivalente des différents groupes de MB lors de l'inhibition de cette navette par l'AOAA, avec un effet sur la prolifération mais également sur la mortalité, suggérant que cette navette semble primordiale pour l'ensemble des groupes de MB. *A contrario*, l'effet de l'inhibition de la navette glycérol-3-phosphate par l'iGP-1 ne montre aucun effet sur la mortalité dans le **groupe non-3** et un effet plutôt bénéfique avec une meilleure viabilité dans le **groupe-3**. Ces résultats mettent en lumière l'hétérogénéité métabolique entre les différents groupes de MB et soulignent le rôle majeur de la navette malate/aspartate.

Nos travaux suggèrent également un effet compensateur de l'expression de mGPDH sur MDH2 et *vice versa*. En effet, l'invalidation de mGPDH entraîne une augmentation d'expression de MDH2, encore plus marqué dans le **groupe 3**, suggérant un lien étroit entre les deux navettes. Ce rôle substituable des deux navettes a été décrit en 2009, par Wibom *et al.* qui ont rapporté le cas d'un patient présentant un défaut inné de l'AGC1, l'isoforme du transporteur aspartate-glutamate principalement active dans le cerveau et les muscles (Wibom et al. 2009). Le patient présentait des troubles du développement neurologique sévère. La concentration de glycérol-3-phosphate dans le sang était élevée et les auteurs pensent que le cycle de glycérol-3-phosphate peut compenser en partie le dysfonctionnement de la navette malate/aspartate au niveau cérébral. Cette compensation a également été démontrée dans un modèle animal reproduisant un déficit en citrine (Saheki et al. 2011). Le phénotype pathogène a été induit par le double knock-out de la citrine et du gène *GPD2* (mGPDH) démontrant que la régulation à la hausse de l'activité de navette du glycérol-3-phosphate était suffisante pour maintenir le transport des équivalents NADH du cytosol aux mitochondries en présence d'une navette malate/aspartate déficiente (Saheki et al. 2007).

Nos résultats traduisent la plasticité métabolique, grâce à laquelle les cellules de MB peuvent engager des voies alternatives pour répondre à leurs besoins spécifiques, et de manière différente en fonction du groupe de MB, en positionnant la navette malate/aspartate comme voie principale de régénération du NAD⁺ dans le MB. Mais cela reste encore à confirmer *in*

in vivo car l'hétérogénéité intra-tumorale du MB reste importante et peut modifier ces caractéristiques métaboliques. Il serait également primordial d'évaluer l'expression et le rôle de ces navettes dans le tissu cérébelleux sain, car utiliser ces navettes comme cibles thérapeutiques potentielles prend encore plus de sens si leur expression est plus élevée dans le tissu tumoral comparativement au tissu sain.

C- L'effet cumulatif des inhibiteurs de navettes

Nous avons mis en évidence dans ce travail une absence de régulation en hypoxie de l'expression de la mGPDH et de la MDH2 dans le **groupe 3**, le rendant de ce fait potentiellement plus sensible aux inhibiteurs de ces deux navettes. Étrangement, l'utilisation isolée d'iGP-1, l'inhibiteur spécifique de la navette glycérol-3-phosphate, n'a pas montré d'effet sur la mortalité cellulaire, avec au contraire une meilleure prolifération des cellules dans les différents groupes de MB. Ce résultat s'explique probablement par une diminution de production de ROS lors du traitement par l'iGP-1, car on sait aujourd'hui que la mGPDH peut être une source de ROS potentiellement importante même dans les tissus typiquement aérobies avec un contenu enzymatique négligeable (Mráček et al. 2014)(Mráček et al. 2009).

L'évaluation d'agents anticancéreux métaboliquement ciblés a révélé que, dans de nombreux cas, la réponse au traitement était moins robuste que prévue, à la fois dans les modèles animaux et en clinique, et que le co-ciblage par différents traitements de la phosphorylation oxydative d'une part et des voies métaboliques compensatrices d'autre part, pourrait améliorer l'efficacité thérapeutique. C'est ce que nous mettons en lumière ici avec un effet cumulatif de la Phenformine associée à l'iGP-1 sur la mortalité cellulaire des cellules du **groupe 3** comparativement au **groupe non-3**. Ceci pourrait s'expliquer par le fait que le **groupe non-3**, exprimant HIF-1, pourrait s'adapter plus facilement en induisant une surexpression de la navette malate/aspartate en réponse à l'inhibition de la navette glycérol-3-phosphate. Ce que fait beaucoup plus difficilement le **groupe 3** ayant un HIF-1 déficient ou inexistant.

L'action de la Phenformine sur la viabilité cellulaire est beaucoup plus marquée dans le **groupe 3** comparativement au **groupe non-3**. Probablement que les mécanismes compensatoires mis en jeu suite au traitement par la Phenformine ne sont pas identiques dans les groupes de MB, et sont différents d'une simple activation de la glycolyse. D'ailleurs, dans notre travail, nous ne mettons pas en évidence d'augmentation de la glycolyse (cf ECAR en Seahorse) secondairement à l'utilisation de la Phenformine. Avec le facteur de transcription HIF-1, MYC

induit de manière coopérative un programme transcriptionnel pour l'adaptation hypoxique (Dang, Le, and Gao 2009). MYC régule l'expression des gènes soit directement, comme les gènes glycolytiques, soit indirectement, comme la répression des microARN miR-23a/b pour augmenter l'expression de la protéine glutaminase (GLS) et le métabolisme de la glutamine. Le **groupe 3** est connu pour avoir comme caractéristique une surexpression de Myc. La littérature décrit la metformine comme un inhibiteur de croissance plus efficace lorsque les cellules utilisent la glutamine plutôt que le glucose comme sources de carbone pour la production d'énergie (Javeshghani et al. 2012) et que des niveaux élevés d'expression de MYC sensibilisent les cellules à l'inhibition de la metformine. La sensibilisation du **groupe 3** à la Phenformine pourrait donc s'expliquer par la surexpression de MYC dans ce groupe et par son appétence pour la glutamine. Des études s'intéressant au glioblastome, mettent également en évidence le rôle important de l'utilisation de la glutamine pour expliquer la plasticité métabolique des différents groupes de glioblastome (Oizel et al. 2017).

D- Importance de la Lactate déshydrogénase (LDH) dans le MB ?

La régénération du NAD⁺ cytosolique n'est pas seulement dépendante des navettes malate/aspartate et glycérol-3-phosphate, la lactate déshydrogénase régénère également le NAD⁺ cytosolique au détriment de l'oxydation mitochondriale de pyruvate. Notre travail démontre clairement que la LDH joue un rôle prépondérant dans la pérennisation de la glycolyse dans le **groupe non-3**, avec un effondrement de la capacité glycolytique lors de l'utilisation du GNE-140 (inhibiteur de la LDH). Cependant, malgré cet effondrement glycolytique, nous ne mettons pas en évidence de baisse de la viabilité dans le **groupe non-3**, comparativement au **groupe 3** dont la mortalité augmente sous traitement par le GNE-140. On sait que la LDHA est abondamment exprimée dans les lignées cellulaires MB comparativement au tissu cérébelleux sain, mais à l'intérieur même des groupes, son expression est variable. En effet, les MB du **groupe 3** expriment des taux de LDHA significativement plus élevés que tous les autres sous-groupes de MB. Nos résultats différents sur l'évolution de la capacité glycolytique des cellules face au traitement par le GNE-140 peuvent s'expliquer par un phénomène dose-dépendant. Probablement qu'avec une dose plus importante de GNE-140 dans le **groupe 3** (car plus forte expression de LDHA) nous aurions eu des résultats similaires à ceux du **groupe non-3**. *A contrario*, l'impact sur la mortalité est plus marqué sur le **groupe 3**. Nos résultats corroborent avec la littérature. Une étude récente a mis en évidence un effet plus marqué sur la mortalité des cellules de **groupe 3** comparativement au **groupe SHH** en traitant

les cellules avec de l'Oxamate (inhibiteur de la LDHA et LDHB) (Valvona and Fillmore 2018). Cette différence d'efficacité pourrait s'expliquer par une plus grande capacité des cellules du **groupe non-3** à switcher sur la phosphorylation oxydative en réponse à l'inhibition de la glycolyse. L'utilisation d'Oxamate et d'autres inhibiteurs de la LDH (GNE-140: triple inhibiteur de la LDH-A, LDH-B et LDH-C) comme approche thérapeutique anti-cancéreuse est prometteuse. Malheureusement, la concentration requise pour avoir des effets significatifs est beaucoup trop élevée pour être considérée pour une utilisation clinique (Le et al. 2010) (Arseneault et al. 2013)(Mazzio et al. 2021). Il semble donc intéressant d'associer à ces inhibiteurs de la LDH d'autres cibles thérapeutiques afin de potentialiser leurs effets. Notre travail confirme cela, en démontrant un effet cumulatif fort sur la prolifération et sur la mortalité cellulaire, de l'ensemble des groupes de MB, en associant au GNE-140 le combo (Phenformine + AOAA) ou (AOAA + iGP-1). Une étude portant sur des lignées cellulaires de cancer du pancréas a mis en évidence que certaines lignées (majoritairement OXPHOS) initialement résistantes au traitement par le GNE-140, avaient une sensibilité augmentée quand ce dernier était associé à la Phenformine (Boudreau et al. 2016).

Au final, nous avons démontré dans notre étude l'importance de la navette malate/asparte dans le MB, et plus précisément la différence d'utilisation des voies de régénération du NAD⁺ cytosolique en fonction des groupes de MB et des conditions d'oxygénation tissulaire. Il apparaît clairement que le co-ciblage de la phosphorylation oxydative par la Phenformine associé aux inhibiteurs des voies de régénération du NAD⁺ (AOAA + GNE-140) est une approche thérapeutique séduisante pour diminuer la viabilité des MB du **groupe 3**. Il est certain que nos résultats nécessitent d'être confirmés dans un premier temps sur un modèle expérimental d'organoïdes de MB puis *in vivo* sur xénogreffes, avant de pouvoir être exportés en recherche clinique.

Discussion générale et perspectives

Les patients atteints de MB du **groupe 3** ont encore aujourd'hui un pronostic qui reste sombre avec une mortalité globale aux environ de 50% et une grande morbidité secondaire aux traitement conventionnel associant chirurgie, radiothérapie et chimiothérapie. Il est urgent de pouvoir développer de nouvelles approches thérapeutiques ciblées sur ce groupe de patients afin d'espérer améliorer leur pronostic. Mon travail de thèse s'est concentré sur la compréhension des différences de métabolisme pouvant exister entre les MB du **groupe 3** comparativement aux autres groupes, dans des conditions expérimentales hypoxiques, reflétant au plus près les conditions physiologiques cérébrales dans lesquelles se développe la tumeur. Nous avons démontré que les voies métaboliques activées en hypoxie ne sont pas contrôlées de la même manière dans le **groupe 3** *versus* les **groupes non-3**, mettant en exergue la place centrale de HIF-2 comme point de contrôle de l'adaptation cellulaire à l'hypoxie dans le **groupe 3**. Une des grandes forces de notre travail a été notamment de travailler dans des conditions d'oxygénation différentes, mimant ainsi l'environnement physiologique et tumoral cérébelleux, élément crucial pour comprendre les phénomènes pathologiques et pouvoir extrapoler à l'*in vivo* les résultats thérapeutiques de l'*in vitro*.

★ HIF-2 à un rôle central dans les MB du groupe 3

L'hétérogénéité intra-tumorale est un facteur important contribuant à la résistance aux traitements anticancéreux. La diversité phénotypique des cellules cancéreuses au sein du microenvironnement tumoral est fortement influencée par des facteurs environnementaux tels que l'hypoxie. L'hypoxie et les facteurs de transcription inductibles par l'hypoxie HIF-1 et HIF-2 sont connus pour être associés aux cellules souches cancéreuses, aux métastases et à la résistance aux médicaments dans la pathologie tumorale. Le rôle de HIF-2 a été très largement mis en avant dans la pathologie tumorale suite aux travaux réalisés dans le cancer du rein (ccRCC), découlant sur la mise en place d'étude clinique de phase 1 testant un inhibiteur de HIF-2 (NCT02293980, A Phase 1, Dose-Escalation Trial of PT2385 Tablets In Patients With Advanced Clear Cell Renal Cell Carcinoma). Mais également dans les tumeurs cérébrales, avec un essai de phase II étudiant l'efficacité du PT2385 dans le traitement des patients atteints de glioblastomes récurrents (NCT03216499). Nos résultats permettent donc d'étendre le potentiel thérapeutique du PT2385 au médulloblastome, et plus particulièrement au **groupe 3**, pour lequel le métabolisme hypoxique est uniquement contrôlé par HIF-2. Une étude exploratoire, non thérapeutique, est en cours visant à évaluer le traceur [18F]PT2385 couplé à une Tomographie

par émission de Positrons/Tomodensitométrie (PET/CT) chez des patients atteints de cancer du rein. L'objectif principal est de corréler les niveaux de HIF-2 α déterminés par [18F]PT2385 PET/CT scan avec les niveaux de HIF-2 α obtenus sur tissus par immunohistochimie (NCT04989959). Si les résultats se révèlent concluants, cette technique pourrait être transposée au MB, permettant de mettre en évidence, avant l'étape de la chirurgie, les patients ayant une tumeur avide pour le PT2385, exprimant fortement HIF-2 α . Elle permettrait alors d'identifier les patients les plus à même de répondre à un traitement associant un inhibiteur de HIF-2 α . Nous savons que l'hétérogénéité intra-tumorale est grande dans le MB, et même si nos résultats présentent les patients du **groupe 3** comme les meilleurs candidats à un traitement par le PT2385, cette technique pourrait potentiellement ouvrir ce traitement à un plus grand nombre de patients.

★ D'autres axes métaboliques à explorer

Le cil primaire

Nous avons fait le choix, dans mon travail de thèse, d'axer nos recherches sur le métabolisme et l'hypoxie. Le métabolisme est un axe de travail majeur de l'équipe dans laquelle j'évolue, et le travail antérieur conduit par le Dr Lucila Fabbri sur le carcinome rénal à cellules claires (ccRCC), le cil primaire et la protéine VDAC-1 nous ouvre également des perspectives intéressantes dans le cadre du MB (**Annexe 4**). Une des caractéristiques du ccRCC est la perte du cil primaire (Nyhan et al. 2008). Les cils primaires sont des organites à structure microtubulaire qui s'étendent de la surface de la cellule vers l'extérieur et jouent un rôle crucial dans la détection et la transduction moléculaire et mécanique des stimuli extracellulaire (Singla and Reiter 2006). Dans son étude, Fabbri *et al.* a mis en évidence, pour la première fois, un groupe de patients atteints de ccRCC dans lesquels la forme clivée en hypoxie de VDAC1 (VDAC1- Δ C) serait responsable de la résorption du cil primaire (Fabbri et al. 2020).

Au niveau du cervelet, le cil primaire serait nécessaire à la prolifération des neurones granulaires cérébelleux (PNG), qui eux même sont considérés aujourd'hui comme cellules progénitrices des MB (Canterini et al. 2017). Mais le rôle du cil primaire dans le développement du MB n'est pas clairement défini. Il semblerait que la disparition du cil primaire soit nécessaire pour la croissance du MB dans les groupes ayant un facteur de transcription Gli2 constitutivement actif, alors que l'ablation génétique du cil primaire bloque la croissance du

MB induit par Smoothed (Smo). Une étude récente a effectivement mis en évidence que la suppression d'Arl13b (une GTPase ciliaire) réduit les niveaux de signalisation SHH en présence de l'oncogène Smo (Bay, Long, and Caspary 2018). La suppression d'Arl13B dans les lignées cellulaires de MB humaines a montré une diminution de la prolifération. Il semblerait donc que le cil primaire induise ou inhibe la formation du MB, selon l'événement oncogène initiateur et que l'expression du cil primaire soit différente selon les groupes de MB. On note une expression importante dans les **groupes non-3** (SHH et WNT), et une absence de cil primaire dans le **groupe 3** (Y.-G. Han et al. 2009). Il n'est pas impossible que l'expression isolée de HIF-2 dans le **groupe 3** des MB puisse jouer un rôle dans la disparition du cil primaire dans ce groupe car récemment, une étude portant sur l'analyse *in vitro* de chondrocytes primaire a montré que HIF-2 α favorise la perte de cils primaires *via* la voie HIF 2 α /AURKA (Aurora kinase A)/NEDD9, et la perte du cil primaire est une caractéristique de l'évolution vers un phénomène pathologique : l'arthrose (Q. Yang et al. 2019).

A la lumière de nos résultats et des travaux antérieur de mon équipe de recherche, il serait intéressant d'essayer de comprendre si, comme dans le cancer du rein, l'absence de cil primaire dans le **groupe 3** peut être une caractéristique du potentiel d'agressivité de la tumeur et si VDAC1- Δ C est impliqué dans la résorption du cil primaire. Connaître le rôle du cil primaire dans la signalisation oncogène du MB pourrait conduire à une meilleure compréhension du développement et du traitement de ces tumeurs.

★ L'ostéopontine

Au cours de mon Master 2 effectué avec le Dr N. Sadaghianloo sous la supervision de N. Mazure, j'ai étudié le rôle de l'ostéopontine (OPN) dans la pathologie vasculaire et plus particulièrement dans la dysfonction des abords vasculaires (fistule artério-veineuse) des patients insuffisants rénaux (**Annexe 1**). L'OPN existe sous une forme soluble et immobile. L'OPN soluble a une fonction dans la survie et la prolifération cellulaire, tandis que la forme immobile de l'OPN fonctionne comme une protéine de la matrice extracellulaire (ECM) et protège les cellules de l'apoptose (Standal, Borset, and Sundan 2004). L'OPN, dans ses différentes isoformes, contient plusieurs régions de liaison, dont un site de liaison au calcium, deux domaines de liaison à l'héparine et une séquence de liaison cellulaire à l'arginine-glycine-aspartic acid (RGD) (Kon et al. 2008)(Reinholt et al. 1990). Les modifications post-traductionnelles de l'OPN, telles que la phosphorylation, la glycosylation et le clivage

protéolytique, entraînent un poids moléculaire compris entre 41 et 71 kDa (Shevde and Samant 2014). Il a été démontré que des variants d'épissage distincts de l'OPN (OPNa, OPN-b et OPN-c) jouent divers rôles dans la progression du cancer. On sait aujourd'hui que l'expression de l'OPN est stimulée par l'hypoxie. Récemment, cette découverte a été confirmée dans le mélanome et le cancer du sein, montrant que l'OPN régule à la hausse l'expression des marqueurs d'hypoxie, améliorant l'angiogenèse tumorale et contribuant à la progression et à l'invasion du cancer (Kale et al. 2015)(Raja et al. 2014). Cependant, la façon dont l'hypoxie influence spécifiquement la libération d'OPN dans la circulation sanguine reste insaisissable. La surexpression de l'OPN dans le tissu tumoral et/ou ses niveaux élevés dans les fluides corporels (sang, bile, urine) des patients ont été associés à un comportement agressif d'une grande variété de cancers de l'adulte, et l'expression de l'OPN s'est avérée être associée à un pronostic plus sombre chez les patients atteints de glioblastome (GBM) (Sreekanthreddy et al. 2010)(Weber, Lett, and Haubein 2010)(Wai and Kuo 2008). Ces résultats suggèrent que l'OPN pourrait jouer un rôle en tant que biomarqueur pronostique potentiel du cancer et servir comme cible thérapeutique prometteuse dans les tumeurs malignes de l'adulte. Une étude récente portant sur le glioblastome met en évidence qu'une hypoxie modérée (5% O₂) régule à la hausse l'expression de l'ostéopontine *via* la stabilisation de HIF-2 α (Nishikawa et al. 2021). La surexpression de l'ostéopontine stimule la prolifération des cellules souches cancéreuses de glioblastome, et l'extinction du gène de l'OPN par siRNA diminue leur prolifération. Il serait intéressant de comprendre le rôle de l'OPN dans le MB, et de savoir si le traitement par PT2385 (inhibiteur de HIF-2 α) entraîne une diminution d'expression d'OPN et si cette variation d'expression d'OPN a un lien direct sur la diminution de prolifération de la tumeur, notamment du **groupe 3**.

★ Les cellules souches cancéreuses

Les cellules souches cancéreuses (CSC) ont été identifiées pour la première fois dans les leucémies en 1973 comme une population distincte de cellules, comprenant des signatures génétiques pro-oncogènes spécifiques, capables de générer des colonies hématopoïétiques malignes. Avec le temps, les CSC ont été progressivement identifiées dans des niches dédiées à de nombreuses autres tumeurs, y compris le MB en 2003 (S. K. Singh et al. 2003). De nombreux articles démontrent le rôle des CSC en tant que moteur principal de l'initiation et de la rechute de MB, et par la suite en tant que cibles thérapeutiques potentielles (J. Wang and Wechsler-Reya 2014). Il a également été mis en évidence que la capacité d'auto-renouvellement

des cellules souches de tumeur cérébrale était plus élevée dans les échantillons cliniques les plus agressifs de médulloblastome (S. K. Singh et al. 2003). Les cellules souches de MB peuvent être identifiées comme des cellules CD133/Prom1 positives, et présentent une capacité marquée de prolifération, d'auto-renouvellement et de différenciation *in vitro*. Une étude récente démontre que l'expression d'AMBRA1 (Autophagy and beclin 1 regulator 1), dépendante des niveaux d'expression de c-MYC, est corrélée au mauvais pronostic des patients atteint de médulloblastome du **groupe 3** (Nazio et al. 2021). De plus, l'inactivation d'AMBRA1 réduit la croissance et la migration des cellules souches au niveau des MB du **groupe 3**. Les cellules souches cancéreuses jouent donc très certainement un rôle important dans l'agressivité du **groupe 3** des MB. On sait aujourd'hui que l'hypoxie améliore l'expression des CSC par rapport aux conditions de normoxie (Eguchi et al. 2018). Par exemple, dans le glioblastome, l'hypoxie augmente l'expression de nombreux marqueurs de CSC, contribuant ainsi à la croissance tumorale (Boyd et al. 2021)(McCord et al. 2009)(P. Wang et al. 2017). Toujours dans le glioblastome, la stabilisation de HIF-2 α entraîne une augmentation d'expression de certains facteurs de cellules souches, notamment Oct4, Sox2 et Nanog. A l'inverse, l'inactivation de HIF-2 α réduit la capacité d'auto-renouvellement des CSC *in vitro* et diminue la croissance tumorale *in vivo* (John M Heddleston et al. 2009b)(Seidel et al. 2010)(Covello et al. 2006)(G. Lee et al. 2016). L'ensemble de ces données, associé aux résultats de mon travail, ouvre des perspectives encore une fois très intéressantes. Cibler HIF-2 avec le PT2385, dans les MB du **groupe 3**, pourrait avoir un effet inhibiteur sur l'auto-renouvellement des CSC et donc entraîner une diminution des capacités d'invasion et de prolifération du groupe le plus agressif.

Comme nous venons de le voir, les perspectives de travail restent grandes afin de mieux appréhender les caractéristiques de développement et de croissance du MB et plus particulièrement du **groupe 3**. Nous avons cependant découvert une caractéristique majeure du métabolisme des MB les plus agressifs, avec une signature hypoxique uniquement dépendante de HIF-2. Nous avons d'ailleurs déposé un brevet sur l'utilisation du PT2385 comme possibilité thérapeutique du MB. Devant l'importance du facteur de transcription HIF dans la mécanistique tumorale, nos résultats semblent importants à prendre en compte dans les futurs travaux sur le MB.

Références

- Albadari, Najah, Shanshan Deng, and Wei Li. 2019. "The Transcriptional Factors HIF-1 and HIF-2 and Their Novel Inhibitors in Cancer Therapy." *Expert opinion on drug discovery* 14(7): 667–82.
- Albanese, Adam et al. 2020. "The Role of Hypoxia-Inducible Factor Post-Translational Modifications in Regulating Its Localisation, Stability, and Activity." *International journal of molecular sciences* 22(1).
- Anastasiadis, Aristotelis G et al. 2002. "Human Hormone-Refractory Prostate Cancers Can Harbor Mutations in the O(2)-Dependent Degradation Domain of Hypoxia Inducible Factor-1alpha (HIF-1alpha)." *Journal of cancer research and clinical oncology* 128(7): 358–62.
- Applebaum, Mark A et al. 2016. "Integrative Genomics Reveals Hypoxia Inducible Genes That Are Associated with a Poor Prognosis in Neuroblastoma Patients." *Oncotarget* 7(47): 76816–26.
- Aprelikova, Olga et al. 2006. "Role of ETS Transcription Factors in the Hypoxia-Inducible Factor-2 Target Gene Selection." *Cancer research* 66(11): 5641–47.
- Aref, Donya, and Sidney Croul. 2013. "Medulloblastoma: Recurrence and Metastasis." *CNS oncology* 2(4): 377–85.
- Arseneault, Robert et al. 2013. "Attenuation of LDHA Expression in Cancer Cells Leads to Redox-Dependent Alterations in Cytoskeletal Structure and Cell Migration." *Cancer letters* 338(2): 255–66.
- Ashley, David M et al. 2012. "Induction Chemotherapy and Conformal Radiation Therapy for Very Young Children with Nonmetastatic Medulloblastoma: Children's Oncology Group Study P9934." *Journal of clinical oncology : official journal of the American Society of Clinical Oncology* 30(26): 3181–86.
- Atlante, A et al. 1999. "Glutamate Neurotoxicity in Rat Cerebellar Granule Cells Involves Cytochrome c Release from Mitochondria and Mitochondrial Shuttle Impairment." *Journal of neurochemistry* 73(1): 237–46.
- Bae, Seong-Hui et al. 2004. "Sumoylation Increases HIF-1alpha Stability and Its Transcriptional Activity." *Biochemical and biophysical research communications* 324(1): 394–400.
- Bagatell, Rochelle et al. 2007. "Phase I Pharmacokinetic and Pharmacodynamic Study of 17-N-Allylamino-17-Demethoxygeldanamycin in Pediatric Patients with Recurrent or Refractory Solid Tumors: A Pediatric Oncology Experimental Therapeutics Investigators Consortium Study." *Clinical cancer research : an official journal of the American Association for Cancer Research* 13(6): 1783–88.
- BAILEY, PERCIVAL. 1925. "MEDULLOBLASTOMA CEREBELLI." *Archives of Neurology & Psychiatry* 14(2): 192.
- Ballabio, Claudio et al. 2020a. "Modeling Medulloblastoma in Vivo and with Human Cerebellar Organoids." *Nature communications* 11(1): 583.
- . 2020b. "Modeling Medulloblastoma in Vivo and with Human Cerebellar Organoids." *Nature communications* 11(1): 583.
- Bay, Sarah N, Alyssa B Long, and Tamara Caspary. 2018. "Disruption of the Ciliary GTPase Arl13b Suppresses Sonic Hedgehog Overactivation and Inhibits Medulloblastoma Formation." *Proceedings of the National Academy of Sciences of the United States of America* 115(7): 1570–75.

- Bellot, Grégory et al. 2009. "Hypoxia-Induced Autophagy Is Mediated through Hypoxia-Inducible Factor Induction of BNIP3 and BNIP3L via Their BH3 Domains." *Molecular and cellular biology* 29(10): 2570–81.
- Benjamin, Don et al. 2018. "Dual Inhibition of the Lactate Transporters MCT1 and MCT4 Is Synthetic Lethal with Metformin Due to NAD⁺ Depletion in Cancer Cells." *Cell reports* 25(11): 3047-3058.e4.
- Bernardini, N et al. 1991. "Comparative Activity of Doxorubicin and Its Major Metabolite, Doxorubicinol, on V79/AP4 Fibroblasts: A Morphofunctional Study." *Experimental and molecular pathology* 55(3): 238–50.
- Bernauer, Carolina et al. 2021. "Hypoxia and Its Therapeutic Possibilities in Paediatric Cancers." *British journal of cancer* 124(3): 539–51.
- Berta, Mélanie A et al. 2007. "SUMOylation of Hypoxia-Inducible Factor-1alpha Reduces Its Transcriptional Activity." *Biochemical and biophysical research communications* 360(3): 646–52.
- Bertout, Jessica A, Shetal A Patel, and M Celeste Simon. 2008. "The Impact of O₂ Availability on Human Cancer." *Nature reviews. Cancer* 8(12): 967–75.
- Birsoy, Kivanç et al. 2014. "Metabolic Determinants of Cancer Cell Sensitivity to Glucose Limitation and Biguanides." *Nature* 508(7494): 108–12.
- . 2015a. "An Essential Role of the Mitochondrial Electron Transport Chain in Cell Proliferation Is to Enable Aspartate Synthesis." *Cell* 162(3): 540–51.
- . 2015b. "An Essential Role of the Mitochondrial Electron Transport Chain in Cell Proliferation Is to Enable Aspartate Synthesis." *Cell* 162(3): 540–51.
- Boiani, Michele, and Hans R Schöler. 2005. "Regulatory Networks in Embryo-Derived Pluripotent Stem Cells." *Nature reviews. Molecular cell biology* 6(11): 872–84.
- Bordt, Evan A. 2018. "The Importance of Controlling in Vitro Oxygen Tension to Accurately Model in Vivo Neurophysiology." *Neurotoxicology* 66: 213–20.
- Boudreau, Aaron et al. 2016. "Metabolic Plasticity Underpins Innate and Acquired Resistance to LDHA Inhibition." *Nature chemical biology* 12(10): 779–86.
- Boyd, Nathaniel H et al. 2021. "Glioma Stem Cells and Their Roles within the Hypoxic Tumor Microenvironment." *Theranostics* 11(2): 665–83.
- Brahimi-Horn, Christiane, Nathalie Mazure, and Jacques Pouyssegur. 2005. "Signalling via the Hypoxia-Inducible Factor-1alpha Requires Multiple Posttranslational Modifications." *Cellular signalling* 17(1): 1–9.
- Brahimi-Horn, M Christiane, Johanna Chiche, and Jacques Pouyssegur. 2007. "Hypoxia and Cancer." *Journal of molecular medicine (Berlin, Germany)* 85(12): 1301–7.
- Brahimi-Horn, M Christiane, and Jacques Pouyssegur. 2009. "HIF at a Glance." *Journal of cell science* 122(Pt 8): 1055–57.
- Brandes, Alba A et al. 2016. "A Phase II Randomized Study of Galunisertib Monotherapy or Galunisertib plus Lomustine Compared with Lomustine Monotherapy in Patients with Recurrent Glioblastoma." *Neuro-oncology* 18(8): 1146–56.
- Bristow, Robert G, and Richard P Hill. 2008. "Hypoxia and Metabolism. Hypoxia, DNA Repair and Genetic Instability." *Nature reviews. Cancer* 8(3): 180–92.
- Brooks, George A. 2020. "Lactate as a Fulcrum of Metabolism." *Redox biology* 35: 101454.
- Brown, H G et al. 2000. "'Large Cell/Anaplastic' Medulloblastomas: A Pediatric Oncology Group Study." *Journal of neuropathology and experimental neurology* 59(10): 857–65.
- von Bueren, André O et al. 2016. "Treatment of Children and Adolescents With Metastatic Medulloblastoma and Prognostic Relevance of Clinical and Biologic Parameters." *Journal of clinical oncology : official journal of the American Society of Clinical Oncology* 34(34): 4151–60.

- Bullen, John W et al. 2016. "Protein Kinase A-Dependent Phosphorylation Stimulates the Transcriptional Activity of Hypoxia-Inducible Factor 1." *Science signaling* 9(430): ra56.
- Cairns, Rob A, Isaac S Harris, and Tak W Mak. 2011. "Regulation of Cancer Cell Metabolism." *Nature reviews. Cancer* 11(2): 85–95.
- Canterini, Sonia et al. 2017. "Shortened Primary Cilium Length and Dysregulated Sonic Hedgehog Signaling in Niemann-Pick C1 Disease." *Human Molecular Genetics* 26(12): 2277–89.
- Cantó, Carles, Keir J Menzies, and Johan Auwerx. 2015. "NAD(+) Metabolism and the Control of Energy Homeostasis: A Balancing Act between Mitochondria and the Nucleus." *Cell metabolism* 22(1): 31–53.
- Carmeliet, Peter. 2005. "Angiogenesis in Life, Disease and Medicine." *Nature* 438(7070): 932–36.
- Cassavaugh, Jessica M et al. 2011. "Negative Regulation of HIF-1 α by an FBW7-Mediated Degradation Pathway during Hypoxia." *Journal of cellular biochemistry* 112(12): 3882–90.
- Cavalli, Florence M G et al. 2017. "Intertumoral Heterogeneity within Medulloblastoma Subgroups." *Cancer cell* 31(6): 737-754.e6.
- Chang, Qing, Igor Jurisica, Trevor Do, and David W Hedley. 2011. "Hypoxia Predicts Aggressive Growth and Spontaneous Metastasis Formation from Orthotopically Grown Primary Xenografts of Human Pancreatic Cancer." *Cancer research* 71(8): 3110–20.
- Chapman, J D, A J Franko, and J Sharplin. 1981. "A Marker for Hypoxic Cells in Tumours with Potential Clinical Applicability." *British journal of cancer* 43(4): 546–50.
- Chau, Cindy H et al. 2005. "Polymorphism in the Hypoxia-Inducible Factor 1 α Gene May Confer Susceptibility to Androgen-Independent Prostate Cancer." *Cancer biology & therapy* 4(11): 1222–25.
- Chen, Wenfang et al. 2016. "Targeting Renal Cell Carcinoma with a HIF-2 Antagonist." *Nature* 539(7627): 112–17.
- Cheng, Jinke, Xunlei Kang, Sui Zhang, and Edward T H Yeh. 2007. "SUMO-Specific Protease 1 Is Essential for Stabilization of HIF1 α during Hypoxia." *Cell* 131(3): 584–95.
- Chin, Alexander L et al. 2018. "Survival Impact of Postoperative Radiotherapy Timing in Pediatric and Adolescent Medulloblastoma." *Neuro-oncology* 20(8): 1133–41.
- Chitneni, Satish K, Gregory M Palmer, Michael R Zalutsky, and Mark W Dewhirst. 2011. "Molecular Imaging of Hypoxia." *Journal of nuclear medicine : official publication, Society of Nuclear Medicine* 52(2): 165–68.
- Cho, Yoon-Jae et al. 2011. "Integrative Genomic Analysis of Medulloblastoma Identifies a Molecular Subgroup That Drives Poor Clinical Outcome." *Journal of clinical oncology : official journal of the American Society of Clinical Oncology* 29(11): 1424–30.
- Choudhry, Hani, and Adrian L Harris. 2018. "Advances in Hypoxia-Inducible Factor Biology." *Cell metabolism* 27(2): 281–98.
- Chowdhury, Subir K R, Adam Gemin, and Gurmit Singh. 2005. "High Activity of Mitochondrial Glycerophosphate Dehydrogenase and Glycerophosphate-Dependent ROS Production in Prostate Cancer Cell Lines." *Biochemical and biophysical research communications* 333(4): 1139–45.
- Cohen, Michael S. 2020. "Interplay between Compartmentalized NAD⁺ Synthesis and Consumption: A Focus on the PARP Family." *Genes & development* 34(5–6): 254–62.
- Corn, Paul G et al. 2005. "Mxi1 Is Induced by Hypoxia in a HIF-1-Dependent Manner and Protects Cells from c-Myc-Induced Apoptosis." *Cancer biology & therapy* 4(11): 1285–94.

- Courtney, Kevin D et al. 2018. "Phase I Dose-Escalation Trial of PT2385, a First-in-Class Hypoxia-Inducible Factor-2 α Antagonist in Patients With Previously Treated Advanced Clear Cell Renal Cell Carcinoma." *Journal of clinical oncology : official journal of the American Society of Clinical Oncology* 36(9): 867–74.
- . 2020. "HIF-2 Complex Dissociation, Target Inhibition, and Acquired Resistance with PT2385, a First-in-Class HIF-2 Inhibitor, in Patients with Clear Cell Renal Cell Carcinoma." *Clinical cancer research : an official journal of the American Association for Cancer Research* 26(4): 793–803.
- Covello, Kelly L et al. 2006. "HIF-2 α Regulates Oct-4: Effects of Hypoxia on Stem Cell Function, Embryonic Development, and Tumor Growth." *Genes & development* 20(5): 557–70.
- Cowman, Sophie, Yuen Ngan Fan, Barry Pizer, and Violaine Sée. 2019. "Decrease of Nibrin Expression in Chronic Hypoxia Is Associated with Hypoxia-Induced Chemoresistance in Some Brain Tumour Cells." *BMC cancer* 19(1): 300.
- Dang, Chi v, Anne Le, and Ping Gao. 2009. "MYC-Induced Cancer Cell Energy Metabolism and Therapeutic Opportunities." *Clinical cancer research : an official journal of the American Association for Cancer Research* 15(21): 6479–83.
- Daugan, Marie, Amélie Dufaÿ Wojcicki, Benoit d'Hayer, and Vincent Boudy. 2016. "Metformin: An Anti-Diabetic Drug to Fight Cancer." *Pharmacological research* 113(Pt A): 675–85.
- Dayan, Frédéric et al. 2006. "The Oxygen Sensor Factor-Inhibiting Hypoxia-Inducible Factor-1 Controls Expression of Distinct Genes through the Bifunctional Transcriptional Character of Hypoxia-Inducible Factor-1 α ." *Cancer research* 66(7): 3688–98.
- . 2009. "Activation of HIF-1 α in Exponentially Growing Cells via Hypoxic Stimulation Is Independent of the Akt/MTOR Pathway." *Journal of cellular physiology* 218(1): 167–74.
- Dobson, Tara H W, and Vidya Gopalakrishnan. 2018. "Preclinical Models of Pediatric Brain Tumors-Forging Ahead." *Bioengineering (Basel, Switzerland)* 5(4).
- Du, Rose et al. 2008. "HIF1 α Induces the Recruitment of Bone Marrow-Derived Vascular Modulatory Cells to Regulate Tumor Angiogenesis and Invasion." *Cancer cell* 13(3): 206–20.
- Duan, Cunming. 2016. "Hypoxia-Inducible Factor 3 Biology: Complexities and Emerging Themes." *American journal of physiology. Cell physiology* 310(4): C260-9.
- Eguchi, Takanori et al. 2018. "Organoids with Cancer Stem Cell-like Properties Secrete Exosomes and HSP90 in a 3D Nanoenvironment." *PloS one* 13(2): e0191109.
- Erecińska, Maria, and Ian A. Silver. 2001. "Tissue Oxygen Tension and Brain Sensitivity to Hypoxia." *Respiration Physiology* 128(3): 263–76.
- Erler, Janine T et al. 2004. "Hypoxia-Mediated down-Regulation of Bid and Bax in Tumors Occurs via Hypoxia-Inducible Factor 1-Dependent and -Independent Mechanisms and Contributes to Drug Resistance." *Molecular and cellular biology* 24(7): 2875–89.
- Eschmann, Susanne-Martina et al. 2005. "Prognostic Impact of Hypoxia Imaging with 18F-Misonidazole PET in Non-Small Cell Lung Cancer and Head and Neck Cancer before Radiotherapy." *Journal of nuclear medicine : official publication, Society of Nuclear Medicine* 46(2): 253–60.
- Evans, Josie M M et al. 2005. "Metformin and Reduced Risk of Cancer in Diabetic Patients." *BMJ (Clinical research ed.)* 330(7503): 1304–5.
- Fabbri, Lucilla et al. 2020. "Identification of a New Aggressive Axis Driven by Ciliogenesis and Absence of VDAC1- Δ C in Clear Cell Renal Cell Carcinoma Patients." *Theranostics* 10(6): 2696–2713.

- Fendt, Sarah-Maria et al. 2013. "Metformin Decreases Glucose Oxidation and Increases the Dependency of Prostate Cancer Cells on Reductive Glutamine Metabolism." *Cancer research* 73(14): 4429–38.
- Ferrer, Isidro, and Noemi Vidal. 2017. "Neuropathology of Cerebrovascular Diseases." *Handbook of clinical neurology* 145: 79–114.
- Fitzpatrick, S M, A J Cooper, and T E Duffy. 1983. "Use of Beta-Methylene-D,L-Aspartate to Assess the Role of Aspartate Aminotransferase in Cerebral Oxidative Metabolism." *Journal of neurochemistry* 41(5): 1370–83.
- Flügel, Daniela, Agnes Görlach, Carine Michiels, and Thomas Kietzmann. 2007. "Glycogen Synthase Kinase 3 Phosphorylates Hypoxia-Inducible Factor 1alpha and Mediates Its Destabilization in a VHL-Independent Manner." *Molecular and cellular biology* 27(9): 3253–65.
- Fu, Xinyu S, Eunis Choi, Glenn J Buble, and Steven P Balk. 2005. "Identification of Hypoxia-Inducible Factor-1alpha (HIF-1alpha) Polymorphism as a Mutation in Prostate Cancer That Prevents Normoxia-Induced Degradation." *The Prostate* 63(3): 215–21.
- Gaber, Timo, Cindy Strehl, and Frank Buttgerit. 2017. "Metabolic Regulation of Inflammation." *Nature reviews. Rheumatology* 13(5): 267–79.
- Gajjar, Amar et al. 2006a. "Risk-Adapted Craniospinal Radiotherapy Followed by High-Dose Chemotherapy and Stem-Cell Rescue in Children with Newly Diagnosed Medulloblastoma (St Jude Medulloblastoma-96): Long-Term Results from a Prospective, Multicentre Trial." *The Lancet. Oncology* 7(10): 813–20.
- . 2006b. "Risk-Adapted Craniospinal Radiotherapy Followed by High-Dose Chemotherapy and Stem-Cell Rescue in Children with Newly Diagnosed Medulloblastoma (St Jude Medulloblastoma-96): Long-Term Results from a Prospective, Multicentre Trial." *The Lancet. Oncology* 7(10): 813–20.
- . 2021. "Outcomes by Clinical and Molecular Features in Children With Medulloblastoma Treated With Risk-Adapted Therapy: Results of an International Phase III Trial (SJMB03)." *Journal of clinical oncology : official journal of the American Society of Clinical Oncology* 39(7): 822–35.
- Garcia-Bermudez, Javier et al. 2018. "Aspartate Is a Limiting Metabolite for Cancer Cell Proliferation under Hypoxia and in Tumours." *Nature cell biology* 20(7): 775–81.
- Gatenby, Robert A, and Robert J Gillies. 2004. "Why Do Cancers Have High Aerobic Glycolysis?" *Nature reviews. Cancer* 4(11): 891–99.
- Gérard, Michael et al. 2019. "Hypoxia Imaging and Adaptive Radiotherapy: A State-of-the-Art Approach in the Management of Glioma." *Frontiers in medicine* 6: 117.
- Gibson, Paul et al. 2010. "Subtypes of Medulloblastoma Have Distinct Developmental Origins." *Nature* 468(7327): 1095–99.
- Gilbertson, Richard J, and David W Ellison. 2008. "The Origins of Medulloblastoma Subtypes." *Annual review of pathology* 3: 341–65.
- Gkotinakou, Ioanna-Maria, Christina Befani, George Simos, and Panagiotis Liakos. 2019. "ERK1/2 Phosphorylates HIF-2 α and Regulates Its Activity by Controlling Its CRM1-Dependent Nuclear Shuttling." *Journal of cell science* 132(7).
- Gladek, I et al. 2017. "HIF1A Gene Polymorphisms and Human Diseases: Graphical Review of 97 Association Studies." *Genes, chromosomes & cancer* 56(6): 439–52.
- Gordan, John D et al. 2007. "HIF-2alpha Promotes Hypoxic Cell Proliferation by Enhancing c-Myc Transcriptional Activity." *Cancer cell* 11(4): 335–47.
- Gordan, John D, Craig B Thompson, and M Celeste Simon. 2007. "HIF and C-Myc: Sibling Rivals for Control of Cancer Cell Metabolism and Proliferation." *Cancer cell* 12(2): 108–13.

- Gottardo, Nicholas G et al. 2014. "Medulloblastoma Down Under 2013: A Report from the Third Annual Meeting of the International Medulloblastoma Working Group." *Acta neuropathologica* 127(2): 189–201.
- Graham, Kaitlin, and Evan Unger. 2018. "Overcoming Tumor Hypoxia as a Barrier to Radiotherapy, Chemotherapy and Immunotherapy in Cancer Treatment." *International journal of nanomedicine* 13: 6049–58.
- Gravel, Simon-Pierre et al. 2014. "Serine Deprivation Enhances Antineoplastic Activity of Biguanides." *Cancer research* 74(24): 7521–33.
- Gu, Y Z et al. 1998. "Molecular Characterization and Chromosomal Localization of a Third Alpha-Class Hypoxia Inducible Factor Subunit, HIF3alpha." *Gene expression* 7(3): 205–13.
- Gui, Dan Y et al. 2016. "Environment Dictates Dependence on Mitochondrial Complex I for NAD⁺ and Aspartate Production and Determines Cancer Cell Sensitivity to Metformin." *Cell metabolism* 24(5): 716–27.
- van Hagen, Martijn, René M Overmeer, Sharareh S Abolvardi, and Alfred C O Vertegaal. 2010. "RNF4 and VHL Regulate the Proteasomal Degradation of SUMO-Conjugated Hypoxia-Inducible Factor-2alpha." *Nucleic acids research* 38(6): 1922–31.
- Hajizadeh, Farnaz et al. 2019. "Hypoxia Inducible Factors in the Tumor Microenvironment as Therapeutic Targets of Cancer Stem Cells." *Life sciences* 237: 116952.
- Han, Young-Goo et al. 2009. "Dual and Opposing Roles of Primary Cilia in Medulloblastoma Development." *Nature medicine* 15(9): 1062–65.
- Han, Zhi-Jian et al. 2018. "The Post-Translational Modification, SUMOylation, and Cancer (Review)." *International journal of oncology* 52(4): 1081–94.
- Hanahan, Douglas, and Robert A Weinberg. 2011. "Hallmarks of Cancer: The next Generation." *Cell* 144(5): 646–74.
- Harris, B H L, A Barberis, C M L West, and F M Buffa. 2015. "Gene Expression Signatures as Biomarkers of Tumour Hypoxia." *Clinical oncology (Royal College of Radiologists (Great Britain))* 27(10): 547–60.
- Heddleston, J M et al. 2010. "Hypoxia Inducible Factors in Cancer Stem Cells." *British journal of cancer* 102(5): 789–95.
- Heddleston, John M et al. 2009a. "The Hypoxic Microenvironment Maintains Glioblastoma Stem Cells and Promotes Reprogramming towards a Cancer Stem Cell Phenotype." *Cell cycle (Georgetown, Tex.)* 8(20): 3274–84.
- . 2009b. "The Hypoxic Microenvironment Maintains Glioblastoma Stem Cells and Promotes Reprogramming towards a Cancer Stem Cell Phenotype." *Cell cycle (Georgetown, Tex.)* 8(20): 3274–84.
- Heidbreder, Marc et al. 2003. "Hypoxia Rapidly Activates HIF-3alpha mRNA Expression." *FASEB journal : official publication of the Federation of American Societies for Experimental Biology* 17(11): 1541–43.
- vander Heiden, Matthew G. 2011. "Targeting Cancer Metabolism: A Therapeutic Window Opens." *Nature reviews. Drug discovery* 10(9): 671–84.
- vander Heiden, Matthew G, Lewis C Cantley, and Craig B Thompson. 2009. "Understanding the Warburg Effect: The Metabolic Requirements of Cell Proliferation." *Science (New York, N.Y.)* 324(5930): 1029–33.
- Hellwig, Sabine, Annette Heinrich, and Knut Biber. 2013. "The Brain's Best Friend: Microglial Neurotoxicity Revisited." *Frontiers in cellular neuroscience* 7: 71.
- Herzog, Julia et al. 2016. "Cyclin-Dependent Kinase 5 Stabilizes Hypoxia-Inducible Factor-1α: A Novel Approach for Inhibiting Angiogenesis in Hepatocellular Carcinoma." *Oncotarget* 7(19): 27108–21.

- Holmquist-Mengelbier, Linda et al. 2006. "Recruitment of HIF-1alpha and HIF-2alpha to Common Target Genes Is Differentially Regulated in Neuroblastoma: HIF-2alpha Promotes an Aggressive Phenotype." *Cancer cell* 10(5): 413–23.
- Hopp, Ann-Katrin, Patrick Grüter, and Michael O Hottiger. 2019. "Regulation of Glucose Metabolism by NAD⁺ and ADP-Ribosylation." *Cells* 8(8).
- Hovestadt, Volker et al. 2019. "Resolving Medulloblastoma Cellular Architecture by Single-Cell Genomics." *Nature* 572(7767): 74–79.
- Hu, Cheng-Jun et al. 2007. "The N-Terminal Transactivation Domain Confers Target Gene Specificity of Hypoxia-Inducible Factors HIF-1alpha and HIF-2alpha." *Molecular biology of the cell* 18(11): 4528–42.
- Huang, L E, J Gu, M Schau, and H F Bunn. 1998. "Regulation of Hypoxia-Inducible Factor 1alpha Is Mediated by an O₂-Dependent Degradation Domain via the Ubiquitin-Proteasome Pathway." *Proceedings of the National Academy of Sciences of the United States of America* 95(14): 7987–92.
- Hubbi, Maimon E et al. 2014. "Cyclin-Dependent Kinases Regulate Lysosomal Degradation of Hypoxia-Inducible Factor 1 α to Promote Cell-Cycle Progression." *Proceedings of the National Academy of Sciences of the United States of America* 111(32): E3325-34.
- Hubert, Christopher G et al. 2016. "A Three-Dimensional Organoid Culture System Derived from Human Glioblastomas Recapitulates the Hypoxic Gradients and Cancer Stem Cell Heterogeneity of Tumors Found In Vivo." *Cancer research* 76(8): 2465–77.
- Hung, Yin Pun, John G Albeck, Mathew Tantama, and Gary Yellen. 2011. "Imaging Cytosolic NADH-NAD(+) Redox State with a Genetically Encoded Fluorescent Biosensor." *Cell metabolism* 14(4): 545–54.
- Hurtado-Bagès, Sarah, Gunnar Knobloch, Andreas G Ladurner, and Marcus Buschbeck. 2020. "The Taming of PARP1 and Its Impact on NAD⁺ Metabolism." *Molecular metabolism* 38: 100950.
- Huszthy, Peter C et al. 2012. "In Vivo Models of Primary Brain Tumors: Pitfalls and Perspectives." *Neuro-oncology* 14(8): 979–93.
- Imai, S, C M Armstrong, M Kaerberlein, and L Guarente. 2000. "Transcriptional Silencing and Longevity Protein Sir2 Is an NAD-Dependent Histone Deacetylase." *Nature* 403(6771): 795–800.
- Ishihama, Sohta et al. 2021. "LPL/AQP7/GPD2 Promotes Glycerol Metabolism under Hypoxia and Prevents Cardiac Dysfunction during Ischemia." *FASEB journal : official publication of the Federation of American Societies for Experimental Biology* 35(12): e22048.
- Ivan, M et al. 2001. "HIFalpha Targeted for VHL-Mediated Destruction by Proline Hydroxylation: Implications for O₂ Sensing." *Science (New York, N.Y.)* 292(5516): 464–68.
- Ivanov, Delyan P, Beth Coyle, David A Walker, and Anna M Grabowska. 2016. "In Vitro Models of Medulloblastoma: Choosing the Right Tool for the Job." *Journal of biotechnology* 236: 10–25.
- Jaakkola, P et al. 2001. "Targeting of HIF-Alpha to the von Hippel-Lindau Ubiquitylation Complex by O₂-Regulated Prolyl Hydroxylation." *Science (New York, N.Y.)* 292(5516): 468–72.
- Jacob, Fadi et al. 2020. "A Patient-Derived Glioblastoma Organoid Model and Biobank Recapitulates Inter- and Intra-Tumoral Heterogeneity." *Cell* 180(1): 188-204.e22.
- Janzer, Andreas et al. 2014. "Metformin and Phenformin Deplete Tricarboxylic Acid Cycle and Glycolytic Intermediates during Cell Transformation and NTPs in Cancer Stem Cells." *Proceedings of the National Academy of Sciences of the United States of America* 111(29): 10574–79.

- Javeshghani, Shiva et al. 2012. "Carbon Source and Myc Expression Influence the Antiproliferative Actions of Metformin." *Cancer research* 72(23): 6257–67.
- Jeong, Joo Won et al. 2002. "Regulation and Destabilization of HIF-1alpha by ARD1-Mediated Acetylation." *Cell* 111(5): 709–20.
- Jiang, Wei et al. 2016. "Repurposing Phenformin for the Targeting of Glioma Stem Cells and the Treatment of Glioblastoma." *Oncotarget* 7(35): 56456–70.
- Jögi, Annika et al. 2004. "Human Neuroblastoma Cells Exposed to Hypoxia: Induction of Genes Associated with Growth, Survival, and Aggressive Behavior." *Experimental cell research* 295(2): 469–87.
- Kahalley, Lisa S et al. 2016. "Comparing Intelligence Quotient Change After Treatment With Proton Versus Photon Radiation Therapy for Pediatric Brain Tumors." *Journal of clinical oncology : official journal of the American Society of Clinical Oncology* 34(10): 1043–49.
- Kalbag, S S, M S Roginsky, Z Jelveh, and S Sulimovici. 1991. "Phorbol Ester, Prolactin, and Relaxin Cause Translocation of Protein Kinase C from Cytosol to Membranes in Human Endometrial Cells." *Biochimica et biophysica acta* 1094(1): 85–91.
- Kale, S et al. 2015. "Osteopontin Signaling Upregulates Cyclooxygenase-2 Expression in Tumor-Associated Macrophages Leading to Enhanced Angiogenesis and Melanoma Growth via A9β1 Integrin." *Oncogene* 34(42): 5408–10.
- Kallio, P J et al. 1998. "Signal Transduction in Hypoxic Cells: Inducible Nuclear Translocation and Recruitment of the CBP/P300 Coactivator by the Hypoxia-Inducible Factor-1alpha." *The EMBO journal* 17(22): 6573–86.
- Kann, Benjamin H et al. 2016. "Postoperative Radiotherapy Patterns of Care and Survival Implications for Medulloblastoma in Young Children." *JAMA oncology* 2(12): 1574–81.
- Key, Jason et al. 2009. "Principles of Ligand Binding within a Completely Buried Cavity in HIF2alpha PAS-B." *Journal of the American Chemical Society* 131(48): 17647–54.
- Khan, Hamidullah et al. 2019. "Metabolic Rewiring in Response to Biguanides Is Mediated by MROS/HIF-1a in Malignant Lymphocytes." *Cell reports* 29(10): 3009-3018.e4.
- KIJIMA, Noriyuki, and Yonehiro KANEMURA. 2016. "Molecular Classification of Medulloblastoma." *Neurologia medico-chirurgica* 56(11): 687–97.
- Kim, Yunho et al. 2016. "Methylation-Dependent Regulation of HIF-1α Stability Restricts Retinal and Tumour Angiogenesis." *Nature communications* 7: 10347.
- Kleihues, Paul et al. 2002. "The WHO Classification of Tumors of the Nervous System." *Journal of neuropathology and experimental neurology* 61(3): 215–25; discussion 226-9.
- Klingenberg, M. 1970. "Localization of the Glycerol-Phosphate Dehydrogenase in the Outer Phase of the Mitochondrial Inner Membrane." *European journal of biochemistry* 13(2): 247–52.
- Koh, Mei Yee, Robert Lemos, Xiuping Liu, and Garth Powis. 2011. "The Hypoxia-Associated Factor Switches Cells from HIF-1α- to HIF-2α-Dependent Signaling Promoting Stem Cell Characteristics, Aggressive Tumor Growth and Invasion." *Cancer research* 71(11): 4015–27.
- Koh, Mei Yee, and Garth Powis. 2012. "Passing the Baton: The HIF Switch." *Trends in biochemical sciences* 37(9): 364–72.
- Köhl, Roman, Jie Zhou, and Bernhard Brüne. 2006. "Reactive Oxygen Species Attenuate Nitric-Oxide-Mediated Hypoxia-Inducible Factor-1alpha Stabilization." *Free radical biology & medicine* 40(8): 1430–42.
- Koivunen, Peppi et al. 2004. "Catalytic Properties of the Asparaginyl Hydroxylase (FIH) in the Oxygen Sensing Pathway Are Distinct from Those of Its Prolyl 4-Hydroxylases." *The Journal of biological chemistry* 279(11): 9899–9904.

- Kon, Shigeyuki et al. 2008. "Syndecan-4 Protects against Osteopontin-Mediated Acute Hepatic Injury by Masking Functional Domains of Osteopontin." *The Journal of experimental medicine* 205(1): 25–33.
- Kool, Marcel et al. 2008. "Integrated Genomics Identifies Five Medulloblastoma Subtypes with Distinct Genetic Profiles, Pathway Signatures and Clinicopathological Features." *PLoS one* 3(8): e3088.
- Koppenol, Willem H, Patricia L Bounds, and Chi v Dang. 2011. "Otto Warburg's Contributions to Current Concepts of Cancer Metabolism." *Nature reviews. Cancer* 11(5): 325–37.
- Koshiji, Minori et al. 2004. "HIF-1 α Induces Cell Cycle Arrest by Functionally Counteracting Myc." *The EMBO journal* 23(9): 1949–56.
- Koza, R A et al. 1996. "Sequence and Tissue-Dependent RNA Expression of Mouse FAD-Linked Glycerol-3-Phosphate Dehydrogenase." *Archives of biochemistry and biophysics* 336(1): 97–104.
- Laclef, Christine. 2014. "Le Cil Primaire, Orchestrateur de La Morphogénèse Cérébrale." *médecine/sciences* 30(11): 980–90.
- Lappin, Terence R, and Frank S Lee. 2019. "Update on Mutations in the HIF: EPO Pathway and Their Role in Erythrocytosis." *Blood reviews* 37: 100590.
- Le, Anne et al. 2010. "Inhibition of Lactate Dehydrogenase A Induces Oxidative Stress and Inhibits Tumor Progression." *Proceedings of the National Academy of Sciences of the United States of America* 107(5): 2037–42.
- Leary, Sarah E S, and James M Olson. 2012. "The Molecular Classification of Medulloblastoma: Driving the next Generation Clinical Trials." *Current opinion in pediatrics* 24(1): 33–39.
- Lee, Eudocia Q et al. 2015. "Phase II Study of Panobinostat in Combination with Bevacizumab for Recurrent Glioblastoma and Anaplastic Glioma." *Neuro-oncology* 17(6): 862–67.
- Lee, Gina et al. 2016. "Dedifferentiation of Glioma Cells to Glioma Stem-like Cells By Therapeutic Stress-Induced HIF Signaling in the Recurrent GBM Model." *Molecular cancer therapeutics* 15(12): 3064–76.
- Lee, KangAe, Huafeng Zhang, et al. 2009. "Acriflavine Inhibits HIF-1 Dimerization, Tumor Growth, and Vascularization." *Proceedings of the National Academy of Sciences of the United States of America* 106(42): 17910–15.
- Lee, KangAe, David Z Qian, et al. 2009. "Anthracycline Chemotherapy Inhibits HIF-1 Transcriptional Activity and Tumor-Induced Mobilization of Circulating Angiogenic Cells." *Proceedings of the National Academy of Sciences of the United States of America* 106(7): 2353–58.
- Lee, Youngsoo et al. 2003. "A Molecular Fingerprint for Medulloblastoma." *Cancer research* 63(17): 5428–37.
- Leigh, B C. 1989. "Attitudes and Expectancies as Predictors of Drinking Habits: A Comparison of Three Scales." *Journal of studies on alcohol* 50(5): 432–40.
- Levine, Arnold J, and Anna M Puzio-Kuter. 2010. "The Control of the Metabolic Switch in Cancers by Oncogenes and Tumor Suppressor Genes." *Science (New York, N.Y.)* 330(6009): 1340–44.
- Levine, H D, and J Sicé. 1976. "Effects of Set, Setting, and Sedatives, on Reaction Time." *Perceptual and motor skills* 42(2): 403–12.
- Li, Qi Fang, Xiang Rui Wang, Yue Wu Yang, and Han Lin. 2006. "Hypoxia Upregulates Hypoxia Inducible Factor (HIF)-3 α Expression in Lung Epithelial Cells: Characterization and Comparison with HIF-1 α ." *Cell research* 16(6): 548–58.

- Li, Yanping, Xiao-Xin Sun, David Z Qian, and Mu-Shui Dai. 2020. "Molecular Crosstalk Between MYC and HIF in Cancer." *Frontiers in cell and developmental biology* 8: 590576.
- Li, Zhiqin, and Sigrid A Langhans. 2021. "In Vivo and Ex Vivo Pediatric Brain Tumor Models: An Overview." *Frontiers in oncology* 11: 620831.
- Li, Zhizhong et al. 2009. "Hypoxia-Inducible Factors Regulate Tumorigenic Capacity of Glioma Stem Cells." *Cancer cell* 15(6): 501–13.
- Lin, Charles Y et al. 2016. "Active Medulloblastoma Enhancers Reveal Subgroup-Specific Cellular Origins." *Nature* 530(7588): 57–62.
- Litchfield, Lacey M et al. 2015. "Hyperglycemia-Induced Metabolic Compensation Inhibits Metformin Sensitivity in Ovarian Cancer." *Oncotarget* 6(27): 23548–60.
- Liu, Ren et al. 2021. "A HIF1 α -GPD1 Feedforward Loop Inhibits the Progression of Renal Clear Cell Carcinoma via Mitochondrial Function and Lipid Metabolism." *Journal of experimental & clinical cancer research : CR* 40(1): 188.
- Liu, Xing et al. 2015. "Repression of Hypoxia-Inducible Factor α Signaling by Set7-Mediated Methylation." *Nucleic acids research* 43(10): 5081–98.
- Louis, David N et al. 2016. "The 2016 World Health Organization Classification of Tumors of the Central Nervous System: A Summary." *Acta neuropathologica* 131(6): 803–20.
- Lu, Renquan et al. 2013. "Lactate Dehydrogenase 5 Expression in Non-Hodgkin Lymphoma Is Associated with the Induced Hypoxia Regulated Protein and Poor Prognosis." *PloS one* 8(9): e74853.
- Luo, Deqing et al. 2019. "Clinicopathological and Prognostic Value of Hypoxia-Inducible Factor-1 α in Patients with Bone Tumor: A Systematic Review and Meta-Analysis." *Journal of orthopaedic surgery and research* 14(1): 56.
- Luo, Weibo et al. 2010. "Hsp70 and CHIP Selectively Mediate Ubiquitination and Degradation of Hypoxia-Inducible Factor (HIF)-1 α but Not HIF-2 α ." *The Journal of biological chemistry* 285(6): 3651–63.
- Maccalli, Cristina, Kakil Ibrahim Rasul, Mamoun Elawad, and Soldano Ferrone. 2018. "The Role of Cancer Stem Cells in the Modulation of Anti-Tumor Immune Responses." *Seminars in cancer biology* 53: 189–200.
- MacDonald, M J. 1981. "High Content of Mitochondrial Glycerol-3-Phosphate Dehydrogenase in Pancreatic Islets and Its Inhibition by Diazoxide." *The Journal of biological chemistry* 256(16): 8287–90.
- Madala, Hanumantha Rao et al. 2020. "Nitrogen Trapping as a Therapeutic Strategy in Tumors with Mitochondrial Dysfunction." *Cancer research* 80(17): 3492–3506.
- Madera, Dmitri et al. 2015. "Prevention of Tumor Growth Driven by PIK3CA and HPV Oncogenes by Targeting MTOR Signaling with Metformin in Oral Squamous Carcinomas Expressing OCT3." *Cancer prevention research (Philadelphia, Pa.)* 8(3): 197–207.
- Madiraju, Anila K et al. 2014. "Metformin Suppresses Gluconeogenesis by Inhibiting Mitochondrial Glycerophosphate Dehydrogenase." *Nature* 510(7506): 542–46.
- di Magno, Laura et al. 2020. "Phenformin Inhibits Hedgehog-Dependent Tumor Growth through a Complex I-Independent Redox/Corepressor Module." *Cell reports* 30(6): 1735-1752.e7.
- Mangraviti, Antonella et al. 2017. "HIF-1 α - Targeting Acriflavine Provides Long Term Survival and Radiological Tumor Response in Brain Cancer Therapy." *Scientific reports* 7(1): 14978.
- Marchiq, Ibtissam et al. 2015. "Genetic Disruption of Lactate/H⁺ Symporters (MCTs) and Their Subunit CD147/BASIGIN Sensitizes Glycolytic Tumor Cells to Phenformin." *Cancer research* 75(1): 171–80.

- Marx, M v, and F D Panzer. 1988. "Recurrent Radiculopathy in an Elderly Woman." *Investigative radiology* 23(2): 147–50.
- Mason, R P. 2006. "Non-Invasive Assessment of Kidney Oxygenation: A Role for BOLD MRI." *Kidney international* 70(1): 10–11.
- Maynard, Mindy A et al. 2005. "Human HIF-3 α 4 Is a Dominant-Negative Regulator of HIF-1 and Is down-Regulated in Renal Cell Carcinoma." *FASEB journal : official publication of the Federation of American Societies for Experimental Biology* 19(11): 1396–1406.
- Mazzio, Elizabeth, Nzinga Mack, Ramesh B Badisa, and Karam F A Soliman. 2021. "Triple Isozyme Lactic Acid Dehydrogenase Inhibition in Fully Viable MDA-MB-231 Cells Induces Cytostatic Effects That Are Not Reversed by Exogenous Lactic Acid." *Biomolecules* 11(12).
- McCord, Amy M et al. 2009. "Physiologic Oxygen Concentration Enhances the Stem-like Properties of CD133+ Human Glioblastoma Cells in Vitro." *Molecular cancer research : MCR* 7(4): 489–97.
- McKenna, Mary C, Helle S Waagepetersen, Arne Schousboe, and Ursula Sonnewald. 2006. "Neuronal and Astrocytic Shuttle Mechanisms for Cytosolic-Mitochondrial Transfer of Reducing Equivalents: Current Evidence and Pharmacological Tools." *Biochemical pharmacology* 71(4): 399–407.
- McKinley, Bruce A., William P. Morris, C. Lee Parmley, and Bruce D. Butler. 1996. "Brain Parenchyma PO Sub 2, PCO Sub 2, and PH during and after Hypoxic, Ischemic Brain Insult in Dogs." *Critical Care Medicine* 24(11): 1858–68.
- Minassian, Lori M, Tiziana Cotechini, Erin Huitema, and Charles H Graham. 2019. "Hypoxia-Induced Resistance to Chemotherapy in Cancer." *Advances in experimental medicine and biology* 1136: 123–39.
- Morabito, Morgane et al. 2019. "An Autocrine ActivinB Mechanism Drives TGF β /Activin Signaling in Group 3 Medulloblastoma." *EMBO molecular medicine* 11(8): e9830.
- Morales, Daniel R, and Andrew D Morris. 2015. "Metformin in Cancer Treatment and Prevention." *Annual review of medicine* 66: 17–29.
- Mottet, Denis et al. 2003. "Regulation of Hypoxia-Inducible Factor-1 α Protein Level during Hypoxic Conditions by the Phosphatidylinositol 3-Kinase/Akt/Glycogen Synthase Kinase 3 β Pathway in HepG2 Cells." *The Journal of biological chemistry* 278(33): 31277–85.
- Mráček, Tomáš et al. 2009. "High Efficiency of ROS Production by Glycerophosphate Dehydrogenase in Mammalian Mitochondria." *Archives of biochemistry and biophysics* 481(1): 30–36.
- Mráček, Tomáš et al. 2014. "ROS Generation and Multiple Forms of Mammalian Mitochondrial Glycerol-3-Phosphate Dehydrogenase." *Biochimica et biophysica acta* 1837(1): 98–111.
- Mráček, Tomáš, Zdeněk Drahota, and Josef Houštěk. 2013. "The Function and the Role of the Mitochondrial Glycerol-3-Phosphate Dehydrogenase in Mammalian Tissues." *Biochimica et biophysica acta* 1827(3): 401–10.
- Mu, Han et al. 2021. "Mild Chronic Hypoxia-Induced HIF-2 α Interacts with c-MYC through Competition with HIF-1 α to Induce Hepatocellular Carcinoma Cell Proliferation." *Cellular oncology (Dordrecht)* 44(5): 1151–66.
- Munksgaard Thorén, Matilda et al. 2017. "Myc-Induced Glutaminolysis Bypasses HIF-Driven Glycolysis in Hypoxic Small Cell Lung Carcinoma Cells." *Oncotarget* 8(30): 48983–95.

- Mylonis, Ilias et al. 2006. "Identification of MAPK Phosphorylation Sites and Their Role in the Localization and Activity of Hypoxia-Inducible Factor-1alpha." *The Journal of biological chemistry* 281(44): 33095–106.
- Mylonis, Ilias, Georgia Chachami, Efrosyni Paraskeva, and George Simos. 2008. "Atypical CRM1-Dependent Nuclear Export Signal Mediates Regulation of Hypoxia-Inducible Factor-1alpha by MAPK." *The Journal of biological chemistry* 283(41): 27620–27.
- Nazio, Francesca et al. 2021. "Targeting Cancer Stem Cells in Medulloblastoma by Inhibiting AMBRA1 Dual Function in Autophagy and STAT3 Signalling." *Acta neuropathologica* 142(3): 537–64.
- Neiva, Ismael, João O Malva, and Jorge Valero. 2014. "Can We Talk about Microglia without Neurons? A Discussion of Microglial Cell Autonomous Properties in Culture." *Frontiers in cellular neuroscience* 8: 202.
- Neumann, Julia E, Fredrik J Swartling, and Ulrich Schüller. 2017. "Medulloblastoma: Experimental Models and Reality." *Acta neuropathologica* 134(5): 679–89.
- Nguyen, Nga Huynh Tran, Anders Bråthe, and Bjørnar Hassel. 2003. "Neuronal Uptake and Metabolism of Glycerol and the Neuronal Expression of Mitochondrial Glycerol-3-Phosphate Dehydrogenase." *Journal of neurochemistry* 85(4): 831–42.
- Nishikawa, Masahiro et al. 2021. "Hypoxia-Induced Phenotypic Transition from Highly Invasive to Less Invasive Tumors in Glioma Stem-like Cells: Significance of CD44 and Osteopontin as Therapeutic Targets in Glioblastoma." *Translational oncology* 14(8): 101137.
- Noguera, Rosa et al. 2009. "HIF-1alpha and HIF-2alpha Are Differentially Regulated in Vivo in Neuroblastoma: High HIF-1alpha Correlates Negatively to Advanced Clinical Stage and Tumor Vascularization." *Clinical cancer research : an official journal of the American Association for Cancer Research* 15(23): 7130–36.
- Nordsmark, M, M Overgaard, and J Overgaard. 1996. "Pretreatment Oxygenation Predicts Radiation Response in Advanced Squamous Cell Carcinoma of the Head and Neck." *Radiotherapy and oncology : journal of the European Society for Therapeutic Radiology and Oncology* 41(1): 31–39.
- Nordsmark, Marianne et al. 2005. "Prognostic Value of Tumor Oxygenation in 397 Head and Neck Tumors after Primary Radiation Therapy. An International Multi-Center Study." *Radiotherapy and oncology : journal of the European Society for Therapeutic Radiology and Oncology* 77(1): 18–24.
- Northcott, Paul A et al. 2017. "The Whole-Genome Landscape of Medulloblastoma Subtypes." *Nature* 547(7663): 311–17.
- van Nostrand, Jeanine L et al. 2020. "AMPK Regulation of Raptor and TSC2 Mediate Metformin Effects on Transcriptional Control of Anabolism and Inflammation." *Genes & development* 34(19–20): 1330–44.
- Nyhan, Michelle J., Gerald C. O'Sullivan, and Sharon L. McKenna. 2008. "Role of the VHL (von Hippel–Lindau) Gene in Renal Cancer: A Multifunctional Tumour Suppressor." *Biochemical Society Transactions* 36(3): 472–78.
- Ohh, M et al. 2000. "Ubiquitination of Hypoxia-Inducible Factor Requires Direct Binding to the Beta-Domain of the von Hippel-Lindau Protein." *Nature cell biology* 2(7): 423–27.
- Oizel, Kristell et al. 2017. "Efficient Mitochondrial Glutamine Targeting Prevails Over Glioblastoma Metabolic Plasticity." *Clinical cancer research : an official journal of the American Association for Cancer Research* 23(20): 6292–6304.
- Ollerenshaw, Martin, Toby Page, John Hammonds, and Andrew Demaine. 2004. "Polymorphisms in the Hypoxia Inducible Factor-1alpha Gene (HIF1A) Are Associated with the Renal Cell Carcinoma Phenotype." *Cancer genetics and cytogenetics* 153(2): 122–26.

- Orr, Adam L et al. 2014. "Novel Inhibitors of Mitochondrial Sn-Glycerol 3-Phosphate Dehydrogenase." *PloS one* 9(2): e89938.
- Packer, R J et al. 1999. "Treatment of Children with Medulloblastomas with Reduced-Dose Craniospinal Radiation Therapy and Adjuvant Chemotherapy: A Children's Cancer Group Study." *Journal of clinical oncology : official journal of the American Society of Clinical Oncology* 17(7): 2127–36.
- Packer, Roger J. 2011. "Risk Stratification of Medulloblastoma: A Paradigm for Future Childhood Brain Tumor Management Strategies." *Current neurology and neuroscience reports* 11(2): 124–26.
- Pagnuzzi-Boncompagni, Marina et al. 2021. "Antiangiogenic Compound Axitinib Demonstrates Low Toxicity and Antitumoral Effects against Medulloblastoma." *Cancers* 14(1): 70.
- Påhlman, Sven, and Sofie Mohlin. 2018. "Hypoxia and Hypoxia-Inducible Factors in Neuroblastoma." *Cell and tissue research* 372(2): 269–75.
- Pasanen, Annika et al. 2010. "Hypoxia-Inducible Factor (HIF)-3 α Is Subject to Extensive Alternative Splicing in Human Tissues and Cancer Cells and Is Regulated by HIF-1 but Not HIF-2." *The international journal of biochemistry & cell biology* 42(7): 1189–1200.
- Pecqueur, Claire et al. 2013. "Targeting Metabolism to Induce Cell Death in Cancer Cells and Cancer Stem Cells." *International journal of cell biology* 2013: 805975.
- Pellerin, Luc et al. 2007. "Activity-Dependent Regulation of Energy Metabolism by Astrocytes: An Update." *Glia* 55(12): 1251–62.
- Percy, Melanie J et al. 2003. "A Common Polymorphism in the Oxygen-Dependent Degradation (ODD) Domain of Hypoxia Inducible Factor-1 α (HIF-1 α) Does Not Impair Pro-564 Hydroxylation." *Molecular cancer* 2: 31.
- Persson, Camilla U et al. 2020. "ARNT-Dependent HIF-2 Transcriptional Activity Is Not Sufficient to Regulate Downstream Target Genes in Neuroblastoma." *Experimental cell research* 388(2): 111845.
- Petruzzelli, Raffaella et al. 2014. "HIF-2 α Regulates NANOG Expression in Human Embryonic Stem Cells Following Hypoxia and Reoxygenation through the Interaction with an Oct-Sox Cis Regulatory Element." *PloS one* 9(10): e108309.
- Pietsch, Torsten et al. 2014. "Prognostic Significance of Clinical, Histopathological, and Molecular Characteristics of Medulloblastomas in the Prospective HIT2000 Multicenter Clinical Trial Cohort." *Acta neuropathologica* 128(1): 137–49.
- Pollak, Michael. 2010. "Metformin and Other Biguanides in Oncology: Advancing the Research Agenda." *Cancer prevention research (Philadelphia, Pa.)* 3(9): 1060–65.
- Puget, Stephanie et al. 2009. "Injuries to Inferior Vermis and Dentate Nuclei Predict Poor Neurological and Neuropsychological Outcome in Children with Malignant Posterior Fossa Tumors." *Cancer* 115(6): 1338–47.
- Pujalte Martin, Marc et al. 2021. "TAXOMET: A French Prospective Multicentric Randomized Phase II Study of Docetaxel Plus Metformin Versus Docetaxel Plus Placebo in Metastatic Castration-Resistant Prostate Cancer." *Clinical genitourinary cancer* 19(6): 501–9.
- Raja, R et al. 2014. "Hypoxia-Driven Osteopontin Contributes to Breast Tumor Growth through Modulation of HIF1 α -Mediated VEGF-Dependent Angiogenesis." *Oncogene* 33(16): 2053–64.
- Ramani, Pramila, Alison Headford, and Margaret T May. 2013. "GLUT1 Protein Expression Correlates with Unfavourable Histologic Category and High Risk in Patients with Neuroblastic Tumours." *Virchows Archiv : an international journal of pathology* 462(2): 203–9.

- Ramaswamy, Vijay et al. 2016. "Risk Stratification of Childhood Medulloblastoma in the Molecular Era: The Current Consensus." *Acta neuropathologica* 131(6): 821–31.
- Ramos, Milagros et al. 2003. "Developmental Changes in the Ca²⁺-Regulated Mitochondrial Aspartate-Glutamate Carrier Aralar1 in Brain and Prominent Expression in the Spinal Cord." *Brain research. Developmental brain research* 143(1): 33–46.
- Ransohoff, Richard M. 2016. "A Polarizing Question: Do M1 and M2 Microglia Exist?" *Nature neuroscience* 19(8): 987–91.
- Raval, Raju R et al. 2005. "Contrasting Properties of Hypoxia-Inducible Factor 1 (HIF-1) and HIF-2 in von Hippel-Lindau-Associated Renal Cell Carcinoma." *Molecular and cellular biology* 25(13): 5675–86.
- Reinholt, F P, K Hulthenby, A Oldberg, and D Heinegård. 1990. "Osteopontin--a Possible Anchor of Osteoclasts to Bone." *Proceedings of the National Academy of Sciences of the United States of America* 87(12): 4473–75.
- Ren, L et al. 2020. "Glutaminase-1 (GLS1) Inhibition Limits Metastatic Progression in Osteosarcoma." *Cancer & metabolism* 8: 4.
- Renfrow, Jaclyn J et al. 2020. "Attenuating Hypoxia Driven Malignant Behavior in Glioblastoma with a Novel Hypoxia-Inducible Factor 2 Alpha Inhibitor." *Scientific reports* 10(1): 15195.
- Rey, Sergio, and Gregg L Semenza. 2010. "Hypoxia-Inducible Factor-1-Dependent Mechanisms of Vascularization and Vascular Remodelling." *Cardiovascular research* 86(2): 236–42.
- Roussel, Martine F, and Jennifer L Stripay. 2020. "Modeling Pediatric Medulloblastoma." *Brain pathology (Zurich, Switzerland)* 30(3): 703–12.
- Rusert, Jessica M et al. 2020. "Functional Precision Medicine Identifies New Therapeutic Candidates for Medulloblastoma." *Cancer research* 80(23): 5393–5407.
- Sadaghianloo, Nirvana et al. 2020. "Co-Culture of Human Fibroblasts, Smooth Muscle and Endothelial Cells Promotes Osteopontin Induction in Hypoxia." *Journal of cellular and molecular medicine* 24(5): 2931–41.
- . 2021. "Hypoxia and Hypoxia-Inducible Factors Promote the Development of Neointimal Hyperplasia in Arteriovenous Fistula." *The Journal of physiology* 599(8): 2299–2321.
- Saheki, Takeyori et al. 2007. "Citrin/Mitochondrial Glycerol-3-Phosphate Dehydrogenase Double Knock-out Mice Recapitulate Features of Human Citrin Deficiency." *The Journal of biological chemistry* 282(34): 25041–52.
- . 2011. "Metabolomic Analysis Reveals Hepatic Metabolite Perturbations in Citrin/Mitochondrial Glycerol-3-Phosphate Dehydrogenase Double-Knockout Mice, a Model of Human Citrin Deficiency." *Molecular genetics and metabolism* 104(4): 492–500.
- Sakadžić, Sava et al. 2010. "Two-Photon High-Resolution Measurement of Partial Pressure of Oxygen in Cerebral Vasculature and Tissue." *Nature methods* 7(9): 755–59.
- Sánchez-López, Elsa et al. "Angiotensin II Regulates Vascular Endothelial Growth Factor via Hypoxia-Inducible Factor-1alpha Induction and Redox Mechanisms in the Kidney." *Antioxidants & redox signaling* 7(9–10): 1275–84.
- Scheuermann, Thomas H et al. 2009. "Artificial Ligand Binding within the HIF2alpha PAS-B Domain of the HIF2 Transcription Factor." *Proceedings of the National Academy of Sciences of the United States of America* 106(2): 450–55.
- Schito, Luana, and Gregg L Semenza. 2016. "Hypoxia-Inducible Factors: Master Regulators of Cancer Progression." *Trends in cancer* 2(12): 758–70.
- Schödel, Johannes et al. 2016. "Hypoxia, Hypoxia-Inducible Transcription Factors, and Renal Cancer." *European urology* 69(4): 646–57.

- Schurr, A, and B M Rigor. 1998. "Brain Anaerobic Lactate Production: A Suicide Note or a Survival Kit?" *Developmental neuroscience* 20(4–5): 348–57.
- Schwalbe, Edward C et al. 2017. "Novel Molecular Subgroups for Clinical Classification and Outcome Prediction in Childhood Medulloblastoma: A Cohort Study." *The Lancet. Oncology* 18(7): 958–71.
- Schwinn, Stefanie et al. 2021. "Cytotoxic Effects and Tolerability of Gemcitabine and Axitinib in a Xenograft Model for C-Myc Amplified Medulloblastoma." *Scientific reports* 11(1): 14062.
- Seidel, Sascha et al. 2010. "A Hypoxic Niche Regulates Glioblastoma Stem Cells through Hypoxia Inducible Factor 2 Alpha." *Brain : a journal of neurology* 133(Pt 4): 983–95.
- Semenza, G L. 2000. "HIF-1: Using Two Hands to Flip the Angiogenic Switch." *Cancer metastasis reviews* 19(1–2): 59–65.
- Semenza, Gregg L. 2012. "Hypoxia-Inducible Factors: Mediators of Cancer Progression and Targets for Cancer Therapy." *Trends in pharmacological sciences* 33(4): 207–14.
- Shackelford, David B et al. 2013. "LKB1 Inactivation Dictates Therapeutic Response of Non-Small Cell Lung Cancer to the Metabolism Drug Phenformin." *Cancer cell* 23(2): 143–58.
- Shen, Chuan et al. 2011. "Genetic and Functional Studies Implicate HIF1 α as a 14q Kidney Cancer Suppressor Gene." *Cancer discovery* 1(3): 222–35.
- Shen, Colette J, and Stephanie A Terezakis. 2021. "The Evolving Role of Radiotherapy for Pediatric Cancers With Advancements in Molecular Tumor Characterization and Targeted Therapies." *Frontiers in oncology* 11: 679701.
- Shevde, Lalita A, and Rajeev S Samant. 2014. "Role of Osteopontin in the Pathophysiology of Cancer." *Matrix biology : journal of the International Society for Matrix Biology* 37: 131–41.
- Sies, Helmut, Carsten Berndt, and Dean P Jones. 2017. "Oxidative Stress." *Annual review of biochemistry* 86: 715–48.
- Silber, J H et al. 1992. "Whole-Brain Irradiation and Decline in Intelligence: The Influence of Dose and Age on IQ Score." *Journal of clinical oncology : official journal of the American Society of Clinical Oncology* 10(9): 1390–96.
- Singh, Gurmit. 2014. "Mitochondrial FAD-Linked Glycerol-3-Phosphate Dehydrogenase: A Target for Cancer Therapeutics." *Pharmaceuticals (Basel, Switzerland)* 7(2): 192–206.
- Singh, Sheila K et al. 2003. "Identification of a Cancer Stem Cell in Human Brain Tumors." *Cancer research* 63(18): 5821–28.
- Singla, Veena, and Jeremy F Reiter. 2006. "The Primary Cilium as the Cell's Antenna: Signaling at a Sensory Organelle." *Science (New York, N.Y.)* 313(5787): 629–33.
- Smythies, James A et al. 2019. "Inherent DNA-Binding Specificities of the HIF-1 α and HIF-2 α Transcription Factors in Chromatin." *EMBO reports* 20(1).
- Soni, Sourabh, and Yogendra S Padwad. 2017. "HIF-1 in Cancer Therapy: Two Decade Long Story of a Transcription Factor." *Acta oncologica (Stockholm, Sweden)* 56(4): 503–15.
- Sreekanthreddy, Peddagangannagari et al. 2010. "Identification of Potential Serum Biomarkers of Glioblastoma: Serum Osteopontin Levels Correlate with Poor Prognosis." *Cancer epidemiology, biomarkers & prevention : a publication of the American Association for Cancer Research, cosponsored by the American Society of Preventive Oncology* 19(6): 1409–22.
- Srinivas, V, L P Zhang, X H Zhu, and J Caro. 1999. "Characterization of an Oxygen/Redox-Dependent Degradation Domain of Hypoxia-Inducible Factor Alpha (HIF-Alpha) Proteins." *Biochemical and biophysical research communications* 260(2): 557–61.

- Standal, Therese, Magne Borset, and Anders Sundan. 2004. "Role of Osteopontin in Adhesion, Migration, Cell Survival and Bone Remodeling." *Experimental oncology* 26(3): 179–84.
- Stiehl, D P et al. 2012. "Non-Canonical HIF-2 α Function Drives Autonomous Breast Cancer Cell Growth via an AREG-EGFR/ErbB4 Autocrine Loop." *Oncogene* 31(18): 2283–97.
- Stone, H B, J M Brown, T L Phillips, and R M Sutherland. 1993. "Oxygen in Human Tumors: Correlations between Methods of Measurement and Response to Therapy. Summary of a Workshop Held November 19-20, 1992, at the National Cancer Institute, Bethesda, Maryland." *Radiation research* 136(3): 422–34.
- Sullivan, Lucas B et al. 2015. "Supporting Aspartate Biosynthesis Is an Essential Function of Respiration in Proliferating Cells." *Cell* 162(3): 552–63.
- . 2018. "Aspartate Is an Endogenous Metabolic Limitation for Tumour Growth." *Nature cell biology* 20(7): 782–88.
- Sung, Ki Woong et al. 2013. "Reduced-Dose Craniospinal Radiotherapy Followed by Tandem High-Dose Chemotherapy and Autologous Stem Cell Transplantation in Patients with High-Risk Medulloblastoma." *Neuro-oncology* 15(3): 352–59.
- Sytinskiĭ, I A et al. "[Aminotransferase and Dehydrogenase Activity in Human Brain Tumours]." *Ukrainskii biokhimiĭeskii zhurnal (1978)* 51(2): 111–16.
- Takeda, Norihiko et al. 2010. "Differential Activation and Antagonistic Function of HIF- α Isoforms in Macrophages Are Essential for NO Homeostasis." *Genes & development* 24(5): 491–501.
- Tamayo, Pablo et al. 2011. "Predicting Relapse in Patients with Medulloblastoma by Integrating Evidence from Clinical and Genomic Features." *Journal of clinical oncology : official journal of the American Society of Clinical Oncology* 29(11): 1415–23.
- Tanaka, J, S Miyawaki, N Maeda, and K Mikoshiba. 1991. "Immunohistochemical Expression of P400 Protein in Purkinje Cells of Sphingomyelinosis Mouse." *Brain & development* 13(2): 110–14.
- Tanimoto, K, Y Makino, T Pereira, and L Poellinger. 2000. "Mechanism of Regulation of the Hypoxia-Inducible Factor-1 Alpha by the von Hippel-Lindau Tumor Suppressor Protein." *The EMBO journal* 19(16): 4298–4309.
- Tanimoto, Keiji et al. 2003. "Hypoxia-Inducible Factor-1alpha Polymorphisms Associated with Enhanced Transactivation Capacity, Implying Clinical Significance." *Carcinogenesis* 24(11): 1779–83.
- Tate, John G et al. 2019. "COSMIC: The Catalogue Of Somatic Mutations In Cancer." *Nucleic acids research* 47(D1): D941–47.
- Tausendschön, Michaela et al. 2015. "Genome-Wide Identification of Hypoxia-Inducible Factor-1 and -2 Binding Sites in Hypoxic Human Macrophages Alternatively Activated by IL-10." *Biochimica et biophysica acta* 1849(1): 10–22.
- Taylor, Michael D et al. 2012. "Molecular Subgroups of Medulloblastoma: The Current Consensus." *Acta neuropathologica* 123(4): 465–72.
- Thakur, Shilpa et al. 2018. "Metformin Targets Mitochondrial Glycerophosphate Dehydrogenase to Control Rate of Oxidative Phosphorylation and Growth of Thyroid Cancer In Vitro and In Vivo." *Clinical cancer research : an official journal of the American Association for Cancer Research* 24(16): 4030–43.
- Thomas, P R et al. 2000. "Low-Stage Medulloblastoma: Final Analysis of Trial Comparing Standard-Dose with Reduced-Dose Neuraxis Irradiation." *Journal of clinical oncology : official journal of the American Society of Clinical Oncology* 18(16): 3004–11.

- Thompson, Eric M et al. 2016. "Prognostic Value of Medulloblastoma Extent of Resection after Accounting for Molecular Subgroup: A Retrospective Integrated Clinical and Molecular Analysis." *The Lancet Oncology* 17(4): 484–95.
- Thompson, Margaret C et al. 2006. "Genomics Identifies Medulloblastoma Subgroups That Are Enriched for Specific Genetic Alterations." *Journal of clinical oncology : official journal of the American Society of Clinical Oncology* 24(12): 1924–31.
- Tian, H, S L McKnight, and D W Russell. 1997. "Endothelial PAS Domain Protein 1 (EPAS1), a Transcription Factor Selectively Expressed in Endothelial Cells." *Genes & development* 11(1): 72–82.
- Titov, Denis v et al. 2016. "Complementation of Mitochondrial Electron Transport Chain by Manipulation of the NAD⁺/NADH Ratio." *Science (New York, N.Y.)* 352(6282): 231–35.
- Trédan, Olivier, Carlos M Galmarini, Krupa Patel, and Ian F Tannock. 2007. "Drug Resistance and the Solid Tumor Microenvironment." *Journal of the National Cancer Institute* 99(19): 1441–54.
- Treins, Caroline et al. 2002. "Insulin Stimulates Hypoxia-Inducible Factor 1 through a Phosphatidylinositol 3-Kinase/Target of Rapamycin-Dependent Signaling Pathway." *The Journal of biological chemistry* 277(31): 27975–81.
- Tuttle, Stephen W et al. 2007. "Detection of Reactive Oxygen Species via Endogenous Oxidative Pentose Phosphate Cycle Activity in Response to Oxygen Concentration: Implications for the Mechanism of HIF-1 α Stabilization under Moderate Hypoxia." *The Journal of biological chemistry* 282(51): 36790–96.
- Valable, Samuel et al. 2017. "Imaging of Brain Oxygenation with Magnetic Resonance Imaging: A Validation with Positron Emission Tomography in the Healthy and Tumoural Brain." *Journal of cerebral blood flow and metabolism : official journal of the International Society of Cerebral Blood Flow and Metabolism* 37(7): 2584–97.
- Valencia-Cervantes, Jesús et al. 2019. "Hypoxia Increases Chemoresistance in Human Medulloblastoma DAOY Cells via Hypoxia-inducible Factor 1 α -mediated Downregulation of the CYP2B6, CYP3A4 and CYP3A5 Enzymes and Inhibition of Cell Proliferation." *Oncology reports* 41(1): 178–90.
- Valvona, Cara J, and Helen L Fillmore. 2018. "Oxamate, but Not Selective Targeting of LDH-A, Inhibits Medulloblastoma Cell Glycolysis, Growth and Motility." *Brain sciences* 8(4).
- Vara-Ciruelos, Diana et al. 2019. "Phenformin, But Not Metformin, Delays Development of T Cell Acute Lymphoblastic Leukemia/Lymphoma via Cell-Autonomous AMPK Activation." *Cell reports* 27(3): 690-698.e4.
- Vaupel, Peter. 2008. "Hypoxia and Aggressive Tumor Phenotype: Implications for Therapy and Prognosis." *The oncologist* 13 Suppl 3: 21–26.
- Vaupel, Peter, Arnulf Mayer, and Michael Höckel. 2004. "Tumor Hypoxia and Malignant Progression." *Methods in enzymology* 381: 335–54.
- Waagepetersen, H S, H Qu, A Schousboe, and U Sonnewald. 2001. "Elucidation of the Quantitative Significance of Pyruvate Carboxylation in Cultured Cerebellar Neurons and Astrocytes." *Journal of neuroscience research* 66(5): 763–70.
- Wahba, H A et al. "Adjuvant Chemotherapy after Reduced Craniospinal Irradiation Dose in Children with Average-Risk Medulloblastoma: A 5-Year Follow-up Study." *Journal of B.U.ON. : official journal of the Balkan Union of Oncology* 18(2): 425–29.
- Wai, Philip Y, and Paul C Kuo. 2008. "Osteopontin: Regulation in Tumor Metastasis." *Cancer metastasis reviews* 27(1): 103–18.
- Wallace, Eli M et al. 2016. "A Small-Molecule Antagonist of HIF2 α Is Efficacious in Preclinical Models of Renal Cell Carcinoma." *Cancer research* 76(18): 5491–5500.

- Wang, G L, B H Jiang, E A Rue, and G L Semenza. 1995. "Hypoxia-Inducible Factor 1 Is a Basic-Helix-Loop-Helix-PAS Heterodimer Regulated by Cellular O₂ Tension." *Proceedings of the National Academy of Sciences of the United States of America* 92(12): 5510–14.
- Wang, Jun, and Robert J Wechsler-Reya. 2014. "The Role of Stem Cells and Progenitors in the Genesis of Medulloblastoma." *Experimental neurology* 260: 69–73.
- Wang, Pan et al. 2017. "HIF1 α Regulates Single Differentiated Glioma Cell Dedifferentiation to Stem-like Cell Phenotypes with High Tumorigenic Potential under Hypoxia." *Oncotarget* 8(17): 28074–92.
- WARBURG, O. 1956a. "On Respiratory Impairment in Cancer Cells." *Science (New York, N.Y.)* 124(3215): 269–70.
- . 1956b. "On the Origin of Cancer Cells." *Science (New York, N.Y.)* 123(3191): 309–14.
- Warfel, Noel A et al. 2013. "CDK1 Stabilizes HIF-1 α via Direct Phosphorylation of Ser668 to Promote Tumor Growth." *Cell cycle (Georgetown, Tex.)* 12(23): 3689–3701.
- Weber, G F, G S Lett, and N C Haubein. 2010. "Osteopontin Is a Marker for Cancer Aggressiveness and Patient Survival." *British journal of cancer* 103(6): 861–69.
- Weigel, Brenda J et al. 2007. "A Phase I Study of 17-Allylaminogeldanamycin in Relapsed/Refractory Pediatric Patients with Solid Tumors: A Children's Oncology Group Study." *Clinical cancer research : an official journal of the American Association for Cancer Research* 13(6): 1789–93.
- Wenthold, R J, K K Skaggs, and R A Altschuler. 1986. "Immunocytochemical Localization of Aspartate Aminotransferase and Glutaminase Immunoreactivities in the Cerebellum." *Brain research* 363(2): 371–75.
- Wheaton, William W et al. 2014. "Metformin Inhibits Mitochondrial Complex I of Cancer Cells to Reduce Tumorigenesis." *eLife* 3: e02242.
- Whillans, D W, and J W Hunt. 1982. "A Rapid-Mixing Comparison of the Mechanisms of Radiosensitization by Oxygen and Misonidazole in CHO Cells." *Radiation research* 90(1): 126–41.
- Wibom, Rolf et al. 2009. "AGC1 Deficiency Associated with Global Cerebral Hypomyelination." *The New England journal of medicine* 361(5): 489–95.
- Wiesener, Michael S et al. 2003. "Widespread Hypoxia-Inducible Expression of HIF-2 α in Distinct Cell Populations of Different Organs." *FASEB journal : official publication of the Federation of American Societies for Experimental Biology* 17(2): 271–73.
- Wigerup, Caroline, Sven Pählman, and Daniel Bexell. 2016. "Therapeutic Targeting of Hypoxia and Hypoxia-Inducible Factors in Cancer." *Pharmacology & therapeutics* 164: 152–69.
- Wilson, William R, and Michael P Hay. 2011. "Targeting Hypoxia in Cancer Therapy." *Nature reviews. Cancer* 11(6): 393–410.
- Wise, David R et al. 2008. "Myc Regulates a Transcriptional Program That Stimulates Mitochondrial Glutaminolysis and Leads to Glutamine Addiction." *Proceedings of the National Academy of Sciences of the United States of America* 105(48): 18782–87.
- Xie, Cen et al. 2018. "Metabolic Profiling of the Novel Hypoxia-Inducible Factor 2 α Inhibitor PT2385 In Vivo and In Vitro." *Drug metabolism and disposition: the biological fate of chemicals* 46(4): 336–45.
- Xie, Na et al. 2020. "NAD⁺ Metabolism: Pathophysiologic Mechanisms and Therapeutic Potential." *Signal transduction and targeted therapy* 5(1): 227.
- Xu, Dazhong et al. 2010. "Plk3 Functions as an Essential Component of the Hypoxia Regulatory Pathway by Direct Phosphorylation of HIF-1 α ." *The Journal of biological chemistry* 285(50): 38944–50.

- Xu, Jingying, Ashley Margol, Shahab Asgharzadeh, and Anat Erdreich-Epstein. 2015. "Pediatric Brain Tumor Cell Lines." *Journal of cellular biochemistry* 116(2): 218–24.
- Xu, Kui, David A Boas, Sava Sakadžić, and Joseph C LaManna. 2017. "Brain Tissue PO₂ Measurement During Normoxia and Hypoxia Using Two-Photon Phosphorescence Lifetime Microscopy." *Advances in experimental medicine and biology* 977: 149–53.
- Xue, G et al. 2015. "C-Myc-Mediated Repression of MiR-15-16 in Hypoxia Is Induced by Increased HIF-2 α and Promotes Tumor Angiogenesis and Metastasis by Upregulating FGF2." *Oncogene* 34(11): 1393–1406.
- Yamazaki, Shintaro et al. 2021. "Newly Established Patient-Derived Organoid Model of Intracranial Meningioma." *Neuro-oncology* 23(11): 1936–48.
- Yang, Lingjian et al. 2018. "Development and Validation of a 28-Gene Hypoxia-Related Prognostic Signature for Localized Prostate Cancer." *EBioMedicine* 31: 182–89.
- Yang, Lingjian, and Catharine MI West. 2019. "Hypoxia Gene Expression Signatures as Predictive Biomarkers for Personalising Radiotherapy." *The British journal of radiology* 92(1093): 20180036.
- Yang, Qining et al. 2019. "Up-Regulated HIF-2 α Contributes to the Osteoarthritis Development through Mediating the Primary Cilia Loss." *International immunopharmacology* 75: 105762.
- Yasinska, Inna M, and Vadim v Sumbayev. 2003. "S-Nitrosation of Cys-800 of HIF-1 α Protein Activates Its Interaction with P300 and Stimulates Its Transcriptional Activity." *FEBS letters* 549(1–3): 105–9.
- Yasui, Hironobu et al. 2010. "Low-Field Magnetic Resonance Imaging to Visualize Chronic and Cycling Hypoxia in Tumor-Bearing Mice." *Cancer research* 70(16): 6427–36.
- Yeh, Joanne I, Unmesh Chinte, and Shoucheng Du. 2008. "Structure of Glycerol-3-Phosphate Dehydrogenase, an Essential Monotopic Membrane Enzyme Involved in Respiration and Metabolism." *Proceedings of the National Academy of Sciences of the United States of America* 105(9): 3280–85.
- Yock, Torunn I et al. 2016. "Long-Term Toxic Effects of Proton Radiotherapy for Paediatric Medulloblastoma: A Phase 2 Single-Arm Study." *The Lancet. Oncology* 17(3): 287–98.
- Yotnda, Patricia, Danli Wu, and Anna May Swanson. 2010. "Hypoxic Tumors and Their Effect on Immune Cells and Cancer Therapy." *Methods in molecular biology (Clifton, N.J.)* 651: 1–29.
- Yu, A C, A Schousboe, and L Hertz. 1982. "Metabolic Fate of ¹⁴C-Labeled Glutamate in Astrocytes in Primary Cultures." *Journal of neurochemistry* 39(4): 954–60.
- Yu, Yancheng, Quanwei Yu, and Xiaojin Zhang. 2019. "Allosteric Inhibition of HIF-2 α as a Novel Therapy for Clear Cell Renal Cell Carcinoma." *Drug discovery today* 24(12): 2332–40.
- Zauner, Alois, Ross Bullock, Xiao Di, and Harold F. Young. 1995. "Brain Oxygen, CO₂, PH, and Temperature Monitoring." *Neurosurgery* 37(6): 1168–77.
- Zhao, Hongyun, Kenneth D Swanson, and Bin Zheng. 2021. "Therapeutic Repurposing of Biguanides in Cancer." *Trends in cancer* 7(8): 714–30.
- Zilli, M A, and G Nisi. 1986. "Simple and Sensitive Method for the Determination of Clobazam, Clonazepam and Nitrazepam in Human Serum by High-Performance Liquid Chromatography." *Journal of chromatography* 378(2): 492–97.

Annexes

Annexe 1: Plasmatic osteopontin and vascular access dysfunction in hemodialysis patients: a cross-sectional, case-control study. J Nephrol. 2021 (PMID: 34468976)

Plasmatic osteopontin and vascular access dysfunction in hemodialysis patients: a cross-sectional, case-control study

Julie Contenti, M.D.^{1,2} Matthieu Durand, M.D, Ph. D^{3,4}.

Sandor Vido, M.D.⁵ Serge Declémy, M.D.⁶, Juliette Raffort, M.D, Ph. D⁷
Joseph Carboni, M.D.⁶ Sophie Bonnet, M.Sc. ^{6,8} Christophe Koelsch, M.Sc.⁹

Réda Hassen-Khodja, M.D.^{2,6} Philippe Gual, Ph.D.²

Nathalie M. Mazure, Ph.D.² and Nirvana Sadaghianloo, M.D., Ph. D.*^{2,6}

1. Department of Emergency Medicine, Centre Hospitalier Universitaire de Nice, Nice, France
2. Centre Méditerranéen de Médecine Moléculaire, INSERM U1065, Université Côte d'Azur, Nice, France
3. Department of Urology and Andrology and Renal transplantation, Centre Hospitalier Universitaire de Nice, Nice, France
4. Institute of research on Cancer and aging of Nice, INSERM U1081-CNRS UMR 7284, Université Côte d'Azur, Nice, France
5. Department of Nephrology and Hemodialysis, Centre Hospitalier Universitaire de Nice, Nice, France
6. Department of Vascular Surgery, Centre Hospitalier Universitaire de Nice, Nice, France
7. Clinical Chemistry Laboratory (J.R), Centre Hospitalier Universitaire de Nice, Nice, France
8. Department of Clinical Research and Innovation, Centre Hospitalier Universitaire de Nice, Nice, France
9. Department of Anesthesiology, Centre Hospitalier Universitaire de Nice, Nice, France

* Corresponding author :

Nirvana SADAGHIANLOO, MD, PhD

Service de Chirurgie Vasculaire - Hôpital Pasteur 1 - Centre Hospitalier Universitaire de Nice - 30

Ave de la voie Romaine - 06000 NICE - FRANCE

Phone : +33 492032941 - Fax : +33 4920 33839 ; email address: sadaghianloo.n@chu-nice.fr

Running title : Osteopontin in AVF stenosis

Keywords (5) : Biomarkers; Hemodialysis access; Osteopontin; Surgical arteriovenous shunt

Word count : Abstract 230; Body 2471

Abstract

Background and aims

Despite recommendations for close follow-up of patients with native arteriovenous fistulas (AVF), up to 10% experience thrombosis each year. We tested the hypothesis that the systemic osteopontin level, a pro-inflammatory mediator related to vascular remodelling and intimal hyperplasia, increases in AVF stenosis.

Methods

Our cross-sectional study compared the level of plasmatic osteopontin (pOPN) between patients with a well-functioning AVF (control group) and patients who required revision of their AVF due to stenosis (stenosis group) (ELISA). Blood samples were collected from the AVF arm but also the opposite arm as a within-subject control.

Results

A total of 76 patients were included in the study. Baseline characteristics were similar between the groups (mean age, 70 years; men, 63%; AVF duration, 39 months), apart from those with type 2 diabetes (T2D) (control group, 33%; stenosis group, 57%; $p=0.04$). pOPN levels were similar between the AVF arm and the opposite arm (551 ± 42 ng/mL vs. 521 ± 41 ng/mL, respectively, $p=0.11$). Patients in the stenosis group displayed a higher pOPN level than patients in the control group (650.2 ± 59.8 ng/mL vs. 460.5 ± 61.2 , respectively, $p= 0.03$). T2D was not a confounding factor in a multivariate analysis ($p= 0.50$).

Conclusions

The increase of pOPN levels in hemodialysis patients was strongly associated to the presence of symptomatic AVF stenosis. Thus, its potential as a diagnostic biomarker should be assessed in a vascular access surveillance program.

Introduction

Despite being the preferred vascular access for hemodialysis patients, arteriovenous fistulas (AVF) present a high rate of dysfunction.¹ AVF dysfunction alters the adequacy of dialysis and negatively impacts the patient's quality of life due to multiple reinterventions.² AVF dysfunction mostly comes from the development of stenosis on the venous limb of the AVF. Stenoses often decrease the Kt/V ratio, increase the recirculation rate, extend the bleeding time, and may eventually lead to AVF thrombosis.^{2,3}

Several surveillance methods have been proposed to detect stenosis before it threatens AVF function.^{3,4} Clinical examination enables detection of a beating AVF or a flat vein, depending on the localisation of the stenosis.⁵ Intradialytic vascular access flow measurement also helps to detect low or decreased flow and therefore underlying stenosis.⁶ Regular duplex ultrasound examination with flow measurement is a robust imaging technique that leads to the qualitative and quantitative assessment of AVF function.⁷ However, these techniques either lack sensitivity, or are expensive, time consuming and poorly accepted by patients and staff.^{8,9} Unfortunately, there is currently no validated blood marker to rapidly predict/diagnose stenosis.

Osteopontin (OPN) is a cytokine/chemokine with pleiotropic functions involved in tissue remodeling, pathological chronic inflammatory processes, carcinogenesis as well as in cardiovascular diseases.¹⁰ OPN plays an important role in the proliferation, migration and accumulation of smooth muscle cells and endothelial cells, which are themselves responsible for vascular remodeling.¹¹ OPN is highly expressed in atherosclerotic plaques.^{12, 13} Significant associations between the circulating OPN level and atheroma plaque formation and high cardiovascular risk have been reported,¹⁴⁻¹⁹ particularly in patients with type 2 diabetes (T2D).^{14, 20} In addition, polymorphisms in the *phosphoprotein 1* (OPN) gene have been associated with subclinical evolution of carotid

artery disease in T2D patients.²¹ Moreover, after coronary angioplasty, higher plasmatic OPN (pOPN) levels have been associated with restenosis in patients.^{15, 22} These data suggest that OPN plays a role in in-stent coronary restenosis, which is associated with excessive intimal proliferation.²³ In arteries, OPN may inhibit calcification by increasing intimal medial thickness.¹⁴ In addition, OPN levels were found to be increased in the venous wall after bypass grafting and AVF creation, suggesting a role in the formation of venous neointimal hyperplasia.²⁴⁻²⁶

We hypothesized that pOPN would be increased in patients with AVF stenosis. It is easily measured in a blood sample withdrawn while cannulating the AVF (with no additional harm or discomfort for the patient), and thus, assessment of pOPN could help the physician to screen patients who need further examination of their AVF.

Materials and methods

Study design

Osteopontin as a marker of stenosis (OSMOSIS) was a prospective, cross-sectional, non-randomized, and controlled study conducted in the University Hospital of Nice (ClinicalTrials.gov Identifier: NCT03270358). The study was conducted in strict accordance with national laws regarding human research and data protection, after declaration to the relevant authorities and the approval of the local ethics committee. Patients gave written informed consent before inclusion.

Setting & participants

Adult patients with end-stage renal disease, who had been under hemodialysis for at least 3 months by the means of the same native upper-arm AVF (radial-cephalic, brachial-cephalic, brachial-basilic) were eligible for the study. Eligibility was screened by the

nephrologist before inclusion. Patients under dialysis for at least 3 months with adequate dialysis parameters and no clinical dysfunction were included in the control group. Patients admitted to the department of vascular surgery for AVF dysfunction and surgical or endovascular treatment of stenosis were included in the stenosis group. Patients were referred for surgical revision of their AVF when one or more of these criteria were seen by the nephrologist: $Q_a < 400 \text{ mL/min}$ or $>20\%$ decrease in Q_a compared to the previous dialysis session; inability of complete dialysis within 4h, recirculation $>20\%$, clinical pulsing in the AVF. Patients with other types of vascular access, patients who had previously received either a stent or a drug-coated balloon in their access, and patient with thrombosed access were not included in the study. Patients were not followed-up for the study after the day of inclusion.

Data collection and sample analysis

Patient characteristics, comorbidities and ongoing medications were recorded upon inclusion. In the control group, a predialysis blood sample was collected after insertion of the dialysis cannula in the AVF and before connection to the dialysis machine. In the stenosis group, a predialysis blood sample was collected at insertion of the sheath in the AVF in the operating room. Sampling was made within 24h of the diagnosis of AVF dysfunction, since patients were referred to the surgical department within 24h. In both groups, simultaneously or immediately following blood collection from the AVF, another blood sample was collected from venipuncture of the contralateral hand of the same patient, to serve as an internal control for the systemic OPN level. Blood samples were centrifuged at 3,000 rpm for 15 min within 30–40 min of blood collection. Each blood sample was aliquoted into multiple vials and stored at -80°C . Plasma samples were diluted 50X in the appropriate buffer prior to analysis. Circulating OPN levels were

evaluated with an ELISA (R&D Systems, Lille, France), as described in the manufacturer's instructions and reported in ng/mL. All samples were analyzed in duplicate, in random order and blinded to the clinical/pathological data. The CV (%) of intra-assay precision and inter assay precision ranged from 2.6 to 4 and 5.4 to 6.6, respectively. The minimum detectable dose of OPN ranged from 0.006 to 0.024 ng/mL. C-reactive protein (CRP) and phosphate concentrations were determined by spectrophotometry (Cobas 8000, Roche Diagnostics, 38240 Meylan, France). Calibrators and quality controls were obtained from Roche Diagnostics. For all assays, quality controls fell within limits defined by the manufacturer.

Statistical analysis

At the time of writing of the study protocol, there were no clear data on the level of circulating OPN in patients under dialysis with an AVF. Based on the data reported from patients with intra-stent stenosis in coronary arteries,²² we hypothesized that a difference of 100 ng/mL in plasmatic OPN level between our two groups would be significant. Seventy-six patients would provide at least 90% power with a risk alpha of 0.05 for comparison of the stenosis group to the control group.

Baseline characteristics between the groups were compared using Pearson's Chi² test for a categorical variable. Continuous variables were reported as mean \pm standard error and compared with a Student's t-test. pOPN levels were compared in each group between the AVF arm and the contralateral arm using a paired t-test. A two-way ANOVA was conducted to examine the effects of AVF group (control or stenosis) and diabetes on the level of pOPN. A ROC curve was used to identify OPN thresholds. A binomial regression model was performed to ascertain the effects of pOPN levels and diabetes on the likelihood that patients have AVF stenosis, and the area under the curve was determined.

p values <0.05 were considered statistically significant. All statistical analyses were performed using SPSS Statistics V.23 (IBM, USA).

Results

Seventy-six patients were included in the study between February 2018 and September 2019 (control, 39 (51%); stenosis, 37 (49%)). Patients' baseline characteristics are reported in Table 1. There was no difference in the AVF vintage between our groups, and a similar percentage of patients had a history of previously abandoned AVF in both groups (Table 1). In the stenosis group, all but three of the patients received endovascular treatment of their stenosis; these three patients had a surgical angioplasty with patch.

In the control group, mean dialysis Kt/V ratio on the day of blood collection was 1.67 (± 0.28) with a range of 1.20 to 2.37, confirming that the AVF was functioning well (Kt/V >1.4). In stenosis group, Kt/V ratio on the day of blood collection was 1,23 (± 0.33) (<1.4) and statistically lower than the control group, which confirm low dialysis efficiency in this group ($p=0.00008$). The markers of depuration and inflammation we measured (Phosphate, Hemoglobin and CRP) were similar between our groups (Table1).

To exclude any local effect of AVF puncture on the level of pOPN and to confirm the systemic circulation of OPN, we first compared the levels of pOPN from samples collected in the AVF arm versus the opposite arm in all patients. As shown in Figure 1A, there was no significant difference between these groups (551 \pm 42 ng/mL vs. 521 \pm 41 ng/mL, respectively, $p =0.11$) (Suppl Table 1). On the basis of these results, the further analyses were conducted on the levels of pOPN in the AVF arm.

Since there were more diabetic patients in the stenosis group (Table 1), diabetes could be a confounding factor. We thus performed a two-way ANOVA to examine the effects of the AVF group (control or stenosis) and diabetes on the level of plasmatic OPN. Levels of

pOPN are reported in Figure 1B. There was no statistically significant interaction between AVF group and diabetes on pOPN levels ($p = 0.89$) indicating that T2D was not a confounding factor. We found that there was a statistically significant main effect of AVF group on pOPN ($F(1,72) = 4.907, p = 0.03$). The unweighted marginal means of pOPN levels for patients in the control group and the stenosis group were 460.5 ± 61.2 and 650.2 ± 59.8 respectively (Figure 1B). The OPN level was higher in the stenosis group compared to the control group with an average increase of 190 ng/mL (CI95%: 18.98-360.4; $p = 0.03$). There was no statistically significant difference in pOPN between diabetic and non-diabetic patients ($F(1,72) = 0.465, p = 0.50$) in this model (Supplementary Figure 1). We conducted a ROC curve analysis to determine the thresholds of pOPN that could lead to the best sensitivity and the best specificity in the prediction of AVF stenosis. The area under the ROC curve (AUC) was 0.70 (95% CI, 0.57 to 0.81). In this model, the level of pOPN had the highest sensitivity at a threshold of 293 ng/mL (89.2% (CI95% : 74.6-97.0); likelihood ratio 2.05) and the highest specificity at a threshold of 567 ng/mL (79.5% (CI95%: 63.5-91.0); likelihood ratio 2.77).

Discussion

In this cross-sectional case-control study, we showed that pOPN was significantly higher in patients with AVF stenosis, independently of their diabetic status. Our results also indicate that a multivariate model including diabetic status and pOPN may help to predict the presence of AVF stenosis.

The role of diabetes in the development of AVF stenosis is controversial. Several previous reports have shown that patients with diabetes have worse AVF maturation.^{27, 28} In ESRD patients, diabetes increases vascular calcification, and calcified arteries may not allow sufficient outward remodeling and sufficient flow to provide a mature AVF. However,

other studies have found that after cannulation, AVF in diabetic patients are similar to AVF in non-diabetic patients, except for dialysis associated hand-ischemia, suggesting that stenosis occurring in mature fistula may not be due to diabetes.^{29, 30} In our study, diabetics were significantly more likely to have stenosis. Therefore, the role of diabetes and vascular calcification in the AVF outcome still needs to be elucidated.

OPN is involved in many calcification processes, including vascular calcification in ESRD patients.³¹⁻³³ OPN has been found to be a marker of diabetes complications (type I and type II), including nephropathy,^{20, 33, 34} retinopathy³⁵ and cardiovascular morbidity and mortality.^{20, 34, 36} However, in a study evaluating several markers of vascular calcification in cardiovascular mortality in patients with end-stage renal disease, Scialla *et al.* did not report significant difference of OPN levels between diabetic and non-diabetic patients (144.9 vs. 159.6 ng/mL, $p = 0.19$).³² While analyzing several calcification markers in patients with vascular access, Lyu *et al.* found that lower levels of fetuin-A and higher levels of OPN and bone morphogenetic protein-7 were associated with greater risk of AVF interventions and were independent of diabetes.³⁷ Ulutas *et al.* also found that low fetuin-A and elevated OPN was not associated with vascular calcifications in hemodialysis patients.³⁸ Therefore, the elevated circulating OPN level in AVF could reflect diabetic vascular calcifications, but also biomineralization or inflammatory events.

We know that serial factors like inflammatory markers or Calcium-Phosphate metabolism could represent an independent risk factor for AVF stenosis³⁹⁻⁴⁰. We were able to measure CRP and phosphate level in our samples and found no significant difference between groups. This finding may suggest that pOPN can be investigated as an independent factor for AVF stenosis and not only related to a broader inflammation status.

OPN has also been described as an emerging inflammatory biomarker in the settings of obesity and its complications (insulin resistance, T2D, and non-alcoholic fatty liver

disease).⁴¹⁻⁴³ Due to its pleiotropic functions at the crossroads of calcium metabolism, glucose metabolism and inflammation, the exact origin of circulating OPN and its role in the development of AVF stenosis is difficult to distinguish. Batko *et al.* studied circulating pOPN and thrombomodulin in ESRD patients and showed that patients in pre-dialysis have less OPN than patients under dialysis.⁴⁴ Although the relationship between thrombomodulin and OPN is complex, these results suggest that phosphate/calcium metabolism is involved in the secretion of OPN, since uremia and inorganic phosphorus affects gene expression of vascular smooth muscle cells.⁴⁵⁻⁴⁷ The pro-inflammatory role of OPN, especially in crosstalk with IL-6 and in the development of fibrosis after tissue damage may also be involved in this process.⁴⁸ Insulin resistance and overweight are frequent in ESRD patients,⁴⁹ and may be confounding factors when analyzing the levels of circulating OPN.⁵⁰ However, previous studies have shown that the increase in local OPN expression in adipose tissue did not correlate with pOPN levels in obese patients.⁴¹ In our study, pOPN levels were not correlated to body mass index, suggesting this analysis can be helpful in all patients regardless of their body weight.

Our study has several strengths, with a prospective design and the use of a dual control (one internal and one external) to analyze the level of pOPN in the AVF arm. But it also has several limitations; in particular, it was a transversal study, with a small sample size and without follow up of the AVF complications and gave no information on the kinetics of pOPN levels over the day or throughout months. We cannot tell if patients with constitutively high OPN level at AVF creation will later be prone to stenosis, or if OPN increases with later development of stenosis, nor if threshold can be identified when the stenosis become significant and needs revision. In further studies, other inflammatory markers and at least one standard method of follow-up should be included in the analysis.

In conclusion, this prospective preliminary study showed that patients with a stenosed AVF have higher levels of pOPN than patients with healthy AVF, independently of their diabetic status. pOPN is a solid candidate in the quest of a biomarker for AVF stenosis that is easy to implement in a dialysis routine. It can now be assessed in a longitudinal study, which will follow the levels of pOPN from creation to failure (or long-term success) of the AVFs.

Acknowledgements

The authors thank Dr Patricia Ferrari and Dr Eric Fontas for their advice regarding the design of the study, and Ms Abby Cuttriss for language editing of the manuscript.

Conflict of Interest Statement

We declare no conflict of interest regarding this study.

Authors' Contributions

J.Co., R.H.K. and N.S. designed the study; J.Co., S.V., S.D., J.R., S.B. and N.S. carried out experiments; M.D., J.Ca, S.B., C.K., P.G., N.M.M. and N.S. analyzed the data; J.Co, N.M.M. and N.S. made the figures and drafted the paper; M.D., S.V, S.D, J.Co, S.B., C.K., R.H.K. and P.G. revised the paper; all authors approved the final version of the manuscript.

Funding

This study was funded by the Centre Hospitalier Universitaire de Nice.

References

1. Bylsma LC, Gage SM, Reichert H, Dahl SLM, Lawson JH. Arteriovenous Fistulae for Haemodialysis: A Systematic Review and Meta-analysis of Efficacy and Safety Outcomes. *Eur J Vasc Endovasc Surg* 2017;54:513-22.
2. Lambie SH, Taal MW, Fluck RJ, McIntyre CW. Analysis of factors associated with variability in haemodialysis adequacy. *Nephrol Dial Transplant* 2004;19:406-12.
3. Vascular Access Work Group. Clinical practice guidelines for vascular access. *Am J Kidney Dis* 2006;48 Suppl 1:S176-247.
4. Tonelli M, Jindal K, Hirsch D, Taylor S, Kane C, Henbrey S. Screening for subclinical stenosis in native vessel arteriovenous fistulae. *J Am Soc Nephrol* 2001;12:1729-33.
5. Tessitore N, Bedogna V, Verlato G, Poli A. Clinical access assessment. *J Vasc Access* 2014;15 Suppl 7:S20-7.
6. Rehman SU, Pupim LB, Shyr Y, Hakim R, Ikizler TA. Intradialytic serial vascular access flow measurements. *Am J Kidney Dis* 1999;34:471-7.
7. Mudoni A, Caccetta F, Caroppo M, Musio F, Accogli A, Zacheo MD, et al. Echo color Doppler ultrasound: a valuable diagnostic tool in the assessment of arteriovenous fistula in hemodialysis patients. *J Vasc Access* 2016;17:446-52.
8. Han A, Min SK, Kim MS, Joo KW, Kim J, Ha J, et al. A Prospective, Randomized Trial of Routine Duplex Ultrasound Surveillance on Arteriovenous Fistula Maturation. *Clin J Am Soc Nephrol* 2016;11:1817-24.
9. Kumbar L, Karim J, Besarab A. Surveillance and monitoring of dialysis access. *Int J Nephrol* 2012;2012:649735.

10. Scatena M, Liaw L, Giachelli CM. Osteopontin: A Multifunctional Molecule Regulating Chronic Inflammation and Vascular Disease. *Arterioscler Thromb Vasc Biol* 2007;27:2302-9.
11. Liaw L, Almeida M, Hart CE, Schwartz SM, Giachelli CM. Osteopontin promotes vascular cell adhesion and spreading and is chemotactic for smooth muscle cells in vitro. *Circ Res* 1994;74:214-24.
12. Golledge J, McCann M, Mangan S, Lam A, Karan M. Osteoprotegerin and osteopontin are expressed at high concentrations within symptomatic carotid atherosclerosis. *Stroke* 2004;35:1636-41.
13. He C, Choi HC, Xie Z. Enhanced tyrosine nitration of prostacyclin synthase is associated with increased inflammation in atherosclerotic carotid arteries from type 2 diabetic patients. *Am J Pathol* 2010;176:2542-9.
14. Ishiyama M, Suzuki E, Katsuda J, Murase H, Tajima Y, Horikawa Y, et al. Associations of coronary artery calcification and carotid intima-media thickness with plasma concentrations of vascular calcification inhibitors in type 2 diabetic patients. *Diabetes Res Clin Pract* 2009;85:189-96.
15. Yilmaz KC, Bal UA, Karacaglar E, Okyay K, Aydinalp A, Yildirim A, et al. Plasma osteopontin concentration is elevated in patients with coronary bare metal stent restenosis. *Acta Cardiol* 2018;73:69-74.
16. Mohamadpour AH, Abdolrahmani L, Mirzaei H, Sahebkar A, Moohebbati M, Ghorbani M, et al. Serum osteopontin concentrations in relation to coronary artery disease. *Arch Med Res* 2015;46:112-7.
17. Abdel-Azeez HA, Al-Zaky M. Plasma osteopontin as a predictor of coronary artery disease: association with echocardiographic characteristics of atherosclerosis. *J Clin Lab Anal* 2010;24:201-6.

18. Ohmori R, Momiyama Y, Taniguchi H, Takahashi R, Kusuhara M, Nakamura H, et al. Plasma osteopontin levels are associated with the presence and extent of coronary artery disease. *Atherosclerosis* 2003;170:333-7.
19. Kadoglou NP, Gerasimidis T, Golemati S, Kapelouzou A, Karayannacos PE, Liapis CD. The relationship between serum levels of vascular calcification inhibitors and carotid plaque vulnerability. *J Vasc Surg* 2008;47:55-62.
20. Yan X, Sano M, Lu L, Wang W, Zhang Q, Zhang R, et al. Plasma concentrations of osteopontin, but not thrombin-cleaved osteopontin, are associated with the presence and severity of nephropathy and coronary artery disease in patients with type 2 diabetes mellitus. *Cardiovasc Diabetol* 2010;9:70.
21. Pleskovic A, Santl Letonja M, Cokan Vujkovic A, Makuc J, Nikolajevic Starcevic J, Petrovic D. Phosphoprotein 1 (osteopontin) gene (rs4754) affects markers of subclinical atherosclerosis in patients with type 2 diabetes mellitus. *Int Angiol* 2018;37:64-70.
22. Kato R, Momiyama Y, Ohmori R, Tanaka N, Taniguchi H, Arakawa K, et al. High plasma levels of osteopontin in patients with restenosis after percutaneous coronary intervention. *Arterioscler Thromb Vasc Biol* 2006;26:e1-2.
23. Srivatsa SS, Fitzpatrick LA, Tsao PW, Reilly TM, Holmes DR, Jr., Schwartz RS, et al. Selective alpha v beta 3 integrin blockade potently limits neointimal hyperplasia and lumen stenosis following deep coronary arterial stent injury: evidence for the functional importance of integrin alpha v beta 3 and osteopontin expression during neointima formation. *Cardiovasc Res* 1997;36:408-28.
24. Kang N, Ng CSH, Hu J, Qiu Z-B, Underwood MJ, Jeremy JY et al. Role of osteopontin in the development of neointimal hyperplasia in vein grafts. *Eur J Cardiothorac Surg* 2012;41:1384-9.

25. Hall MR, Yamamoto K, Protack CD, Tsuneki M, Kuwahara G, Assi R, et al. Temporal regulation of venous extracellular matrix components during arteriovenous fistula maturation. *J Vasc Access* 2015;16:93-106.
26. Abeles D, Kwei S, Stavrakis G, Zhang Y, Wang ET, Garcia-Cardena G. Gene expression changes evoked in a venous segment exposed to arterial flow. *J Vasc Surg* 2006;44:863-70.
27. Woodside KJ, Bell S, Mukhopadhyay P, Repeck KJ, Robinson IT, Eckard AR, et al. Arteriovenous Fistula Maturation in Prevalent Hemodialysis Patients in the United States: A National Study. *Am J Kidney Dis* 2018;71:793-801.
28. Zarkowsky DS, Arhuidese IJ, Hicks CW, Canner JK, Qazi U, Obeid T, et al. Racial/Ethnic Disparities Associated With Initial Hemodialysis Access. *JAMA Surg* 2015;150:529-36.
29. Allon M, Robbin ML, Umphrey HR, Young CJ, Deierhoi MH, Goodman J, et al. Preoperative arterial microcalcification and clinical outcomes of arteriovenous fistulas for hemodialysis. *Am J Kidney Dis* 2015;66:84-90.
30. Smith GE, Gohil R, Chetter IC. Factors affecting the patency of arteriovenous fistulas for dialysis access. *J Vasc Surg* 2012;55:849-55.
31. Nitta K, Ishizuka T, Horita S, Hayashi T, Ajiro A, Uchida K, et al. Soluble osteopontin and vascular calcification in hemodialysis patients. *Nephron* 2001;89:455-8.
32. Scialla JJ, Kao WH, Crainiceanu C, Sozio SM, Oberai PC, Shafi T, et al. Biomarkers of vascular calcification and mortality in patients with ESRD. *Clin J Am Soc Nephrol* 2014;9:745-55.
33. Al-Rubeaan K, Siddiqui K, Al-Ghonaim MA, Youssef AM, Al-Sharqawi AH, AlNaqeb D. Assessment of the diagnostic value of different biomarkers in relation to various stages of diabetic nephropathy in type 2 diabetic patients. *Sci Rep* 2017;7:2684.

34. Gordin D, Forsblom C, Panduru NM, Thomas MC, Bjerre M, Soro-Paavonen A, et al. Osteopontin is a strong predictor of incipient diabetic nephropathy, cardiovascular disease, and all-cause mortality in patients with type 1 diabetes. *Diabetes Care* 2014;37:2593-600.
35. Zhang X, Chee WK, Liu S, Tavintharan S, Sum CF, Lim SC, et al. Association of plasma osteopontin with diabetic retinopathy in Asians with type 2 diabetes. *Mol Vis* 2018;24:165-73.
36. Zwakenberg SR, van der Schouw YT, Schalkwijk CG, Spijkerman AMW, Beulens JWJ. Bone markers and cardiovascular risk in type 2 diabetes patients. *Cardiovasc Diabetol* 2018;17:45.
37. Lyu B, Banerjee T, Scialla JJ, Shafi T, Yevzlin AS, Powe NR, et al. Vascular Calcification Markers and Hemodialysis Vascular Access Complications. *Am J Nephrol* 2018;48:330-8.
38. Ulutas O, Taskapan MC, Dogan A, Baysal T, Taskapan H. Vascular calcification is not related to serum fetuin-A and osteopontin levels in hemodialysis patients. *Int Urol Nephrol* 2018;50:137-42.
39. Olsson LF, Odselius R, Ribbe E, Hegbrant j. Evidence of calcium phosphate depositions in stenotic arteriovenous fistulas. *Am J Kidney Dis* 2001;38(2):377-83.
40. Chou CY, Kuo HL, Yung YF, Liu YL, Huang CC. C-reactive protein predicts vascular access thrombosis in hemodialysis patients. *Blood Purif* 2006;24(4):342-6.
41. Bertola A, Deveaux V, Bonnafous S, Rousseau D, Anty R, Wakkach A, et al. Elevated expression of osteopontin may be related to adipose tissue macrophage accumulation and liver steatosis in morbid obesity. *Diabetes* 2009;58:125-33.
42. Kahles F, Findeisen HM, Bruemmer D. Osteopontin: A novel regulator at the cross roads of inflammation, obesity and diabetes. *Mol Metab* 2014;3:384-93.

43. Lund, S.A., Giachelli, C.M., Scatena, M. The role of osteopontin in inflammatory processes. *J Cell Commun Signal* 2009;3:311-22.
44. Batko K, Krzanowski M, Gajda M, Dumnicka P, Fedak D, Woziwodzka K, et al. Endothelial injury is closely related to osteopontin and TNF receptor-mediated inflammation in end-stage renal disease. *Cytokine* 2019;121:154729.
45. Wu-Wong JR, Nakane M, Ma J, Ruan X, Kroeger PE. Elevated phosphorus modulates vitamin D receptor-mediated gene expression in human vascular smooth muscle cells. *Am J Physiol Renal Physiol* 2007;293:F1592-604.
46. Son BK, Akishita M, Iijima K, Ogawa S, Arai T, Ishii H, et al. Thrombomodulin, a novel molecule regulating inorganic phosphate-induced vascular smooth muscle cell calcification. *J Mol Cell Cardiol* 2013;56:72-80.
47. Pedersen TX, Madsen M, Junker N, Christoffersen C, Vikesa J, Bro S, et al. Osteopontin deficiency dampens the pro-atherogenic effect of uraemia. *Cardiovasc Res* 2013;98:352-9.
48. Shimodaira T, Matsuda K, Uchibori T, Sugano M, Uehara T, Honda T. Upregulation of osteopontin expression via the interaction of macrophages and fibroblasts under IL-1b stimulation. *Cytokine* 2018;110:63-9.
49. United States Renal Data System. 2018 USRDS annual data report: Epidemiology of kidney disease in the United States. National Institutes of Health, National Institute of Diabetes and Digestive and Kidney Diseases, Bethesda, MD, 2018.
50. Daniele G, Winnier D, Mari A, Bruder J, Fourcaudot M, Pengou Z, et al. The potential role of the osteopontin-osteocalcin-osteoprotegerin triad in the pathogenesis of prediabetes in humans. *Acta Diabetol* 2018;55:139-48.

51. Kiefer, F.W., Zeyda, M., Todoric, J., Huber, J., Geyeregger, R., Weichhart, T., et al. Osteopontin expression in human and murine obesity: extensive local up-regulation in adipose tissue but minimal systemic alterations. *Endocrinology* 2008;149:1350-7.

Tables

Table 1. Baseline characteristics of patients.

* Statistical significance, $p < 0.05$.

AVF, arteriovenous fistula; BMI, Body Mass Index; CRP, C-reactive protein; SEM, standard error of the mean.

Variable	Control (N=39)	Stenosis (N=37)	p value
	N or mean (% or SEM)	N or mean (% or SEM)	
Age (years)	71 ± 2.0	67 ± 2.8	0.25
Sex			
Male	23 (59)	25 (68)	0.44
Female	16 (41)	12 (32)	
Comorbidities and BMI			
Diabetes	13 (33)	21 (57)	0.04*
Hypertension	31 (80)	32 (87)	0.42
Dyslipidemia	26 (67)	18 (59)	0.14
Coronary disease	17 (44)	10 (27)	0.13
BMI (kg/m ²)	25.9 ± 0.9	26.4 ± 1.0	0.70

Treatment			
Anticoagulant	8 (21)	5 (14)	0.27
Antiplatelet	20 (51)	20 (54)	0.81
Statin	23 (59)	16 (46)	0.25
Beta-blocker	22 (56)	16 (46)	0.36
Angiotensin-converting enzyme inhibitor	11 (28)	8 (23)	0.60
AVF			
Age of AVF (months)	38 ± 4.6	41.4 ± 5.9	0.61
History of previously abandoned AVF	12 (31)	10 (27)	0.72
Biomarkers			
Hemoglobin (g/dL)	11.3 ± 1.5	10.9 ± 2.9	0.06
CRP (mg/L)	6.6 ± 6.5	10.1 ± 19.1	0.12
Phosphate (mmol/L)	1.2 ± 0.4	1.3 ± 0.4	0.83

Figure legends

Figure 1. Levels of plasmatic osteopontin (pOPN) in patients with arteriovenous fistulas (AVF). A. Comparison between the mean pOPN in the AVF arm and the opposite arm (without AVF) of the same patient (551 ± 42 ng/mL vs. 521 ± 41 ng/mL, respectively, $p = 0.11$, paired t-test). B. Two-way ANOVA analysis of mean pOPN in control patients and stenosis patients, with analysis of interaction of diabetes.

Annexe 2: Co-culture of human fibroblasts, smooth muscle and endothelial cells promotes osteopontin induction in hypoxia. *J Cell Mol Med.* 2020.


Received: 31 July 2019 | Revised: 20 November 2019 | Accepted: 23 November 2019

DOI: 10.1111/jcmm.14905

ORIGINAL ARTICLE

WILEY

Co-culture of human fibroblasts, smooth muscle and endothelial cells promotes osteopontin induction in hypoxia

Nirvana Sadaghianloo^{1,2} | Julie Contenti^{1,3} | Maeva Dufies⁴ | Julien Parola¹ |
Matthieu Rouleau⁵ | Shinrong Lee^{6,7} | Jean-François Peyron¹ | Lucilla Fabbri¹ |
Réda Hassen-Khodja² | Jacques Pouysségur^{1,4} | Frédéric Bost¹ | Elixène Jean-Baptiste² |
Alan Dardik^{6,7} | Nathalie M. Mazure¹ 

¹Université Côte d'Azur, Institute for Research on Cancer and Aging of Nice (IRCAN), CNRS-UMR 7284-Inserm U1081, Centre Antoine Lacassagne, University of Nice Sophia-Antipolis, Nice, France

²Department of Vascular Surgery, Centre Hospitalier Universitaire de Nice, Nice, France

³Department of Emergency Medicine, Centre Hospitalier Universitaire de Nice, Nice, France

⁴Centre Scientifique de Monaco (CSM), Monaco, Monaco

⁵Faculty of Medicine, LP2M, CNRS-UMR 7370, Nice, France

⁶Department of Surgery and the Vascular Biology and Therapeutics Program, Yale University, New Haven, CT, USA

⁷Department of Vascular Surgery, VA Connecticut Healthcare Systems, West Haven, CT, USA

Correspondence

Nirvana Sadaghianloo and Nathalie M. Mazure, INSERM U1065, C3M, 151 Route de St Antoine de Ginestière, BP2 3194, 06204 Nice Cedex 03, France.
Emails: sadaghianloo.n@chu-nice.fr; mazure@unice.fr

Present address

Nirvana Sadaghianloo, Julie Contenti, Lucilla Fabbri, Réda Hassen-Khodja, Elixène Jean-Baptiste and Nathalie M. Mazure, Centre de Méditerranéen de Médecine Moléculaire (C3M), INSERM U1065, Université Côte d'Azur, Nice Cedex 03, France

Funding information

Fondation Flavien; Société Française de Chirurgie Vasculaire et Endovasculaire; Fondation ARC pour la Recherche sur le Cancer; Fondation de France; La Ligue contre le Cancer

Abstract

Arteriovenous fistulas (AVFs) are the preferred vascular access for haemodialysis of patients suffering from end-stage renal disease, a worldwide public health problem. However, they are prone to a high rate of failure due to neointimal hyperplasia and stenosis. This study aimed to determine if osteopontin (OPN) was induced in hypoxia and if OPN could be responsible for driving AVF failure. Identification of new factors that participate in remodelling of AVFs is a challenge. Three cell lines representing the cells of the three layers of the walls of arteries and veins, fibroblasts, smooth muscle cells and endothelial cells, were tested in mono- and co-culture in vitro for OPN expression and secretion in normoxia compared to hypoxia after silencing the hypoxia-inducible factors (HIF-1 α , HIF-2 α and HIF-1/2 α) with siRNA or after treatment with an inhibitor of NF- κ B. None of the cells in mono-culture showed OPN induction in hypoxia, whereas cells in co-culture secreted OPN in hypoxia. The changes in oxygenation that occur during AVF maturation up-regulate secretion of OPN through cell-cell interactions between the different cell layers that form AVF, and in turn, these promote endothelial cell proliferation and could participate in neointimal hyperplasia.

KEYWORDS

arteriovenous fistula, hypoxia, hypoxia-inducible factor, metabolism, osteopontin

This is an open access article under the terms of the Creative Commons Attribution License, which permits use, distribution and reproduction in any medium, provided the original work is properly cited.

© 2019 The Authors. *Journal of Cellular and Molecular Medicine* published by Foundation for Cellular and Molecular Medicine and John Wiley & Sons Ltd.

J Cell Mol Med. 2020;24:2931–2941.

wileyonlinelibrary.com/journal/jcmm | 2931

1 | INTRODUCTION

Renal failure is a major public health problem with increasing incidence every year. Patients with end-stage renal disease require either kidney transplantation or haemodialysis to sustain life. Arteriovenous fistula (AVF) is the preferred vascular access for haemodialysis.¹ However, only 50% of AVF remain functional six months after creation, which increases the morbidity-mortality of patients.² Several clinical factors seem to play a role in the dysfunction of AVFs, including female gender, age, or diabetes. Histologically, dysfunction most frequently results from neointimal hyperplasia (NH), which is responsible for stenosis.³ Different mechanisms including the differentiation of fibroblasts into myofibroblasts, proliferation of smooth muscle cells and endothelial cell activation have been identified in NH of AVF. Following surgery, changes in tissue oxygenation result in (a) an increase of arterial O₂ partial pressure (pO₂), from 35 to 45 mm Hg in the venous blood and from 73 to 100 mm Hg in the arterial blood, and (b) a decrease in the oxygen (O₂) concentration in the venous wall, as seen by the stabilization of the hypoxia-inducible factor (HIF) in the venous limb of the AVF in several models.⁴ Rupture of the *vasa vasorum* during surgical dissection may contribute to the induction of hypoxia, thereby stabilizing HIF.⁵ HIFs are dimeric protein complexes that consist of an α -subunit (HIF-1 α or HIF-2 α) and a β -subunit (HIF-1 β or HIF-2 β),⁶ and are major regulators of cellular adaptation to hypoxia. HIF-1 α is expressed ubiquitously, whereas HIF-2 α is primarily detected in endothelial cells but is also selectively highly expressed in a limited number of tissues.⁷ There is increasing evidence supporting the contribution of the HIF pathway, both the protective and destructive effects, to the pathogenesis of diseases affecting the vascular wall including atherosclerosis,^{8,9} arterial aneurysms,¹⁰⁻¹² pulmonary hypertension,¹³⁻¹⁵ vascular graft failure,^{4,16-18} chronic venous diseases^{19,20} and vascular malformation.^{21,22} Furthermore, increased expression of VEGF-A, a target HIF-1 α gene, may contribute to NH, through increased proliferation of smooth muscle cells. A recent study has shown that reducing VEGF-A gene expression during AVF formation reduces NH.²³

Although HIFs are involved in the regulation of the oxygen homeostasis, NF- κ B, a major transcription factor that responds to cellular stress, is also activated by hypoxia.²⁴ The most abundant cytoplasmic form of the NF- κ B complex is an inactive heterotrimeric form composed of p50 and p65 subunits, and the inhibitor I κ B- α . Stimulus-induced degradation of I κ B- α is critical for nuclear translocation of NF- κ B and induction of transcription of target genes.²⁵ In rat models, overexpression of NF- κ B was found following vascular injury and correlated to thickening of the intima compared to that of control vessels.²⁶

Osteopontin (OPN) is a SIBLING protein (Small Integrin Binding Ligand N-linked Glycoproteins), which was initially identified as a bone matrix protein that links bone cells to the extracellular matrix.²⁷ OPN exists in two isoforms, a secreted (sOPN) and an intracellular form (iOPN), that have distinct biological functions.²⁸ At the protein level, OPN has a molecular weight of about 60 kD. This protein undergoes multiple post-translational modifications by

phosphorylation and glycosylation variables that can explain the previously described variability in the apparent molecular weights (from 25 to 75 kD).²⁹ OPN is involved in multiple processes including tissue remodelling, regulation of cellular immunity, pathological chronic inflammatory processes, carcinogenesis as well as cardiovascular diseases.³⁰ OPN is also involved in several vascular diseases promoting angiogenesis, in parallel with vascular endothelial growth factor (VEGF), through enhanced endothelial cell migration, proliferation and subsequent formation of capillaries, which are essential requirements for the process of angiogenesis. In particular, it has been found to be expressed in vascular smooth muscle cells of human restenotic lesions and stenotic vascular lesions.³¹ Significant association between the level of plasma circulating OPN and atheroma plaque formation has been reported.³² Moreover, high OPN levels in patients with stenosis have been described after coronary angioplasty compared to patients without stenosis.³³ Interestingly, Hall et al³⁴ have shown a 40-fold increase in OPN expression in the early stages of AVF maturation in a mouse model of AVF. In addition, constitutive overexpression of OPN in mice was found to result in increased neointima formation after cuffing of the femoral artery.³⁵ Finally, structural changes were noted on the OPN-null background including disorganized collagen and increased vessel wall compliance.³⁶ Altogether, these data suggest that OPN may play a role in the development of vascular stenosis associated with excessive intimal proliferation. Reactive oxygen species (ROS)³⁷ and hyperglycaemia³⁸ induce *in vivo* expression of OPN in pancreatic epithelial cells, and also in vascular smooth muscle cells. Even though up-regulation of OPN in hypoxia has been shown to be dependent^{39,40} or independent⁴¹ of HIF-1 regulation, OPN expression is enhanced under hypoxia through different mechanisms,⁴² leading to co-expression with VEGF.⁴³ Moreover, we reported that the oxidative stress generated during early maturation of an AVF stabilized the HIF-1 α protein and thus activated HIF-target genes such as *Vegf-A*, *Nox-2* and *Ho-1*.⁴⁴

Given that changes in the oxygen concentration occur during surgical creation of an AVF in parallel to OPN overexpression, we suggested that OPN is induced by hypoxia and thus could contribute to the failure of AVF maturation due to NH and juxta-anastomotic stenosis. We postulated that regulation of OPN through silencing of HIFs or NF- κ B could promote AVF maturation. Finally, we describe an all-human *in vitro* cell model of co-culture that induces OPN in hypoxia but only under conditions of cell-cell interaction.

2 | MATERIALS AND METHODS

2.1 | Cell culture and co-culture

Normal human fibroblasts (NHf; gifted by Dr Cédric Gaggioli, IRCAN) were grown in Dulbecco's modified eagle medium (DMEM, Gibco) supplemented with 10% foetal bovine serum (FBS), penicillin (10 U/mL) and streptomycin (10 μ g/mL), and used between

passages 3 and 10. Human umbilical vein smooth muscle cells (HUVSMC) were grown on poly-L-lysine-coated dishes in full smooth muscle cell medium (ScienCell Research Laboratories) and used between passages 1-6. Human umbilical vein endothelial cells (HUVEC; Gibco, Thermo Fisher Scientific) were grown on gelatin-coated dishes in endothelial cell growth medium supplemented with SingleQuots™ (Lonza), penicillin (10 U/mL) and streptomycin (10 µg/mL), and used between passages 1 and 6. Mesenchymal stromal cells (MSCs) were isolated from bone marrow aspirate obtained from healthy donors and expanded in alpha-MEM medium (Gibco; Thermo Fisher Scientific) supplemented with 5% HyClone foetal bovine serum (Thermo Fisher Scientific) while fulfilling uniformly minimal MSC criteria. Their osteoblast differentiation was obtained after 3 weeks of culture in the StemPro Osteogenesis Differentiation kit (Thermo Fisher Scientific) according to the manufacturer's instructions. For normoxia, cells were maintained in a humid incubator at 37°C with 5% CO₂ and air. For hypoxia, cells were transferred to an *Invivo*₂ hypoxic workstation (Baker Ruskinn Global) set at 37°C, 5% CO₂ and 1% O₂.

To model the AVF microenvironment, different combinations of direct co-cultures of cells (100 000 cells/well) were used: NHF/HUVSMC, NHF/HUVEC, HUVSMC/HUVEC and NHF/HUVSMC/HUVEC. The same total number of cells was used for both these combinations and the mono-cultures. For combinations of NHF/HUVSMC, NHF/HUVEC and HUVSMC/HUVEC, a ratio of 1 to 1 was used with 50% of each cell line. For NHF/HUVSMC/HUVEC, the ratio was still 1 to 1 but with 33% of each cell line.

2.2 | Tissue collection

Studies on human samples received authorization from regulatory boards and the local ethics committee. Informed consent was obtained from patients regarding the collection of samples and data. Deidentified matured patent human AVF samples were provided by Yale Vascular Surgery. Samples were obtained after ≥6 months of haemodialysis during surgical revision of the fistula resulting from severe anastomotic stenosis.⁴⁵ The samples analysed are of a segment of normally remodelling patent vein from the fistulae. Control veins were obtained from renal disease patients at the time of initial AVF creation. Sample procurement with informed consent was approved by Human Investigation Committee of Yale University Institutional Review Board HIC No. 1005006865. Tissues were fixed in formalin and embedded in paraffin.

2.3 | Pharmacological inhibitors and chemicals

Recombinant human OPN was from R&D system and was used at 1 µg/mL. Inhibition of the NF-κB activity was conducted with a specific inhibitor (inhibitor of IKK2 (AS602868), iNF-κB), a gift from Dr JF Peyron.

2.4 | RNAi transfection

Cells were plated at 70% confluence and transfected the following day using Lipofectamine RNAiMAX™ (Thermo Fisher Scientific) according to the manufacturer's protocol, at a 50 nmol/L final concentration of RNAi. The set of RNAi sequences (Eurogentec) targeting human were as follows: SIMA (siCtl) (forward) 5'-CCUACAUCGCCGAUCGAUGAUG-3', siHIF-1α (forward) 5'-CUGAUGACCAGCAACUUGA-3',⁴⁶⁻⁴⁸ siHIF-2α (forward) 5'-CAGCAUCUUUGAUAGCAGU-3',⁴⁸ siOPN#1 (forward) 5'-GUUUCACAGCCACAAGGAC-3', siOPN#2 (forward) 5'-GCCACAAGCAGUCCAGAUU-3'.

2.5 | Immunoblotting

Protein immunodetection was performed as previously //described.⁴⁹ Briefly, cells were lysed in 1.5X SDS buffer, and if exposed to hypoxia, they were lysed while inside the hypoxic chamber. Proteins (40 µg) were separated on 7.5% SDS-polyacrylamide gels and transferred onto polyvinylidene difluoride membranes (Millipore). Blots were blocked in 5% milk in Tris-HCl/NaCl buffer and incubated with antibodies at 4°C overnight. Immunoreactive signals were revealed with horseradish peroxidase (HRP)-conjugated antibodies (Promega) using the Pierce™ ECL Western blotting system (Thermo Fisher Scientific). The antibody against HIF-1α was produced in our laboratory and used at 1:1000. The antibody against HIF-2α (NB100-122) was purchased from Novus Biologicals (Littleton) and used at 1:1000. The antibody against OPN (AF 14-33OP) was purchased from R&D System and used at 1:500. The antibody against β-tubulin (T4026; Sigma-Aldrich) was used at a 1:2000 dilution as a loading control.

2.6 | RNA extraction and quantitative real-time PCR

For patient samples, total RNA was extracted with the RNeasy FFPE Kit (Qiagen). For cells, total RNA was extracted and reverse transcribed (SuperScript II Reverse Transcriptase; Invitrogen), and real-time RT-PCR was performed on an StepOnePlus Fast real-time PCR system (Sybr Green, Applied Biosystems) on triplicates as described. Results were normalized to the housekeeping gene *36B4* on the same plate. Differences in gene expression were calculated using the 2^{-ΔΔCt} method.

Human primer sequences used were: OPN (Eurogentec) (forward: 5'-CAGGCTGATTCTGGAAGTTCTGA-3'; reverse: 5'-GGGCTAGGAGATTCTGCTTCTGA-3'), *GLUT1* (Eurogentec) (forward: 5'-TTCAGTGTGTCGCTGTTT-3'; reverse: 5'-TCACACTGGGAA TCAGCCCC-3') and *rpL0* (Sigma) (forward: 5'-CAGCTTGGCTACC CAACTGTT-3'; reverse: 5'-GGCCAGGACTCGTTTGTACC-3').

2.7 | ELISA

The concentration of human OPN was determined by ELISA (kit DuoSet ELISA Human osteopontin, R&D systems DY1433) using NHF, HUVMC and HUVEC conditioned culture media according to the manufacturer's instructions. Cells were plated at 50% confluence and treated the following day with H₂O₂ (50 µmol/L), glucose (50 mmol/L) and inhibitor of IKK2 (AS602868), iNF-κB⁵⁰ for 48 hours. Treatment with phosphate-buffered saline (PBS) was used as control.

2.8 | Immunofluorescence

Human vein and AVF samples were sectioned at 5 µm and mounted onto glass slides. After heating overnight at 55°C, deparaffinization was accomplished through a series of xylene and graded ethanol soaks. Sections were heated in citric acid buffer (pH 6.0) at 100°C for 10 minutes for antigen retrieval, then washed and permeabilized with 0.1% Tween-20 in phosphate-buffered saline (PBS-T). Antigens were blocked with 2% bovine serum albumin in PBS-T for 60 minutes at room temperature. Sections were then incubated with the following primary antibodies diluted in antibody diluent (Agilent Dako S3022) overnight at 4°C: anti-OPN (1:500, Abcam, ab8448), anti-alpha-smooth muscle actin (1 µg/mL, Invitrogen 14-9760-80). Sections were treated with secondary antibodies goat anti-rabbit Alexa-Fluor-568 (Life Technologies) and chicken anti-mouse Alexa-Fluor-488 diluted 1:400 for 1 hour at room temperature. Sections were then stained with ProLong™ Gold Antifade Mountant with DAPI (Thermo Fisher), and coverslips were applied. Digital fluorescence images were captured with the EVOS FL Auto 2 cell imaging system (Thermo Fisher) at 40x, with subsequent image analysis done with ImageJ software (NIH). Osteopontin fluorescence was background-subtracted and normalized to smooth muscle cell area (determined by area fraction of alpha-smooth muscle cell actin immunofluorescence). The background was obtained from negative control sections, that is without the primary antibody. The value of this negative signal was subtracted from the signal obtained from the red channel (OPN) using the primary antibody. Samples were analysed with ImageJ, and whole sections were analysed; 3-5 sections were analysed for each sample and the mean value computed for each specimen.

2.9 | Statistics

All values are the means ± SEM. Statistical analyses were performed using Student's *t* test in Microsoft Excel. The *P* values are indicated. All categorical data used numbers and percentages. Quantitative data were presented using the median and range or mean. Differences between groups were evaluated using the chi-square test for categorical variables and Student's *t* test for continuous variables. Analyses were performed using SPSS 16.0 statistical software (SPSS Inc.). All statistical tests were two-sided, and *P*-values < .05 indicated statistical significance whereas *P*-values between .05 and .10 indicated a statistical tendency.

3 | RESULTS

We suggested that OPN plays a role in intimal hyperplasia of AVF; thus, we searched *in vitro* for OPN expression in hypoxia (1% O₂) in comparison to normoxia in cells (NHF, HUVMC and HUVEC) representative of those involved in AVF maturation. We investigated silencing of HIFs and inhibition of NF-κB *in vitro* in these cells to see if these transcription factors down-regulated OPN expression in hypoxia.

3.1 | Intracellular OPN (iOPN) is not induced in hypoxic cells

First, we evaluated the level of expression of OPN in AVF patients. Both expressions of OPN mRNA (Figure 1A) and OPN immunoreactivity (Figure 1B) in the AVF were significantly increased, compared to control veins, confirming our previous results and the potential role of OPN in AVF maturation.³⁴ Knowing that OPN has two isoforms, intracellular OPN (iOPN) and soluble OPN (sOPN), we first characterized iOPN by immunoblot in different cellular models. Recombinant OPN (recOPN) was used to quantitate the expression (Figure 1C). Human bone marrow mesenchymal cells osteoblasts (Figure 1D) and LNCap cells (Figure 1E) were examined as controls, since these two models are known to express OPN. Moreover, OPN is known as a biomarker for prostate cancer and for its role in tumour progression.⁵¹ The antibody against OPN detected recOPN at the concentrations of 50 and 16.6 ng and at a relative molecular weight of 70 kDa (Figure 1C). Human bone marrow mesenchymal cells and osteoblasts showed high expression of iOPN in normoxia after 48 hours incubation. Since iOPN is expressed in LNCap, we evaluated potential hypoxic induction of iOPN in these cells and observed a slight induction (twofold; Figure 1E). As HIF-1 is the key protein responsible for cellular adaptation to hypoxia, we checked whether HIF-1 was involved in the induction of iOPN. Using siRNA to silence HIF-1α, we showed that, in the absence of HIF-1α, iOPN expression was still present. Only siRNA#2 to OPN completely abolished iOPN expression. Subsequent experiments were done with this siRNA to OPN. NHF (representing the adventitia; Figure 1F), HUVMC (representing smooth muscle cells associated with elastic fibres) (Figure 1G) and HUVEC (representing the endothelium) (Figure 1H), the three cell lines that compose the three layers of the arteries and veins, were tested for iOPN expression. Although HIF-1α and HIF-2α were detected in hypoxic conditions, 1% O₂ for 48 hours, none of these cells expressed iOPN. These cells did not express iOPN in either normoxia or hypoxia 0.2% O₂ (data not shown). Transfection of NHF (Figure 1F), HUVMC (Figure 1G) and HUVEC (Figure 1H) with siRNA to HIF-1α and/or HIF-2α strongly diminished the amount of these two subunits and the silencing of HIF-1α slightly increased the detection level of HIF-2α and *vice versa*. Thus, we silenced both subunits to completely abolish the HIF activity.

These results suggest that iOPN expression is below the detectable level of 16.6 ng, (Figure 1C) in NHF, and weakly expressed in HUVMC and HUVEC.

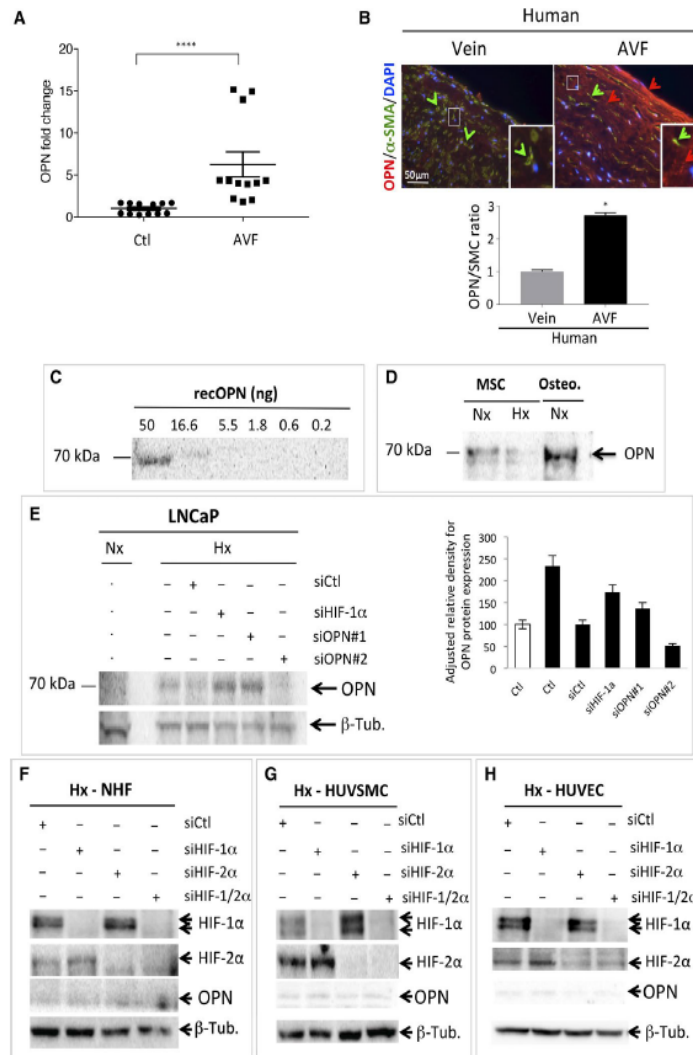


FIGURE 1 Osteopontin (OPN) is weakly expressed in NHF, HUVMSC and HUVEC and is not induced in hypoxia. **A**, Levels of OPN mRNA in AVF patients (n = 12) compared to control veins (Ctl). ****, $P < .0001$ (Test Mann-Whitney). **B**, Representative immunofluorescence of OPN (red staining and arrow) and alpha-smooth muscle actin (α -SMA—green staining and arrows) of human control upper-arm vein and venous limb of a mature AVF. Osteopontin quantification of group data (vein, n = 3; AVF, n = 2), unpaired t test, $P < .01$ (right). **C**, Quantitative immunoblotting to detect recombinant OPN protein. Serial dilutions from 50 to 0.2 ng were used. **D**, Bone marrow mesenchymal (MSC) and osteoblast (Osteo.) cell lysates analysed by immunoblotting for OPN as indicated. **E**, LNCaP cells were transfected with control siRNA (siCtl), siHIF-1 α (40 nmol/L), siOPN#1 (40 nmol/L) and siOPN#2 (40 nmol/L) and incubated in normoxia (Nx) or hypoxia 1% O₂ (Hx) for 48 h. Cell lysates were analysed by immunoblotting for OPN or β -tubulin as indicated. Quantification of the signal to OPN is shown using ImageJ (OPN/ β -tubulin). **F–H**, NHF (**F**), HUVMSC (**G**) and HUVEC (**H**) cells were transfected with control siRNA (siCtl), siHIF-1 α (40 nmol/L), siHIF-2 α (40 nmol/L) and siHIF1/2 α (40 nmol/L + 40 nmol/L), incubated in hypoxia 1% O₂ (Hx) for 48 h. AVF, Arteriovenous fistula; HUVEC, human umbilical vein endothelial cells; HUVMSC, Human umbilical vein smooth muscle cells; NHF, normal human fibroblasts

3.2 | Secreted OPN (sOPN) is not induced in hypoxic cells

We then tested for sOPN in these cells using an ELISA. Two different kits were used, one that measured sOPN in nanograms (Figure 2A) and one in picograms (Figure 2B). No sOPN was detected in NHF,

HUVMSC and HUVEC, at nanogram levels when using recOPN as reference, in normoxia or hypoxia or in conditions that are supposed to induce OPN such as H₂O₂ or glucose^{52,53} (Figure 2A). No cell death was observed in these conditions (data not shown). A more sensitive kit detected sOPN in NHF (Figure 2B), HUVMSC (Figure 2C) but not in HUVEC (Figure 2D). HNF and HUVMSC

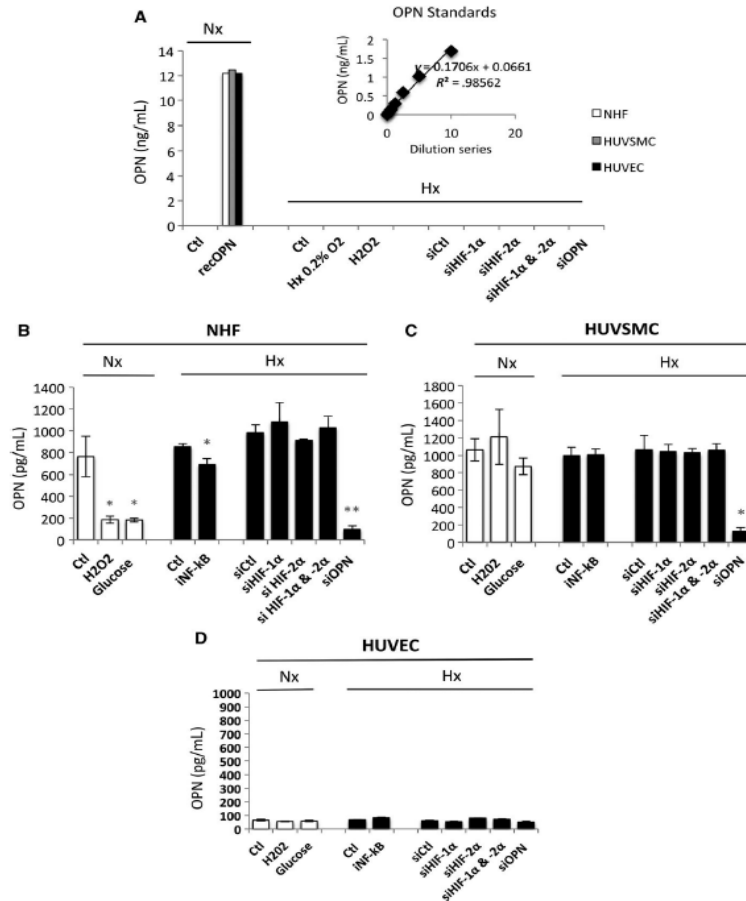


FIGURE 2 Production of OPN by NHF, HUVSMC and HUVEC in normoxia compared to hypoxia. (A) Histograms representing the level of OPN produced *in vitro* by NHF, HUVSMC and HUVEC after 48 h in culture, detected by ELISA using a Quantikine ELISA Human Osteopontin immunoassay. The mean \pm SEM is representative of three independent experiments expressed as nanograms per millilitre. Cells were cultured in the absence (Ctl) or presence of recombinant OPN (recOPN) in normoxia. Cells were cultured in the absence (Hx 0.2% O₂) or presence of H₂O₂ (50 μ mol/L) for 48 h or transfected with control siRNA (siCtI), siHIF-1 α (40 nmol/L), siHIF-2 α (40 nmol/L), siHIF-1/2 α (40 nmol/L + 40 nmol/L) or siOPN (40 nmol/L), and incubated in hypoxia 0.1% O₂ (Hx). (B–D) Histograms representing the level of OPN produced *in vitro* by NHF (B), HUVSMC (C) and HUVEC (D) after 48 h in culture using a DuoSet ELISA Human osteopontin immunoassay. The mean \pm SEM is representative of three independent experiments expressed as picograms per millilitre. Cells were cultured in the absence (Ctl) or presence of H₂O₂ (50 μ mol/L), glucose (50 mmol/L) for 48 h, or transfected with control siRNA (siCtI) with addition of glucose (Gluc) + siOPN (40 nmol/L) in normoxia. Cells were cultured in the absence (Ctl) or presence of an inhibitor to NF- κ B (iNF- κ B) (10 μ mol/L) for 48 h or transfected with control siRNA (siCtI), siHIF-1 α (40 nmol/L), siHIF-2 α (40 nmol/L), siHIF-1/2 α (40 nmol/L + 40 nmol/L) or siOPN (40 nmol/L), and incubated in hypoxia 1% O₂ (Hx) for 48 h. The mean \pm SEM is representative of three independent experiments carried out in triplicate. HUVEC, human umbilical vein endothelial cells; HUVSMC, Human umbilical vein smooth muscle cells; NHF, normal human fibroblasts; OPN, osteopontin

showed a similar level of sOPN in normoxia, 765 and 1060 pg/mL, respectively. siRNA to OPN (siOPN), used as a control, abolished secretion of OPN. However, no stimuli known to increase OPN, including H₂O₂ or glucose, activated sOPN in normoxia. Hypoxic conditions did not increase sOPN and silencing of HIF-1 α and/or HIF-2 α did not block secretion of OPN in NHF and HUVSMC. However,

inhibition of NF- κ B activity with a specific inhibitor (inhibitor of IKK2 (AS602868), iNF- κ B) slightly, but statistically, decreased secretion of OPN from 850 to 700 pg/mL.

These results confirm weak expression of both iOPN (Figure 1) and sOPN in these cells and show that sOPN was not detected in HUVEC. They also confirm that these two forms are not induced

under hypoxic conditions *via* HIFs. However, they show that NF- κ B participates in OPN regulation to some extent.

3.3 | mRNA expression of OPN is not induced in hypoxic cells

As we were unable to detect hypoxic induction of either iOPN or sOPN, we tested an even more sensitive technique to measure OPN. Using real-time qPCR, we quantified the endogenous expression of OPN in normoxia and hypoxia (Figure 3). As a control for hypoxia, the glucose transporter 1 (GLUT1) mRNA expression was evaluated (Figure 3A,3,3). Two- to threefold induction at the mRNA level of GLUT1 was observed in NHF (Figure 3A) and HUVEC (Figure 3E). A decrease in GLUT1 expression was observed with the HIF-2 α -directed siRNA in NHF and HUVMC, whereas both siRNAs to HIF-1 α and/or HIF-2 α decreased GLUT1 expression in HUVEC suggesting shared regulation by HIF-1 and HIF-2 in these cells. siRNA to HIF-1 α and HIF-2 α abolished endogenous expression of both HIF-1 α and HIF-2 α as shown in Figure S1. Intriguingly, the mRNA level of GLUT1 was systematically increased when OPN was silenced, suggesting negative control of GLUT1 by OPN. Thus, we quantified the endogenous expression of OPN in NHF (Figure 3B), HUVMC (Figure 3D) and HUVEC (Figure 3F). For the first time, we observed an increase of OPN mRNA levels in the presence of glucose in HUVMC and HUVEC but not in NHF. However, no induction under conditions of hypoxia was detected in NHF, HUVMC and HUVEC. A slight decrease in OPN expression was observed in NHF and HUVMC in the presence of iNF- κ B confirming that NF- κ B participates in OPN regulation. A twofold induction was observed at the mRNA level for OPN in hypoxia in NHF with siHIF-1 α and siHIF-1/2 α compared to the control siRNA suggesting that HIF-1 α only could repress OPN. Similarly, a threefold induction was observed at the mRNA level for OPN in hypoxia in HUVEC with siHIF-1 α , but also with siHIF-2 α and siHIF-1/2 α . However, siRNA to OPN did not affect the mRNA level of OPN under these conditions; therefore, these results (Figure 3F) are not specific to OPN expression and reflect non-specific amplification due to undetectable OPN expression in HUVEC (Figure 2D).

We thus confirmed that mRNA expression of OPN is not induced in hypoxia in the three cell lines tested.

3.4 | Co-culture favours OPN induction in hypoxia

Finally, given that a potential link between OPN and AVF has been shown early in the maturation process in a mouse model where the three layers of cells are juxtaposed, we co-cultured cells using different combinations: NHF/HUVMC, NHF/HUVEC, HUVMC/HUVEC and NHF/HUVMC/HUVEC (Figure 4). The mRNA expression of OPN in NHF, HUVMC and HUVEC was higher than that of NHF/HUVMC, NHF/HUVEC, HUVMC/HUVEC and NHF/HUVMC/HUVEC co-cultures (Figure 4A). Co-culture of HUVMC/HUVEC clearly increased the level of OPN expression. We then quantified

the endogenous expression of OPN in normoxia and hypoxia in the absence or presence of siRNA compared to control siRNA or siOPN (Figure 4B). Co-cultures of NHF/HUVMC and NHF/HUVEC exposed to hypoxia showed a twofold increase in OPN expression. Cell-cell interaction between HUVMC and HUVEC showed high basal expression of OPN, 16-fold induction, compared to the other co-cultures in which no induction was found in hypoxia. Finally, all the cell types together presented intermediate expression, fourfold induction in normoxia, but still no induction in hypoxia.

Therefore, we measured sOPN in the different combinations using ELISA (Figure 4C). For the first time, sOPN induction was observed in all co-culture combinations in hypoxia. Moreover, the presence of HUVEC in combination with NHF (2.3-fold induction), HUVMC (2.7-fold induction) or NHF/HUVMC (2.4-fold induction) seemed to stimulate more sOPN induction in hypoxia compared to the combination without HUVEC (NHF/HUVMC, 1.5-fold induction). Finally, we showed that OPN down-regulation did not alter cell proliferation of NHF, HUVMC and HUVEC, whereas recombinant human OPN only increased HUVEC proliferation (Figure 4D) suggesting that HUVEC cells were sensitive to OPN and could directly contribute to the pathological NH.

These results strongly suggest that in the absence of cell-cell interaction, OPN expression is not induced in hypoxia. Moreover, HUVEC cells, which do not express OPN, are central to the process of NH.

4 | DISCUSSION

The main objective of this study was to determine whether OPN was induced in hypoxia and thus could be responsible for driving the failure of AVF maturation due to NH and juxta-anastomotic stenosis. We first used cell mono-layers grown on tissue culture plastic to examine hypoxic production of OPN observed in AVF, which is the approach used by the majority of research groups. Mono-cultures are less complex to perform but certainly less adapted to, and not very representative of, the physiological extracellular microenvironment present in humans. While the expression of OPN has been shown to be increased during early AVF maturation⁵⁴ or throughout maturation⁵⁴ under hypoxic conditions,⁴⁴ none of the three cell lines forming the three layers of the artery and vein walls expressed iOPN or sOPN.

However, this is the first time that a study has shown that cell-cell communication or interaction between NHF, HUVMC and HUVEC is essential for OPN induction in hypoxia. Co-culture allows investigation of cell-cell interactions and is therefore more representative of human *in vivo*-like tissue models.⁵⁵ Interestingly, all co-cultures showed induction of OPN in hypoxia, whereas none of the mono-cultures showed OPN induction. However, we noted that co-cultures containing HUVEC produced more OPN. Although we do not know which cell line(s) produced the OPN, it is interesting to note that the amount of sOPN in mono-culture conditions was barely detectable and 10 times lower in HUVEC than in NHF or HUVMC. Moreover, siRNA directed to OPN in NHF and HUVMC

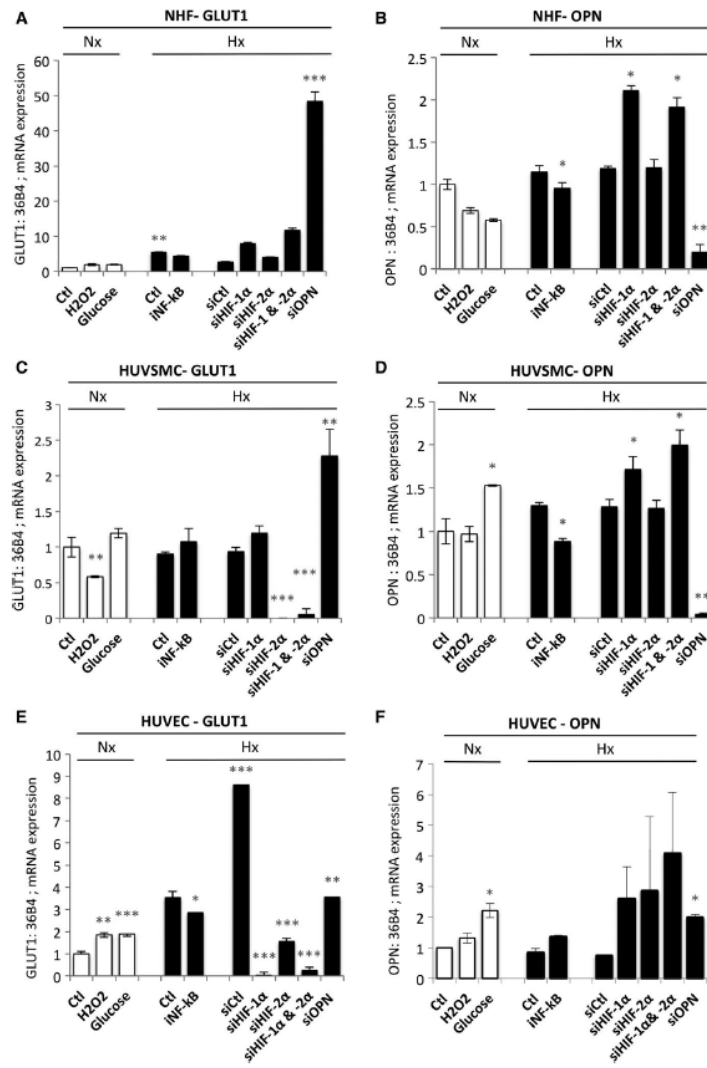


FIGURE 3 Expression of OPN mRNA in NHF, HUVMSC and HUVEC is not induced in hypoxia. (A, C and E) Histograms represent the expression of the mRNA of GLUT-1 in NHF (A), HUVMSC (C) and HUVEC (E). The mean \pm SEM is representative of three independent experiments. Cells were cultured in the absence (Ctl) or presence of H₂O₂ (50 μ mol/L), or glucose (50 mmol/L) for 48 h, or transfected with control siRNA (siCtl) and glucose (Gluc) + siOPN (40 nmol/L) in normoxia. Cells were cultured in the absence (Ctl) or presence of an inhibitor to (iNF-kB) (10 μ mol/L) for 48 h or transfected with control siRNA (siCtl), siHIF-1 α (40 nmol/L), siHIF-2 α (40 nmol/L), siHIF-1/2 α (40 nmol/L + 40 nmol/L) or siOPN (40 nmol/L), and incubated in hypoxia 1% O₂ (Hx) for 48 h. (B, D and F) Histograms represent the expression of the mRNA of OPN in NHF (B), HUVMSC (D) and HUVEC (F). The mean \pm SEM is representative of three independent experiments. Cells were cultured in the absence (Ctl) or presence of H₂O₂ (50 μ mol/L), glucose (50 mmol/L) for 48 h, or transfected with control siRNA (siCtl) and glucose (Gluc) + siOPN (40 nmol/L) in normoxia. Cells were cultured in the absence (Ctl) or presence of iNF-kB (10 μ mol/L) for 48 h or transfected with control siRNA (siCtl), siHIF-1 α (40 nmol/L), siHIF-2 α (40 nmol/L), siHIF-1/2 α (40 nmol/L + 40 nmol/L) or siOPN (40 nmol/L), and incubated in hypoxia 1% O₂ (Hx) for 48 h. HUVEC, human umbilical vein endothelial cells; HUVMSC, Human umbilical vein smooth muscle cells; NHF, normal human fibroblasts; OPN, osteopontin

totally abolished OPN at the mRNA level, whereas it had no effect on HUVEC suggesting that the mRNA level of OPN was extremely low in HUVEC. However, OPN was only induced in the presence of

HUVEC in the co-culture. Moreover, HUVEC cells were the most sensitive to the presence of OPN as it increased their proliferation. However, were the HUVEC cells the only ones producing OPN? If

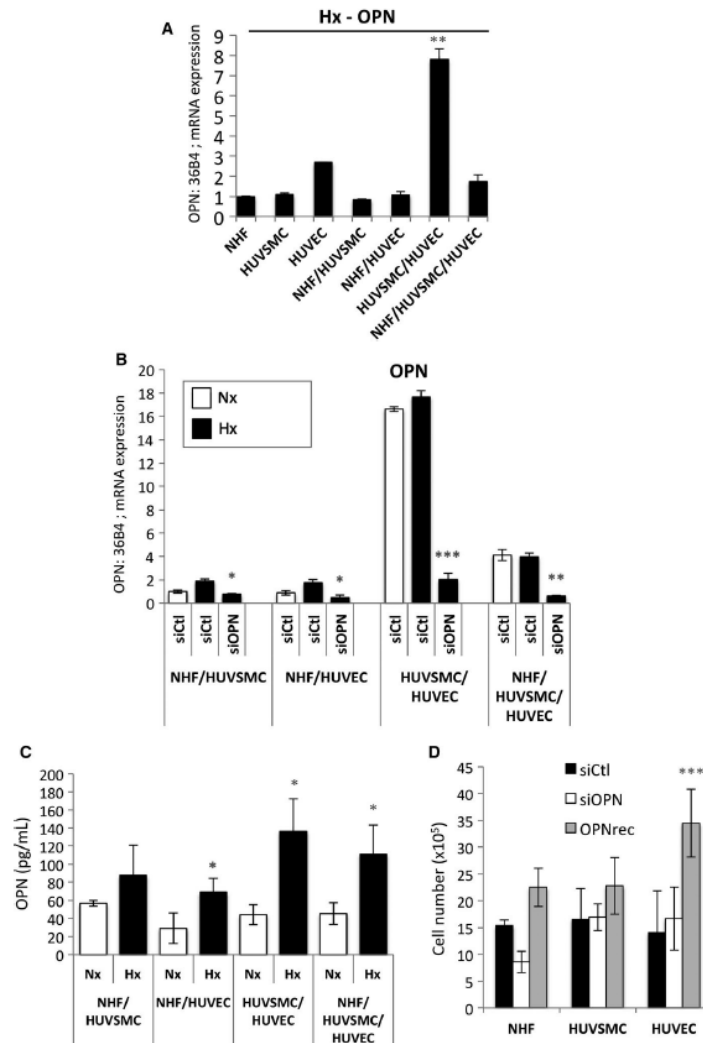


FIGURE 4 Co-culture induced OPN expression in hypoxia. (A) Histograms represent the expression of the mRNA of OPN in mono- and co-cultures after 48 h in hypoxia 1% O₂ (Hx). The mean ± SEM is representative of three independent experiments. (B) Histograms represent the expression of the mRNA of OPN in co-culture (mean ± SD of values from three independent experiments). Co-culture with NHF/HUVSMC, NHF/HUVEC, HUVSMC/HUVEC, NHF/HUVSMC/HUVEC were transfected with control siRNA (siCtI) in normoxia (Nx) or transfected with control siRNA (siCtI) or siOPN (40 nmol/L), and incubated in hypoxia 1% O₂ (Hx) for 48 h. (C) Histograms represent the level of OPN produced in vitro in co-culture of NHF/HUVSMC, NHF/HUVEC, HUVSMC/HUVEC and NHF/HUVSMC/HUVEC, after 48 h in culture detected with a DuoSet ELISA Human osteopontin immunoassay. The mean ± SEM is representative of three independent experiments expressed as picograms per millilitre. (D) NHF-, HUVSMC- and HUVEC cells were transfected with control siRNA (siCtI) in normoxia (Nx) or transfected with siOPN (40 nmol/L) or in the presence of recombinant human OPN (OPNrec-1 µg/mL) and incubated in normoxia for 48 h. Cell lines were seeded at the same density and incubated in for 48 h. The mean ± SEM is representative of two independent experiments carried out in duplicate. HUVEC, human umbilical vein endothelial cells; HUVSMC, Human umbilical vein smooth muscle cells; NHF, normal human fibroblasts; OPN, osteopontin

this is the case, the regulation of OPN production in HUVEC may be a consequence of specific cellular interactions and regulation. Hall et al³⁴ showed a 40-fold increase in OPN expression in the

endothelium of veins of AVF relative to control veins suggesting OPN production was mainly in the intima. In this murine AVF model, they also showed increased expression of matrix metalloproteinases

(MMPs, MMP3 and MMP9) early on after AVF creation and subsequent decreased expression after 21 days. They proposed that such a balance could favour AVF failure and stenosis. When OPN was co-localized with members of the MMP family, it was shown to induce the expression of MMP9,⁵⁶ one of the two MMPs identified by Hall et al⁵⁴. In our model, hypoxic induction of OPN, an active player in tissue remodelling and a response to vascular injury and inflammation, may modulate the activity of MMPs, which are responsible for degradation and accumulation of the ECM, and thus contribute to AVF failure and NH.

In conclusion, changes in oxygenation that occur during AVF maturation may up-regulate secretion of OPN, possibly via endothelial cells or at least through cell-cell interactions of the different cell layers that form AVF, and in turn increase inflammation and promote endothelial cell proliferation.

ACKNOWLEDGEMENTS

This research was supported by a grant from the Société Française de Chirurgie Vasculaire et Endovasculaire. The Institut National de la Santé et de la Recherche Médicale (INSERM) supervised the collection and analysis of patient's samples. The team was supported by grants from the Fondation Flavien, the Fondation ARC, La Ligue contre le Cancer and Fondation de France. We thank Abby Cuttriss for the language editing of the manuscript.

CONFLICT OF INTEREST

The authors declare that they have no conflicting interests.

AUTHOR CONTRIBUTIONS

N.S., J.C., AD and NMM: conception and design, data analysis and interpretation, manuscript writing and editing; J.C., M.D., Ju.P., L.F.: data collection and assembly; M.R. and JFP: provided reagents and cells, data analysis and interpretation; R.H-K, Ja.P., FB E.J-B: data analysis and interpretation, manuscript editing and final approval of manuscript.

DATA AVAILABILITY STATEMENT

I confirm that my article contains a Data Availability Statement even if no data are available (list of sample statements) unless my article type does not require one (eg, Editorials, Corrections, Book Reviews, etc). I confirm that I have included a citation for available data in my references section, unless my article type is exempt.

ORCID

Nathalie M. Mazure  <https://orcid.org/0000-0003-1350-7161>

REFERENCES

- Vascular Access Work Group. Clinical practice guidelines for vascular access. *Am J Kidney Dis.* 2006;48(Suppl 1):S176-S247.
- Al-Jaishi AA, Oliver MJ, Thomas SM, et al. Patency rates of the arteriovenous fistula for hemodialysis: a systematic review and meta-analysis. *Am J Kidney Dis.* 2014;63:464-478.
- Brahmbhatt A, Remuzzi A, Franzoni M, Misra S. The molecular mechanisms of hemodialysis vascular access failure. *Kidney Int.* 2016;89:303-316.
- Misra S, Shergill U, Yang B, Janardhanan R, Misra KD. Increased expression of HIF-1alpha, VEGF-A and its receptors, MMP-2, TIMP-1, and ADAMTS-1 at the venous stenosis of arteriovenous fistula in a mouse model with renal insufficiency. *J Vasc Interv Radiol.* 2010;21:1255-1261.
- Sadaghianloo N, Contenti J, Dardik A, Mazure NM. Role of hypoxia and metabolism in the development of neointimal hyperplasia in arteriovenous fistulas. *Int J Mol Sci.* 2019;20:5387.
- Brahimi-Horn M, Laferrrière J, Mazure N, Pouyssegur J. In: Marmè D, Fusenig N eds., *Tumor Angiogenesis*. Springer;2007:171-194.
- Patel SA, Simon MC. Biology of hypoxia-inducible factor-2alpha in development and disease. *Cell Death Differ.* 2008;15:628-634.
- Bitto A, DeCaridi G, Polito F, et al. Evidence for markers of hypoxia and apoptosis in explanted human carotid atherosclerotic plaques. *J Vasc Surg.* 2010;52:1015-1021.
- Sluimer JC, Daemen MJ. Novel concepts in atherogenesis: angiogenesis and hypoxia in atherosclerosis. *J Pathol.* 2009;218:7-29.
- Erdozain OJ, Pegrum S, Winrow VR, Horrocks M, Stevens CR. Hypoxia in abdominal aortic aneurysm supports a role for HIF-1alpha and Ets-1 as drivers of matrix metalloproteinase upregulation in human aortic smooth muscle cells. *J Vasc Res.* 2011;48:163-170.
- Hu XH, Yang J, Liu CW, Zhang ZS, Zhang Q. The expression and significance of hypoxia-inducible factor-1 alpha and related genes in abdominal aorta aneurysm. *Zhonghua wai ke za zhi [Chinese Journal of Surgery]*. 2004;42:1509-1512.
- Sakata N, Nabeshima K, Iwasaki H, et al. Possible involvement of myofibroblast in the development of inflammatory aortic aneurysm. *Pathol Res Pract.* 2007;203:21-29.
- Brusselmans K, Compennolle V, Tjwa M, et al. Heterozygous deficiency of hypoxia-inducible factor-2alpha protects mice against pulmonary hypertension and right ventricular dysfunction during prolonged hypoxia. *J Clin Invest.* 2003;111:1519-1527.
- Hanze J, Weissmann N, Grimminger F, Seeger W, Rose F. Cellular and molecular mechanisms of hypoxia-inducible factor driven vascular remodeling. *Thromb Haemost.* 2007;97:774-787.
- Tuder RM, Chacon M, Alger L, et al. Expression of angiogenesis-related molecules in plexiform lesions in severe pulmonary hypertension: evidence for a process of disordered angiogenesis. *J Pathol.* 2001;195:367-374.
- Hughes D, Fu AA, Puggioni A, et al. Adventitial transplantation of blood outgrowth endothelial cells in porcine haemodialysis grafts alleviates hypoxia and decreases neointimal proliferation through a matrix metalloproteinase-9-mediated pathway—a pilot study. *Nephrol Dial Transplant.* 2009;24:85-96.
- Lee ES, Bauer GE, Caldwell MP, Santilli SM. Association of artery wall hypoxia and cellular proliferation at a vascular anastomosis. *J Surg Res.* 2000;91:32-37.
- Santilli SM, Wernsing SE, Lee ES. Transarterial wall oxygen gradients at a prosthetic vascular graft to artery anastomosis in the rabbit. *J Vasc Surg.* 2000;31:1229-1239.
- Evans CE, Humphries J, Mattock K, et al. Hypoxia and upregulation of hypoxia-inducible factor 1[alpha] stimulate venous thrombus recanalization. *Arterioscler Thromb Vasc Biol.* 2010;30:2443-2451.
- Evans CE, Humphries J, Waltham M, et al. Upregulation of hypoxia-inducible factor 1 alpha in local vein wall is associated with enhanced venous thrombus resolution. *Thromb Res.* 2011;128:346-351.
- Comati A, Beck H, Halliday W, Snipes GJ, Plate KH, Acker T. Upregulation of hypoxia-inducible factor (HIF)-1alpha and HIF-2alpha in leptomeningeal vascular malformations of Sturge-Weber syndrome. *J Neuropathol Exp Neurol.* 2007;66:86-97.
- Gao P, Zhu Y, Ling F, et al. Nonischemic cerebral venous hypertension promotes a pro-angiogenic stage through HIF-1 downstream genes and leukocyte-derived MMP-9. *J Cereb Blood Flow Metab.* 2009;29:1482-1490.

23. Nieves Torres EC, Yang B, Janardhanan R., et al. Adventitial delivery of lentivirus-shRNA-ADAMTS-1 reduces venous stenosis formation in arteriovenous fistula. *PLoS ONE*. 2014;9:e94510.
24. D'Ignazio L, Rocha S. Hypoxia Induced NF-kappaB. *Cells*. 2016;5:p11-E10.
25. Oeckinghaus A, Ghosh S. The NF-kappaB family of transcription factors and its regulation. *Cold Spring Harb Perspect Biol*. 2009;1:a000034.
26. Miyake T, Aoki M, Morishita R. Inhibition of anastomotic intimal hyperplasia using a chimeric decoy strategy against NFkappaB and E2F in a rabbit model. *Cardiovasc Res*. 2008;79:706-714.
27. Sodek J, Ganss B, McKee MD. Osteopontin. *Crit Rev Oral Biol Med*. 2000;11:279-303.
28. Singh M, Foster CR, Dalal S, Singh K. Role of osteopontin in heart failure associated with aging. *Heart Fail Rev*. 2010;15:487-494.
29. Hao C, Cui Y, Owen S, et al. Human osteopontin: potential clinical applications in cancer (review). *Int J Mol Med*. 2017;39:1327-1337.
30. Okamoto H, Imanaka-Yoshida K. Matricellular proteins: new molecular targets to prevent heart failure. *Cardiovasc Ther*. 2012;30:e198-e209.
31. O'Brien ER, Garvin MR, Stewart DK, et al. Osteopontin is synthesized by macrophage, smooth muscle, and endothelial cells in primary and restenotic human coronary atherosclerotic plaques. *Arterioscler Thromb*. 1994;14:1648-1656.
32. Momiyama Y, Ohmori R, Fayad ZA, et al. Associations between plasma osteopontin levels and the severities of coronary and aortic atherosclerosis. *Atherosclerosis*. 2010;210:668-670.
33. Yan X, Sano M, Lu L, et al. Plasma concentrations of osteopontin, but not thrombin-cleaved osteopontin, are associated with the presence and severity of nephropathy and coronary artery disease in patients with type 2 diabetes mellitus. *Cardiovasc Diabetol*. 2010;9:70.
34. Hall MR, Yamamoto K, Protack CD, et al. Temporal regulation of venous extracellular matrix components during arteriovenous fistula maturation. *J Vasc Access*. 2015;16:93-106.
35. Isoda K, Nishikawa K, Kamezawa Y, et al. Osteopontin plays an important role in the development of medial thickening and neointimal formation. *Circ Res*. 2002;91:77-82.
36. Myers DL, Harmon KJ, Lindner V, Liaw L. Alterations of arterial physiology in osteopontin-null mice. *Arterioscler Thromb Vasc Biol*. 2003;23:1021-1028.
37. Lyle AN, Joseph G, Fan AE., et al. Reactive oxygen species regulate osteopontin expression in a murine model of postischemic neovascularization. *Arterioscler Thromb Vasc Biol*. 2012;32:1383-1391.
38. Ito M, Makino N, Matsuda A, et al. High glucose accelerates cell proliferation and increases the secretion and mRNA expression of osteopontin in human pancreatic duct epithelial cells. *Int J Mol Sci*. 2017;18:807.
39. Potier E, Ferreira E, Andriamanalijaona R., et al. Hypoxia affects mesenchymal stromal cell osteogenic differentiation and angiogenic factor expression. *Bone*. 2007;40:1078-1087.
40. Wu C, Zhou Y, Chang J, Xiao Y. Delivery of dimethylallyl glycine in mesoporous bioactive glass scaffolds to improve angiogenesis and osteogenesis of human bone marrow stromal cells. *Acta Biomater*. 2013;9:9159-9168.
41. Sahai S, Williams A, Skiles ML, Blanchette JO. Osteogenic differentiation of adipose-derived stem cells is hypoxia-inducible factor-1 independent. *Tissue Eng Part A*. 2013;19:1583-1591.
42. Zhou Y, Guan X, Yu M, et al. Angiogenic/osteogenic response of BMMSCs on bone-derived scaffold: effect of hypoxia and role of PI3K/Akt-mediated VEGF-VEGFR pathway. *Biotechnol J*. 2014;9:944-953.
43. Ramchandani D, Weber GF. Interactions between osteopontin and vascular endothelial growth factor: Implications for cancer. *Biochim Biophys Acta*. 2015;1855:202-222.
44. Sadaghianloo N, Yamamoto K, Bai H, et al. Increased oxidative stress and hypoxia inducible factor-1 expression during arteriovenous fistula maturation. *Ann Vasc Surg*. 2017;41:225-234.
45. Xie Y, Ostriker AC, Jin Y., et al. LMO7 is a negative feedback regulator of transforming growth factor beta signaling and fibrosis. *Circulation*. 2019;139:679-693.
46. Brahimi-Horn MC, et al. Expression of a truncated active form of VDAC1 in lung cancer associates with hypoxic cell survival and correlates with progression to chemotherapy resistance. *Can Res*. 2012;72:2140-2150.
47. Chiche J, Ilc K, Laferriere J, et al. Hypoxia-inducible carbonic anhydrase IX and XII promote tumor cell growth by counteracting acidosis through the regulation of the intracellular pH. *Can Res*. 2009;69:358-368.
48. Dayan F, Roux D, Brahimi-Horn MC, Pouyssegur J, Mazure NM. The oxygen sensor factor-inhibiting hypoxia-inducible factor-1 controls expression of distinct genes through the bifunctional transcriptional character of hypoxia-inducible factor-1alpha. *Can Res*. 2006;66:3688-3698.
49. Brahimi-Horn MC, Lacas-Gervais S, Adaixo R., et al. Local mitochondrial-endolysosomal microfusion cleaves the voltage-dependent anion channel 1 to promote survival in hypoxia. *Mol Cell Biol*. 2015;35:1491-1505.
50. Lagadec P, Griessinger E, Nawrot MP, et al. Pharmacological targeting of NF-kappaB potentiates the effect of the topoisomerase inhibitor CPT-11 on colon cancer cells. *Br J Cancer*. 2008;98:335-344.
51. Zhang Y, et al. Suppressing tumorigenicity of prostate cancer cells by inhibiting osteopontin expression. *Int J Oncol*. 2011;38:1083-1091.
52. Cai M, Bompada P, Atac D, et al. Epigenetic regulation of glucose-stimulated osteopontin (OPN) expression in diabetic kidney. *Biochem Biophys Res Commun*. 2016;469:108-113.
53. Lyle AN, Remus EW, Fan AE., et al. Hydrogen peroxide regulates osteopontin expression through activation of transcriptional and translational pathways. *J Biol Chem*. 2014;289:275-285.
54. Abeles D, Kwei S, Stavrakis G, et al. Gene expression changes evoked in a venous segment exposed to arterial flow. *J Vasc Surg*. 2006;44:863-870.
55. Goers L, Freemont P, Polizzi KM. Co-culture systems and technologies: taking synthetic biology to the next level. *J R Soc Interface*. 2014;11:20140065.
56. Yang M, Jiang C, Chen H, et al. The involvement of osteopontin and matrix metalloproteinase-9 in the migration of endometrial epithelial cells in patients with endometriosis. *Reprod Biol Endocrinol*. 2015;13:95.

SUPPORTING INFORMATION

Additional supporting information may be found online in the Supporting Information section.

How to cite this article: Sadaghianloo N, Contenti J, Dufies M, et al. Co-culture of human fibroblasts, smooth muscle and endothelial cells promotes osteopontin induction in hypoxia. *J Cell Mol Med*. 2020;24:2931-2941. <https://doi.org/10.1111/jcmm.14905>

Annexe 3: Role of hypoxia and metabolism in the development of neointimal hyperplasia in arteriovenous fistulae. Int J Mol Sci. 2019




International Journal of
Molecular Sciences



Review

Role of Hypoxia and Metabolism in the Development of Neointimal Hyperplasia in Arteriovenous Fistulas

Nirvana Sadaghianloo ^{1,2,*}, Julie Contenti ^{1,3}, Alan Dardik ^{4,5} and Nathalie M. Mazure ^{1,2} 

¹ Centre de Méditerranéen de Médecine Moléculaire (C3M), Université Côte d'Azur, INSERM U1065, 151 Route de St Antoine de Ginesière, BP2 3194, 06204 Nice CEDEX 03, France; contenti.j@chu-nice.fr (J.C.); mazure@unice.fr (N.M.M.)

² Department of Vascular Surgery, Centre Hospitalier Universitaire de Nice, 06000 Nice, France

³ Department of Emergency Medicine, Centre Hospitalier Universitaire de Nice, 06000 Nice, France

⁴ Department of Surgery and the Vascular Biology and Therapeutics Program, Yale University, New Haven, CT 06520, USA; alan.dardik@yale.edu

⁵ Department of Surgery, VA Connecticut Healthcare Systems, West Haven, CT 06516, USA

* Correspondence: sadaghianloo.n@chu-nice.fr

Received: 4 October 2019; Accepted: 25 October 2019; Published: 29 October 2019



Abstract: For patients with end-stage renal disease requiring hemodialysis, their vascular access is both their lifeline and their Achilles heel. Despite being recommended as primary vascular access, the arteriovenous fistula (AVF) shows sub-optimal results, with about 50% of patients needing a revision during the year following creation. After the AVF is created, the venous wall must adapt to new environment. While hemodynamic changes are responsible for the adaptation of the extracellular matrix and activation of the endothelium, surgical dissection and mobilization of the vein disrupt the *vasa vasorum*, causing wall ischemia and oxidative stress. As a consequence, migration and proliferation of vascular cells participate in venous wall thickening by a mechanism of neointimal hyperplasia (NH). When aggressive, NH causes stenosis and AVF dysfunction. In this review we show how hypoxia, metabolism, and flow parameters are intricate mechanisms responsible for the development of NH and stenosis during AVF maturation.

Keywords: arteriovenous fistula; hypoxia; hypoxia-inducible factor; metabolism; neointimal hyperplasia

1. End-Stage Renal Disease and Arteriovenous Fistulas

1.1. Chronic Kidney Disease

Chronic kidney disease (CKD) describes the gradual loss of kidney function. At the stage of kidney failure, also called end-stage renal disease (ESRD) renal function must be replaced by either a new functioning kidney or an artificial kidney in order to maintain life. The main etiology of CKD is related to the diabetes-metabolic syndrome-obesity bundle and hypertension. As the prevalence of these diseases is growing exponentially worldwide, so is CKD [1]. In 2016, 124,675 new cases of ESRD were reported in the USA, with a total of nearly 500,000 patients receiving dialysis treatment and over 200,000 patients living with a kidney transplant [2]. Hemodialysis is the most commonly utilized therapeutic approach for the treatment of ESRD in the majority of countries [3]. Current hemodialysis devices run at a flow of 300 to 400 mL/min, meaning that the blood flow should be at least 500 to 600 mL/min [4]. As a comparison, the standard blood flow rate in a forearm radial artery is less than 40 mL/min [5]. Several types of vascular access have been designed and used for that purpose.

1.2. Arteriovenous fistulas (AVFs)

Hemodialysis arteriovenous fistulas (AVFs) are direct communications between a vein and an artery of the patient (Figure 1), first described in 1966, by Brescia et al. [6]. Bringing the arterial flow to the vein induces a large increase in the venous flow. With progressive maturation, which usually takes around six weeks, the venous wall becomes thicker, the venous diameter larger (>5–6 mm), and the venous flow reaches 600 to 1200 mL/min [5].

AVFs are considered the optimal vascular access for hemodialysis because of their potential for durability, lower risk of infection, and reduced need for intervention to ensure patency compared to grafts or catheters; however, literature and registries reveal a high prevalence of failure of newly placed fistulas never becoming functional (early failure) [4,7]. Based on the United States Renal Data System (USRDS), among AVFs placed between June 2014 and May 2016, 39% failed to mature sufficiently for use in dialysis. Of those that matured and were finally used, the median time to the first use was 108 days [2]. Late failure worsens the outcome of these AVFs, with a recent systematic review and meta-analysis reporting that primary patency rates of AVFs were 60% at 1 year and 51% at 2 years, meaning almost half of the patients had at least one reintervention on their AVF to maintain patency [8]. Secondary patency rates of 71% at 1 year and 64% at 2 years, meaning 30–40% of all AVFs were abandoned after a short time [8]. These reinterventions add to the burden of hemodialysis patients, already tired by the disease, the 3-times a week visit to the dialysis facility, the dialysis sessions themselves, and all the burden of vascular access monitoring [9]. Vascular access care is also responsible for a significant proportion of health care costs, in particular in the first year of hemodialysis. In the USRDS report, the cost of hemodialysis treatment was evaluated in the US at \$90,971 per patient per year [2].

These data show that even the AVF, the best vascular access for hemodialysis, is clearly sub-optimal for a permanent treatment. The vascular access and dialysis community needs to better understand and correct the mechanisms leading to AVF failure.

2. Pathophysiology of AVFs

2.1. How AVFs Mature

During AVF creation, the surgeon directly connects the artery, a high-pressure pulsatile flow conduit, to a vein, which is ordinarily a low-pressure steady flow conduit (Figure 1). The pressure gradient results in an immediate increase in flow in both the artery and vein. The resulting hemodynamic change initiates a vascular remodeling response within both vessels. Pressure in the venous segment increases upon AVF creation and remains relatively constant during the time course of remodeling and thereafter. Outward remodeling is thought to be mediated by the venous endothelium and adventitia that sense these hemodynamic forces and integrates them to allow successful adaptation without loss of luminal area and vessel patency [10]. Venous diameter expansion is a critical element of outward remodeling and predicts the clinical success of AVF [11].

The venous wall is composed of three layers (Figure 2A) [12]. The external layer, called the adventitia, acts like a thin but resistant envelope to the vessel. It is composed of extracellular matrix (ECM), fibroblasts and immune cells. *Vasa vasorum*, small vessels, also run around the vein within the adventitia, to bring arterial blood flow to the venous wall [13]. The middle layer, called the media, is made of smooth muscle cells (SMC) and some extracellular fibers. The internal layer, also called intima, is composed of endothelial cells. During remodeling, hemodynamic changes and surgical injuries have an impact on all three layers of the venous wall. Endothelial and adventitial signaling induces, in turn, structural changes in the cells and the ECM, which affect the venous caliber and thickness (Figure 2B,C). Lack of outward remodeling and/or excess in wall thickening creates a disequilibrium that leads to AVF non-maturation and early failure (Figure 2D) [12].

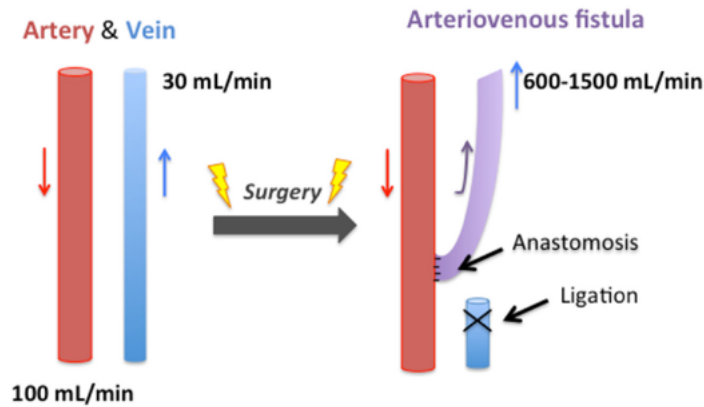
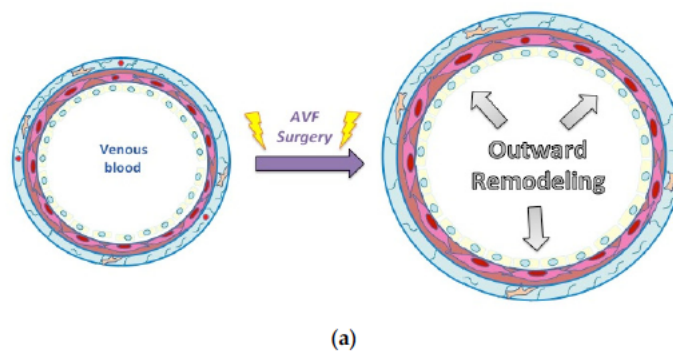


Figure 1. A fistula is direct communication between a vein and an artery, frequently on the upper limb of the patient. This communication is made by the surgeon with the help of a suture. The vein is dissected and ligated its extremity, and sewn to the artery. The arterial blood (red arrow) flows into the vein (blue arrow) through this anastomosis. The fistula matures, and the blood flow in the fistula (purple arrow) reaches around 1 L per minute.

2.2. Flow and Hemodynamic Parameters in AVF

The increased hemodynamics of arterial flow that increases vessel wall shear stress (WSS) are critical events after AVF creation that promotes AVF adaptation [14]. In a patient-specific end-to-side fistula, image-based computational fluid dynamics studies showed laminar flow within the arterial limb and a complex multi-directional and reciprocating flow field on the inner side of the swing segment in the proximal venous limb [15]. Wall thickening is predisposed to occur in the inner wall of the venous segment near the anastomosis and has a strong inverse correlation with magnitudes of shear stress, but is also related to flow patterns [16]. Although data is sparse in the venous vasculature and venous cells, studies on the arterial vasculature have shown that disturbed flow, with low and reciprocating WSS, is known to induce selective expression of atherogenic and thrombogenic genes that are pro-oxidant, proinflammatory, procoagulant, and proapoptotic in endothelial cells [17,18], and to stimulate vascular smooth muscle cell migration and proliferation, all of which may enhance wall thickening [19–21].



(a)
Figure 2. Cont.

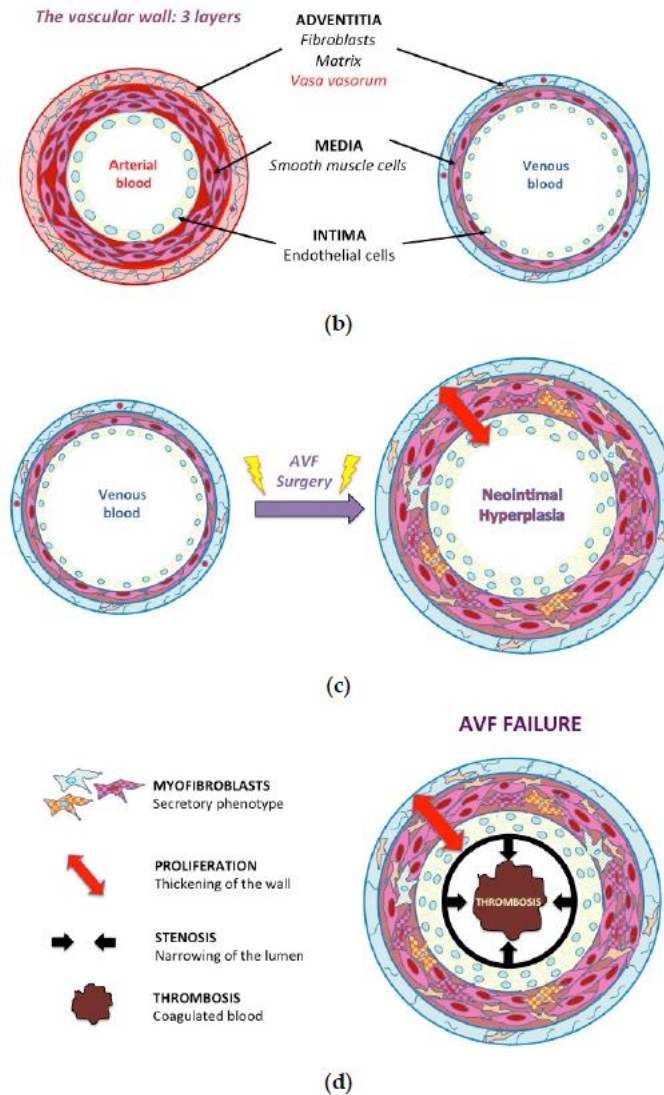


Figure 2. Mechanisms of venous wall remodeling. (a) Similar to the arterial wall, the venous wall is composed of three layers: the external layer, called the adventitia, composed of extracellular matrix (ECM), fibroblasts, immune cells, and *vasa vasorum*. The middle layer, called the media, is made of smooth muscle cells (SMC) and some extracellular fibers. The internal layer, also called intima, is composed of endothelial cells. (b) and (c), upon arteriovenous fistula (AVF) creation, in response to the altered hemodynamic environment, several structural changes occur in the vessel wall. Surgery induces endothelial denudation, matrix reorganization to accommodate outward expansion but also vascular SMC proliferation and migration, contributing to NH formation. (d) Aggressive intimal hyperplasia induces stenosis (narrowing) of the vessel that can provoke thrombosis (occlusion).

3. Neointimal Hyperplasia in AVF

3.1. Definitions

Wall thickening is the adaptation of the vessel wall to increased pressure and abnormal WSS. This process involves the expansion of all the vessel layers via ECM deposition, cell proliferation and migration [22]. The thickening of the venous wall composed of these matrix proteins and proliferative and secretive cells is called neointimal hyperplasia (NH). Excessive neointimal hyperplasia causes stenosis. As a consequence of stenosis, the blood flow may be diminished and the AVF becomes unusable for dialysis. In extreme cases, stenosis may cause thrombosis, a complete occlusion of the vessel because of non-circulating blood (Figure 2D). Several types of cells are involved in NH, including ECs, SMCs, and adventitial fibroblasts [23].

3.2. Role of Endothelial Cells

The release of chemotactic and inflammatory mediators from the endothelium during surgical manipulation and hemodynamic variation are substantial during the initial phase of adaptation [24]. Directly after AVF creation, high magnitudes of arterial flow result in both passive vascular distention and nitric oxide (NO) synthesis by endothelial cells with subsequent vascular SMC relaxation, resulting in acute vasodilation [25,26]. NO is produced by endothelial nitric oxide synthase (eNOS) and may contribute to adaptive vein wall remodeling through its anti-inflammatory, anti-thrombotic, and antiproliferative properties. Both eNOS and inducible nitric oxide synthase (iNOS) are upregulated in the AVF, and pharmacological inhibition of eNOS results in increased monocyte chemoattractant protein-1 and interleukin (IL) 8, leading to NH [27]. Endothelin-1 (ET-1) is an inflammatory mediator of vasoconstriction and endothelial proliferation. ET-1 expression is upregulated in the venous wall and within areas of NH in AVF as well as in the plasma of patients with chronic renal failure and hemodialysis. ET-1 may mediate wall thickening in response to localized hemodynamic forces [28,29]. Selectins facilitate leukocyte adhesion. P-selectin is present on ECs and platelets, and E-selectin is present on ECs. Intercellular adhesion molecule (ICAM) and vascular cell adhesion molecule (VCAM) facilitate additional binding and migration [30]. P-selectin and E-selectin expression are both upregulated early after AVF creation, followed by decreased P-selectin expression after 1 month [27]. VCAM-1, but not ICAM-1, is highly expressed in thrombosed and stenotic AVF [31].

3.3. Role of Smooth Muscle Cells

The canonical origin of proliferating cells in NH is the vessel media that contains SMC. Endothelial and smooth muscle cell injury, consequences of hemodynamic stress and mechanical injury, results in the migration of SMCs from the media into the intima, where the SMC proliferate and differentiate into a secretory phenotype (myofibroblasts). This process of injury, followed by migration, proliferation and differentiation, is orchestrated by a large number of mediators, such as cell cycle regulators (p27-p16 [32], p38 mitogen-activated protein kinase [33]) and growth factors (vascular endothelial growth factor (VEGF) [34], platelet derived growth factor (PDGF) [27], basic fibroblast growth factor (bFGF) [35,36], insulin-like growth factor-1 (IGF-1) [37], etc.). Expression of adhesion molecule β -catenin and proto-oncogene c-Myc is increased one week after AVF creation, correlating with decreased adhesion molecule N-cadherin, associated with vascular SMC proliferation [38]. Vascular SMC may also become resistant to NO, decreasing vascular SMC relaxation and preventing AVF maturation by reducing outward remodeling [39]. As shown recently, mature SMCs are keys to the equilibrium between medial wall thickening (proliferation of differentiated SMCs that promotes maturation) and neointimal hyperplasia (dedifferentiated SMCs that cause NH and failure) [40]. Interestingly, vascular SMCs from the proximal artery may also contribute to venous NH: in a murine AVF model, increased Notch signaling could drive migration of these cells to the venous outflow tract [41].

3.4. Role of Fibroblasts

More recent studies have shown that the adventitial fibroblasts are critical during venous adaptation to arterial flow and help maintain venous wall integrity and hemostasis after surgical creation of the AVF [23,42]. Fibroblast precursors residing in the venous adventitia sense the abrupt changes in mechanical forces produced by the arterial flow to rapidly adjust their genomic expression program to help increase vascular resistance [43]. They differentiate into myofibroblasts, form matrix bundles of contractile microfilaments and extensive cell-to-matrix attachment sites, and secrete matrix metalloproteinases (MMPs), collagen, and ECM proteins that strengthen the fistula wall. Recent data suggest that NH in AVFs consists mainly of smooth muscle α -actin-positive, vimentin-positive and desmin-negative myofibroblasts that have probably migrated from the adventitial layer [23,44]. Analysis of venous segments of failed AVF has shown increased adventitial fibrosis, myofibroblast activation, and capillary rarefaction [45].

3.5. Role of Inflammatory Cells

Inflammatory cells and cytokines, such as CD68-positive macrophages, CD3-positive lymphocytes, IL-6, IL-8, and monocyte chemo-attractant protein-1 are also known to be part of the NH process in AVFs [29,46–48]. This inflammatory state, exacerbated by CKD and dialysis, leads towards the up-regulation of numerous growth factors and cytokines, such as insulin-like growth factor-1, platelet-derived growth factor and basic fibroblast growth factor [27,37]. They all play a significant role in the stimulation of cell proliferation and migration. Even transforming growth factor- β 1, usually known for its anti-inflammatory properties, is produced by ECs, vascular SMCs and inflammatory cells within the venous wall, leading to ECM deposition. These cells also participate in NH in AVFs [36,37,49].

3.6. Role of Extracellular Matrix

The equilibrium between ECM degradation and accumulation is closely related to the maturation process of AVFs. In a murine AVF model, Hall et al. showed that initial ECM degradation occurs early after AVF creation, coincident with an early increase in expression of matrix metalloproteinases (MMP-2 and -9) and tissue inhibitor of metalloproteinase-1 (TIMP-1) [50]. Although the role of TIMP-1 is not clear, an imbalance in MMP and TIMP may contribute to AVF failure [51]. By day 7, there is an increase in collagen and elastin production and a change in patterns of MMP expression. By day 21, expression of MMPs is reduced and expression of larger structural and non-collagenous matrix proteins, such as fibronectin and perlecan, is increased. Other studies have shown that decreased expression of MMP-1, MMP-3, and MMP-9 is linked to increased AVF failure and stenosis [52]. Giachelli et al. have found that the expression of osteopontin (OPN) was up-regulated in the development of NH in a model of arterial balloon-injury. OPN was originally identified as matrix protein in bones, facilitating cell adhesion and migration, but this secreted protein has also been found in several experimental models of AVF maturation [50,53]. Its pro-inflammatory properties may favor vascular remodeling and development of NH [54].

3.7. Dissection Injury: Ischemia and Oxidative Stress

Hemodynamic changes and surgery-induced mechanical injury to the venous wall have been proposed as the etiology of juxta-anastomotic stenosis and maturation failure of AVF; however, a more recent theory proposes that hypoxia and oxidative stress may also play a role. Starting from the observation that during traditional AVF creation the vein is dissected free from the surrounding tissue, and that this same dissected segment is responsible for the majority of stenosis, researchers hypothesized that the rupture of the vasa vasorum during surgical dissection may induce hypoxia, low oxygen (O_2) concentration, in the venous wall [12,34] (Figure 3). Additionally, the O_2 partial pressure (pO_2) in the venous blood is approximately 35–45 mmHg. However, after AVF creation, pO_2 in the

fistula increases to the level of arterial pO_2 (73–100 mmHg). Thus it is possible that interruption of the arterial blood supply followed by the sudden increase in luminal pO_2 causes an ischemia-reperfusion phenomenon within the venous wall. Both of these phenomena provoke oxidative stress and stimulate numerous signaling pathways [36]. Interestingly, Joddar et al. have shown that arterial levels of oxygen stimulate NH in veins via a ROS-dependent mechanism [55]. In addition, two computational studies suggest that hypoxic segments of vessels may be linked to hemodynamic patterns and may correlate with stenosis [56,57]. Thus the two pathophysiological theories, flow and ischemia, may be related.

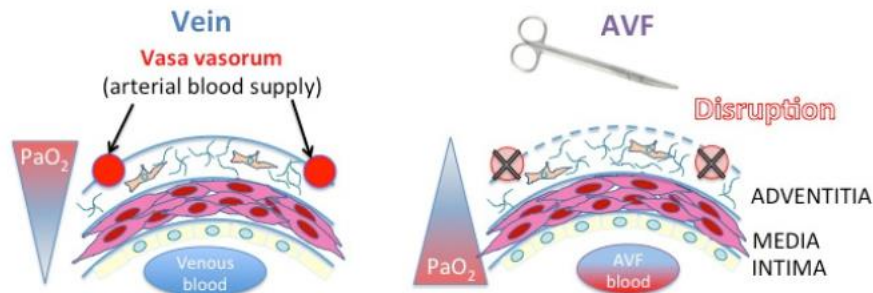


Figure 3. Changes in the venous wall after surgery: The *vasa vasorum* disruption creates a new oxygen gradient. The *vasa vasorum* in the adventitia provides oxygenated blood to the wall, whereas the intima is in contact with a venous blood low in oxygen. During surgery, the vein is dissected, disrupting the *vasa vasorum*, and potentially decreasing oxygen levels. On the other side, oxygenated arterial blood mixed to venous blood potentially creates an inversion of the oxygen gradient.

4. The Hypoxic Pathway in AVF

4.1. Hypoxia-Inducible Factors (HIFs), Keys to the Hypoxic Environment

Maintaining oxygen homeostasis is essential for the survival of all aerobic organisms. Therefore, a change in pO_2 is a major physiological stimulus that elicits rapid cellular responses. HIFs are key transcription factors that regulate the cellular response to hypoxic injury by stimulating the transcription of genes that help restore O_2 and maintain effective energy production [58]. HIFs belong to the large family of basic-helix-loop-helix transcription factors and bind DNA as a heterodimer composed of one oxygen-regulated α -subunit (isoforms HIF-1 α , HIF-2 α , or HIF-3 α) and two β stable subunits (HIF-1 β or aryl hydrocarbon receptor nuclear translocator (ARNT), and HIF-2 β or ARNT2) [59,60].

4.2. Oxygen-Dependent Regulation of HIFs

The discovery of molecular mechanisms behind oxygen-dependent regulation of HIFs was rewarded in 2019 by the Nobel Prize in Physiology or Medicine. In well-oxygenated cells, the HIF- α subunits are constantly and rapidly degraded by hydroxylation of proline residues within the oxygen-dependent degradation domain of HIF- α , with one of the shortest half-lives (less than 5 min) among cellular proteins (Figure 4A) [59,61,62]. Prolyl hydroxylation targets the HIF- α proteins for proteasomal degradation by promoting their interaction with the protein von Hippel-Lindau (pVHL) (Figure 4A) [59,61,63–65]. This post-translational modification of HIF- α is carried out by a family of prolyl hydroxylase enzymes, the prolyl hydroxylase domain proteins (PHD1, PHD2, PHD3) (Figure 4A) [61,62,66]. Since these enzymes bind oxygen directly, they are critical oxygen sensors within the hypoxic response pathway [67]. In hypoxia, these enzymes being inactivated, HIF- α proteins are not degraded and accumulate in cells (Figure 4B) [68]. An additional hydroxylation of an asparaginyl moiety at the end of the COOH-terminal transactivation domain of HIF-1 α or HIF-2 α subunit is catalyzed by an enzyme called factor-inhibiting HIF-1 (FIH-1) [69,70]. In normoxia, FIH-1 abrogates HIF transcriptional activity by inhibiting the binding of coactivators such as p300 and

C-AMP Response Element-binding protein [71–73]. Under hypoxia, PHD inactivation causes HIF- α accumulation, and FIH-1 inactivation allows HIF transcriptional activity. While the HIF- β /ARNT subunits are constitutively expressed in the nucleus, the HIF- α subunits found in the cytoplasm have sensitivity towards O₂. When the HIF- α subunit is stabilized and active, it leaves the cytoplasm to enter the nucleus, binds its β -subunit and cofactors, and induces the transcription of a large number of genes (1–2% of all human genes) (Figure 4B) [61]. All these genes have in common a hypoxia-responsive element (HRE: 5' -RCGTG-3') as an enhancer, either in their promoter, in the 3' untranslated region, or in introns [58–76]. These genes have key biological roles such as cell survival (*ADM* [77], *cyclin D1* [78], *BNIP3* [79], *NIX* [80]), cell proliferation (*cyclin G2* [81], *IGF2* [82], *TGF α* [83], *NOS2* [84]), cell motility (*AMF/GPI* [83], *LRP1* [81]), cytoskeletal structure and ECM (*vimentin* [83], some keratins [83]), erythropoiesis (*EPO*) [85], pH regulation (*carbonic anhydrase 9 and 12*) [86], nucleotide metabolism (*adenylate kinase 4*) [87], amino acid metabolism (*transglutaminase 2*) [81], iron metabolism (*transferrin* [88], *ceruleoplasmin* [89]), and glucose and energy metabolism (*HK2* [90], *GLUT1* [91], *GAPDH* [92], *LDHA* [93], *leptin* [94]).

A number of HIF-target genes also control angiogenesis: (VEGF [95], VEGF receptor (VEGFR)-1 and -2 [96]), vascular remodeling (angiopoietin-2 and -4, TIE1, TIE2) [97] and vascular tone (HO1 [98], NOS2 [84], ET1 [81]). As such, HIF pathways have been of great scientific interest for more than two decades, in particular in the fields of development [99,100], cancer [101,102] and cardiovascular diseases [103].

4.3. Oxygen-Independent Regulation of HIFs

HIF- α can also be stabilized in normoxic conditions as a consequence of cell injury and oxidative stress. Several O₂-independent mechanisms of HIF regulation have been identified such as receptor for activated C kinase 1 (RACK1) [104], carboxyl terminus of Hsc70-interaction protein (CHIP) and heat shock protein-70 (HSP70) [105], hypoxia-associated factor (HAF) [106], and Sirtuin-7 (SIRT7) [107]. They all mediate ubiquitination and proteasomal degradation. HIF-1 α responds also to non-hypoxic stimuli [68], including hormones like insulin [108,109], growth factors such as IGF-1 [110] or PDGF [111], vasoactive peptides such as nitric-oxide (NO) [112,113] or angiotensin 2 [111,114] and cytokines such as tumor necrosis factor- α (TNF- α) [115]. It is assumed that these O₂-independent stimuli contribute to an autocrine role in proliferation, survival or tissue repair, allowing early adaptation to variations in the cell environment.

Since many of these stimuli induce reactive oxygen species (ROS) production as part of their signaling cascade, it has been hypothesized that ROS participate directly in HIF stabilization [116]. Incubation of cells with H₂O₂ leads to the stabilization of HIF- α proteins and activation of HIF target genes even when O₂ levels are high [117,118]. Furthermore, exposing keratinocytes to ultra-violet B irradiation activates HIF-1 α through generation of mitochondrial ROS [119]. Using *junD*-deficient cells that exhibit chronic oxidative stress, Gerald et al. discovered ROS-dependent iron-mediated regulation of PHD enzymes [120]. Since enhanced H₂O₂ levels promote the oxidation of Fe(II) to Fe(III) through the Fenton reaction, it reduces the cellular pool of Fe(II) and increases even more drastically the proportion of active PHD. PHD and FIH-1 not only directly sense O₂ concentrations, as discussed above, but are also regulated by ROS (mostly H₂O₂) and metabolites through modulation of iron availability [120–122] and 2-OG accessibility [121], respectively. In addition to PHD inactivation, ROS has also been shown to act on HIF expression via activation of kinases [123]. ROS-induced HIF- α stabilization was reversed in various studies by iron supplementation, reducing agents or antioxidant compounds. Treating cells with anti-oxidant compounds, such as the free radical scavenger *N*-acetylcysteine [124–126], glutathione [126], or vitamins E and C [127,128], markedly attenuates HIF- α protein accumulation and expression of HIF target genes in various cell types, including hepatoma cells [124], vascular SMC [129], myocardial cells [127], gastric epithelial cells [125], renal tubuloepithelial cells [114], and macrophages [126]. Therefore, oxidative stress could trigger activation of HIF even in well-oxygenated conditions, thereby mimicking hypoxia signaling.

4.4. HIF-1 vs. HIF-2

The expression of HIF-2 α was first believed to be restricted to blood vessels and in particular to vascular endothelial cells [85,130,131]. Since then, the expression of HIF-2 α has been found in several tissues, including hypoxic kidney, lung, colonic epithelia, hepatocytes, macrophages, muscle cells and astrocytes [132]. Some early studies showed that besides common target genes, each HIF- α isoform seems to have unique targets [133,134], and this transcriptional specificity may reside in the NH₂-terminal transactivation domain, suggesting that HIF- α interactions with transcriptional co-factors are key to determine differential gene activation [135]. However, recent studies have shown that the mechanisms leading to selective gene transactivation are highly context specific. The individual HIFs have specific temporal and functional roles: HIF-1 drives the initial response to hypoxia (<24h) and HIF-2 drives the chronic response (>24 h) [136,137]. They can also exhibit antagonistic functions on the same final target. While HIF-1 α deletion in macrophages reduced the expression of iNOS and consequent production of NO [138], activation of HIF-2 α in the same cell type will reduce the pool of L-arginine (the source of NO) by inducing arginase 1 [139].

The selective expression of HIF-1 α vs. HIF-2 α is the result of a complex regulation process rather than the sole consequence of cell type or O₂-dependant stabilization of HIF- α subunits. HIF-1 α vs. HIF-2 α expression can be regulated selectively at the level of transcription, translation, or protein stability [133]. Lin et al. have shown that chromatin remodeling via differential acetylation of core histones in the promoter of HIF-1 α or -2 α may regulate their transcription [140]. Another well-known regulator of HIF-1 α gene transcription is nuclear factor-KB (NF-KB), but it has not been shown to control HIF-2 α [141]. As above, the phosphatidylinositol-3-kinases/protein kinase B/mechanistic target of rapamycin (PI3K/AKT/mTOR) pathway regulates HIF α gene translation. However, Toschi et al. have shown that, in the same renal clear cell carcinoma cell line, HIF-1 α expression was both mTOR complex 1 and 2 (mTORC1, mTORC2)-dependent, whereas HIF-2 α was only mTORC2 dependent [142]. As for the stability of HIF- α subunits, HAF binds and leads HIF-1 α towards proteasomal degradation under normoxic and hypoxic conditions in a pVHL-independent manner, but does not decrease HIF-2 α levels [106]. In contrast, HAF binds HIF2 α at a distinct C-terminal region and promotes HIF-2 α transcriptional activity: cells switch from a HIF-1 α to a HIF-2 α transcriptional program [59,137]. In addition, HSP70 and CHIP bind and degrade HIF-1 α (but not HIF-2 α) under conditions of prolonged hypoxia in cultured cells, whereas rapid reoxygenation destabilizes both HIF-1 α and HIF-2 α proteins via the PHD-pVHL-proteasome pathway (Figure 4) [59,105]. This is one mechanism by which HIF-2 is considered to be the effector of prolonged hypoxia, whereas HIF-1 drives the initial response to hypoxia [59]. Other mechanisms of HIF differential regulation include sirtuins (SIRT1–7), a family of redox-sensitive, NAD⁺-dependent deacetylases and/or adenosine diphosphate (ADP)-ribosyltransferases, which are known to regulate complex changes in gene expression, metabolism, and redox status in mammalian cells [143]. SIRT1 acts at a post-translational level: forming a complex with HIF-2 α , SIRT1 deacetylates lysine residues in the N-TAD, which enhances HIF-2 α transcriptional activity [59,144]. However, deacetylation of lysine residues in HIF-1 α results in the repression of the HIF-1 α transcriptional activity [145]; these opposing effects of SIRT1 may result in a switch towards either HIF-1 α or -2 α transcriptional programs in response to a metabolic switch in hypoxic tumors. The authors propose a mechanism of positive feedback in which under hypoxia HIF-1 α promotes glycolysis, reducing NAD⁺/NADH (nicotinamide adenine dinucleotide, oxidized and reduced forms, respectively) ratios and inhibiting SIRT1, thereby further increasing the HIF-1 α activity and presumably decreasing the HIF-2 α activity [145]. Given the disparate actions and differential regulation of HIF-1 and -2, targeting the hypoxic pathway needs to determine whether broad or selective inhibition is required, depending on the cell type and the expected effect.

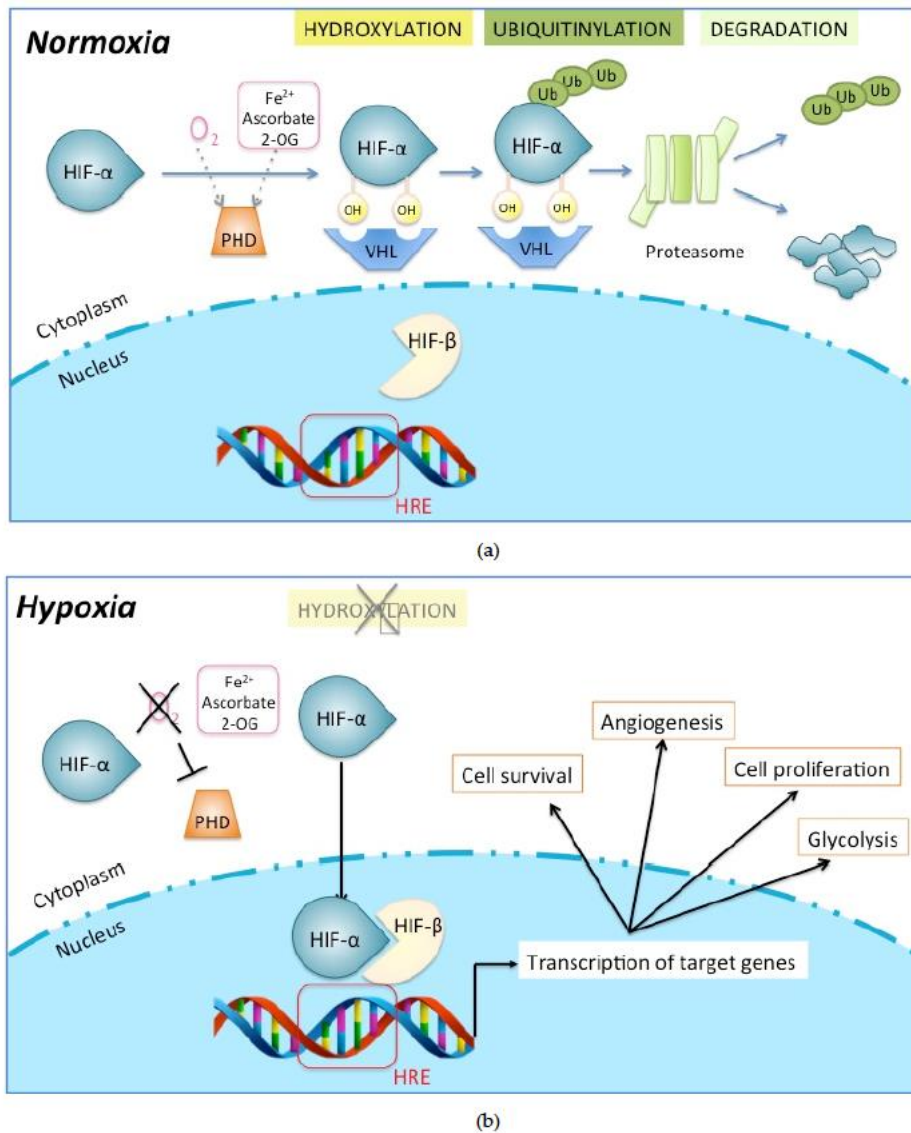


Figure 4. Molecular mechanisms of oxygen sensing and signaling. (a) In normoxia, hypoxia-inducible factor- α subunit (HIF- α) is hydroxylated through a combination of α -ketoglutarate, molecular oxygen (O_2), one or more of the prolyl hydroxylase (PHD) isoenzymes and the asparaginyl hydroxylase factor inhibiting HIF (grey dotted arrow). The von Hippel-Lindau protein (VHL)-containing E3 ubiquitin ligase targets the α -subunit for polyubiquitinylation and degradation in the proteasome. (b) In hypoxia, low oxygen (black cross line) causes inactivation of PHD (black T arrow). The α -subunit is no longer hydroxylated (grey cross line) and becomes stabilized. In the nucleus, HIF- α binds to the HIF- β subunit and with the help of cofactors, the complex becomes transcriptionally active upon binding to the hypoxia-responsive element (HRE, red box) consensus sequence on the promoter of target genes. HIF-target genes are numerous, with key roles in cell survival, angiogenesis, proliferation, and glycolysis.

5. HIF and Cell Metabolism

Metabolism comprises a series of interconnected pathways that can function in the presence or absence of O_2 . Two of them, glycolysis and oxidative phosphorylation (OXPHOS) are represented in Figure 5. During glycolytic metabolism 1 molecule of glucose is converted into 2 molecules of pyruvate and generates 2 molecules of ATP and NADH. Lactate dehydrogenase A (LDHA) further reduces pyruvate into lactate [146]. During OXPHOS, 1 molecule of glucose is converted into 2 molecules of pyruvate, which are transported into the mitochondria, converted to acetyl coenzyme A and oxidized to CO_2 in the Krebs cycle. The NADH and $FADH_2$ generated in this process provide electrons to the electron transport chain in the inner mitochondrial membrane (respiratory cytochromes) [147]. Electrons are added to O_2 at complex IV (cytochrome c oxidase or COX), finally generating 38 molecules of ATP per molecule of glucose (Figure 5).

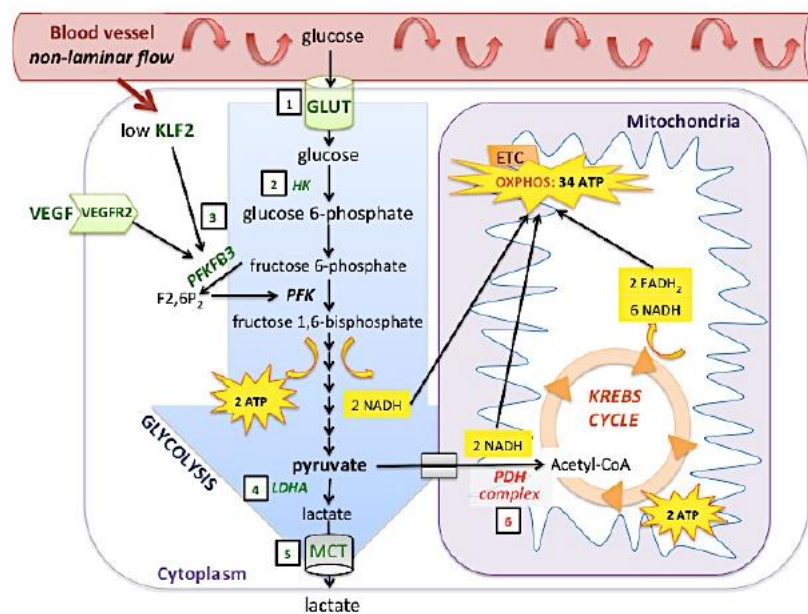


Figure 5. Glucose metabolism is regulated by hypoxia-inducible factors (HIFs). During glycolysis, glucose enters the cytoplasm through the glucose transporter (GLUT) and is transformed into glucose 6-phosphate by hexokinase (HK). Eight successive enzymatic reactions then occur to produce 2 molecules of pyruvate, 2 ATP and 2 NADH. At the end, cytosolic pyruvate has two possibilities: transformation into lactate by the enzyme lactate dehydrogenase A (LDHA)—lactate being then exported through the monocarboxylate transporter (MCT), or transferred into the mitochondria and transformed into Acetyl-CoA via the pyruvate dehydrogenase complex (PDH complex). In the second option, Acetyl-coA goes into the Krebs cycle to produce 2 ATP, 6 NADH, and 2 $FADH_2$. NADH and $FADH_2$ will further be used in redox reactions in the electron transport chain (ETC) to produce more ATP via oxidative phosphorylation (OXPHOS). HIF intervenes in several steps during glucose metabolism: by inducing GLUT it allows more entry of glucose (1) and by inducing hexokinase (2) and PFKFB3 (3), it enhances glycolysis. Note that non-laminar blood flow decreases the expression of Kruppel-like factor 2 (KLF2), which has otherwise an inhibitory action on HIF-1 and PFKFB3 expression. VEGF and its receptor VEGFR2 are also induced by HIF-1 and enhance PFKFB3 expression. Further, pyruvate is pushed towards lactate transformation by up-regulation of LDHA (4) and some isoforms of MCT (5). At the same time, HIF prevents the PDH complex from transforming pyruvate into Acetyl-coA (6). Green: activation by HIF, Red: inhibition by HIF.

5.1. Metabolic Adaptation to Hypoxia

Metabolic adaptation to hypoxia involves mainly a switch from oxidative (aerobic) to glycolytic (anaerobic) metabolism by cells. With this energy compensation, the cell continues to generate ATP and, despite the hypoxia, try to meet the metabolic demands and maintain the expenditure of energy of normoxic conditions. During hypoxia, HIF-1 stimulates glycolysis through the up-regulation of key glycolytic genes, including *GLUT1*, *GLUT3*, *HK1*, *HK2*, and *LDHA* [148]. HIFs also reduce mitochondrial O₂ consumption by attenuating glucose oxidation: they up-regulate the expression of pyruvate dehydrogenase kinase, which inhibits the activity of the pyruvate dehydrogenase complex (PDH complex), a key enzyme regulating the entry of pyruvate into the Krebs cycle through conversion to acetyl CoA [149,150]. Finally, the subunit composition of COX is altered in hypoxic cells by increased expression of the COX4-2 subunit, which optimizes the COX activity under hypoxic conditions, and increases degradation of the COX4-1 subunit by the LON protease, which optimizes the COX activity under aerobic conditions [146].

5.2. Metabolism of Endothelial Cells

The metabolism of ECs has been largely studied in the domain of cancer and atherosclerosis but is also of great interest in the problematic AVF. All ECs (arterial, venous, microvascular) are preferentially glycolytic, rather than OXPHOS since 85% of their ATP is produced by converting glucose into lactate [151,152]. One hypothesis is that downregulation of OXPHOS metabolism protects them from excessive ROS and oxidative stress [152]. At the same time, they save O₂ to enhance the diffusion of oxygen to perivascular cells [152]. In addition, glycolysis produces less ATP but with faster kinetics, which is necessary for the rapid revascularization of hypoxic tissues when needed [153]. A hypoxic environment stimulates EC proliferation, and hypoxic proliferation of ECs increases glycolysis because of HIF-1 upregulation (both hypoxia- and growth factor- induced) [151].

5.3. Shear Stress, Hypoxia, and Metabolism in Endothelial Cells

Interestingly, hemodynamics and shear stress also play a role in EC metabolism. Laminar shear stress induces Kruppel-like factor-2 (KLF2) in ECs [154], whereas non-laminar (disturbed or turbulent) flow inhibits KLF2 (Figure 5). KLF2 is a zinc-finger transcription factor that maintains anti-proliferative and anti-inflammatory phenotypes of quiescent ECs. By inactivating p65 (subunit of NF- κ B), KLF2 down-regulates cell adhesion (E-selectin) and prothrombotic molecules (thrombomodulin), inhibits VEGFR2, and up-regulates eNOS [155–159]. Doddaballapur et al. showed that laminar shear-stress induced KLF2 reduces glucose uptake and represses the key glycolytic enzyme 6-phosphofructo-2-kinase/fructose-2,6-bisphosphatase 3 (PFKFB3) [160]. This enzyme produces fructose-2,6-bisphosphate (F2,6P2), a strong allosteric activator of phosphofructokinase-1 (PFK1), a rate-limiting enzyme of glycolysis (Figure 5) [161]. Thereby, glycolytic metabolism is limited and blood flow keeps ECs in a resting state [162]. Kawanami et al. showed that KLF2 expression is also induced in hypoxic ECs, and over-expression of KLF2 inhibits HIF-1 α (but not HIF-2 α) stabilization and downstream expression of ANG2, IL-8 and VEGF [163]. Conversely, inhibition of KLF2 increases HIF-1 α and its target-gene expression [163]. As such, KLF2 links hemodynamics, hypoxia and metabolism in ECs.

6. HIF and Vascular Diseases

In vascular pathology, hypoxia is typically the consequence of altered, destroyed or absent blood vessels leading to tissue ischemia. The mechanisms of the HIF response have therefore been studied in ischemic vascular diseases, such as myocardial infarction (consequence of obstruction of coronary arteries) or peripheral vascular disease (PAD, consequence of obstruction of arteries going to the limbs) [164,165].

Besides tissue ischemia, mechanisms of hypoxia and ischemia can occur within the vascular wall itself, with implications for diseases such as atherosclerosis [166], arterial aneurysm [167], chronic venous insufficiency [168] and thromboembolism [169,170]. There is growing evidence that the HIF pathway is implicated—for better or for worse—in the response of the vascular wall to inadequate oxygenation and/or increased cellular oxygen, a demand secondary to various stresses or injuries [171,172].

6.1. HIF and Atherosclerosis

Atherosclerosis is a condition in which fatty deposits (plaques) develop in the arterial wall, leading to stenosis and ultimately to thrombosis of the vessel [173]. Atherosclerotic plaques are mainly composed of cholesterol, other lipids, calcium, fibrin and inflammatory cells [174]. Oxygen diffusion through space-occupying atherosclerotic plaques could be limited due to wall thickening. Hypoxia could also originate from the high oxygen demand of metabolically active inflammatory cells, such as macrophage foam cells that play a pivotal role in this disease [175]. Detection of HIF-1 α and activation of its target genes occurs in atherosclerotic plaques [166,176]. During atherogenesis (plaque build-up), hypoxia increases angiogenesis [166], releases pro-inflammatory mediators [177], activates MMPs [178], forms reactive oxygen species [179], and oxidizes low-density lipoprotein [180,181]. Necrotic cores within atherosclerotic plaques can lead to plaque instability and thromboembolic complications. The HIF-1 α protein is found in tissue surrounding atherosclerotic arteries, inflammatory macrophages [166] and arterial SMCs around these necrotic cores [182,183]. Proangiogenic HIF-target genes, such as VEGF-A, are responsible for intra-plaque neoangiogenesis, contributing to plaque instability [184]. HIF-1 activity also alters the lipid metabolism of macrophages and vascular SMC [172,176,185]. Finally, besides hypoxia, several non-hypoxic stimuli of HIF have also been found in plaques and plaque macrophages, such as inflammation, ROS, vasoactive and thrombotic factors [129,186,187].

6.2. HIF and NH in Vascular Grafts

The role of the HIF pathway in the development of NH has also been studied. When atherosclerotic lesions occupy a long segment of the artery, surgeons frequently use a graft to bypass the lesion and provide blood to distal tissues. Either venous or prosthetic, these grafts are prone to NH. Although vein grafts and prosthetic grafts are not identical, because of different hemodynamics and oxygen tension, the characteristics of NH in vein grafts are similar to those of NH that form in AVFs [188]. In studies with animal models, grafts showed increased hypoxia within the vessel wall in regions of neointimal hyperplasia [189,190]. A study using a porcine model showed an association of HIF-1 α expression with the degree of neointimal hyperplasia in grafts, and suggested that reducing hypoxia might inhibit venous NH formation, possibly by reducing the phenotypic switch of fibroblasts to myofibroblasts [191]. Paradoxically, increased activation of the HIF pathway may also protect against NH formation. Nakao et al. studied the role of carbon monoxide, a physiologically important vasodilator that acts via cyclic guanosine monophosphate, in the formation of NH [192]. They showed that a vein graft placed immediately after harvest led to less NH than if the graft was rinsed with lactated Ringer for 2 h prior to surgical placement. However, if the lactated Ringer solution was saturated with carbon monoxide, it significantly inhibited NH compared to the untreated control. The effects of carbon monoxide in inhibiting NH formation seemed to be associated with increased HIF-1 α and VEGF expression a few hours after grafting. This effect, including the induction of VEGF, was reversed by treatment with YC-1, a HIF-1 α inhibitor, supporting the conclusion that these effects were mediated through the activation of the HIF pathway. These apparently contradictory studies suggest that, at least in the setting of vein graft NH, transient activation of the HIF pathway may protect the wall from hypoxia, whereas chronic activation may maintain the ongoing NH process. Carbon monoxide may also display vasoconstrictor effects depending on oxygen and metabolic homeostasis, including ROS production, highlighting the important role of metabolism in the vascular wall [193].

6.3. HIF and NH in Vascular Access

Both prosthetic arteriovenous graft and AVF failure may be associated with increased activation of the HIF pathway. Misra et al. investigated HIF-1 α and several target genes in stenotic segments from prosthetic grafts compared with AVFs [194]. The authors compared the expression of HIF-1 α , several MMPs and TIMPs, and macrophage migration inhibitory factor (MIF), a proinflammatory factor that regulates proliferation and migration of vascular SMC, which is affected by HIF-1 α in human vascular SMCs exposed to hypoxia [195]. Specimens from patients with prosthetic grafts expressed significantly more HIF-1 α , MIF, TIMP-1, pro-MMP-2, and pro-MMP-9 compared with control veins. Pro-MMP-9 was also up-regulated in AVFs compared with control samples. The expression of MIF and TIMP-1 was significantly increased in prosthetic graft specimens compared with AVFs. Expression of HIF-1 α in AVFs seemed to be higher than in controls although the differences reported in this study were not statistically significant. The authors concluded that there were major differences in the expression HIF-1 α , and proteins regulated by HIF-1 in specimens removed from patients with prosthetic grafts and AVFs. They consequently developed porcine and mouse models of vascular access failure and found that HIF-1 α and HIF-1-associated protein expression were increased in failed conduits compared with controls [196–198].

6.4. HIF Target Genes in Vascular Access

We previously studied oxidative stress and HIF-1 expression in a murine model of AVF maturation. Our team used a microarray analysis to show downregulation of 27 of the 83 genes involved in the OXPHOS pathway, downregulation of 12 of the 18 genes involved in mitochondrial long-chain fatty acid beta-oxidation, and 10 of the 13 genes involved in mitochondrial unsaturated fatty acid beta-oxidation, suggesting the presence of oxidative stress during early AVF maturation [199], and which was consistent with previous research [36]. We then showed increased excreted hydrogen peroxide, nitrotyrosine staining, and NOX-2 (nicotinamide adenine dinucleotide phosphate oxidase - 2) staining in the venous limb of the AVF during early maturation compared to control veins, confirming the presence of oxidative stress during AVF maturation. We also showed up-regulation of HIF-1 α mRNA and protein expression in AVFs. Immunofluorescence of the AVF showed increased immunoreactivity of HIF-1-associated heme oxygenase-1 (HO-1) and VEGF-A, at both days 3 and 7 compared with control veins [199].

Interestingly, recent research has shown that expression of the HIF-1-target *HO1* is related to AVF function [200–203]. HO-1 is a cytoprotective and rate-limiting enzyme responsible for heme degradation, generating free iron, biliverdin, and carbon monoxide. Biliverdin is subsequently converted to bilirubin by biliverdin reductase, and free iron is rapidly sequestered by ferritin [204]. Bilirubin is a free radical scavenger that blocks lipid peroxidation [205]. HO has antioxidant, anti-inflammatory, anti-apoptotic, and angiogenic functions through its reactive products [98,204]. HO-1 is an inducible isoform, whereas HO-2 is expressed constitutively. Patients with *HO-1* gene polymorphisms characterized by long GT repeats, resulting in less HO-1 production, were more likely to have worse AVF patency [200,201]. In a murine model of AVF, Junco et al. showed that *HO-1* gene expression was markedly induced in the vascular SMCs. *HO-1* knockout mice had reduced patency and increased expression of pro-inflammatory and pro-oxidant mediators, such as MCP-1, MMP-2, and MMP-9 [206]. Subsequently, Kang et al., using the same model, showed that the adventitial delivery of an adeno-associated viral gene *HO-1* improved AVF blood flow and decreased venous wall thickness [203]. A functional AVF also requires HO-2 [202]. Shear stress also regulates HO-1 activity, with high flow inducing HO-1 to generate NO and mitochondria-derived hydrogen peroxide. Low flow induces lower levels of HO-1 that lead to macrophage infiltration and superoxide production within the vessel wall. However, the authors did not report whether these results were HIF-dependent. While they suggest an important role for HO in promoting outward remodeling and in preventing NH [207], we may think that HIF expression in this setting would be beneficial.

VEGF-A is necessary at low concentrations to promote endothelial cell health, NO and prostacyclin production, vasodilation, antithrombosis, and suppression of SMC proliferation but promotes angiogenesis and vasculogenesis at high concentrations [13]. Increased VEGF expression has been associated with early AVF thrombosis in human patients [208], and the VEGF-936C/C gene polymorphism has been associated with a 5.54-fold increase in risk of late AVF thrombosis [209]. Adventitial delivery of a lentivirus inhibiting VEGF-A expression decreases cell proliferation, inhibits NH and increases patency in a mouse model of AVF [34]. Systemic VEGF receptor gene transfer in rats decreases carotid artery restenosis, suggesting the utility of targeting this pathway to inhibit NH [210].

7. HIFs as Therapeutic Targets

Several experimental studies have shown that inhibiting the HIF-1 target gene VEGF decreases NH [34]. Further studies are needed to understand if the HIF pathway should be inhibited or activated in this setting. These studies can evaluate the broad range of therapeutic agents tested in other fields, in particular in cancer, since pharmacological targeting of HIF has been a major field of research these past two decades [101,211].

7.1. O₂ Treatment

In a study using a rabbit iliac AVF model, Lata et al. demonstrated that NH is inhibited by the administration of 30% supplemental oxygen [212]. Based on the pattern of SMC proliferation, they suggested that 21 days of oxygen supplementation would be enough to control the initial burst of proliferation and subsequent NH. Further experiments by the same team demonstrated that HIF-1 α was stabilized, VEGFR-2 up-regulated, and plasma VEGF-A was increased in rabbits with AVFs placed in normoxia [213]. In addition, these markers were significantly decreased when rabbits with AVFs were placed in 30% oxygen chambers for 21 days after surgery. Plasma collected in the hyperoxic group induced significantly less SMC and EC proliferation *in vitro* [213]. These results support the role of hypoxia and HIF-1 stabilization in NH. However, translation of this treatment to humans would mean wearing a nasal cannula all day. It is likely that it would be very difficult to convince patients who already carry a heavy medical burden to use supplemental oxygen therapy. Paradoxically, several studies conducted in different non-vascular experimental settings and cell types have shown that absolute hyperoxia induces HIF stabilization and activation of HIF targets [214–218]. The putative mechanisms may involve oxidative stress and ROS production, consequences of disturbed mitochondrial metabolism. In the AVF, both hypoxia (induced by the rupture of the vasa vasorum) and relative hyperoxia (induced by an increase in blood PaO₂) may cause HIF stabilization, with a balance between the two mechanisms over the maturation period potentially leading towards NH and AVF dysfunction. Future studies may use ROS scavengers and/or regulate other metabolic targets to discriminate between the two mechanisms.

7.2. Pharmacological Treatment

Many existing drugs or drugs used in clinical trials can specifically, but mostly non-specifically, target HIF at different points of its regulation [219,220].

7.2.1. HIF Inhibition

According to their putative mechanism of action, HIF inhibitors can be divided into agents that modulate (Figure 6):

- HIF transcriptional activity, such as the FDA-approved chemotherapeutic drug PD-341 (Bortezomib, impairs binding of p300 to HIF1- α by enhancing the binding of HIF-1 to HIF1- α) [221],
- HIF- α mRNA expression, such as the experimental compounds EZN-2968 (antisense oligonucleotide) [222] and aminoflavone (ligand of aryl hydrocarbon receptor) [223],

- HIF- α protein translation, such as FDA-approved chemotherapeutic drug topotecan (camptothecin analog, inhibitor of topoisomerase I) [211,224], experimental compound EZN-2208 (derived from irinotecan, another camptothecin analog) [225], FDA-approved cardiac glycoside digoxin [226], and FDA-approved chemotherapeutic drugs temsirolimus and everolimus (mTOR inhibitors) [227–229],
- HIF- α protein degradation, such as Hsp90 inhibitors [230,231] or histone deacetylase (HDAC) inhibitors [232],
- HIF DNA binding, such as echinomycin (a cyclic peptide of the family of quinoxaline antibiotics) [233] and anthracyclines (such as the FDA-approved chemotherapeutic drug doxorubicin) [234].

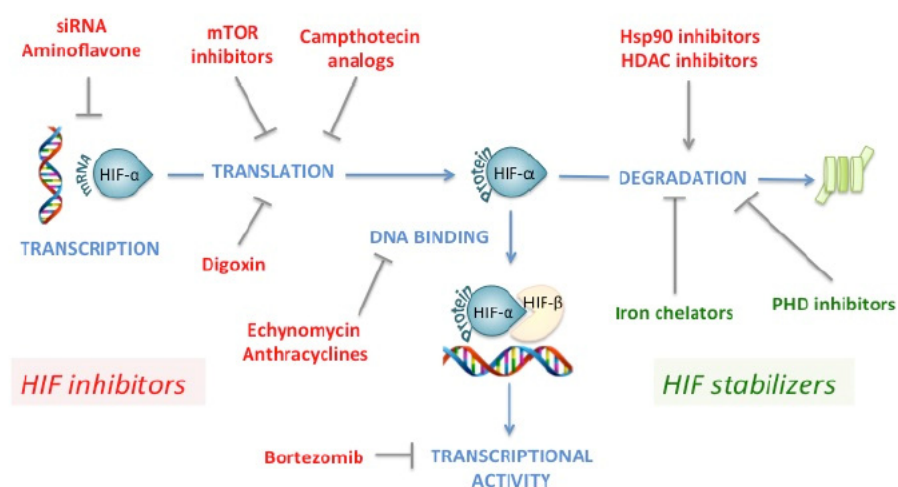


Figure 6. Pharmacological treatments targeting the HIF pathway. Green: stabilization of HIF- α , red: destabilization of HIF- α . Blue arrows: physiological process, grey arrows: activation, grey T arrows: inhibition.

7.2.2. HIF Activation

One of the easiest ways to stabilize HIF- α is to act on the repressing enzymes PHDs and FIH-1. These enzymes being dependent on Fe(II) and 2-OG, iron chelators such as desferioxamine [34] and 2-OG analogs such as dimethylxallylglycine (DMOG) [63] have been used in many experimental studies to stabilize HIF-1 α . Importantly, these therapeutics are not isoform specific as the compounds inhibit all PHDs and therefore, all HIF- α . In the setting of atherosclerosis and treatment of PAD, experimental studies evaluated intramuscular injection of AdCA5 and intravenous administration of bone marrow-derived angiogenic cells that were cultured in the presence of the PHD inhibitor DMOG. The combined therapy increased perfusion, motor function and limb salvage in aged mice subjected to femoral artery ligation [165,235]. Based on these promising findings, a Phase I dose-escalation human clinical trial was performed using an adenoviral delivery system to deliver the active form of HIF1- α into the lower extremity of patients with critical limb ischemia. In addition, the therapy was well tolerated [236]. However, in a trial evaluating the efficacy of intramuscular administration of three different doses of Ad2/HIF1A/VP16 on walking time in patients with PAD and intermittent claudication, there was no significant clinical improvement when comparing the placebo and each HIF1- α dosage group [237]. This led to the conclusion that gene therapy with intramuscular administration of Ad2/HIF1A/VP16 was not an effective treatment for patients with intermittent claudication [237]. Although the reasons underlying failure remain unclear, concerns include the efficacy of gene transfer, including whether the gene transfer was increasing HIF to sufficient levels in the critical tissue

compartment. For the treatment of CKD-induced anemia, promising compounds targeting PHD (Roxadustat, Vadadustat, Daprodustat, Molidustat) have been tested in patients with significant improvement of their hemoglobin level (mainly as a consequence of HIF-1-induced expression of EPO) [238–240]. These inhibitors are likely to become an important tool for the management of anemia in patients with CKD, where the oral route is a significant advantage. However, long-term safety of HIF activation must be determined, in particular with regards to HIF pathway tumorigenicity. Further studies are ongoing [238].

8. Conclusions

Increasing evidence shows that in AVFs, NH induced by upstream hemodynamic changes is linked to downstream metabolic disruption, involving the regulation of the response to hypoxia. Unfortunately, the common denominator of most HIF inhibitors and activators described so far is the lack of specificity, which indicates that they inhibit multiple targets and that HIF inhibition cannot be easily separated from other activities exerted by these agents [241]. Moreover, the majority of drugs primarily target HIF-1, although they may also act on HIF-2. One of the challenges of pharmacologically targeting the HIF pathway is to identify which isoforms are responsible for the disease and to find an isoform-specific drug. One of the most striking advances in the field is the successful targeting of HIF-2 in renal cell carcinoma, using a small molecule called PT2399, specifically designed to inhibit the binding of HIF-2 α to the HIF- β subunit [242–245].

Besides finding HIF specific, isoform specific molecules, one major challenge will be to target delivery of these drugs to specific organs, to limit off-target and secondary effects.

Author Contributions: N.S., J.C., A.D., and N.M.M. conceptualized, wrote, and reviewed the article.

Funding: N.S.: J.C. and N.M.M. were supported by grants from the Fondation Flavien, the Fondation ARC, La Ligue contre le Cancer, Fondation de France, and the Société Française de Chirurgie Vasculaire et Endovasculaire. A.D. was supported by NIH grants R01HL128406 and R01HL144476.

Conflicts of Interest: The authors declare no conflict of interest.

Abbreviations

ADM	Adrenomedullin
ADP	Adenosine DiPhosphate
AKT	Protein kinase B
AMF/GPI	Autocrine Motility Factor/Glucose-6-Phosphate Isomerase
AMP	Adenosine MonoPhosphate
ANG	ANGiopoietin
ARNT	Aryl hydrocarbon Receptor Nuclear Translocator
ATP	Adenosine TriPhosphate
AVF	ArterioVenous Fistula
bFGF	basic Fibroblast Growth Factor
BNIP3	BCL2/adenovirus E1B 19 kDa protein-Interacting Protein 3
CHIP	Carboxyl terminus of Hsp70-interacting protein
CKD	Chronic Kidney Disease
COX	Cytochrome C Oxidase
CREB	C-AMP Response Element-binding protein
DMOG	DiMethylOxalylGlycine
DNA	Deoxyribonucleic acid
EC	Endothelial Cells
ECM	Extra-Cellular Matrix
eNOS	endothelial Nitric Oxide Synthase
EPO	ErythroPOeitin
ESRD	End-Stage Renal Disease

ET-1	Endothelin-1
FAD	Flavin Adenine Dinucleotide
FDA	Food & Drug Administration
FIH	Factor Inhibiting HIF
GLUT	GLUCose Transporter
HAF	Hypoxia-Associated Factor
HDAC	Histone DeACetylase
HIF	Hypoxia-Inducible Factor
HK	HexoKinase
HO-1	Heme Oxygenase-1
HRE	Hypoxia-Responsive Element
Hsp	Heat-shock protein
ICAM	InterCellular Adhesion Molecule
IGF	Insulin-like Growth Factor
IL	InterLeukine
iNOS	inducible Nitric Oxide Synthase
KLF2	Kruppel-Like Factor 2
LDHA	Lactate DeHydrogenase A
LRP1	Low density lipoprotein recpetor-related protein 1
MCT	MonoCarboxylate Transporter
MMP	Matrix MetalloProteinase
mRNA	messenger RiboNucleic Acid
mTOR	mechanistic Target Of Rapamycin
mTORC	mTOR Complex
NAD	Nicotinamide Adenine Dinucleotide
NADH	Reduced form of NAD
NF-KB	Nuclear Factor-KB
NH	Neointimal Hyperplasia
NO	Nitric Oxide
NOX	Nicotinamide adenine dinucleotide phosphate oxidase
OPN	Osteopontin
PAD	Peripheral Arterial Disease
PDGF	Platelet Derived Growth Factor
PDH	Pyruvate DeHydrogenase
PFK	PhospoFructoKinase
PFKFB3	6-PhosphoFructo-2-Kinase/Fructose-2,6-Bisphosphatase 3
PHD	Prolyl Hydroxylase Domain
PI3K	Phosphatidylinositol-3-kinases
RACK	Receptor for Activated Protein Kinase C
ROS	Reactive Oxygen Species
SIRT	Sirtuin
SMC	Smooth Muscle Cells
TGF	Transforming-Growth Factor
TIE	Tyrosine kinase with Immunoglobulin-like and EGF-like domains
TIMP	Tissue Inhibitor of MetalloProteinase
TNF	Tumor Necrosis Factor
USRDS	United States Renal Data System
VCAM	Vascular Cell Adhesion Molecule
VEGF	Vascular Endothelial Growth Factor
VHL	von Hippel-Lindau
WSS	Wall Shear Stress

References

- Jha, V.; Garcia-Garcia, G.; Iseki, K.; Li, Z.; Naicker, S.; Plattner, B.; Saran, R.; Wang, A.Y.; Yang, C.W. Chronic kidney disease: Global dimension and perspectives. *Lancet* **2013**, *382*, 260–272. [CrossRef]
- United States Renal Data System. *2018 USRDS Annual Data Report: Epidemiology of Kidney Disease in the United States*; National Institutes of Health, National Institute of Diabetes and Digestive and Kidney Diseases: Bethesda, MD, USA, 2018; Available online: <https://www.usrds.org/adr.aspx> (accessed on 3 October 2019).
- Czyzewski, L.; Sanko-Resmer, J.; Wyzgal, J.; Kurowski, A. Assessment of health-related quality of life of patients after kidney transplantation in comparison with hemodialysis and peritoneal dialysis. *Am. Transpl.* **2014**, *19*, 576–585.
- Vascular Access Work, G. Clinical practice guidelines for vascular access. *Am. J. Kidney Dis.* **2006**, *48* (Suppl. 1), S176–S247.
- Konner, K.; Nonnast-Daniel, B.; Ritz, E. The arteriovenous fistula. *J. Am. Soc. Nephrol.* **2003**, *14*, 1669–1680. [CrossRef]
- Brescia, M.J.; Cimino, J.E.; Appel, K.; Hurwicz, B.J. Chronic hemodialysis using venipuncture and a surgically created arteriovenous fistula. *N. Engl. J. Med.* **1966**, *275*, 1089–1092. [CrossRef]
- Dember, L.M.; Beck, G.J.; Allon, M.; Delmez, J.A.; Dixon, B.S.; Greenberg, A.; Himmelfarb, J.; Vazquez, M.A.; Gassman, J.J.; Greene, T.; et al. Effect of clopidogrel on early failure of arteriovenous fistulas for hemodialysis: A randomized controlled trial. *JAMA* **2008**, *299*, 2164–2171. [CrossRef]
- Al-Jaishi, A.A.; Oliver, M.J.; Thomas, S.M.; Lok, C.E.; Zhang, J.C.; Garg, A.X.; Kosa, S.D.; Quinn, R.R.; Moist, L.M. Patency rates of the arteriovenous fistula for hemodialysis: A systematic review and meta-analysis. *Am. J. Kidney Dis.* **2014**, *63*, 464–478. [CrossRef]
- Hedin, U. Vascular access: A never-ending story. *J. Cardiovasc. Surg. (Torino)* **2014**, *55*, 793–801.
- Roy-Chaudhury, P.; Spergel, L.M.; Besarab, A.; Asif, A.; Ravani, P. Biology of arteriovenous fistula failure. *J. Nephrol.* **2007**, *20*, 150–163.
- Feldman, H.L.; Joffe, M.; Rosas, S.E.; Burns, J.E.; Knauss, J.; Brayman, K. Predictors of successful arteriovenous fistula maturation. *Am. J. Kidney Dis.* **2003**, *42*, 1000–1012. [CrossRef]
- Rothuizen, T.C.; Wong, C.; Quax, P.H.A.; van Zonneveld, A.J.; Rabelink, T.J.; Rotmans, J.I. Arteriovenous access failure: More than just intimal hyperplasia? *Nephrol. Dial. Transplant.* **2013**, *28*, 1085–1092. [CrossRef] [PubMed]
- Hu, H.; Patel, S.; Hanisch, J.J.; Santana, J.M.; Hashimoto, T.; Bai, H.; Kudze, T.; Foster, T.R.; Guo, J.; Yatsula, B.; et al. Future research directions to improve fistula maturation and reduce access failure. *Semin. Vasc. Surg.* **2016**, *29*, 153–171. [CrossRef] [PubMed]
- Remuzzi, A.; Ene-Iordache, B. Novel paradigms for dialysis vascular access: Upstream hemodynamics and vascular remodeling in dialysis access stenosis. *Clin. J. Am. Soc. Nephrol.* **2013**, *8*, 2186–2193. [CrossRef] [PubMed]
- Browne, L.D.; Bashar, K.; Griffin, P.; Kavanagh, E.G.; Walsh, S.R.; Walsh, M.T. The Role of shear stress in arteriovenous fistula maturation and failure: A systematic review. *PLoS ONE* **2015**, *10*, e0145795. [CrossRef]
- Jia, L.; Wang, L.; Wei, F.; Yu, H.; Dong, H.; Wang, B.; Lu, Z.; Sun, G.; Chen, H.; Meng, J.; et al. Effects of wall shear stress in venous neointimal hyperplasia of arteriovenous fistulae. *Nephrology (Carlton)* **2015**, *20*, 335–342. [CrossRef]
- Chiu, J.-J.; Chien, S. Effects of disturbed flow on vascular endothelium: Pathophysiological basis and clinical perspectives. *Physiol. Rev.* **2011**, *91*, 327–387. [CrossRef]
- Dai, G.; Kaazempur-Mofrad, M.R.; Natarajan, S.; Zhang, Y.; Vaughn, S.; Blackman, B.R.; Kamm, R.D.; Garcia-Cardena, G.; Gimbrone, M.A., Jr. Distinct endothelial phenotypes evoked by arterial waveforms derived from atherosclerosis-susceptible and -resistant regions of human vasculature. *Proc. Natl. Acad. Sci. USA* **2004**, *101*, 14871–14876. [CrossRef]
- Fan, L.; Karino, T. Effect of a disturbed flow on proliferation of the cells of a hybrid vascular graft. *Biorheology* **2010**, *47*, 31–38.
- Fan, L.; Sakai, J.; Bessho, S.; Wada, S.; Karino, T. Effect of a disturbed flow on adhesion of monocytes to a model of an arterial wall. *Biorheology* **2010**, *47*, 15–29.

21. Ene-Iordache, B.; Cattaneo, L.; Dubini, G.; Remuzzi, A. Effect of anastomosis angle on the localization of disturbed flow in side-to-end fistulae for haemodialysis access. *Nephrol. Dial. Transplant.* **2013**, *28*, 997–1005. [[CrossRef](#)]
22. Muto, A.; Model, L.; Ziegler, K.; Eghbalieh, S.D.; Dardik, A. Mechanisms of vein graft adaptation to the arterial circulation: Insights into the neointimal algorithm and management strategies. *Circ. J.* **2010**, *74*, 1501–1512. [[CrossRef](#)] [[PubMed](#)]
23. Roy-Chaudhury, P.; Wang, Y.; Krishnamoorthy, M.; Zhang, J.; Banerjee, R.; Munda, R.; Heffelfinger, S.; Arend, L. Cellular phenotypes in human stenotic lesions from haemodialysis vascular access. *Nephrol. Dial. Transplant.* **2009**, *24*, 2786–2791. [[CrossRef](#)] [[PubMed](#)]
24. Tseng, C.N.; Karlof, E.; Chang, Y.T.; Lengquist, M.; Rotzius, P.; Berggren, P.O.; Hedin, U.; Eriksson, E.E. Contribution of endothelial injury and inflammation in early phase to vein graft failure: The causal factors impact on the development of intimal hyperplasia in murine models. *PLoS ONE* **2014**, *9*, e98904. [[CrossRef](#)] [[PubMed](#)]
25. Kang, H.Y.; Fan, Y.B.; Deng, X.Y. Vascular smooth muscle cell glycocalyx modulates shear-induced proliferation, migration, and NO production responses. *Am. J. Physiol. Heart C* **2011**, *300*, H76–H83. [[CrossRef](#)]
26. Pike, D.; Shiu, Y.T.; Cho, Y.F.; Le, H.; Somarathna, M.; Isayeva, T.; Guo, L.; Symons, J.D.; Kevil, C.G.; Totenhagen, J.; et al. The effect of endothelial nitric oxide synthase on the hemodynamics and wall mechanics in murine arteriovenous fistulas. *Sci. Rep.* **2019**, *9*, 4299. [[CrossRef](#)]
27. Croatt, A.J.; Grande, J.P.; Hernandez, M.C.; Ackerman, A.W.; Katusic, Z.S.; Nath, K.A. Characterization of a model of an arteriovenous fistula in the rat: The effect of L-NAME. *Am. J. Pathol.* **2010**, *176*, 2530–2541. [[CrossRef](#)]
28. Jones, G.T.; van Rij, A.M.; Packer, S.G.; Walker, R.J.; Stehbens, W.E. Venous endothelial changes in therapeutic arteriovenous fistulae. *Atherosclerosis* **1998**, *137*, 149–156. [[CrossRef](#)]
29. Nath, K.A.; Kanakiriya, S.K.; Grande, J.P.; Croatt, A.J.; Katusic, Z.S. Increased venous proinflammatory gene expression and intimal hyperplasia in an aorto-caval fistula model in the rat. *Am. J. Pathol.* **2003**, *162*, 2079–2090. [[CrossRef](#)]
30. Schepers, A.; Eefting, D.; Bonta, P.I.; Grimbergen, J.M.; de Vries, M.R.; van Weel, V.; de Vries, C.J.; Egashira, K.; van Bockel, J.H.; Quax, P.H. Anti-MCP-1 gene therapy inhibits vascular smooth muscle cells proliferation and attenuates vein graft thickening both in vitro and in vivo. *Arterioscler. Thromb. Vasc. Biol.* **2006**, *26*, 2063–2069. [[CrossRef](#)]
31. Chang, C.J.; Ko, Y.S.; Ko, P.J.; Hsu, L.A.; Chen, C.F.; Yang, C.W.; Hsu, T.S.; Pang, J.H. Thrombosed arteriovenous fistula for hemodialysis access is characterized by a marked inflammatory activity. *Kidney Int.* **2005**, *68*, 1312–1319. [[CrossRef](#)]
32. Tsui, L.V.; Camrud, A.; Mondesire, J.; Carlson, P.; Zayek, N.; Camrud, L.; Donahue, B.; Bauer, S.; Lin, A.; Frey, D.; et al. p27-p16 fusion gene inhibits angioplasty-induced neointimal hyperplasia and coronary artery occlusion. *Circ. Res.* **2001**, *89*, 323–328. [[CrossRef](#)] [[PubMed](#)]
33. Ohashi, N.; Matsumori, A.; Furukawa, Y.; Ono, K.; Okada, M.; Iwasaki, A.; Miyamoto, T.; Nakano, A.; Sasayama, S. Role of p38 mitogen-activated protein kinase in neointimal hyperplasia after vascular injury. *Arterioscler. Thromb. Vasc. Biol.* **2000**, *20*, 2521–2526. [[CrossRef](#)] [[PubMed](#)]
34. Yang, B.; Janardhanan, R.; Vohra, P.; Greene, E.L.; Bhattacharya, S.; Withers, S.; Roy, B.; Nieves Torres, E.C.; Mandrekar, J.; Leof, E.B.; et al. Adventitial transduction of lentivirus-shRNA-VEGF-A in arteriovenous fistula reduces venous stenosis formation. *Kidney Int.* **2014**, *85*, 289–306. [[CrossRef](#)] [[PubMed](#)]
35. Lindner, V.; Reidy, M.A. Proliferation of smooth muscle cells after vascular injury is inhibited by an antibody against basic fibroblast growth factor. *Proc. Natl. Acad. Sci. USA* **1991**, *88*, 3739–3743. [[CrossRef](#)]
36. Weiss, M.F.; Scivittaro, V.; Anderson, J.M. Oxidative stress and increased expression of growth factors in lesions of failed hemodialysis access. *Am. J. Kidney Dis.* **2001**, *37*, 970–980. [[CrossRef](#)]
37. Stracke, S.; Konner, K.; Kostlin, I.; Friedl, R.; Jehle, P.M.; Hombach, V.; Keller, F.; Waltenberger, J. Increased expression of TGF-beta1 and IGF-I in inflammatory stenotic lesions of hemodialysis fistulas. *Kidney Int.* **2002**, *61*, 1011–1019. [[CrossRef](#)]
38. Nath, K.A.; Grande, J.P.; Kang, L.; Juncos, J.P.; Ackerman, A.W.; Croatt, A.J.; Katusic, Z.S. ss-Catenin is markedly induced in a murine model of an arteriovenous fistula: The effect of metalloproteinase inhibition. *Am. J. Physiol. Renal Physiol.* **2010**, *299*, F1270–F1277. [[CrossRef](#)]

39. Geenen, I.L.; Kolk, F.F.; Molin, D.G.; Wagenaar, A.; Compeer, M.G.; Tordoir, J.H.; Schurink, G.W.; De Mey, J.G.; Post, M.J. Nitric oxide resistance reduces arteriovenous fistula maturation in chronic kidney disease in rats. *PLoS ONE* **2016**, *11*, e0146212. [[CrossRef](#)]
40. Zhao, J.; Jourdain, F.L.; Xue, M.; Conti, D.; Lopez-Soler, R.I.; Ginnan, R.; Asif, A.; Singer, H.A.; Jourdain, D.; Long, X. Dual function for mature vascular smooth muscle cells during arteriovenous fistula remodeling. *J. Am. Heart Assoc.* **2017**, *6*, e004891. [[CrossRef](#)]
41. Liang, M.; Wang, Y.; Liang, A.; Mitch, W.E.; Roy-Chaudhury, P.; Han, G.; Cheng, J. Migration of smooth muscle cells from the arterial anastomosis of arteriovenous fistulas requires Notch activation to form neointima. *Kidney Int.* **2015**, *88*, 490–502. [[CrossRef](#)]
42. Duque, J.C.; Vazquez-Padron, R.I. Myofibroblasts: The ideal target to prevent arteriovenous fistula failure? *Kidney Int.* **2014**, *85*, 234–236. [[CrossRef](#)] [[PubMed](#)]
43. Coen, M.; Gabbiani, G.; Bochaton-Piallat, M.L. Myofibroblast-mediated adventitial remodeling: An underestimated player in arterial pathology. *Arterioscler. Thromb. Vasc. Biol.* **2011**, *31*, 2391–2396. [[CrossRef](#)] [[PubMed](#)]
44. Wang, Y.; Krishnamoorthy, M.; Banerjee, R.; Zhang, J.; Rudich, S.; Holland, C.; Arend, L.; Roy-Chaudhury, P. Venous stenosis in a pig arteriovenous fistula model—anatomy, mechanisms and cellular phenotypes. *Nephrol. Dial. Transplant.* **2008**, *23*, 525–533. [[CrossRef](#)] [[PubMed](#)]
45. Simone, S.; Loverre, A.; Cariello, M.; Divella, C.; Castellano, G.; Gesualdo, L.; Pertosa, G.; Grandaliano, G. Arteriovenous fistula stenosis in hemodialysis patients is characterized by an increased adventitial fibrosis. *J. Nephrol.* **2014**, *27*, 555–562. [[CrossRef](#)] [[PubMed](#)]
46. Liang, A.; Wang, Y.; Han, G.; Truong, L.; Cheng, J. Chronic kidney disease accelerates endothelial barrier dysfunction in a mouse model of an arteriovenous fistula. *Am. J. Physiol. Renal Physiol.* **2013**, *304*, F1413–F1420. [[CrossRef](#)]
47. Wasse, H.; Huang, R.; Naqvi, N.; Smith, E.; Wang, D.; Husain, A. Inflammation, oxidation and venous neointimal hyperplasia precede vascular injury from AVF creation in CKD patients. *J. Vasc. Access.* **2012**, *13*, 168–174. [[CrossRef](#)]
48. Juncos, J.P.; Grande, J.P.; Kang, L.; Ackerman, A.W.; Croatt, A.J.; Katusic, Z.S.; Nath, K.A. MCP-1 Contributes to arteriovenous fistula failure. *J. Am. Soc. Nephrol.* **2011**, *22*, 43–48. [[CrossRef](#)]
49. Ikegaya, N.; Yamamoto, T.; Takeshita, A.; Watanabe, T.; Yonemura, K.; Miyaji, T.; Ohishi, K.; Furuhashi, M.; Maruyama, Y.; Hishida, A. Elevated erythropoietin receptor and transforming growth factor-beta1 expression in stenotic arteriovenous fistulae used for hemodialysis. *J. Am. Soc. Nephrol.* **2000**, *11*, 928–935.
50. Hall, M.R.; Yamamoto, K.; Protack, C.D.; Tsuneki, M.; Kuwahara, G.; Assi, R.; Brownson, K.E.; Bai, H.; Madri, J.A.; Dardik, A. Temporal regulation of venous extracellular matrix components during arteriovenous fistula maturation. *J. Vasc. Access.* **2015**, *16*, 93–106. [[CrossRef](#)]
51. Lee, E.S.; Shen, Q.; Pitts, R.L.; Guo, M.; Wu, M.H.; Sun, S.C.; Yuan, S.Y. Serum metalloproteinases MMP-2, MMP-9, and metalloproteinase tissue inhibitors in patients are associated with arteriovenous fistula maturation. *J. Vasc. Surg.* **2011**, *54*, 454–459. [[CrossRef](#)]
52. Lin, C.C.; Yang, W.C.; Chung, M.Y.; Lee, P.C. Functional polymorphisms in matrix metalloproteinases-1, -3, -9 are associated with arteriovenous fistula patency in hemodialysis patients. *Clin. J. Am. Soc. Nephrol.* **2010**, *5*, 1805–1814. [[CrossRef](#)] [[PubMed](#)]
53. Kokubo, T.; Ishikawa, N.; Uchida, H.; Chasnoff, S.E.; Xie, X.; Mathew, S.; Hruska, K.A.; Choi, E.T. CKD Accelerates development of neointimal hyperplasia in arteriovenous fistulas. *J. Am. Soc. Nephrol.* **2009**, *20*, 1236–1245. [[CrossRef](#)] [[PubMed](#)]
54. Scatena, M.; Liaw, L.; Giachelli, C.M. Osteopontin: A multifunctional molecule regulating chronic inflammation and vascular disease. *Arterioscler. Thromb. Vasc. Biol.* **2007**, *27*, 2302–2309. [[CrossRef](#)] [[PubMed](#)]
55. Joddar, B.; Firstenberg, M.S.; Reen, R.K.; Varadharaj, S.; Khan, M.; Childers, R.C.; Zweier, J.L.; Gooch, K.J. Arterial levels of oxygen stimulate intimal hyperplasia in human saphenous veins via a ROS-dependent mechanism. *PLoS ONE* **2015**, *10*, e0120301. [[CrossRef](#)] [[PubMed](#)]
56. Sun, N.; Wood, N.B.; Hughes, A.D.; Thom, S.A.; Xu, X.Y. Fluid-wall modelling of mass transfer in an axisymmetric stenosis: Effects of shear-dependent transport properties. *Ann. Biomed. Eng.* **2006**, *34*, 1119–1128. [[CrossRef](#)] [[PubMed](#)]

57. Iori, F.; Grechy, L.; Corbett, R.W.; Gedroyc, W.; Duncan, N.; Caro, C.G.; Vincent, P.E. The effect of in-plane arterial curvature on blood flow and oxygen transport in arterio-venous fistulae. *Phys. Fluids (1994)* **2015**, *27*, 031903. [[CrossRef](#)] [[PubMed](#)]
58. Semenza, G.L. Hypoxia-inducible factor 1 (HIF-1) pathway. *Sci. STKE* **2007**, *2007*, cm8. [[CrossRef](#)]
59. Koh, M.Y.; Powis, G. Passing the baton: The HIF switch. *Trends Biochem. Sci.* **2012**, *37*, 364–372. [[CrossRef](#)]
60. Wenger, R.H. Cellular adaptation to hypoxia: O₂-sensing protein hydroxylases, hypoxia-inducible transcription factors, and O₂-regulated gene expression. *FASEB J.* **2002**, *16*, 1151–1162. [[CrossRef](#)]
61. Eltzschig, H.K.; Bratton, D.L.; Colgan, S.P. Targeting hypoxia signalling for the treatment of ischaemic and inflammatory diseases. *Nat. Rev. Drug Discov.* **2014**, *13*, 852–869. [[CrossRef](#)]
62. Epstein, A.C.; Gleadle, J.M.; McNeill, L.A.; Hewitson, K.S.; O'Rourke, J.; Mole, D.R.; Mukherji, M.; Metzen, E.; Wilson, M.I.; Dhanda, A.; et al. Elegans EGL-9 and mammalian homologs define a family of dioxygenases that regulate HIF by prolyl hydroxylation. *Cell* **2001**, *107*, 43–54. [[CrossRef](#)]
63. Jaakkola, P.; Mole, D.R.; Tian, Y.M.; Wilson, M.I.; Gielbert, J.; Gaskell, S.J.; von Kriegsheim, A.; Hebestreit, H.E.; Mukherji, M.; Schofield, C.J.; et al. Targeting of HIF- α to the von Hippel-Lindau ubiquitylation complex by O₂-regulated prolyl hydroxylation. *Science* **2001**, *292*, 468–472. [[CrossRef](#)] [[PubMed](#)]
64. Lisztwan, J.; Imbert, G.; Wirbelauer, C.; Gstaiger, M.; Krek, W. The von Hippel-Lindau tumor suppressor protein is a component of an E3 ubiquitin-protein ligase activity. *Genes Dev.* **1999**, *13*, 1822–1833. [[CrossRef](#)] [[PubMed](#)]
65. Ivan, M.; Kondo, K.; Yang, H.; Kim, W.; Valiando, J.; Ohh, M.; Salic, A.; Asara, J.M.; Lane, W.S.; Kaelin, W.G., Jr. HIF α targeted for VHL-mediated destruction by proline hydroxylation: Implications for O₂ sensing. *Science* **2001**, *292*, 464–468. [[CrossRef](#)] [[PubMed](#)]
66. Bruick, R.K.; McKnight, S.L. A conserved family of prolyl-4-hydroxylases that modify HIF. *Science* **2001**, *294*, 1337–1340. [[CrossRef](#)] [[PubMed](#)]
67. Mazure, N.M.; Brahimi-Horn, M.C.; Berta, M.A.; Benizri, E.; Bilton, R.L.; Dayan, F.; Ginouves, A.; Berra, E.; Pouyssegur, J. HIF-1: Master and commander of the hypoxic world. A pharmacological approach to its regulation by siRNAs. *Biochem. Pharmacol.* **2004**, *68*, 971–980. [[CrossRef](#)] [[PubMed](#)]
68. Brahimi-Horn, M.C.; Pouyssegur, J. HIF at a glance. *J. Cell Sci.* **2009**, *122*, 1055–1057. [[CrossRef](#)]
69. Lando, D.; Peet, D.J.; Gorman, J.J.; Whelan, D.A.; Whitelaw, M.L.; Bruick, R.K. FIH-1 is an asparaginyl hydroxylase enzyme that regulates the transcriptional activity of hypoxia-inducible factor. *Genes Dev.* **2002**, *16*, 1466–1471. [[CrossRef](#)]
70. Mahon, P.C.; Hirota, K.; Semenza, G.L. FIH-1: A novel protein that interacts with HIF-1 α and VHL to mediate repression of HIF-1 transcriptional activity. *Genes Dev.* **2001**, *15*, 2675–2686. [[CrossRef](#)]
71. Lando, D.; Peet, D.J.; Whelan, D.A.; Gorman, J.J.; Whitelaw, M.L. Asparagine hydroxylation of the HIF transactivation domain a hypoxic switch. *Science* **2002**, *295*, 858–861. [[CrossRef](#)]
72. Dayan, F.; Roux, D.; Brahimi-Horn, M.C.; Pouyssegur, J.; Mazure, N.M. The oxygen sensor factor-inhibiting hypoxia-inducible factor-1 controls expression of distinct genes through the bifunctional transcriptional character of hypoxia-inducible factor-1 α . *Cancer Res.* **2006**, *66*, 3688–3698. [[CrossRef](#)] [[PubMed](#)]
73. Kung, A.L.; Wang, S.; Klco, J.M.; Kaelin, W.G.; Livingston, D.M. Suppression of tumor growth through disruption of hypoxia-inducible transcription. *Nat. Med.* **2000**, *6*, 1335–1340. [[CrossRef](#)]
74. Tazuke, S.I.; Mazure, N.M.; Sugawara, J.; Carland, G.; Faessen, G.H.; Suen, L.F.; Irwin, J.C.; Powell, D.R.; Giaccia, A.J.; Giudice, L.C. Hypoxia stimulates insulin-like growth factor binding protein 1 (IGFBP-1) gene expression in HepG2 cells: A possible model for IGFBP-1 expression in fetal hypoxia. *Proc. Natl. Acad. Sci. USA* **1998**, *95*, 10188–10193. [[CrossRef](#)] [[PubMed](#)]
75. Pugh, C.W.; Tan, C.C.; Jones, R.W.; Ratcliffe, P.J. Functional analysis of an oxygen-regulated transcriptional enhancer lying 3' to the mouse erythropoietin gene. *Proc. Natl. Acad. Sci. USA* **1991**, *88*, 10553–10557. [[CrossRef](#)] [[PubMed](#)]
76. Wang, G.L.; Semenza, G.L. Purification and characterization of hypoxia-inducible factor 1. *J. Biol. Chem.* **1995**, *270*, 1230–1237. [[CrossRef](#)]
77. Frede, S.; Freitag, P.; Otto, T.; Heilmaier, C.; Fandrey, J. The proinflammatory cytokine interleukin 1 β and hypoxia cooperatively induce the expression of adrenomedullin in ovarian carcinoma cells through hypoxia inducible factor 1 activation. *Cancer Res.* **2005**, *65*, 4690–4697. [[CrossRef](#)]

78. Zatyka, M.; da Silva, N.F.; Clifford, S.C.; Morris, M.R.; Wiesener, M.S.; Eckardt, K.U.; Houlston, R.S.; Richards, F.M.; Latif, F.; Maher, E.R. Identification of cyclin D1 and other novel targets for the von Hippel-Lindau tumor suppressor gene by expression array analysis and investigation of cyclin D1 genotype as a modifier in von Hippel-Lindau disease. *Cancer Res.* **2002**, *62*, 3803–3811.
79. Mazure, N.M.; Pouyssegur, J. Atypical BH3-domains of BNIP3 and BNIP3L lead to autophagy in hypoxia. *Autophagy* **2009**, *5*, 868–869. [[CrossRef](#)]
80. Sowter, H.M.; Ratcliffe, P.J.; Watson, P.; Greenberg, A.H.; Harris, A.L. HIF-1-dependent regulation of hypoxic induction of the cell death factors BNIP3 and NIX in human tumors. *Cancer Res.* **2001**, *61*, 6669–6673.
81. Wykoff, C.C.; Pugh, C.W.; Maxwell, P.H.; Harris, A.L.; Ratcliffe, P.J. Identification of novel hypoxia dependent and independent target genes of the von Hippel-Lindau (VHL) tumour suppressor by mRNA differential expression profiling. *Oncogene* **2000**, *19*, 6297–6305. [[CrossRef](#)]
82. Feldser, D.; Agani, F.; Iyer, N.V.; Pak, B.; Ferreira, G.; Semenza, G.L. Reciprocal positive regulation of hypoxia-inducible factor 1alpha and insulin-like growth factor 2. *Cancer Res.* **1999**, *59*, 3915–3918. [[PubMed](#)]
83. Krishnamachary, B.; Berg-Dixon, S.; Kelly, B.; Agani, F.; Feldser, D.; Ferreira, G.; Iyer, N.; LaRusch, J.; Pak, B.; Taghavi, P.; et al. Regulation of colon carcinoma cell invasion by hypoxia-inducible factor 1. *Cancer Res.* **2003**, *63*, 1138–1143. [[PubMed](#)]
84. Jung, F.; Palmer, L.A.; Zhou, N.; Johns, R.A. Hypoxic regulation of inducible nitric oxide synthase via hypoxia inducible factor-1 in cardiac myocytes. *Circ. Res.* **2000**, *86*, 319–325. [[CrossRef](#)] [[PubMed](#)]
85. Wang, G.L.; Semenza, G.L. General involvement of hypoxia-inducible factor 1 in transcriptional response to hypoxia. *Proc. Natl. Acad. Sci. USA* **1993**, *90*, 4304–4308. [[CrossRef](#)]
86. Wykoff, C.C.; Beasley, N.J.; Watson, P.H.; Turner, K.J.; Pastorek, J.; Sibtain, A.; Wilson, G.D.; Turley, H.; Talks, K.L.; Maxwell, P.H.; et al. Hypoxia-inducible expression of tumor-associated carbonic anhydrases. *Cancer Res.* **2000**, *60*, 7075–7083.
87. Greijer, A.E.; van der Groep, P.; Kemming, D.; Shvarts, A.; Semenza, G.L.; Meijer, G.A.; van de Wiel, M.A.; Belien, J.A.; Van Diest, P.J.; van der Wall, E. Up-regulation of gene expression by hypoxia is mediated predominantly by hypoxia-inducible factor 1 (HIF-1). *J. Pathol.* **2005**, *206*, 291–304. [[CrossRef](#)]
88. Rolfs, A.; Kvietikova, I.; Gassmann, M.; Wenger, R.H. Oxygen-regulated transferrin expression is mediated by hypoxia-inducible factor-1. *J. Biol. Chem.* **1997**, *272*, 20055–20062. [[CrossRef](#)]
89. Mukhopadhyay, C.K.; Mazumder, B.; Fox, P.L. Role of hypoxia-inducible factor-1 in transcriptional activation of ceruloplasmin by iron deficiency. *J. Biol. Chem.* **2000**, *275*, 21048–21054. [[CrossRef](#)]
90. Menendez, M.T.; Teygong, C.; Wade, K.; Florimond, C.; Blader, I.J. siRNA Screening Identifies the Host Hexokinase 2 (HK2) Gene as an Important Hypoxia-Inducible Transcription Factor 1 (HIF-1) Target Gene in *Toxoplasma gondii*-Infected Cells. *mBio* **2015**, *6*, e00462. [[CrossRef](#)]
91. Ebert, B.L.; Firth, J.D.; Ratcliffe, P.J. Hypoxia and mitochondrial inhibitors regulate expression of glucose transporter-1 via distinct Cis-acting sequences. *J. Biol. Chem.* **1995**, *270*, 29083–29089. [[CrossRef](#)]
92. Graven, K.K.; Bellur, D.; Klahn, B.D.; Lowrey, S.L.; Amberger, E. HIF-2alpha regulates glyceraldehyde-3-phosphate dehydrogenase expression in endothelial cells. *Biochim. Biophys. Acta* **2003**, *1626*, 10–18. [[CrossRef](#)]
93. Firth, J.D.; Ebert, B.L.; Pugh, C.W.; Ratcliffe, P.J. Oxygen-regulated control elements in the phosphoglycerate kinase 1 and lactate dehydrogenase A genes: Similarities with the erythropoietin 3' enhancer. *Proc. Natl. Acad. Sci. USA* **1994**, *91*, 6496–6500. [[CrossRef](#)] [[PubMed](#)]
94. Grosfeld, A.; Andre, J.; Hauguel-De Mouzon, S.; Berra, E.; Pouyssegur, J.; Guerre-Millo, M. Hypoxia-inducible factor 1 transactivates the human leptin gene promoter. *J. Biol. Chem.* **2002**, *277*, 42953–42957. [[CrossRef](#)] [[PubMed](#)]
95. Tsuzuki, Y.; Fukumura, D.; Oosthuysen, B.; Koike, C.; Carmeliet, P.; Jain, R.K. Vascular endothelial growth factor (VEGF) modulation by targeting hypoxia-inducible factor-1alpha-> hypoxia response element-> VEGF cascade differentially regulates vascular response and growth rate in tumors. *Cancer Res.* **2000**, *60*, 6248–6252.
96. Das, B.; Yeager, H.; Tsuchida, R.; Torkin, R.; Gee, M.F.; Thorner, P.S.; Shibuya, M.; Malkin, D.; Baruchel, S. A hypoxia-driven vascular endothelial growth factor/Flt1 autocrine loop interacts with hypoxia-inducible factor-1alpha through mitogen-activated protein kinase/extracellular signal-regulated kinase 1/2 pathway in neuroblastoma. *Cancer Res.* **2005**, *65*, 7267–7275. [[CrossRef](#)]

97. Yamakawa, M.; Liu, L.X.; Date, T.; Belanger, A.J.; Vincent, K.A.; Akita, G.Y.; Kuriyama, T.; Cheng, S.H.; Gregory, R.J.; Jiang, C. Hypoxia-inducible factor-1 mediates activation of cultured vascular endothelial cells by inducing multiple angiogenic factors. *Circ. Res.* **2003**, *93*, 664–673. [[CrossRef](#)]
98. Kim, Y.M.; Pae, H.O.; Park, J.E.; Lee, Y.C.; Woo, J.M.; Kim, N.H.; Choi, Y.K.; Lee, B.S.; Kim, S.R.; Chung, H.T. Heme oxygenase in the regulation of vascular biology: From molecular mechanisms to therapeutic opportunities. *Antioxid. Redox Signal.* **2011**, *14*, 137–167. [[CrossRef](#)]
99. Shimoda, L.A.; Semenza, G.L. HIF and the lung: Role of hypoxia-inducible factors in pulmonary development and disease. *Am. J. Respir. Crit. Care Med.* **2011**, *183*, 152–156. [[CrossRef](#)]
100. Semenza, G.L.; Agani, F.; Iyer, N.; Kotch, L.; Laughner, E.; Leung, S.; Yu, A. Regulation of cardiovascular development and physiology by hypoxia-inducible factor 1. *Ann. NY Acad. Sci.* **1999**, *874*, 262–268. [[CrossRef](#)]
101. Semenza, G.L. Targeting HIF-1 for cancer therapy. *Nat. Rev. Cancer* **2003**, *3*, 721–732. [[CrossRef](#)]
102. Schito, L.; Semenza, G.L. Hypoxia-Inducible Factors: Master Regulators of Cancer Progression. *Trends Cancer* **2016**, *2*, 758–770. [[CrossRef](#)] [[PubMed](#)]
103. Semenza, G.L. Hypoxia-inducible factor 1 and cardiovascular disease. *Annu. Rev. Physiol.* **2014**, *76*, 39–56. [[CrossRef](#)] [[PubMed](#)]
104. Baek, J.H.; Liu, Y.V.; McDonald, K.R.; Wesley, J.B.; Hubbi, M.E.; Byun, H.; Semenza, G.L. Spermidine/spermine-N1-acetyltransferase 2 is an essential component of the ubiquitin ligase complex that regulates hypoxia-inducible factor 1alpha. *J. Biol. Chem.* **2007**, *282*, 23572–23580. [[CrossRef](#)] [[PubMed](#)]
105. Luo, W.; Zhong, J.; Chang, R.; Hu, H.; Pandey, A.; Semenza, G.L. Hsp70 and CHIP selectively mediate ubiquitination and degradation of hypoxia-inducible factor (HIF)-1alpha but not HIF-2alpha. *J. Biol. Chem.* **2010**, *285*, 3651–3663. [[CrossRef](#)]
106. Koh, M.Y.; Darnay, B.G.; Powis, G. Hypoxia-associated factor, a novel E3-ubiquitin ligase, binds and ubiquitinates hypoxia-inducible factor 1alpha, leading to its oxygen-independent degradation. *Mol. Cell. Biol.* **2008**, *28*, 7081–7095. [[CrossRef](#)]
107. Hubbi, M.E.; Hu, H.; Kshitiz, Gilkes, D.M.; Semenza, G.L. Sirtuin-7 inhibits the activity of hypoxia-inducible factors. *J. Biol. Chem.* **2013**, *288*, 20768–20775. [[CrossRef](#)]
108. Zelzer, E.; Levy, Y.; Kahana, C.; Shilo, B.Z.; Rubinstein, M.; Cohen, B. Insulin induces transcription of target genes through the hypoxia-inducible factor HIF-1alpha/ARNT. *EMBO J.* **1998**, *17*, 5085–5094. [[CrossRef](#)]
109. Treins, C.; Giorgetti-Peraldi, S.; Murdaca, J.; Semenza, G.L.; Van Obberghen, E. Insulin stimulates hypoxia-inducible factor 1 through a phosphatidylinositol 3-kinase/target of rapamycin-dependent signaling pathway. *J. Biol. Chem.* **2002**, *277*, 27975–27981. [[CrossRef](#)]
110. Fukuda, R.; Hirota, K.; Fan, F.; Jung, Y.D.; Ellis, L.M.; Semenza, G.L. Insulin-like growth factor 1 induces hypoxia-inducible factor 1-mediated vascular endothelial growth factor expression, which is dependent on MAP kinase and phosphatidylinositol 3-kinase signaling in colon cancer cells. *J. Biol. Chem.* **2002**, *277*, 38205–38211. [[CrossRef](#)]
111. Richard, D.E.; Berra, E.; Pouyssegur, J. Nonhypoxic pathway mediates the induction of hypoxia-inducible factor 1alpha in vascular smooth muscle cells. *J. Biol. Chem.* **2000**, *275*, 26765–26771.
112. Kohl, R.; Zhou, J.; Brune, B. Reactive oxygen species attenuate nitric-oxide-mediated hypoxia-inducible factor-1alpha stabilization. *Free Radic. Biol. Med.* **2006**, *40*, 1430–1442. [[CrossRef](#)] [[PubMed](#)]
113. Sandau, K.B.; Fandrey, J.; Brune, B. Accumulation of HIF-1alpha under the influence of nitric oxide. *Blood* **2001**, *97*, 1009–1015. [[CrossRef](#)] [[PubMed](#)]
114. Sanchez-Lopez, E.; Lopez, A.F.; Esteban, V.; Yague, S.; Egidio, J.; Ruiz-Ortega, M.; Alvarez-Arroyo, M.V. Angiotensin II regulates vascular endothelial growth factor via hypoxia-inducible factor-1alpha induction and redox mechanisms in the kidney. *Antioxid. Redox Signal.* **2005**, *7*, 1275–1284. [[CrossRef](#)] [[PubMed](#)]
115. Hellwig-Burgel, T.; Rutkowski, K.; Metzen, E.; Fandrey, J.; Jelkmann, W. Interleukin-1beta and tumor necrosis factor-alpha stimulate DNA binding of hypoxia-inducible factor-1. *Blood* **1999**, *94*, 1561–1567. [[CrossRef](#)]
116. Pouyssegur, J.; Mehta-Grigoriou, F. Redox regulation of the hypoxia-inducible factor. *Biol. Chem.* **2006**, *387*, 1337–1346. [[CrossRef](#)]
117. Chandel, N.S.; McClintock, D.S.; Feliciano, C.E.; Wood, T.M.; Melendez, J.A.; Rodriguez, A.M.; Schumacker, P.T. Reactive oxygen species generated at mitochondrial complex III stabilize hypoxia-inducible factor-1alpha during hypoxia: A mechanism of O2 sensing. *J. Biol. Chem.* **2000**, *275*, 25130–25138. [[CrossRef](#)]

118. Brauchle, M.; Funk, J.O.; Kind, P.; Werner, S. Ultraviolet B and H₂O₂ are potent inducers of vascular endothelial growth factor expression in cultured keratinocytes. *J. Biol. Chem.* **1996**, *271*, 21793–21797. [[CrossRef](#)]
119. Rezvani, H.R.; Dedieu, S.; North, S.; Belloc, F.; Rossignol, R.; Letellier, T.; de Verneuil, H.; Taieb, A.; Mazurier, F. Hypoxia-inducible factor-1alpha, a key factor in the keratinocyte response to UVB exposure. *J. Biol. Chem.* **2007**, *282*, 16413–16422. [[CrossRef](#)]
120. Gerald, D.; Berra, E.; Frapart, Y.M.; Chan, D.A.; Giaccia, A.J.; Mansuy, D.; Pouyssegur, J.; Yaniv, M.; Mechta-Grigoriou, F. JunD reduces tumor angiogenesis by protecting cells from oxidative stress. *Cell* **2004**, *118*, 781–794. [[CrossRef](#)]
121. Lu, H.; Dalgard, C.L.; Mohyeldin, A.; McFate, T.; Tait, A.S.; Verma, A. Reversible inactivation of HIF-1 prolyl hydroxylases allows cell metabolism to control basal HIF-1. *J. Biol. Chem.* **2005**, *280*, 41928–41939. [[CrossRef](#)]
122. Knowles, H.J.; Mole, D.R.; Ratcliffe, P.J.; Harris, A.L. Normoxic stabilization of hypoxia-inducible factor-1alpha by modulation of the labile iron pool in differentiating U937 macrophages: Effect of natural resistance-associated macrophage protein 1. *Cancer Res.* **2006**, *66*, 2600–2607. [[CrossRef](#)] [[PubMed](#)]
123. Wang, G.L.; Jiang, B.H.; Semenza, G.L. Effect of protein kinase and phosphatase inhibitors on expression of hypoxia-inducible factor 1. *Biochem. Biophys. Res. Commun.* **1995**, *216*, 669–675. [[CrossRef](#)] [[PubMed](#)]
124. Tacchini, L.; Dansi, P.; Matteucci, E.; Desiderio, M.A. Hepatocyte growth factor signalling stimulates hypoxia inducible factor-1 (HIF-1) activity in HepG2 hepatoma cells. *Carcinogenesis* **2001**, *22*, 1363–1371. [[CrossRef](#)] [[PubMed](#)]
125. Park, J.H.; Kim, T.Y.; Jong, H.S.; Kim, T.Y.; Chun, Y.S.; Park, J.W.; Lee, C.T.; Jung, H.C.; Kim, N.K.; Bang, Y.J. Gastric epithelial reactive oxygen species prevent normoxic degradation of hypoxia-inducible factor-1alpha in gastric cancer cells. *Clin. Cancer Res.* **2003**, *9*, 433–440.
126. Shatrov, V.A.; Sumbayev, V.V.; Zhou, J.; Brune, B. Oxidized low-density lipoprotein (oxLDL) triggers hypoxia-inducible factor-1alpha (HIF-1alpha) accumulation via redox-dependent mechanisms. *Blood* **2003**, *101*, 4847–4849. [[CrossRef](#)] [[PubMed](#)]
127. Zhu, X.Y.; Rodriguez-Porcel, M.; Bentley, M.D.; Chade, A.R.; Sica, V.; Napoli, C.; Caplice, N.; Ritman, E.L.; Lerman, A.; Lerman, L.O. Antioxidant intervention attenuates myocardial neovascularization in hypercholesterolemia. *Circulation* **2004**, *109*, 2109–2115. [[CrossRef](#)] [[PubMed](#)]
128. Rodriguez, J.A.; Nespereira, B.; Perez-Ilzarbe, M.; Eguinoa, E.; Paramo, J.A. Vitamins C and E prevent endothelial VEGF and VEGFR-2 overexpression induced by porcine hypercholesterolemic LDL. *Cardiovasc. Res.* **2005**, *65*, 665–673. [[CrossRef](#)]
129. Gorlach, A.; Diebold, I.; Schini-Kerth, V.B.; Berchner-Pfannschmidt, U.; Roth, U.; Brandes, R.P.; Kietzmann, T.; Busse, R. Thrombin activates the hypoxia-inducible factor-1 signaling pathway in vascular smooth muscle cells: Role of the p22(phox)-containing NADPH oxidase. *Circ. Res.* **2001**, *89*, 47–54. [[CrossRef](#)]
130. Semenza, G.L.; Wang, G.L. A nuclear factor induced by hypoxia via de novo protein synthesis binds to the human erythropoietin gene enhancer at a site required for transcriptional activation. *Mol. Cell. Biol.* **1992**, *12*, 5447–5454. [[CrossRef](#)]
131. Tian, H.; McKnight, S.L.; Russell, D.W. Endothelial PAS domain protein 1 (EPAS1), a transcription factor selectively expressed in endothelial cells. *Genes Dev.* **1997**, *11*, 72–82. [[CrossRef](#)]
132. Wiesener, M.S.; Jurgensen, J.S.; Rosenberger, C.; Scholze, C.K.; Horstrup, J.H.; Warnecke, C.; Mandriota, S.; Bechmann, I.; Frei, U.A.; Pugh, C.W.; et al. Widespread hypoxia-inducible expression of HIF-2alpha in distinct cell populations of different organs. *FASEB J.* **2003**, *17*, 271–273. [[CrossRef](#)] [[PubMed](#)]
133. Keith, B.; Johnson, R.S.; Simon, M.C. HIF1alpha and HIF2alpha: Sibling rivalry in hypoxic tumour growth and progression. *Nat. Rev. Cancer* **2011**, *12*, 9–22. [[CrossRef](#)] [[PubMed](#)]
134. Hu, C.J.; Wang, L.Y.; Chodosh, L.A.; Keith, B.; Simon, M.C. Differential roles of hypoxia-inducible factor 1alpha (HIF-1alpha) and HIF-2alpha in hypoxic gene regulation. *Mol. Cell. Biol.* **2003**, *23*, 9361–9374. [[CrossRef](#)] [[PubMed](#)]
135. Hu, C.J.; Sataur, A.; Wang, L.; Chen, H.; Simon, M.C. The N-terminal transactivation domain confers target gene specificity of hypoxia-inducible factors HIF-1alpha and HIF-2alpha. *Mol. Biol. Cell* **2007**, *18*, 4528–4542. [[CrossRef](#)] [[PubMed](#)]

136. Holmquist-Mengelbier, L.; Fredlund, E.; Lofstedt, T.; Noguera, R.; Navarro, S.; Nilsson, H.; Pietras, A.; Vallon-Christersson, J.; Borg, A.; Gradin, K.; et al. Recruitment of HIF-1alpha and HIF-2alpha to common target genes is differentially regulated in neuroblastoma: HIF-2alpha promotes an aggressive phenotype. *Cancer Cell* **2006**, *10*, 413–423. [[CrossRef](#)]
137. Koh, M.Y.; Lemos, R., Jr.; Liu, X.; Powis, G. The hypoxia-associated factor switches cells from HIF-1alpha- to HIF-2alpha-dependent signaling promoting stem cell characteristics, aggressive tumor growth and invasion. *Cancer Res.* **2011**, *71*, 4015–4027. [[CrossRef](#)]
138. Doedens, A.L.; Stockmann, C.; Rubinstein, M.P.; Liao, D.; Zhang, N.; DeNardo, D.G.; Coussens, L.M.; Karin, M.; Goldrath, A.W.; Johnson, R.S. Macrophage expression of hypoxia-inducible factor-1 alpha suppresses T-cell function and promotes tumor progression. *Cancer Res.* **2010**, *70*, 7465–7475. [[CrossRef](#)]
139. Takeda, N.; O'Dea, E.L.; Doedens, A.; Kim, J.W.; Weidemann, A.; Stockmann, C.; Asagiri, M.; Simon, M.C.; Hoffmann, A.; Johnson, R.S. Differential activation and antagonistic function of HIF-1alpha isoforms in macrophages are essential for NO homeostasis. *Genes Dev.* **2010**, *24*, 491–501. [[CrossRef](#)]
140. Lin, Q.; Cong, X.; Yun, Z. Differential hypoxic regulation of hypoxia-inducible factors 1alpha and 2alpha. *Mol. Cancer Res.* **2011**, *9*, 757–765. [[CrossRef](#)]
141. Rius, J.; Guma, M.; Schachtrup, C.; Akassoglou, K.; Zinkernagel, A.S.; Nizet, V.; Johnson, R.S.; Haddad, G.G.; Karin, M. NF-kappaB links innate immunity to the hypoxic response through transcriptional regulation of HIF-1alpha. *Nature* **2008**, *453*, 807–811. [[CrossRef](#)]
142. Toschi, A.; Lee, E.; Gadir, N.; Ohh, M.; Foster, D.A. Differential dependence of hypoxia-inducible factors 1 alpha and 2 alpha on mTORC1 and mTORC2. *J. Biol. Chem.* **2008**, *283*, 34495–34499. [[CrossRef](#)] [[PubMed](#)]
143. Finkel, T.; Deng, C.X.; Mostoslavsky, R. Recent progress in the biology and physiology of sirtuins. *Nature* **2009**, *460*, 587–591. [[CrossRef](#)] [[PubMed](#)]
144. Dioum, E.M.; Chen, R.; Alexander, M.S.; Zhang, Q.; Hogg, R.T.; Gerard, R.D.; Garcia, J.A. Regulation of hypoxia-inducible factor 2alpha signaling by the stress-responsive deacetylase sirtuin 1. *Science* **2009**, *324*, 1289–1293. [[CrossRef](#)] [[PubMed](#)]
145. Lim, J.H.; Lee, Y.M.; Chun, Y.S.; Chen, J.; Kim, J.E.; Park, J.W. Sirtuin 1 modulates cellular responses to hypoxia by deacetylating hypoxia-inducible factor 1alpha. *Mol. Cell* **2010**, *38*, 864–878. [[CrossRef](#)] [[PubMed](#)]
146. Semenza, G.L. Oxygen-dependent regulation of mitochondrial respiration by hypoxia-inducible factor 1. *Biochem. J.* **2007**, *405*, 1–9. [[CrossRef](#)]
147. Bhargava, P.; Schnellmann, R.G. Mitochondrial energetics in the kidney. *Nat. Rev. Nephrol.* **2017**, *13*, 629–646. [[CrossRef](#)]
148. Iyer, N.V.; Kotch, L.E.; Agani, F.; Leung, S.W.; Laughner, E.; Wenger, R.H.; Gassmann, M.; Gearhart, J.D.; Lawler, A.M.; Yu, A.Y.; et al. Cellular and developmental control of O2 homeostasis by hypoxia-inducible factor 1 alpha. *Genes Dev.* **1998**, *12*, 149–162. [[CrossRef](#)]
149. Kim, J.W.; Tchernyshyov, I.; Semenza, G.L.; Dang, C.V. HIF-1-mediated expression of pyruvate dehydrogenase kinase: A metabolic switch required for cellular adaptation to hypoxia. *Cell Metab.* **2006**, *3*, 177–185. [[CrossRef](#)]
150. Papandreou, I.; Cairns, R.A.; Fontana, L.; Lim, A.L.; Denko, N.C. HIF-1 mediates adaptation to hypoxia by actively downregulating mitochondrial oxygen consumption. *Cell Metab.* **2006**, *3*, 187–197. [[CrossRef](#)]
151. Rohlenova, K.; Veys, K.; Miranda-Santos, I.; De Bock, K.; Carmeliet, P. Endothelial cell metabolism in health and disease. *Trends Cell Biol.* **2018**, *28*, 224–236. [[CrossRef](#)]
152. De Bock, K.; Georgiadou, M.; Carmeliet, P. Role of endothelial cell metabolism in vessel sprouting. *Cell Metab.* **2013**, *18*, 634–647. [[CrossRef](#)] [[PubMed](#)]
153. Helmlinger, G.; Endo, M.; Ferrara, N.; Hlatky, L.; Jain, R.K. Formation of endothelial cell networks. *Nature* **2000**, *405*, 139–141. [[CrossRef](#)] [[PubMed](#)]
154. Dekker, R.J.; van Soest, S.; Fontijn, R.D.; Salamanca, S.; de Groot, P.G.; VanBavel, E.; Pannekoek, H.; Horrevoets, A.J. Prolonged fluid shear stress induces a distinct set of endothelial cell genes, most specifically lung Kruppel-like factor (KLF2). *Blood* **2002**, *100*, 1689–1698. [[CrossRef](#)] [[PubMed](#)]
155. Lin, Z.; Kumar, A.; SenBanerjee, S.; Staniszewski, K.; Parmar, K.; Vaughan, D.E.; Gimbrone, M.A., Jr.; Balasubramanian, V.; Garcia-Cardena, G.; Jain, M.K. Kruppel-like factor 2 (KLF2) regulates endothelial thrombotic function. *Circ. Res.* **2005**, *96*, e48–e57. [[CrossRef](#)] [[PubMed](#)]
156. Chiplunkar, A.R.; Curtis, B.C.; Eades, G.L.; Kane, M.S.; Fox, S.J.; Haar, J.L.; Lloyd, J.A. The Kruppel-like factor 2 and Kruppel-like factor 4 genes interact to maintain endothelial integrity in mouse embryonic vasculogenesis. *BMC Dev. Biol.* **2013**, *13*, 40. [[CrossRef](#)]

157. Tuomisto, T.T.; Lumivuori, H.; Kansanen, E.; Hakkinen, S.K.; Turunen, M.P.; van Thienen, J.V.; Horrevoets, A.J.; Levenon, A.L.; Yla-Herttuala, S. Simvastatin has an anti-inflammatory effect on macrophages via upregulation of an atheroprotective transcription factor, Kruppel-like factor 2. *Cardiovasc. Res.* **2008**, *78*, 175–184. [[CrossRef](#)]
158. Sweet, D.R.; Fan, L.; Hsieh, P.N.; Jain, M.K. Kruppel-Like Factors in Vascular Inflammation: Mechanistic Insights and Therapeutic Potential. *Front. Cardiovasc. Med.* **2018**, *5*, 6. [[CrossRef](#)]
159. Bhattacharya, R.; Senbanerjee, S.; Lin, Z.; Mir, S.; Hamik, A.; Wang, P.; Mukherjee, P.; Mukhopadhyay, D.; Jain, M.K. Inhibition of vascular permeability factor/vascular endothelial growth factor-mediated angiogenesis by the Kruppel-like factor KLF2. *J. Biol. Chem.* **2005**, *280*, 28848–28851. [[CrossRef](#)]
160. Doddaballapur, A.; Michalik, K.M.; Manavski, Y.; Lucas, T.; Houtkooper, R.H.; You, X.; Chen, W.; Zeiher, A.M.; Potente, M.; Dimmeler, S.; et al. Laminar shear stress inhibits endothelial cell metabolism via KLF2-mediated repression of PFKFB3. *Arterioscler. Thromb. Vasc. Biol.* **2015**, *35*, 137–145. [[CrossRef](#)]
161. De Bock, K.; Georgiadou, M.; Schoors, S.; Kuchnio, A.; Wong, B.W.; Cantelmo, A.R.; Quaegebeur, A.; Ghesquiere, B.; Cauwenberghs, S.; Eelen, G.; et al. Role of PFKFB3-driven glycolysis in vessel sprouting. *Cell* **2013**, *154*, 651–663. [[CrossRef](#)]
162. Schoors, S.; De Bock, K.; Cantelmo, A.R.; Georgiadou, M.; Ghesquiere, B.; Cauwenberghs, S.; Kuchnio, A.; Wong, B.W.; Quaegebeur, A.; Goveia, J.; et al. Partial and transient reduction of glycolysis by PFKFB3 blockade reduces pathological angiogenesis. *Cell Metab.* **2014**, *19*, 37–48. [[CrossRef](#)] [[PubMed](#)]
163. Kawanami, D.; Mahabeshwar, G.H.; Lin, Z.; Atkins, G.B.; Hamik, A.; Haldar, S.M.; Maemura, K.; Lamanna, J.C.; Jain, M.K. Kruppel-like factor 2 inhibits hypoxia-inducible factor 1alpha expression and function in the endothelium. *J. Biol. Chem.* **2009**, *284*, 20522–20530. [[CrossRef](#)] [[PubMed](#)]
164. Resar, J.R.; Roguin, A.; Voner, J.; Nasir, K.; Henneby, T.A.; Miller, J.M.; Ingersoll, R.; Kasch, L.M.; Semenza, G.L. Hypoxia-inducible factor 1alpha polymorphism and coronary collaterals in patients with ischemic heart disease. *Chest* **2005**, *128*, 787–791. [[CrossRef](#)] [[PubMed](#)]
165. Bosch-Marce, M.; Okuyama, H.; Wesley, J.B.; Sarkar, K.; Kimura, H.; Liu, Y.V.; Zhang, H.; Strazza, M.; Rey, S.; Savino, L.; et al. Effects of aging and hypoxia-inducible factor-1 activity on angiogenic cell mobilization and recovery of perfusion after limb ischemia. *Circ. Res.* **2007**, *101*, 1310–1318. [[CrossRef](#)] [[PubMed](#)]
166. Sluimer, J.C.; Gasc, J.M.; van Wanroij, J.L.; Kisters, N.; Groeneweg, M.; Sollewijn Gelpke, M.D.; Cleutjens, J.P.; van den Akker, L.H.; Corvol, P.; Wouters, B.G.; et al. Hypoxia, hypoxia-inducible transcription factor, and macrophages in human atherosclerotic plaques are correlated with intraplaque angiogenesis. *J. Am. Coll. Cardiol.* **2008**, *51*, 1258–1265. [[CrossRef](#)]
167. Vorp, D.A.; Lee, P.C.; Wang, D.H.; Makaroun, M.S.; Nemoto, E.M.; Ogawa, S.; Webster, M.W. Association of intraluminal thrombus in abdominal aortic aneurysm with local hypoxia and wall weakening. *J. Vasc. Surg.* **2001**, *34*, 291–299. [[CrossRef](#)]
168. Lee, J.D.; Lai, C.H.; Yang, W.K.; Lee, T.H. Increased expression of hypoxia-inducible factor-1alpha and metallothionein in varicocele and varicose veins. *Phlebology* **2012**, *27*, 409–415. [[CrossRef](#)]
169. Evans, C.E.; Humphries, J.; Mattock, K.; Waltham, M.; Wadoodi, A.; Saha, P.; Modarai, B.; Maxwell, P.H.; Smith, A. Hypoxia and upregulation of hypoxia-inducible factor 1(alpha) stimulate venous thrombus recanalization. *Arterioscler. Thromb. Vasc. Biol.* **2010**, *30*, 2443–2451. [[CrossRef](#)]
170. Evans, C.E.; Humphries, J.; Waltham, M.; Saha, P.; Mattock, K.; Patel, A.; Ahmad, A.; Wadoodi, A.; Modarai, B.; Burnand, K.; et al. Upregulation of hypoxia-inducible factor 1 alpha in local vein wall is associated with enhanced venous thrombus resolution. *Thromb. Res.* **2011**, *128*, 346–351. [[CrossRef](#)]
171. Semenza, G.L. Hypoxia-inducible factors in physiology and medicine. *Cell* **2012**, *148*, 399–408. [[CrossRef](#)]
172. Lim, C.S.; Kiriakidis, S.; Sandison, A.; Paleolog, E.M.; Davies, A.H. Hypoxia-inducible factor pathway and diseases of the vascular wall. *J. Vasc. Surg.* **2013**, *58*, 219–230. [[CrossRef](#)] [[PubMed](#)]
173. Hansson, G.K. Inflammation, atherosclerosis, and coronary artery disease. *N. Engl. J. Med.* **2005**, *352*, 1685–1695. [[CrossRef](#)] [[PubMed](#)]
174. Lusis, A.J. Atherosclerosis. *Nature* **2000**, *407*, 233–241. [[CrossRef](#)] [[PubMed](#)]
175. Murdoch, C.; Muthana, M.; Lewis, C.E. Hypoxia regulates macrophage functions in inflammation. *J. Immunol.* **2005**, *175*, 6257–6263. [[CrossRef](#)]
176. Parathath, S.; Mick, S.L.; Feig, J.E.; Joaquin, V.; Grauer, L.; Habel, D.M.; Gassmann, M.; Gardner, L.B.; Fisher, E.A. Hypoxia is present in murine atherosclerotic plaques and has multiple adverse effects on macrophage lipid metabolism. *Circ. Res.* **2011**, *109*, 1141–1152. [[CrossRef](#)]

177. Cramer, T.; Yamanishi, Y.; Clausen, B.E.; Forster, I.; Pawlinski, R.; Mackman, N.; Haase, V.H.; Jaenisch, R.; Corr, M.; Nizet, V.; et al. HIF-1 α is essential for myeloid cell-mediated inflammation. *Cell* 2003, 112, 645–657. [CrossRef]
178. Burke, B.; Giannoudis, A.; Corke, K.P.; Gill, D.; Wells, M.; Ziegler-Heitbrock, L.; Lewis, C.E. Hypoxia-induced gene expression in human macrophages: Implications for ischemic tissues and hypoxia-regulated gene therapy. *Am. J. Pathol.* 2003, 163, 1233–1243. [CrossRef]
179. Lobanova, E.M.; Tahanovich, A.D. Hydrogen peroxide metabolism in alveolar macrophages after exposure to hypoxia and heat. *Physiol. Res.* 2006, 55, 569–575.
180. Rydberg, E.K.; Krettek, A.; Ullstrom, C.; Ekstrom, K.; Svensson, P.A.; Carlsson, L.M.; Jonsson-Rylander, A.C.; Hansson, G.I.; McPheat, W.; Wiklund, O.; et al. Hypoxia increases LDL oxidation and expression of 15-lipoxygenase-2 in human macrophages. *Arterioscler. Thromb. Vasc. Biol.* 2004, 24, 2040–2045. [CrossRef]
181. Lattimore, J.D.; Wilcox, I.; Nakhla, S.; Langenfeld, M.; Jessup, W.; Celermajer, D.S. Repetitive hypoxia increases lipid loading in human macrophages—a potentially atherogenic effect. *Atherosclerosis* 2005, 179, 255–259. [CrossRef]
182. Luque, A.; Turu, M.; Juan-Babot, O.; Cardona, P.; Font, A.; Carvajal, A.; Slevin, M.; Iborra, E.; Rubio, F.; Badimon, L.; et al. Overexpression of hypoxia/inflammatory markers in atherosclerotic carotid plaques. *Front. Biosci.* 2008, 13, 6483–6490. [CrossRef] [PubMed]
183. Vink, A.; Schoneveld, A.H.; Lamers, D.; Houben, A.J.; van der Groep, P.; van Diest, P.J.; Pasterkamp, G. HIF-1 α expression is associated with an atheromatous inflammatory plaque phenotype and upregulated in activated macrophages. *Atherosclerosis* 2007, 195, e69–e75. [CrossRef] [PubMed]
184. Higashida, T.; Kanno, H.; Nakano, M.; Funakoshi, K.; Yamamoto, I. Expression of hypoxia-inducible angiogenic proteins (hypoxia-inducible factor-1 α , vascular endothelial growth factor, and E26 transformation-specific-1) and plaque hemorrhage in human carotid atherosclerosis. *J. Neurosurg.* 2008, 109, 83–91. [CrossRef] [PubMed]
185. Jiang, G.; Li, T.; Qiu, Y.; Rui, Y.; Chen, W.; Lou, Y. RNA interference for HIF-1 α inhibits foam cells formation in vitro. *Eur. J. Pharmacol.* 2007, 562, 183–190. [CrossRef] [PubMed]
186. Blouin, C.C.; Page, E.L.; Soucy, G.M.; Richard, D.E. Hypoxic gene activation by lipopolysaccharide in macrophages: Implication of hypoxia-inducible factor 1 α . *Blood* 2004, 103, 1124–1130. [CrossRef] [PubMed]
187. Cramer, T.; Johnson, R.S. A novel role for the hypoxia inducible transcription factor HIF-1 α : Critical regulation of inflammatory cell function. *Cell Cycle* 2003, 2, 192–193. [CrossRef]
188. Lu, D.Y.; Chen, E.Y.; Wong, D.J.; Yamamoto, K.; Protack, C.D.; Williams, W.T.; Assi, R.; Hall, M.R.; Sadaghianloo, N.; Dardik, A. Vein graft adaptation and fistula maturation in the arterial environment. *J. Surg. Res.* 2014, 188, 162–173. [CrossRef]
189. Lee, E.S.; Bauer, G.E.; Caldwell, M.P.; Santilli, S.M. Association of artery wall hypoxia and cellular proliferation at a vascular anastomosis. *J. Surg. Res.* 2000, 91, 32–37. [CrossRef]
190. Santilli, S.M.; Wernsing, S.E.; Lee, E.S. Transarterial wall oxygen gradients at a prosthetic vascular graft to artery anastomosis in the rabbit. *J. Vasc. Surg.* 2000, 31, 1229–1239. [CrossRef]
191. Hughes, D.; Fu, A.A.; Puggioni, A.; Glockner, J.E.; Anwer, B.; McGuire, A.M.; Mukhopadhyay, D.; Misra, S. Adventitial transplantation of blood outgrowth endothelial cells in porcine haemodialysis grafts alleviates hypoxia and decreases neointimal proliferation through a matrix metalloproteinase-9-mediated pathway—A pilot study. *Nephrol. Dial. Transplant.* 2009, 24, 85–96. [CrossRef]
192. Nakao, A.; Huang, C.S.; Stolz, D.B.; Wang, Y.; Franks, J.M.; Tochigi, N.; Billiar, T.R.; Toyoda, Y.; Tzeng, E.; McCurry, K.R. Ex vivo carbon monoxide delivery inhibits intimal hyperplasia in arterialized vein grafts. *Cardiovasc. Res.* 2011, 89, 457–463. [CrossRef] [PubMed]
193. Rochette, L.; Cottin, Y.; Zeller, M.; Vergely, C. Carbon monoxide: Mechanisms of action and potential clinical implications. *Pharmacol. Ther.* 2013, 137, 133–152. [CrossRef] [PubMed]
194. Misra, S.; Fu, A.A.; Rajan, D.K.; Juncos, L.A.; McKusick, M.A.; Bjarnason, H.; Mukhopadhyay, D. Expression of hypoxia inducible factor-1 α , macrophage migration inhibition factor, matrix metalloproteinase-2 and -9, and their inhibitors in hemodialysis grafts and arteriovenous fistulas. *J. Vasc. Interv. Radiol.* 2008, 19, 252–259. [CrossRef] [PubMed]

195. Fu, H.; Luo, F.; Yang, L.; Wu, W.; Liu, X. Hypoxia stimulates the expression of macrophage migration inhibitory factor in human vascular smooth muscle cells via HIF-1 α dependent pathway. *BMC Cell Biol.* **2010**, *11*, 66. [[CrossRef](#)]
196. Misra, S.; Fu, A.A.; Puggioni, A.; Glockner, J.F.; McKusick, M.A.; Bjarnason, H.; Mukhopadhyay, D. Proteomic Profiling in Early Venous Stenosis Formation in a Porcine Model of Hemodialysis Graft. *J. Vasc. Interv. Radiol.* **2009**, *20*, 241–251. [[CrossRef](#)] [[PubMed](#)]
197. Misra, S.; Fu, A.A.; Puggioni, A.; Glockner, J.F.; Rajan, D.K.; McKusick, M.A.; Bjarnason, H.; Mukhopadhyay, D. Increased Expression of Hypoxia-inducible Factor-1 α in venous stenosis of arteriovenous polytetrafluoroethylene grafts in a chronic renal insufficiency porcine model. *J. Vasc. Interv. Radiol.* **2008**, *19*, 260–265. [[CrossRef](#)] [[PubMed](#)]
198. Misra, S.; Shergill, U.; Yang, B.; Janardhanan, R.; Misra, K.D. Increased Expression of HIF-1 α , VEGF-A and Its Receptors, MMP-2, TIMP-1, and ADAMTS-1 at the venous stenosis of arteriovenous fistula in a mouse model with renal insufficiency. *J. Vasc. Interv. Radiol.* **2010**, *21*, 1255–1261. [[CrossRef](#)] [[PubMed](#)]
199. Sadaghianloo, N.; Yamamoto, K.; Bai, H.; Tsuneki, M.; Protack, C.D.; Hall, M.R.; Declémy, S.; Hassen-Khodja, R.; Madri, J.; Dardik, A. Increased oxidative stress and hypoxia inducible factor-1 expression during arteriovenous fistula maturation. *Ann. Vasc. Surg.* **2017**, *41*, 225–234. [[CrossRef](#)]
200. Lin, C.C.; Chung, M.Y.; Yang, W.C.; Lin, S.J.; Lee, P.C. Length polymorphisms of heme oxygenase-1 determine the effect of far-infrared therapy on the function of arteriovenous fistula in hemodialysis patients: A novel physiogenomic study. *Nephrol. Dial. Transplant.* **2013**, *28*, 1284–1293. [[CrossRef](#)]
201. Lin, C.C.; Yang, W.C.; Lin, S.J.; Chen, T.W.; Lee, W.S.; Chang, C.F.; Lee, P.C.; Lee, S.D.; Su, T.S.; Fann, C.S.; et al. Length polymorphism in heme oxygenase-1 is associated with arteriovenous fistula patency in hemodialysis patients. *Kidney Int.* **2006**, *69*, 165–172. [[CrossRef](#)]
202. Kang, L.; Grande, J.P.; Farrugia, G.; Croatt, A.J.; Katusic, Z.S.; Nath, K.A. Functioning of an arteriovenous fistula requires heme oxygenase-2. *Am. J. Physiol. Renal Physiol.* **2013**, *305*, F545–F552. [[CrossRef](#)] [[PubMed](#)]
203. Kang, L.; Grande, J.P.; Hillestad, M.L.; Croatt, A.J.; Barry, M.A.; Katusic, Z.S.; Nath, K.A. A new model of an arteriovenous fistula in chronic kidney disease in the mouse: Beneficial effects of upregulated heme oxygenase-1. *Am. J. Physiol. Renal Physiol.* **2016**, *310*, F466–F476. [[CrossRef](#)] [[PubMed](#)]
204. Lever, J.M.; Boddu, R.; George, J.F.; Agarwal, A. Heme oxygenase-1 in kidney health and disease. *Antioxid. Redox Signal.* **2016**, *25*, 165–183. [[CrossRef](#)] [[PubMed](#)]
205. Adin, C.A.; Croker, B.P.; Agarwal, A. Protective effects of exogenous bilirubin on ischemia-reperfusion injury in the isolated, perfused rat kidney. *Am. J. Physiol. Renal Physiol.* **2005**, *288*, F778–F784. [[CrossRef](#)]
206. Juncos, J.P.; Tracz, M.J.; Croatt, A.J.; Grande, J.P.; Ackerman, A.W.; Katusic, Z.S.; Nath, K.A. Genetic deficiency of heme oxygenase-1 impairs functionality and form of an arteriovenous fistula in the mouse. *Kidney Int.* **2008**, *74*, 47–51. [[CrossRef](#)]
207. Freidja, M.L.; Toutain, B.; Caillon, A.; Desquret, V.; Lambert, D.; Loufrani, L.; Procaccio, V.; Henrion, D. Heme oxygenase 1 is differentially involved in blood flow-dependent arterial remodeling: Role of inflammation, oxidative stress, and nitric oxide. *Hypertension* **2011**, *58*, 225–231. [[CrossRef](#)]
208. Zohny, S.F.; Abd el-Fattah, M. Evaluation of circulating vascular endothelial growth factor and soluble adhesion molecules as reliable predictors of native arteriovenous fistula thrombosis in chronic hemodialysis patients. *Clin. Biochem.* **2008**, *41*, 1175–1180. [[CrossRef](#)]
209. Candan, F.; Yildiz, G.; Kayatas, M. Role of the VEGF 936 gene polymorphism and VEGF-A levels in the late-term arteriovenous fistula thrombosis in patients undergoing hemodialysis. *Int. Urol. Nephrol.* **2014**, *46*, 1815–1823. [[CrossRef](#)]
210. Ohtani, K.; Egashira, K.; Hiasa, K.; Zhao, Q.; Kitamoto, S.; Ishibashi, M.; Usui, M.; Inoue, S.; Yonemitsu, Y.; Sueishi, K.; et al. Blockade of vascular endothelial growth factor suppresses experimental restenosis after intraluminal injury by inhibiting recruitment of monocyte lineage cells. *Circulation* **2004**, *110*, 2444–2452. [[CrossRef](#)]
211. Rapisarda, A.; Uranchimeg, B.; Scudiero, D.A.; Selby, M.; Sausville, E.A.; Shoemaker, R.H.; Melillo, G. Identification of small molecule inhibitors of hypoxia-inducible factor 1 transcriptional activation pathway. *Cancer Res.* **2002**, *62*, 4316–4324.
212. Lata, C.; Green, D.; Wan, J.; Roy, S.; Santilli, S.M. The role of short-term oxygen administration in the prevention of intimal hyperplasia. *J. Vasc. Surg.* **2013**, *58*, 452–459. [[CrossRef](#)] [[PubMed](#)]

213. Wan, J.; Lata, C.; Santilli, A.; Green, D.; Roy, S.; Santilli, S. Supplemental oxygen reverses hypoxia-induced smooth muscle cell proliferation by modulating HIF- α and VEGF levels in a rabbit arteriovenous fistula model. *Ann. Vasc. Surg.* **2014**, *28*, 725–736. [[CrossRef](#)] [[PubMed](#)]
214. Terraneo, L.; Paroni, R.; Bianciardi, P.; Giallongo, T.; Carelli, S.; Gorio, A.; Samaja, M. Brain adaptation to hypoxia and hyperoxia in mice. *Redox Biol.* **2017**, *11*, 12–20. [[CrossRef](#)] [[PubMed](#)]
215. Terraneo, L.; Virgili, E.; Caretti, A.; Bianciardi, P.; Samaja, M. In vivo hyperoxia induces hypoxia-inducible factor-1 α overexpression in LNCaP tumors without affecting the tumor growth rate. *Int. J. Biochem. Cell Biol.* **2014**, *51C*, 65–74. [[CrossRef](#)]
216. Marconi, G.D.; Zara, S.; De Colli, M.; Di Valerio, V.; Rapino, M.; Zaramella, P.; Dedja, A.; Macchi, V.; De Caro, R.; Porzionato, A. Postnatal hyperoxia exposure differentially affects hepatocytes and liver haemopoietic cells in newborn rats. *PLoS ONE* **2014**, *9*, e105005. [[CrossRef](#)]
217. Zara, S.; Macchi, V.; De Caro, R.; Rapino, M.; Cataldi, A.; Porzionato, A. pPKC α mediated-HIF-1 α activation related to the morphological modifications occurring in neonatal myocardial tissue in response to severe and mild hyperoxia. *Eur. J. Histochem.* **2012**, *56*, e2. [[CrossRef](#)]
218. Vandegriff, K.D.; Malavalli, A.; Lohman, J.; Young, M.A.; Terraneo, L.; Virgili, E.; Bianciardi, P.; Caretti, A.; Samaja, M. Impact of acellular hemoglobin-based oxygen carriers on brain apoptosis in rats. *Transfusion* **2014**, *54*, 45–54. [[CrossRef](#)]
219. Wigerup, C.; Pahlman, S.; Bexell, D. Therapeutic targeting of hypoxia and hypoxia-inducible factors in cancer. *Pharmacol. Ther.* **2016**, *164*, 152–169. [[CrossRef](#)]
220. Melillo, G. Targeting hypoxia cell signaling for cancer therapy. *Cancer Metastasis Rev.* **2007**, *26*, 341–352. [[CrossRef](#)]
221. Shin, D.H.; Chun, Y.S.; Lee, D.S.; Huang, L.E.; Park, J.W. Bortezomib inhibits tumor adaptation to hypoxia by stimulating the FIH-mediated repression of hypoxia-inducible factor-1. *Blood* **2008**, *111*, 3131–3136. [[CrossRef](#)]
222. Greenberger, L.M.; Horak, I.D.; Filpula, D.; Sapra, P.; Westergaard, M.; Frydenlund, H.F.; Albaek, C.; Schroder, H.; Orum, H. A RNA antagonist of hypoxia-inducible factor-1 α , EZN-2968, inhibits tumor cell growth. *Mol. Cancer Ther.* **2008**, *7*, 3598–3608. [[CrossRef](#)] [[PubMed](#)]
223. Terzuoli, E.; Puppo, M.; Rapisarda, A.; Uranchimeg, B.; Cao, L.; Burger, A.M.; Ziche, M.; Melillo, G. Aminoflavone, a ligand of the aryl hydrocarbon receptor, inhibits HIF-1 α expression in an AhR-independent fashion. *Cancer Res.* **2010**, *70*, 6837–6848. [[CrossRef](#)] [[PubMed](#)]
224. Rapisarda, A.; Uranchimeg, B.; Sordet, O.; Pommier, Y.; Shoemaker, R.H.; Melillo, G. Topoisomerase I-mediated inhibition of hypoxia-inducible factor 1: Mechanism and therapeutic implications. *Cancer Res.* **2004**, *64*, 1475–1482. [[CrossRef](#)] [[PubMed](#)]
225. Sapra, P.; Zhao, H.; Mehlig, M.; Malaby, J.; Kraft, P.; Longley, C.; Greenberger, L.M.; Horak, I.D. Novel delivery of SN38 markedly inhibits tumor growth in xenografts, including a camptothecin-11-refractory model. *Clin. Cancer Res.* **2008**, *14*, 1888–1896. [[CrossRef](#)] [[PubMed](#)]
226. Zhang, H.; Qian, D.Z.; Yan, Y.S.; Lee, K.; Gao, P.; Ren, Y.R.; Rey, S.; Hammers, H.; Chang, D.; Pili, R.; et al. Digoxin and other cardiac glycosides inhibit HIF-1 α synthesis and block tumor growth. *Proc. Natl. Acad. Sci. USA* **2008**, *105*, 19579–19586. [[CrossRef](#)] [[PubMed](#)]
227. Del Bufalo, D.; Ciuffreda, L.; Trisciuglio, D.; Desideri, M.; Cognetti, F.; Zupi, G.; Milella, M. Antiangiogenic potential of the Mammalian target of rapamycin inhibitor temsirolimus. *Cancer Res.* **2006**, *66*, 5549–5554. [[CrossRef](#)] [[PubMed](#)]
228. Manegold, P.C.; Paringer, C.; Kulka, U.; Krimmel, K.; Eichhorn, M.E.; Wilkowski, R.; Jauch, K.W.; Guba, M.; Bruns, C.J. Antiangiogenic therapy with mammalian target of rapamycin inhibitor RAD001 (everolimus) increases radiosensitivity in solid cancer. *Clin. Cancer Res.* **2008**, *14*, 892–900. [[CrossRef](#)]
229. Majumder, P.K.; Febbo, P.G.; Bikoff, R.; Berger, R.; Xue, Q.; McMahon, L.M.; Manola, J.; Brugarolas, J.; McDonnell, T.J.; Golub, T.R.; et al. mTOR inhibition reverses Akt-dependent prostate intraepithelial neoplasia through regulation of apoptotic and HIF-1-dependent pathways. *Nat. Med.* **2004**, *10*, 594–601. [[CrossRef](#)]
230. Isaacs, J.S.; Jung, Y.J.; Mimnaugh, E.G.; Martinez, A.; Cuttitta, F.; Neckers, L.M. Hsp90 regulates a von Hippel Lindau-independent hypoxia-inducible factor-1 α -degradative pathway. *J. Biol. Chem.* **2002**, *277*, 29936–29944. [[CrossRef](#)]

231. Hur, E.; Kim, H.H.; Choi, S.M.; Kim, J.H.; Yim, S.; Kwon, H.J.; Choi, Y.; Kim, D.K.; Lee, M.O.; Park, H. Reduction of hypoxia-induced transcription through the repression of hypoxia-inducible factor-1 α /aryl hydrocarbon receptor nuclear translocator DNA binding by the 90-kDa heat-shock protein inhibitor radicicol. *Mol. Pharmacol.* **2002**, *62*, 975–982. [CrossRef]
232. Ellis, L.; Hammers, H.; Pili, R. Targeting tumor angiogenesis with histone deacetylase inhibitors. *Cancer Lett.* **2009**, *280*, 145–153. [CrossRef] [PubMed]
233. Kong, D.; Park, E.J.; Stephen, A.G.; Calvani, M.; Cardellina, J.H.; Monks, A.; Fisher, R.J.; Shoemaker, R.H.; Melillo, G. Echinomycin, a small-molecule inhibitor of hypoxia-inducible factor-1 DNA-binding activity. *Cancer Res.* **2005**, *65*, 9047–9055. [CrossRef] [PubMed]
234. Lee, K.; Qian, D.Z.; Rey, S.; Wei, H.; Liu, J.O.; Semenza, G.L. Anthracycline chemotherapy inhibits HIF-1 transcriptional activity and tumor-induced mobilization of circulating angiogenic cells. *Proc. Natl. Acad. Sci. USA* **2009**, *106*, 2353–2358. [CrossRef] [PubMed]
235. Rey, S.; Lee, K.; Wang, C.J.; Gupta, K.; Chen, S.; McMillan, A.; Bhise, N.; Levchenko, A.; Semenza, G.L. Synergistic effect of HIF-1 α gene therapy and HIF-1-activated bone marrow-derived angiogenic cells in a mouse model of limb ischemia. *Proc. Natl. Acad. Sci. USA* **2009**, *106*, 20399–20404. [CrossRef] [PubMed]
236. Rajagopalan, S.; Olin, J.; Deitcher, S.; Pieczek, A.; Laird, J.; Grossman, P.M.; Goldman, C.K.; McEllin, K.; Kelly, R.; Chronos, N. Use of a constitutively active hypoxia-inducible factor-1 α transgene as a therapeutic strategy in no-option critical limb ischemia patients: Phase I dose-escalation experience. *Circulation* **2007**, *115*, 1234–1243. [CrossRef]
237. Creager, M.A.; Olin, J.W.; Belch, J.J.; Moneta, G.L.; Henry, T.D.; Rajagopalan, S.; Annex, B.H.; Hiatt, W.R. Effect of hypoxia-inducible factor-1 α gene therapy on walking performance in patients with intermittent claudication. *Circulation* **2011**, *124*, 1765–1773. [CrossRef]
238. Gupta, N.; Wish, J.B. Hypoxia-inducible factor prolyl hydroxylase inhibitors: A potential new treatment for anemia in patients with CKD. *Am. J. Kidney Dis.* **2017**, *69*, 815–826. [CrossRef]
239. Brigandi, R.A.; Johnson, B.; Oei, C.; Westerman, M.; Olbina, G.; de Zoysa, J.; Roger, S.D.; Sahay, M.; Cross, N.; McMahon, L.; et al. A novel hypoxia-inducible factor-prolyl hydroxylase inhibitor (GSK1278863) for anemia in CKD: A 28-day, phase 2A randomized trial. *Am. J. Kidney Dis.* **2016**, *67*, 861–871. [CrossRef]
240. Provenzano, R.; Besarab, A.; Wright, S.; Dua, S.; Zeig, S.; Nguyen, P.; Poole, L.; Saikali, K.G.; Saha, G.; Hemmerich, S.; et al. Roxadustat (FG-4592) versus epoetin alfa for anemia in patients receiving maintenance hemodialysis: A phase 2, randomized, 6- to 19-week, open-label, active-comparator, dose-ranging, safety and exploratory efficacy study. *Am. J. Kidney Dis.* **2016**, *67*, 912–924. [CrossRef]
241. Onnis, B.; Rapisarda, A.; Melillo, G. Development of HIF-1 inhibitors for cancer therapy. *J. Cell. Mol. Med.* **2009**, *13*, 2780–2786. [CrossRef]
242. Chen, W.; Hill, H.; Christie, A.; Kim, M.S.; Holloman, E.; Pavia-Jimenez, A.; Homayoun, F.; Ma, Y.; Patel, N.; Yell, P.; et al. Targeting renal cell carcinoma with a HIF-2 antagonist. *Nature* **2016**, *539*, 112–117. [CrossRef] [PubMed]
243. Scheuermann, T.H.; Li, Q.; Ma, H.W.; Key, J.; Zhang, L.; Chen, R.; Garcia, J.A.; Naidoo, J.; Longgood, J.; Frantz, D.E.; et al. Allosteric inhibition of hypoxia inducible factor-2 with small molecules. *Nat. Chem. Biol.* **2013**, *9*, 271–276. [CrossRef] [PubMed]
244. Cho, H.; Du, X.; Rizzi, J.P.; Liberzon, E.; Chakraborty, A.A.; Gao, W.; Carvo, L.; Signoretti, S.; Bruick, R.K.; Josey, J.A.; et al. On-target efficacy of a HIF-2 α antagonist in preclinical kidney cancer models. *Nature* **2016**, *539*, 107–111. [CrossRef] [PubMed]
245. Wallace, E.M.; Rizzi, J.P.; Han, G.; Wehn, P.M.; Cao, Z.; Du, X.; Cheng, T.; Czerwinski, R.M.; Dixon, D.D.; Goggin, B.S.; et al. A small-molecule antagonist of HIF2 α is efficacious in preclinical models of renal cell carcinoma. *Cancer Res.* **2016**, *76*, 5491–5500. [CrossRef] [PubMed]



© 2019 by the authors. Licensee MDPI, Basel, Switzerland. This article is an open access article distributed under the terms and conditions of the Creative Commons Attribution (CC BY) license (<http://creativecommons.org/licenses/by/4.0/>).

Annexe 4: Identification of a new aggressive axis driven by ciliogenesis and absence of VDAC-deltaC in clear cell Carcinoma patients. Theranostics. 2020

Theranostics 2020, Vol. 10, Issue 6

2696



Theranostics

2020; 10(6): 2696-2713. doi: 10.7150/thno.41001

Research Paper

Identification of a new aggressive axis driven by ciliogenesis and absence of VDAC1- Δ C in clear cell Renal Cell Carcinoma patients

Lucilla Fabbri^{1,2*}, Maeva Dufies^{3*}, Sandra Lacas-Gervais⁴, Betty Gardie⁵, Sophie Gad-Lapiteau⁷, Julien Parola^{1, 8}, Nicolas Nottet², Monique Meyenberg Cunha de Padua², Julie Contenti², Delphine Borchellini⁸, Jean-Marc Ferrero^{2,8}, Nathalie Rioux Leclercq⁹, Damien Ambrosetti¹⁰, Baharia Mograbi¹, Stéphane Richard¹¹, Julien Viotti¹², Emmanuel Chamorey¹², Nirvana Sadaghianloo^{1, 2, 13}, Matthieu Rouleau¹⁴, William J. Craigen¹⁵, Bernard Mari¹⁶, Stéphan Clavel², Gilles Pagès^{1, 3}, Jacques Pouysségur^{1, 3}, Frédéric Bost² and Nathalie M. Mazure^{1, 2*}

1. Université Côte d'Azur (UCA), CNRS-UMR 7284-Inserm U1081, IRCAN, Centre Antoine Lacassagne, 33 Ave. de Valombrose, 06189 Nice, France.
2. Present address: Université Côte d'Azur (UCA), INSERM U1065, CSM, 151 Route de St Antoine de Ginestière, BP2 3194, 06204 Nice Cedex 03, France.
3. Medical Biology Department, Centre Scientifique de Monaco (CSM), Monaco.
4. Université Côte d'Azur (UCA), Centre Commun de Microscopie Appliquée, Nice, France.
5. Institut du thorax, INSERM, CNRS, Univ. Nantes, Nantes, France.
6. Ecole Pratique des Hautes Etudes, EPHE, PSL Research University, Paris, France.
7. INSERM UMR 1186, Integrative Tumor Immunology and Genetic Oncology, Gustave Roussy, EPHE, PSL, Fac. de médecine - Univ. Paris-Sud, Université Paris-Saclay, 114 rue Edouard Vaillant, 94800 Villejuif, France.
8. Centre Antoine Lacassagne, Oncology Department, Nice, France.
9. Rennes University Hospital, Department of Pathology, Rennes, France.
10. Centre Hospitalier Universitaire de Nice, Department of Pathology, Nice, France.
11. REDIR Center, Department of Urology, AP-HP, Bicêtre Hospital, 78 Rue du Général Leclerc, 94270 Le Kremlin-Bicêtre.
12. Centre Antoine Lacassagne, Statistics Department, Nice, France.
13. Centre Hospitalier Universitaire de Nice, Department of Vascular Surgery, Nice, France.
14. Université Côte d'Azur (UCA), CNRS-UMR 7370, LP2M, Nice, France.
15. Department of Molecular and Human Genetics, The Mitochondrial Diagnostic Laboratory, Baylor College of Medicine, Houston, TX 77030, USA.
16. Université Côte d'Azur (UCA), CNRS, IPMC, FHUOncoAge, 06560 Valbonne, France.

* These authors contributed equally to this paper.

✉ Corresponding author: mazure@unice.fr

© The author(s). This is an open access article distributed under the terms of the Creative Commons Attribution License (<https://creativecommons.org/licenses/by/4.0/>). See <http://ivyspring.com/terms> for full terms and conditions.

Received: 2019.10.08; Accepted: 2020.01.09; Published: 2020.02.03

Abstract

Rationale: Renal cell carcinoma (RCC) accounts for about 2% of all adult cancers, and clear cell RCC (ccRCC) is the most common RCC histologic subtype. A hallmark of ccRCC is the loss of the primary cilium, a cellular antenna that senses a wide variety of signals. Loss of this key organelle in ccRCC is associated with the loss of the von Hippel-Lindau protein (VHL). However, not all mechanisms of ciliopathy have been clearly elucidated.

Methods: By using RCC4 renal cancer cells and patient samples, we examined the regulation of ciliogenesis *via* the presence or absence of the hypoxic form of the voltage-dependent anion channel (VDAC1- Δ C) and its impact on tumor aggressiveness. Three independent cohorts were analyzed. Cohort A was from PREDIR and included 12 patients with hereditary pVHL mutations and 22 sporadic patients presenting tumors with wild-type pVHL or mutated pVHL; Cohort B included tissue samples from 43 patients with non-metastatic ccRCC who had undergone surgery; and Cohort C was composed of 375 non-metastatic ccRCC tumor samples from The Cancer Genome Atlas (TCGA) and was used for validation. The presence of VDAC1- Δ C and legumain was determined by immunoblot. Transcriptional regulation of IFT20/GLII expression was evaluated by qPCR. Ciliogenesis was detected using both mouse anti-acetylated α -tubulin and rabbit polyclonal ARL13B antibodies for immunofluorescence.

Results: Our study defines, for the first time, a group of ccRCC patients in which the hypoxia-cleaved form of VDAC1 (VDAC1- Δ C) induces resorption of the primary cilium in a Hypoxia-Inducible Factor-1 (HIF-1)-dependent manner. An additional novel group, in which the primary cilium is re-expressed or maintained, lacked VDAC1- Δ C yet maintained glycolysis, a signature of epithelial-mesenchymal transition (EMT) and more aggressive tumor progression, but was independent to VHL. Moreover, these patients were less sensitive to sunitinib, the first-line treatment for ccRCC, but were potentially suitable for immunotherapy, as indicated by the immunophenoscore and the presence of PDL1 expression.

Conclusion: This study provides a new way to classify ccRCC patients and proposes potential therapeutic targets linked to metabolism and immunotherapy.

Key words: Ciliopathy, clear cell Renal Cell Carcinoma, immunotherapy, HIFs, poor prognosis, primary cilium, Voltage-Dependent Anion Channel 1, VDAC1.

Introduction

Among the many dysfunctions of tumor cells, the decreased prevalence or loss of the primary cilium, a small sensory organelle in which many signaling factors are known to be concentrated, is being increasingly recognized [1-3]. This cilia loss redefines cancer as a form of ciliopathy [4-6]. The primary cilium (PC) is a single protrusion emerging from the apical surface of the cell membrane of nearly all mammalian cells during interphase. It senses external signals from the microenvironment and initiates corresponding signaling cascades to the rest of the cell, such as the Hedgehog (Hh) and Wntless (Wnt) pathways [7-11]. Its structure is built of a microtubule-based axoneme, which confers mechanical strength and guides the transport of molecules *via* motor-dependent intraflagellar transport (IFT). Any defects in the structure, the activity or the function of the PC affect multiple systems, the consequences of which can be devastating or even life-threatening. There are many phenotypes that are associated with ciliopathies, including renal diseases [12], with the kidneys being among the organs that are most highly affected. A spectrum of renal diseases have been associated with ciliopathic syndromes, including a morphologically heterogeneous group of disorders that have been classified as polycystic kidney disease, renal medullary cystic disease, cystic renal dysplasia and, more recently, renal cell carcinoma [13-15]. The von Hippel-Lindau (VHL) protein is encoded by a known tumor suppressor gene, and has been shown to be necessary to maintain cilia [13, 14]. Mutations or deletions in the *VHL* gene, in addition to methylation, are characteristic features of: (i) a rare hereditary tumor disease caused by germline alterations of the *VHL* gene [16] and (ii) sporadic clear cell renal cell carcinoma (ccRCC) lacking cilia [17]. The VHL protein, a component of an E3 ubiquitin ligase complex, ubiquitylates HIFs and targets them for degradation by the proteasome [18]. Interestingly, ccRCCs that are deficient in pVHL cluster into tumors

that express either both HIF-1 α and -2 α or HIF-2 α only.

The voltage-dependent anion channel 1 (VDAC1) is the most abundant protein of the mitochondrial outer membrane. VDAC1 has fundamental functions in regulating energy production, calcium signaling and promoting apoptotic signaling [19, 20]. A strong relationship between VDAC and hexokinase, the first enzyme of glycolysis, confirms the interconnection between the regulation of glycolysis and mitochondrial respiration. We have further described the role of VDAC1 under hypoxic conditions, in a HIF-1-dependent manner, and showed that a cleaved form of VDAC1 (VDAC1- Δ C) plays a role in promoting resistance to apoptosis, in increasing metabolism and thus in cancer cell survival [21, 22]. We characterized its cleavage by the asparagine endopeptidase (Legumain, LGMN) at asparagine 214 to produce VDAC1- Δ C [23]. We also showed that the knockout of *Vdac1* in murine embryonic fibroblasts (MEFs) expressing oncogenic RAS potentiates tumor development in mice by promoting metabolic reprogramming, accelerating vascular destabilization and inflammation [23]. Finally, a new function for members of the VDAC family has recently been discovered: centrosomal VDAC3 associates with the centrosome *via* Mps1, a protein kinase that plays a role in centriole assembly [24], and this complex leads to aberrant ciliogenesis [24, 25]. A similar function has also been described for the centrosomal form of VDAC1. The authors showed that VDAC1 and VDAC3 both negatively modulate PC but with non-redundant functions. However, the mechanisms by which VDACS act on ciliogenesis are unknown.

In the present study, we therefore sought to explore the function of mitochondrial VDAC1- Δ C in the context of ccRCC cells and patients, a rare cancer where ciliopathy and HIF stabilization co-exist. We hypothesized that mitochondrial VDAC1- Δ C could control ciliogenesis. Interestingly, we identified a

new group of ccRCC patients in which the primary cilium is re-expressed giving rises to increased tumor aggressiveness. This group is also characterized by the absence of VDAC1-ΔC.

Materials and Methods

Cell culture

RCC4/pVHL and 786-O cells were grown in Dulbecco's Modified Eagle's Medium (DMEM) (Gibco-BRL) supplemented with 5% fetal bovine serum with penicillin G (50U/ml) and streptomycin sulfate (50μg/ml). A498 RCC cell lines were purchased from the ATCC (March 3, 2013). The RCC10 cell line was a kind gift from Dr. W.H. Kaelin (Dana-Farber Cancer Institute, Boston, MA). Normal epithelial HK2 cells were a kind gift from Dr I. Rubera (LP2M, Nice, France).

An INVIVO₂ 200 anaerobic workstation (Ruskin Technology Biotrace International Plc) set at 1 % oxygen, 94 % nitrogen and 5 % carbon dioxide was used for hypoxic conditions.

Pharmacological inhibitors and chemicals

3BP was from Sigma. Sunitinib was from Centre Antoine Lacassagne.

RNA interference

The 21-nucleotide RNAs were chemically synthesized (Eurogentec, Seraing, Belgium) and previously described. The siRNA sequences, all validated, were as follows: siCt1 (forward) 5'-CCU-ACA-UCC-CGA-UCG-AUG-AUG-TT-3' [26], siVDAC1 (forward) 5'-GAUACACUCAGACUCUAA-3' [22, 27], siHIF-1α (forward) 5'-CUG-AUG-ACC-AGC-AAC-UUG-ATT-3' [22, 26, 28], siHIF-2α (forward) 5'-CAG-CAU-CUU-UGA-UAG-CAG-UTT-3' [26]. siLGMN also known as AEP has been described previously [27]. siIFT20 and siGLI1 were from Mission esiRNA Sigma, and were a heterogenous mixture of siRNAs that all target the same mRNA sequence.

Quantitative real-time PCR analysis

For tumor samples, total RNA was extracted with the RNeasy FFPE Kit (QIAGEN, Hilden, Germany). For cells, total RNA was extracted with the RNeasy Mini Kit (QIAGEN, Hilden, Germany). The amount of RNA was evaluated with a NanoDrop™ spectrophotometer (ThermoFisher Scientific, Waltham, MA USA). One μg of total RNA was used for reverse transcription, using the QuantiTect Reverse Transcription kit (QIAGEN, Hilden, Germany), with a blend of oligo (dT) and random primers to prime first-strand synthesis. SYBR master mix plus (Eurogentec, Liege, Belgium) and specific

oligonucleotides (Sigma Aldrich) were used for qPCR. Primer sequences used are: *GLI1* (forward: 5'-TGCAGTAAAGCCTTCAGCAATG-3'; reverse: 5'-TTTTTCGAGCGAGCTAGGAT-3'), *IFT20* (forward: 5'-GGTATCGGGTTGAATATGAAG-3'; reverse: 5'-GACATAGGTCATTGGTCAAG-3'), *LGMN* (forward: 5'-ACTATGATGAGAAGAGGTCC-3'; reverse: 5'-GGTGGAGATIGTTTTGTTTC3'); *PDL1* (forward: 5'-ATGCCCCATACAACAAAATC-3'; reverse: 5'-GACATGTCAGTTCATGTTTCAG3'); *STAT3* primers was a kind gift from Dr J. Gilleron (C3M, Nice).

Immunoblotting

Cells were lysed in 1.5x Laemmli buffer and the protein concentration determined using the BCA assay. 40 μg of protein from whole cell extracts was resolved by SDS-PAGE and transferred onto a PVDF membrane (Millipore). Membranes were blocked in 5% non-fat milk in TN buffer (50 mM Tris-HCl pH 7.4, 150 mM NaCl) and incubated in the presence of the primary and then secondary antibodies in 5% non-fat milk in TN buffer. The rabbit polyclonal antibody to central regions of VDAC1 was purchased from Abcam (ab15895). Rabbit polyclonal anti-HIF-1α antibody (antiserum 2087) was produced and characterized in our laboratory [29]. The antibodies against HIF-2α (NB100-122) and ARL13b (NBP2-15463) were purchased from Novus Biologicals (Littleton, CA). Mouse anti-acetylated α-tubulin (T7451), anti-β-tubulin, HSP90 and β-actin were from Sigma. ECL signals were normalized to either β-tubulin or HSP90. Anti-LGMN antibody (AF2058) was from R&D system. After washing in TN buffer containing 1 % Triton-X100 and then in TN buffer, immunoreactive bands were visualized with the ECL system (Amersham Biosciences).

Immunocytochemistry

Cells were fixed in 3% paraformaldehyde and permeabilized with Triton X-100. Primary antibodies included mouse anti-acetylated α-tubulin (Sigma-Aldrich, Basel, Switzerland; 1:400 dilution); rabbit anti-Arl13b (Novusbio, Abingdon, United Kingdom; 1:400 dilution). Alexa Fluor 594- and 488-conjugated secondary goat anti-mouse or goat anti-rabbit antibodies (Molecular Probes, Carlsbad, CA) were used at 1:400. Cells were visualized by wide-field, fluorescence microscopy using a DM5500B upright stand (Leica, Germany) with a 40X oil objective NA 1.00. The cubes used were A4 (excitation filter BP 360/40, dichroic mirror 400, emission filter BP 470/40), L5 (BP 480/40, 505, BP 527/30), and TX2 (BP 560/40, 595, BP645/75). Acquisitions were done with an Orca-ER camera (Hamamatsu, Japan). Cells

were also visualized using the confocal microscope, Axiovert 200M inverted stand (Zeiss, Germany). Objectives 10X dry NA 0.3 and/or 25X multi immersion (oil, glycerol, water) NA 0.75, and/or 40X oil 1.3 NA and/or 63X oil 1.4 NA were used. The LASERS used were diode 405 nm, and/or Argon 488 nm, and/or HeNe 543 nm. The microscope was equipped with an automated xy stage for mosaic acquisitions.

Cilia frequency was counted manually from scans using a 40X digital zoom for 100-300 nuclei.

Immunohistochemistry

Normal and renal cell carcinoma tissue sections (5 μ m) were obtained from the Department of Pathology of Centre Hospitalier Universitaire de Nice, Nice (France). The sections had been formal fixed within 1h of surgery, for a total of 72h before being paraffin-embedded. After dewaxing, rehydrating, antigen retrieval was achieved by boiling in 0.01 M citrate buffer for 20 min. For immunofluorescence detection of primary cilia, sections were incubated with mouse anti-acetylated α -tubulin (Sigma-Aldrich, Basel, Switzerland; 1:50 dilution), rabbit anti-Arl13b (Novusbio, Abingdon, United Kingdom; 1:50 dilution) or rabbit anti-PDL1 (eBioscience ThermoFisher Scientific, Waltham, USA; 1:10 dilution) primary antibodies, then followed by goat anti-mouse secondary antibodies conjugated to Alexa 594 and goat anti-rabbit secondary antibodies conjugated to Alexa 488 (Molecular Probes, Invitrogen, Basel, Switzerland; 1:100 dilution). Nuclei were labeled with 2 mg/mL 4-6-diamidino-2-phenylindole (DAPI). Cilium counting was performed by focusing up and down on the microscope to capture cilia and nuclei that lay in different focal planes within the section. Images were obtained using an Axiovert 200M inverted stand (Zeiss, Germany) with a 40X oil objective 1.3 NA with samples mounted in an immersion medium (water). A diode 405 nm, Argon 488 nm and HeNe 543 nm laser was used. Optical sections were 0.3 μ m thick and stacks were made encompassing a Z-plane depth of 0.5 μ m. The number of cilia was counted manually from scans using a 40X digital zoom for at least 500 nuclei.

FACS analysis

For determination of IFT20 expression in RCC4+pVHL-, RCC4-, RCC4 siCtl-, RCC4 siVDAC1-, RCC4 siLGMN- cells, cellular suspensions (1×10^6 cells) were resuspended in 4% PFA for 15 min and washed 3 times in cold PBS/BSA 0.1%. Cell suspensions were then incubated with a polyclonal rabbit anti-IFT20 (1 μ g/ 1×10^6 cells; Proteintech) for 1 h at 4°C in PBS/BSA 0.1% buffer. After washing, cells

were incubated with Alexa 488-conjugated secondary goat anti-rabbit antibody (μ g/ 1×10^6 cells;) for 30 min and washed prior to analysis. Samples were collected with Miltenyi MCSQuant10 (Bergisch Gladbach, Germany) and analyzed with FlowJo Software. Secondary antibody in the control experiment was identical to that described *supra*.

Invasion assay

The invasion assay was performed using cell culture inserts with 8.0 μ m pore transparent PET membrane coated with 10 μ g/mL fibronectin. Inserts were coated with 2 μ g/ μ L of Matrigel and incubated for 3 h at 37 °C in a CO₂ incubator. Briefly, overnight serum-starved cells (8×10^4 cells) were seeded into the top chamber in medium without FBS, while medium with 10% FBS was present in the bottom chamber. The cells were incubated for 24 h. Media and remaining cells were removed from the top chamber with a cotton swab and washed twice with PBS. The bottom chamber was aspirated and washed twice with PBS. Inserts were fixed with 4% PFA. Invasiveness was assayed in triplicate for each condition, in at least three independent experiments. Cells that invaded the Matrigel and migrated through the filter and adhered to the lower surface were stained for 10 min with 0.5% crystal violet in 25% methanol. Inserts were rinsed in distilled water until no additional stain leached and were air-dried overnight. Crystal violet was extracted from the invading cells by adding 600 μ L of 0.1 M sodium citrate in 10% acetic acid. Absorbance was measured spectrophotometrically at 585 nm using the Spectronic GENESYS 5 (Milton Roy, Rochester, NY).

Tumor spheroid invasion assay

A cell suspension of 15×10^3 cells/mL was prepared and 200 μ L aliquots were put in 24 wells containing solidified agarose 1% and incubated at 37°C for 48h. Spheroids containing 3000 cells each were placed on the inside of the cover of a culture dish and incubated at 37°C. Formed spheroids were transferred into wells containing matrigel 25% + 1 mg/mL 3D collagen I gel and left to grow for the designated time (24h, 48h and 72h). Diameters of the spheroids were monitored by an Evos optical microscope. Cell invasion through the surrounding collagen was measured using the ImageJ software and the final spheroid size was compared to the initial size at time zero. At least 8 spheroids were analyzed per condition and at least three independent experiments were performed.

CAM assay

Fertilized chicken eggs (*Gallus gallus*) (EARL Morizeau, Dangers, France) were handled as previously described [30]. On embryonic day 9, a

plastic ring was placed on the CAM, and 1 million RCC4 or RCC4+pVHL cells in 20 μ L of medium were deposited on the surface. Digital photos were taken under a stereomicroscope.

Wound-healing assay

The equivalent number of RCC4 and RCC4+pVHL cells were seeded and incubated for 24 h. Cells were photographed at the time of insert removal (0 h), then 8 h, 16 h and 20 h after. The percentage of the scratched area at each time point was calculated with ImageJ.

Immunophenoscore

Immunophenoscore is a predictor of the response to checkpoint blockade established by Charoentong et al. based on a panel of immune genes for classification of patients likely to respond to therapy with antibodies targeting CTLA-4 and PD-1 with superior performance [31].

Patients and cohorts

RCC was classified according to the tumor, node and metastasis (TNM) system developed by the American Joint Committee on Cancer (AJCC). RCC was classified from Stage I to Stage IV according to the TN and a prognostic score.

Stages

- stage I: T1 N0 M0
- stage II: T2 N0 M0
- stage III: T3 or N1 with M0
- stage IV: T4 or M1

Patients from Nice (Table S1)

Tissue samples from 19 patients with ccRCC who had undergone surgery in the Urology and Pathology Departments of the Nice University Hospital were selected. For each patient, a piece of fresh tumor was embedded in paraffin (IF) and a piece was immediately frozen (immunoblot). For each patient, tumor diagnosis was based on pathology and on cytogenetic analyses, as defined by the 2016 World Health Organization criteria. This prospective study was approved by the institutional review board and was conducted in accordance with the Declaration of Helsinki.

Cohort A (PREDIR; Table S2)

A series of 32 renal tumors were obtained thanks to the PREDIR Center (French Kidney Cancer Consortium coordinated by S. Richard) composed of 12 VHL tumor-associated and 22 sporadic RCC that were verified as clear-cell renal cell carcinomas. Part of the microarray transcriptome analysis of this series

has been previously reported [32].

Cohort B (Table S3)

Tissue samples from 43 patients with ccRCC who had undergone surgery in the Urology Department of the Rennes University Hospital were selected. As defined by the 2016 World Health Organization criteria, diagnosis was based on the pathology and on cytogenetic analyses. This retrospective study was approved by the institutional review board and was conducted in accordance with the Declaration of Helsinki.

Cohort C (TCGA) has been previously described [33].

Gene expression microarray analysis

Normalized RNA sequencing (RNA-Seq) data produced by The Cancer Genome Atlas (TCGA) were downloaded from cBioportal (www.cbioportal.org, TCGA Provisional; RNA-Seq V2). Different parameters were available for 375 ccRCC tumor samples, with information for VHL status (methylation, mutation and deletion) [34, 35]. We performed a differential expression analysis between patients with a "primary cilium" signature and patients with a "no primary cilium" signature using the Bioconductor package DESeq2.

The results published here are in whole or in part based upon data generated by the TCGA Research Network: <http://cancergenome.nih.gov/>.

Database analysis

To assess the effect of the presence or absence of the primary cilium in ccRCC from Cohort C, we performed a differential analysis between the group expressing the primary cilium (n=48 patients) and the group expressing no primary cilium (n=327 patients) by computing the ratio and p-values obtained with a Wilcoxon rank sum test. We then performed a functional and pathway enrichment analysis on differentially expressed genes (p-value < 0.05 and absolute ratio > 0.7) based on Reactome databases using the geneSCF tool [36]. The terms are considered significant only if enriched with a p-value < 0.05.

Statistics

All values are the mean \pm SEM. Statistical analyses were performed using the Student's *t* test in Microsoft Excel. The *p* values are indicated. All categorical data used numbers and percentages. Quantitative data were presented using the median and range or mean. Differences between groups were evaluated using the chi square test for categorical variables and the Student's *t* test for continuous variables. Analyses were performed using SPSS 16.0

statistical software (SPSS Inc., Chicago, Ill). All statistical tests were two-sided, and p -values <0.05 indicated statistical significance whereas p -values between 0.05 and 0.10 indicated a statistical tendency.

Statistics for patients

The Student's t -test was used to compare continuous variables and chi-square test, or Fisher's exact test (when the conditions for use of the χ^2 -test were not fulfilled), were used for categorical variables. To guarantee the independence of the primary cilium as a prognostic factor, the multivariate analysis was performed using Cox regression adjusted to the stage and age. DFS was defined as the time from surgery to the appearance of metastasis. OS was defined as the time between surgery and the date of death from any cause, censoring those alive at last follow-up. The Kaplan-Meier method was used to produce survival curves and analyses of censored data were performed using Cox models. All analyses were performed using R software, version 3.2.2 (Vienna, Austria, <https://www.r-project.org/>).

Results

Low VDAC1 and LGMN expression levels are linked to poor prognosis in ccRCC patients

By interacting with hexokinase, or members of the Bcl-2 family, VDAC1 supports glycolysis and apoptosis is prevented. VDAC is thus involved in determining cellular survival or death, which is particularly relevant to cancer cells. To explore its possible role in ccRCC (kidney renal clear cell carcinoma, KIRC), we first interrogated the Gene Expression Profiling Interactive Analysis (GEPIA) human dataset. Interestingly, the patients' overall survival (OS; Figure 1A) and disease-free survival (DFS; Figure 1B) plots revealed a direct correlation between low levels of VDAC1 and a poor prognosis. As we had previously shown a link between the asparagine endopeptidase (LGMN) and VDAC1 in hypoxia (Supplementary Fig. S1A) [27, 37], we also explored the expression level of LGMN in the same cohort of ccRCC patients. Similar to VDAC1, both OS (Figure 1C) and DFS (Figure 1D) showed a strong correlation between low levels of LGMN and a poor prognosis. We obtained 19 tissue samples of ccRCC patients from the Pathology Department of Nice (CHU; Table S1). Fourteen out of 19 (73.7%) were classified with high VDAC1 expression and the presence of VDAC1- Δ C in tumor tissues (defined as group A) whereas five out of 19 (26.3%) were classified with a low level of VDAC1 and the absence of VDAC1- Δ C (defined as group B; Figure 1E-F). In group A, VDAC1- Δ C and LGMN were present in

tumor (T) tissues, except for patients #7 and #12 (Supplementary Fig. S1B). In contrast, group B showed no VDAC1- Δ C in tumor (T) tissues in parallel with weak or absent expression of LGMN. Moreover, LGMN protein expression (Figure 1E) also correlated to its mRNA level (Figure 1G). Of the 19 tissue samples from the ccRCC patients, HIF-2 and sometimes HIF-1 was present in each group suggesting that this classification does not depend on the HIF status (Figure S1C). VDAC1- Δ C expression was also analyzed in ccRCC cell lines. HK2, kidney epithelial cells from normal kidney, did not express VDAC1- Δ C under normoxic conditions (Figure 1H). As previously shown [38], analysis of VHL mutant RCC4 cell lines, in which the wild-type VHL gene has been restored (RCC4+pVHL), and thus mimicking normoxia with no stabilization of either HIF-1 α or -2 α , showed no VDAC1- Δ C whereas RCC4 cells with both stabilization of HIF-1 α or -2 α expressed VDAC1- Δ C. Moreover, LGMN was expressed in each cell line with higher expression in cells defective for pVHL (Figure 1H).

These results suggest a strong link between VDAC1/VDAC1- Δ C and LGMN in the ccRCC context and describe two groups of ccRCC patients with distinct prognoses.

The presence of VDAC1- Δ C in RCC4 and 786-O cells decreases or abolishes ciliation

As ccRCC is associated with the loss of VHL function, deregulation of the hypoxia pathway and the loss of primary cilia [39], we investigated a potential role of VDAC1 in ciliogenesis. Using mouse anti-acetylated α -tubulin (which are microtubule proteins that are enriched in the axonemes of most primary cilium), rabbit polyclonal ARL13B antibodies counterstained with DAPI for immunofluorescence (Figure 2A), and electron microscopy (Figure 2B) we found the presence of primary cilia in RCC4+pVHL and RCC4 cells only. A high proportion of ciliated cells were observed in RCC4+pVHL and RCC4 cells (between 60% to 32%), whereas no primary cilia were detected in 786-O, RCC10 and A498 (Figure 2C). RCC4 had 50% fewer primary cilia compared to RCC4+pVHL in similar conditions of proliferation. Cell proliferation was tested as the primary cilium is highly dependent on the cell cycle. RCC4 and RCC4+pVHL were cultured in the presence or absence of serum where cell growth was arrested (Figure 2D). No significant difference was observed between the two cell types. Following experiments were performed in the absence of serum in order to magnify the number of ciliated cells. However, as RCC4+pVHL and RCC4 cells presented a lower percentage of ciliated cells, these results suggest that

ciliogenesis and cell cycle could be deregulated and uncoupled in these tumoral cells. The knockdown of HIF-1 α alone or both HIF-1 α and -2 α using specific siRNAs, decreased the expression of VDAC1- Δ C and concomitantly increased the percentage of ciliated cells compared to siCtl (Figure 2E). However, the knockdown of HIF-2 α alone had no effect on VDAC1- Δ C and the primary cilium. Finally, siRNA targeting VDAC1 in the RCC4 cell line statistically increased the percentage of ciliated cells by more than

1.4-fold (Figure 2F). In order to block the hypoxic cleavage of VDAC1, LGMN was silenced in RCC4 cells (Figure 2G). VDAC1- Δ C totally disappeared and cells expressed a higher percentage of primary cilia, which was similar to what we have observed by downregulating VDAC1 expression.

These results strongly suggested that VDAC1- Δ C controls resorption of the primary cilium in the HIF-1/LGMN-dependent model of ccRCC.

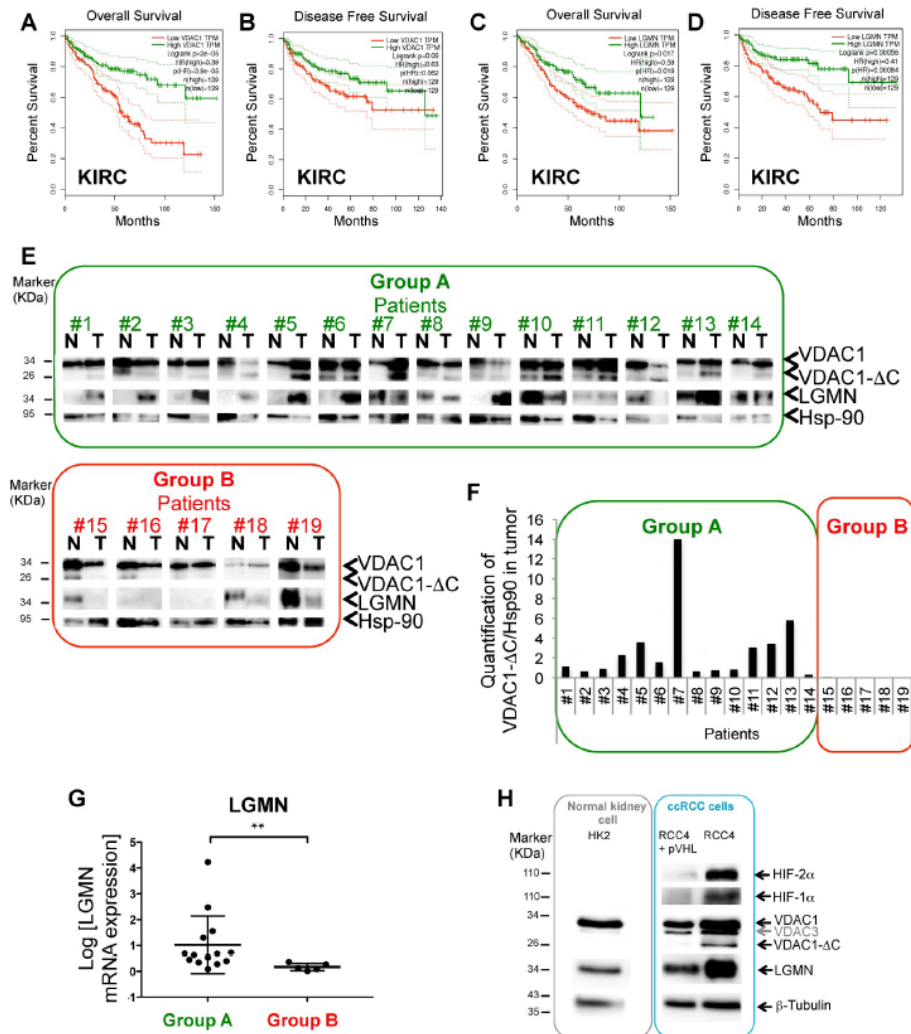


Figure 1. **A** and **B**, Overall survival (**A**) and Disease free survival (**B**) for VDAC1 expression was calculated from Kidney renal clear cell carcinoma (KIRC) (Gepia.cancer-pku.cn) using the third quartile for the cutoff. **C** and **D**, Overall survival (**C**) and Disease free survival (**D**) for LGMN expression was calculated from KIRC. **E**, Tissues lysates (Normal (N), Tumoral (T)) of 19 patients were analyzed by immunoblotting for VDCA1 and LGMN. Hsp-90 was used as a loading control. Group A: high level of VDAC1 + VDAC1- Δ C and LGMN in T. Group B: low level of VDAC1 and absence of VDAC1- Δ C and LGMN. **F**, Expression of VDAC1- Δ C and Hsp-90 proteins was quantified in tumoral tissues (T) and VDAC1- Δ C/Hsp-90 ratio was obtained in each patient. **G**, Graphic representation of LGMN mRNA expression in patients from Group A compared to patients from Group B. **H**, HK2, RCC4+pVHL, RCC4, cell lysates were analyzed by immunoblotting for HIF-2 α , HIF-1 α , LGMN and VDCA1. β -tubulin and Hsp-90 were used as a loading control.

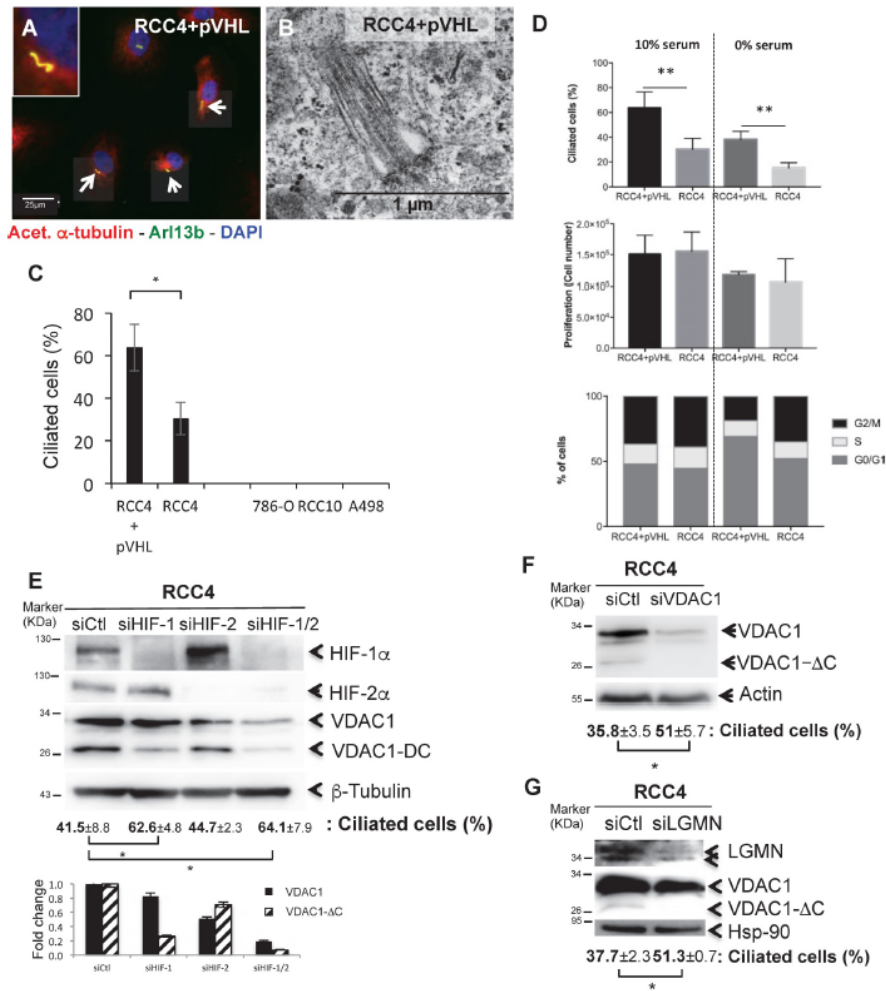


Figure 2. The presence of VDAC1-DC in ccRCC cells decreases or abolishes ciliation. **A.** Triple immunofluorescence labeling and merged images with acetylated α -tubulin (Acet. α -tubulin in red), Arl13b (in green) and DAPI (in blue). **B.** Electron microscopy of RCC4+pVHL cells. **C.** Quantitative analysis of the ciliation percentage was assessed by confocal fluorescence microscopy (n=100-300 cells). **D.** Both cell lines were seeded at the same density and incubated in Nx for 48h with or without serum. Percentage of ciliated cells, proliferation and FACS analysis were measured. The mean \pm SEM is representative of three independent experiments carried out in duplicate. **E, F and G.** RCC4 cells were transfected with control siRNA (siCtl), **(E)** siHIF-1 α , siHIF-2 α and siHIF-1/2 α , **(F)** siVDAC1 and **(G)** siLGMN. Cell lysates were analyzed by immunoblotting for HIF-1 α , HIF-2 α , VDAC1, LGMN and β -tubulin/Actin or HSP90 were used as a loading control. Quantitative analysis of the ciliation percentage was assessed by confocal fluorescence microscopy (n=100-300 cells). A * p<0.05 shows significant differences. Quantification of VDAC1 and VDAC1- Δ C protein levels (E). Experiments have been proceeded without serum.

The GLI1/IFT20 signature correlates to the primary cilium and VDAC1

To further reinforce the link between VDAC1- Δ C and the percentage of ciliated cells, we evaluated the expression of genes involved in the biogenesis and the activity of the primary cilium. The analysis of our transcriptomic data in WT MEF in hypoxia versus normoxia [23] highlighted differences in the expression of genes related to the primary cilium.

Given that mRNA levels of the *GLI1* transcription factor and the intraflagellar transport protein 20 (*IFT20*) had been shown to be modified in hypoxia, -0.59 and +0.91 respectively ([23], NCBI Gene Expression Omnibus (GEO) (<http://www.ncbi.nlm.nih.gov/geo/>) under the series record number GSE63247) and because this combination, among all those tested, proved to be a fair reflect of the presence or absence of the primary cilium, we chose to examine these two genes as indicators for the activity and

formation of the primary cilium. The less ciliated RCC4 cells had low expression levels of both *GLI1* and *IFT20* and could be classified as *GLI1*-/*IFT20*- cells in comparison to the more ciliated RCC4+pVHL cells (Figure 3A). Similarly, IFT20 protein abundance was decreased in RCC4 compared to RCC4+pVHL cells demonstrating a clear correlation between the mRNA and protein levels of IFT20 (Figure S2A). Moreover, a cell invasion assay to evaluate aggressiveness

demonstrated that RCC4 cells were less invasive compared to RCC4+pVHL cells (Figure 3B). This result was also confirmed using the three-dimensional, *in vitro*, chicken chorioallantoic membrane (CAM) assay and a migration assay (Figure S3).

Moreover, the RCC4+pVHL cells presented an epithelial-mesenchymal transition signature with higher expression of *TWIST*, *SNAIL* and *SLUG*

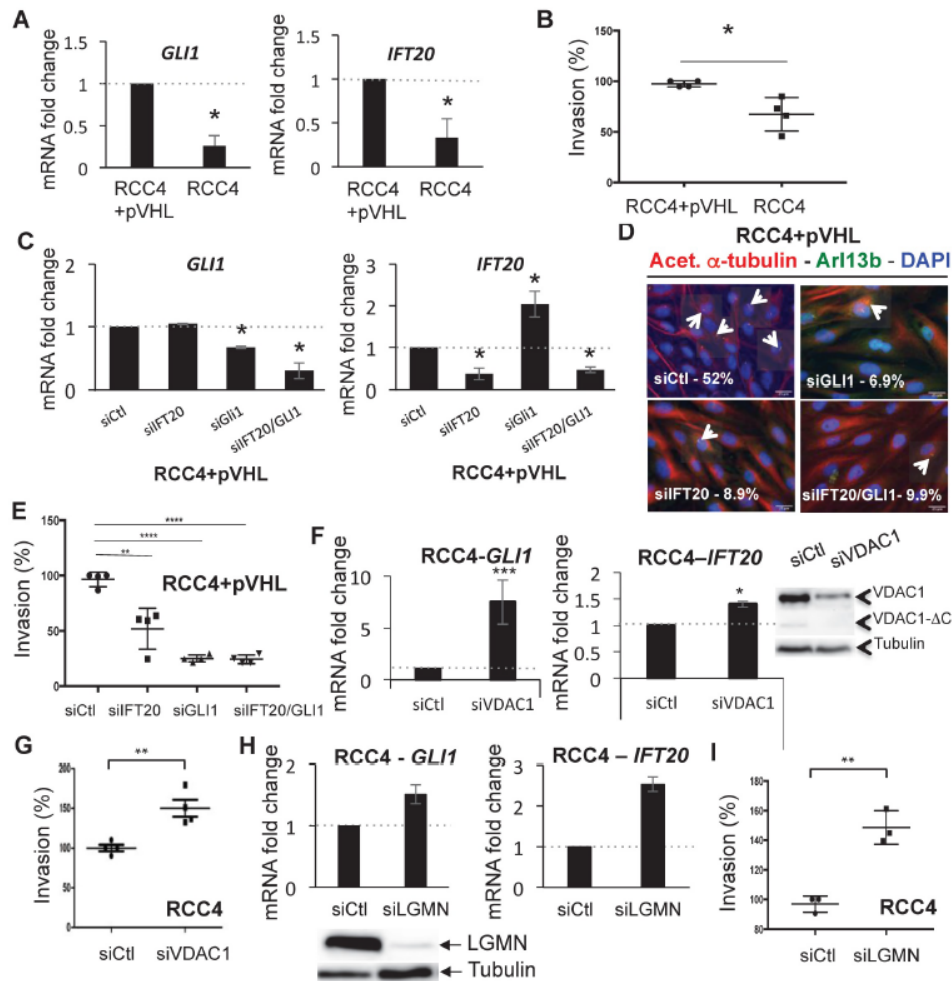


Figure 3. *GLI1/IFT20* signature is correlated to primary cilium and *VDAC1*. **A**, Histograms represent the expression of the mRNA of *GLI1* (left panel) and *IFT20* (right panel) in RCC4 cells compared to RCC4+pVHL in Nx. **B**, Graphic representation of the Boyden chamber cell-based invasion assay using RCC4+pVHL and RCC4 cells. **C**, RCC4+pVHL cells were transfected with control siRNA (siCtrl), si*GLI1* (40nM), si*IFT20* (40nM) and si*IFT20/GLI1* (40nM+40nM). Quantitative analysis of the ciliation percentage in RCC4+pVHL cells was assessed by confocal fluorescence microscopy (n=100-300 cells). **D**, Triple immunofluorescence labeling and merged images with acetylated α -tubulin (Acet. α -tubulin in red), Arl13b (in green) and DAPI (in blue). **E**, Graphic representation of the Boyden chamber cell-based invasion assay using RCC4+pVHL cells transfected with control siRNA (siCtrl), si*GLI1* (40nM), si*IFT20* (40nM) and si*IFT20/GLI1* (40nM+40nM). **F**, Histograms represent the expression of the mRNA of *GLI1* (left panel) and *IFT20* (right panel) in RCC4 cells transfected with siRNA *VDAC1*. Cell lysates from the same experiment were analyzed by immunoblotting. **G**, Graphic representation of the Boyden chamber cell-based invasion assay using RCC4 cells transfected with siRNA *VDAC1* compared to Ctl (siCtrl). **H**, Histograms represent the expression of the mRNA of *GLI1* (left panel) and *IFT20* (right panel) in RCC4 cells transfected with siRNA *LGMN*. Cell lysates from the same experiment were analyzed by immunoblotting. **I**, Graphic representation of the Boyden chamber cell-based invasion assay using RCC4 cells transfected with siRNA *LGMN* compared to Ctl (siCtrl). The mean \pm SEM is representative of three independent experiments. A * $p < 0.05$, ** $p < 0.005$ and *** $p < 0.0005$ show significant differences. Experiments have been proceeded without serum.

compared to RCC4 cells reinforcing the aggressivity profile often associated with EMT with a concomitant increase in glycolytic capacity. We then knocked down *GLI1* and *IFT20* in RCC4+pVHL cells (Figure 3C), and observed no change in the expression of *VDAC1* or *VDAC1-ΔC* (Figure S2B) but a decrease in the presence of primary cilia (Figure 3D) associated with decreased invasion (Figure 3E). Moreover, knocking down *GLI1* and *IFT20* in RCC4 cells (Figure S2C) also increased expression of *VDAC1* and, subsequently, increased expression of *VDAC1-ΔC* (Figure S2D). In contrast, RCC4 cells transfected with siRNA to *VDAC1* presented a gene expression profile of *GLI1+* and *IFT20+* cells and overexpression of *IFT20* compared to siRNA to *Ctl* (Figure 3F and Figure S2E). Moreover, in these cells, downregulation of *VDAC1* was sufficient to increase the invasive potential (Figure 3G). RCC4 cells transfected with siRNA targeting *LGGMN* presented a *GLI1+/IFT20+* signature and overexpression of *IFT20* (Figure 3H and Figure S2E) and were more aggressive (Figure 3I), which was similar to what we observed by downregulating *VDAC1*. To confirm the impact of the primary cilium on invasion, we silenced an independent marker of the primary cilium structure, *KIF3A*. RCC4+pVHL cells transfected with siRNA to *KIF3A* showed a significant decrease in ciliated cells, which was linked to a decrease in invasion (Figure S2F). In parallel, we overexpressed *GLI1* and *IFT20* in RCC4 cells (Figure S4A), and observed a reproducible increase in the percentage of ciliated cells (5%) (Figure S4B) associated with increased invasion (Figure S4C). Moreover, overexpression of *LGGMN* in RCC4+pVHL cells (Figure S4D) led to a *GLI1-* and *IFT20+* gene expression profile (Figure S4E) correlated with a decreased percentage of ciliated cells (Figure S4F) and decreased invasion potential (Figure S4G).

These results demonstrated that downregulation of *GLI1* and/or *IFT20* expression correlated with the decrease or absence of primary cilia expression in ccRCC cells with *VDAC1-ΔC* expression and *vice versa*. Moreover, the decrease in *VDAC1/VDAC1-ΔC* expression in RCC4 cells increased the percentage of ciliated cells and was correlated with increased invasive potential.

The 2-gene signature is predictive of the presence of both the *VDAC1-ΔC* and the primary cilium in ccRCC patients

To further confirm the value of the *GLI1* and *IFT20* signature obtained *in vitro*, this marker combination was tested on the 19 tissue samples and slides previously described (Figure 1E and Table 1). Four groups were formed on the basis of the expression patterns of these two genes: group 1 with

four patients (*GLI1+/IFT20-*), group 2 with five patients (*GLI1-/IFT20-*), group 3 with five patients (*GLI1-/IFT20+*) and group 4 with five patients (*GLI1+/IFT20+*; Figure 4A). On the basis of *GLI1* and *IFT20* expression at the mRNA level, but also at the protein level for *IFT20* only (Figure S5), and our previous results in ccRCC cell lines, 14 out of 19 (73.7%) from the previous group A, were found to have a “no primary cilium” signature, whereas 5 out of 19 (26.3%) from the previous group B, were classified with a “primary cilium” signature. As expected, we confirmed that the *GLI1+/IFT20-*, *GLI1-/IFT20-* and *GLI1-/IFT20+* signatures were linked to the presence of *VDAC1-ΔC* and the absence of the primary cilium, while the *GLI1+/IFT20+* signature was linked to the absence of *VDAC1-ΔC* and the increased presence of the primary cilium (8-18%; Figure 4A-C).

Table 1. Patient characteristics included in the study and multivariate analysis.

A

	Total	No primary cilium	Primary cilium	p value
Number	375	327	48	
Gender				ns
Female	135 (36%)	124 (38.8%)	11 (22.9%)	
Male	240 (64%)	203 (61.2%)	37 (77.1%)	
Age	61 (26-90)	61 (29-90)	58.5 (26-85)	ns
Tumor stage				<0.0001
1/2	259 (69.6%)	245 (74.9%)	14 (31.1%)	
3/4	113 (30.4%)	82 (25.1%)	31 (68.9%)	
Fuhrman grade				<0.01
1/2	189 (51.1%)	174 (54%)	15 (31.2%)	
3/4	181 (49.9%)	148 (46%)	33 (68.8%)	
DFS (months)	84.2	89.8	52	<0.0001
OS (months)	NR	NR	62.8	<0.0001

B

Univariate analysis	p value for DFS	p value for OS
Gender	ns	ns
Age	<0.0001	<0.0001
Tumor stage (1/2 vs 3/4)	<0.0001	<0.0001
Fuhrman grade (1/2 vs 3/4)	<0.01	<0.0001
Primary cilium (no vs yes)	<0.0001	<0.0001

C

DFS	Description	Hazard ratio [IC 95% OR]	p value
Biological parameters			
Primary cilium	no yes	2.438 [1.458-4.09]	7.10E-04
Clinical parameters			
Tumor stage	1 and 2 3 and 4	1.802 [1.173-2.768]	7.10E-03
Patient parameters			
Age		1.039 [1.033-1.07]	2.70E-08

D

OS	Description	Hazard ratio [IC 95% OR]	p value
Biological parameters			
Primary cilium	no yes	2.158 [1.367-3.406]	9.70E-04
Clinical parameters			
Tumor stage	1 and 2 3 and 4	2.13 [1.47-3.085]	6.10E-05
Patient parameters			
Age		1.039 [1.023-1.055]	4.70E-07

A, Patient characteristics and univariate analysis with the Fisher or K2 test. Statistical significance (*p* values) are indicated. B, Univariate analysis of primary cilium, tumor stage, Fuhrman grade, age and PFS or OS. Statistical significance (*p* values) is indicated. C and D, Multivariate analysis of primary cilium, tumor stage, age and PFS (C) or OS (D). The multivariate analysis was performed using Cox regression adjusted to the tumor stage and age. Statistical significance (*p* values) is indicated.

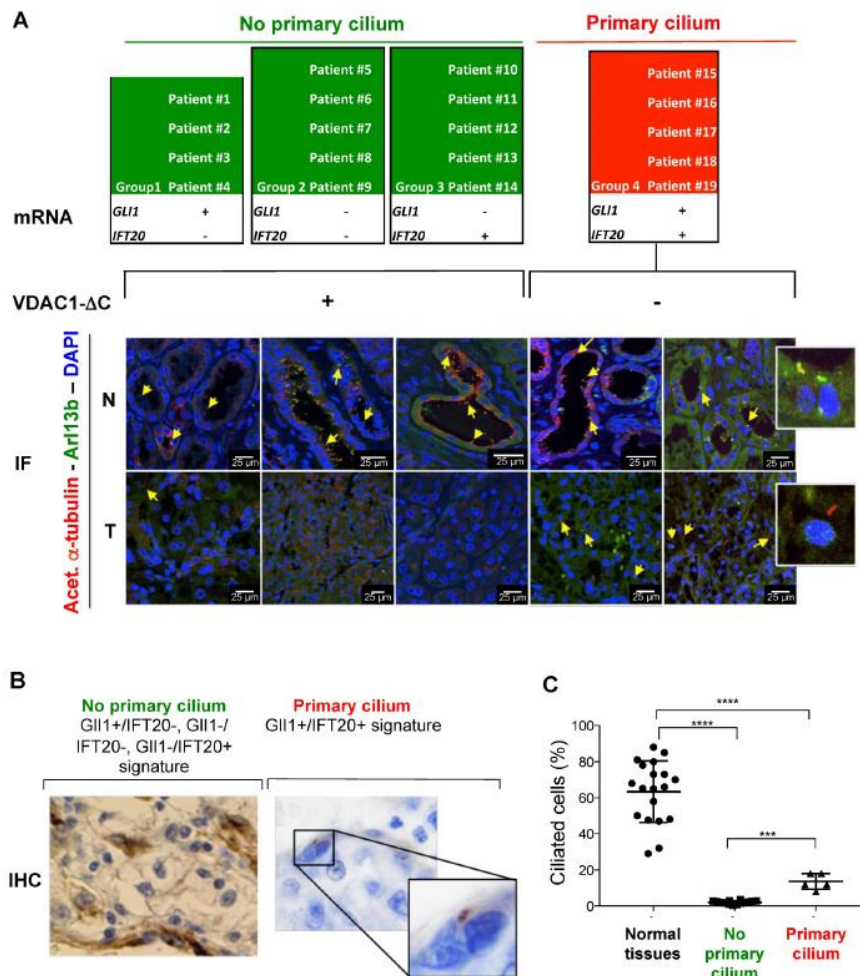


Figure 4. Identification and validation of the 2-gene signature predictive of the presence of VDAC1-ΔC and the primary cilium of ccRCC patients from 19 ccRCC patients. **A.** The mRNA (2-gene signature) and immunofluorescence (Acetyl. a-Tubulin, Arl13b and DAPI) of tumors samples of 12 patients were studied to evaluate the prediction model of the absence or presence of the primary cilium. Normal tissues (N) and tumoral tissues (T). **B.** Representative image of immunohistochemistry (IHC) analysis of the 19 patients studied to evaluate a prediction model of the absence or presence of the primary cilium. **C.** Percentage of ciliated cells in normal and tumor tissues from patients. A **** p<0.0005 show significant differences.

These results clearly demonstrate that this 2-gene expression signature provides a new form of classification, according to the presence or absence of the primary cilium and depending on VDAC1-ΔC. Moreover, our results unexpectedly uncovered one group of patients in which cancer cells expressed the primary cilium in a ciliopathic disease.

The tumors in the primary cilium re-expression groups are more aggressive than tumors with ciliopathy

To investigate the possibility of predicting the prognosis of ccRCC patients based on the presence of

the primary cilium, we tested if this two gene signature could be used to classify patients from three cohorts. First, a cohort of patients from PREDIR (Cohort A) was used with 12 patients with hereditary pVHL mutations and 22 sporadic patients presenting tumors with wild-type pVHL and mutated pVHL (Figure S6, Table S2). Tissue samples from 43 patients with non-metastatic ccRCC who had undergone surgery (Urology Department of the Rennes University Hospital; Cohort B; Table S3) [40] and 375 non-metastatic ccRCC tumor samples produced by The Cancer Genome Atlas (TCGA; Cohort C; www.cbioportal.org, TCGA Provisional; RNA-Seq

V2) [33] were analyzed. The same four gene signature groups were obtained (Figure 5A). In Cohort A, 100% of the pVHL patients had a signature with no primary cilium (GLI1-/IFT20- and GLI1+/IFT20-), whereas two patients with a primary cilium signature (GLI1+/IFT20+) were found in sporadic patients. No patient presented the group 3 signature in this cohort. For group 4, two (Cohort A) + nine (Cohort B) + 48 (Cohort C) patients were identified. This group

represented a low percentage of patients with the primary cilium signature, 5.9%, 20.9% and 12.8% respectively. In Cohort C, GLI1+/IFT20+ mRNA expression (primary cilium) correlated with shorter DFS (median survival of TCGA, 52 months versus 89.8 months (p<0.0001) compared to the GLI1+/IFT20-, GLI1-/IFT20- or GLI1-/IFT20+ signature (no primary cilium; Figure 5B).

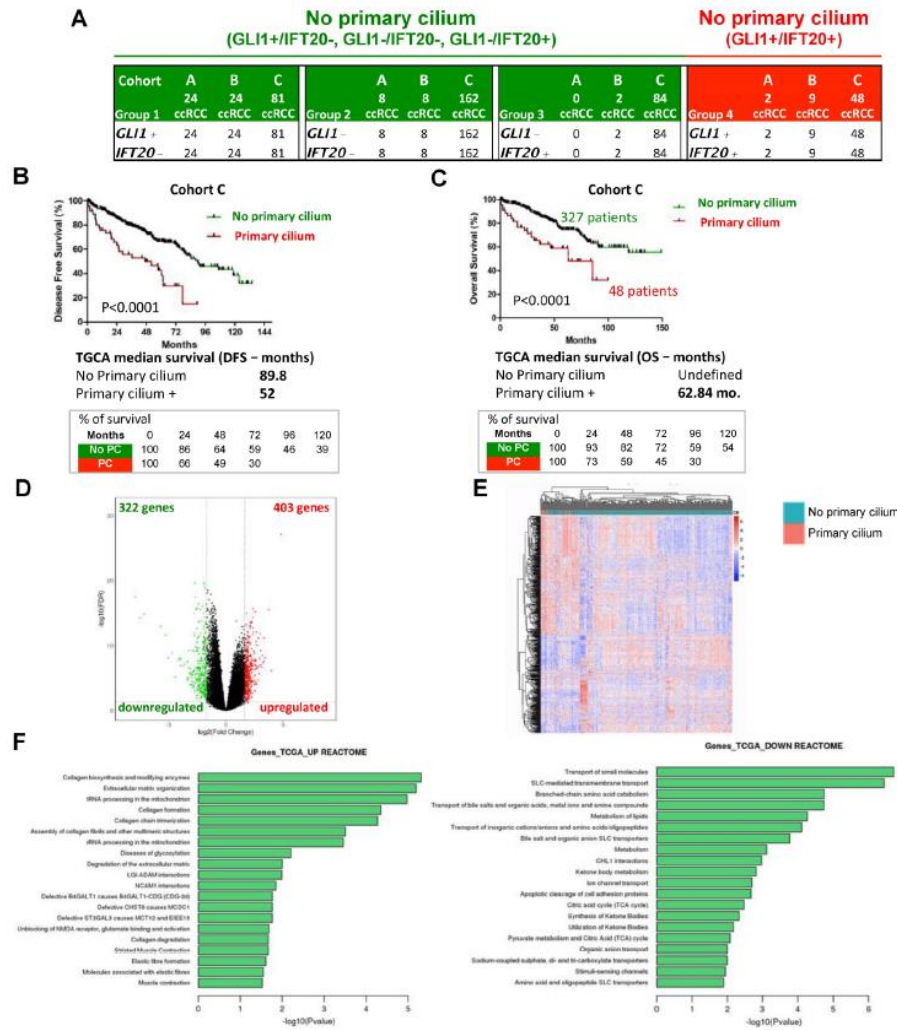


Figure 5. Identification and validation of the 2-gene signature predictive of the presence of primary cilia and of the aggressiveness of tumors of ccRCC patients from Cohort B and from TCGA (Cohort C). **A**, Amount of intra-tumor GLI1- and IFT20- from the Cohort B and Cohort C. **B**, Disease free survival for the primary cilium signature was calculated from patients of the cohort C using the GLI1/IFT20 signature (less or greater than the third quartile). **C**, Overall survival for the primary cilium signature was calculated from patients of the TCGA cohort C using the GLI1/IFT20 signature (less or greater than the third quartile). **D**, Volcano plot showing the distribution of differentially expressed transcripts. **E**, Heatmap comparing the normalized log2 expression (z score) of the differentially expressed genes between the 48 patients with primary cilium expression and the 327 patients with no primary cilium signature to obtain differentially expressed genes. A Wilcoxon test was performed to obtain a p-value showing the differential significance between the two groups. **F**, Graph of the top 20 enriched Reactome pathways from up-regulated and down-regulated genes.

Moreover, *GLI1+ /IFT20+* mRNA expression also correlated with shorter OS (median survival of cohort B, 101 months versus superior to 150 months ($p=0.09$) and median survival of TCGA, 62.84 months versus greater than 150 months ($p<0.0001$)) compared to the no primary cilium signature (Figure S7A and Figure 5C), strongly demonstrating that tumors expressing more primary cilia and without VDAC1- Δ C were more aggressive in a ciliopathy model; thus confirming our *in vitro* findings. We found high median survival in both groups 1 and 2 (> 150 months), whereas group 3 presented a lower OS (118.8 months; Figure S7B). We also established a correlation between the primary cilium and VDAC1 (Figure S7C). Patients with no primary cilium expressed a higher level of VDAC1 mRNA, whereas patients with primary cilia expressed a low level of VDAC1 mRNA, similar to the groups A and B that we characterized in Figure 1E. We observed a similar expression level for LGMN mRNA (Figure S7D). Using the tumor proliferation marker KI67 (MKI67) to assess tumor growth, we observed no correlation ($p=0.3573$) between the absence or the presence of the primary cilium and proliferation, demonstrating that the presence of the primary cilium did not impact the proliferation status of the tumor (Figure S7E). As expected, tumors with stabilization of HIF-2 α only presented a tendency to be more aggressive (OS median survival: 72.38 months versus undefined, $p=0.1035$) compared to those expressing both HIF-1 α /2 α Supplementary (Figure S7F). A volcano plot analysis to further explore the difference between patients with a primary cilium signature and patients with “no primary cilium” signature showed the expression of 403 genes to be UP (1.8%) and 322 DOWN (1.5%) when the mRNAs were significantly differentially expressed (Figure 5D). The results of hierarchical cluster analyses showed distinguishable mRNA expression profiles between the “primary cilium” patients and the “no primary cilium” patients (Figure 5E). Pathway analysis showed that the positively expressed mRNAs in these ccRCC patients were involved in collagen biosynthesis and its modifying enzymes, ECM organization, collagen formation/degradation, degradation of the ECM, whereas the negatively expressed mRNAs were involved in transport of small molecules, solute-carrier-mediated transmembrane transport, metabolism of lipids, and the TCA cycle. The UP mRNA signature pathways strongly suggested involvement of EMT (epithelial-mesenchymal transition; Figure 5F), which was confirmed by analyzing the expression patterns of individual genes such as *SNAIL*, *SLUG*, *TWIST1*, *TWIST2*, *TBX2* and *FN1* (Figure S8). However, the DOWN mRNAs

indicated complete metabolic reprogramming (Figure 5F). An in depth analysis of the TCGA database revealed 310 patients with pVHL- ccRCC and 65 patients with pVHL+ ccRCC defined *via* deletions, mutations and promoter methylation in pVHL (Figure S9). Among the pVHL- tumors, 250 ccRCC tumors in the TCGA expressed both HIF-1 and -2 but 60 expressed only HIF-2. Using the primary cilium signature, we characterized two sub-groups, no primary cilium (PC-) and primary cilium (PC+) in each category. The PC+ group contained a low number of patients (10.4%, 21.7% and 13.8%) compared to the PC- group and showed lower median survival. We also found that the majority of PC+ patients were mostly at advanced tumor stages (stage 3/4-66%) rather than stage 1/2 (34%), whereas we observed the opposite with PC- patients, 25.2% and 74.8% respectively (Table S4). Group 4 of PC+ patients presented a more aggressive pattern with increases in pathways for extracellular matrix modifications coupled with decreased OXPHOS and lipid metabolism but maintenance of glycolysis, which would favor EMT.

Finally, *in silico* transcriptomic data showed that the primary cilium signature correlates with tumor stage and, to a lesser extent, with the Furhman grade (Table 1A). The “primary cilium” signature, Furhman grade, tumor stage and age have an impact on DFS and OS (univariate analysis, Table 1B). The “primary cilium” signature represented a marker for DFS (Table 1C) and OS (Table 1D) independent of the tumor stage and age in a multivariate analysis. As an example, hazard ratios show that PC+ patients will be twice as metastatic as PC- patients (Hazard ratio = 2.448, DFS; Table 1C) and will die faster (Hazard ratio = 2.13, OS; Table 1D).

These results highlight that tumors from ccRCC patients expressing primary cilia with a *GLI1+ /IFT20+* signature but not VDAC1- Δ C are significantly more aggressive and are characterized by a poor prognosis. In this context, the increased presence of primary cilia in tumors is clearly a cancer promoter and the maintenance of glycolysis seems to be crucial to support this aggressiveness.

The tumors of primary cilium re-expression groups should respond to anti-glycolysis treatments and have a higher score indicative of better response to immunotherapy

Sunitinib (sunitinib malate, Sutent®, SU11248, Pfizer Inc.), a vascular endothelial growth factor receptor inhibitor, is widely used for patients with metastatic RCC, mostly in first-line treatment. Despite sunitinib's clinical efficacy, patients eventually develop drug resistance and disease progression

[41-45]. We thus checked if patients with tumors presenting the primary cilium, a *GLI1*/*IFT20* signature and no *VDAC1-ΔC* are resistant or sensitive to sunitinib. Analysis of these patients from the clinical trial SUVEGIL (Clinical trials.gov Identifier: NCT00943839), who had been treated with sunitinib, revealed that they had a lower survival rate than the groups with no primary cilium (Figure 6A and B, Table S5). To reinforce these results, *in vitro* experiments were conducted using *RCC4* and *RCC4+pVHL* cells in the absence or presence of sunitinib. We found that cells with *VDAC1-ΔC* were significantly more sensitive to treatment than

RCC4+pVHL cells (Figure S10A). *RCC4-*, *RCC4* *siVDAC1-* and *RCC4* *siLGMN-* cells were also treated with 5 μM of sunitinib (Figure S10B). Although sensitive to sunitinib, we found that *RCC4* cells with *VDAC1-ΔC* had a lower percentage of ciliated cells and were characterized by a “no primary cilium” signature, and were slightly more sensitive to treatment than cells with less *VDAC1* or no *VDAC1-ΔC* with a higher percentage of cilia and with a “primary cilium” signature. This was similar to the observations of patients from group 4 with more primary cilia.

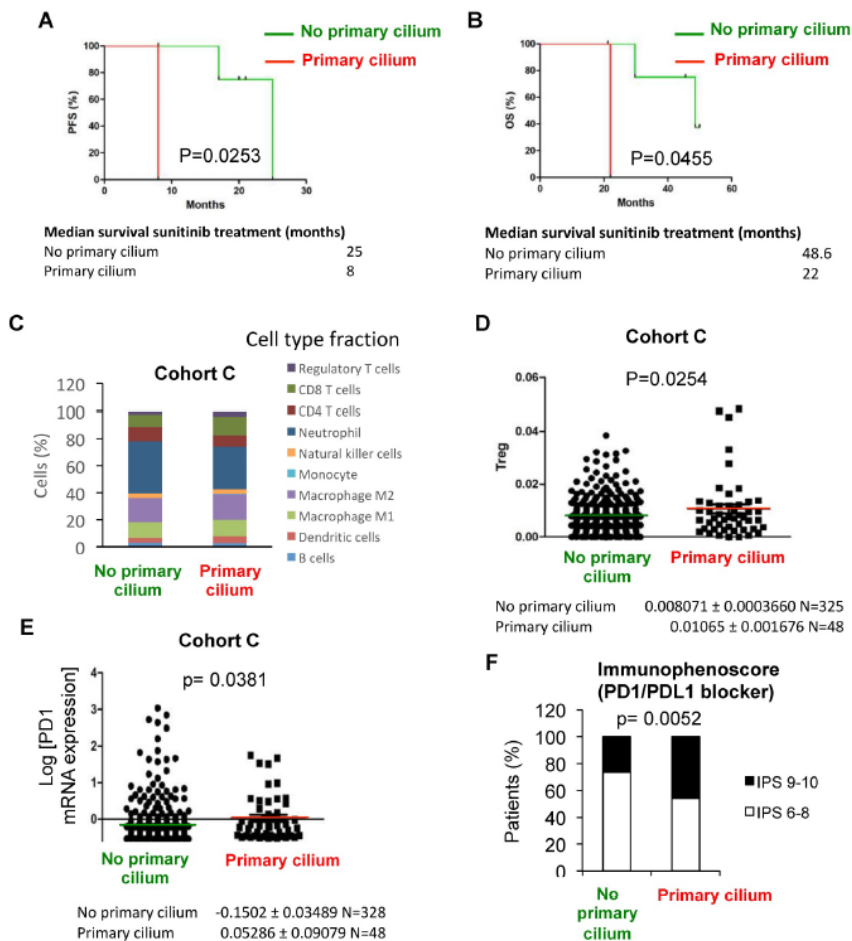


Figure 6. Patients with primary cilium signature present a higher immunogenicity compared to no primary cilium signature and a better response to immunotherapy. **A** and **B**. Progression-free-survival (PFS) (**A**) and Overall survival (OS) (**B**) for the primary cilium signature was calculated from patients of the TCGA cohort C treated with sunitinib using the *GLI1/IFT20* signature. PFS and OS were calculated from patient subgroups with *GLI1/IFT20* mRNA levels that were less or greater than the third quartile. Statistical significance (p-value) is indicated. The median survival is also indicated. **C**. *In silico* analysis of immune cell type fraction (%) according to the primary signature status (no primary cilium and primary cilium). **D**. *In silico* analysis of regulatory T lymphocytes (T reg) fraction (%) according to the primary signature status (no primary cilium and primary cilium). **E**. Tumors from patients with no primary cilium signature and tumors from patients with primary cilium were compared. The level of PD1 mRNA was determined by RNAseq for the TCGA cohort. Statistical significance (p value) is indicated. **F**. Distribution of ccRCC patients from the TCGA database depending on the primary cilium signature and immunophenoscore. p-value between no primary cilium and primary cilium is indicated.

As group 4 of “primary cilium” patients present a decrease in OXPHOS and lipid metabolism but maintenance of glycolysis, we used 3-Bromopyruvate (3BP), a halogenated analog of pyruvic acid that enters cells in the same way as lactate molecules, *via* monocarboxylic acid transporters, to block glycolysis in *in vitro* experiments. As expected, RCC4+pVHL cells and RCC4 siVDAC1 or RCC4 siLGMN with no VDAC1- Δ C, all characterized by an increase in primary cilia expression, were highly sensitive to 25 μ M of 3BP compared to RCC4 or RCC4 siCtl (Figure S10C and D). Moreover, the aggressiveness of RCC4 siVDAC1 or siLGMN treated with 3BP was decreased compared to the control (Figure S10E and F), suggesting a potential therapeutic use of glycolysis inhibitors.

Finally, as immunotherapy has become increasingly common for the treatment of clear cell RCC, we investigated the immune profile for each group. Slight differences were observed in the relative fraction of major immune cell types in “primary cilium” patients compared to “no primary cilium” patients of the TCGA cohort (Figure 6C) and a significantly higher proportion of T regulatory lymphocytes (Treg) was observed in the “primary cilium” patient group (Figure 6D). To reinforce these results, PD1 mRNA expression was significantly increased in the “primary cilium” patient group (Figure 6E). Furthermore, the immunophenoscore (Figure 6F), used as a predictor of response to anti-programmed cell death protein 1 (anti-PD1) treatment, was favorable for the “primary cilium” patient group. In the analysis of groups A and B from Figure 1G, we also observed a significant increase of PD-L1 mRNA expression in the “primary cilium” patient group B (Figure S11A) associated with increased frequency of cytoplasmic PDL1 punctae within vesicle-like structures in patient tumor sections (Figure S11B). These results clearly showed the specific immunotherapeutic potential for the “primary cilium” patient group.

Considered together, these results suggest that sunitinib is not the best treatment for patients re-expressing primary cilium. Our results indicate two therapeutic approaches, glycolysis inhibitors (3BP) and/or anti-PD1, that could be used in the first or second line only for the patients that present the strong “primary cilium” signature and for whom sunitinib is unfortunately less effective.

Discussion

Our data describe i) a new mechanism for the control of ciliogenesis that is driven by VDAC1- Δ C, the form of VDAC1 that is produced in hypoxia and ii) a new group of ccRCC patients in which the

primary cilium is re-expressed, giving rise to greater tumor aggressiveness.

The role of VDAC in metabolic homeostasis and cell death has been studied extensively [19, 20, 46-54]. However, new functions for VDAC1 as a ciliogenesis controller have been discovered, with Majumder *et al.* recently showing that centrosomal VDAC3 is associated with the centrosome *via* Mps1, a protein kinase that plays a role in centriole assembly [24]. The Mps1-VDAC3 complex, and also centrosomal VDAC1, were involved in the negative regulation of ciliogenesis. However, these results are not directly comparable because Majumder *et al.* used a retinal cell model rather than cancer cell models and we studied mitochondrial VDAC1 instead of centrosomal VDAC1. Our preliminary results have shown that VDAC1 is in close proximity to the centrosome (data not shown) suggesting that VDAC1 could directly participate in ciliogenesis, a mechanism that we are exploring further. We focused on the role of VDAC1- Δ C formation and the involvement of HIF-1. We have previously shown that VDAC1- Δ C formation is mitochondrial and is dependent on nuclear HIF-1 α in a lung cancer model [22]. However, it has been demonstrated that VDAC1- Δ C formation can also be triggered by the physical association of HIF-1 α with the mitochondrial outer membrane and a mortalin/VDAC1/HK2 complex under conditions that inhibit ERK activity and HIF-1 α phosphorylation [55]. Thus, we checked the subcellular localization of HIFs in RCC4 and the ERK activation status in patients. Our data clearly showed that HIFs are present in the nucleus of the RCC4 cells, as previously observed in LS174 cells, whereas P-ERK1/2 was observed in both Group A and Group B (data not shown) strongly suggesting that this mechanism is cell-type specific and does not occur in our ccRCC model.

Since 2012, we have been investigating the role of VDAC1- Δ C in hypoxia [22, 23, 27] and under iron deprivation conditions [56]. Our study describes, for the first time, a VDAC1- Δ C-dependent mechanism in which kidney cancer cells can maintain glycolysis in the presence of the EMT signature, which promotes survival of cells surrounded by an unfavorable microenvironment. Our study definitively shows that the hypoxic 2-gene expression signature, which we characterized, is closely related to the formation of VDAC1- Δ C and the absence or decreased prevalence of the primary cilium. The global OS allowed us to classify patients, by differentiating levels of tumor aggressiveness. However, we also described a new group of patients (group 4: *GLI1+/IFT20+*) expressing/re-expressing the primary cilium in a ciliopathy context. We demonstrated that patients

belonging to this group had much more aggressive tumors than patients with few or no primary cilia. The tumors in this group could be directly derived from healthy tissue but the expression of the EMT genes made the tumors of these patients more aggressive. In the first cohort we studied (Cohort A-PREDIR), the *GLI1+/IFT20+* signature was observed only in sporadic patients, suggesting that such expression/re-expression was impossible in patients with VHL mutations at the germinal level. However, the cohort of VHL patients was too small to draw conclusions.

Interestingly, we also found that each group (pVHL-/HIF-1+/HIF-2+, pVHL-/HIF-2+ and pVHL+) from the TCGA database presented 10.4, 21.7 and 13.8% of patients, respectively, with a *GLI1+/IFT20+* signature. The median survival of these patients was lower than for patients with a “no primary cilium” signature. Moreover, patients with this *GLI1+/IFT20+* signature presented a significant correlation between aggressiveness and lower VDAC1 expression. Similarly, in our study, siRNA to VDAC1 and LGMN in RCC4 cells shifted the signature in *GLI1+/IFT20+* and increased the primary cilium expression. These cells were characterized by higher invasion than siRNA to control cells suggesting a more aggressive phenotype. The same invasive behavior was found in RCC4+pVHL cells. The tumor aggressiveness in these patients could be the result of the combination of a switch to EMT process activation, re-expression or maintenance of the primary cilium, together with a decrease in VDAC1 and LGMN expression and thus the disappearance of the cleaved form of VDAC1.

In patients who express/re-express the primary cilium, it is unlikely that the primary cilium is the only force associated with aggressiveness. Indeed, we characterized a signature related to EMT that can explain the aggressive phenotype of the tumors of these patients. Moreover, metabolic remodeling was impacted, and although cancer metabolism is a hallmark of cancer, it has been shown that aberrant metabolism supports EMT [57, 58]. In the signature of the present study, lipid metabolism and the TCA signature were down-regulated in line with observations made by Hakimi *et al.* for ccRCC patients [59]. However, the expression of glycolytic enzymes was not modified, strongly suggesting that this metabolic pathway was favored in the cancer cells of group 4 patients. It is therefore possible to envisage specific treatment for these groups: Temsirolimus [60] or Everolimus, specific inhibitors of mTOR [61] that block proliferation, in combination with small molecule inhibitors that prevent EMT such as EW-7197 or IN-1130, through a block in TGF β 1 and 2, have already been used in metastatic breast and lung

cancer [62]. By maintaining only one metabolic pathway, cancer cells with a *GLI1+/IFT20+* signature offer a metabolic vulnerability that we would be wise to exploit. We have shown that inhibitors of glycolysis such as 3-bromopyruvate, used as a proof-of-concept, or inhibitors of lactate production (dichloroacetate, FX11, AZD-3965) [58] are of interest.

Finally, an immune-checkpoint inhibitor such as atezolizumab or nivolumab (an anti-PD-L1 or PD1 inhibitor) alone or in combination with glycolysis inhibitors could be evaluated on “primary cilium” patients who exhibit such reduced overall survival. Indeed, the presence of PD-L1 in group B strongly suggests an important role in promoting tumor progression. We have proposed several hypotheses to explain such expression patterns. Firstly, Noman and Chouaib have revealed the binding of HIF-1 α to the PD-L1 promoter [63], although we showed that absence of the primary cilium is driven by the pVHL/HIF/hypoxia axis, we showed that the resurgence of primary cilia in patients from group 4 was independent of HIF-1, HIF-2 and pVHL. Secondly, it has been reported that PDL1 works predominantly in lactate-enriched tumor micro-environments [64]. As tumors of patients from group 4 maintain glycolysis, and thus lactate production, this suitable microenvironment may protect cancer cells and thus could participate in the activation of PD-L1. Thirdly, epigenetic regulation has been revealed to be involved in PD-L1 expression in cancer cells [65]. MiRs, P53 and STAT3 were reported to epigenetically regulate PD-L1 expression. As ccRCC patients are mainly p53 wild type, we focused on STAT3 and observed a significant ($p < 0.001$) increase in STAT3 expression in patients from group 4 (data not shown). Understanding what regulates PDL1 in patients expressing primary cilia will be thus an important avenue of research going forward.

This novel classification of *GLI1+/IFT20+* ccRCC patients should have an impact on clinical practice, not only in characterizing new subgroups of ccRCC patients, but also in offering new combinations of treatments that are much more effective and more specific for a specific group of ccRCC patients.

Supplementary Material

Supplementary figures and tables.
<http://www.thno.org/v10p2696s1.pdf>

Acknowledgments

This research was supported by grants from the Fondation Flavien, the Fondation ARC, La Ligue contre le Cancer and Fondation de France. This work has been also supported by the French government, through the UCA^{JEDI} Investments in the Future project

managed by the National Research Agency (ANR) with the reference number ANR-15-IDEX-01. This study was conducted as part of the Centre Scientifique de Monaco Research Program, funded by the Government of the Principality of Monaco. The funders had no role in study design, data collection and analysis, decision to publish, or preparation of the manuscript. We acknowledge the excellent support of the Nice-Sophia Antipolis Functional Genomics Platform, the microscopy facility of C3M-INSERM U1065 (the help of Maeva Gesson is acknowledged) and the Cancerpole PACA. The authors would like to thank the "Centre de Ressources Biologiques" from Necker and Saint Joseph Hospitals (Paris, France) and Bicêtre Hospital (Le Kremlin-Bicêtre, France) for the samples of the PREDIR cohort, and Dr Sophie Ferlicot, Dr Virginie Verkarre and Dr Vincent Molinié for their histological analyses. We thank Abby Cuttriss (Office of International Scientific Visibility, Université Côte d'Azur).

Author Contributions

Conceptualization, L.F., M.D. and N.M.M.; Methodology, S.L.-G. and N.M.M.; Formal Analysis, N.N., B.M. and M.D.; Investigation, L.F., M.D., S.L.-G., J.P., M.M.C.deP., J.C., D.A., S.C., B. M., N.S., M.R., N.M.M.; Writing – Original Draft, N.M.M.; Writing – Review & Editing, L.F., M.D., S.C., F.B. and N.M.M.; Funding Acquisition, G.P., J.P. and N.M.M.; Resources, B.G., S.G.-L., N.R.L. and W.J.C.; Supervision, N.M.M.

Competing Interests

The authors have declared that no competing interest exists.

References

- Fliegauf M, Benzing T, Omran H. When cilia go bad: cilia defects and ciliopathies. *Nat Rev Mol Cell Biol.* 2007; 8: 880-93.
- Gradilone SA, Pisarello MJL, LaRusso NF. Primary Cilia in Tumor Biology: The Primary Cilium as a Therapeutic Target in Cholangiocarcinoma. *Curr Drug targets.* 2017; 18: 958-63.
- Fabbri L, Bost F, Mazure NM. Primary Cilium in Cancer Hallmarks. *Int J Mol Sci.* 2019; 20.
- Michaud EJ, Yoder BK. The primary cilium in cell signaling and cancer. *Cancer Res.* 2006; 66: 6463-7.
- Hassounah NB, Bunch TA, McDermott KM. Molecular pathways: the role of primary cilia in cancer progression and therapeutics with a focus on Hedgehog signaling. *Clin Cancer Res.* 2012; 18: 2429-35.
- Gerhardt C, Leu T, Lier JM, Ruther U. The cilia-regulated proteasome and its role in the development of ciliopathies and cancer. *Cilia.* 2016; 5: 14.
- Badano JL, Mitsuma N, Beales PL, Katsanis N. The ciliopathies: an emerging class of human genetic disorders. *Annual review of genomics and human genetics.* 2006; 7: 125-48.
- Gerdes JM, Davis EE, Katsanis N. The vertebrate primary cilium in development, homeostasis, and disease. *Cell.* 2009; 137: 32-45.
- Hynes M, Stone DM, Dowd M, Pitts-Meek S, Goddard A, Gurney A, et al. Control of cell pattern in the neural tube by the zinc finger transcription factor and oncogene Gli-1. *Neuron.* 1997; 19: 15-26.
- Ruiz I, Altaba A. Gli proteins encode context-dependent positive and negative functions: implications for development and disease. *Development.* 1999; 126: 3205-16.
- Berbari NF, O'Connor AK, Haycraft CJ, Yoder BK. The primary cilium as a complex signaling center. *Curr Biol.* 2009; 19: R526-35.
- Fry AM, Leaper MJ, Bayliss R. The primary cilium: guardian of organ development and homeostasis. *Organogenesis.* 2014; 10: 62-8.
- Plotnikova OV, Golemis EA, Pugacheva EN. Cell cycle-dependent ciliogenesis and cancer. *Cancer Res.* 2008; 68: 2058-61.
- Thoma CR, Frew IJ, Krek W. The VHL tumor suppressor: riding tandem with GSK3beta in primary cilium maintenance. *Cell Cycle.* 2007; 6: 1809-13.
- Chapman JR, Wong G. Cancer in patients with inherited ciliopathies: polycystic kidney disease. *Lancet Oncol.* 2016; 17: 1343-5.
- Richard S, Gardie B, Couve S, Gad S. Von Hippel-Lindau: how a rare disease illuminates cancer biology. *Semin Cancer Biol.* 2013; 23: 26-37.
- Esteban MA, Harten SK, Tran MG, Maxwell PH. Formation of primary cilia in the renal epithelium is regulated by the von Hippel-Lindau tumor suppressor protein. *J Am Soc Nephrol.* 2006; 17: 1801-6.
- Brahimi-Horn M, Laferrière J, Mazure N, Pouyssegur J. Hypoxia and tumour progression. In: Marmé D, Fussenig N, editors. *Tumor Angiogenesis.* Springer ed: Springer; 2007. p. 171-94.
- Shoshan-Barmatz V, Knuta H, Lemasters JJ. Editorial: Uncovering the Function of the Mitochondrial Protein VDAC in Health and Disease: From Structure-Function to Novel Therapeutic Strategies. *Front Oncol.* 2017; 7: 320.
- Shoshan-Barmatz V, Krelin Y, Shteinfer-Kuzmine A, Arif T. Voltage-Dependent Anion Channel 1 As an Emerging Drug Target for Novel Anti-Cancer Therapeutics. *Front Oncol.* 2017; 7: 154.
- Chiche J, Rouleau M, Gounon P, Brahimi-Horn MC, Pouyssegur J, Mazure NM. Hypoxic enlarged mitochondria protect cancer cells from apoptotic stimuli. *J Cell Physiol.* 2010; 222: 648-57.
- Brahimi-Horn MC, Ben-Hail D, Ilie M, Gounon P, Rouleau M, Hofman V, et al. Expression of a truncated active form of VDAC1 in lung cancer associates with hypoxic cell survival and correlates with progression to chemotherapy resistance. *Cancer Res.* 2012; 72: 2140-50.
- Brahimi-Horn MC, Giuliano S, Saland E, Lacas-Gervais S, Sheiko T, Pelletier J, et al. Knockout of Vdac1 activates hypoxia-inducible factor through reactive oxygen species generation and induces tumor growth by promoting metabolic reprogramming and inflammation. *Cancer Metab.* 2015; 3: 8.
- Majumder S, Cash A, Fisk HA. Non-Overlapping Distributions and Functions of the VDAC Family in Ciliogenesis. *Cells.* 2013; 4: 351-53.
- Majumder S, Slabodnick M, Pike A, Marquardt J, Fisk HA. VDAC3 regulates centriole assembly by targeting Mps1 to centrosomes. *Cell Cycle.* 2012; 11: 3666-78.
- Dayan F, Roux D, Brahimi-Horn MC, Pouyssegur J, Mazure NM. The oxygen sensor factor-inhibiting hypoxia-inducible factor-1 controls expression of distinct genes through the bifunctional transcriptional character of hypoxia-inducible factor-1alpha. *Cancer Res.* 2006; 66: 3688-98.
- Brahimi-Horn MC, Lacas-Gervais S, Adaxio R, Ilc K, Rouleau M, Notte A, et al. Local mitochondrial-endolysosomal microfusion cleaves the voltage-dependent anion channel 1 to promote survival in hypoxia. *Mol Cell Biol.* 2015; 35: 1491-505.
- Chiche J, Ilc K, Laferrière J, Trotter E, Dayan F, Mazure NM, et al. Hypoxia-inducible carbonic anhydrase IX and XII promote tumor cell growth by counteracting acidosis through the regulation of the intracellular pH. *Cancer Res.* 2009; 69: 338-68.
- Richard DE, Berra E, Gothie E, Roux D, Pouyssegur J. p42/p44 mitogen-activated protein kinases phosphorylate hypoxia-inducible factor 1alpha (HIF-1alpha) and enhance the transcriptional activity of HIF-1. *J Biol Chem.* 1999; 274: 32631-7.
- Vu BT, Shahin SA, Croissant J, Fatiev Y, Matsumoto K, Le-Hoang Doan T, et al. Chick chorioallantoic membrane assay as an in vivo model to study the effect of nanoparticle-based anticancer drugs in ovarian cancer. *Sci Rep.* 2018; 8: 8524.
- Charoentong P, Finotello F, Angelova M, Mayer C, Efreanova M, Rieder D, et al. Pan-cancer Immunogenomic Analyses Reveal Genotype-Immunophenotype Relationships and Predictors of Response to Checkpoint Blockade. *Cell Rep.* 2017; 18: 248-62.
- Gattoliat C-H, Couvè S, Maurice G, Orsà C, Droin N, Chiquet M, et al. Integrative analysis of dysregulated microRNAs and mRNAs in multiple recurrent synchronized renal tumors from patients with von Hippel-Lindau disease. *Int J Oncol.* 2018.
- Dufies M, Nollet M, Ambrosetti D, Traboulsi W, Viotti J, Borchiellini D, et al. Soluble CD146 is a predictive marker of pejorative evolution and of sunitinib efficacy in clear cell renal cell carcinoma. *Theranostics.* 2018; 8: 2447-58.
- Chen F, Zhang Y, Senbabaoglu Y, Ciriello G, Yang L, Reznik E, et al. Multilevel Genomics-Based Taxonomy of Renal Cell Carcinoma. *Cell Rep.* 2016; 14: 2476-89.
- Ricketts CJ, De Cubas AA, Fan H, Smith CC, Lang M, Reznik E, et al. The Cancer Genome Atlas Comprehensive Molecular Characterization of Renal Cell Carcinoma. *Cell Rep.* 2018; 23: 3698.
- Subhash S, Kanduri C. GeneSCF: a real-time based functional enrichment tool with support for multiple organisms. *BMC bioinformatics.* 2016; 17: 365.
- Pahima H, Reina S, Tadmor N, Dadon-Klein D, Shteinfer-Kuzmine A, Mazure NM, et al. Hypoxic-induced truncation of voltage-dependent anion channel 1 is mediated by both asparagine endopeptidase and calpain 1 activities. *Oncotarget.* 2018; 9: 12825-41.
- Berra E, Richard DE, Gothie E, Pouyssegur J. HIF-1-dependent transcriptional activity is required for oxygen-mediated HIF-1alpha degradation. *FEBS Lett.* 2001; 491: 85-90.

